THE UNIVERSITY *of* EDINBURGH

A STUDY OF RADIONUCLIDES, LEAD AND LEAD ISOTOPE RATIOS IN SCOTTISH SEA LOCH SEDIMENTS

TRACY MARJORY SHIMMIELD

PhD Thesis
University of Edinburgh
1993

ABSTRACT

This research involved the study of sediment cores from Loch Etive, Loch Long, Loch Goil and Loch Fyne with the aims of investigating the geochemistry of natural, and manmade radionuclides and heavy metals within the sea loch environment. The main aims of the research were to determine accumulation rates and the extent of mixing within these sediments and to assess the fluxes, sources and temporal variations in input of pollutant heavy metals to these environments. In recent years it has been suggested that Pb is mobile in sea loch sediments which questions the validity of applying ^{210}Pb dating in this environment. This has important implications with respect to interpreting sediment cores to assess temporal trends of pollutant inputs and investigating the rates of physical and biogeochemical processes that are taking place in the coastal environment. Hence, one of the aims of this research was to determine whether Pb was mobile in these sediments. The ^{206}Pb/^{207}Pb isotope ratio can potentially be used to determine the extent of pollutant Pb input from leaded petrol to the environment and a further objective of the work was to investigate the isotopic signature of pollutant Pb in the sediment.

Concentration of ^{210}Pb, ^{226}Ra, ^{228}Ra, ^{228}Th, ^{238}U, ^{137}Cs, ^{134}Cs and ^{241}Am in the sediments were analysed using gamma spectroscopy and the heavy metals, Pb, Zn and Cu were determined using X-ray Fluorescence. Stable Pb isotope ratios were determined using Inductively coupled plasma Mass spectrometry.

The results obtained indicated that Pb is not subject to diagenetic mobility in these sediments and that ^{210}Pb profiles can be used to determine sedimentation rates for most of the sediment cores. It was not possible to determine accumulation rates for the two cores from Loch Fyne by ^{210}Pb dating, and in this case the sedimentation rate was assessed by correlating the maximum concentration of ^{137}Cs in the sediments with the maximum ^{137}Cs discharge from Sellafield, BNFL's reprocessing plant located on the Cumbrian coast. The flux of ^{210}Pb to the lochs varied significantly suggesting that there has been sediment focusing of fine and/or organic rich material to the deeper sites, resulting in an enhanced flux of ^{210}Pb to these sediments. Sellafield waste radionuclides also provided useful chronologies by relating sediment maximum concentrations to maxima in the discharges. ^{137}Cs was

observed to be subject to diffusive movement, invalidating the use of its total depth of penetration as a chronological indicator.

The temporal trends of pollutant metal input agreed well with known historical trends and the Pb isotope profiles indicated that the onset of deposition from pollutant Pb from petrol occurred in the late 1920's. The maximum input of Pb from petrol peaked in the early 1980's and since then there has been a decrease in this input. The two sea lochs which were closest to the industrial centre of Glasgow exhibited a large anthropogenic pollutant input, confirming that these sediments have been highly perturbed by human activities, either directly as a result of sludge dumping or due to changes in land use (eg. road construction, deforestation, etc.) in the catchment.. All the sea lochs reflected a change in the supply of material to the sediments over the last eighty years, indicating that increased anthropogenic activity has had an effect on these environments.

ACKNOWLEDGEMENTS

I wish to express my sincerest gratitude to both my supervisors, Dr A B MacKenzie for his expert advice and unending enthusiasm at every stage of this work and Dr N B Price for his expert advice on sampling techniques and for his patience in explaining sedimentary geology to an analytical chemist.

I would also like to thank the staff and students of SURRC for the many helpful discussions and for helping me retain my sanity during the writing of this thesis. Special thanks must go to M.Kerr and I. Woodburn, with out whose help this thesis would not have seen the light of day.

Thanks go to Dr G Fitton and Mrs D James of Edinburgh University for there help with the XRF analysis. I would also like to thank J.Smith for his expert help in obtaining the sediment cores. Thanks must also go to the Dunstafnage Marine Laboratory who provided the boats from which to collect the samples.

I am very grateful to the Scottish Universities for allowing me to undertake this research.

Finally , without the support and continuous encouragement of my family and friends, I could not have undertaken this study and I wish to express my profound gratitude to them.

CONTENTS LIST

LIST OF TABLES

LIST OF FIGURES

CHAPTER 1

Introduction

1.1 *The study area and general aspects of fjord geochemistry*

1.1.1 *Outline*

This project involved a study of natural and manmade radionuclides, stable lead isotopes and selected heavy metals in the sediments of four sea lochs (fjords) situated on the west coast of Scotland: Loch Etive, Loch Fyne, Loch Long and Loch Goil (Figure 1.1).

The sea lochs of the west coast of Scotland offer a particularly interesting environment in which to study the geochemistry of radionuclides and other trace elements, since major variations in water depth, sediment type and redox conditions occur over short distances. The sea lochs are of inherent scientific interest and, as with much of the UK coastal environment, are subject to significant pollutant input so it is important to investigate the geochemical behaviour of pollutants in this environment and to develop models which can quantitatively describe the physical processes, (eg. sediment fluxes and mixing) taking place.

The aims of the research were to investigate the geochemistry of selected radionuclides and lead within this environment and to use the radionuclides themselves as tracers in the study of physical and biogeochemical processes taking place within the sediments.

1.1.2 *The Fjordic Environment of the West Coast of Scotland*

The coastal marine environment is of major scientific importance and interest since it represents the interface between the terrestrial and marine systems

and, as such, plays an important role in the transport of material from the land to the oceans. Coastal sediments are also often a major repository for pollutants, both from direct local input and from more distant sources via marine transport or atmospheric deposition. The waters and sediments of the coastal marine system can exhibit major variations in geochemical and biogeochemical conditions over comparatively short distances and it is important to characterise the influence of such variations on the geochemical behaviour of pollutants, including radionuclides and heavy metals, in attempting to determine their long term fate.

Sea lochs are a particular type of coastal environment, being long, narrow sea inlets often lying between steep mountain slopes. The Scottish west coast contains many sea lochs which are glaciated valleys that have become flooded by the sea, owing to a relative rise in sea level after the melting of the Pleistocene ice sheets. Due to glacial action they are characterised by deeply gouged basins of U-shaped cross section separated from the open sea by sills of solid rock (Stamp, 1969). In general, sea lochs have restricted circulation, particularly if they have well developed sills, and the degree of brackishness and stratification of the water is influenced to a large extent by the ratio of the volume of freshwater input to the total volume of the loch. Such restricted circulation can result in stratification and lead to oxygen depleted conditions in the water column. As a consequence of the restricted circulation of water, hydrographic conditions in a sea loch can often exert a dominant control on the availability of nutrients and dissolved oxygen and hence on the biological activity, which in turn will affect the supply of materials to the underlying sediments and consequently the composition of those sediments. A sea loch, as an estuary, can be classified with respect to the degree of mixing within the water column as being vertically mixed, slightly stratified, or highly stratified. The particular sea lochs investigated in this study were chosen to give a range of contrasting geochemical regimes as outlined below.

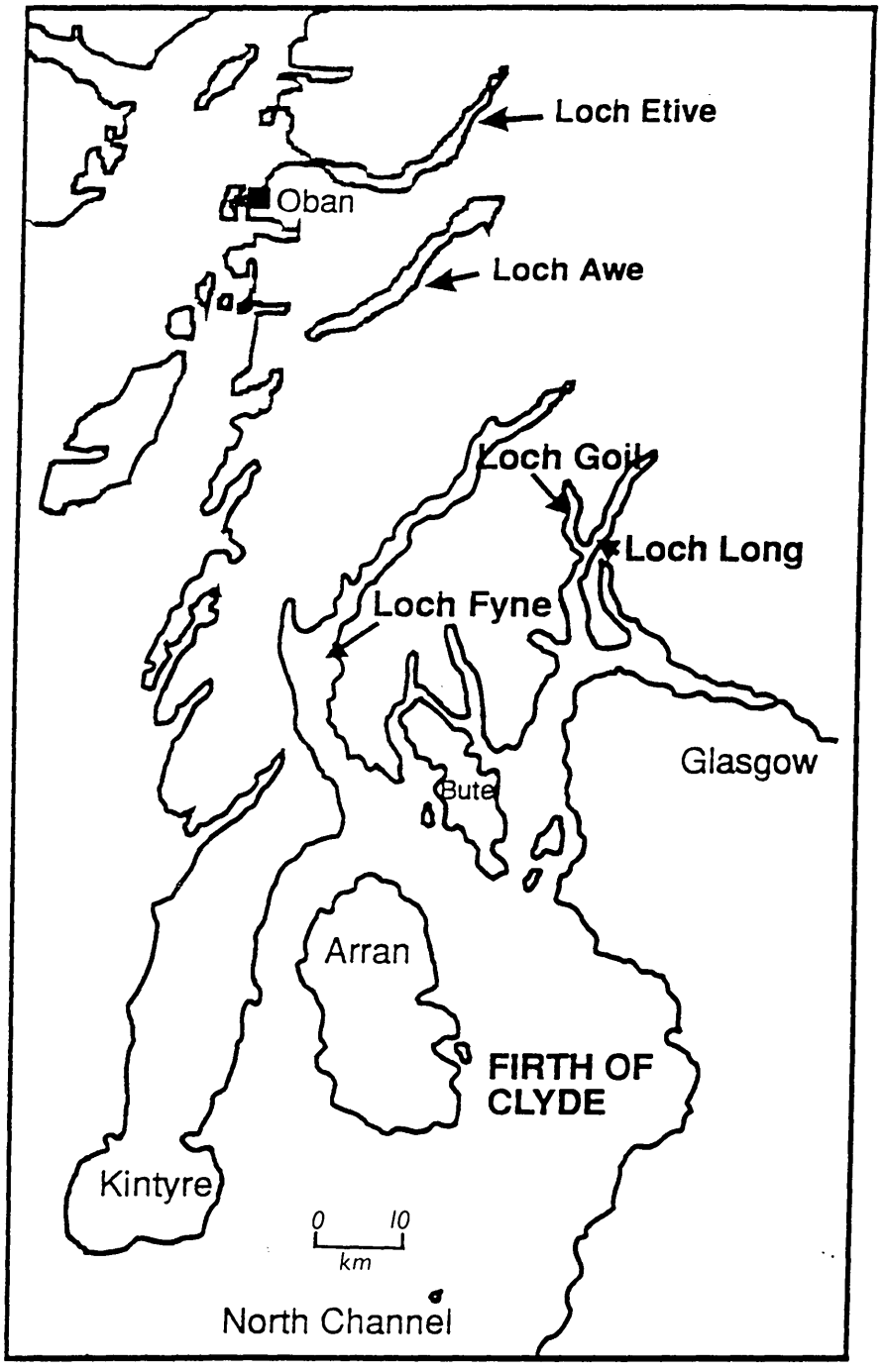

Figure 1.1 **Map of South West of Scotland showing Loch Etive, Loch Fyne, Loch Long and Loch Goil**

Loch Etive is the most northerly of the lochs studied and has a restricted opening to the Firth of Lorne at its seaward end via a shoal choked sill with a length of approximately 4 km and an average water depth of about 10 m (Figure 1.1.). It is a narrow loch, being 28 km long from the head to the Falls of Lora at Connel, and has a water surface area of approximately 26 km^2 (Figure 1.2.).

The loch is divided into two main basins, by a sill at Bonawe, with the maximum depths of the inner and seaward basins being 170 m and 60 m respectively. This division of the loch is matched by variations in the geology and topography of the area, the inner basin being encompassed by the granite mountains of the Etive Ring Complex, which rise to over 1000 m, and the outer basin being surrounded by low rolling hills consisting of andesitic lavas.

The catchment area of 1400 km^2 of the loch is large in comparison with other sea lochs of the Scottish west coast which are typically of the order of 200 km^2. The two main fresh water inputs to Loch Etive are the River Etive, (40%), which drains the extensive peatlands of Rannoch moor, entering at the head of the loch, and the River Awe (60%) entering at Bonawe. The flow of the River Awe has been controlled since 1963 by a hydroelectric scheme which uses Loch Awe as a reservoir. Secondary sources of freshwater are the rivers Kinglass, Liver and Noe which flow into the south side of the loch.

The large catchment (1400 km^2) and small surface area of the loch (26 km^2), in conjunction with a high rainfall (200 cm y^{-1}), combine to give a freshwater input which is significant relative to the volume of the loch and which produces an intense halocline in the upper waters, resulting in surface salinities at the landward end of the loch between 5‰ and 21‰ in winter and summer respectively. (Malcolm, 1981).

Loch Etive is highly stratified (Figure 1.3.) and there are three main water masses in the loch. Nearest the surface is a brackish layer which extends

from the head of the loch to the outer basin in winter but is confined to the inner basin in summer.

Below the brackish layer is water of intermediate salinity 20-28‰ which extends down to the bottom of the outer basin but is confined to the top 60 m of the water column in the inner basin by a secondary halocline. Below this halocline, the deep water has a salinity of greater than 28‰ and is depleted in dissolved oxygen. This deep water is confined to the inner basin and is only renewed when the salinity of the intermediate water is equal to or greater than that of the deep water. Deep water renewal of the inner basin of Loch Etive is described in detail by Edwards and Edelsten (1977).

The magnitude of contemporary local pollutant inputs is negligible as there is only a small amount of raw sewage discharged into the coastal waters. This, combined with the fact that the only active industry near the loch is the quarrying of granite at Bonawe, results in a low regional input of pollutants in comparison with the other three sea lochs considered in this study. During the 18th and 19th centuries, however, iron smelting was carried out at the loch side and the use of trees as fuel resulted in massive deforestation of the surrounding area with a potential effect on the input of material to the loch at the time. Iron smelting was first carried out in 1730 by Irish iron-masters with a furnace in Glen Kinglass. Later a furnace was built at Bonawe by iron masters from the Lake District which operated until 1870, with peak production of 15 tons of pig iron per day being achieved in 1840 (Malcolm, 1981). Iron ore for the furnaces was brought from Ireland and Cumbria to take advantage of the ready supply of wood around the loch.

The sediments of Loch Etive have a surficial layer of brown flocculant material, this layer being thickest in the outer basin. Below the surface layer the sediments are uniform grey/ black clayey silts. In the Firth of Lorne the sediments consist of uniform grey clays without the surficial flocculant layer, and are coarser than the majority of the Etive basin sediments (Ridgway, 1984).

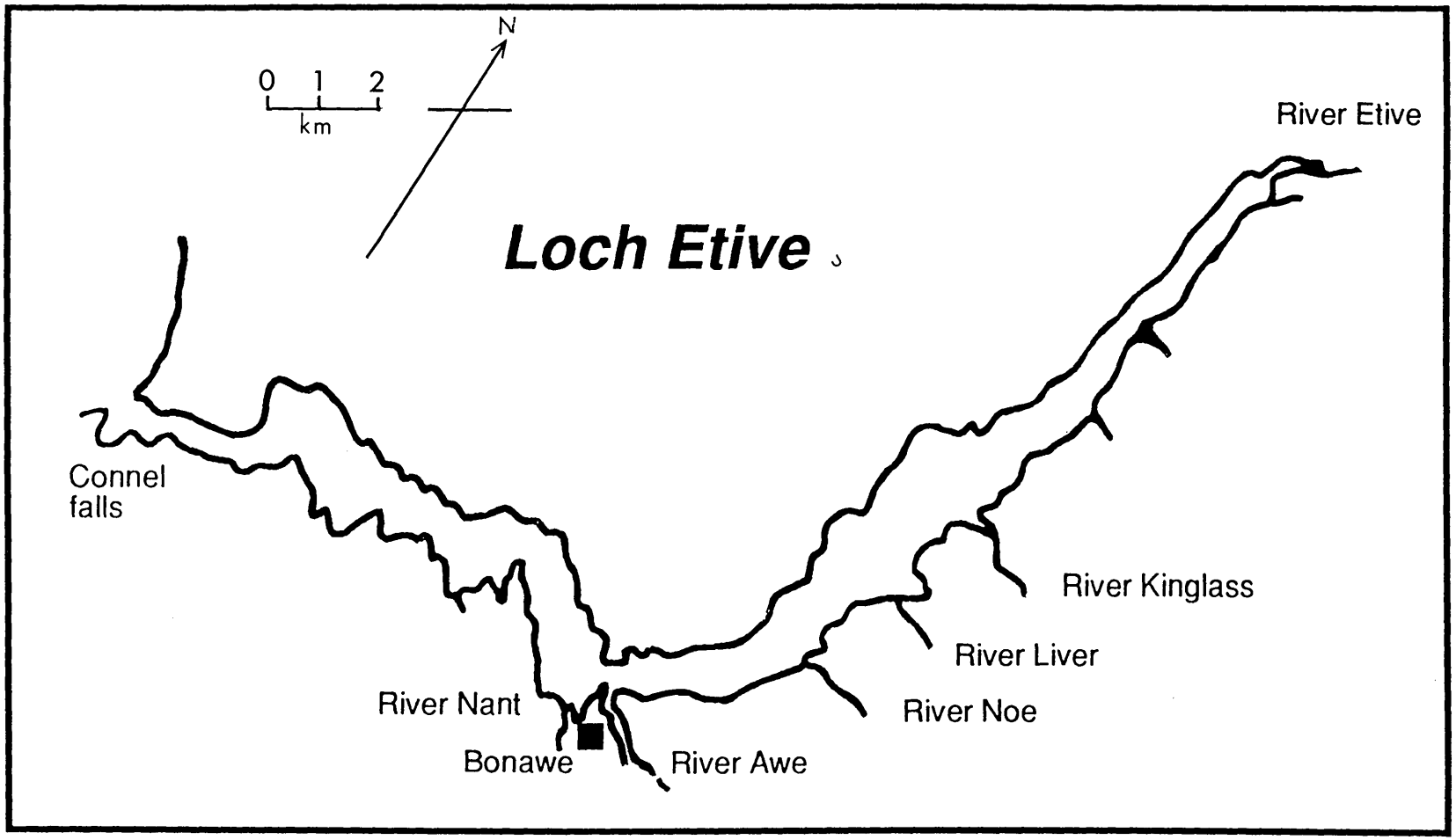

Figure 1.2 Loch Etive

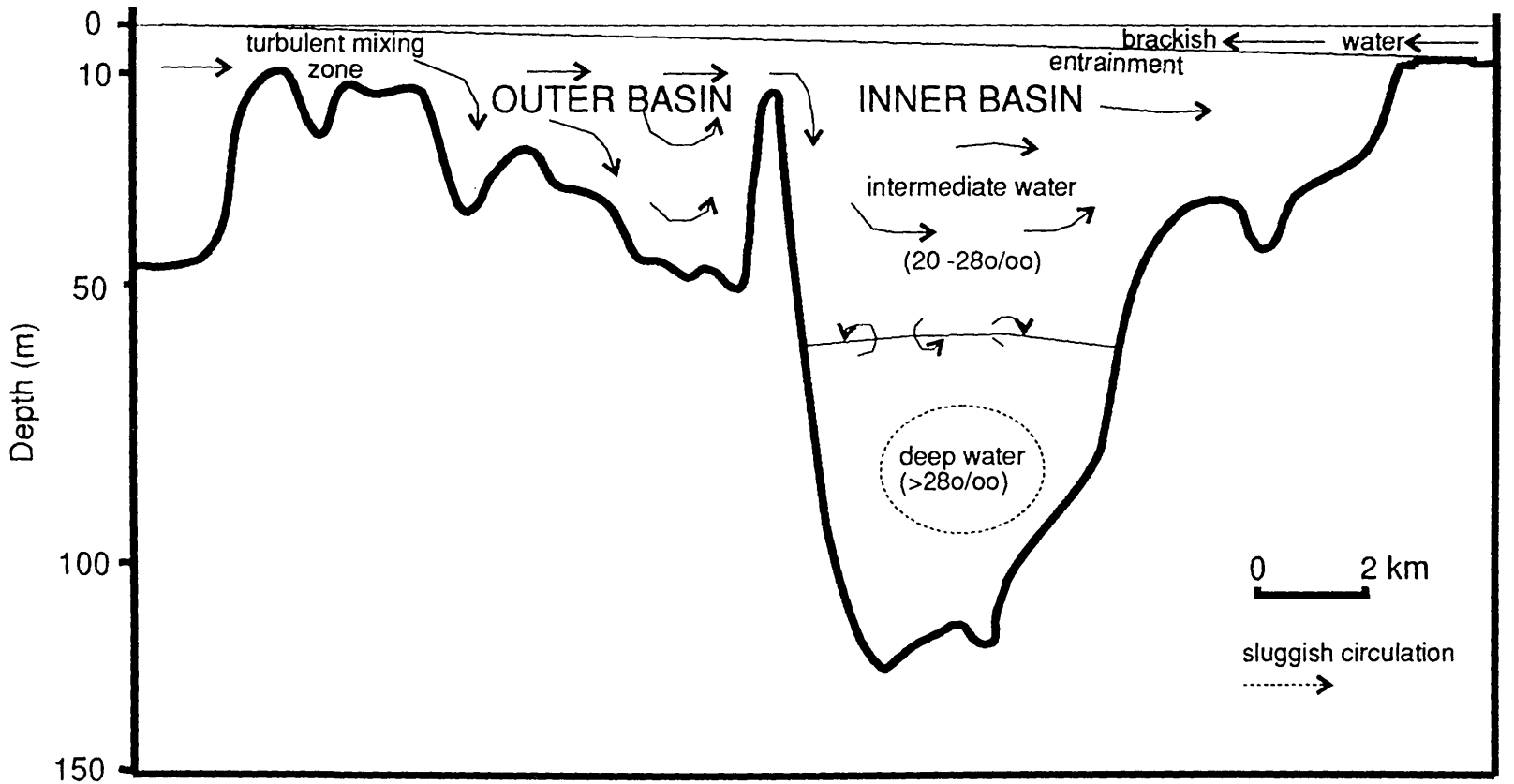

Figure 1.3. Bathymetry of Loch Etive

The other lochs studied, Fyne, Long and Goil are contained within the Clyde Sea Area (Figure 1.4.), which is a semi-enclosed water body, comprising the Clyde Estuary, the Firth of Clyde and a series of sea lochs and covers an area of over 2500 km^2 with a mainland catchment area of 8265 km^2. The most significant component of the catchment with respect to the sea lochs, is the 2000 km^2 area draining the highlands of Argyll, which contains a large number of small mountain streams but no large rivers. The remainder of the catchment comprises the Clyde basin, which is the largest freshwater input into the Clyde Sea Area and the Loch Lomond catchment which has an area of 785 km^2. The whole of the Loch Lomond catchment drains via the River Leven to the Clyde estuary (NERC, 1974).

Loch Fyne, the largest and deepest of the lochs sea of the Clyde Sea Area, is separated from the Atlantic Ocean by the narrow peninsula of Kintyre and is approximately 61 km long and 7.5 km wide at the southern end where it opens into the Firth of Clyde. It is divided into two main basins at Otter Spit where the water depth is reduced to 30m by a morainic gravel sill, the inner loch having a maximum depth of 135 m and the outer loch having a maximum depth of 185 m.

The main freshwater contributions are from the Rivers Fyne, Shira and Aray, but their inputs are insignificant relative to the volume of the loch ($9747x10^6$ m^3) (Edwards and Sharples, 1991). As a consequence, brackish water conditions do not occur to any great extent and there is no seasonal stratification of the water column in Loch Fyne. The loch is bordered by quartzites, phyllites, tuffs, schists and limestones of Middle and Late Dalradian age with low grade (chlorite-garnet) Barrovian metamorphism (Calvert and Price, 1970). Glacial sands and gravels are widespread around the margins of the loch with bottom sediments ranging from red to brown gravelly, shelly sands on the shelves to brown silty clays in deeper water. Manganese nodules are present in the sediments of Loch Fyne, but are mainly found in the deepest part of the southern basin (Calvert and Price,

1970).

Loch Goil is a steep sided loch, consisting of a single basin of length 8 km, average width 1.2 km and maximum depth of 86 m and a volume of $306x10^6$ m^3 (Edwards and Sharples, 1991). It opens into Loch Long via a narrow entrance sill with a water depth of 13 m. The major fresh water inputs to the loch are the River Goil and the Lettermay burn. The surface waters of the loch are well oxygenated but as a consequence of its shallow sill depth, sheltered position and lack of disturbance the water becomes stratified in summer months, resulting in differences in temperature, salinity and dissolved oxygen between surface and deep waters. Under stratified conditions the deep waters suffer severe oxygen depletion during summer (5% saturation has been recorded) (pers. com. Best,1992).

MacKenzie (1977) used ^{137}Cs and ^{134}Cs as tracers of the water circulation to show that oxygen depleted conditions develop by interruption of the normal pattern of outward flow of low salinity surface water and corresponding deeper inflow of higher salinity water when the depth of the pycnocline is greater than the sill depth, preventing renewal of the deeper water. Under these conditions, decay of organic debris rapidly depletes the oxygen content of the deep water. This situation generally arises in midsummer due to heating and freshwater input to the surface water at a time when biological activity is high. When the loch is not stratified, renewal of the deep water occurs over a timescale of a month or less. However, when stratification develops, little renewal of the deep water may occur over several months. Nevertheless even under stratified conditions internal mixing within the oxygen depleted water probably occurs in less than 2 months.

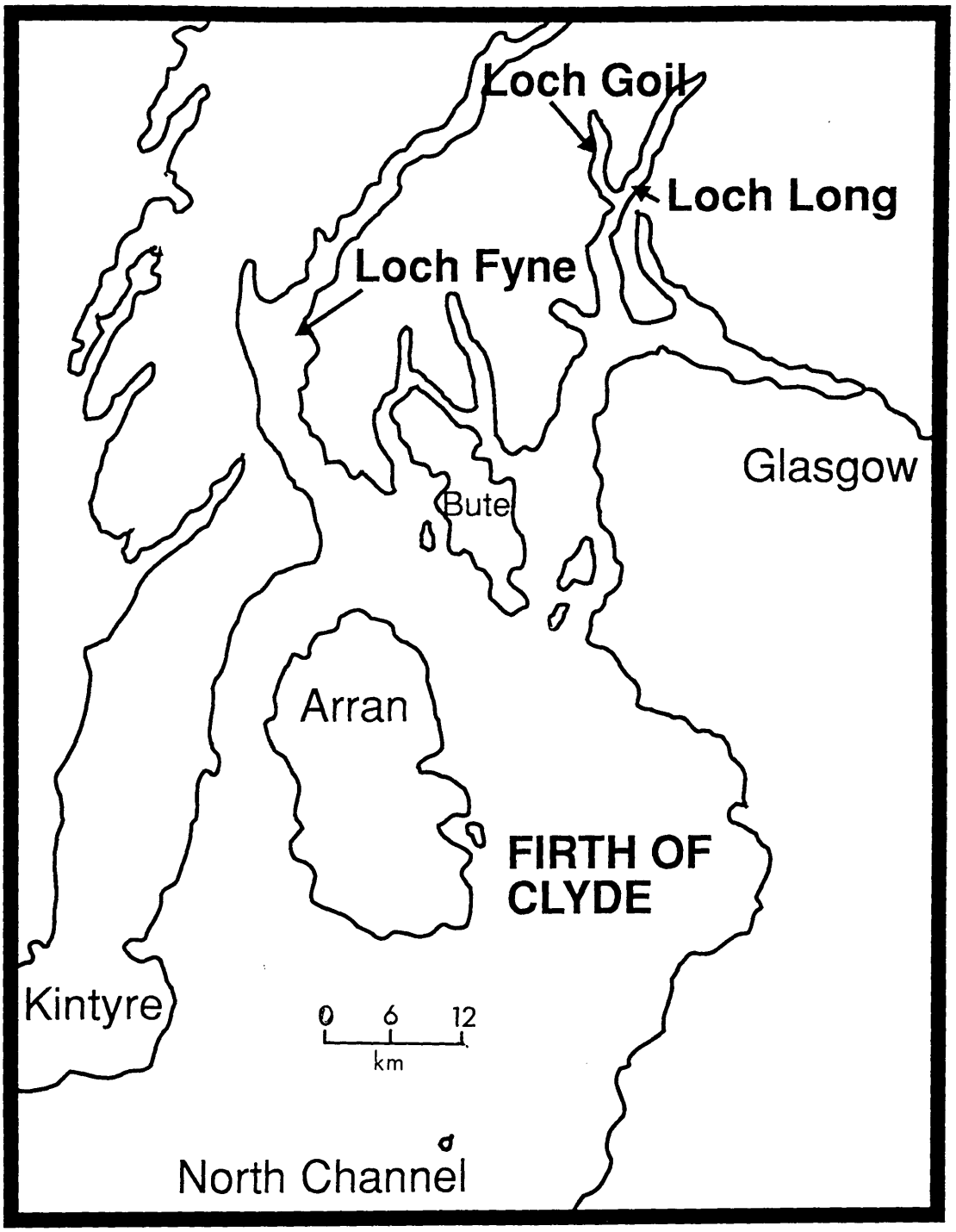

Figure 1.4. Map of the Clyde Sea Area

Loch Long is a narrow loch of length 27 km and maximum depth of 97 m and volume of $805x10^6$ m^3, (Edwards and Sharples, 1991) which opens into the Firth of Clyde at its southern end. Where the loch connects with the mouth of Loch Goil the water depth is approximately 70 m. The only freshwater inputs from the Rivers Loin, Core and Finnart are low relative to the volume of the loch so, as with Loch Fyne, brackish water conditions do not occur to any great extent. As a result of the fjordic structure, there is little disturbance of the deep waters which occasionally become oxygen depleted (~20% saturation). The sediment types range from muddy sand to muddy sandy gravel. Silty clays constitute a major fraction of the sediments in deeper waters (NERC, 1974).

There has been and is little industry around the sea lochs themselves but, they have been affected by pollutant inputs from the major industrial centre of west Central Scotland.

The function of Glasgow as a major industrial centre since the 19^{th} century has resulted in pollution of the surrounding atmosphere, rivers, estuary and the Firth of Clyde. The main sources of pollutant inputs to the area are domestic sewage, (total catchment population > 2.5 million) and industrial effluent from the Rivers Clyde and Leven, inflow from the Irish Sea and atmospheric deposition. A redistribution of polluted sediments results from the dumping, near the mouth of Loch Long, of sediment, high in metal concentration, dredged from the River Clyde navigation channel (NERC , 1974).

1.1.3 *Fjordic Geochemical Processes*

A diverse range of geochemical processes occur within the estuarine environment and these have been described in detail by many authors, e.g. Grasshoff (1975), Riley and Chester (1975) and Chester (1990), and the following section is restricted to consideration of only the main processes

operating in the sea lochs under study.

Sea lochs are an interface where fresh water and saline water mix and are consequently complex environments in which there is a continuous spectrum of salinities. The changes in ionic strength, pH and Eh, which occur during mixing of saline and fresh water, and the abundance of suspended solids with active adsorption sites leads to the partitioning of elements, transported by the rivers, between the aqueous and solid phases. Some dissolved species are simply diluted, i.e behave conservatively, whereas others undergo reactions that lead to their addition to, or removal from, the dissolved phase. The particulate material can act as either a source of dissolved components, by release into solution during mixing, or as a sink for dissolved components, which are removed from solution during mixing.

a) **Water Column Processes**

The water in a sea loch is eventually flushed out, with the time scale for this ranging from days to months, so the only permanent sink for elements in this system is the sediment.

The composition of the river water flowing into the sea lochs depends on the sources of the dissolved and suspended particulates which is governed to a large extent by the geology of the catchment. Other factors which can affect the composition of river waters are decomposition of organic material, wet and dry atmospheric deposition and in some cases pollutant inputs.

Aqueous phase/solid phase portioning of elements in sea lochs is controlled by an interacting set of physical, chemical and biological processes which include sorption/ desorption by suspended particles, scavenging, precipitation, ion exchange, flocculation or aggregation and uptake via biological processes. The extent to which such processes occur is controlled by the geochemical conditions of the sea loch, e.g. pH, redox potential, salinity, and the concentrations of complexing ligands, nutrients, organic components and particulate matter (Kester et al., 1975; Aston, 1978; Li et al.,

1984; Duinker, 1986; Kester et al., 1986; Chester et al., 1990). The removal of dissolved species from solution by precipitation and hydrolysis requires the solubility product of the element in question to be exceeded. However, removal by scavenging (or coprecipitation), surface sorption, ion exchange and biological uptake can occur at concentrations which are less than that of the solubility product.

There are two main types of removal of trace elements from the water column, namely scavenging and nutrient mediated mechanisms. Scavenging is considered to be an external cycling process in which the distribution of a trace element is controlled by the input and a rapid scavenging by particulate phases throughout the water column, onto which may be superimposed the effects of other processes such as those that affect the trace element sources at the sediment/water interface. The distribution of trace metals involved in the nutrient cycles shows a surface depletion and a subsurface enrichment in dissolved concentrations and such metals are considered to be involved in internal cycling processes. Trace element distributions may be considered to be controlled by either mechanism or by a combination of both, but the point of importance is that removal of dissolved species involves uptake on particulate matter.

Precipitation in sea lochs is important in the removal of elements from solution eg. the removal of manganese and iron by the formation of oxyhydroxide precipitates. Iron and manganese have a very active chemistry in sea lochs, as discussed below, resulting in the formation of relatively large quantities of oxyhydroxides. These compounds have a very high affinity for scavenging trace elements and effectively concentrate a number of heavy metals and radionuclides (Murray and Irvine, 1895; Buchowiecki and Cherry, 1967; Skei, 1983; Hamilton-Taylor and Price, 1983; Sawlan and Murray, 1983; Malcolm, 1985; Peterson and Carpenter, 1986; Cochran et al., 1986; Shimmield and Price, 1986; Williams et al.,1988; Todd et al., 1988; Shimmield and Pedersen, 1990).

Such processes, combined with particle accumulation, result in the retention of selected elements in the sea loch sediments. However, processes such as sediment resuspension and diagenetic release followed by the flushing out of interstitial waters can recycle these elements back into the overlying water. The addition of components to the dissolved phase takes place when desorption from particle surfaces, dissolution and re-dissolution of minerals and the degradation of organic matter take place. Dissolved components are stabilized by complexation and chelation reactions with inorganic and organic ligands, and components that remain in solution will be removed from the sea loch during tidal flushing. Investigations of estuaries and river deltas, (Duinker et al, 1979; Trefry and Presley, 1976; Milliman et al, 1975; Brewers and Yeats,1977) have shown that only a small amount of the total particulate matter entering such systems is transported to the open ocean and that approximately 90% of the river particulate matter reaching the land/sea margin is retained in estuaries.

The distribution of particulate material in estuaries is dependent on water circulation, gravitational settling, and sediment deposition and resuspension. In a partially stratified fjord, the landward flow of water is strong enough to move suspended material, which may include both fluvial and marine suspended particulates up the fjord to the head of the salt intrusion. At this point a turbidity maximum may develop in the region where suspended solids can be transported from both up stream and down stream. This is a region which is important for dissolved/particulate interaction as the suspended particulate concentration is high (Chester,1990).

b) **Biological Processes**

Biological processes have an important role in aqueous phase/suspended particulate partioning, controlling the water chemistry and in part, determining the flux of elements to the sediments.

The estuarine biomass is formed as a result of primary production which is related to the supply of nutrients and the turbidity of the waters. Williams

(1981), estimated that the global internal estuarine photo-production is about 5.2×10^{14}g y^{-1} which is approximately 1.5% of the total annual marine production. Rivers transport about 2×10^{14} g y^{-1} of carbon into estuaries which is of the same order of magnitude as that resulting from primary production. Of the carbon that is introduced into the estuarine environment only a proportion enters into recycling processes, and according to Reuther (1981), much of the imported carbon is refractory.

Biological processes are important since heavy metals and radionuclides can be taken up by active biological processes or by surface uptake and transferred to the sediments via faecal pellets or settling remains of organisms. The supply of organic matter to the sea loch sediments varies seasonally due to the effect of plankton blooms. These occur in the spring and summer months and result in an increased supply of marine organic carbon to the sediments. The plankton can also concentrate dissolved elements from the water and are therefore involved in the aqueous/solid phase partioning of elements in the sea loch environment. Thus, the degree of biological activity governs the quantity of decaying organic matter, which is a strong reducing agent, in both the water and (as discussed below) the sediment and consequently has a major influence on redox conditions.

c) **Sediment Processes**

It is important to establish if a pollutant species remains in the sediment after uptake or is transferred back into the overlying water. Sea loch sediments are subjected to a number of processes which can result in the recycling of deposited elements back into the water column, including dissolution and diffusion of elements in interstitial waters, flushing (advective flow) of interstitial waters into the overlying water column, resuspension of surface sediments and bioturbation.

Chemical, physical and biological processes occur within the interstitial water/sediment system which can lead to the formation of new and altered mineral phases and to changes in the water composition. These processes

involve the degradation of organic matter, diffusion, advection and sediment compaction and are collectively known as sediment diagenesis. Diagenesis can take place at or close to the sediment/water interface or at greater depths during continual burial and it is important to evaluate the influence of diagenetic reactions on the chemical fluxes between the sediments and the overlying water.

Chemical diagenesis in sediments depends on a number of environmental factors, the most important of these being, the accumulation rate, the depth to which the sediment is mixed, the amount and composition of organic matter present and its rate of degradation, and the geochemical conditions of the overlying water.

Many researchers have described diagenesis in marine sediments, (Froelich et al., 1979; Jahnke et al., 1982; Galloway and Bender 1982, Wilson et al., 1985; Stumm and Morgan 1981) and it is generally accepted that there is a general order in which the oxidants are utilised as follows: oxygen > nitrate ≥ manganese oxide > iron oxides > sulphate. Finally, methane is formed, and this sequence of degradation can be represented by reactions taking place at increasing depth in the sediment as follows;

dissolved O_2	$CH_2O + O_2 \rightarrow CO_2 + H_2O$
denitrification	$5CH_2O + 4NO_3^- \rightarrow 2N_2 + 4HCO_3^- + CO_2 + 3H_2O$
manganese oxides	$CH_2O + 2MnO_2 + 3CO_2 + H_2O \rightarrow 2Mn^{2+} + 4HCO_3^-$
iron oxides	$CH_2O + 4Fe(OH)_3 + 7CO_2 \rightarrow 4Fe^{2+} + 8HCO_3^- + 3H_2O$
sulphate reduction	$2CH_2O + SO_4^{2-} \rightarrow H_2S + 2HCO_3^-$
methane production	$2CH_2O + 2H_2O \rightarrow 2CO_2 + 8(H)$ **followed by**
	$8(H) + CO_2 \rightarrow CH_4 + 2H_2O$

To evaluate the geochemical behaviour of elements within the sediment/pore water system it is necessary to be able to evaluate the redox condition of the sediment. The measurement of the redox potential using electrodes has been employed to assess the redox condition of the sediment (Pearson and

Stanley, 1979; Becking et al., 1960) but there are problems with this method due to the poisoning of the electrodes, and erroneous results may be obtained due to the high ionic content of the pore waters (Guppy and Atkinson,1989) The most commonly used indicators of diagenesis in sediments are Mn, Fe and sulphate/sulphide and by observing the concentrations of these elements in the pore waters and solid phases, the extent to which the diagenetic sequence has proceeded can be ascertained.

In sea loch sediments major changes in redox potential can occur at or near the sediment/ water interface, since they usually have a high organic content which leads to intense bacterial activity, resulting in the sediments becoming anoxic at relatively shallow depths. In these sediments aerobic decomposition of organic matter takes place at or close to the sediment/ water interface, nitrate reduction in the top few centimetres, sulphate reduction over the next tens of centimetres, and methane production below the depth where sulphate disappears (Berner, 1980).

The sea loch sediments act as a sink for trace elements/pollutants, effectively concentrating them and resulting in the sediments themselves becoming a potential source of pollutants if there is a change in environmental conditions. For example, on resuspension, previously buried sediments are transferred from an anoxic environment to oxic waters which will result in the oxidation of reduced sediments and may involve the release of enriched trace elements into the water column (Murray and Irvine, 1895; Malcolm, 1981; Sawlan and Murray, 1983; Peterson and Carpenter, 1986; Cochrane et al., 1986; Todd et al., 1988; Shimmield and Pederson, 1990; Paalmann et al., 1991; Shimmield et al., 1991).

The organic matter in sediments is composed of a wide range of compounds (Degens and Moper, 1976), and is derived from terrestrial, marine and anthropogenic sources. Ertel and Hedges (1985) concluded that organic material in marine sediments exists in a number of forms including discrete organic particles, surface films on inorganic phases and as integral

components of inorganic phases. In addition there are a number of dissolved organic components which are present in the interstitial waters of sediments.

Much of the organic material that accumulates in sea lochs is land derived and is more refractory than marine derived organic matter e.g. lignin from vascular plants can remain well preserved in sediments for hundreds of years (Chester, 1990). Marine derived organics are formed within the marine environment largely from the photosynthetic fixation of carbon during primary production. Hence, there are two types of organic material reaching the surface sediments of the sea loch, a fraction that is utilised by bacteria and a fraction that is retained in the sediment and undergoes only minor modification.

The magnitude of the flux of organic matter to the sediment and the rate of sediment accumulation largely determine the amount of organic matter within the sediment that is available to be degraded by bacteria which will utilise the various oxidants. The diagenetic sequence passes through each of the oxidant utilization stages successively in a down column direction, thus setting up a vertical gradient within the sediment column.

The chemical composition of sediment pore waters is controlled by a number of inter-related factors including, the nature of the original trapped fluid, diffusion of elements within the pore water, reactions involving the sediment and pore water and reactions occurring at the sediment/water interface. This results in changes in the concentration of the pore water relative to the overlying water, and diffusion gradients will be set up under which the components will diffuse from high to low concentration regions. The fate of an element in the sediment system is related to its redox sensitivity, either directly as in the case of manganese or indirectly through association with either organic or inorganic ligands which are susceptible to redox changes.

The first investigation of marine interstitial waters was published by Sir John Murray in conjunction with R. Irvine (Murray et al., 1895) who squeezed fluids

from a shallow "blue mud" from the Scottish Coast and found that, although the major components of the interstitial water were similar in their relative proportions to those of sea water, oxygen had been depleted, sulphate had been lost, and the bicarbonate content had increased. The results indicated that the oxidation of organic carbon to CO_2 balanced most of the reduction of sulphate to form sulphide. Murray also found appreciable amounts of manganese in the pore waters and he revised his earlier concept of a largely volcanic origin for deep-sea manganese nodules, and suggested that, together with river-borne and volcanic supplies of Mn, a major source of the element might be diffusion into sea water from terrigenous sediments undergoing diagenetic reduction.

It has become apparent from many studies (eg. Klinkhammer et al., 1982; Sawlan and Murray, 1983) that the position in the sediment at which elements are released can be critical in controlling their subsequent fate in the sediment/pore water system. Elements released into the pore water can migrate either upward or downward, and the shapes of the concentration profiles are often indicative of the flux direction.

The oxic release of metals from their organic carriers can lead to concentrations in upper pore waters that are high relative to both underlying pore waters and overlying sea water, so the concentration gradient can result in both a downward migration of the metals into the sediment and upward migration into the sea water. Under these conditions metals can diffuse out into the sea water, they can be incorporated into the solid phase at the sediment surface, or they can diffuse downwards and be incorporated into solids at depth.

Sub-oxic processes usually occur at depth except in the case of sediments which are reducing to the surface, as can be the case in sea lochs, and result in the release of trace elements from the secondary oxidants into the interstitial waters. The concentrations of elements involved in such processes are consequently greater in the zone of sub-oxic diagenesis than higher up

the sediment column, and the concentration gradients set up lead to migration via diffusion through the pore waters. A large fraction of the metals released during sub-oxic diagenesis does in fact diffuse and is then re-incorporated in the sediment by deposition in the oxic zone.

In strongly reducing sediments with a sub oxic zone lying near the surface, the maximum dissolved Mn concentration is found close to the sediment/seawater interface. In such systems, the dissolved Mn can diffuse into the overlying water. However, in oxic sediments there is a decrease in the pore water Mn concentration in the oxic zone, indicating removal of the element from solution to the solid phases. This is confirmed by the shape of solid phase Mn profiles in the sediments.

The reactions involved in the diagenesis of Mn can be related to pore water/solid phase changes and can be expressed as follows;

$$Mn^{2+}\ (\text{soluble}) + \underset{\text{reduction}}{\overset{\text{oxidation}}{\rightleftarrows}} MnO_x\ (\text{solid hydrous oxide})$$

where x is generally less than 2. This reaction governs the diagenetic mobility of Mn in sediments and the general conditions that control both the solid phase and the dissolved Mn can be described in terms of the model proposed by Lynn and Bonatti (1965).

In this model, first generation manganese oxides are deposited at the sediment surface and are subsequently buried below the redox boundary where they are reduced. This results in the production of dissolved Mn^{2+} which diffuses upwards, along a concentration gradient in the pore water, and is oxidised and precipitated in the upper sediment layer as hydrous, second generation Mn oxides. As sedimentation proceeds, the second generation oxides are again buried below the redox boundary and the cycle starts again. The overall result of the Mn recycling is the trapping of the Mn in the solid phase in a narrow zone at the position in the sediment where the potential

is equal to that of the Mn^{2+}/Mn^{4+} couple. This general description of Mn behaviour was refined by Froelich et al. (1979), who proposed that the depth of the maximum Mn concentration in the solid phase is controlled by the downwards diffusion of oxygen. In a steady state system the concentration of the Mn peak (solid phase) will increase until the sedimentary input of reactive Mn is equivalent to the amount being reduced and released into the pore water. Such a steady state system would display the highly concentrated Mn peak near the top of the dissolved Mn^{2+} gradient (Figure 1.5.) (Froelich et al., 1979). Steady state Mn diagenesis has also been described by the Burdige and Gieskes model,(Burdige and Geiskes, 1983) in which the sediment column is divided into four distinct zones: (Figure 1.5.).

(a) an **oxidised zone**, in which Mn oxides accumulate and the dissolved Mn^{2+} concentration is essentially zero; (b) a **Mn oxidation zone**, where the dissolved Mn^{2+} profile increases with depth and is concave upwards as a result of the diffusion of Mn^{2+} from below the Mn^{2+}/Mn^{4+} redox boundary and its removal by oxidation in the oxidised zone as solid hydrous Mn oxide, resulting in an increase in solid phase Mn with depth; (c) the **Mn reduction zone**. In this zone as the solid Mn oxides are buried below the redox boundary they undergo reduction, Mn^{2+} is released into the pore waters and the dissolved Mn^{2+} profiles are concave downwards. The pore water Mn^{2+} concentration therefore increases with depth while solid phase Mn concentrations decrease and finally (d) the **equilibrium zone** in which the dissolved Mn concentration reaches a maximum and may in fact decrease with depth perhaps due to the formation of a secondary Mn carbonate mineral. Mn in the reduced state is known to occur as concretions of $MnCO_3$ in marine sediments both in shallow waters (Zen,1959; Manheim, 1961; Calvert and Price, 1971) and in the deep ocean (Lynn and Bonatti, 1965). The composition comprises an admixture of the 3-phase system $MnCO_3$ -- $CaCO_3$-- $MgCO_3$ and often has almost equi-molecular proportions of Mn and Ca carbonates with subordinate amounts of Mg and Fe. The presence of this carbonate phase in sediments implies a high activity of both Mn^{2+} and bicarbonate ions in the pore water environment.

The models described above have been successfully applied to field situations and were able to predetermine the presence of Mn peaks in deep-sea sediments displaying an upper oxic zone separated from a lower reducing zone by a redox boundary.

Fe and sulphate exhibit a similar behaviour to Mn but the redox cycling takes place at lower redox potentials and consequently they occur further down the diagenetic sequence. Mn and Fe oxides are effective scavengers of heavy metals and radionuclides and these elements will be released on redissolution of the oxides, and the processes therefore have the potential for redistribution of scavenged elements in the sediment pore/water system. However, the reduction of sulphate to sulphide is complicated by the formation of metal sulphides which can also scavenge elements from the pore waters. Sulphate reduction can be responsible for an increase in the concentration of dissolved Ba, which is released as $BaSO_4$ is reduced.
The halogen elements Br and I can also be used as indicators of degradation of organic matter in sediments since they are dominantly contained in organic matter (Vinogradov, 1939; Sugawara and Teradda, 1957; Shishkina and Pavlova, 1965.). Where sediment accumulation is constant and the material sedimenting is of uniform lithology, the loss of I with respect to carbon follows an exponential decrease with depth and the $I/C_{(org)}$ ratio has been used to indicate the extent of oxidation of organic matter in sediments during early diagenesis (Price et al., 1970).

Surface sediment acts as a reservoir for metals with many occurring as organically bound complexes, and the (I/C_{org})/metal profile therefore may give some indication about processes affecting the metals in these sediments. Price and Calvert (1973) observed that the depletion of Zn, Cu, Pb and I with depth in a profile of rapidly forming oxic marine sediments from Loch Fyne was such that below 25cm (where the sediments are essentially free of Mn and Fe oxyhydroxides), Zn, Cu and Pb attained constant values. Variations in the concentration ratios of these metals to organic carbon were found to be depth dependent, with the extent of variation being Zn > Cu >Pb >> I.

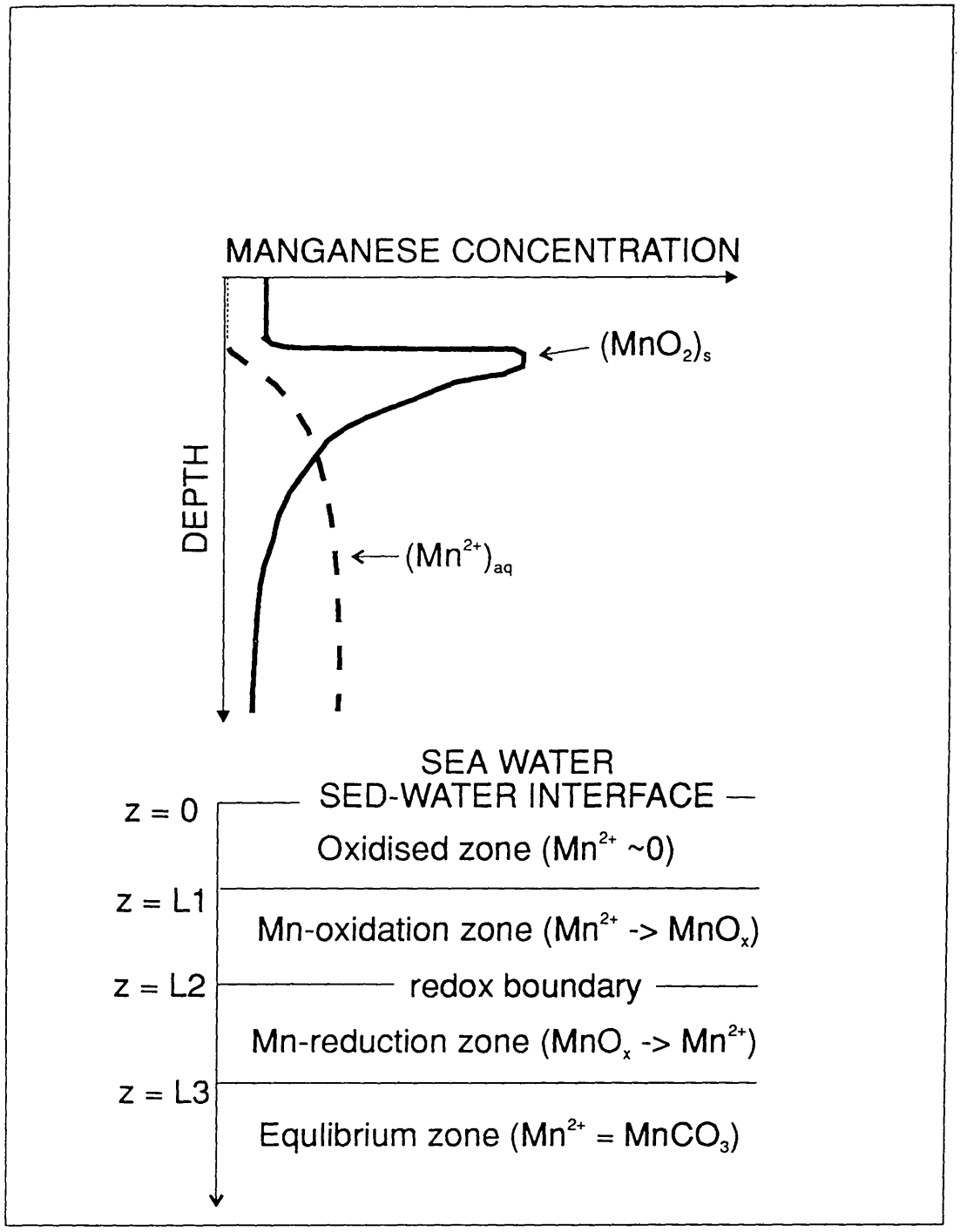

Figure 1.5. Schematic of Mn diagenesis in sediment

Such behaviour may imply a breakdown and release of metal-organic substances from the sediment during burial. This observation has implications for the redistribution of heavy metals and radionuclides in
the sea loch environment and has raised important implications with respect to the dating of such sediments by ^{210}Pb as discussed by Ridgway and Price (1987) and Urban et al., (1990). If Pb is mobile in sea loch sediments it invalidates the method of ^{210}Pb dating for these sediments which limits the possibility of obtaining chronologies for sediment cores from these environments and hence, limits the interpretation of the heavy metal and radionuclide profiles.

Berner (1980) describes a theoretical approach to early diagenesis. In which he considers physical, biological and chemical processes in turn and applies mathematical models to each. In this approach, the major process of benthic boundary diffusion is considered to be bioturbation, which is the mixing of sediments by the activities of benthic organisms. The simplest way to treat bioturbation is a box model approach assuming total mixing This approach assumes that there is fast mixing over a certain depth, resulting in the sediment properties being uniform from the sediment/ water interface down to the fixed depth of mixing. This model also assumes that changes in the properties of the sediment added at the sediment/ water interface are immediately detected at the bottom of the box but are damped by the mixing (Berger and Heath, 1968). A more complex approach, allowing for decreasing biological activity with depth, is to model it as a random mixing process (Goldberg and Koide, 1962; Berger and Heath, 1968; Hanor and Marshall, 1971; Guinasso and Schink, 1975; Peng et al., 1977; Nozaki, et al., 1977).

If the only diagenetic process affecting the solids is bioturbation then it can be represented mathematically by:

$$\frac{dC}{dt} = \frac{F(t) - \omega C_s}{L}$$

where C_s= concentration in the zone of bioturbation (box) of solid substance under study in terms of mass per unit volume of total sediment (solids plus pore water)

t = time

F(t) = depositional flux to sediment surface of substance under study (mass area^{-1} time^{-1})

ω = rate of depositional burial of total sediment (compactive flow of pore water is ignored)

L = thickness (depth) of box which is assumed to be constant with time.

The record of depositional changes, as modified by bioturbation,is fixed at the time the sediment passes downward by burial below the zone of bioturbation, therefore the buried record can be used to deduce F(t), the depositional flux of a component to the sediment surface.

Box modelling can be used to describe the record left after bioturbational mixing of a pulse input of a pollutant and to describe bioturbational mixing of materials undergoing chemical reaction or radioactive decay, (Santschi et al., 1983; Nozaki et al., 1977; Peng et al., 1977; MacKenzie and Scott, 1982).

Sea lochs exhibit a wide range of geochemical conditions over relatively short distances making them ideal sites for investigating the behaviour of heavy metal and radionuclides with respect to changing environmental conditions. The sea lochs investigated in this study experience some or all of the following; brackish conditions, restricted water circulation, seasonally intense biological production and, in some cases, seasonal oxygen depletion resulting in the sediment types ranging from oxic to anoxic. The interpretation of sediment core data depends on being able to fit a chronology to the depth profiles to determine whether they reflect a historical record of pollution or in fact are indicating that geochemical and biogeochemical conditions are resulting in redistribution of the pollutants. The uncertainty over the behaviour of Pb in these environments has important implications with respect to ^{210}Pb

dating and one of the main aims of this research was to determine the mobility or immobility of Pb within the sea lochs of the west coast of Scotland.

1.2 *Radionuclides in the coastal marine environment*

1.2.1 *Introduction*

Radionuclides have become well established as tracers of marine processes (Jefferies et al., 1973; Robbins and Edington, 1975; Aaby et al., 1978; Baxter and McKinley, 1978; Benninger et al., 1979; Clifton and Hamilton, 1979; Bowen et al., 1980; Stanners and Aston, 1981; McKinley et al., 1981; Chanton et al., 1983; Carpenter et al., 1984; Shell and Barnes, 1986, Cochran et al., 1986; MacKenzie et al., 1987; Bonnet and Cambray., 1989) and manmade radionuclides constitute an important class of pollutants in the nearshore environment (McKinley et al., 1979; Aston and Stanners, 1981; Aston et al., 1981; Carpenter and Beasley, 1981; Cambray and Eakins., 1982; Cook et al., 1984; Pentreath et al., 1984; Jones et al., 1984; MacKay et al., 1985; Assinder et al., 1985; Williams et al., 1987; Walker and McKay, 1991; McDonald et al., 1992; MacKenzie et al., 1993) The following sections will include a brief description of the relevant aspects of the use of natural and manmade radionuclides as tracers and a description of the major sources of manmade radionuclides to the study area.

1.2.2 *Natural Radionuclides*

Radionuclides occur in nature both as cosmic ray produced species such as ^{14}C and primordial radionuclides such as ^{40}K and ^{238}U, ^{235}U and ^{232}Th (Lillie, 1986), which are the parents of the three radioactive decay series shown in Figure 1.6. The genetic relationship between two or more successive nuclei is described by the terms parent and daughter nuclide. For example, the decay of ^{238}U produces the daughter radionuclide of ^{234}Th (Freidlander et al, 1981). The different nuclides in the decay chains exhibit marked variations

in geochemical behaviour and this can lead to their separation during geochemical processes. Investigation of the systematics of decay or ingrowth of radionuclides in such disequilibrium situations has become well established in marine science in the study of rates of processes such as sediment accumulation and water circulation (Ivanovich and Harmon, 1992) Moreover, the ^{238}U, ^{235}U and ^{232}Th decay chains respectively end in the stable lead isotopes ^{206}Pb, ^{207}Pb and ^{208}Pb and the relative abundances of these isotopes can be used in geochronological studies (Faure, 1986) and in identification of pollutant Pb from different sources (Delves, 1988, Sugden, 1993). A brief outline of the systematics of radioactive decay and ingrowth during natural decay series disequilibrium is provided below, with more detailed treatments being given in Wehr et al.,(1966) Freidlander et al, (1981) and Keller , (1988).

In sequential decay of a parent nuclide **X** and shorter half life daughter nuclide **Y**: $\mathbf{X \rightarrow Y}$

Separation of **Y** from **X** will result in the decay of Y according to the basic radionuclide decay equation:

$$(A_Y)_T = (A_Y)_0 \, e^{-\lambda_Y t}$$

$A_{Y(T)}$ = activity of daughter nuclide at time t

$A_{Y(O)}$ = activity of daughter nuclide at time zero

λ_y = decay constant of daughter nuclide

t = time

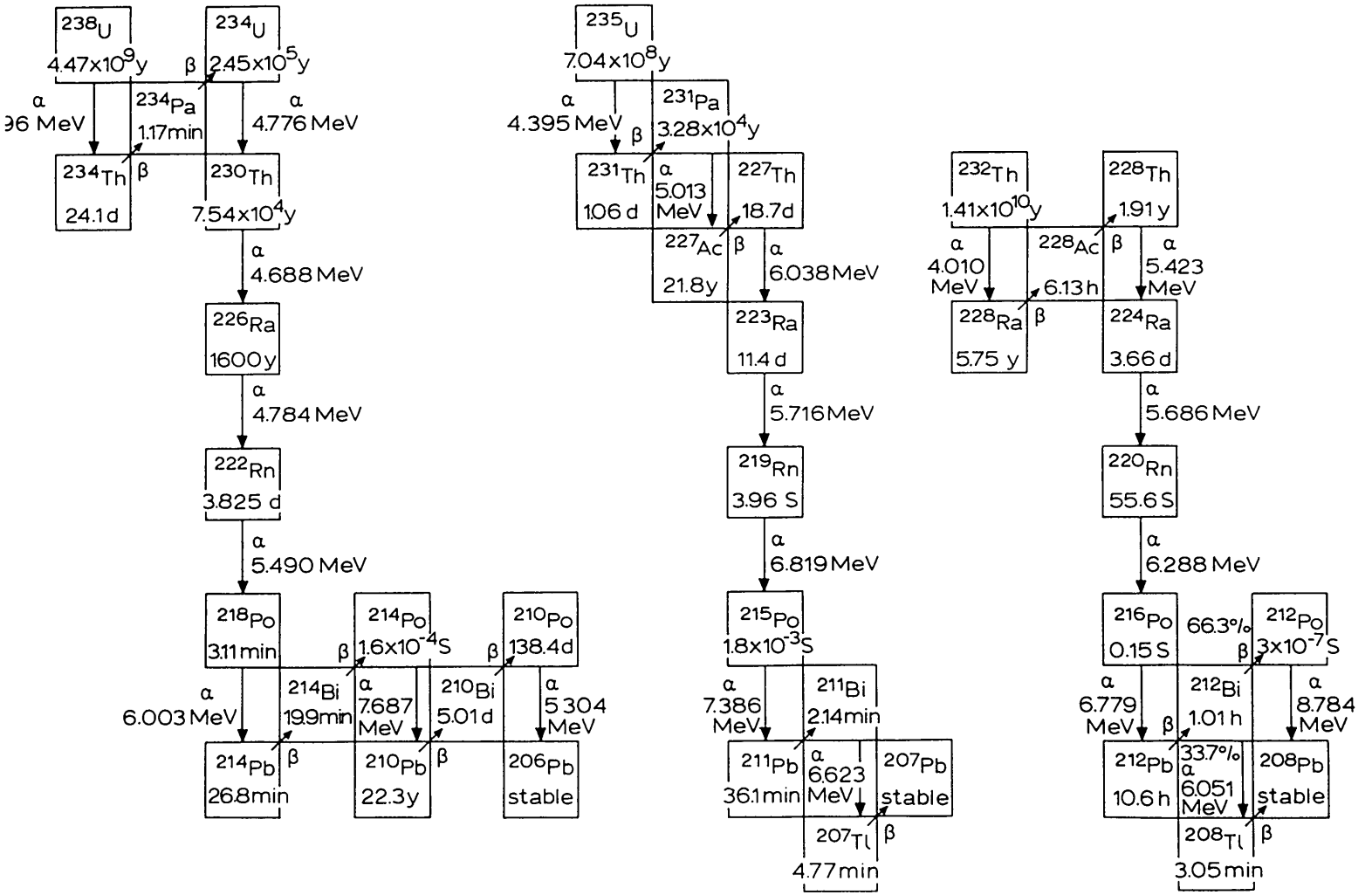

Figure 1.6. Natural Decay Series

If the parent is separated, then the daughter activity will grow in, but the daughter will be simultaneously be subject to decay. Under these conditions, the rate of decay of the daughter nuclide is;

$$\frac{dN_Y}{dt} = -\frac{dN_X}{dt} - \lambda_Y N_Y = \lambda_X N_X - \lambda_Y N_Y$$

where N_X and N_Y are the numbers of atoms of nuclides X and Y respectively, at a given time. Combining the above equations and differentiating;

$$N_Y = \frac{\lambda_X}{\lambda_Y - \lambda_X} N_{X_{(0)}} \left(e^{-\lambda_X t} - e^{-\lambda_Y t}\right) + N_{Y(0)} e^{-\lambda_Y t}$$

where $N_{X(0)}$ and $N_{Y0)}$ are the numbers of atoms of nuclides X and Y present at time zero.

The activity of the daughter radionuclide is given by;

$$A_Y = \frac{\lambda_Y}{\lambda_Y - \lambda_X} A_{X(0)} \left(e^{-\lambda_X t} - e^{-\lambda_Y t}\right)$$

Detailed description of the ingrowth of the daughter activity to the initially pure parent fraction are described in Freidlander et al. (1981), and two cases are of relevance to the present work:

(a) **secular equilibrium** in which $(t_{1/2})_X >> (t_{1/2})_Y$ (X=parent; Y=daughter), in which the growth to equilibrium is described by ;

$$A_Y = A_X \left(1 - e^{-\lambda_Y t}\right)$$

and at equilibrium $A_Y = A_X$

(b) **transient equilibrium** in which $(t_{1/2})_X > (t_{1/2})_Y$ in which the growth to equilibrium is described by;

$$A_Y = \frac{\lambda_X}{\lambda_Y - \lambda_X} A_{X(0)} e^{-\lambda_X t} \left(1 - e^{-(\lambda_Y - \lambda_X)t}\right)$$

and equilibrium is reached when

$$(1 - e^{-(\lambda_y - \lambda_x)t}) = 1$$

1.2.3 *Natural decay series disequilibrium in the coastal marine environment.*

Natural decay series disequilibrium in the marine environment arises from differential aqueous/solid phase partioning of the radionuclides. For radionuclides such as uranium, which can exist in different oxidation states, the redox conditions can be important in determining whether the nuclide will be in the aqueous or solid phase.

The degree of solubility of a radionuclide (or indeed any element) is governed by the nature of its interactions with water molecules, ligands and solid phase surfaces and such interactions are determined largely by size and the charge of the ion. For example, the extent of hydration of an ion is proportional to its charge (Z) and inversely proportional to its radius. The factor Z/r, known as ionic potential, can be used qualitatively to determine the degree of solubility of an ion (Mason, 1966) and ionic potentials of a selection of radionuclides are given in Table 1.1. (Henderson, 1982; Greenwood and Earnshaw, 1984)

ION	IONIC POTENTIAL	SOLUBILITY
Ra^{2+}	1.35	generally soluble
Th^{4+}	4.25	generally insoluble
Po^{4+}	4.25	generally insoluble
U^{4+}	4.49	generally insoluble
Pb^{2+}	5.16	generally insoluble
U^{6+}	8.22	generally soluble

Table 1.1 Ionic potentials for selected radionuclides

At low values of ionic potential, simple hydration occurs which results in a very high degree of solubility. However, at higher values, hydrolysis can occur which results in a low degree of solubility. Finally, at very high values oxy ion formation occurs which results in a high degree of solubility. In addition ionic potential governs attraction to surfaces and ions with a low Ionic potential have a low degree of surface reactivity compared to ions with higher ionic potential which have a very high degree of reactivity, while ions with very high ionic potential (resulting in oxy ion formation) have a higher degree of solubility. U^{6+}, Ra and Rn exhibit relatively high solubility whereas all other natural decay series radionuclides are highly insoluble. This leads to the separation of parent/ daughter pairs, providing useful tracers for a number of marine processes as follows; $^{234}U/^{238}U$ which is used as a dating tool and to study radionuclide migration and transport processes, $^{230}Th/^{234}U$ which is used in chronological studies and $^{234}Th/^{238}U$ which is used to study particle scavenging and euphotic zone production.

In the deep ocean U has a uniform distribution, with an average concentration of 3.3 ppb, which is attributed to the fact that it is thought to exist as the stable $[UO_2(CO_3)_3]^{4-}$ complex (Starik and Kolyadin, 1957). However, this theory is questioned by Krylov et al., (1985) who regard the hydroxide complex as the most stable uranium complex in seawater. This is in comparison to ^{232}Th which has an average concentration of 0.7×10^{-4} ppb in the ocean which is than would be expected from its solubility product (Bruno and Sellin, 1992)

Radium also has considerable mobility within the marine environment (Burton, 1975: Kigoshi, 1971; Somayajulu and Church, 1973; Mackenzie, 1977; Li et al., 1977; Cochran and Kirshnaswami, 1980; Huh et al., 1987). Many studies of ^{226}Ra and ^{228}Ra have shown that radium diffuses into the pore waters of sediments into overlying water resulting in disequiliberia between Ra and insoluble Th parents. There is an increase in concentration of ^{226}Ra found in coastal and fjordic waters (MacKenzie et al., 1979, Li et al., 1977; Todd et al., 1988) and these elevated concentrations can be used to study the mixing of nearshore and oceanic water masses (Ku and Lin, 1976; MacKenzie et al., 1979, Elsinger et al., 1984 Ku and Lin, 1976). Ra solubility also results in its fractionation from its much less soluble

descendant (via a series of short lived nuclides) ^{210}Pb (Figure 1.6.) and this is of particular importance in the coastal marine environment where ^{210}Pb is used to investigate sediment accumulation and mixing rates (Koide et al., 1973; Robbins and Edgington, 1975; Appleby and Oldfield, 1978; Benninger et al., 1979; Clifton and Hamilton, 1979; Swan et al., 1982; Chanton et al., 1983; Smith Briggs, 1983; Carpenter et al., 1987; Ridgway and Price, 1987; Santschi et al., 1987; Gubala et al., 1990; Sugden, 1993) and in the deep ocean where it is used to study the residence time of particles in the water column and sediment mixing processes (Nozaki et al., 1976; Bacon et al., 1976; Chung, 1987; Thomson et al, 1993).

As a consequence of their different solubilities ^{210}Pb unsupported by ^{226}Ra is added to sediments. The unsupported ^{210}Pb has two sources, namely atmospheric deposition from ^{222}Rn decay and in situ production in the water column via ^{226}Ra decay. Radon is a noble gas and as such can diffuse out of soils into the atmosphere where it then decays to ^{210}Pb. The ^{210}Pb then attaches to particles which are removed from the atmosphere and transported to the sediments. Any ^{210}Pb produced in the water column from the decay of its parent nuclide ^{226}Ra will be scavenged by particulate matter and transported to the sediment surface. A summary of the pathways of ^{210}Pb to sediments based upon Santschi et al (1989), is given in Figure 1.7. In the nearshore environment atmospheric input is dominant but in deep ocean situations water column production becomes more important. In addition, a 'supported' component must be considered since detrital minerals will contain ^{226}Ra in equilibrium with ^{210}Pb. Another possible source of ^{210}Pb to the sediments of the sea lochs is from the river input to the system but this is will be minor in comparison with other inputs.

To enable the activity of ^{210}Pb in sediments to be used as an indicator of sedimentation rates some assumptions must be made, namely (1) the flux of ^{210}Pb to the sediment is constant, (2) there is no post depositional movement of ^{210}Pb, and (3) that the excess ^{210}Pb can be calculated from the ^{226}Ra and the total ^{210}Pb activities of the sediment (Wan et al, 1987).

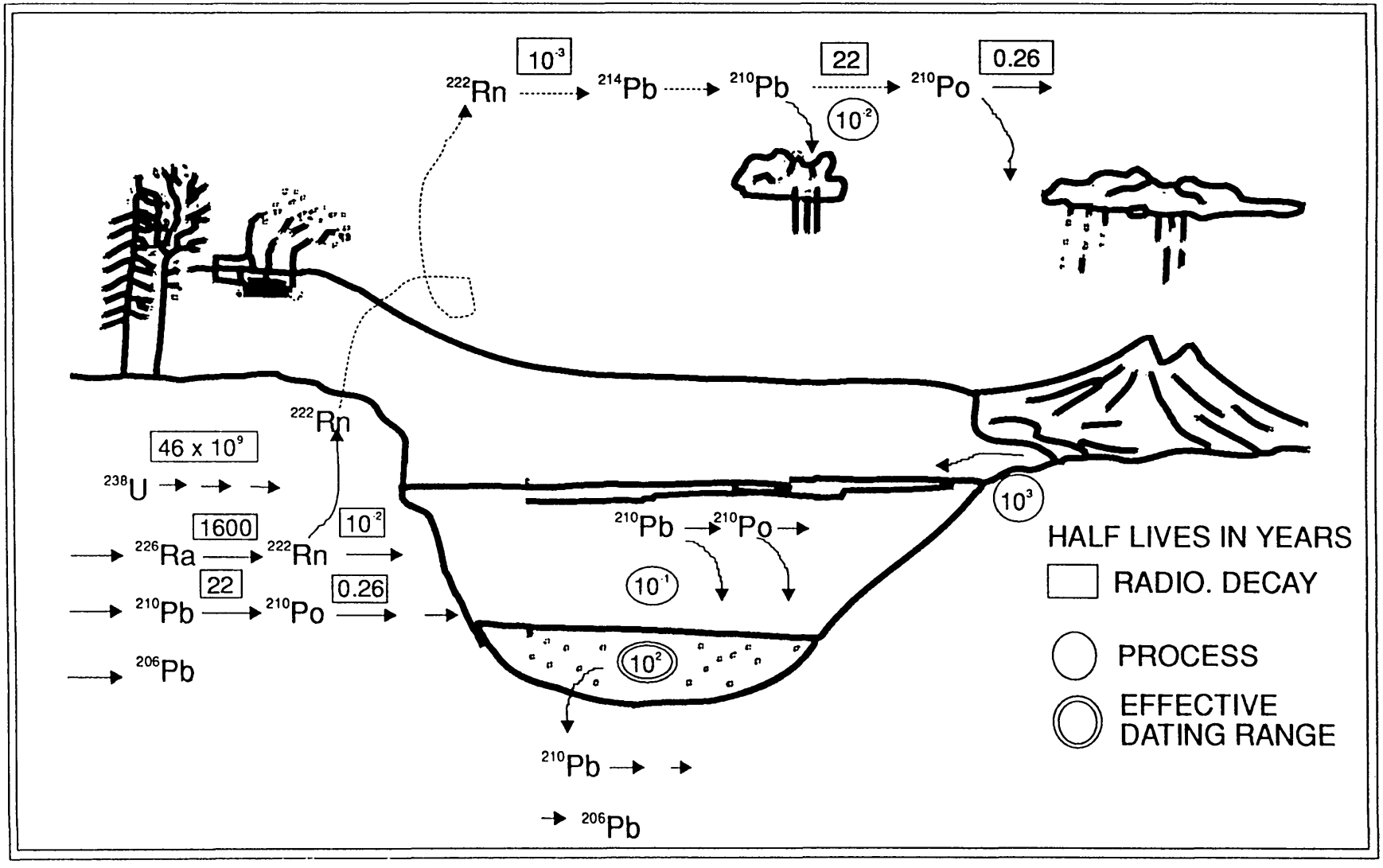

Figure 1.7. Pathways of ^{210}Pb to sediments (Santschi et al, 1989)

The two most commonly used models to calculate sedimentation rates and ages are the *constant rate of supply model* (CRS) (Appleby and Oldfield, 1978) and the *constant initial concentration model* (CIC) Robbins and Edginton, 1975). Both models depend on the assumption that the flux of ^{210}Pb to the sediment is constant and that the ^{210}Pb and ^{226}Ra are non-mobile. The CRS model can be used when sedimentation rates are variable, in comparison to the CIC model where the sedimentation rate must be constant.

The CIC model can be used to obtain sedimentation rates from measured activities of ^{210}Pb in the sediment by using a form of the general radioactive decay equation;

$$A_y = A_0\, e^{(-\lambda t)}$$

where A_y= activity of excess ^{210}Pb at depth y

A_0 = initial activity of excess ^{210}Pb at the surface.

λ = decay constant for ^{210}Pb

t = time in years

the equation can be transformed to;

$$\ln A_y = \ln A_0 - \lambda t$$

and time $t = z/\varpi$

z = weight of sediment (g cm^{-2})

ϖ = sediment accumulation rate (g cm^{-2} y^{-1})

the equation can then be rewritten as

$$\ln A_y = -(\frac{\lambda}{\omega})\, z + \ln A_0$$

The above equation is of the form **y = mx + c**, where $\ln A_0$ represents the constant c and $-(\lambda/\omega)$ is the gradient m, therefore by plotting ln A versus z and calculating the gradient the sedimentation rate can be calculated from $\omega = -(\lambda/m)$.

The CRS method assumes that the flux of excess ^{210}Pb supply to the sediment is

constant with time (Appleby and Oldfield, 1978), thus, the age (t) for a horizon at depth n is calculated from

$$\Sigma(excess^{210}Pb)_n = n_t(1-e^{-\lambda_{210}t})$$

where Σ(excess ^{210}Pb)$_n$ = total excess activity of ^{210}Pb from surface to depth n

n_t = total excess ^{210}Pb in the core.

In the ^{210}Pb dating of nearshore sediments the ^{210}Pb profile may be perturbed by Pb mobility, Ra mobility or sediment mixing. Mixing can either be treated as a homogeneously mixed box to a certain depth or can be considered as partial mixing that decreases with depth. Both types of mixing models are discussed in detail by Berner (1980).

In near shore sediments bioturbation can be particularly important and the effects of this must be taken into account when determining sedimentation rates. Radionuclides can also be used to calculate biodiffusion rates. If the sedimentation rate and decay constant are known then the following equation can be used to calculate D_B, the biodiffusion coefficient and P, a constant.

$$D_B\frac{\partial^2 A_S}{\partial x^2} - \omega\frac{\partial A_S}{\partial x} - \lambda A_S + P = 0$$

As discussed above, ^{226}Ra is relatively soluble and is mobile in the pore waters of sediments and has been used as a tracer of solute transport processes and irrigation in coastal sediments (Martin et al, 1987). The ^{226}Ra in the pore waters may be removed to the sediment depending on the concentrations of Fe and Mn and the redox condition of the sediment. It is well documented that radium is associated with Fe-Mn oxyhydroxides (Kadko, 1981, Moore et al., 1981, Huh and Ku, 1984) and the excess ^{210}Pb cannot therefore simply be calculated by subtracting the constant ^{210}Pb activity at depth.

^{210}Pb dating has been successfully applied to obtain chronologies for nearshore sediment by a number of investigators (Koide et al.,1973; Robbins and Edgington, 1975; Clifton and Hamilton, 1979; Benninger et al., 1979; Chanton et al., 1983; Malcolm, 1981; Swan et al., 1982; Ridgway, 1982; Sugden, 1993; Bryant, 1993) and in particular, it has been applied to Loch Etive by Malcolm (1981) and Ridgway (1983). Ridgway and Price (1987) questioned the ^{210}Pb chronologies obtained for sediment cores from Loch Etive and suggested that Pb might be mobile in this environment. However, this was based on chronologies obtained from the total depth of penetration of ^{137}Cs, and recent observations of Cs diffusion raise questions over the validity of this approach.

Pb mobility has also been suggested by Benoit et al., (1990) and Benoit et al., (1991), and since non- mobility of Pb is one of the necessary assumptions in ^{210}Pb dating, its mobility could invalidate the method. ^{210}Pb is a widely used and important tracer for mixing and accumulation studies and it is therefore important to verify whether or not it is mobile and this is of particular importance in the environment where mobility has been suggested.

While radium isotopes are soluble in seawater, thorium isotopes exhibit a very low solubility giving rise to radioactive disequilibrium in which ^{228}Ra and ^{226}Ra activities in seawater are virtually unsupported by their thorium parents. Studies by Moore (1969) indicated that the source of ^{228}Ra to the surface waters of the oceans is the near shore sediments of the continental shelf and continental rise. Mackenzie et al (1979) found elevated concentrations of ^{226}Ra and ^{228}Ra in the waters of the Clyde Sea area, the concentrations being maximal near the sediment surface and with activity ratio of about 1.5 for ^{228}Ra/^{226}Ra. Mackenzie (1977) found enhanced concentrations of ^{226}Ra in the bottom waters and sediments of Loch Goil and this may place limitations on applying ^{210}Pb dating to the sediments of Loch Goil.

Disequilibrium between ^{228}Ra and ^{228}Th has been used to study many different processes taking place within the marine environment. ^{228}Ra, with a half life of 5.7 years, is ideally suited for studying natural processes on a timescale of 1 to 30 years. The main processes studied within the deep ocean are the scavenging of

^{228}Th from surface waters of the oceans and residence times of particles within the surface waters (Broecker et al., 1973; Reid et al., 1979; Li et al., 1980;), vertical eddy diffusion (Li et al., 1980) and thermocline mixing (Moore, 1972). Within the coastal marine environment the disequilibrium has been used to a) determine the effect of bioturbation on surface sediments (Carpenter at al., 1984); b) determine the involvement of Th in the redox cycling of Mn and Fe (Todd et al., 1988); c) particle scavenging (Santschi et al., 1983, Cochrane et al., 1987) and d) sedimentation rates in undisturbed surface sediments (Koide et al., 1973; Bruland et al., 1981).

In conclusion, natural radionuclides have considerable potential for study of nearshore sediments and, in particular, ^{210}Pb is of major importance in the study of mixing and accumulation rates within this environment. However, it is necessary to investigate the mobility of both ^{210}Pb and ^{226}Ra in the study area. Previous work undertaken in the Clyde Sea Area used short cores (Craib) and gravity cores (that did not collect the sediment surface) to investigate sedimentation and mixing rates (Swan, 1978; Smith-Briggs, 1983) which limited the assessment of accumulation rates. Therefore, the study of longer, gravity, cores is necessary to determine the accumulation rates for this area.

1.3 *Manmade Radionuclides*

1.3.1. *Outline*

There are three main sources of manmade radionuclides to the marine environment of the West Coast of Scotland. These are, atmospheric fallout resulting from nuclear bomb testing, 1945-1975, (Carter et al, 1977), discharges from BNFL's nuclear fuel reprocessing plant at Sellafield, previously known as Windscale, 1952-present day, (Cambray, 1981) and finally the most recent source, fallout from the Chernobyl reactor accident in April 1986, (Fry et al, 1986). Weapons testing fallout was much greater source of nuclides than either Chernobyl or Sellafield which were approximately the same in terms of total inventories. However, in terms of local influences, Sellafield being a point source release, is of much greater significance in the study area than either weapons testing fallout or Chernobyl fallout, which were

distributed globally. There are also some minor sources of radionuclides to the Clyde Sea Area including magnox and AGR nuclear reactors at Hunterston and the British Naval base at Faslane which is involved with nuclear submarines. An American Naval base operated in the Holy Loch until 1992, which was also involved with nuclear submarines.

The main manmade radionuclides of interest in this study are listed in Table 1.2. The $^{134}Cs/^{137}Cs$ activity ratio can be used as a tracer of water movement and as a potential tracer of sediment processes. ^{241}Pu is the parent of ^{241}Am and therefore its distribution will have an affect on the distribution of ^{241}Am, which has the potential to be used as a tracer of sediment processes. Finally, all these nuclides are of interest as they provide additional information on dispersion and distribution of radionuclides within the coastal marine environment.

Cs isotopes have been shown to be highly soluble and to remain largely in solution in sea water (Broecker et al., 1966; Jefferies et al., 1973; Baxter et al., 1979; Livingston and Bowen, 1979; Swan et al., 1982), in contrast, Pu and Am isotopes are mainly associated with particulate phases (Hetherington, 1975; Hetherington, 1978; Edgington, 1980 Pentreath et al., 1984). Pu exists in two main oxidation states, Pu^{4+} which is insoluble and Pu^{5+} which is relatively soluble (Lovett and

NUCLIDE	$t_{1/2}$(years)	SOURCE
^{134}Cs	2.1	Sellafield, Chernobyl fallout
^{137}Cs	30.17	Sellafield, bomb fallout, Chernobyl fallout
^{241}Pu	14.4	Sellafield, bomb fallout
^{241}Am	441	Sellafield, bomb fallout

Table 1.2 Manmade radionuclides, half lives and sources

Nelson, 1978) and results in Pu being more widely distributed within the marine environment.

1.3.2. *Sellafield*

Nuclear fuel reprocessing at BNFL's plant situated at Sellafield in Cumbria (Figure 1.8.), has resulted in the discharge of waste radionuclides into the Irish Sea since 1952, with a pronounces maximum in discharge levels occurring between 1973 and 1975 (Figure 1.9.)(MAFF, 1971-1991; BNFL 1977-1989).Allowing for radioactive decay and ingrowth, it can be calculated that by 1990, the discharge had generated environmental inventories of approximately 3×10^4 TBq of ^{137}Cs, 6.8×10^2 TBq of $^{239,240}Pu$ and 8.9×10^2 TBq of ^{241}Am (BNFL , 1977-1989; MAFF, 1971-1991; Cambray, 1982).

Most of the radiocaesium remains in solution in sea water and is transported out of the Irish Sea on a timescale of a year or less. (Jefferies et al., 1973; Baxter et al., 1979; McKinley et al., 1981). About 10% of the radiocaesium is associated with the sediments of the Irish Sea (Smith et al., 1980; Miller et al., 1982; Pentreath et al., 1984; Jones et al., 1984) mainly in an area of fine sediment lying off the Cumbrian coast. In contrast to the radiocaesium, almost all of the discharged ^{241}Am is incorporated in sediment close to the discharge point (Day and Cross, 1981; Aston and Stanners, 1982; Pentreath et al., 1984). Most of the plutonium is also incorporated into the sediment as Pu^{4+}, but a small fraction exists as the more soluble Pu^{5+} and is transported in solution with the radiocaesium (Hetherington, 1975; Nelson and Lovett, 1978; Pentreath et al., 1984, 1986). The wide distribution of a fraction of the plutonium due to the solubility of its oxidised form has important implications for the distribution of ^{241}Am, since decay of Sellafield ^{241}Pu provides an *in situ* source of ^{241}Am in the environment. (Day and Cross, 1981). There are two main transport mechanisms of Sellafield waste radionuclides in the marine environment namely, solution transport of dissolved radionuclides and transport of contaminated sediment from the Irish sea. Redistribution of contaminated sediment is restricted largely to the area within the Irish Sea to the south and east of Burrow Head (Mackenzie et al., 1987; McDonald et al., 1990; Mackenzie et al., 1993; MacKenzie and Scott, 1993) and radionuclide supply to the sea lochs of the west coast of Scotland can be regarded as being by solution transport, which will affect

Cs and Pu^{5+} but not Am or Pu^{4+}. It is well documented that the 'plume' of dissolved radiocaesium from Sellafield travels northwards from the Irish Sea around the west coast of Scotland (Jefferies et al., 1973; Wilson, 1974; Mitchell, 1975; Hetherington, 1976; Livingston and Bowen, 1977), undergoing relatively slow dilution and dispersal during transit. The transport of radiocaesium from Sellafield to the Clyde Sea Area and its partitioning between water and Scottish coastal sediments has been studied previously (McKinley et al., 1981; Swan et al., 1982; McKay and Baxter, 1985; McKay et al., 1986.). In the 1970's, Baxter et al., (1979) found that the transit time of radiocaesium from Sellafield to the Clyde area was approximately 8 months and that Firth of Clyde seawater had a composition consisting of approximately 92% Irish Sea water, 7% Atlantic water and 1 % freshwater. They also reported that approximately 30% of the Sellafield radiocaesium output passes into the Clyde Sea Area with a maximum of 0.3 % of the output of radiocaesium being incorporated in the Clyde Sea Area sediments.

From their studies of radiocaesium in the Clyde Sea Loch sediments Swan et al., (1982) reported that a maximum of 0.025% of ^{137}Cs in Clyde waters finds a "permanent" sink in its sediments and that the average residence time of caesium in coastal waters is approximately 950 years which is short compared to the residence time of 10^4-10^6 years for caesium in open ocean. They also reported that sedimentation rates obtained from radiocaesium distributions in the sediment were in good agreement with ^{210}Pb sedimentation rates for the Clyde Sea Area cores. The calculation of sedimentation rates using the ^{137}Cs concentration was achieved by assuming that the observed vertical trends reflect past variations of nuclide concentrations in particles deposited from the overlying water column and comparing the ^{137}Cs profiles with data for the Sellafield discharge, decay corrected to the time of collection of the cores (1977). Swan et al., (1982) obtained sedimentation rates in a deep station from Loch Goil of 0.2 g cm^{-2} y^{-1} from both ^{210}Pb and ^{137}Cs profiles and 0.12 g cm^{-2} y^{-1} and 0.15 g cm^{-2} y^{-1} from ^{210}Pb and ^{137}Cs profiles respectively for a shallow station in Loch Goil and concluded that the sedimentation rates observed from both ^{137}Cs and ^{210}Pb were in good agreement.

Ridgway and Price (1987) also investigated the use of both ^{137}Cs and ^{210}Pb profiles

Figure 1.8. Location of Sellafield, BNFL's reprocessing plant

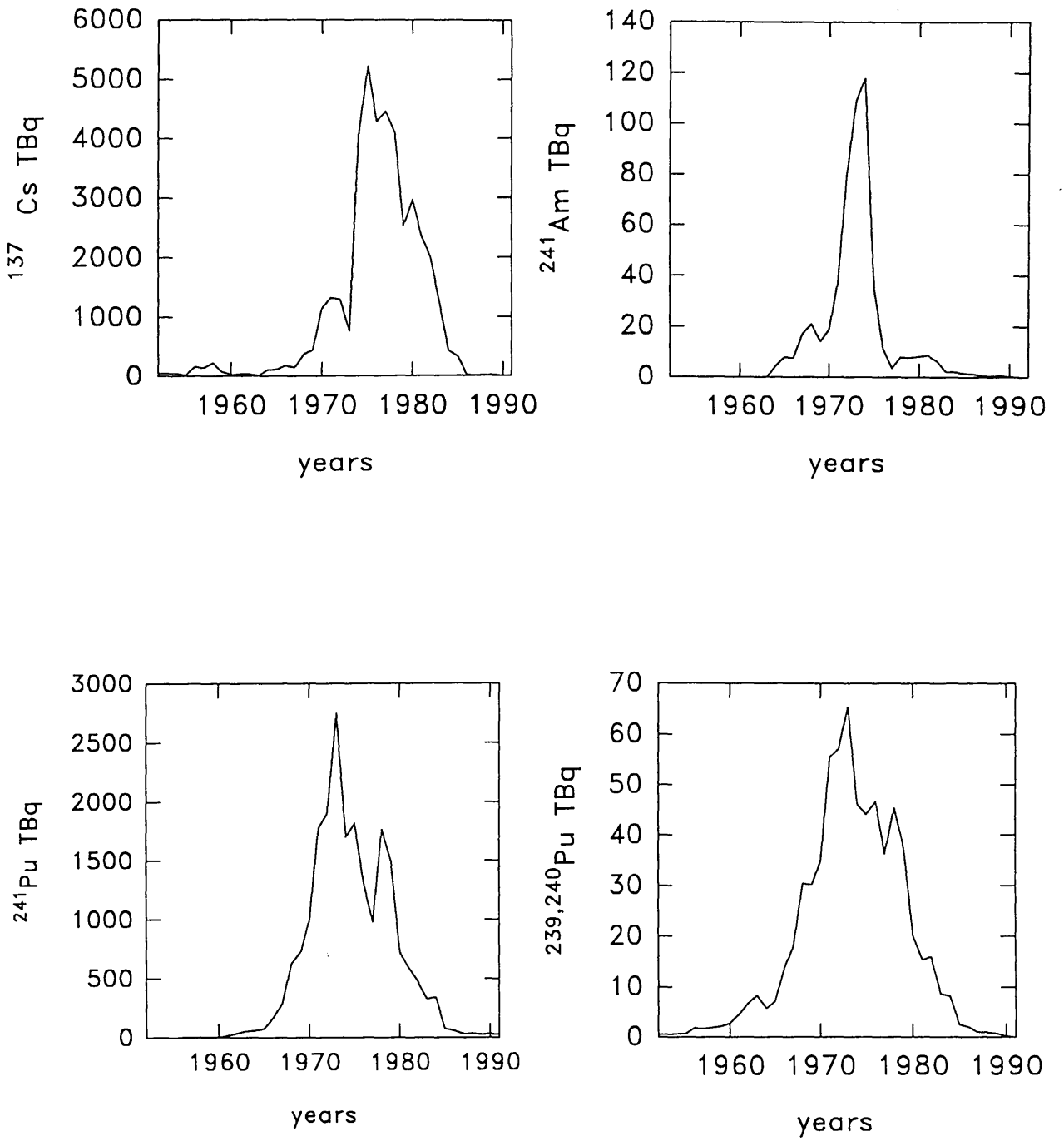

Figure 1.9. Discharge data for ^{137}Cs, ^{241}Am ^{241}Pu and $^{239,240}Pu$ from BNFL

to investigate sedimentation rates in Loch Etive. However, in this case the authors used the depth of penetration of ^{137}Cs to calculate sedimentation rates and observed a two to three fold discrepancy between the ^{137}Cs and ^{210}Pb chronologies. They obtained chronologies for four gravity cores, from Loch Etive, by equating the depth to which ^{137}Cs penetrated in the sediment, to the start of the Sellafield discharge in 1952, and applied this to interpret the concentration profiles of Zn, Cu and Pb.

Using this chronology they obtained dates of apparent onset of metal enrichment in these sediments which ranged from 1932 to 1962 and contented that there was diagenetic loss of metals, including Pb, during burial. This obviously has major implications in the use of ^{210}Pb dating for sediment cores within this environment. The sedimentation rates obtained by Ridgway and Price (1987) from ^{210}Pb dating were 0.33 cm^{-1} y^{-1} and 0.86 cm^{-1} y^{-1} for the outer and inner basins of Loch Etive respectively which can be compared to those calculated from the ^{137}Cs profiles which were 1.21 and 1.07 cm^{-1} y^{-1} respectively.

MacKay and Baxter (1985) studied the sediments of Loch Goil and Loch Etive and found that ^{137}Cs was incorporated in clays and that organic and oxide coatings prevented release of ^{137}Cs from clay mineral exchange sites. Sellafield waste radionuclides are thus well established as tracers of water movement and sediment processes in the study area. Therefore from previous studies it can be seen that radionuclides emanating from BNFL plc. at Sellafield are detectable in the sediments of the sea lochs of the west coast of Scotland and due to the decrease in discharge from Sellafield (Figure 1.9.), the concentrations of these decreases should be reflected in more recently acquired sediment cores (Kershaw et al., 1990).

1.3.2 *Bomb testing and Chernobyl fallout*

During the 30 year span from 1945 to 1975, approximately, 800 nuclear detonations were announced with a cumulative yield of 325 Mt (Carter and Moghissi, 1976). Radionuclide fallout from bomb testing has been dispersed globally and has introduced radiocaesium, plutonium and americium to the environment. Almost no ^{241}Am was released during bomb detonations, but it has grow in from weapons

testing ^{241}Pu in the environment. ^{137}Cs which is a fission product is present in the bomb fallout but ^{134}Cs which is a neutron activation product is not produced by nuclear detonations and is therefore not present in the fallout.

Another source of radioactive fallout is from the Chernobyl accident. The accident at the nuclear power station in Chernobyl, near Kiev, on 26th of April 1986, led to substantial quantities of radioactive material being released to the atmosphere. Table 1.3. gives the estimated inventories of radionuclides released from Sellafield, nuclear weapons testing and Chernobyl.

	SELLAFIELD		WEAPONS TESTING		CHERNOBYL	
Nuclide	Activity (Bq)	Weight (kg)	Activity (Bq)	Weight (kg)	Activity (Bq)	Weigh t (kg)
^{137}Cs	3.0×10^{16}	9.4	1.3×10^{18}	406	4×10^{16}	12.5
$^{239,240}Pu$	6.8×10^{14}	253	8.9×10^{15}	3900		
^{241}Am	8.9×10^{14}	7.0	3.0×10^{15}	24		

Table 1.3 Comparison of radionuclide discharges from Sellafield, weapons testing and Chernobyl (BNFL, 1977-89; Cambray, 1982; NRPB, 1984; Joseph et al., 1971; Hardy et al., 1973; NRPB, 1986)

Many studies have been undertaken to determine the effect of the Chernobyl fallout in the soils and sediments of the U.K. (Fry et al., 1986; Camplin et al., 1986; Clark et al., 1988; McDonald et al., 1992). The release of ^{137}Cs and ^{134}Cs from Chernobyl resulted in a change in the $^{134}Cs/^{137}Cs$ ratio in environmental materials, the Chernobyl ratio being approximately 0.55 (Horrill et al., 1988) in comparison to 0.073 for the 1986 Sellafield ratio (BNFL, 1987). However, the Chernobyl deposition had a small and transient effect on radiocaesium concentrations in seawater (MAFF, 1986).

In summary, the West Coast of Scotland is contaminated by radionuclides, in particular radiocaesium from Sellafield and it is important to characterise the behaviour of radionuclides to evaluate the long term implications of the discharge of

nuclear waste. The radionuclides have a potential use as tracers of sediment processes eg. mixing and accumulation rates, but there is a possible conflict between ^{137}Cs and ^{210}Pb chronologies and hence there is a need for research in this area.

1.4 *Lead and Lead isotopes in the environment*

1.4.1 *Lead in the environment*

Lead is a natural trace constituent and is widely distributed in the environment but it is also one of the major environmental pollutants of the 19th and 20th century. The crustal abundance of lead is 15 mg/kg (Kesler, 1978), occurring primarily in potassium feldspars and micas in igneous rocks and in lead minerals such as galena, cerrusite, anglesite and pyromorphite but only galena is sufficiently abundant to be mined commercially for lead (Kesler, 1978).

Lead is relatively easily extracted from ores and this made its use widespread in many ancient civilizations, with the largest pre-industrial use being by the Romans (Nriagu, 1978: Harrison et al., 1984). The industrial revolution saw the worldwide production of lead escalate and more recent uses of metallic lead include Pb/acid cells and radiation shielding. Lead compounds are used in paints, varnishes, plastics and insecticides. The 1920's saw the addition of tetra-alkyl lead additives to petrol as an anti-knock agent (Guthrie, 1960) which resulted in the widespread dispersal of lead from this source to the environment.

The major sources of input of lead to the environment due to anthropogenic activities are heavy industry, e.g. steel and iron production, fossil fuel combustion, refuse incineration and lead from exhaust emissions from petrol driven engines. Nriagu (1989, 1991) calculated that anthropogenic global emissions of lead to the atmosphere in 1983 (332×10^9g/y) were 28 times larger than natural sources (12×10^9 g/y) and that lead from exhaust emissions accounted for 75% of the total atmospheric lead emissions in that year. With respect to the U.K., in the early 1980's lead derived from alkyllead anti-knock compounds accounted for 90% of the 7590

$\times 10^6$ g/y of lead emitted to the atmosphere (Jones et al., 1991). However, more recent work has shown a decrease in the concentration of deposited pollutant lead in rural herbage in the U.K. following the reduction of the maximum permissible lead content of petrol from 0.40 to 0.15 g/l at the beginning of 1986 (Jones et al., 1991).

1.4.2 *Stable lead isotopes*

There are four stable isotopes of lead ^{204}Pb, ^{206}Pb, ^{207}Pb and ^{208}Pb, which have an average abundance in the earths crust of 1:17:15:37. Three of the isotopes are radiogenic (^{206}Pb, ^{207}Pb and ^{208}Pb) and are the stable end products of the natural decay series of ^{238}U, ^{235}U and ^{232}Th respectively (Figure 1.6.) while ^{204}Pb is a primordial nuclide.

Variations in the $^{206}Pb/^{207}Pb$ ratios of ore deposits are related to their U and Th content and their ages. In lead ore deposits which are 1000 million years old the $^{206}Pb/^{207}Pb$ ratios are $\sim$1.10 and in 30 million year old deposits $^{206}Pb/^{207}Pb$ are $\sim$1.30 (Maring et al., 1987). Table 1.4. gives the $^{206}Pb/^{207}Pb$ ratios for selected world ores and Table 1.5 gives the $^{206}Pb/^{207}Pb$ and the $^{208}Pb/^{206}Pb$ ratios in the principal lead mining areas of Scotland during the 19th century. Pollutant lead from different sources such as industrial emissions and car exhaust fumes retains the original isotopic signature of the lead ore from which it was derived. Therefore by using lead isotope ratios it should be possible to determine the different sources of pollutant lead, although mixing of ores during industrial processes could present problems.

The isotopic signature of the leaded petrol is determined by the ores used in the manufacture of the alkyllead additive and the dominant U.K. manufacturer, Associated Octel, uses a 70:30 mixture of Australian and British Columbian ores with a $^{206}Pb/^{207}Pb$ ratio of 1.04 and 1.16 respectively giving a net $^{206}Pb/^{207}Pb$ ratio of 1.076 (Delves, 1988). Delves (1988) obtained a $^{206}Pb/^{207}Pb$ ratio of 1.065 $\pm$ 0.003 for petrol from Southampton and Edinburgh in 1988. Sugden (1993) who was, in part, testing Delves hypothesis on the use of $^{206}Pb/^{207}Pb$ ratios

Ore Deposit	$^{206}Pb/^{207}Pb$
CANADA	
Buchans, Newfoundland	1.15
MEXICO	
Durango	1.20
Taxaco	1.19
PERU	
Casapalea	1.20
AUSTRALIA	
Mt. Isa	1.04
Broken Hill	1.04
USA	
Mississippi Valley, Missouri	1.39

Table 1.4 $^{206}Pb/^{207}Pb$ **ratios in lead bearing ores (Brown, 1962)**

Location	$^{206}Pb/^{207}Pb$	$^{208}Pb/^{206}Pb$
DUMFRIESSHIRE		
Wanlockhead	1.170	2.090
ARGYLLSHIRE		
Strontian	1.172	2.081
Islay (Mulreesh)	1.162	2.095
Islay (Ballygrant)	1.168	2.088
PERTHSHIRE		
Tyndrum	1.144	2.121
KIRKCUDBRIGHTSHIRE		
Minnigaff	1.170	2.096

Table 1.5 Lead isotope ratios in lead mined in Scotland in the 19th century (Moorbath, 1962)

to determine the source of pollutant lead, carried out an extensive study of lead isotope ratios in environmental materials including petrol, atmospheric particulates, street dust, coal and lead ore related samples which gave mean $^{206}Pb/^{207}Pb$ ratios of 1.082, 1.094, 1.108, 1.185 and 1.173 respectively. It can be seen that the urban air particulates and the street dust have $^{206}Pb/^{207}Pb$ ratios are similar to that of petrol and this suggests that petrol is the dominant Pb source term for these materials.

Sugden (1993) also studied peat and freshwater lake sediment cores in order to establish historical deposition trends of lead. Omborotrophic peat cores were studied to determine the atmospheric deposition of lead and Sugden (1993) concluded that the profiles supported the established view that lead is strongly bound and relatively immobile in unsaturated ombrotrophic peat (Livett et al., 1979; Schell et al., 1986). The results from peat cores taken from rural and remote locations in Scotland showed a 10-20 fold enhancement in the fluxes of lead deposited from the atmosphere since 1800, with a maximum flux occurring between 1930 to 1960, and also exhibited a significant reduction in $^{206}Pb/^{207}Pb$ ratios over the last 50 years which can be attributed to increasing contributions from car exhaust emissions of particulate lead derived from alkyllead petrol additives. The estimated contributions of petrol lead to atmospheric lead fluxes ranged from 27-47% at rural locations to 35-57%in North Uist during the last 20-25 years. The sediment cores indicated that lead from heavy industry and the combustion of coal, with a $^{206}Pb/^{207}Pb$ ratio of 1.17-1.18, dominated lead inputs to the sediments during the 19th and early 20th centuries (Sugden, 1993). The sediment cores also showed a similar decrease of $^{206}Pb/^{207}Pb$ ratio towards the surface as the peat cores and this was attributed to the effect of lead from petrol which has a low $^{206}Pb/^{207}Pb$ ratio.

Stable Pb isotope and total Pb and ^{210}Pb data for peat and sediment cores thus allow historical trends of deposition to be established which are consistent with historical inputs (eg. industrial revolution, the addition of alkyl lead to petrol, and the increased usage of cars). Different pollutant sources of Pb can, at least in part, be identified and there is a potential for the application of stable Pb isotope ratios in the study of Pb geochemistry in the marine environment (Elbaz-Poulichet et al., 1984, 1986.)

1.5 *Aims of Research*

The main aims of this research were as follows;

1) To study radionuclide geochemistry and the use of radionuclides as tracers of mixing and accumulation processes in Scottish sea loch sediments.

2) To investigate heavy metal distributions and geochemistry and in particular to determine whether Pb is diagenetically mobile in these sediments.

3) To investigate the isotopic composition of Pb and, thereby, to attempt to distinguish pollutant Pb from natural Pb and to assign a heavy industry or petrol origin to the pollutant Pb.

4) By combing the information derived from the above aspects of the work to attempt to establish historical trends of heavy metal deposition and to evaluate anthropogenic influences on the study area.

5) To investigate the suitability of ICP-MS in the analysis of pore waters and to use concentrations of redox sensitive metals to evaluate the redox conditions of the sediment.

CHAPTER 2

Experimental

2.1 *Sample Collection*

2.1.1 *Outline*

The main objective of the sampling programme was to collect sediment cores from Loch Etive and sea lochs within the Clyde Sea Area, which a) retained the vertical integrity of the sediment b) provided an undisturbed sediment water interface and c) represented sediment deposition over a period of several hundred years. Cores were obtained at three sites in Loch Etive, two sites in Loch Fyne and one site in each of Loch Long and Loch Goil (Fig. 2.1 and 2.2). The gravity corer used was a modified version of the Kemp corer (Kemp *et al.*, 1976), which enables 4 inch diameter cores to be collected satisfying the above criteria.

An archived set of surface samples of Loch Etive sediment taken every 0.5 mile from the head of the loch to the sea on 1/11/81, was also analysed by gamma spectroscopy.

In addition to sediment collection, pore water samples were extracted from the Clyde sediments. The method of collection is described in detail below. Salinity and temperature readings were taken at regular intervals down the water column at each sampling site and at the Clyde Sea area sampling sites, water was additionally collected for determination of dissolved oxygen profiles.

2.1.2 *Loch Etive*

Sample collection was conducted from the Dunstaffnage Marine Laboratory research vessel ***Seol Mara*** on 12/9/86. Water column salinity and temperature readings were taken using an electronic switchgear T/S probe.

Three gravity cores were obtained from Loch Etive from the locations indicated in Fig. 2.1. Core 1 was from the outer basin and cores 2 and 3 were from the inner basin, with core 3 being from the deepest part of the basin.

The sediment cores were extruded and cut into 1 cm vertical sections for the first 10 cm depth, 2 cm sections until 50 cm depth and then 5 cm sections until the end of the core. The samples were placed into pre-weighed glass jars and transported to the laboratory where they were weighed and then oven dried (50°C) for two days. The samples were then re-weighed to obtain the dry weight of the sediment. Thereafter the sediments were ground using a tema mill and stored in sealed plastic jars.

2.1.3 *Clyde Sea Area*

Sampling in the Clyde Sea Area was performed from the Dunstaffnage Marine Laboratory research vessel ***Callunus*** during 23/6/88 - 29/6/88. At each sampling location the temperature of the water column at different depth intervals was measured using an electronic switchgear T/S probe.

Unfortunately the salinity probe was not operational so no salinity data are available for these sites. Water samples, collected using 10 l N.I.O. bottles, were analyzed for oxygen using the method of Strickland and Parsons (1975). Four sediment cores were collected from sea lochs within the Clyde Sea Area from the locations shown in Fig 2.2. The Decca coordinates for the sampling sites and the sampling dates are given in Table 2.1.

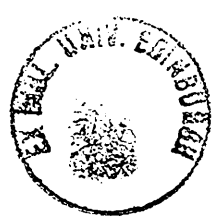

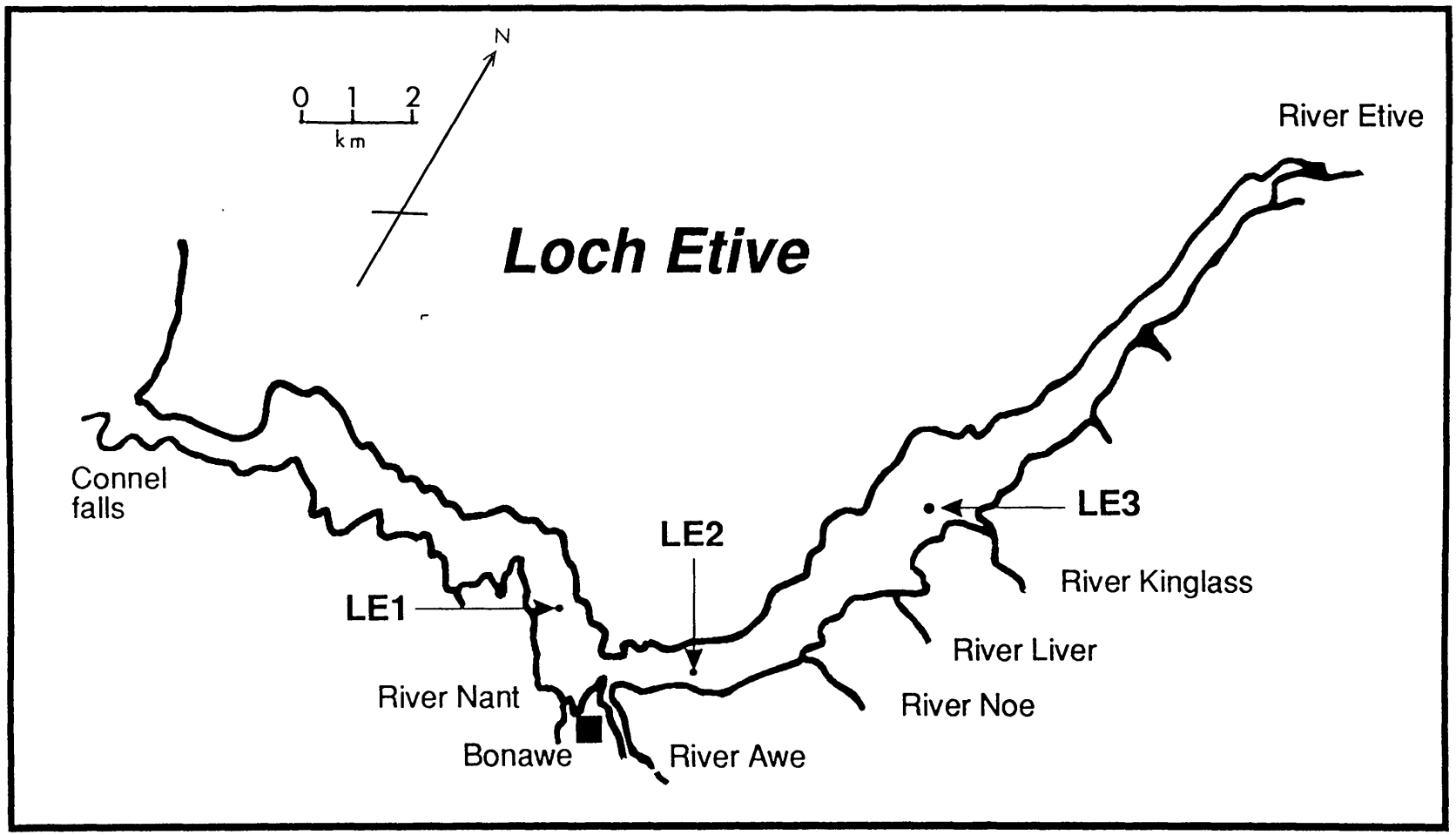

Figure 2.1. Location of sampling sites in Loch Etive

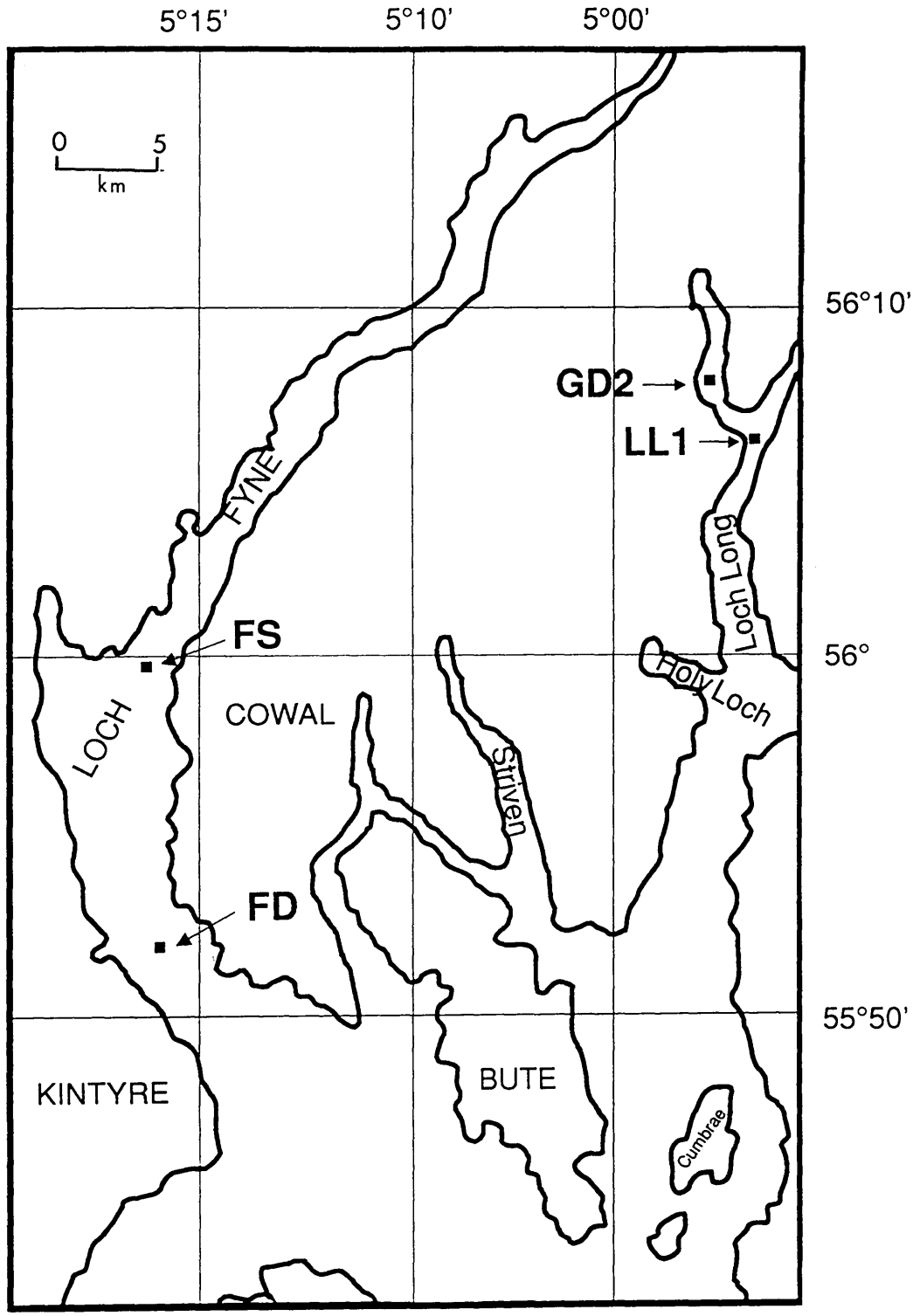

Figure 2.2. Sampling locations for sea lochs in the Clyde Sea Area

CORE (Code)	DATE	COORDINATES
Loch Fyne shallow (FS)	24/6/88	55,59.19N 5,22.07W
Loch Fyne Deep (FD)	23/6/88	55,51.86N 5,20.89W
Loch Long (LL)	28/6/88	56,05.07N 4,51.88W
Loch Goil (LG)	29/6/88	56,08.02N 4,53.48W

Table 2.1 Sampling locations, dates and codes for sediment cores collected from sea lochs in the Clyde Sea Area

The cores were collected using the gravity corer described above, and were immediately introduced into a glove box filled to a positive pressure with nitrogen. The oxygen content of the glove box was monitored using a Beckmann oxygen meter and was found to be < 0.1%. The water overlying the sediment, normally 20-30 cm in depth, was syphoned off and the cores were then extruded and divided into 1 cm or 2 cm vertical sections. A small sub-sample of sediment was removed from each section for water content analysis after which the samples were placed in 250 ml nitrogen filled centrifuge bottles. The bottles were then sealed and removed from the glove box, centrifuged for approximately 10 minutes at 6500 rpm and returned to the glove box for the pore water to be removed and filtered. Pore water was extracted by syringe filtering the samples through a combination of 5 micron and 1.2 micron Sartorius membrane minifilters which had been previously tested for contamination by syringing high purity water through a set and analysing the filtered water by ICP-MS. The combination of filters allowed the samples to be filtered relatively easily as the larger particles were removed before the 1.2 micron filter thus preventing fast clogging of the finer filter. Standard 5 ml sterile plastic syringes were used and a new syringe and set of filters was used for each sample. In some cases more than one set of filters was required.

The filtered samples were split into two aliquots, one of which was placed in a pre-washed plastic bottle containing 0.1 ml of 16M. Aristar nitric acid and the other in a pre-washed bottle without acid. The acidified samples were analyzed for metal concentrations by ICP-MS and the unacidified samples for nutrient concentrations by HPLC. The nutrient pore water samples were kept at 4°C aboard ship and were frozen on return to the laboratory. The availability of nitrogen on board the vessel was limited, so not all of the cores were section in nitrogen to the end of the core. Core FD was sectioned in nitrogen until the end of the core at 43 cm, core FS was sectioned until 30 cm depth before the nitrogen feed to the glove box was turned off. Cores LL and GD had a positive-pressure, nitrogen atmosphere to depths 30 cm and 44 cm respectively. After the nitrogen flow was turned off, the oxygen content in the glove box did not increase immediately, but to prevent ambiguity in interpretation of the data the cut off point of inert conditions was considered to be when the nitrogen flow was turned off.

After the sediments were centrifuged they were removed and placed in pre-weighed plastic containers. The sediments were then dried and ground using a mechanical agate mortar and pestle after which they were stored in sealed plastic containers. The samples collected for water content analysis were weighed before and after drying and then added to the bulk sample before grinding.

2.2.1 *Gamma Spectroscopy*

The sediment samples were analyzed for manmade and natural radionuclides by gamma spectroscopy. This involved the detection of gamma radiation emitted from the radionuclides in the sample using germanium semiconductor detectors. The principles and use of semiconductor detectors are well established and have been described in detail by many authors (e.g. Friedlander et al., 1981; Ehmann and Vance, 1991; Parry, 1991; MacKenzie,1991) so the present treatment is limited to a brief description of the technique and the detectors used. Possible interferences, sources of error and methods of calibration of the detectors (which are of critical

importance in obtaining accurate and precise results) are described in detail.

The principle interaction of gamma radiation with matter is with electrons, but this process is inefficient resulting in the specific ionization of gamma radiation being low and the range being high. There are three main types of interaction: **1)** the *photoelectric effect*, in which the total energy of the gamma radiation is transferred to an electron (the ejected electron is essentially a β^- particle which gives rise to further ionization); **2)** *Compton scattering*, in which there is partial transfer of the gamma photon energy to an electron and **3)** *pair production*, in which gamma rays of energy $\geq$ 1.022 MeV can spontaneously produce a β^+ and a β^- particle. The most important process with respect to gamma spectroscopy is the photoelectric effect, the efficiency of which decreases with increasing gamma photon energy and increases approximately in proportion to Z^5 of the absorber, where Z is the average atomic mass.

The Loch Etive samples were analyzed using an EG&G Ortec Ge(Li) detector and the Clyde Sea Area samples were analyzed using a Canberra (high purity) Intrinsic Ge detector. In both cases the ionization, or electron excitation, produced by the interaction of gamma photons with the detector material gives rise to voltage pulses which are amplified and detected electronically. The relative detection efficiencies, resolution and operational hardware and software for the two systems are given in Table 2.2. Spectra were analysed using either the Minigam2 (Ortec system) or MicroSampo (Canberra system) software package which calculate the energy, shape and area of the peaks and construct a report file listing energies in KeV, counts per second (cps) and % counting error at each of the detected energies.

Detector	EG&G Ortec Ge(Li)	Canberra Intrinsic Ge
relative efficiency @ 1.33 MeV	26.1 %	30 %
resolution @ 1.33 MeV	2.1 KeV	1.9 KeV
hardware	ADCAM 918 Multichannel buffer Locland 286 computer	Model 1510 Signal processor System 100 MCA IBM-AT Computer
software	Minigam 2	MicroSampo

Table 2.2 Description of counting systems

The accuracy and precision in gamma spectroscopy are highly dependent upon a number of factors, the effects of which must be characterised as follows.

1) Background:

The main contributions to background arise from natural cosmic radiation and radiations emitted from primordial and cosmic ray produced radionuclides. Part of the background can also be attributed to manmade radionuclides from fallout which are incorporated into many materials such as steel. In order to minimise background, 4" lead shielding was used with a Cu/Cd lining to minimise interferences arising from fluorescent Pb x-rays emitted from the Pb shielding.

2) Counting geometry:

The detection efficiency, which is defined as,

$$\%\ detection\ efficeny = \left(\frac{observed\ counting\ rate}{source\ disintegration\ rate}\right) * 100$$

varies in proportion to $1/d^2$ where d is the distance of a point source from the detector. It is therefore essential that the counting geometry is accurately defined and highly reproducible.

In the analysis of the cores obtained from Loch Etive, a perspex sample holder was constructed to fit closely over the aluminium can which protects the Ge(Li) crystal, ensuring a high degree of sample position reproducibility. The holder was large enough to allow the complete sample from each depth to be counted, thus maximising the number of counts and minimising the counting error. The samples were weighed into the holder and the depth of the sample accurately measured. The samples for the Clyde sea lochs were pressed into discs using a pressure of 20 tonnes which minimised geometry variations and improved the detection efficiency by decreasing the sample depth.

3) Self adsorption:

Self adsorption of gamma photons within samples (Miller, 1987, Cutshall, 1983, Gäggeler et al, 1976, Bjurman et al, 1987), is related to the Z value and sample density. This effect is of particular importance for low energy gamma photons and, since self adsorption of the radiation by the photoelectric effect varies approximately in proportion to Z^5, changes in Z value and density between samples can introduce an error. This effect may be of importance in coastal sediments where the effect of diagenesis can result in concentrating elements at the surface of the sediment core.

4) Counting Statistics:

Even when using the lowest possible background, tightly defined geometry and accounting for self absorption an intrinsic uncertainty remains based upon the statistical uncertainty associated with the number of observed counts, N. The standard deviation (σ) of which is equal to $\sqrt{N}$. This uncertainty applies to counts in the peak, the background and the compton continuum and ultimately determines the detection limit. Background radiation was therefore kept at a minimum and suitable counting statistics error to the lowest practical value.

2.2.2 *Calibration of the detection efficiency*

The Radionuclides analysed are given in Table 2.3 along with their energies and half live ($t_{1/2}$) values. Some radionuclides have more than one gamma energy, e.g. ^{134}Cs (604 KeV, 765 KeV) and ^{226}Ra (186 KeV, 609 KeV). The energies chosen gave the greatest count rate with minimum interference effects.

Radionuclide	$t_{1/2}$ (y)	Energy (KeV)	Radionuclide	$t_{1/2}$ (y)	Energy (KeV)
^{210}Pb	22.3	46	^{134}Cs	2.1	604
^{241}Am	441	59	^{226}Ra	1600	609
^{238}U	4.49×10^9	63	^{137}Cs	30.2	661
^{228}Th	1.913	238	^{228}Ra	5.75	911

Table 2.3 Radionuclides analysed and their respective halflives and energies

a) Ge(Li) Detector

Calibration of the detection efficiency for the radionuclides of interest was carried out by spiking sediment from 60-80 cm depth in a core from Loch Fyne which was ground to give a homogeneous bulk sediment. Five 55 g aliquots were taken the first of which was left unspiked and counted to give the "blank" count rate. The other aliquots were spiked with radionuclides as defined in Table 2.4

The spiked sediments were prepared by slurrying 55 g aliquots of sediment with approximately 200 ml of distilled water in a 2 l pyrex beaker. The radionuclide spikes were then added and the sample stirred after which a freeze drier was used to remove the water and leave the sediment dry and free flowing. The gamma spectrum of water removed from the freeze drier was recorded to verify that there was no detectable loss of radionuclides. The spiked sediment samples were then carefully transferred to sealed

Aliquot	Radionuclide added	Activity (Bq)
1	no radionuclides added	
2	^{134}Cs ^{137}Cs ^{241}Am	373 354.1 96.0
3	^{226}Ra ^{210}Pb	230.9 66.2
4	^{228}Th ^{228}Ra	48.0 48.0
5	^{238}U ^{234}Th	106.0 106.0

Table 2.4 Spiked sediment activity data

containers.

A series of counts, each of 48 hours duration, of spiked and unspiked sediment samples was then carried out for a range of sample depths and the detection efficiencies for individual radionuclides for each depth calculated from:

$$\%\ counting\ efficency = \left(\frac{Acps_{(x)} - Bcps_{(x)}}{dps}\right) * 100$$

where

$Acps_{(x)}$ = count rate (cps) of the spiked sample at depth x mm
$Bcps_{(x)}$ = count rate (cps) of the unspiked sample at depth x mm
dps = spike activity (disintegrations per second)

The % counting error (% CE) was calculated from

$$\left(\frac{\sqrt{(e\ Acps)^2 + (e\ Bcps)^2}}{Acps}\right) * 100$$

where e Acps = counting error of the spiked sample in cps

e Bcps = counting error of the unspiked sample in cps

Acps = cps of the spiked sample

The % total error on the counting efficiency was calculated as follows

$$\%\ eff.\ err. = \sqrt{(\ \%\ CE\ )^2 + (\ \%\ SE\ )^2 + (\ 1\ )}$$

where % CE = % counting error

% SE = % error on the spike

1% encompasses pipetting and weighing errors

The measured detection efficiencies are given in Tables 2.5, 2.6 and 2.7

Depth (mm)	^{134}Cs	% error	^{137}Cs	% error	^{241}Am	% error
4	2.95	1.3	3.00	2.1	6.55	2.1
6.5	2.88	1.4	2.81	2.1	5.81	2.3
11	2.68	1.6	2.51	2.2	5.04	2.5
24	2.08	1.4	1.91	2.1	3.68	2.3
27	1.89	1.6	1.80	2.1	3.55	2.4

Table 2.5 Measured detection efficiencies for the Ge(Li) detector

depth (mm)	^{210}Pb	% error	^{226}Ra	% error
4	0.57	5.7	0.91	3.5
6	0.45	4.6	0.84	3.4
10	0.37	5.1	0.76	3.4
18	0.31	4.4	0.65	3.4
24	0.25	3.6	0.58	3.4
28	0.23	4.3	0.57	3.4

Table 2.6 Measured detection efficiencies for the Ge(Li) detector

depth	^{228}Th	% error	^{228}Ra	% error	Depth (mm)	^{238}U	% error
4	3.65	3.6	0.64	3.7	4	0.54	4.4
6	3.38	3.6	0.59	3.6	6	0.51	3.4
10	3.05	3.6	0.55	3.8	10	0.43	3.5
19	2.60	3.5	0.45	3.6	18	0.33	3.6
25	2.38	3.5	0.40	3.6	25	0.28	3.6
28	2.30	3.5	0.39	3.6	28	0.26	3.4

Table 2.7 Measured detection efficiencies for the Ge(Li) detector

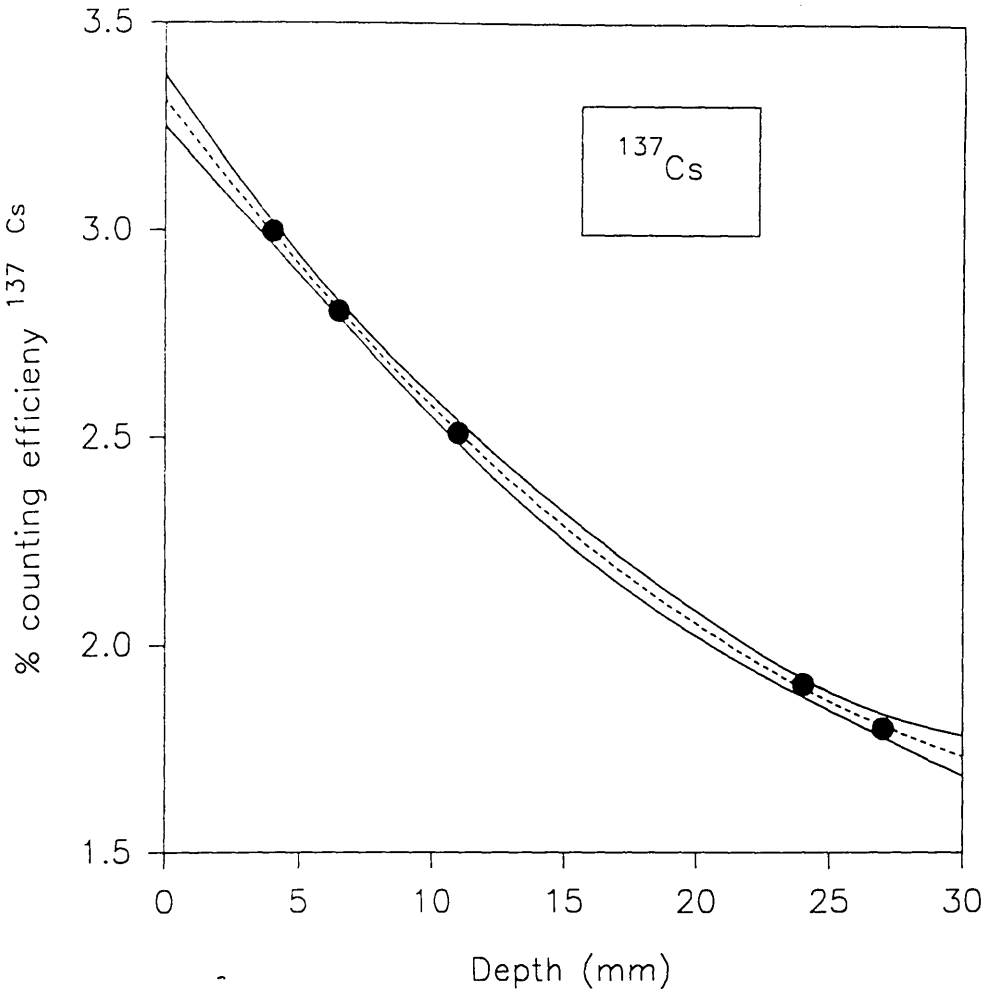

Figure 2.2. ^{137}Cs counting efficiencies

Nuclide	Energy (KeV)	Ortec Ge(Li) detector
^{210}Pb	46	7.5800 E-04
^{241}Am	59	0
^{238}U	63	1.4560 E-03
^{228}Th	238	6.0350 E-03
^{134}Cs	6.4	1.2751 E-04
^{226}Ra	6.9	1.6240 E-03
^{137}Cs	661	1.7670 E-03
^{228}Ra	911	1.2280 E-03

Table 2.8 Typical background count rates(cps) for the Ge(Li) detector

depth (mm)	^{134}Cs	^{137}Cs	^{241}Am	^{210}Pb	^{226}Ra	^{228}Th	^{228}Ra	^{238}U
2 mm (~5 g)	0.6	5.0	6.8	9.2	15.4	6.1	18.6	10.9
4 mm (~10 g)	0.3	2.5	3.7	5.3	8.1	3.2	9.7	5.8
10 mm (~16 g)	0..2	1.8	2.9	4.4	6.0	2.4	7.0	4.6
25 mm (~40 g)	0.1	1.0	1.6	3.0	3.1	1.2	3.8	2.9

Table 2.9 Detection limits Bq kg^{-1} for the Ortec Ge(Li) detector

A 2^{nd} order polynomial regression line was then fitted to the measured detection efficiencies and regression plots covering the depth range 1 -30 mm obtained for each nuclide. A typical regression plot is given in Fig. 2.3 with the 95% confidence limits shown.

Background counts were recorded regularly with the sample holder in place but with no sample and the detection limits for each nuclide were calculated to be 3 σ of the background counts. Table 2.8 gives typical background count rates in cps for the Ge(Li) detector.

The detection limits in Bq kg^{-1} for each radionuclide are given in Table 2.9. for selected sample depths.

2.2.3 *Accuracy of analysis using the Ge(Li) detector*

To evaluate the accuracy of the gamma spectrometry analysis, two IAEA marine sediment standards were analysed. The activities of some of the radionuclides were low and a result could only be obtained by taking relatively large samples. Even so, in some cases the concentrations were too low for analysis. The certified values and minimum weight required to detect the radionuclides on the basis of the calculated limits of detection are given in Table 2.10. The results obtained for IAEA standard SD-A-1 and SD-N-2 are given in Tables 2.11 and 2.12.

Radionuclide (energy)	SD-A-1 certified value and range (Bq\kg)	min. weight required	SD-N-2 certified value and range (Bq/kg)	mini. weight required
^{210}Pb (46 KeV)	**70** (58-88)	*5 g	not applicable	not applicable
^{241}Am (59 KeV)	not applicable	not applicable	**0.0039** (0.0022-0.0048)	ND by γ spec.
^{238}U (63 KeV)	**7.3** (6.3-9.3)	40 g	**4.2** (3.7-4.8)	> 40 g
^{228}Th (238 KeV)	**12.3** (10.2-12.9)	> 5 g	**4.9** (4.5-5.4)	> 10 g
^{134}Cs (604 KeV)	not applicable	not applicable	not applicable	not applicable
^{226}Ra (609 KeV)	**74.9** (55-85)	* 5 g	**4.4** (4.2-4.8)	>16 g
^{137}Cs (661 KeV)	not applicable	not applicable	**0.89** (0.5-1.0)	> 40 g
^{228}Ra (911 KeV)	**12.3** (10.2-12.9)	> 10 g	**4.9** (4.5-5.4)	> 40 g

* NB. in these cases 5 g does not represent the minimum detectable activity but was the minimum mass to ensure source reproducibility in the geometry used.

Table 2.10 Certified values of IAEA standards and minimum weight required for analysis by gamma spectroscopy

Sample	Weight	^{210}Pb	^{238}U	^{228}Th	^{226}Ra	^{228}Ra
SD-A-1	15.9930	54.5 ± 5.8	nd	10.4 ± 2.7	65.2 ± 2.1	10.6 ± 1.5
SD-A-1	37.5608	64.1 ± 7.3	nd	11.0 ± 4.3	63.9 ± 3.2	10.3 ± 1.6

Table 2.11 Results obtained for analysis of standard reference material SD-A-1

Sample	Weight	^{228}Th	^{226}Ra	^{137}Cs	^{228}Ra
SD-N-2	11.8077	5.6 ± 0.5	4.7 ± 1.0	BDL	BDL
SD-N-2	28.4878	5.7 ± 0.5	6.5 ± 1.8	BDL	BDL
SD-N-2	48.9663	4.4 ± 0.2	7.1 ± 0.7	0.63 ± 0.1	5.8 ±1.1

Table 2.12 Results obtained for analysis of standard reference material SD-N-2

From the above data it was concluded that the analytical method provided results within the quoted range of the standard, indicating a satisfactory accuracy for the method. The ^{226}Ra results for SD-N-2 are outwith the certified range, although within the correct order of magnitude. This probably reflects the difficulty in analysing samples of ^{226}Ra concentrations less than 10 Bq kg^{-1}.

2.2.4 *Calibration of the Canberra Intrinsic Ge detector*

The above procedure used in earlier stages of the research, was time consuming, since count rates were low and was subject to potential experimental error since depth measurements were difficult to achieve accurately for small samples and there was the possibility of cross contamination between samples. In the later stages of the study dealing with the Clyde sea lochs, it was therefore decided to press the sediment samples into uniform discs using a 4.8 cm diameter die with a pressure of 20 tons. In order to avoid potential errors in interpolating between calibration points, integral sample weights were used with, four sample sizes being selected,

namely 5, 10, 15 and 20 g, to cover the range of sediment weights within sections from the top to the bottom of a core. The height of the sources was thus minimised and made highly reproducible, with the depths of the pressed discs being constant for each weight at 2 mm, 3.5 mm, 5 mm and 7 mm for 5, 10, 15 and 20 g sources respectively. This procedure improved the detection efficiency relative to loose powdered samples by giving a smaller source and minimised density and geometry variations. Each pressed disc was placed in a sealed 5 cm diameter plastic container and located centrally on the detector.

The detector was calibrated as above using unspiked and spiked Loch Fyne sediment which was pressed into 5, 10, 15 and 20 g discs. The counting efficiencies and errors were calculated as above. Typical background count rates for the intrinsic Ge detector are given in Table 2.13. and the radionuclide detection efficiencies for the pressed discs are given in Tables 2.14., 2.15. and 2.16.

Nuclide	Energy (KeV)	Canberra Intrinsic Ge detector
^{210}Pb	46	4.3727×10^{-3}
^{241}Am	59	0
^{238}U	63	3.2772×10^{-3}
^{228}Th	238	9.7544×10^{-3}
^{134}Cs	6.4	2.6925×10^{-3}
^{226}Ra	6.9	5.3453×10^{-3}
^{137}Cs	661	1.4290×10^{-3}
^{228}Ra	911	4.4175×10^{-3}

Table 2.13 Typical background count rates (cps) for the intrinsic Ge detector

Sample size (g)	^{134}Cs	% error	^{137}Cs	% error	^{241}Am	% error
5	2.88	1.7	3.65	2.2	5.78	2.4
10	2.75	1.3	3.48	2.1	5.07	2.5
15	2.65	1.4	3.30	2.1	4.82	2.8
20	2.52	1.4	3.16	2.2	4.51	2.7

Table 2.14 Detection efficiencies for pressed disc geometries

Sample size (g)	^{210}Pb	% error	^{226}Ra	% error
5	0.28	6.9	1.07	4.7
10	0.26	5.2	1.07	3.9
15	0.20	6.5	1.03	3.7
20	0.20	11.1	1.08	4.3

Table 2.15 Detection efficiencies for pressed disc geometries

Sample size (g)	^{228}Th	% error	^{228}Ra	% error	^{238}U	% error
5	3.8	3.7	0.77	4.0	0.43	3.9
10	3.7	3.7	0.77	3.9	0.40	4.0
15	3.34	3.7	0.72	3.7	0.40	3.9
20	3.45	3.7	0.70	3.6	0.37	4.2

Table 2.16 Detection efficiencies for pressed disc geometries

2.2.5 *Accuracy and precision of analysis using the Intrinsic Ge detector*

The IAEA standard SD-A-1 was counted in the four geometries used to evaluate the accuracy of the analysis Table 2.17. gives the detection limits for each radionuclide for the 4 geometries and Table 2.18. gives the certified values and the results for analysis of pressed disc samples.

Sample	^{210}Pb	^{241}Am	^{238}U	^{226}Ra	^{228}Th	^{134}Cs	^{137}Cs	^{228}Ra
5	51.5	3.5	20.6	8.4	4.0	2.6	1.5	9.7
10	27.7	2.0	10.8	4.2	2.0	1.4	0.8	4.9
15	24.0	1.4	7.4	2.9	1.5	1.0	0.6	3.5
20	18.0	1.0	6.0	2.1	1.1	0.8	0.4	2.7

Table 2.17 Radionuclide detection limits for pressed discs (Bq kg^{-1})

Radionuclide	SD-A-1 certified value (range)	5 g disc Bq/kg	10 g disc Bq/kg	15 g disc Bq/kg	20 g disc Bq/kg
^{210}Pb	70 Bq/kg (58 - 88)	70.8 ± 6.2	63.8 ± 5.4	87.3 ± 6.5	82.9 ± 9.8
^{226}Ra	74.9 Bq/kg (55 - 85)	67.6 ± 3.8	64.3 ± 3.2	66.1 ± 2.7	60.6 ± 2.9
^{228}Th	12.3 Bq/kg (10.2-12.9)	BDL	BDL	12.9 ± 0.6	10.2 ± 0.5
^{228}Ra	12.3 Bq/kg (10.9-15.6)	BDL	BDL	BDL	11.3 ± 0.5
^{238}U	7.3 Bq/kg (6.3-9.3)	BDL	BDL	BDL	BDL

Table 2.18 Results for SD-A-1 measured in pressed disc geometry

From the above results it was concluded that the accuracy of the analytical procedure was satisfactory and would give an answer within error of the true result. The precision of the gamma spectroscopy analysis was evaluated by counting the same sample 10 times and the results for the repeated analysis are given in Table 2.19.

Sample	^{137}Cs	^{241}Am	^{210}Pb	^{228}Th	^{228}Ra
1	570.5 ± 21.6	7.0 ± 0.3	93.0 ± 11.3	34.8 ± 1.5	32.4 ± 1.3
2	565.2 ± 23.1	7.4 ± 0.4	104.1 ±12.4	34.6 ± 1.4	32.0 ±1.4
3	576.0 ± 22.1	6.8 ± 0.4	84.8 ± 10.2	34.1 ± 1.5	33.8 ± 1.6
4	562.8 ± 23.3	6.8 ± 0.3	95.6 ± 11.2	35.6 ± 1.5	34.9 ± 1.5
5	565.8 ± 21.6	6.6 ± 0.5	87.5 ± 10.6	34.5 ± 1.4	38.1 ± 1.5
6	576.1 ± 21.7	7.8 ± 0.8	96.3 ± 12.5	36.4 ± 1.5	37.9 ± 1.7
7	584.9 ± 22.2	7.6 ± 0.8	90.7 ±10.7	37.1 ± 1.5	34.3 ± 1.5
8	580.6 ± 21.9	7.2 ± 0.8	90.4 ±11.8	39.4 ± 1.6	34.1 ± 1.8
9	573.5 ± 22.4	6.7 ± 0.5	102.2 ± 12.8	37.3 ± 1.9	32.6 ± 1.7
10	581.3 ± 21.8	7.0 ± 0.4	105.0 ± 13.1	35.7 ± 1.8	35.6 ± 1.6

Table 2.19 Repeat analysis for gamma counting precision

2.3.1 *Principles of Inductively Coupled Plasma -Mass Spectrometry (ICP-MS)*

Inductively coupled plasma mass spectrometry is a relatively new technique in which a sample is ionised by an argon plasma and the resulting ions are analysed using a quadrupole mass spectrometer. This method of analysis allows concentration and isotopic measurements to be carried out on samples which have low concentrations of analyte elements. There are three commonly employed methods of sample introduction used in ICP-MS, namely liquid nebulisation, electrothermal vapourisation and laser ablation. The first is the most widely used method of sample introduction and entails the sample being in a solution which is introduced into the plasma using a Meinhart nebuliser (Fig. 2.3). Electrothermal vapourisation also requires the sample to be in solution but has the advantage of being able to cope with

higher solid concentrations. Finally, laser ablation is used for analysis of solid samples and in this technique a laser is used to vapourise a small sample of the solid which is then carried by Ar gas into the plasma. The main disadvantage of laser ablation is the difficulty in the calibration of the technique to obtain quantitative results. The history, development and use of ICP-MS to analyse a wide range of sample types have been described in detail by Date and Gray (1989) and Jarvis (1991) and the following section provides a brief description of the operating principles and analytical methods used in ICP-MS using liquid nebulisation.

Samples are generally prepared for analysis in a solution of 2% HNO_3 with a maximum dissolved solids content of 0.2%. The solid concentration of the solution is limited to 0.2 % as higher concentrations block the sampling cones and coat the electrostatic lenses, resulting in a decrease in the sensitivity of the instrument. HNO_3 is normally used as the solvent as the it forms a smaller number of molecular ions than other acid solvents such as HCl and HF. The sample solutions are introduced into the ICP-MS using a peristaltic pump which injects the sample into a stream of Ar to form an aerosol. The Ar gas containing the sample is injected into the core of a high temperature plasma (10000 K), sustained by radiofrequency fields, where energy is transferred from the plasma to the sample, dissociating, atomising and finally ionising it.

The plasma core containing the sample ions is extracted into a reduced pressure region through a Ni sampling cone with a 1 mm orifice. A portion of the extracted plasma passes through a Ni mini skimmer with a 0.75 mm orifice where there is a further drop in pressure.

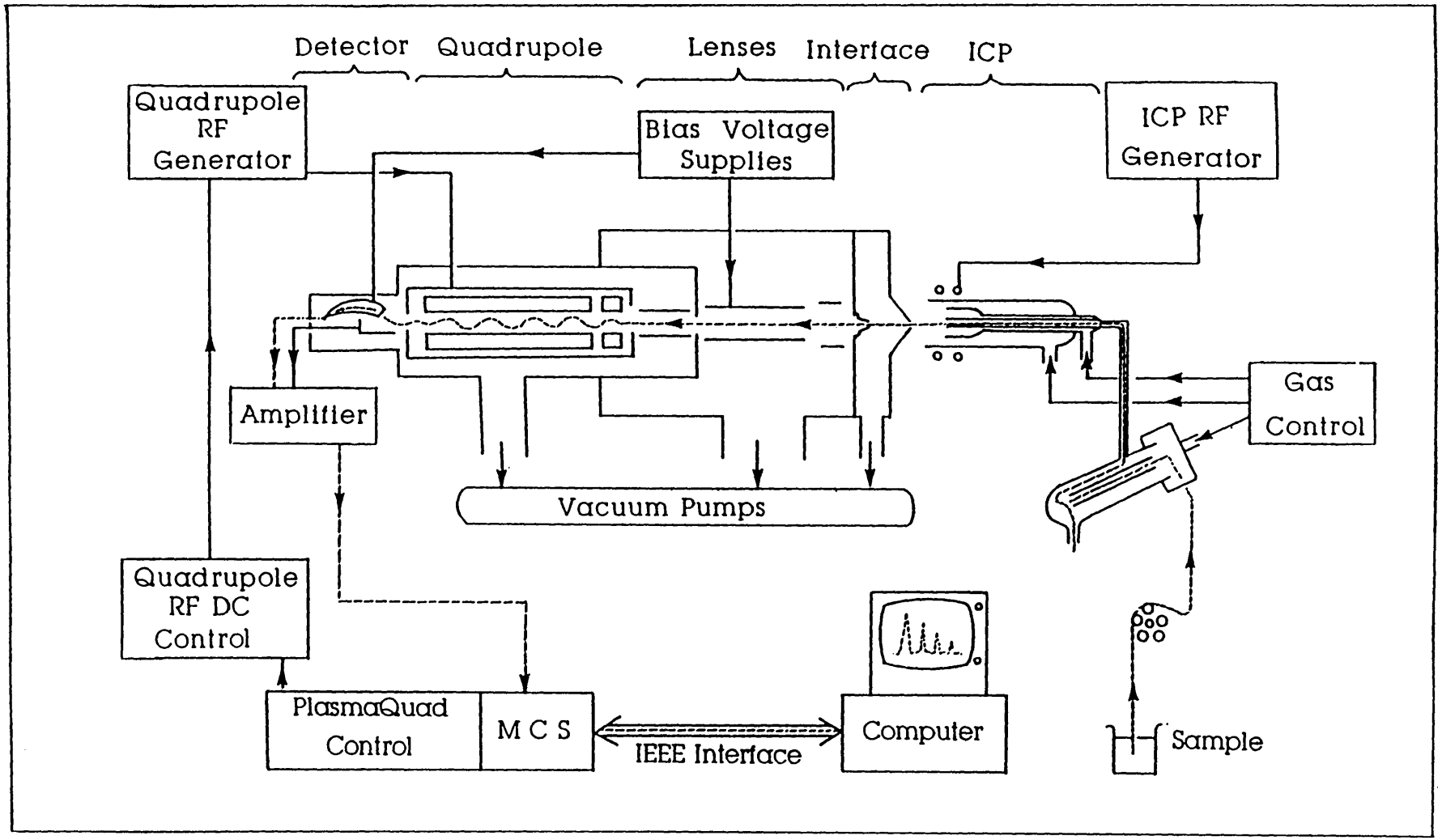

Figure 2.4. Schematic diagram of an ICP-MS Instrument

The extraction process utilises a system of electrostatic lenses which transports the positively charged ions to a quadrapole mass filter. The quadrapole transmits only ions of a particular, selected mass to charge ratio and the transmitted ions are detected by an ion detector, with the number of ions registered being proportional to the concentration of the element in the sample. Each naturally occurring element has a unique and simple pattern of nearly integer mass to charge ratios corresponding to its stable isotopes which allows easy identification of the elements in the sample (VG Elemental, 1988).

Most elements have at least one isotope which is not overlapped by isotopes of any other elements. However, spectral interferences do occur in ICP-MS and result from the formation of doubly charged ions, molecular oxide ions, molecular ions derived from the Ar gas, molecular species derived from the sample solvent and combination ions (Olivares, J.A. and Houk, R.S., 1986; Long, S.E. and Brown, R.M., 1986; Houk, 1986; Longerich et al., 1987; Date et al., 1987, Wilson et al., 1988; Gilson et al., 1988; Jarvis et al., 1992; Evans and Giglio, 1993.). The majority of these interfering species are however present at very low levels and, if the matrix of the sample is known, their effects can be minimised and the sample spectra interpreted accordingly.

The three major advantages of ICP-MS are the sensitivity of the technique, the rapid through put of samples, and the diverse range of sample types that can be analysed (Dean, J.R. and Ebdon, I., 1987; Lyon, et al., 1988, Jarvis, K.E., 1988, Riddle et al., 1988, Delves, 1988, McCurdy, 1990, Toole et al., 1990, Moore et al., 1990).

The technique is very sensitive with detection limits in the range of 0.02-0.7 ppb (Selby et al., 1987) and can be setup to perform semiquantitative (typically ± 30% accuracy), quantitative and isotopic analysis. A

semiquantitative analysis is one in which an internal standard, usually In, of a known concentration is added and the response of the internal standard is used to calculate the concentrations of other elements in the sample. This is achieved by using a mass/ response calibration curve that covers the entire mass range. The response curve of the instrument can change from day to day and to obtain reasonable semiquantitative results a new response curve must be calculated daily. A quantitative analysis uses standards of a known concentration of the analyte elements to construct a calibration curve which is then used to calculate the sample concentrations. Finally, an isotope ratio analysis can be performed by either scanning the mass range of interest or by using the peak jumping mode of analysis. The scanning mode was repeated continuous scans over the entire mass range of the isotopes of interest whereas in peak jumping mode the quadrapole successively detects selected peaks and 'jumps' from one isotope to the next. The scanning mode gives more precise analyses but peak jumping is faster and requires smaller samples.

Analysis time using ICP-MS is short, with a typical semiquantitative analysis taking approximately 6 minutes to perform, including 2 minutes for sample uptake, 1 minute to acquire the sample spectrum and 3 minute wash time between samples. The time to perform each quantitative and isotopic analysis depends on the number of scans carried out for each sample. A quantitative measurement has usually 3 scans per sample compared to 5 scans for an isotope ratio measurement, giving sample processing times of 10 and 15 minutes respectively. The amount of sample solution needed to carry out an analysis depends on the rate of delivery of the peristaltic pump and the number of scans performed on each sample. Typically, the sample volumes required for semiquantitative, quantitative or isotopic analysis are 4, 6 and 10 ml respectively. Isotopic ratios can be determined on samples of volume smaller than 10 ml by using the peak jumping mode of the VG software but as discussed above this method is not as precise as peak

scanning and tends to give larger errors on the isotope ratios obtained.

2.3.2 *ICP-MS Analysis Performed*

The analyses performed for this research by ICP-MS included determination of Pb isotope ratios of the seven sediment cores collected, multielement analysis of the pore waters collected from the sea lochs within the Clyde Sea Area. The ICP-MS instrument used in this research was a VG Elemental PQ1 Plasmaquad coupled to a Gilson 222 automatic sampler (Fig 2.3). The instrument was controlled, the sample scans performed and data stored and analysed using the VG Elemental Plasmaquad software version 3.1b. and an IBM-AT computer.

2.3.3 *Stable Lead Isotope Ratio Measurements by ICP-MS*

Lead has four naturally occurring isotopes three of which are radiogenic, ^{206}Pb (24.1%), ^{207}Pb (22.1%) and ^{208}Pb (52.3%) and one which is non radiogenic, ^{204}Pb (1.4%). The use of Pb isotopes in geological dating is well established (Faure, 1986) but ICP-MS does not have sufficient precision to be used in the analysis of samples for dating. However, more recently the potential of ICP-MS analysis in environmental studies has been recognised due to its ability to determine characteristic stable isotope ratios of different sources of pollutant Pb (Petit et al., 1984; Flegal, A.R., 1987; Delves, 1988; Delves, T.H. and Campbell, M.J.; 1988; Flegal, et al., 1989; Viczian et al., 1990; Sugden et al., 1991; Sugden, C.L., 1993).

There are three important experimental parameters to consider when making Pb isotope measurements using ICP-MS, namely; the mass bias of the analysis, the dead time and the resolution of the instrument.

The mass bias is the difference that may occur between the measured isotopic ratio and the true value as a function of the difference in mass between the two isotopes and can be accounted for by using a standard lead solution of known isotopic composition, in this case NBS 981. It is essential that the standard solution is measured frequently within the sample analysis protocol to ensure that there is no mass bias drift within the run of analyses. At high count rates the electron multiplier and pulse counting systems used in ICP-MS instruments record fewer events than actually occur and the time interval during which the detection system is unable to resolve successive pulses is termed the *dead time* of the instrument. The result of dead time is that the signal response becomes non-linear above a certain count rate, typically 1×10^6 cps (Jarvis et al., 1992). Dead time correction on early ICP-MS systems was approximately 110 ns in comparison to 20 ns for modern instruments. To obtain accurate isotope measurements when using the scanning mode of operation the resolution must be such that there is no overlap of adjacent peaks. The higher the resolution the lower the sensitivity i.e. less cps.

The precision of a measurement at low concentrations of Pb is limited by counting statistics and in solutions containing low concentrations, the Pb in the sample must be pre-concentrated, normally by ion- exchange methods. In this study the lowest Pb concentration was approximately 20 ppb in solution for samples at depth in the sediment cores and a maximum of approximately 500 ppb in solution for surface samples. The precision of the $^{206}Pb/^{207}Pb$ ratio for the samples analysed was normally less than 0.5% RSD.

2.3.4 *Sample preparation and analysis conditions for Isotope Ratio measurements*

The samples were prepared by totally dissolving approximately 0.1 g of

sediment using 4 ml of 16M HNO_3, 2 ml of 40% HF acid and 1 ml of 12M HCl acid in a Floyd microwave digestion system with pressure control. The system consists of 12 teflon vessels in a carousel, one of which is monitored for pressure. With every 10 samples a blank and an in house standard sediment HL/LG were included to check for contamination problems and to evaluate the precision of the sample preparation procedure. All acids used were Aristar grade and the samples were microwaved for 30 minutes at 30% of full power and 25 minutes at 50 % of full power. The dissolved samples were then transferred to teflon beakers and taken to dryness. The samples were re-dissolved in 0.5 ml 12M HCl and 2 ml 40% HNO_3 and finally diluted to 100 ml in a volumetric flask using high purity water. The samples were stored in sealed polypropylene bottles.

The operational parameters of the instrument are given in Table 2.20.
The samples were analysed in batches of 22, comprising 20 sediment samples and 2 HL/LG samples, with the aid of a Gilson 222 autosampler. Each sample run consisted of a 2% HNO_3 blank , a standard of known Pb isotope ratios, a wash sample (2% HNO_3) and then a sample blank. The samples were then analysed with a *check* being included after every 3 samples. The check was the same solution as the standard which was the NBS 981 isotopic lead standard at approximately 100 ppb Pb concentration. After each sample run the sample spectra were analysed and the data assessed for drift using the check samples. If the check was not within error of the expected result then the check was reassigned as a standard and later checks used to assess the rest of the procedure. In these cases if the latter checks did not conform to the certified values, the samples were reanalysed.

2.3.5 *Accuracy and precision of Pb isotope ratio analysis*

The certified values for NBS 981 for $^{206/207}Pb$, $^{208/207}Pb$ and $^{208/206}Pb$, isotopic lead standard are 1.0933 ± 0.00039, 2.3704 ± 0.0009 and 2.1681 ± 0.0008

PlasmaQuad operating parameters		
Plasma ——		
R.f. power		
	Forward	1.35 kW
	Reflected	< 10 W
Gas controls		
	Auxiliary	0.55 l min^{-1}
	Coolant	14 l min^{-1}
	Nebulizer	0.73 l min^{-1}
Nebulizer		
	Meinhart : concentric type	
Spray Chamber	Scott-type double bypass, water cooled (ambient)	
Ion Sampling ——		
Sampling cone	Nickel with 1.0 mm orifice	
Skimmer cone	Nickel with 0.75 mm orifice	
Sampling distance	10 mm from load coil	
Optimization ——		
	The lenses were adjusted to maximize the ^{115}In signal	
Vacuum ——		
Expansion stage	2.4 mbar	
Intermediate	$< 1 \times 10^{-4}$ mbar	
Analyser	4.6×10^{-6} mbar	
Data acquisition ——		
Peak scanning		
Sweeps	1600	
Dwell time	80 μs	
Channels	512	
Dead Time	20 ns	

Table 2.20 Operational parameters of the PlasmaQuad PQ1

respectively.

Tables 2.21. and 2.22. give the results for repeated analysis of NBS 981 and the in house sediment standard HL/LG.

There are three different methods of considering the precision of the Pb isotope measurements, namely: the error on a single analysis which depends on counting statistics, the within run variation; and the between run variation. All of these factors must be considered as the isotope ratio analysis of an entire sediment core which has typically 40 samples, took several runs to complete.

The results in table 2.21 give mean values of 1.093, 2.374, and 2.174 for the $^{206/207}$Pb, $^{208/207}$Pb and $^{206/208}$ Pb respectively, with the precision being 0.19%, 0.70% and 0.69%. These results compare favourably with the certified values. The results in table 2.22. give mean values of 1.1522, 2.4404 and 2.1184 for the $^{206/207}$Pb, $^{208/207}$Pb and $^{206/208}$ Pb respectively for the in house reference sediment, with the precision being, 0.18%, 0.84% and 0.90%. This indicated that the sediment HL/LG was homogeneous and was satisfactory to use as an in house standard and provided confidence that the sampling procedure employed provided representative samples of the sediment. The within run precision are given for runs 2,5,6 and 7 in Table 2.23. These runs were chosen as they had between 7 and 10 checks in each run.

DATE	206/207	± ERROR	208/207	± ERROR	208/206	± ERROR
12/8/92	1.09635	0.00292	2.36858	0.00229	2.16042	0.00579
12/8/92	1.09037	0.00254	2.37657	0.00572	2.17959	0.00909
12/8/92	1.09325	0.00563	2.36646	0.01329	2.16459	0.00946
12/8/92	1.09553	0.01234	2.41699	0.01795	2.20861	0.01115
12/8/92	1.09812	0.0099	2.39603	0.01707	2.8442	0.03322
12/8/92	1.09002	0.0023	2.41822	0.00462	2.22082	0.00577
12/8/92	1.09195	0.00158	2.40496	0.00402	2.20473	0.00569
12/8/92	1.09308	0.00211	2.40804	0.00427	2.20529	0.00376
12/8/92	1.08916	0.00367	2.41427	0.00832	2.21894	0.00661
12/8/92	1.0974	0.00278	2.41034	0.00671	2.19869	0.00513
23/9/92	1.09514	0.00227	2.37042	0.00348	2.16449	0.00647
23/9/92	1.09191	0.00227	2.36734	0.0075	2.16805	0.00279
23/9/92	1.09437	0.00112	2.36937	0.0025	2.16503	0.00179
23/9/92	1.09254	0.00283	2.37364	0.0055	2.17258	0.00228
1/10/92	1.09105	0.00238	2.37884	0.00525	2.1803	0.00392
1/10/92	1.09023	0.0028	2.38281	0.00327	2.18558	0.0035
1/10/92	1.0928	0.00244	2.38345	0.003	2.18104	0.00417
1/10/92	1.09233	0.00323	2.38506	0.00387	2.18347	0.00714
1/10/92	1.09234	0.00243	2.38094	0.0055	2.17966	0.00305
1/10/92	1.09559	0.00178	2.38644	0.00503	2.17821	0.00556
12/10/92	1.09364	0.00128	2.37126	0.00302	2.16826	0.00254
12/10/92	1.09317	0.0017	2.37342	0.00249	2.17118	0.00299
12/10/92	1.09386	0.00167	2.37062	0.00326	2.16719	0.0033
12/10/92	1.0952	0.00107	2.37331	0.00246	2.16699	0.00251
12/10/92	1.09473	0.00111	2.37032	0.00324	2.1652	0.00242
12/10/92	1.09414	0.00153	2.36734	0.00191	2.16364	0.00294

Table 2.21 Repeated analyses of NBS 981

DATE	206/207	± ERROR	206/208	± ERROR	207/208	± ERROR
12/10/92	1.09411	0.00162	2.36682	0.00404	2.16323	0.00262
15/10/92	1.09423	0.0014	2.3708	0.00363	2.16668	0.00409
15/10/92	1.09354	0.00359	2.036997	0.00696	2.16728	0.00186
15/10/92	1.09365	0.00164	2.37347	0.00385	2.17026	0.00172
15/10/92	1.0921	0.00255	2.37278	0.00456	2.17271	0.00398
15/10/92	1.09227	0.00152	2.372	0.00158	2.17165	0.00253
15/10/92	1.09356	0.00248	2.37294	0.00694	2.16997	0.00525
4/11/92	1.09331	0.00179	2.36309	0.00351	2.16139	0.0044
4/11/92	1.09311	0.00132	2.37283	0.00385	2.1707	0.00331
4/11/92	1.09072	0.00301	2.36706	0.00225	2.17017	0.00565
4/11/92	1.0918	0.00234	2.36288	0.00318	2.1642	0.00398
4/11/92	1.09164	0.00243	2.35929	0.00348	2.16122	0.00341
4/11/92	1.09129	0.00128	2.363	0.00522	2.16532	0.00375
4/11/92	1.09142	0.00129	2.36267	0.00355	2.16475	0.00255
4/11/92	1.09403	0.00073	2.36222	0.00568	2.15918	0.00542
4/11/92	1.0894	0.00163	2.33333	0.00321	2.14185	0.00288
4/11/92	1.09105	0.0019	2.37397	0.00202	2.17584	0.00314
4/11/92	1.09041	0.001	2.35041	0.00458	2.15551	0.00543
4/11/92	1.09042	0.00126	2.34613	0.00127	2.15158	0.00326
6/11/92	1.09141	0.00262	2.36378	0.00762	2.16578	0.00454
6/11/92	1.0931	0.00116	2.36457	0.00504	2.16317	0.00286
16/11/92	1.0919	0.00290	2.3675	0.0067	2.16822	0.00250
16/11/92	1.09246	0.00373	2.36446	0.00556	2.16436	0.00883
16/11/92	1.09196	0.00282	2.36457	0.00481	2.16543	0.00290
16/11/92	1.09036	0.00105	2.36227	0.00211	2.1665	0.00285

Table 2.21 Repeated analyses of NBS 981(continued)

Sample	206/207	± ERROR	208/207	± ERROR	208/206	± ERROR
1	**1.1528**	0.0046	**2.43765**	0.00808	**2.11454**	0.00285
2	**1.15102**	0.00442	**2.43332**	0.00811	**2.11405**	0.0056
3	**1.15012**	0.00481	**2.46502**	0.03319	**2.14547**	0.02513
4	**1.15332**	0.00174	**2.48065**	0.00441	**2.15311**	0.00416
5	**1.1492**	0.00426	**2.48987**	0.00717	**2.16886**	0.00649
6	**1.15718**	0.00153	**2.45403**	0.00429	**2.12073**	0.00395
7	**1.1548**	0.00136	**2.43969**	0.00409	**2.11265**	0.00145
8	**1.15146**	0.00166	**2.43449**	0.00564	**2.11425**	0.00733
9	**1.15432**	0.0014	**2.43481**	0.0049	**2.10928**	0.00322
10	**1.15239**	0.0015	**2.45244**	0.00411	**2.12812**	0.00212
11	**1.15042**	0.00217	**2.44412**	0.00601	**2.12453**	0.00311
12	**1.15273**	0.00132	**2.43384**	0.00185	**2.11136**	0.0027
13	**1.15297**	0.00089	**2.42916**	0.00218	**2.10685**	0.00048
14	**1.1543**	0.00244	**2.43809**	0.00479	**2.11223**	0.00477
15	**1.1508**	0.00087	**2.42947**	0.0057	**2.11109**	0.00401
16	**1.15094**	0.00084	**2.42605**	0.00377	**2.10788**	0.00382
17	**1.15035**	0.00177	**2.40622**	0.00505	**2.09171**	0.0013
18	**1.15117**	0.00208	**2.39865**	0.00194	**2.08365**	0.00397

Table 2.22 Repeated analyses of *in-house* sediment standard HL/LG

RUN	% precision $^{206/207}$Pb	% precision $^{208/207}$ Pb	% precision $^{208/206}$Pb
2	0.33	0.32	0.57
5	0.06	0.11	0.13
6	0.08	0.06	0.11
7	0.12	0.49	0.42

Table 2.23 Within run precision for Pb isotope ratio results

The within run precision for the isotope ratios was generally less than 0.5%. The error on the Pb isotope results was calculated as ;

$$\%e = \sqrt{(a)^2 + (b)^2}$$

where %e =% error

a is the % RAD on the measurement and

b is the % within run precision

Finally, reference material SRM 1646 was analysed ten times to evaluate the accuracy and precision of the analysis. Table 2.24 gives the isotope ratios obtained. The overall mean isotope ratios are 1.196, 2.467 and 2.069 for $^{206/207}$Pb, $^{208/207}$Pb and $^{208/206}$Pb respectively and the standard deviations are 0.82%, 0.38% and 0.50%. Reported values for SRM 1646 are 1.2006 ± 0.0148 for $^{206/207}$Pb and 2.078 ± 0.0158 for $^{208/206}$Pb (Viczián et al., 1990). From the above data it was concluded that the analytical method provided results within the quoted range of the standard, indicating a satisfactory accuracy for the method.

SAMPLE	206/207	error	208/207	error	208/206	error
SRM 1646 1	1.2070	0.0042	2.4736	0.0107	2.0549	0.0110
SRM 1646 2	1.2008	0.0039	2.4765	0.0085	2.0679	0.0048
SRM 1646 3	1.1966	0.0030	2.4713	0.0086	2.0709	0.0086
SRM 1646 4	1.1965	0.0052	2.4697	0.0198	2.0697	0.0108
SRM 1646 5	1.1936	0.0083	2.4622	0.0168	2.0684	0.0022
SRM 1646 6	1.21023	0.0094	2.4798	0.0152	2.0546	0.0094
SRM 1646 7	1.1780	0.0053	2.4525	0.0124	2.0876	0.0037
SRM 1646 8	1.1973	0.0052	2.4715	0.0096	2.0699	0.0078
SRM 1646 9	1.1821	0.0053	2.4533	0.0138	2.0810	0.0097
SRM 1646 10	1.1970	0.0063	2.4604	0.0208	2.0610	0.0091

Table 2.24 Repeated analyses of SRM 1645 for Pb isotope ratios

2.3.6 *Analysis of pore waters by ICP-MS*

As mentioned above the maximum solid or salt content of solutions analysed by ICP-MS should not exceed 0.2 %. The pore waters had salinites varying from 16 ‰ to 30 ‰ and were consequently diluted by a factor of twenty. The pore waters were analysed for the following elements, Li, Cu, Ba, B, Rb, Sr, Pb, Mn, Mo, U, Fe, Zn, and Sn but it was found that Pb was below detection limits in the pore water. The Zn and Sn results also indicated contamination which was thought to have come from the neoprene plug of the syringes. As there are no certified pore water solutions it was difficult to check the accuracy of the analysis. To check for drift a mixed standard solution was analysed after every five sample solutions and samples were repeated throughout the pore water analyses. Tables 2.26., 2.27., 2.28. and 2.29. give the results for 'check' runs within the time span of analysis of cores FS, FD, LL and GD respectively, while table 2.30. gives the results for repeated analyses of a sample. The tables also give the standard deviations for each core.

Date	Li (ppb)	Ba (ppb)	B (ppb)	Rb (ppb)	Sr (ppb)	Mn (ppb)	Mo (ppb)	U (ppb)
5/2/90	26.7	12.5	129.6	13.3	1287.6	275.2	5.1	1.1
5/2/90	27.4	12.5	127.4	13.6	1329.4	260.8	5.2	1.0
5/2/90	26.4	12.4	129.8	13.0	1290.5	254.4	5.1	1.1
8/2/90	28.5	12.4	120.7	14.5	1356.6	291.9	5.5	1.0
8/2/90	28.2	12.3	131.1	13.4	1279.6	272.1	5.3	0.9
8/2/90	28.9	12.6	138.9	13.2	1302.1	257.2	5.2	1.5
Std. Dev.	1.0	0.1	5.9	0.5	29.6	14.1	0.2	0.1
mean	27.7	12.5	129.6	13.5	1307.6	268.6	5.2	1.1
% std. Dev	**3.7**	**0.8**	**4.5**	**3.9**	**2.3**	**5.2**	**2.9**	**7.6**

Table 2.26 Repeated analyses of check solution for core FS

Date	Li (ppb)	Ba (ppb)	B (ppb)	Rb (ppb)	Sr (ppb)	Mn (ppb)	Mo (ppb)	U (ppb)
3/11/89	29.7	12.2	168.9	13.5	1311.2	279.1	5.3	1.1
4/11/89	31.9	12.3	180.8	14.1	1314.7	297.6	5.4	1.1
4/11/89	30.0	12.5	151.9	13.3	1371.3	276.0	5.4	1.1
4/11/89	28.1	12.7	155.6	13.3	1296.3	272.9	5.1	1.3
5/11/89	29.3	12.3	162.5	13.4	1270.0	273.1	6.5	1.1
16/11/89	25.6	12.4	178.9	15.0	1405.0	314.2	6.0	1.2
std. dev	2.1	0.2	11.9	0.7	50.3	16.8	0.5	1.1
mean	29.7	12.2	168.9	13.5	1311.2	279.1	5.3	0.1
% std. dev	**7.1**	**1.5**	**7.1**	**5.0**	**3.8**	**6.0**	**9.6**	**7.8**

Table 2.27 Repeated analyses of check solution for core FD

Date	Li (ppb)	Ba (ppb)	B (ppb)	Rb (ppb)	Sr (ppb)	Mn (ppb)	Mo (ppb)	U (ppb)
17/11/89	31.9	12.9	158.1	13.5	1285.3	279.9	5.4	1.1
17/11/89	29.5	12.5	154.5	13.8	1376.5	279.7	5.4	1.2
23/11/89	28.2	12.5	145.7	11.9	1347.8	282.8	4.7	1.1
23/11/89	28.6	12.4	154.1	14.0	1329.2	286.1	5.4	1.0
24/11/89	28.2	12.0	142.0	12.1	1300.4	280.2	5.3	1.0
std. dev.	1.6	0.3	6.7	1.0	36.5	2.7	0.3	0.1
mean	29.3	12.4	150.9	13.0	1327.8	281.7	5.2	1.1
%std. dev.	**5.3**	**2.6**	**4.5**	**7.5**	**2.7**	**1.0**	**5.7**	**7.8**

Table 2.28 Repeated analyses of check solution for core LL

Date	Li (ppb)	Ba (ppb)	B (ppb)	Rb (ppb)	Sr (ppb)	Mn (ppb)	Mo (ppb)	U (ppb)
8/1/90	27.6	12.5	132.8	12.8	1322.0	261.6	4.7	1.2
8/1/90	30.4	12.4	151.0	14.7	1242.6	261.3	5.3	1.0
11/1/89	27.1	12.4	123.6	13.0	1299.3	256.2	5.3	1.1
11/1/89	26.9	12.6	129.9	12.5	1268.8	248.3	5.2	1.2
30/1/90	24.4	12.2	126.9	13.1	1297.7	268.2	5.5	0.9
30/1/90	26.5	11.9	126.1	13.1	1300.3	259.0	5.4	1.0
30/1/90	23.8	12.3	126.8	13.1	1298.1	260.1	5.2	1.2
std. dev	2.1	0.2	9.7	0.7	27.9	6.3	0.3	0.1
mean	26.5	12.3	129.5	13.1	1284.8	258.2	5.2	1.1
% std. dev.	**7.8**	**1.8**	**7.5**	**5.0**	**2.2**	**2.4**	**5.0**	**11.3**

Table 2.29 Repeated analyses of check solution for core GD

Date	Li (ppb)	Ba (ppb)	B (ppb)	Rb (ppb)	Sr (ppb)	Mn (ppb)	Mo (ppb)	U (ppb)
23/11/89	168.80	33.40	4705.50	171.20	7285.30	11583.80	11.30	0.60
8/1/90	178.40	30.50	5028.70	145.40	8202.30	13690.40	19.00	0.40
5/2/90	228.6	32.1	5416.8	130.4	8346.7	14858.5	15.4	0.4
5/2/90	204.7	32	5219.3	139.9	8184.3	13880.2	14.5	0.3
5/2/90	186.6	32	5166.8	125.3	7524.2	12694.7	15.1	0.5
std. dev.	23.7	1.0	264.3	17.9	471.8	1247.1	2.7	0.
mean	193.4	32.0	5107.4	142.4	7908.6	13341.5	15.1	0.4
% std. dev.	**12.2**	**3.2**	**5.2**	**12.6**	**6.0**	**9.3**	**18.2**	**25.9**

Table 2.30 Repeated analyses of sample LL 14-16

2.4.1 *Bulk sediment analysis by X-Ray Fluorescence*

XRF analysis was performed to provide geochemical data to assist in interpretation of radionuclide and Pb isotope data.

XRF analysis of bulk sediment sample analyses was carried out using the Department of Earth Sciences and Geophysics, Edinburgh XRF service facility University (by Dr. G. Fitton and D. James).

The ground samples were pressed into discs with boric acid backing for trace element determination (Shimmield, 1985) and fused into glass discs for major element analysis (Norrish and Hutton, 1969). The analyses were performed by a Philips PW1250 sequential automatic spectrometer using international rock standards for calibration. Typical precision for major and minor elements using the above instrument are quoted in Shimmield et al. (1990) and are reproduced in table 2.31.

function	Si (wt. %)	Al (wt. %)	Ca (wt. %)	Ti (wt. %)	Ba (ppm)
mean (n=8)	26.24	7.99	1.14	0.45	2736
1σ	0.12	0.03	0.01	0.004	36.83
% precision (% rsd,1σ)	0.5	0.4	1.0	1.0	1.3
accuracy	± 0.097	± 0.075	± 0.048	± 0.009	± 42.5

Table 2.31 XRF typical precision and accuracy (Shimmield et al., 1990)

CHAPTER 3

RESULTS

3.1 *Results*

This chapter contains the results for cores LE 1, LE 2 and LE 3 from Loch Etive, (Tables 3.1. to 3.19) and cores LL1, GD2, FS and FD (Tables 3.20 to 3.47), from the Clyde Sea Area.

station	depth fathoms	^{210}Pb	+/-	^{226}Ra	+/-	excess ^{210}Pb	+/-	^{228}Th	+/-	^{232}Th
1	42	114	18	11.5	2.3	104	18	32	2	38
2	12	168	21	2.3	2.3	173	22	15	2	33
3	12	157	21	17.7	2.3	143	22	16	3	23
4	na	na	na	na	na	na	na	na	na	na
5	26	368	25	3.8	3.1	378	26	35	2	46
6	30	232	25	8.5	3.0	230	26	29	2	44
7	30	286	25	7.7	2.3	286	26	23	2	39
8	27	275	21	9.2	2.3	273	22	26	2	na
9	na	na	na	na	na	na	na	na	na	na
10	58	107	16	10.0	2.3	100	16	22	1	30
11	68	211	18	nd	nd	211	18	60	3	38
12	68	321	18	7.6	2.5	315	18	104	3	48
13	76	300	18	23.8	3.1	283	18	111	3	39
14	54	407	21	29.2	3.0	382	21	151	3	35
15	53	311	21	20.8	2.3	294	21	134	3	44
16	57	289	21	14.6	2.3	274	21	99	2	45
17	42	136	18	13.1	2.3	126	18	44	3	38
18	24	275	18	23.8	3.1	257	18	58	2	46
19	23	279	18	20.0	3.1	259	18	59	2	56
20	18	229	18	6.2	2.3	225	18	47	2	56
21	16	125	18	19.2	3.1	108	18	36	2	47
22	23	250	18	9.2	2.3	246	18	49	2	64
23	20	343	21	4.6	2.3	345	21	52	2	47
24	15	279	18	5.4	2.3	278	18	39	2	50
25	12	250	21	19.2	2.3	235	21	36	2	42

Table 3.1 Loch Etive surface transect natural radionuclide concentrations (Bq kg^{-1})

station	depth fathoms	% organics	Cs-137	+/-	Cs-134	+/-	Am-241	+/-
1	42	3.4	275	3	9.1	1.1	4.5	1.3
2	12	3.8	173	2	5.3	1.2	2.3	1.2
3	12	2.9	125	2	5.5	1.2	2.0	1.2
4	na	na	na	na	na	na	na	na
5	26	6.2	353	3	12.7	1.5	7.0	1.5
6	30	4.9	272	3	7.7	1.0	4.1	1.4
7	30	5.4	292	3	8.5	1.5	3.8	1.4
8	27	5.0	300	3	12.6	1.3	8.0	1.4
9	na	na	na	na	na	na	na	na
10	58	1.8	120	2	3.5	1.0	3.4	1.2
11	68	5.3	201	3	nd	1.0	4.2	0.7
12	68	6.0	236	3	6.9	1.0	4.8	1.3
13	76	6.4	195	2	7.9	1.2	3.9	1.4
14	54	6.6	220	3	5.6	1.0	4.9	1.3
15	53	6.3	223	3	5.2	1.1	2.8	1.5
16	57	6.3	238	2	4.7	0.9	3.1	1.2
17	42	3.1	160	2	8.2	1.1	3.0	1.2
18	24	6.7	208	2	8.4	1.1	2.8	1.3
19	23	7.2	195	3	4.0	1.0	3.2	1.2
20	18	6.2	172	2	4.5	0.9	2.3	1.2
21	16	3.1	88	2	2.6	1.0	nd	nd
22	23	6.8	173	2	3.9	0.8	nd	nd
23	20	7.3	212	3	4.3	1.2	1.9	1.1
24	15	7.2	195	2	2.8	0.8	3.2	1.0
25	12	5.6	196	3	4.3	1.0	2.9	1.2

Table 3.2 Loch Etive surface transect manmade radionuclide conmcentrations (Bq kg^{-1}) and % organic content

LE1			LE2			LE3		
DEPTH (m)	TEMP (°C)	SALINITY (‰)	DEPTH (m)	TEMP (°C)	SALINITY (‰)	DEPTH (m)	TEMP (°C)	SALINITY (‰)
0	13.8	24.1	0	12.4	15.9	0	11.8	22.7
1	13.2	24.7	1	12.1	22.4	1	11.8	23.0
2	13	26.2	2	11.9	22.9	2	12.2	24.5
3	13	27.5	3	12.6	26.1	3	12.4	26.4
4	12.8	28.1	4	12.5	26.9	4	12.4	26.7
5	12.6	28.1	5	12.4	27.3	5	12.3	27.2
6	12.6	28.2	6	12.3	27.5	6	12.3	27.4
7	12.6	28.2	7	12.2	27.6	7	12	27.5
8	12.6	28.5	8	12.2	27.9	8	12.2	27.6
9	12.5	28.8	9	12	27.9	9	12.2	27.6
10	12.5	29.0	10	12	27.9	10	12.2	27.7
15	12.5	29.5	15	12	28.1	15	12.2	28.1
20	12.5	29.6	20	12	28.1	20	12.2	28.4
25	12.5	29.6	25	12.2	28.1	25	12.2	28.5
30	12.4	29.8	30	12.1	28.5	30	12.2	28.6
25	12.4	29.8	35	12.1	28.6	35	11.8	28.8
40	12.4	29.9	40	12.1	28.8	40	11	29.0
45	12.4	29.9	45	12	29.0	45	10	29.0
50	12.4	30.0	50	11.5	29.1	50	9.6	29.2
54	12.4	30.0	55	10.2	29.2	55	9.4	29.2
			60	9.8	29.5	60	9.2	29.5
			65	9.3	29.5	65	9.2	29.5
			70	9.1	29.7	70	9.2	29.6

Table 3.3 Loch Etive, Temperature and Salinity readings at stations 1, 2 and 3

LE 1 DEPTH (cm)	g/cm2	LOI (%)	LE 2 DEPTH (cm)	g/cm2	LOI (%)	LE 3 DEPTH	g/cm2	LOI (%)
0.5	0.06	18.98	0.5	0.18	12.40	0.5	0.05	18.79
1.5	0.21	19.96	1.5	0.45	12.61	1.5	0.14	19.60
2.5	0.39	18.89	2.5	0.72	12.17	2.5	0.25	17.70
3.5	0.60	18.46	3.5	1.06	12.29	3.5	0.37	17.54
4.5	0.82	19.45	4.5	1.41	12.90	4.5	0.50	17.54
5.5	1.04	17.98	5.5	1.75	12.77	5.5	0.67	16.76
6.5	1.26	17.05	6.5	2.08	12.94	6.5	0.80	17.19
7.5	1.50	17.12	7.5	2.42	13.32	7.5	0.98	16.98
8.5	1.75	16.10	8.5	2.76	13.13	8.5	1.15	16.47
10.5	2.19	15.35	9.5	3.13	13.74	9.5	1.32	16.89
13.0	2.90	16.33	11.0	3.68	14.64	11.0	1.69	17.54
15.0	3.37	16.26	13.0	4.20	13.61	13.0	2.07	15.61
17.0	3.83	17.16	15.0	4.76	14.58	15.0	2.48	16.06
19.0	4.30	16.99	17.0	5.36	15.22	17.0	2.84	17.57
21.0	4.77	15.64	19.0	5.93	14.34	19.0	3.18	15.35
23.0	5.29	16.35	21.0	6.51	13.90	21.0	3.54	16.11
25.0	5.77	15.96	23.0	7.13	14.71	23.0	3.92	15.88
27.0	6.34	15.22	25.0	7.56	13.65	25.0	4.30	14.28
29.0	6.87	15.72	27.0	8.13	14.04	27.0	4.71	15.20
31.0	7.37	16.03	29.0	8.77	14.62	29.0	5.19	13.46
33.0	7.91	15.46	31.0	9.41	13.57	31.0	5.68	15.96
35.0	8.43	16.15	33.0	10.06	14.32	33.0	6.13	18.20
37.0	8.96	16.02	35.0	10.71	14.73	35.0	6.64	17.99
39.0	9.45	15.66	37.0	11.41	13.51	37.0	7.10	17.87
41.0	9.99	16.66	39.0	12.01	13.50	39.0	7.52	17.97
43.0	10.52	16.89	41.0	12.64	14.10	41.0	7.95	18.61
45.0	11.08	16.89	43.0	13.31	13.62	41.0	8.35	16.40
47.0	11.56	18.19	45.0	13.97	12.66	43.0	8.75	16.57
49.0	12.16	17.58	47.0	14.65	13.16	45.0	9.21	17.46
52.5	12.89	16.62	49.0	15.40	13.33	47.0	9.64	15.09
			52.5	16.24	12.61	52.5	10.33	16.54
			57.5	17.14	10.72	57.5	10.82	15.78
						63.5	11.24	16.10

Table 3.3a Loch Etive, % loss on ignition results

	LE1		LE2		LE3	
DEPTH (cm)	POROSITY	g/cm2	POROSITY	g/cm2	POROSITY	g/cm2
0.5	0.93	0.06	0.88	0.18	0.95	0.05
1.5	0.91	0.21	0.86	0.45	0.93	0.14
2.5	0.90	0.39	0.85	0.72	0.93	0.25
3.5	0.89	0.60	0.84	1.06	0.93	0.37
4.5	0.88	0.82	0.84	1.41	0.92	0.50
5.5	0.89	1.04	0.84	1.75	0.92	0.67
6.5	0.89	1.26	0.84	2.08	0.91	0.80
7.5	0.88	1.50	0.84	2.42	0.91	0.98
8.5	0.88	1.75	0.84	2.76	0.91	1.15
9.5	0.88	1.97	0.84	3.13	0.91	1.32
11	0.87	2.41	0.84	3.68	0.90	1.69
13	0.87	2.90	0.84	4.2	0.89	2.07
15	0.86	3.37	0.84	4.76	0.88	2.48
17	0.84	3.83	0.84	5.36	0.90	2.84
19	0.82	4.30	0.84	5.93	0.91	3.18
21	0.86	4.77	0.84	6.51	0.90	3.54
23	0.86	5.29	0.84	7.13	0.90	3.92
25	0.86	5.77	0.83	7.56	0.89	4.30
27	0.86	6.34	0.83	8.13	0.89	4.71
29	0.86	6.87	0.82	8.77	0.87	5.19
31	0.85	7.37	0.83	9.41	0.88	5.68
33	0.85	7.91	0.82	10.06	0.88	6.13
35	0.85	8.43	0.84	10.71	0.89	6.64
37	0.85	8.96	0.83	11.41	0.89	7.10
39	0.87	9.45	0.82	12.01	0.90	7.52
41	0.87	9.99	0.82	12.64	0.90	7.95
43	0.81	10.52	0.82	13.31	0.89	8.35
45	0.82	11.08	0.82	13.97	0.88	8.75
47	0.82	11.56	0.80	14.65	0.88	9.21
49	0.83	12.16	0.80	15.4	0.87	9.64
52.5	0.77	12.89	0.79	16.24	0.84	10.33
57.5			0.79	17.14	0.86	10.82
62.5					0.87	11.24

Table 3.4 Loch Etive, Porosity and cumulative weights for cores LE 1, LE 2, LE 3

Depth (cm)	g cm^{-2}	^{210}Pb	+/-	^{226}Ra	+/-	excess^{210}Pb	+/-	^{228}Th	+/-	^{228}Ra	+/-	^{238}U	+/-
0.5	0.06	337.1	23.7	13.2	2.8	347.8	79.2	43.6	3.0	58.0	6.7	99.5	22.6
1.5	0.21	324.5	7.9	36.7	4.4	313.2	38.4	37.1	2.5	33.8	4.9	ND	ND
2.5	0.39	348.9	7.5	24.0	3.7	349.9	54.7	34.4	2.4	35.7	5.3	ND	ND
3.5	0.60	284.2	7.1	28.7	2.8	278.1	28.4	38.2	1.9	31.6	3.1	ND	ND
4.5	0.82	291.3	6.4	40.7	4.8	269.9	32.3	37.3	2.3	30.6	4.0	ND	ND
5.5	1.04	308.9	7.7	27.6	3.8	306.2	43.2	34.7	2.2	32.0	3.8	ND	ND
6.5	1.26	282.1	6.2	35.9	3.1	265.3	24.1	35.1	1.9	39.9	3.6	ND	ND
7.5	1.50	261.1	6.6	34.5	2.7	246.8	20.7	37.1	1.8	36.9	2.8	ND	ND
8.5	1.75	227.5	5.0	32.8	3.9	209.7	25.3	33.8	2.2	37.1	4.6	ND	ND
11.0	2.41	173.6	3.9	35.3	3.1	149.0	13.6	40.4	1.9	39.8	3.2	44.7	9.2
15.0	3.37	154.3	4.0	34.1	2.8	131.0	11.2	43.5	2.1	47.6	3.7	38.5	10.6
17.0	3.83	143.3	3.7	35.3	3.1	117.7	10.7	43.2	2.0	34.6	3.0	41.2	11.2
19.0	4.30	146.2	3.9	25.1	2.8	132.0	15.1	42.4	2.0	41.7	3.5	56.0	11.5
21.0	4.77	117.0	3.0	28.0	2.7	97.0	9.9	42.7	2.0	43.1	3.5	41.4	11.0
23.0	5.29	100.6	2.6	34.5	2.9	72.1	6.4	42.2	2.0	44.7	3.4	74.7	11.1
25.0	5.77	70.2	1.6	31.9	2.8	41.3	3.8	48.2	2.2	43.8	3.5	74.0	12.0
27.0	6.34	42.8	1.1	39.9	2.9	3.1	0.2	45.6	2.0	47.1	3.4	87.1	11.3
29.0	6.87	39.4	1.0	31.9	3.1	8.1	0.8	47.2	2.2	50.1	3.8	72.2	12.3
31.0	7.37	ND	ND	35.6	3.1	ND	ND	48.5	2.2	51.9	3.8	75.8	11.6
33.0	7.91	32.0	0.8	34.9	2.7	-3.1	-0.3	50.7	2.2	45.4	3.4	70.6	10.1
35.0	8.43	ND	ND	26.6	2.7	ND	ND	49.5	2.2	42.7	3.4	93.5	12.0
37.0	8.96	28.2	0.7	37.5	2.3	-10.2	-0.7	52.3	2.1	48.9	2.8	105.0	8.2
41.0	9.99	ND	ND	39.5	3.2	ND	ND	47.6	2.2	45.2	3.5	106.6	12.6
43.0	10.52	ND	ND	29.9	2.8	ND	ND	47.5	2.2	47.6	3.7	92.9	13.6
47.0	11.56	ND	ND	35.9	2.2	ND	ND	48.4	1.9	45.3	2.7	89.4	7.5
49.0	12.16	ND	ND	40.8	3.5	ND	ND	61.1	2.7	52.3	4.4	119.6	15.2
52.5	12.89	ND	ND	26.5	1.8	ND	ND	41.9	1.7	42.2	2.7	75.1	8.4

Table 3.5 Loch Etive core LE 1, natural radionuclide concentrations (Bq kg^{-1})

DEPTH (cm)	g cm^{-2}	^{137}Cs	+/-	^{134}Cs	+/-	^{241}Am	+/-
0.5	0.06	297.6	8.2	30.9	5.6	7.8	1.9
1.5	0.21	284.5	7.5	29.5	0.5	8.8	1.5
2.5	0.39	289.3	7.4	12.8	0.3	11.4	1.5
3.5	0.60	312.9	7.4	ND	ND	7.8	0.9
4.5	0.82	308.3	7.8	ND	ND	8.1	1.3
5.5	1.04	293.7	7.4	12.5	0.3	8.7	1.3
6.5	1.26	310.9	7.3	ND	ND	8.8	1.0
7.5	1.50	302.4	6.9	6.3	0.2	6.5	0.7
8.5	1.75	286.3	7.2	nd	nd	nd	nd
11.0	2.41	218.9	5.2	nd	nd	3.7	0.8
15.0	3.37	139.4	3.6	nd	nd	nd	nd
17.0	3.83	88.4	2.5	nd	nd	nd	nd
19.0	4.30	61.1	2.0	nd	nd	nd	nd
21.0	4.77	42.9	1.5	nd	nd	nd	nd
23.0	5.29	32.0	1.3	nd	nd	nd	nd
25.0	5.77	25.2	1.2	nd	nd	nd	nd
27.0	6.34	23.7	1.0	nd	nd	nd	nd
29.0	6.87	24.8	1.2	nd	nd	nd	nd
31.0	7.37	26.3	1.2	nd	nd	nd	nd
33.0	7.91	13.7	0.9	nd	nd	nd	nd
35.0	8.43	10.2	0.8	nd	nd	nd	nd
37.0	8.96	7.2	0.5	nd	nd	nd	nd
41.0	9.99	4.7	0.6	nd	nd	nd	nd
43.0	10.52	3.5	0.6	nd	nd	nd	nd
47.0	11.56	2.7	0.3	nd	nd	nd	nd
49.0	12.16	0.8	0.2	nd	nd	nd	nd
52.5	12.89	0.7	0.2	nd	nd	nd	nd

Table 3.6 Loch Etive core LE 1, manmade radionuclide concentrations (Bq kg^{-1})

Depth (cm)	g cm^{-2}	$^{206}Pb/^{207}Pb$	+/-	$^{208}Pb/^{207}Pb$	+/-	$^{208}Pb^{206}Pb$	+/-
0.5	0.06	1.1489	0.0044	2.4320	0.0070	2.1168	0.0121
1.5	0.21	1.1491	0.0022	2.4318	0.0079	2.1163	0.0039
2.5	0.39	1.1513	0.0053	2.4337	0.0126	2.1139	0.0045
3.5	0.60	1.1534	0.0039	2.4381	0.0051	2.1138	0.0079
4.5	0.82	1.1527	0.0040	2.4345	0.0048	2.1121	0.0091
5.5	1.04	1.1490	0.0027	2.4297	0.0083	2.1147	0.0061
6.5	1.26	1.1542	0.0016	2.4425	0.0065	2.1162	0.0057
7.5	1.50	1.1515	0.0037	2.4265	0.0102	2.1072	0.0035
8.5	1.75	1.1506	0.0013	2.4234	0.0041	2.1062	0.0047
9.5	1.97	1.1598	0.0063	2.4359	0.0057	2.1003	0.0073
11.0	2.41	1.1535	0.0042	2.4162	0.0161	2.0947	0.0069
13.0	2.90	1.1546	0.0017	2.4493	0.0046	2.1137	0.0025
15.0	3.37	1.1516	0.0025	2.4438	0.0030	2.1145	0.0027
17.0	3.83	1.1655	0.0057	2.4476	0.0094	2.1000	0.0093
19.0	4.30	1.1632	0.0041	2.4411	0.0048	2.0986	0.0043
21.0	4.77	1.1631	0.0042	2.4382	0.0126	2.0936	0.0113
23.0	5.29	1.1701	0.0053	2.4539	0.0079	2.0972	0.0059
25.0	5.77	1.1717	0.0019	2.4597	0.0072	2.0993	0.0051
27.0	6.34	1.1758	0.0042	2.4626	0.0103	2.0944	0.0049
29.0	6.87	1.1763	0.0067	2.4594	0.0161	2.0908	0.0095
31.0	7.37	1.1769	0.0039	2.4513	0.0112	2.0827	0.0052
33.0	7.91	1.1744	0.0021	2.4468	0.0073	2.0833	0.0051
35.0	8.43	1.1732	0.0061	2.4323	0.0083	2.0732	0.0083
37.0	8.96	1.1780	0.0056	2.4840	0.0116	2.0927	0.0075
39.0	9.45	1.1740	0.0060	2.4824	0.0034	2.0984	0.0094
41.0	9.99	1.1670	0.0112	2.4233	0.0295	2.0765	0.0112
43.0	10.52	1.1767	0.0028	2.5062	0.0098	2.1299	0.0067
45.0	11.08	1.1767	0.0068	2.4584	0.0091	2.0894	0.0145
47.0	11.56	1.1813	0.0040	2.4693	0.0100	2.0904	0.0077
49.0	12.16	1.1821	0.0050	2.4668	0.0082	2.0867	0.0119
52.5	12.89	1.1825	0.0048	2.4716	0.0102	2.0902	0.0078

Table 3.7 Loch Etive core LE 1, Pb isotope ratios

DEPTH (cm)	g cm^{-2}	V (ppm)	Ba (ppm)	Sc (ppm)	La (ppm)	Nd (ppm)	Ce (ppm)	Cr (ppm)	Ni (ppm)
0.5	0.06								
1.5	0.21	130.2	424.0	12.5	46.0	38.9	96.5	88.4	40.0
2.5	0.39	134.1	437.2	11.9	45.4	38.6	101.3	89.2	41.4
3.5	0.60	138.6	445.3	13.0	46.6	40.1	104.2	90.2	42.6
4.5	0.82	131.0	437.2	12.3	45.0	37.8	100.5	86.7	38.5
5.5	1.04	138.0	455.1	12.9	46.1	39.9	106.5	90.6	42.4
6.5	1.26	141.8	456.0	14.5	49.2	38.9	105.5	92.8	42.3
7.5	1.50	140.8	459.1	13.4	47.4	41.7	107.4	102.2	82.8
8.5	1.75	141.4	467.7	13.6	48.7	41.8	111.0	110.3	114.2
10.5	1.97	140.1	473.0	13.5	46.9	40.6	109.3	102.8	76.0
13.0	2.90	136.8	473.7	15.0	48.9	41.7	108.0	96.2	43.6
15.0	3.37	132.9	478.0	14.5	46.8	40.8	105.8	93.9	42.8
17.0	3.83	130.6	469.9	13.0	46.4	41.3	104.4	94.9	43.8
19.0	4.30	128.9	486.6	13.5	47.5	40.5	103.6	94.2	43.6
21.0	4.77	124.1	461.6	12.7	46.3	37.6	95.9	89.7	41.0
23.0	5.29	120.8	462.4	12.7	46.2	38.4	99.4	89.1	42.1
25.0	5.77	129.0	504.0	15.4	46.3	41.1	101.6	96.6	45.5
27.0	6.34	122.2	475.1	14.8	44.4	39.3	99.7	93.1	46.3
29.0	6.87	124.7	505.7	13.8	46.1	40.9	104.9	95.8	44.4
31.0	7.37	124.1	498.5	14.2	45.6	41.3	108.2	95.0	43.6
33.0	7.91	125.3	504.5	13.0	48.3	41.2	104.7	94.2	44.4
35.0	8.43	130.8	470.6	13.1	47.4	41.5	105.7	89.3	41.7
37.0	8.96	135.7	481.8	14.3	46.7	41.2	104.0	90.4	42.8
39.0	9.45	136.1	474.1	14.5	47.2	41.2	105.9	92.6	43.1
41.0	9.99	131.7	488.8	13.4	45.9	41.1	106.5	94.2	42.4
43.0	10.52	135.3	465.3	14.1	45.8	41.7	106.2	94.9	42.7
45.0	11.08	136.0	451.7	13.8	45.5	38.9	101.2	93.4	43.2
47.0	11.56	139.2	462.4	15.0	46.8	40.5	103.0	96.3	44.7
49.0	12.16	134.0	448.6	12.6	46.1	38.8	100.9	93.1	43.4
52.5	12.89	132.5	443.5	13.7	46.5	39.6	97.5	96.6	44.4

Table 3.8 Loch Etive core LE 1, XRF trace element results.

DEPTH (cm)	g cm^{-2}	Cu (ppm)	Zn (ppm)	Pb (ppm)	Th (ppm)	Rb (ppm)	Sr (ppm)	Y (ppm)	Zr (ppm)	Nb (ppm)
0.5	0.06									
1.5	0.21	9.5	221.3	96.1	15.1	93.7	230.3	22.3	151.6	11.9
2.5	0.39	13.3	229.7	97.2	15.8	97.6	228.4	24.0	157.4	11.1
3.5	0.60	16.3	241.2	97.4	17.6	100.2	225.3	24.9	163.2	11.8
4.5	0.82	6.5	222.5	92.2	16.2	92.2	212.2	23.0	145.2	11.2
5.5	1.04	15.5	237.5	99.0	15.8	98.9	228.8	24.4	155.0	11.5
6.5	1.26	15.0	240.2	96.8	17.0	98.7	221.7	24.1	164.4	11.3
7.5	1.50	14.0	237.3	96.2	15.6	97.9	218.7	25.2	167.1	11.6
8.5	1.75	18.0	242.4	94.0	17.4	100.0	216.0	26.4	171.7	12.3
10.5	1.97	18.0	236.6	90.1	16.7	100.3	218.0	25.7	179.3	12.3
13.0	2.90	14.6	233.0	88.0	15.4	100.5	216.3	25.1	174.6	12.1
15.0	3.37	12.7	225.1	85.5	15.3	98.4	211.7	24.6	171.6	11.9
17.0	3.83	13.8	223.6	83.8	15.4	101.2	217.6	25.2	179.8	12.4
19.0	4.30	14.9	219.8	83.1	14.7	100.7	218.1	24.8	181.3	12.2
21.0	4.77	8.6	205.0	77.5	15.2	95.6	215.6	23.9	179.8	12.1
23.0	5.29	11.4	202.1	75.7	14.3	98.2	224.5	24.5	191.6	12.2
25.0	5.77	15.4	201.1	75.9	14.8	103.1	255.8	25.4	201.1	12.6
27.0	6.34	14.2	164.4	60.9	14.4	99.8	289.3	25.3	195.0	12.3
29.0	6.87	12.9	140.4	49.8	15.5	102.3	244.4	25.8	196.7	12.9
31.0	7.37	10.2	135.4	49.2	17.4	103.5	234.2	25.6	198.2	13.4
33.0	7.91	10.4	125.2	46.2	16.8	105.7	246.8	25.8	187.2	13.2
35.0	8.43	9.7	104.8	37.8	15.3	98.1	287.7	24.9	166.2	11.8
37.0	8.96	7.3	105.4	37.9	16.7	102.6	223.2	25.2	171.3	12.9
39.0	9.45	6.2	105.2	37.6	16.5	102.8	224.9	25.2	183.6	13.2
41.0	9.99	4.8	102.0	35.2	16.0	99.3	229.0	24.5	190.5	13.1
43.0	10.52	7.2	102.3	34.4	15.3	98.5	238.4	25.1	177.7	11.8
45.0	11.08	7.7	102.3	33.7	15.4	99.5	225.2	24.5	174.1	12.9
47.0	11.56	8.5	105.3	34.9	14.4	102.0	212.8	25.1	170.6	12.2
49.0	12.16	6.5	102.6	34.9	16.7	100.4	209.0	24.4	167.3	12.6
52.5	12.89	8.2	101.5	31.0	13.9	102.0	210.7	24.5	176.6	12.8

Table 3.8 Loch Etive core LE 1, XRF trace element results (continued)

DEPTH (cm)	g cm^{-2}	Si (%)	Al (%)	Fe (%)	Mg (%)	Ca (%)	Na (%)	K (%)	Ti (%)	Mn (%)	P (%)
0.5	0.06	22.93	6.97	4.88	1.62	1.29	1.11	1.81	0.52	0.08	0.22
1.5	0.21	22.94	7.16	4.87	1.65	1.43	1.09	1.86	0.53	0.07	0.21
2.5	0.39	23.13	7.23	5.11	1.69	1.30	1.20	1.98	0.53	0.06	0.21
3.5	0.60	23.41	7.36	5.14	1.69	1.19	1.15	1.99	0.54	0.06	0.18
4.5	0.82	21.34	6.75	4.62	1.61	1.32	0.89	1.73	0.48	0.05	0.16
5.5	1.04	22.91	7.13	5.07	1.64	1.54	1.24	2.07	0.53	0.06	0.20
6.5	1.26	23.65	7.36	4.87	1.69	1.19	1.20	2.12	0.55	0.05	0.17
7.5	1.50	23.89	7.41	4.70	1.68	1.10	1.35	2.13	0.55	0.05	0.17
8.5	1.75	24.11	7.54	4.90	1.71	1.06	1.37	2.18	0.56	0.05	0.14
10.5	1.97	24.19	7.54	4.91	1.71	1.12	1.37	2.20	0.57	0.05	0.13
13.0	2.90	24.64	7.75	4.66	1.79	1.01	1.89	2.26	0.57	0.05	0.12
15.0	3.37	24.02	7.79	4.62	1.69	1.05	1.58	2.21	0.57	0.05	0.12
17.0	3.83	24.18	7.60	4.80	1.69	1.04	1.48	2.16	0.59	0.05	0.12
19.0	4.30	24.35	7.58	4.64	1.65	1.01	1.50	2.13	0.59	0.04	0.13
21.0	4.77	24.76	7.31	4.23	1.61	1.09	1.40	2.10	0.56	0.04	0.12
23.0	5.29	24.84	7.43	4.56	1.63	1.18	1.42	2.07	0.58	0.05	0.11
25.0	5.77	25.36	7.58	4.70	1.55	1.76	0.68	2.15	0.60	0.05	0.11
27.0	6.34	24.42	7.33	4.91	1.52	2.25	0.85	2.13	0.57	0.05	0.11
29.0	6.87	24.82	7.58	4.99	1.62	1.38	1.07	2.18	0.60	0.05	0.11
31.0	7.37	24.82	7.72	4.76	1.65	1.20	1.13	2.22	0.62	0.05	0.11
33.0	7.91	24.62	7.75	4.94	1.71	1.52	1.09	2.25	0.60	0.06	0.11
35.0	8.43	23.38	7.22	4.58	1.59	2.66	1.13	2.08	0.56	0.05	0.12
37.0	8.96	23.45	7.53	4.85	1.71	1.13	1.42	2.16	0.61	0.04	0.11
39.0	9.45	24.02	7.64	4.88	1.68	1.12	1.23	2.25	0.61	0.05	0.11
41.0	9.99	24.21	7.60	4.51	1.67	1.18	1.10	2.21	0.62	0.05	0.11
43.0	10.52	23.67	7.51	4.59	1.70	1.61	1.44	2.17	0.61	0.05	0.11
45.0	11.08	22.96	7.43	5.00	1.69	1.35	1.48	2.21	0.59	0.05	0.11
47.0	11.56	23.10	7.49	5.04	1.71	1.08	1.40	2.26	0.60	0.05	0.11
49.0	12.16	22.86	7.45	5.07	1.74	1.05	1.42	2.20	0.60	0.05	0.11
52.5	12.89	23.10	7.35	5.10	1.72	1.14	1.69	2.23	0.58	0.05	0.10

Table 3.9 Loch Etive core LE 1, XRF major element results

DEPTH (cm)	g cm^{-2}	^{210}Pb	+/-	^{226}Ra	+/-	excess^{210}Pb	+/-	^{228}Th	+/-	^{228}Ra	+/-	^{238}U	+/-
0.5	0.18	104.4	13.3	29.9	3.4	74.6	10.2	55.0	3.2	31.2	4.0	41.0	10.0
1.5	0.45	93.5	12.0	30.3	3.1	63.2	8.7	45.3	2.6	34.1	3.7	nd	nd
2.5	0.72	94.1	11.4	32.5	3.0	61.6	7.9	42.8	2.5	33.1	3.6	41.4	9.1
3.5	1.06	107.1	6.0	30.5	1.8	78.1	4.6	38.7	1.7	33.8	2.2	38.5	4.2
4.5	1.41	96.9	9.0	30.1	2.3	68.0	6.7	40.5	2.0	33.8	2.8	43.0	6.8
5.5	1.75	90.8	11.0	31.9	3.0	60.4	7.8	41.3	2.4	32.7	3.5	39.4	9.1
6.5	2.08	85.8	11.8	33.9	3.3	53.2	7.8	45.1	2.6	45.0	4.0	49.7	11.0
7.5	2.42	69.0	11.1	29.9	2.9	39.9	6.8	39.9	2.3	40.1	3.6	55.0	4.6
8.5	2.76	65.2	4.8	32.4	1.7	33.4	2.6	43.1	1.8	35.3	2.2	54.3	10.1
9.5	3.13	53.3	10.1	36.3	3.1	17.5	3.5	47.1	2.5	31.5	3.5	80.4	10.9
11.0	3.68	52.6	8.9	39.0	3.1	14.0	2.5	46.2	2.2	42.8	3.3	72.4	5.3
13.0	4.20	37.3	3.8	32.2	1.6	5.2	0.6	42.5	1.7	37.7	2.2	76.1	8.3
15.0	4.76	34.0	6.6	32.3	2.1	1.8	0.4	47.2	2.0	36.9	2.5	87.9	11.9
17.0	5.36	0.0	nd	27.4	2.4	-28.2	0.0	46.4	2.2	40.2	3.2	90.2	7.4
19.0	5.93	24.0	5.6	27.7	1.8	-3.8	-0.9	50.0	2.1	44.1	2.8	27.9	3.6
21.0	6.51	8.2	0.4	31.6	2.0	-24.1	-1.1	55.8	2.3	39.8	2.6	39.4	5.1
23.0	7.13	23.7	5.0	30.3	1.6	-6.8	-1.5	46.6	1.9	40.5	2.3	93.3	6.0
25.0	7.56	0.0	nd	39.7	3.2	-42.3	0.0	49.5	2.3	38.1	3.3	77.3	11.0
27.0	8.13	28.0	7.8	31.2	2.5	-3.3	-1.0	53.8	2.5	36.4	3.1	62.2	8.6
29.0	8.77	0.0	nd	24.5	2.8	-25.8	0.0	55.5	2.7	35.7	3.2	102.8	12.4
31.0	9.41	0.0	nd	34.4	2.5	-36.7	0.0	46.4	2.0	41.0	3.0	76.7	9.5
33.0	10.06	31.3	7.0	34.2	2.4	-3.1	-0.7	46.5	2.0	41.2	2.8	78.0	9.2
35.0	10.71	22.8	4.2	32.5	1.8	-10.4	-2.0	46.3	1.8	42.6	2.3	74.9	6.1
37.0	11.41	19.7	4.8	34.9	1.9	-16.2	-4.1	45.8	1.8	39.1	2.4	72.7	7.0
39.0	12.01	16.3	2.9	32.2	1.5	-17.0	-3.1	45.1	1.7	42.8	2.1	60.0	4.4
41.0	12.64	18.9	3.8	35.6	1.8	-17.9	-3.8	48.3	1.9	41.1	2.3	55.3	5.0
43.0	13.31	18.6	4.5	31.7	1.8	-14.1	-3.5	47.9	1.9	38.5	2.3	44.5	5.6
45.0	13.97	19.6	5.5	32.9	2.1	-14.2	-4.2	46.8	1.9	40.8	2.3	63.2	6.7
47.0	14.65	0.0	nd	33.5	1.9	-36.0	0.0	46.1	1.9	35.1	2.3	43.1	6.4
49.0	15.40	0.0	nd	38.0	2.5	-40.9	0.0	50.1	2.2	37.3	2.7	48.7	7.8
52.5	16.24	0.0	nd	42.7	2.8	-45.9	0.0	43.9	2.0	39.9	2.9	49.1	8.3
57.5	17.14	24.7	3.7	33.6	1.7	-9.5	-1.5	42.8	1.7	40.4	2.1	35.2	4.4

Table 3.10 Loch Etive core LE 2, natural radionuclide concentrations (Bq kg^{-1})

DEPTH (cm)	g cm^{-2}	^{137}Cs	+/-	^{134}Cs	+/-	^{241}Am	+/-
0.5	0.18	128.8	3.7	5.2	0.9	nd	nd
1.5	0.45	155.1	4.0	nd	0.0	nd	nd
2.5	0.72	164.9	4.2	3.0	0.7	nd	nd
3.5	1.06	183.6	4.2	1.3	0.2	2.4	0.4
4.5	1.41	184.0	4.4	nd	nd	nd	nd
5.5	1.75	171.4	4.3	2.7	0.6	nd	nd
6.5	2.08	198.8	5.0	nd	nd	nd	nd
7.5	2.42	162.6	4.1	1.9	0.6	nd	nd
8.5	2.76	145.6	3.3	2.1	0.3	nd	nd
9.5	3.13	123.1	3.3	3.3	0.7	nd	nd
11.0	3.68	106.5	2.8	nd	nd	nd	nd
13.0	4.20	95.7	2.2	1.1	0.2	nd	nd
15.0	4.76	56.7	1.6	1.3	0.3	nd	nd
17.0	5.36	37.3	1.3	nd	nd	nd	nd
19.0	5.93	23.5	0.8	0.9	0.3	nd	nd
21.0	6.51	53.2	1.4	3.1	0.4	nd	nd
23.0	7.13	13.7	0.6	nd	nd	nd	nd
25.0	7.56	8.9	0.7	nd	nd	nd	nd
27.0	8.13	5.1	0.5	4.2	0.6	nd	nd
29.0	8.77	5.8	0.6	nd	nd	nd	nd
31.0	9.41	4.6	0.5	nd	nd	nd	nd
33.0	10.06	1.8	0.3	nd	nd	nd	nd
35.0	10.71	2.6	0.3	nd	nd	nd	nd
37.0	11.41	2.0	0.3	nd	nd	nd	nd
39.0	12.01	1.3	0.1	nd	nd	nd	nd
41.0	12.64	1.9	0.2	nd	nd	nd	nd
43.0	13.31	1.8	0.2	nd	nd	nd	nd
45.0	13.97	2.1	0.3	nd	nd	nd	nd
47.0	14.65	0.7	0.1	nd	nd	nd	nd
49.0	15.40	1.2	0.2	nd	nd	nd	nd
52.5	16.24	0.9	0.2	nd	nd	nd	nd
57.5	17.14	0.7	0.1	nd	nd	nd	nd

Table 3.11 Loch Etive core LE 2 manmade radionuclide concentrations (Bq kg^{-1})

DEPTH (cm)	g cm^{-2}	$^{206}Pb/^{207}Pb$	+/-	$^{208}Pb/^{207}Pb$	+/-	$^{208}Pb/^{206}Pb$	+/-
0.5	0.18	1.1568	0.0031	2.4106	0.0028	2.0840	0.0046
1.5	0.45	1.1625	0.0042	2.4128	0.0073	2.0755	0.0066
2.5	0.72	1.1593	0.0026	2.4137	0.0045	2.0820	0.0034
3.5	1.06	1.1625	0.0016	2.4139	0.0073	2.0765	0.0040
4.5	1.41	1.1650	0.0033	2.4212	0.0039	2.0782	0.0033
5.5	1.75	1.1633	0.0028	2.4126	0.0054	2.0739	0.0043
6.5	2.08	1.1626	0.0038	2.4123	0.0047	2.0749	0.0030
7.5	2.42	1.1648	0.0050	2.4159	0.0044	2.0741	0.0098
8.5	2.76	1.1634	0.0048	2.4020	0.0078	2.0647	0.0074
9.5	3.13	1.1675	0.0040	2.3962	0.0075	2.0524	0.0055
11.0	3.68	1.1716	0.0033	2.4182	0.0049	2.0641	0.0041
13.0	4.20	1.1704	0.0031	2.4286	0.0068	2.0750	0.0022
15.0	4.76	1.1757	0.0036	2.4217	0.0099	2.0597	0.0061
17.0	5.36	1.1772	0.0051	2.4211	0.0144	2.0567	0.0049
19.0	5.93	1.1844	0.0064	2.4246	0.0128	2.0470	0.0060
21.0	6.51	1.1786	0.0101	2.4226	0.0169	2.0556	0.0079
23.0	7.13	1.1834	0.0063	2.4225	0.0075	2.0471	0.0098
25.0	7.56	1.1817	0.0070	2.4316	0.0098	2.0577	0.0106
27.0	8.13	1.1781	0.0066	2.4225	0.0096	2.0563	0.0100
29.0	8.77	1.1873	0.0045	2.4939	0.0073	2.1005	0.0033
31.0	9.41	1.1869	0.0060	2.4617	0.0160	2.0741	0.0090
33.0	10.06	1.1748	0.0036	2.4540	0.0075	2.0889	0.0065
35.0	10.71	1.1768	0.0045	2.4565	0.0120	2.0875	0.0040
37.0	11.41	1.1855	0.0028	2.4539	0.0106	2.0698	0.0058
39.0	12.01	1.1788	0.0061	2.4534	0.0196	2.0812	0.0128
41.0	12.64	1.1816	0.0048	2.4837	0.0084	2.1021	0.0044
43.0	13.31	1.1780	0.0042	2.4790	0.0078	2.1044	0.0101
45.0	13.97	1.1824	0.0099	2.4908	0.0122	2.1066	0.0120
47.0	14.65	1.1801	0.0026	2.4847	0.0063	2.1056	0.0096
49.0	15.40	1.1835	0.0051	2.4552	0.0139	2.0745	0.0141
52.5	16.24	1.1795	0.0087	2.4565	0.0144	2.0827	0.0205

Table 3.12 Loch Etive core LE 2, Pb isotope ratios.

Depth (cm)	g cm^{-2}	V (ppm)	Ba (ppm)	Sc (ppm)	La (ppm)	Nd (ppm)	Ce (ppm)	Cr (ppm)	Ni (ppm)
0.5	0.18	117.8	528.8	12.7	48.8	40.1	99.9	80.5	38.6
1.5	0.45	124.4	535.6	13.8	49.7	42.5	108.4	84.2	39.2
2.5	0.72	124.7	539.2	14.1	50.8	42.9	109.7	84.1	39.1
3.5	1.06	126.7	550.2	14.1	51.2	44.0	110.9	83.8	40.5
4.5	1.41	126.8	546.2	14.2	53.2	44.1	115.0	88.6	39.9
5.5	1.75	128.6	548.9	12.9	51.2	42.5	111.6	86.4	40.4
6.5	2.08	128.4	564.0	13.2	51.5	44.1	116.7	85.3	39.9
7.5	2.42	128.7	551.0	13.5	51.3	43.4	111.7	86.1	39.9
8.5	2.76	128.0	560.5	12.8	49.8	43.5	110.8	86.1	40.7
9.5	3.13	128.9	558.2	13.4	50.9	43.7	112.5	85.8	40.1
11.0	3.68	127.2	550.4	12.6	54.1	44.4	111.4	94.8	80.4
13.0	4.20	125.3	545.5	12.8	49.3	42.7	114.2	97.1	96.2
15.0	4.76	129.5	538.2	12.7	51.0	42.1	112.4	93.9	82.2
17.0	5.36	134.6	515.9	12.0	50.8	42.3	108.3	93.3	81.5
19.0	5.93	135.3	502.5	13.1	50.0	42.4	112.5	92.9	74.7
21.0	6.51	136.3	494.6	13.0	52.6	41.4	108.3	97.9	81.3
23.0	7.13	136.9	497.1	13.9	50.1	42.0	108.8	98.3	90.6
25.0	7.56	137.3	490.6	14.3	52.3	41.0	109.6	100.5	98.1
27.0	8.13	139.3	488.7	13.8	50.8	41.7	112.4	106.7	123.5
29.0	8.77	134.3	472.6	12.8	52.9	42.3	109.4	100.9	98.2
31.0	9.41	134.2	465.1	12.5	51.6	42.3	111.2	99.7	84.6
33.0	10.06	141.9	472.9	13.6	51.1	42.0	111.7	100.0	88.9
35.0	10.71	139.5	465.9	13.1	50.9	41.5	108.9	97.3	76.4
37.0	11.41	140.5	480.8	13.9	52.1	41.9	110.2	97.9	80.7
39.0	12.01	136.4	473.9	12.8	50.9	41.3	110.1	98.7	85.6
41.0	12.64	136.8	473.4	13.0	53.2	43.4	108.3	98.4	82.0
43.0	13.31	135.0	466.1	12.7	51.2	40.1	107.4	98.6	81.6
45.0	13.97	129.7	469.8	13.6	53.2	42.2	109.2	102.7	111.5
47.0	14.65	130.7	457.8	12.6	46.7	41.2	105.1	98.3	85.8
49.0	15.40	129.4	465.7	12.5	47.0	39.8	102.5	92.7	63.3
52.5	16.24	127.0	478.8	12.6	48.1	37.9	103.4	92.2	74.2
57.5	17.14	123.5	480.7	12.7	47.3	38.5	97.4	90.3	60.7

Table 3.13 Loch Etive core LE 2, XRF trace element results

Depth (cm)	g cm^{-2}	Cu (ppm)	Zn (ppm)	Pb (ppm)	Th (ppm)	Rb (ppm)	Sr (ppm)	Y (ppm)	Zr (ppm)	Nb (ppm)
0.5	0.18	12.7	164.5	54.6	14.4	84.7	293.1	24.2	256.3	12.6
1.5	0.45	13.4	165.8	53.5	13.9	86.3	282.8	25.7	249.0	12.8
2.5	0.72	15.1	172.0	58.1	14.8	86.4	284.7	25.4	264.4	12.6
3.5	1.06	15.0	177.3	60.2	15.0	88.4	284.2	26.4	258.4	12.9
4.5	1.41	14.5	174.8	59.5	14.6	88.3	283.4	25.8	252.1	12.7
5.5	1.75	15.4	176.3	59.9	13.8	88.6	283.6	25.9	251.8	12.8
6.5	2.08	14.3	171.5	60.5	15.2	88.2	282.4	26.2	251.2	12.8
7.5	2.42	13.7	164.3	58.1	14.9	89.4	287.3	25.5	247.7	13.0
8.5	2.76	13.9	163.1	59.2	16.1	90.2	282.0	25.6	241.8	12.4
9.5	3.13	13.0	148.3	56.2	15.0	90.7	285.0	26.2	242.8	13.1
11.0	3.68	11.6	135.3	49.9	16.2	91.3	283.8	25.8	233.0	13.0
13.0	4.20	10.5	126.2	44.9	14.0	89.0	287.5	25.5	233.9	13.0
15.0	4.76	9.4	113.8	37.4	14.6	88.6	281.0	24.9	231.9	12.7
17.0	5.36	8.6	107.6	33.5	14.4	90.4	266.6	25.5	227.5	12.4
19.0	5.93	7.6	107.1	30.7	14.7	91.2	262.8	25.6	226.0	12.5
21.0	6.51	7.3	106.4	27.6	13.1	91.6	256.5	25.3	225.2	13.0
23.0	7.13	6.8	104.9	27.9	14.3	92.4	252.0	25.0	223.8	12.4
25.0	7.56	5.2	105.0	25.6	13.4	91.2	245.7	25.5	225.0	12.3
27.0	8.13	5.1	102.5	25.1	13.6	91.9	237.1	24.8	218.9	12.1
29.0	8.77	4.0	101.4	25.7	13.9	90.9	239.2	24.7	224.3	12.1
31.0	9.41	4.2	103.8	25.0	14.2	92.2	239.9	25.2	232.2	13.1
33.0	10.06	6.5	104.6	26.5	13.0	93.3	237.2	25.2	214.5	12.7
35.0	10.71	2.3	102.2	24.3	13.2	90.3	234.8	25.5	215.9	12.1
37.0	11.41	5.8	103.7	24.7	14.1	94.8	240.1	25.8	225.7	12.3
39.0	12.01	4.8	101.1	23.7	14.3	93.6	240.8	25.2	222.6	12.1
41.0	12.64	4.0	101.6	23.4	15.0	94.2	233.8	25.0	226.0	12.0
43.0	13.31	2.9	99.7	24.0	14.0	92.8	236.4	25.0	220.3	12.1
45.0	13.97	4.1	98.7	21.8	12.5	94.4	234.2	25.3	234.8	11.7
47.0	14.65	5.0	98.7	23.7	14.1	94.5	233.4	25.7	229.2	12.2
49.0	15.40	2.8	96.6	22.8	13.8	92.7	231.5	25.2	223.9	12.2
52.5	16.24	5.2	93.5	21.8	13.9	94.4	244.9	24.3	238.5	12.2
57.5	17.14	4.8	91.6	21.2	12.7	96.0	247.3	24.3	250.7	12.2

Table 3.13 Loch Etive core LE 2, XRF trace element results (cont'd)

Depth (cm)	g cm^{-2}	Si (%)	Al (%)	Fe (%)	Mg (%)	Ca (%)	Na (%)	K (%)	Ti (%)	Mn (%)	P (%)
0.5	0.18	26.00	7.01	4.87	1.61	1.19	1.70	1.99	0.60	0.11	0.15
1.5	0.45	26.20	7.13	4.63	1.59	1.19	1.74	1.99	0.60	0.06	0.13
2.5	0.72	26.29	7.16	4.46	1.57	1.19	1.78	2.02	0.61	0.06	0.13
3.5	1.06	26.32	7.18	4.44	1.58	1.20	1.77	2.04	0.62	0.06	0.13
4.5	1.41	26.16	7.27	4.30	1.59	1.20	1.69	2.02	0.61	0.06	0.13
5.5	1.75	26.11	7.30	4.46	1.56	1.20	1.61	2.08	0.62	0.05	0.13
6.5	2.08	26.02	7.32	4.38	1.56	1.20	1.74	2.07	0.62	0.06	0.13
7.5	2.42	25.86	7.33	4.38	1.57	1.19	1.68	2.08	0.62	0.05	0.13
8.5	2.76	25.74	7.31	4.43	1.59	1.19	1.71	2.10	0.62	0.06	0.13
9.5	3.13	25.58	7.42	4.42	1.62	1.20	1.74	2.12	0.63	0.05	0.13
11.0	3.68	25.50	7.51	4.52	1.63	1.19	1.76	2.08	0.63	0.05	0.13
13.0	4.20	25.75	7.24	4.49	1.56	1.19	1.67	2.07	0.61	0.05	0.13
15.0	4.76	25.54	7.23	4.62	1.54	1.18	1.62	2.04	0.61	0.05	0.12
17.0	5.36	25.21	7.33	4.84	1.58	1.14	1.57	2.03	0.61	0.05	0.12
19.0	5.93	25.02	7.27	4.88	1.61	1.14	1.62	2.07	0.61	0.06	0.11
21.0	6.51	25.21	7.39	4.81	1.61	1.14	1.56	2.10	0.61	0.05	0.11
23.0	7.13	25.31	7.32	4.97	1.60	1.13	1.53	2.04	0.60	0.06	0.11
25.0	7.56	25.06	7.30	4.74	1.63	1.10	1.62	2.13	0.59	0.05	0.10
27.0	8.13	25.46	7.36	4.76	1.63	1.10	1.55	2.15	0.60	0.05	0.10
29.0	8.77	26.08	7.42	4.78	1.61	1.10	1.60	2.10	0.59	0.06	0.10
31.0	9.41	25.55	7.29	5.06	1.59	1.09	1.50	2.11	0.59	0.06	0.10
33.0	10.06	26.11	7.57	5.12	1.71	1.10	1.76	2.16	0.59	0.06	0.10
35.0	10.71	25.18	7.32	4.77	1.62	1.13	1.46	2.08	0.59	0.06	0.10
37.0	11.41	25.65	7.43	5.09	1.59	1.10	1.54	2.18	0.59	0.06	0.10
39.0	12.01	25.71	7.30	4.96	1.57	1.09	1.66	2.17	0.57	0.06	0.10
41.0	12.64	25.71	7.35	4.73	1.60	1.10	1.58	2.15	0.58	0.06	0.10
43.0	13.31	25.92	7.31	4.54	1.57	1.12	1.59	2.12	0.57	0.05	0.10
45.0	13.97	25.87	7.27	4.91	1.57	1.11	1.59	2.19	0.57	0.05	0.10
47.0	14.65	25.89	7.24	4.95	1.55	1.13	1.65	2.21	0.57	0.05	0.09
49.0	15.40	25.82	7.26	4.76	1.57	1.27	1.70	2.14	0.57	0.06	0.09
52.5	16.24	26.82	7.18	4.83	1.46	1.14	1.65	2.15	0.56	0.06	0.09
57.5	17.14	27.40	7.24	4.63	1.44	1.15	1.63	2.26	0.55	0.05	0.09

Table 3.14 Loch Etive core LE 2, XRF major element results

DEPTH	g cm^{-2}	^{210}Pb	+/-	^{226}Ra	+/-	excess ^{210}Pb	+/-	^{228}Th	+/-	^{228}Ra	+/-	^{238}U	+/-
0.5	0.05	418.7	52.6	276.9	22.3	141.8	25.3	186.1	12.2	379.7	28.9	256.5	53.4
1.5	0.14	330.0	38.1	29.1	5.7	301.1	71.5	124.9	6.3	124.5	11.1	68.3	21.0
2.5	0.25	340.0	17.6	34.0	2.9	306.3	31.8	111.7	4.5	57.5	4.5	39.7	6.2
3.5	0.37	308.5	26.3	34.4	4.8	275.3	47.0	88.5	4.7	44.9	5.8	nd	nd
4.5	0.50	316.1	27.1	41.2	5.4	276.2	44.9	80.3	4.3	50.4	6.2	nd	nd
5.5	0.67	299.2	17.9	46.5	3.4	254.1	25.2	62.0	2.8	50.1	4.0	41.0	7.5
6.5	0.80	211.5	16.1	43.1	4.1	170.5	21.8	51.6	2.6	43.1	4.4	nd	nd
7.5	0.98	277.1	17.0	28.5	2.8	250.4	30.1	55.5	2.6	44.5	3.8	37.1	7.0
8.5	1.15	265.7	16.7	41.5	3.6	226.6	25.4	49.6	2.4	42.2	3.8	37.5	7.6
9.5	1.32	272.7	19.4	35.3	3.5	240.1	30.8	51.8	2.8	46.5	4.9	nd	nd
11.0	1.69	269.0	19.3	28.8	2.9	242.9	31.2	52.9	2.5	42.0	3.7	37.6	9.0
13.0	2.07	249.6	20.6	32.3	3.4	220.0	30.2	50.4	2.6	40.5	4.3	nd	nd
15.0	2.48	206.1	18.6	34.4	3.9	173.9	25.9	51.9	2.6	44.5	4.2	nd	nd
17.0	2.84	201.5	18.3	40.0	3.6	163.6	22.1	46.7	2.4	55.7	4.8	nd	nd
19.0	3.18	155.0	15.8	38.4	3.8	118.2	17.7	43.4	2.3	46.5	4.3	nd	nd
21.0	3.54	140.7	16.8	41.8	4.1	100.1	16.4	47.0	2.4	43.5	4.5	38.8	11.5
23.0	3.92	143.5	15.9	38.5	3.8	106.4	16.7	42.2	2.2	41.0	3.0	nd	nd
25.0	4.30	84.1	8.3	34.5	2.4	50.2	6.5	43.5	1.9	37.8	3.1	42.8	6.5
27.0	4.71	8.1	0.4	41.2	3.7	-33.5	-3.6	51.9	2.5	50.2	3.2	nd	nd
29.0	5.19	79.2	8.7	40.7	2.4	39.0	5.2	47.5	3.6	46.0	2.2	58.6	7.0
31.0	5.68	66.2	8.2	36.6	2.4	31.7	4.7	41.4	1.8	43.3	3.1	52.9	7.3
33.0	6.13	49.7	8.0	34.0	2.2	16.9	3.1	43.4	1.9	41.7	3.0	61.2	8.1
35.0	6.64	43.9	4.2	31.6	1.6	13.1	1.5	37.3	1.5	38.3	2.2	54.3	4.4
37.0	7.10	63.7	8.5	30.4	2.1	35.4	5.7	45.2	1.9	53.0	3.4	52.6	7.8
39.0	7.52	54.7	5.4	38.4	2.0	17.3	2.1	47.3	1.9	52.5	2.9	46.6	5.0
41.0	7.95	8.0	0.4	52.0	3.4	-46.9	-4.1	52.5	2.3	60.7	4.2	80.6	10.7
43.0	8.35	65.0	11.7	35.7	3.2	31.1	6.7	46.1	2.2	55.7	4.3	45.6	9.0
45.0	8.75	54.8	6.3	39.2	2.2	16.7	2.3	46.6	1.9	46.2	2.8	45.4	5.7
47.0	9.21	8.7	2.0	32.6	2.9	-25.5	-6.6	46.6	2.2	44.8	3.9	37.4	10.3
49.0	9.64	51.6	2.5	40.7	3.3	11.6	1.1	42.3	2.0	40.9	3.7	45.1	11.1
52.5	10.33	35.9	8.6	30.7	2.3	5.6	1.5	35.7	1.7	29.0	2.7	64.7	9.2
57.5	10.82	43.5	11.2	32.8	2.7	11.4	3.3	42.1	2.0	45.2	3.8	43.2	10.2
63.5	11.24	43.6	11.0	40.7	3.4	3.1	0.9	42.5	2.0	41.3	3.7	52.7	9.9

Table 3.15 Loch Etive core LE 3, natural radionuclide concentrations (Bq kg^{-1})

DEPTH (cm)	g cm^{-2}	^{137}Cs	+/-	^{134}Cs	+/-	^{241}Am	+/-
0.5	0.05	248.2	10.0	22.6	5.0	nd	nd
1.5	0.14	269.3	7.6	nd	nd	nd	nd
2.5	0.25	286.9	6.7	4.3	0.6	7.0	0.8
3.5	0.37	298.9	7.9	5.8	1.5	7.1	1.9
4.5	0.50	302.7	8.0	4.0	1.2	9.2	1.9
5.5	0.67	299.8	7.0	2.3	0.5	5.7	0.9
6.5	0.80	291.9	6.9	nd	nd	nd	nd
7.5	0.98	301.5	7.0	nd	nd	7.6	0.9
8.5	1.15	286.4	6.8	nd	nd	6.1	1.0
9.5	1.32	269.3	6.7	nd	nd	4.9	1.1
11.0	1.69	256.4	6.1	nd	nd	5.1	1.0
13.0	2.07	222.3	5.5	nd	nd	5.5	1.2
15.0	2.48	170.1	4.5	nd	nd	nd	nd
17.0	2.84	118.8	3.3	nd	nd	nd	nd
19.0	3.18	79.8	2.4	nd	nd	nd	nd
21.0	3.54	49.8	1.9	nd	nd	nd	nd
23.0	3.92	33.6	1.5	nd	nd	nd	nd
25.0	4.30	19.4	1.2	nd	nd	nd	nd
27.0	4.71	11.9	0.8	nd	nd	nd	nd
29.0	5.19	8.1	0.5	nd	nd	nd	nd
31.0	5.68	5.1	0.5	nd	nd	nd	nd
33.0	6.13	5.0	0.5	nd	nd	nd	nd
35.0	6.64	4.5	0.3	nd	nd	nd	nd
37.0	7.10	7.4	0.6	nd	nd	nd	nd
39.0	7.52	4.8	0.4	nd	nd	nd	nd
41.0	7.95	5.8	0.9	nd	nd	nd	nd
43.0	8.35	2.5	0.4	nd	nd	nd	nd
45.0	8.75	2.9	0.3	nd	nd	nd	nd
47.0	9.21	3.3	0.5	nd	nd	nd	nd
49.0	9.64	2.3	0.4	nd	nd	nd	nd
52.5	10.33	1.0	0.2	nd	nd	nd	nd
57.5	10.82	1.1	0.2	nd	nd	nd	nd
63.5	11.24	1.2	0.2	nd	nd	nd	nd

Table 3.16 Loch Etive core LE 3, manmade radionuclide concentrations (Bq kg^{-1})

DEPTH (cm)	g cm^{-2}	$^{206}Pb/^{207}Pb$	+/-	$^{208}Pb/^{207}Pb$		$^{208}Pb/^{206}Pb$	+/-
0.5	0.05	1.1518	0.0036	2.4251	0.0049	2.1054	0.0076
1.5	0.14	1.1541	0.0040	2.4257	0.0062	2.1018	0.0031
3.5	0.37	1.1573	0.0033	2.4326	0.0023	2.1019	0.0072
4.5	0.50	1.1580	0.0035	2.4406	0.0028	2.1070	0.0061
5.5	0.67	1.1583	0.0034	2.4390	0.0091	2.1056	0.0093
6.5	0.80	1.1576	0.0018	2.4371	0.0080	2.1052	0.0068
7.5	0.98	1.1534	0.0027	2.4230	0.0096	2.1007	0.0044
8.5	1.15	1.1530	0.0047	2.4225	0.0113	2.1010	0.0028
9.5	1.32	1.1530	0.0047	2.4254	0.0099	2.1035	0.0046
11.0	1.69	1.1601	0.0047	2.4379	0.0133	2.1015	0.0045
13.0	2.07	1.1621	0.0099	2.4393	0.0174	2.0990	0.0094
15.0	2.48	1.1611	0.0074	2.4389	0.0135	2.1006	0.0051
17.0	2.84	1.1560	0.0044	2.4259	0.0113	2.0985	0.0029
19.0	3.18	1.1592	0.0040	2.4223	0.0153	2.0896	0.0064
21.0	3.54	1.1654	0.0050	2.4418	0.0138	2.0953	0.0072
23.0	3.92	1.1627	0.0062	2.4372	0.0147	2.0961	0.0048
25.0	4.30	1.1675	0.0074	2.4408	0.0144	2.0906	0.0053
27.0	4.71	1.1698	0.0068	2.4475	0.0135	2.0922	0.0020
29.0	5.19	1.1687	0.0059	2.4441	0.0184	2.0913	0.0077
31.0	5.68	1.1680	0.0062	2.4449	0.0178	2.0932	0.0075
33.0	6.13	1.1760	0.0057	2.4544	0.0133	2.0871	0.0051
35.0	6.64	1.1768	0.0059	2.4609	0.0144	2.0912	0.0022
37.0	7.10	1.1713	0.0074	2.4480	0.0214	2.0899	0.0082
39.0	7.52	1.1721	0.0101	2.4462	0.0237	2.0871	0.0042
41.0	7.95	1.1735	0.0061	2.4496	0.0140	2.0875	0.0020
43.0	8.35	1.1766	0.0073	2.4508	0.0222	2.0829	0.0070
45.0	8.75	1.1694	0.0070	2.4481	0.0214	2.0934	0.0070
47.0	9.21	1.1765	0.0066	2.4511	0.0173	2.0833	0.0071
49.0	9.64	1.1729	0.0061	2.4540	0.0107	2.0922	0.0064
52.5	10.33	1.1682	0.0102	2.4502	0.0318	2.0974	0.0125
57.5	10.82	1.1786	0.0096	2.4568	0.0242	2.0846	0.0069
63.5	11.24	1.1527	0.0065	2.4386	0.0174	2.1157	0.0042

Table 3.17 Loch Etive core LE 3, Pb isotope ratios

DEPTH (cm)	g cm^{-2}	V (ppm)	Ba (ppm)	Sc (ppm)	La (ppm)	Nd (ppm)	Ce (ppm)	Cr (ppm)	Ni (ppm)
0.5	0.05	NA	NA	NA	NA	NA	NA	NA	NA
1.5	0.14	NA	NA	NA	NA	NA	NA	NA	NA
2.5	0.25	NA	NA	NA	NA	NA	NA	NA	NA
3.5	0.37	NA	NA	NA	NA	NA	NA	NA	NA
4.5	0.50	158.3	486.0	12.2	51.1	42.5	115.6	81.1	40.6
5.5	0.67	155.2	476.9	12.5	52.7	42.2	114.9	79.5	40.4
6.5	0.80	159.1	481.7	12.6	51.2	43.4	117.2	78.4	40.0
7.5	0.98	160.1	476.0	12.3	54.7	43.2	116.5	78.9	41.0
8.5	1.15	159.4	463.1	11.9	56.2	42.8	113.3	78.6	41.4
9.5	1.32	158.5	472.6	13.1	52.7	42.5	113.4	77.5	41.4
11.0	1.69	155.3	451.4	12.4	54.7	40.9	111.9	85.3	69.4
13.0	2.07	153.1	489.0	13.3	54.0	43.9	120.4	86.7	86.4
15.0	2.48	148.8	486.7	13.0	53.3	41.4	111.1	87.7	70.6
17.0	2.84	148.1	464.6	12.1	54.3	42.9	114.4	85.8	72.5
19.0	3.18	144.9	490.8	12.4	54.2	42.3	110.3	85.9	73.7
21.0	3.54	144.1	484.8	12.4	54.1	42.2	108.4	86.5	91.6
23.0	3.92	149.5	523.0	11.5	53.7	42.3	113.2	87.9	83.6
25.0	4.30	150.9	562.7	13.5	49.6	41.4	108.6	89.9	94.3
27.0	4.71	150.4	536.1	12.5	50.5	43.5	111.5	85.8	81.3
29.0	5.19	151.4	615.3	12.6	51.4	40.3	107.7	81.2	85.4
31.0	5.68	156.1	583.1	11.4	50.6	41.8	111.1	82.0	65.9
33.0	6.13	153.6	558.0	11.8	51.4	40.9	111.0	78.2	68.7
35.0	6.64	149.7	604.8	13.2	47.5	37.0	97.2	73.2	72.2
37.0	7.10	146.7	545.2	12.1	50.3	39.8	108.0	84.1	84.5
39.0	7.52	148.3	528.7	12.9	51.4	41.3	110.9	79.1	62.5
41.0	7.95	145.9	523.1	12.3	49.0	40.2	110.7	79.6	61.3
43.0	8.35	142.9	536.7	12.6	48.9	38.3	109.0	83.0	84.7
45.0	8.75	143.5	569.6	12.5	49.1	41.0	106.9	78.3	66.2
47.0	9.21	140.7	568.8	11.8	46.6	39.6	106.9	77.9	68.9
49.0	9.64	133.8	626.0	11.1	46.0	38.2	103.3	90.3	138.2
52.5	10.33	140.2	735.1	11.1	41.2	34.7	92.8	55.8	41.0
57.5	10.82	133.6	621.0	11.1	45.8	38.7	99.7	95.9	156.0
63.5	11.24	143.1	563.6	10.8	48.1	37.5	105.9	75.7	77.7

Table 3.18 Loch Etive core LE 3, XRF trace element results

DEPTH (cm)	g cm^{-2}	Cu (ppm)	Zn (ppm)	Pb (ppm)	Th (ppm)	Rb (ppm)	Sr (ppm)	Y (ppm)	Zr (ppm)	Nb (ppm)
0.5	0.05	NA	NA	75.0	NA	NA	NA	NA	NA	NA
1.5	0.14	NA	NA	78.6	NA	NA	NA	NA	NA	NA
2.5	0.25	NA	NA	NA	NA	NA	NA	NA	NA	NA
3.5	0.37	NA	NA	80.7	NA	NA	NA	NA	NA	NA
4.5	0.50	12.6	239.1	95.7	15.5	83.8	256.3	23.8	153.5	11.0
5.5	0.67	14.5	240.5	85.6	15.0	85.4	259.4	24.0	155.5	11.1
6.5	0.80	15.3	242.0	86.5	16.2	84.6	257.8	24.5	157.7	11.3
7.5	0.98	15.0	245.7	88.7	16.3	85.6	250.3	24.2	143.4	10.9
8.5	1.15	15.5	243.5	88.7	15.1	85.5	250.3	24.8	138.6	11.4
9.5	1.32	15.7	241.3	87.2	15.5	85.0	253.3	23.9	142.7	11.0
11.0	1.69	14.3	238.2	86.4	16.2	84.3	244.6	24.6	146.8	10.9
13.0	2.07	18.9	229.8	81.4	14.9	85.8	255.7	25.8	170.8	10.6
15.0	2.48	15.0	218.7	80.7	15.7	85.3	253.0	24.8	158.0	11.0
17.0	2.84	11.6	221.0	83.0	15.9	86.5	247.2	23.8	151.3	10.6
19.0	3.18	11.1	217.0	79.4	17.5	87.4	260.7	24.7	165.1	11.7
21.0	3.54	12.8	218.5	81.0	16.4	87.6	264.5	24.7	155.5	11.3
23.0	3.92	13.3	209.0	79.1	15.5	87.9	295.9	24.6	165.3	11.7
25.0	4.30	14.1	194.2	72.3	14.4	85.5	335.1	25.0	183.5	11.3
27.0	4.71	13.7	191.9	69.2	16.4	85.2	318.1	25.1	182.6	11.2
29.0	5.19	11.2	165.7	60.8	14.9	81.0	399.7	23.6	215.9	11.4
31.0	5.68	11.5	162.7	61.5	12.9	82.9	375.5	23.0	187.3	11.2
33.0	6.13	10.7	158.4	60.6	15.4	81.8	355.2	23.2	186.1	11.0
35.0	6.64	8.8	133.6	49.4	11.8	74.7	439.1	21.1	213.4	10.9
37.0	7.10	7.6	146.6	58.0	15.7	82.7	319.8	22.6	162.3	10.8
39.0	7.52	6.7	141.0	57.1	15.6	83.6	305.4	23.1	169.8	10.4
41.0	7.95	7.2	134.6	51.8	15.7	83.8	301.6	23.7	175.1	10.9
43.0	8.35	9.4	127.1	49.6	15.1	83.8	326.1	23.8	185.3	11.1
45.0	8.75	7.6	119.1	45.8	14.5	81.0	362.1	23.4	192.9	11.1
47.0	9.21	6.3	115.9	44.2	14.7	79.6	377.3	22.9	218.5	11.2
49.0	9.64	7.8	109.1	42.0	13.8	78.4	413.7	22.4	247.1	11.9
52.5	10.33	4.3	81.2	28.4	8.6	63.3	546.2	18.7	311.0	11.3
57.5	10.82	5.8	98.3	33.7	11.9	81.1	384.5	22.8	225.1	11.1
63.5	11.24	7.0	95.3	38.3	13.5	78.8	380.6	22.7	234.3	11.2

Table 3.18 Loch Etive core LE 3, XRF trace element results (cont'd)

DEPTH (cm)	g cm^{-2}	Si (%)	Al (%)	Fe (%)	Mg (%)	Ca (%)	Na (%)	K (%)	Ti (%)	Mn (%)	P (%)
0.5	0.05	21.19	6.62	5.57	1.65	1.11	1.21	1.73	0.48	1.69	0.23
1.5	0.14	21.24	6.60	5.09	1.72	2.20	1.31	1.74	0.49	0.80	0.20
2.5	0.25	22.25	6.88	5.25	1.82	1.15	1.34	1.90	0.51	0.71	0.18
3.5	0.37	22.59	6.97	5.32	1.80	1.16	1.31	1.97	0.52	0.57	0.16
4.5	0.50	22.78	7.04	5.01	1.79	1.27	1.36	1.93	0.54	0.47	0.16
5.5	0.67	22.79	7.07	5.23	1.76	1.23	1.53	2.00	0.54	0.50	0.15
6.5	0.80	22.71	6.99	5.19	1.77	1.32	1.44	1.96	0.53	0.54	0.15
7.5	0.98	22.68	7.00	5.13	1.75	1.24	1.57	1.99	0.53	0.62	0.15
8.5	1.15	22.64	6.97	5.22	1.76	1.24	1.45	2.00	0.53	0.65	0.15
9.5	1.32	22.65	7.02	5.32	1.74	1.23	1.36	1.99	0.53	0.66	0.15
11.0	1.69	22.92	6.97	5.30	1.75	1.19	1.55	1.97	0.52	0.49	0.14
13.0	2.07	23.45	7.18	5.14	1.75	1.11	1.84	2.06	0.55	0.33	0.14
15.0	2.48	23.12	7.13	5.04	1.77	1.15	1.78	2.04	0.55	0.35	0.14
17.0	2.84	23.01	7.22	5.27	1.78	1.13	1.46	2.00	0.55	0.36	0.13
19.0	3.18	23.01	7.20	5.34	1.76	1.15	1.50	2.07	0.55	0.35	0.13
21.0	3.54	22.92	7.20	5.24	1.80	1.19	1.74	2.02	0.56	0.41	0.13
23.0	3.92	23.67	7.48	4.71	1.72	1.17	1.71	2.10	0.58	0.27	0.13
25.0	4.30	24.23	7.62	4.84	1.74	1.34	1.81	2.15	0.59	0.25	0.12
27.0	4.71	23.69	7.44	4.75	1.73	1.25	2.00	2.11	0.59	0.22	0.12
29.0	5.19	24.02	7.66	4.45	1.66	1.46	1.95	2.13	0.62	0.22	0.11
31.0	5.68	23.82	7.62	4.44	1.68	1.57	1.85	2.08	0.61	0.23	0.12
33.0	6.13	23.26	7.48	4.74	1.71	1.43	1.82	1.95	0.60	0.23	0.12
35.0	6.64	23.69	7.62	4.53	1.56	1.65	1.58	1.89	0.63	0.19	0.11
37.0	7.10	23.25	7.44	4.67	1.73	1.36	1.70	2.04	0.60	0.32	0.12
39.0	7.52	22.87	7.33	4.70	1.77	1.29	1.85	2.06	0.59	0.35	0.12
41.0	7.95	23.12	7.39	4.72	1.78	1.33	1.63	1.98	0.60	0.35	0.12
43.0	8.35	22.87	7.32	5.10	1.76	1.37	1.68	2.05	0.60	0.39	0.12
45.0	8.75	23.30	7.44	4.82	1.74	1.47	1.71	2.00	0.62	0.32	0.12
47.0	9.21	23.20	7.49	4.69	1.69	1.62	1.70	1.93	0.62	0.32	0.12
49.0	9.64	23.60	7.58	4.73	1.65	1.58	2.00	2.01	0.64	0.26	0.12
52.5	10.33	22.85	7.47	4.44	1.56	1.91	2.28	1.83	0.71	0.14	0.11
57.5	10.82	24.17	7.52	4.70	1.68	1.51	1.72	2.00	0.64	0.23	0.12
63.5	11.24	22.66	7.27	4.95	1.71	1.53	1.98	1.96	0.62	0.34	0.12

Table 3.19 Loch Etive core LE 3, XRF major element results

LL1 (70 m)		GD2 (79 m)		FS (86 m)		FD (185 m)	
DEPTH (m)	TEMP °C	DEPTH (m)	TEMP °C	DEPTH (m)	TEMP °C	DEPTH (m)	TEMP °C
0	13.80	0	13.20	0	9.70	0	10.80
1	13.70	1	12.90	1	9.70	1	10.80
2	13.70	2	12.80	2	9.70	2	10.80
3	13.70	3	12.80	3	9.70	3	10.80
4	13.70	4	12.70	4	9.60	4	10.80
5	12.80	5	12.65	5	9.50	5	10.85
6	12.40	6	12.60	6	9.40	6	10.10
7	11.40	7	11.00	7	9.10	7	9.40
8	9.05	8	9.60	8	9.10	8	8.00
9	8.60	9	9.05	9	8.90	9	8.90
10	8.60	10	8.60	10	8.80	10	8.80
12	8.20	12	8.20	12	8.60	12	8.40
14	8.00	14	8.00	14	8.50	14	8.20
16	8.00	16	7.95	16	8.40	16	8.20
18	8.00	18	7.95	18	8.30	18	8.20
20	8.00	20	8.00	20	8.20	20	8.00
22	8.00	22	8.05	22	8.20	22	8.00
24	8.00	24	8.00	24	8.20	24	8.00
26	7.95	26	7.85	26	8.10	26	8.00
28	7.90	28	7.85	28	8.00	28	8.00
30	7.90	30	7.80	30	8.00	30	8.00
32	7.90	32	7.65	32	8.00	32	8.00
34	7.90	34	7.55	34	7.80	34	7.80
36	7.80	36	7.30	36	7.80	36	7.90
38	7.80	38	7.20	38	7.80	38	8.00
40	7.80	40	7.15	40	7.80	40	8.00
42	7.80	42	7.10	42	7.80	45	8.00
44	7.80	44	7.00	44	7.70	50	7.60
46	7.80	46	7.00	46	7.70	55	7.60
48	7.80	48	6.90	48	7.70	60	7.60
50	7.80	50	6.90	50	7.70	65	7.60
52	7.80	52	6.90	55	7.60	70	7.50
54	7.80	54	6.90	60	7.60	75	7.50
56	7.80	56	6.90	65	7.60	80	7.50
58	7.80	58	6.90	70	7.60	85	7.40
60	7.80	60	6.90	75	7.40		
		62	6.85	80	7.40		
		64	6.85	85	7.40		
		66	6.85				
		68	6.85				
		70	6.85				
		72	6.85				
		74	6.85				

Table 3.20 Temperature readings at stations LL1, GD2, FS and FD

LL1		GD2		FS		FD	
DEPTH (m)	dissolved O_2 mg atoms/l	DEPTH (m)	dissolved O_2 mg atoms/l	DEPTH (m)	dissolved O_2 mg atoms/l	DEPTH (m)	dissolved O_2 mg atoms/l
0	0.84	0	0.73	0	0.61	0	0.68
5	0.80	5	0.62	5	0.54	5	0.67
10	0.62	10	0.49	10	0.41	10	0.55
15	0.49	15	0.44	15	0.62	15	0.53
20	0.40	20	0.48	20	0.63	20	0.45
25	0.41	25	0.44	25	0.55	25	0.49
30	0.37	30	0.46	30	0.54	30	0.50
35	0.42	40	0.39	40	0.61	35	0.50
40	0.37	50	0.39			40	0.52
45	0.44	60	0.4			45	0.49
50	0.36	70	0.37			50	0.50
55	0.12	75	0.35			55	0.49
						60	0.50
						65	0.48
						70	0.48
						75	0.48
						80	0.49
						85	0.48
						90	0.48
						100	0.49
						110	0.49
						120	0.48
						130	0.49
						140	0.50

Table 3.21 Dissolved oxygen concentrations at stations LL1, GD2, FS and FD

LL1 DEPTH (m)	g cm^{-2}	GD2 DEPTH (m)	g cm^{-2}	FS DEPTH (m)	g cm^{-2}	FD DEPTH (m)	g cm^{-2}
0.5	0.18	0.5	0.20	0.5	0.28	0.5	0.08
1.5	0.65	1.5	0.36	1.5	0.60	1.5	0.42
2.5	1.14	2.5	0.68	2.5	1.05	2.5	0.63
3.5	1.56	3.5	0.98	3.5	1.59	3.5	0.96
4.5	1.93	4.5	1.23	4.5	2.27	4.5	1.34
5.5	2.50	5.5	1.53	5.5	2.86	5.5	1.75
6.5	2.92	6.5	1.81	6.5	3.46	6.5	2.08
7.5	3.43	7.5	2.12	7.5	4.12	7.5	2.54
8.5	3.99	8.5	2.51	8.5	4.84	8.8	2.92
9.5	4.56	9.5	2.87	9.5	5.50	9.5	3.41
11	5.16	11.0	3.36	11.0	6.74	10.5	3.84
13	5.69	13.0	4.08	13.0	7.99	11.5	4.19
15	6.19	15.0	4.67	15.0	9.18	12.5	4.64
17	6.74	17.0	5.31	17.0	10.50	13.5	5.24
19	7.32	19.0	5.68	19.0	11.80	14.5	5.81
21	7.95	21.0	6.26	21.0	12.87	15.5	6.42
23	8.47	23.0	6.82	23.0	13.90	16.5	7.09
25	8.99	25.0	7.43	25.0	15.02	17.5	7.68
27	9.53	27.0	7.81	27.0	16.11	18.5	8.33
29	10.13	29.0	8.18	29.0	17.17	19.5	8.88
31	10.69	31.0	8.67	31.0	18.26	21.0	9.81
33	11.19	33.0	9.12	33.0	19.29	23.0	10.94
35	11.78	35.0	9.69	35.0	20.38	25.0	12.22
37	12.34	37.0	10.23	37.0	21.48	27.0	13.20
39	13.04	39.0	10.77	39.0	22.49	29.0	14.02
41	13.65	41.0	11.29	41.0	23.38	31.0	15.06
43	14.34	43.0	11.72	43.0	24.39	33.0	15.91
45	14.91	45.0	12.24	45.0	25.49	35.0	16.97
47	15.52	47.0	12.71	47.0	26.46	37.0	18.28
49	15.88	49.0	13.17	49.0	27.51	39.0	19.24
51	16.44	51.0	13.63	51.0	28.62	41.0	20.39
53	16.95	53.0	14.07	53.0	29.65	43.5	21.88
55	17.56	55.0	14.59	55.0	30.69		
57	18.14	57.0	14.98	57.0	31.66		
59	18.72	59.0	15.52	59.0	32.65		
61	19.26	61.0	15.93	61.0	33.60		
63	19.86	63.0	16.40	63.0	34.53		
65	20.44	65.0	16.95	65.0	35.65		
67	21.03	67.0	17.46	67.0	36.97		
69	21.63	69.0	17.95				
71	22.16	71.5	18.74				
73	22.76						
75	23.38						
77	24.01						
79	24.70						

Table 3.22 Clyde Sea Area cumulative weights

LL1			GD2			FS			FD		
DEPTH (cm)	g cm^{-2}	LOI (%)	DEPTH (cm)	g cm^{-2}	LOI (%)	DEPTH (cm)	g cm^{-2}	LOI (%)	DEPTH (cm)	g cm^{-2}	LOI
0.5	0.18	15.4	0.5	0.20	19.6	0.5	0.28	6.8	0.5	0.08	7.9
1.5	0.65	15.0	1.5	0.36	20.4	1.5	0.60	6.8	1.5	0.42	8.3
2.5	1.14	15.2	2.5	0.68	19.9	2.5	1.05	7.1	2.5	0.63	9.3
3.5	1.56	15.2	3.5	0.98	19.9	3.5	1.59	7.0	3.5	0.96	9.6
4.5	1.93	15.4	4.5	1.23	18.2	4.5	2.27	6.9	4.5	1.34	9.1
5.5	2.50	15.4	5.5	1.53	19.0	5.5	2.86	6.9	5.5	1.75	8.6
6.5	2.92	15.6	6.5	1.81	20.4	6.5	3.46	6.5	6.5	2.08	9.4
7.5	3.43	15.1	7.5	2.12	20.6	7.5	4.12	7.1	7.5	2.54	9.6
8.5	3.99	14.9	8.5	2.51	18.5	8.5	4.84	6.6	8.8	2.92	9.8
9.5	4.56	14.2	9.5	2.87	20.1	9.5	5.50	6.3	9.5	3.41	9.8
11.0	5.16	14.3	11.0	3.36	19.9	11.0	6.74	6.1	10.5	3.84	11.0
13.0	5.69	15.0	13.0	4.08	18.5	13.0	7.99	7.0	11.5	4.19	10.5
15.0	6.19	15.2	15.0	4.67	19.8	15.0	9.18	6.7	12.5	4.64	10.6
17.0	6.74	15.0	17.0	5.31	19.1	17.0	10.50	6.8	13.5	5.24	12.8
19.0	7.32	15.3	19.0	5.68	18.2	19.0	11.80	5.8	14.5	5.81	9.3
21.0	7.95	15.4	21.0	6.26	18.0	21.0	12.87	6.0	15.5	6.42	12.0
23.0	8.47	14.6	23.0	6.82	17.9	23.0	13.90	6.1	16.5	7.09	10.3
25.0	8.99	14.9	25.0	7.43	18.1	25.0	15.02	5.5	17.5	7.68	9.5
27.0	9.53	14.6	27.0	7.81	16.7	27.0	16.11	5.8	18.5	8.33	8.6
29.0	10.13	14.8	29.0	8.18	16.9	29.0	17.17	6.1	19.5	8.88	7.8
31.0	10.69	14.6	31.0	8.67	17.1	31.0	18.26	6.7	21.0	9.81	8.9
33.0	11.19	14.8	33.0	9.12	17.0	33.0	19.29	6.8	23.0	10.94	9.8
35.0	11.78	14.4	35.0	9.69	15.4	35.0	20.38	7.1	25.0	12.22	8.6
37.0	12.34	14.4	37.0	10.23	15.3	37.0	21.48	6.6	27.0	13.20	8.5
39.0	13.04	14.3	39.0	10.77	15.8	39.0	22.49	6.9	29.0	14.02	7.9
41.0	13.65	14.4	41.0	11.29	15.2	41.0	23.38	7.2	31.0	15.06	8.4
43.0	14.34	14.2	43.0	11.72	15.4	43.0	24.39	7.0	33.0	15.91	7.6
45.0	14.91	13.9	45.0	12.24	15.5	45.0	25.49	7.0	35.0	16.97	7.5
47.0	15.52	13.9	47.0	12.71	15.4	47.0	26.46	7.3	37.0	18.28	8.2
49.0	15.88	14.0	49.0	13.17	15.1	49.0	27.51	6.2	39.0	19.24	7.5
51.0	16.44	13.6	51.0	13.63	15.4	51.0	28.62	6.6	41.0	20.39	9.2
53.0	16.95	13.5	53.0	14.07	15.3	53.0	29.65	6.8	43.5	21.88	
55.0	17.56	13.5	55.0	14.59	15.2	55.0	30.69	6.4			
57.0	18.14	12.9	57.0	14.98	15.3	57.0	31.66	6.7			
59.0	18.72	13.1	59.0	15.52	15.4	59.0	32.65	6.9			
61.0	19.26	13.4	61.0	15.93	15.6	61.0	33.60	6.7			
63.0	19.86	13.4	63.0	16.40	15.1	63.0	34.53	7.3			
65.0	20.44	13.0	65.0	16.95	15.3	65.0	35.65	7.4			
67.0	21.03	13.2	67.0	17.46	15.3	67.0	36.97	7.0			
69.0	21.63	13.4	69.0	17.95	15.5						
71.0	22.16	13.5	71.5	18.74	15.9						
73.0	22.76	13.3									
75.0	23.38	13.0									
77.0	24.01	12.6									
79.0	24.70	12.7									

3.23 Clyde Sea Area cores, % loss on ignition results

DEPTH (cm)	g cm^{-2}	^{210}Pb	+/-	^{226}Ra	+/-	excess ^{210}Pb	+/-
0.5	0.18	141.2	11.9	23.9	1.3	124.9	12.6
1.5	0.65	133.8	11.1	32.5	1.5	107.9	10.1
2.5	1.14	116.7	14.8	31.0	1.5	91.4	12.5
3.5	1.56	102.4	12.7	25.6	1.4	81.9	11.0
4.5	1.93	133.8	11.9	27.9	1.3	112.9	11.4
5.5	2.50	109.1	13.2	29.1	1.5	85.3	11.2
6.5	2.92	109.5	9.4	38.8	1.7	75.5	7.3
7.5	3.43	115.5	13.8	26.6	1.3	94.9	12.3
8.5	3.99	116.4	13.9	27.9	1.4	94.5	12.3
9.5	4.56	110.4	13.8	29.6	1.5	86.3	11.6
11.0	5.16	105.0	13.1	26.2	1.4	84.1	11.4
13.0	5.69	88.1	10.9	27.3	1.4	65.0	8.7
15.0	6.19	102.9	12.1	28.3	1.4	79.7	10.1
17.0	6.74	57.4	6.9	20.3	1.0	39.7	5.2
19.0	7.32	58.6	7.1	22.5	1.1	38.6	5.0
21.0	7.95	52.0	6.5	29.1	1.4	24.5	3.3
23.0	8.47	56.3	6.9	27.5	1.3	30.8	4.1
25.0	8.99	82.7	10.1	28.7	1.4	57.9	7.7
27.0	9.53	64.6	7.9	28.1	1.4	39.2	5.1
29.0	10.13	62.5	8.2	30.2	1.5	34.7	4.8
31.0	10.69	56.6	6.8	29.1	1.4	29.5	3.8
33.0	11.19	53.9	7.0	28.1	1.4	27.7	3.9
35.0	11.78	83.3	10.6	27.2	1.7	60.1	8.5
37.0	12.34	34.9	4.7	23.8	1.2	11.9	1.7
39.0	13.04	40.0	4.9	29.1	1.4	11.8	1.5
41.0	13.65	31.7	4.6	32.6	1.9	-0.9	-0.1
43.0	14.34	42.9	5.6	28.7	1.4	15.3	2.1
45.0	14.91	23.1	3.2	32.4	1.6	-10.0	-1.5
47.0	15.52	26.2	3.4	29.3	1.4	-3.3	-0.5
49.0	15.88	37.7	4.6	29.6	1.4	8.7	1.1
51.0	16.44	56.8	12.1	28.7	1.4	30.3	6.6
53.0	16.95	27.9	3.8	27.2	1.3	0.7	0.1
55.0	17.56	38.3	4.9	29.5	1.4	9.4	1.3
57.0	18.14	35.9	4.6	30.3	1.5	6.1	0.8
59.0	18.72	32.1	4.2	30.5	1.5	1.7	0.2
61.0	19.26	48.1	6.5	31.8	1.6	17.5	2.5
63.0	19.86	40.0	5.2	27.3	1.4	13.3	1.9
65.0	20.44	35.8	4.4	26.6	1.3	9.7	1.3
67.0	21.03	24.7	3.0	28.0	1.4	-3.5	-0.5
69.0	21.63	48.0	6.0	28.6	1.4	20.5	2.7
71.0	22.16	34.7	4.4	27.0	1.3	8.1	1.1
73.0	22.76	52.1	6.4	29.0	1.4	24.3	3.2
75.0	23.38	30.3	4.4	28.7	1.6	1.7	0.3
77.0	24.01	26.6	4.0	29.6	1.8	-3.1	-0.5
79.0	24.70	55.1	6.7	29.1	1.4	27.3	3.6

Table 3.24 Loch Long core LL1, natural radionuclide concentrations (Bq kg^{-1})

DEPTH (cm)	g cm^{-2}	^{228}Th	+/-	^{228}Ra	+/-	^{238}U	+/-
0.5	0.18	46.0	1.9	38.8	1.8	96.4	15.0
1.5	0.65	45.6	1.9	42.0	1.8	47.2	3.9
2.5	1.14	41.6	1.7	37.2	1.5	44.9	4.0
3.5	1.56	45.1	1.9	27.6	1.6	ND	0.0
4.5	1.93	43.1	1.9	42.3	2.1	76.5	19.6
5.5	2.50	54.4	2.3	34.8	1.6	54.7	6.0
6.5	2.92	47.9	2.4	42.1	1.9	54.4	5.6
7.5	3.43	38.1	1.5	37.3	1.5	54.2	9.9
8.5	3.99	37.2	1.5	34.2	1.5	47.8	4.2
9.5	4.56	36.5	1.6	34.5	1.5	48.8	4.4
11.0	5.16	39.4	1.6	36.3	1.6	51.0	5.2
13.0	5.69	39.6	1.7	34.5	1.5	45.3	7.1
15.0	6.19	39.4	1.7	35.3	1.4	52.1	4.9
17.0	6.74	25.7	1.1	26.4	1.1	41.0	2.5
19.0	7.32	28.8	1.2	28.3	1.1	49.9	4.6
21.0	7.95	42.0	1.8	40.6	1.7	50.8	2.9
23.0	8.47	39.8	1.6	36.8	1.5	46.7	3.5
25.0	8.99	37.4	1.8	34.1	1.5	53.3	6.7
27.0	9.53	38.7	1.6	38.6	1.5	44.1	9.7
29.0	10.13	40.1	1.8	40.7	2.1	50.4	3.8
31.0	10.69	39.1	1.6	37.3	1.5	56.4	4.3
33.0	11.19	39.8	1.6	35.0	1.6	53.7	5.3
35.0	11.78	37.5	1.8	31.2	1.5	49.0	8.8
37.0	12.34	40.9	1.7	41.7	1.8	39.3	4.4
39.0	13.04	40.9	1.7	39.2	1.6	52.8	3.5
41.0	13.65	44.8	2.0	39.0	1.9	67.9	7.1
43.0	14.34	42.5	1.8	43.0	1.8	62.6	6.0
45.0	14.91	43.2	1.8	40.8	1.7	51.5	3.7
47.0	15.52	41.3	1.7	35.8	1.5	63.7	4.0
49.0	15.88	43.2	1.7	41.5	1.7	52.8	4.4
51.0	16.44	43.7	2.0	40.0	1.9	52.7	5.6
53.0	16.95	44.5	1.8	35.8	1.6	50.9	6.0
55.0	17.56	42.4	1.7	37.1	1.5	64.6	3.6
57.0	18.14	42.0	1.7	39.2	1.7	47.5	8.5
59.0	18.72	40.3	1.7	37.6	1.6	64.5	6.6
61.0	19.26	42.0	1.8	44.5	1.8	67.4	5.1
63.0	19.86	39.5	1.6	39.7	1.8	64.3	4.9
65.0	20.44	39.6	1.7	36.9	1.5	56.4	3.1
67.0	21.03	41.9	1.7	38.0	1.5	52.8	11.6
69.0	21.63	42.5	1.7	36.0	1.5	41.6	10.5
71.0	22.16	43.1	1.7	40.1	1.7	49.7	5.2
73.0	22.76	39.7	1.8	41.3	1.7	48.0	4.3
75.0	23.38	45.9	1.9	39.7	1.9	63.1	5.7
77.0	24.01	47.7	2.2	44.1	2.3	37.3	6.4
79.0	24.70	44.7	1.8	39.1	1.6	62.0	4.2

Table 3.24 Loch Long core LL1, natural radionuclide concentrations (Bq kg^{-1}) (continued)

DEPTH (cm)	g cm^{-2}	^{137}Cs	+/-	^{134}Cs	+/-	^{241}Am	+/-	^{60}Co	+/-
0.5	0.18	392.8	16.4	12.3	0.6	11.0	1.1	37.5	3.9
1.5	0.65	415.8	16.1	14.4	0.6	9.8	0.4	8.3	0.8
2.5	1.14	454.6	17.0	18.3	0.6	10.4	0.4	3.9	0.4
3.5	1.56	457.1	17.7	10.0	0.6	11.0	1.0	8.2	0.9
4.5	1.93	511.4	20.2	6.5	0.4	9.7	0.8	8.5	0.9
5.5	2.50	575.9	21.6	6.9	0.4	9.3	0.6	4.5	0.5
6.5	2.92	574.1	22.1	9.5	0.4	9.4	0.5	9.2	1.0
7.5	3.43	623.7	23.4	6.7	0.3	9.0	0.6	4.8	0.5
8.5	3.99	666.1	25.0	3.4	0.2	8.2	0.4	2.9	0.3
9.5	4.56	641.2	24.0	5.0	0.3	7.1	0.4	2.4	0.2
11.0	5.16	581.3	21.8	1.7	0.1	7.0	0.4	3.6	0.4
13.0	5.69	398.8	15.0	0.2	0.0	4.7	0.5	3.4	0.4
15.0	6.19	286.3	11.0	nd	nd	2.6	0.2	0.2	0.02
17.0	6.74	127.4	4.8	2.1	0.1	2.8	0.2	20.1	2.0
19.0	7.32	145.3	5.5	1.5	0.1	2.2	0.2	14.5	1.5
21.0	7.95	180.3	6.8	nd	nd	nd	nd	0.7	0.08
23.0	8.47	146.5	5.5	1.1	0.1	nd	nd	nd	nd
25.0	8.99	113.7	4.3	nd	nd	nd	nd	0.6	0.07
27.0	9.53	90.0	3.4	nd	nd	nd	nd	nd	nd
29.0	10.13	84.4	3.2	1.8	0.1	nd	nd	nd	nd
31.0	10.69	71.2	2.7	0.6	0.0	nd	nd	nd	nd
33.0	11.19	49.6	1.9	nd	nd	nd	nd	nd	nd
35.0	11.78	22.9	0.9	nd	nd	nd	nd	nd	nd
37.0	12.34	7.5	0.4	nd	nd	nd	nd	nd	nd
39.0	13.04	5.1	0.2	nd	nd	nd	nd	nd	nd
41.0	13.65	6.1	0.4	nd	nd	nd	nd	nd	nd
43.0	14.34	4.6	0.3	nd	nd	nd	nd	nd	nd
45.0	14.91	7.0	0.4	nd	nd	nd	nd	nd	nd
47.0	15.52	6.4	0.3	nd	nd	nd	nd	nd	nd
49.0	15.88	8.2	0.4	nd	nd	nd	nd	nd	nd
51.0	16.44	10.6	0.5	nd	nd	nd	nd	nd	nd
53.0	16.95	10.5	0.5	nd	nd	nd	nd	nd	nd
55.0	17.56	14.6	0.7	nd	nd	nd	nd	nd	nd
57.0	18.14	13.3	0.6	nd	nd	nd	nd	nd	nd
59.0	18.72	14.1	0.6	nd	nd	nd	nd	nd	nd
61.0	19.26	14.2	0.6	nd	nd	nd	nd	nd	nd
63.0	19.86	18.6	0.8	nd	nd	nd	nd	nd	nd
65.0	20.44	19.2	0.8	nd	nd	nd	nd	nd	nd
67.0	21.03	10.3	0.4	nd	nd	nd	nd	nd	nd
69.0	21.63	4.4	0.3	nd	nd	nd	nd	nd	nd
71.0	22.16	2.8	0.2	nd	nd	nd	nd	nd	nd
73.0	22.76	1.4	0.1	nd	nd	nd	nd	nd	nd
75.0	23.38	nd	nd	nd	nd	nd	nd	nd	nd
77.0	24.01	2.5	0.3	nd	nd	nd	nd	nd	nd
79.0	24.70	10.9	0.5	nd	nd	nd	nd	nd	nd

Table 3.25 Loch Long core LL1, manmade radionuclide concentrations (Bq kg^{-1})

DEPTH (cm)	g cm^{-2}	$^{206}Pb/^{207}Pb$	+/-	$^{208}Pb/^{207}Pb$	+/-	$^{208}Pb/^{206}Pb$	+/-
0.5	0.18	1.1554	0.0041	2.4799	0.0020	2.1487	0.0066
1.5	0.65	1.1549	0.0023	2.4808	0.0040	2.1504	0.0037
2.5	1.14	1.1511	0.0022	2.4836	0.0039	2.1596	0.0056
3.5	1.56	1.1538	0.0024	2.4775	0.0013	2.1493	0.0039
4.5	1.93	1.1545	0.0013	2.4838	0.0032	2.1537	0.0042
5.5	2.50	1.1526	0.0032	2.4904	0.0023	2.1629	0.0051
6.5	2.92	1.1514	0.0028	2.4901	0.0072	2.1650	0.0040
7.5	3.43	1.5538	0.0050	2.4884	0.0034	2.1560	0.0086
8.5	3.99	1.1532	0.0019	2.4909	0.0032	2.1622	0.0035
9.5	4.56	1.1515	0.0040	2.4895	0.0045	2.1642	0.0096
11.0	5.16	1.5542	0.0041	2.4849	0.0040	2.1529	0.0108
13.0	5.69	1.5594	0.0026	2.4898	0.0033	2.1562	0.0068
15.0	6.19	1.1623	0.0028	2.4870	0.0043	2.1419	0.0024
17.0	6.74	1.1603	0.0023	2.4890	0.0026	2.1473	0.0035
19.0	7.32	1.1600	0.0016	2.4899	0.0054	2.1487	0.0035
21.0	7.95	1.1508	0.0177	2.4574	0.0076	2.1353	0.0059
23.0	8.47	1.5143	0.0021	2.4650	0.0008	2.1408	0.0036
25.0	8.99	1.1574	0.0024	2.4425	0.0044	2.1104	0.0010
27.0	9.53	1.1612	0.0075	2.4470	0.0035	2.1074	0.0031
29.0	10.13	1.1614	0.0016	2.4508	0.0060	2.1101	0.0028
31.0	10.69	1.1607	0.0015	2.4499	0.0017	2.1107	0.0031
33.0	11.19	1.1642	0.0011	2.4545	0.0037	2.1083	0.0024
35.0	11.78	1.1662	0.0017	2.4554	0.0029	2.1055	0.0019
37.0	12.34	1.1652	0.0177	2.4568	0.0057	2.1086	0.0029
39.0	13.04	1.1653	0.0035	2.4523	0.0064	2.1044	0.0035
41.0	13.65	1.1674	0.0039	2.4551	0.0065	2.1031	0.0027
43.0	14.34	1.1679	0.0027	2.4532	0.0023	2.1006	0.0040
45.0	14.91	1.1702	0.0027	2.4591	0.0020	2.1014	0.0045
47.0	15.52	1.1731	0.0042	2.4625	0.0080	2.0992	0.0048
49.0	15.88	1.1746	0.0022	2.4634	0.0052	2.0973	0.0024
51.0	16.44	1.1729	0.0017	2.4606	0.0033	2.0980	0.0050
53.0	16.95	1.1748	0.0028	2.4620	0.0038	2.0957	0.0029
55.0	17.56	1.1740	0.0033	2.4629	0.0059	2.0979	0.0044
57.0	18.14	1.1763	0.0028	2.4611	0.0077	2.0923	0.0054
59.0	18.72	1.1735	0.0005	2.4552	0.0043	2.0921	0.0032
61.0	19.26	1.1742	0.0020	2.4572	0.0031	2.0925	0.0054
63.0	19.86	1.1764	0.0036	2.4593	0.0048	2.0906	0.0054
65.0	20.44	1.1746	0.0032	2.4577	0.0067	2.0923	0.0031
67.0	21.03	1.1758	0.0027	2.4573	0.0050	2.0899	0.0056
69.0	21.63	1.1700	0.0042	2.4547	0.0053	2.0979	0.0031
71.0	22.16	1.1741	0.0007	2.4584	0.0059	2.0938	0.0039
73.0	22.76	1.1781	0.0106	2.5033	0.0055	2.1249	0.0034
75.0	23.38	1.1778	0.0005	2.5066	0.0022	2.1282	0.0021
77.0	24.01	1.1787	0.0038	2.5052	0.0042	2.1254	0.0066
79.0	24.70	1.1718	0.0009	2.4365	0.0035	2.0793	0.0023

Table 3.26 Loch Long core LL1, Pb isotope ratios

DEPTH (cm)	g cm^{-2}	V (ppm)	Ba (ppm)	Sc (ppm)	La (ppm)	Nd (ppm)	Ce (ppm)	Cr (ppm)	Ni (ppm)
0.5	0.18	181	536	16	41	38	89	363	60
1.5	0.65	172	511	16	39	35	90	335	57
2.5	1.14	184	534	17	42	36	87	374	62
3.5	1.56	186	538	17	44	37	93	385	64
4.5	1.93	183	535	16	42	37	92	384	61
5.5	2.50	185	545	16	43	37	93	386	62
6.5	2.92	191	539	18	43	37	93	438	84
7.5	3.43	186	550	18	44	38	92	400	63
8.5	3.99	190	549	18	43	38	93	412	62
9.5	4.56	189	556	18	43	38	91	414	64
11.0	5.16	200	586	17	44	39	98	441	67
13.0	5.69	199	574	18	44	40	98	449	65
15.0	6.19	202	570	16	45	40	100	454	65
17.0	6.74	203	583	16	46	39	97	455	67
19.0	7.32	200	561	18	45	38	97	427	65
21.0	7.95	200	557	17	45	40	98	390	65
23.0	8.47	202	550	18	47	39	95	364	64
25.0	8.99	204	543	18	45	40	97	345	63
27.0	9.53	201	548	17	47	39	96	321	65
29.0	10.13	202	542	18	48	39	95	293	63
31.0	10.69	204	538	16	46	40	96	290	69
33.0	11.19	207	542	18	47	40	96	270	67
35.0	11.78	233	607	20	50	48	109	300	83
37.0	12.34	205	531	18	44	40	97	255	64
39.0	13.04	206	519	18	52	40	99	254	67
41.0	13.65	203	510	18	54	40	95	249	68
43.0	14.34	204	510	18	51	39	95	238	67
45.0	14.91	202	509	18	45	41	99	229	69
47.0	15.52	198	515	17	44	41	100	224	67
49.0	15.88	194	513	18	45	40	99	217	67
51.0	16.44	196	514	18	43	40	97	344	133
53.0	16.95	196	501	18	43	40	97	209	67
55.0	17.56	194	496	17	45	38	91	199	68
57.0	18.14	196	490	18	44	41	99	193	71
59.0	18.72	196	485	17	44	40	99	190	67
61.0	19.26	191	477	18	43	40	98	176	67
63.0	19.86	198	503	19	42	40	98	181	71
65.0	20.44	193	485	18	42	38	96	172	68
67.0	21.03	184	467	16	42	38	95	159	70
69.0	21.63	188	478	18	41	40	97	157	66
71.0	22.16	184	469	18	42	40	98	151	65
73.0	22.76	187	472	17	44	38	94	152	66
75.0	23.38	190	463	18	44	39	98	148	65
77.0	24.01	192	465	18	44	40	97	153	70
79.0	24.70	193	475	18	44	40	102	148	68

Table 3.27 Loch Long core LL1, trace element XRF results

DEPTH (cm)	g cm^{-2}	Cu (ppm)	Zn (ppm)	Pb (ppm)	Th (ppm)	Rb (ppm)	Sr (ppm)	Y (ppm)	Zr (ppm)	Nb (ppm)
0.5	0.18	59	436	318	17	106	189	26	166	16
1.5	0.65	54	402	287	16	103	177	25	170	15
2.5	1.14	64	460	337	16	110	170	27	172	16
3.5	1.56	67	469	347	15	111	177	28	175	16
4.5	1.93	62	458	339	17	108	160	26	176	16
5.5	2.50	63	467	348	16	109	162	26	170	16
6.5	2.92	64	469	347	17	108	161	27	167	16
7.5	3.43	65	479	355	17	109	156	28	177	17
8.5	3.99	65	485	364	17	109	152	28	179	17
9.5	4.56	66	491	361	16	109	151	27	178	17
11.0	5.16	72	526	388	18	115	158	28	184	17
13.0	5.69	69	533	401	19	112	150	28	170	17
15.0	6.19	65	539	409	18	111	146	27	169	15
17.0	6.74	67	556	425	19	113	149	27	172	16
19.0	7.32	61	535	414	20	110	147	26	168	16
21.0	7.95	58	513	409	19	108	155	26	167	16
23.0	8.47	57	492	389	19	109	155	26	172	17
25.0	8.99	56	465	366	18	109	144	26	169	16
27.0	9.53	55	448	360	18	110	147	27	173	17
29.0	10.13	52	426	346	16	109	142	26	169	16
31.0	10.69	57	437	357	17	113	148	28	173	17
33.0	11.19	53	412	339	19	111	140	27	174	17
35.0	11.78	81	478	398	20	133	169	32	205	20
37.0	12.34	50	394	337	18	110	143	27	167	16
39.0	13.04	52	384	336	17	112	146	29	171	16
41.0	13.65	53	377	339	18	112	145	28	172	16
43.0	14.34	50	340	321	18	113	146	27	171	17
45.0	14.91	51	302	296	17	115	151	28	177	17
47.0	15.52	49	296	289	17	114	147	28	178	16
49.0	15.88	48	283	277	17	113	145	28	179	18
51.0	16.44	51	286	280	17	113	143	26	178	17
53.0	16.95	51	272	280	17	115	147	27	179	17
55.0	17.56	46	245	264	17	118	146	26	181	17
57.0	18.14	42	213	237	17	117	144	27	181	16
59.0	18.72	41	215	240	15	116	144	27	181	17
61.0	19.26	37	194	218	16	117	144	28	175	17
63.0	19.86	40	188	217	16	122	145	27	178	18
65.0	20.44	35	180	195	16	119	141	28	176	18
67.0	21.03	28	159	166	16	117	142	27	172	18
69.0	21.63	29	158	164	15	117	142	26	171	18
71.0	22.16	28	149	160	16	115	142	26	168	17
73.0	22.76	29	153	162	16	116	145	27	172	18
75.0	23.38	27	147	146	15	118	141	26	173	18
77.0	24.01	28	147	138	16	119	140	27	179	19
79.0	24.70	28	154	125	14	120	138	27	178	18

Table 3.27 Loch Long core LL1, trace element XRF result (continued)

DEPTH (cm)	g cm^{-2}	Si (%)	Al (%)	Fe (%)	Mg (%)	Ca (%)	Na (%)	K (%)	Ti (%)	Mn (%)	P (%)
0.5	0.18	20.74	8.69	6.20	1.65	1.72	2.62	2.14	0.68	0.407	0.181
1.5	0.65	22.21	8.54	5.92	1.58	1.39	2.31	2.07	0.68	0.284	0.170
2.5	1.14	20.99	8.82	6.61	1.65	1.19	2.24	2.23	0.69	0.245	0.180
3.5	1.56	21.50	9.04	6.68	1.69	1.33	2.29	2.23	0.70	0.279	0.183
4.5	1.93	21.59	8.97	6.26	1.67	1.09	2.29	2.20	0.71	0.226	0.173
5.5	2.50	20.96	8.71	6.40	1.62	1.29	2.29	2.21	0.70	0.189	0.148
6.5	2.92	21.40	8.99	6.30	1.65	1.15	2.18	2.21	0.71	0.174	0.179
7.5	3.43	21.69	8.99	6.44	1.65	1.04	2.29	2.25	0.71	0.175	0.160
8.5	3.99	21.98	9.02	6.30	1.62	1.09	2.23	2.24	0.71	0.167	0.140
9.5	4.56	22.25	9.00	6.35	1.60	1.00	2.16	2.26	0.72	0.159	0.134
11.0	5.16	22.68	9.50	6.77	1.71	1.07	2.14	2.38	0.73	0.170	0.140
13.0	5.69	21.40	9.26	6.54	1.65	1.03	2.17	2.31	0.73	0.154	0.131
15.0	6.19	21.32	9.27	6.38	1.66	0.98	2.20	2.30	0.72	0.160	0.130
17.0	6.74	21.35	9.28	6.56	1.68	0.97	2.19	2.35	0.73	0.168	0.129
19.0	7.32	21.33	9.27	6.07	1.67	0.98	2.32	2.29	0.73	0.178	0.134
21.0	7.95	21.36	9.28	6.21	1.66	1.02	2.21	2.28	0.73	0.258	0.173
23.0	8.47	21.50	9.31	6.25	1.66	1.01	2.26	2.29	0.73	0.246	0.159
25.0	8.99	21.55	9.36	6.01	1.65	0.92	2.25	2.28	0.74	0.229	0.139
27.0	9.53	21.62	9.38	6.25	1.67	0.89	2.23	2.29	0.74	0.218	0.145
29.0	10.13	21.38	9.32	6.10	1.69	0.86	2.26	2.27	0.73	0.221	0.140
31.0	10.69	21.52	9.45	6.54	1.69	0.89	2.17	2.33	0.74	0.253	0.138
33.0	11.19	21.74	9.51	6.24	1.67	0.86	2.21	2.30	0.75	0.173	0.123
35.0	11.78	26.41	11.78	7.88	2.10	1.13	2.63	2.81	0.91	0.221	0.141
37.0	12.34	21.50	9.49	6.32	1.69	0.98	2.19	2.30	0.75	0.186	0.116
39.0	13.04	21.55	9.54	6.50	1.70	0.96	2.20	2.33	0.75	0.184	0.114
41.0	13.65	21.47	9.50	6.49	1.70	0.99	2.16	2.31	0.75	0.194	0.112
43.0	14.34	21.58	9.59	6.33	1.68	0.99	2.22	2.32	0.76	0.204	0.113
45.0	14.91	21.89	9.80	6.47	1.73	1.06	2.23	2.36	0.76	0.242	0.111
47.0	15.52	21.81	9.66	6.41	1.67	0.99	2.06	2.35	0.77	0.217	0.109
49.0	15.88	21.86	9.68	6.35	1.67	0.94	2.13	2.32	0.77	0.221	0.107
51.0	16.44	21.96	9.69	6.25	1.63	0.94	2.02	2.34	0.77	0.255	0.110
53.0	16.95	21.99	9.69	6.47	1.66	0.94	2.06	2.34	0.77	0.259	0.108
55.0	17.56	22.09	10.01	6.32	1.72	0.88	2.11	2.38	0.78	0.312	0.110
57.0	18.14	21.80	9.77	6.20	1.64	0.87	2.03	2.37	0.78	0.302	0.110
59.0	18.72	21.99	9.91	6.07	1.66	0.87	2.12	2.38	0.79	0.313	0.110
61.0	19.26	21.81	9.96	6.05	1.67	0.89	2.14	2.37	0.78	0.347	0.109
63.0	19.86	22.92	10.63	6.30	1.85	0.79	2.22	2.48	0.81	0.307	0.116
65.0	20.44	21.85	10.09	6.14	1.70	0.77	2.12	2.42	0.79	0.291	0.110
67.0	21.03	21.89	10.06	6.24	1.69	0.78	2.17	2.39	0.78	0.268	0.119
69.0	21.63	21.79	9.96	6.17	1.68	0.85	2.20	2.36	0.78	0.329	0.108
71.0	22.16	21.67	9.93	6.14	1.68	0.87	2.19	2.36	0.77	0.337	0.107
73.0	22.76	21.77	9.97	6.14	1.70	0.89	2.25	2.38	0.77	0.397	0.109
75.0	23.38	21.67	9.98	6.12	1.70	0.78	2.18	2.37	0.78	0.231	0.105
77.0	24.01	22.38	10.29	6.15	1.70	0.72	2.11	2.41	0.80	0.169	0.109
79.0	24.70	22.37	10.35	6.06	1.69	0.65	2.17	2.42	0.80	0.177	0.112

Table 3.28 Loch Long core LL1, XRF major element results

DEPTH (cm)	g cm^{-2}	^{210}Pb	+/-	^{226}Ra	+/-	excess ^{210}Pb.	+/-
0.5	0.20	275.8	25.6	118.2	8.2	163.2	18.9
1.5	0.36	247.1	22.9	137.8	7.9	113.2	12.3
2.5	0.68	279.2	24.8	80.5	4.2	205.8	21.2
3.5	0.98	258.6	18.1	77.0	4.0	188.1	16.4
4.5	1.23	197.5	15.6	79.6	4.3	122.1	11.7
5.5	1.53	242.6	18.3	70.7	4.0	178.1	16.7
6.5	1.81	195.5	18.9	69.8	3.3	130.3	14.1
7.5	2.12	130.4	11.5	75.9	4.0	56.5	5.8
8.5	2.51	195.1	25.0	68.7	3.6	131.0	18.1
9.5	2.87	131.2	16.8	63.2	3.4	70.5	9.8
11.0	3.36	147.8	18.6	53.2	2.8	98.1	13.4
13.0	4.08	127.7	16.0	55.4	2.7	75.0	10.1
15.0	4.67	109.0	13.9	49.8	2.5	61.5	8.4
17.0	5.31	96.3	12.0	47.3	2.3	52.5	7.0
19.0	5.68	77.4	12.6	45.8	2.4	33.0	5.6
21.0	6.26	78.4	10.2	52.9	2.6	26.5	3.7
23.0	6.82	72.2	9.1	48.2	2.3	25.7	3.5
25.0	7.43	61.9	7.8	47.3	2.3	15.2	2.1
27.0	7.81	51.0	6.6	46.6	2.2	4.7	0.6
29.0	8.18	62.7	8.6	49.4	2.4	13.8	2.0
31.0	8.67	57.8	7.5	49.3	2.6	8.7	1.2
33.0	9.12	31.2	4.2	50.0	2.4	-19.5	-2.8
35.0	9.69	34.4	4.4	49.2	2.4	-15.4	-2.1
37.0	10.23	37.5	5.5	51.2	2.4	-14.2	-2.2
39.0	10.77	35.0	4.9	51.5	2.4	-17.2	-2.5
41.0	11.29	63.7	8.4	53.3	2.7	10.9	1.5
43.0	11.72	77.6	9.8	48.0	2.3	30.8	4.2
45.0	12.24	38.1	5.2	51.7	2.5	-14.2	-2.1
47.0	12.71	36.2	4.9	52.3	2.5	-16.8	-2.4
49.0	13.17	42.4	6.0	50.2	2.5	-8.1	-1.2
51.0	13.63	58.7	7.5	49.7	2.3	9.4	1.3
53.0	14.07	42.1	5.6	52.3	2.6	-10.6	-1.5
55.0	14.59	51.7	6.9	52.3	2.5	-0.7	-0.1
57.0	14.98	76.4	9.9	53.2	2.8	24.3	3.4
59.0	15.52	27.4	4.0	35.1	1.9	-8.1	-1.3
61.0	15.93	63.1	5.8	64.0	2.6	-0.8	-0.1
63.0	16.40	66.8	8.8	52.0	2.8	15.4	2.2
65.0	16.95	61.8	7.9	53.5	2.5	8.7	1.2
67.0	17.46	39.7	5.2	55.5	2.9	-16.5	-2.3
69.0	17.95	54.5	6.9	55.5	2.6	-1.0	-0.1
71.5	18.74	51.8	6.5	50.5	2.4	1.4	0.2

Table 3.29 Loch Goil core GD2, natural radionuclide concentrations (Bq kg^{-1})

DEPTH (cm)	g cm^{-2}	^{228}Th	+/-	^{228}Ra	+/-	^{236}U	+/-
0.5	0.20	90.1	4.5	90.6	4.6	192.0	25.6
1.5	0.36	107.0	4.9	61.5	3.9	nd	nd
2.5	0.68	65.9	3.0	54.3	2.8	115.4	29.8
3.5	0.98	51.2	2.5	29.1	1.8	95.2	12.0
4.5	1.23	56.0	2.6	36.8	2.0	86.4	9.2
5.5	1.53	44.9	2.2	28.8	1.6	nd	nd
6.5	1.81	43.2	2.1	39.6	2.1	nd	nd
7.5	2.12	47.6	2.2	39.4	2.1	89.2	9.0
8.5	2.51	44.0	2.0	33.0	1.9	77.5	9.4
9.5	2.87	41.9	2.0	43.6	2.2	nd	nd
11.0	3.36	42.1	1.7	34.8	1.6	83.2	5.7
13.0	4.08	38.3	1.8	38.8	1.8	71.5	7.2
15.0	4.67	37.4	1.6	31.1	1.3	75.8	6.5
17.0	5.31	36.5	1.5	33.7	1.4	66.5	4.4
19.0	5.68	34.9	1.5	31.0	1.5	75.6	5.4
21.0	6.26	40.4	1.7	35.7	1.6	68.2	11.1
23.0	6.82	39.8	3.0	36.5	1.7	68.0	4.8
25.0	7.43	40.5	1.6	37.2	1.5	71.2	4.5
27.0	7.81	40.4	1.6	32.6	1.3	78.1	5.1
29.0	8.18	40.2	1.7	37.8	1.6	79.3	5.2
31.0	8.67	42.1	1.8	36.7	1.5	70.8	5.7
33.0	9.12	43.7	1.9	33.5	1.4	77.1	5.1
35.0	9.69	43.6	1.9	40.6	1.7	78.8	5.9
37.0	10.23	45.4	1.9	40.1	1.6	80.7	5.6
39.0	10.77	45.7	1.8	40.5	1.7	67.4	8.2
41.0	11.29	45.1	1.9	43.1	1.9	75.2	9.2
43.0	11.72	43.9	1.9	42.1	1.7	92.8	7.0
45.0	12.24	44.4	1.9	39.0	1.7	74.7	5.2
47.0	12.71	45.0	1.9	39.2	1.8	74.6	14.9
49.0	13.17	44.7	1.9	41.9	2.0	83.8	7.5
51.0	13.63	44.5	1.9	45.0	1.8	67.2	12.2
53.0	14.07	45.0	2.0	39.9	1.6	57.5	4.3
55.0	14.59	44.9	1.9	42.6	6.8	55.5	4.0
57.0	14.98	41.0	1.6	42.0	1.9	60.3	4.1
59.0	15.52	23.3	1.0	21.5	1.0	38.7	3.5
61.0	15.93	48.3	1.9	45.2	1.8	55.2	3.9
63.0	16.40	48.4	2.0	41.8	2.0	55.7	5.5
65.0	16.95	46.6	1.9	40.7	1.6	62.6	5.0
67.0	17.46	48.3	2.1	37.8	1.7	62.0	6.9
69.0	17.95	48.0	1.9	40.9	1.6	55.6	3.8
71.5	18.74	44.8	1.8	41.0	1.6	51.9	3.7

Table 3.29 Loch Goil core GD2, natural radionuclide concentrations (Bq kg^{-1}) continued

DEPTH (cm)	g cm^{-2}	^{137}Cs	+/-	^{134}Cs	+/-	^{241}Am	+/-
0.5	0.20	666.6	15.4	57.1	2.6	nd	nd
1.5	0.36	760.6	17.0	6.0	0.4	nd	nd
2.5	0.68	881.0	18.5	7.4	0.5	16.9	4.3
3.5	0.98	897.6	18.8	1.5	0.1	16.3	1.3
4.5	1.23	920.3	19.3	2.9	0.3	16.3	1.0
5.5	1.53	913.6	19.7	2.1	0.2	15.3	1.1
6.5	1.81	424.4	8.9	1.2	0.1	nd	nd
7.5	2.12	282.2	6.3	nd	nd	nd	nd
8.5	2.51	211.2	4.5	1.7	0.2	nd	nd
9.5	2.87	141.2	3.1	nd	nd	nd	nd
11.0	3.36	101.8	2.3	nd	nd	nd	nd
13.0	4.08	79.2	2.1	nd	nd	nd	nd
15.0	4.67	103.2	2.4	nd	nd	nd	nd
17.0	5.31	118.6	2.6	nd	nd	nd	nd
19.0	5.68	106.6	2.3	nd	nd	nd	nd
21.0	6.26	94.1	2.1	nd	nd	nd	nd
23.0	6.82	49.2	1.1	nd	nd	nd	nd
25.0	7.43	38.6	0.9	nd	nd	nd	nd
27.0	7.81	43.7	1.0	nd	nd	nd	nd
29.0	8.18	34.7	0.8	nd	nd	nd	nd
31.0	8.67	25.3	0.7	nd	nd	nd	nd
33.0	9.12	16.3	0.5	nd	nd	nd	nd
35.0	9.69	8.0	0.4	nd	nd	nd	nd
37.0	10.23	5.3	0.2	nd	nd	nd	nd
39.0	10.77	4.4	0.2	nd	nd	nd	nd
41.0	11.29	4.0	0.2	nd	nd	nd	nd
43.0	11.72	4.4	0.3	nd	nd	nd	nd
45.0	12.24	5.1	0.2	nd	nd	nd	nd
47.0	12.71	3.0	0.2	nd	nd	nd	nd
49.0	13.17	2.1	0.2	nd	nd	nd	nd
51.0	13.63	1.3	0.1	nd	nd	nd	nd
53.0	14.07	1.7	0.2	nd	nd	nd	nd
55.0	14.59	0.6	0.1	nd	nd	nd	nd
57.0	14.98	0.8	0.1	nd	nd	nd	nd
59.0	15.52	0.3	0.0	nd	nd	nd	nd
61.0	15.93	0.4	0.0	nd	nd	nd	nd
63.0	16.40	0.2	0.0	nd	nd	nd	nd
65.0	16.95	0.2	0.0	nd	nd	nd	nd
67.0	17.46	nd	nd	nd	nd	nd	nd
69.0	17.95	0.1	0.0	nd	nd	nd	nd
71.5	18.74	0.5	0.0	nd	nd	nd	nd

Table 3.30 Loch Goil core GD2, manmade radionuclide concentrations (Bq kg^{-1})

DEPTH (cm)	g cm^{-2}	$^{206}Pb/^{207}Pb$	+/-	$^{208}Pb/^{207}Pb$	+/-	$^{208}Pb/^{206}Pb$	+/-
0.5	0.20	1.1449	0.0019	2.3710	0.0172	2.0710	0.0179
1.5	0.36	1.1470	0.0025	2.4124	0.0086	2.1033	0.0074
2.5	0.68	1.1448	0.0021	2.4333	0.0089	2.1256	0.0057
3.5	0.98	1.1452	0.0022	2.4537	0.0071	2.1426	0.0077
4.5	1.23	1.1452	0.0008	2.4576	0.0043	2.1459	0.0037
5.5	1.53	1.1515	0.0037	2.4423	0.0033	2.1210	0.0089
6.5	1.81	1.1507	0.0027	2.4420	0.0027	2.1222	0.0069
7.5	2.12	1.1540	0.0019	2.4438	0.0030	2.1178	0.0051
8.5	2.51	1.1568	0.0024	2.4477	0.0047	2.1158	0.0083
9.5	2.87	1.1589	0.0011	2.4400	0.0030	2.1055	0.0021
11.0	3.36	1.1573	0.0021	2.4377	0.0032	2.1064	0.0050
13.0	4.08	1.1536	0.0011	2.4456	0.0071	2.1199	0.0073
15.0	4.67	1.1556	0.0035	2.4429	0.0054	2.1140	0.0078
17.0	5.31	1.1574	0.0032	2.4486	0.0058	2.1156	0.0068
19.0	5.68	1.1647	0.0037	2.4479	0.0041	2.1015	0.0088
21.0	6.26	1.1599	0.0025	2.4433	0.0066	2.1065	0.0054
23.0	6.82	1.1595	0.0016	2.4481	0.0055	2.1114	0.0031
25.0	7.43	1.1644	0.0024	2.4521	0.0085	2.1059	0.0055
27.0	7.81	1.1678	0.0023	2.4556	0.0074	2.1028	0.0035
29.0	8.18	1.1735	0.0058	2.4549	0.0096	2.0920	0.0130
31.0	8.67	1.1784	0.0035	2.4958	0.0062	2.1203	0.0076
33.0	9.12	1.1775	0.0054	2.5062	0.0087	2.1307	0.0026
35.0	9.69	1.1722	0.0095	2.4901	0.0255	2.1266	0.0121
37.0	10.23	1.1704	0.0268	2.4910	0.0125	2.1306	0.0132
39.0	10.77	1.1725	0.0031	2.4976	0.0063	2.1324	0.0070
41.0	11.29	1.1746	0.0019	2.4990	0.0057	2.1297	0.0042
43.0	11.72	1.1725	0.0044	2.5049	0.0123	2.1385	0.0075
45.0	12.24	1.1709	0.0032	2.5040	0.0074	2.1407	0.0039
47.0	12.71	1.1721	0.0020	2.5099	0.0058	2.1437	0.0069
49.0	13.17	1.1724	0.0018	2.4977	0.0086	2.1326	0.0071
51.0	13.63	1.1722	0.0039	2.5005	0.0055	2.1354	0.0086
53.0	14.07	1.1682	0.0039	2.4970	0.0304	2.1398	0.0305
55.0	14.59	1.1681	0.0049	2.5034	0.0073	2.1455	0.0091
57.0	14.98	1.1695	0.0033	2.5009	0.0047	2.1407	0.0053
59.0	15.52	1.1214	0.0044	2.4503	0.0064	2.1873	0.0071
61.0	15.93	1.1716	0.0011	2.5153	0.0068	2.1491	0.0041
63.0	16.40	1.1711	0.0032	2.4731	0.0581	2.1140	0.0536
65.0	16.95	1.1714	0.0030	2.5060	0.0024	2.1415	0.0053
67.0	17.46	1.1702	0.0034	2.4954	0.0074	2.1347	0.0072
69.0	17.95	1.1729	0.0011	2.5053	0.0048	2.1383	0.0053
71.5	18.74	1.1724	0.0041	2.5007	0.0091	2.1351	0.0088

Table 3.31 Loch Goil core GD2, Pb isotope results

DEPTH (cm)	g cm^{-2}	V (ppm)	Ba (ppm)	Sc (ppm)	La (ppm)	Nd (ppm)	Ce (ppm)	Cr (ppm)	Ni (ppm)
0.5	0.20								
1.5	0.36	219	509	14	41	35	87	300	55
2.5	0.68	229	523	15	44	37	92	348	58
3.5	0.98	228	537	15	44	37	94	344	58
4.5	1.23	228	557	16	41	36	92	339	59
5.5	1.53	235	525	15	41	34	89	341	59
6.5	1.81	235	492	15	41	32	83	356	60
7.5	2.12	250	502	16	41	36	88	424	62
8.5	2.51	254	520	16	44	38	92	445	65
9.5	2.87	254	506	17	44	38	96	430	65
11.0	3.36	261	535	16	46	38	94	425	76
13.0	4.08	264	520	16	44	38	97	392	69
15.0	4.67	260	495	15	45	38	93	294	63
17.0	5.31	258	461	16	42	35	84	241	63
19.0	5.68	270	493	17	45	38	94	240	65
21.0	6.26	264	493	16	45	38	92	248	61
23.0	6.82	266	513	17	45	40	98	255	63
25.0	7.43	259	503	17	46	39	99	235	63
27.0	7.81	252	488	16	47	41	98	222	63
29.0	8.18	244	477	17	46	38	93	208	61
31.0	8.67	242	500	17	45	37	91	209	60
33.0	9.12	243	493	17	46	40	99	207	63
35.0	9.69	248	523	18	48	41	104	197	66
37.0	10.23	235	532	20	47	41	104	158	65
39.0	10.77	228	521	19	46	40	102	149	62
41.0	11.29	233	514	19	48	41	102	152	63
43.0	11.72	229	519	19	49	40	99	148	64
45.0	12.24	228	515	19	48	41	105	147	64
47.0	12.71	227	509	18	49	41	101	144	62
49.0	13.17	228	520	18	49	42	102	141	64
51.0	13.63	225	507	18	48	41	101	136	63
53.0	14.07	220	491	17	47	42	101	135	64
55.0	14.59	221	500	18	48	42	105	130	63
57.0	14.98	218	501	18	47	39	99	127	62
59.0	15.52	219	503	18	48	41	101	127	61
61.0	15.93	218	495	18	48	41	100	128	62
63.0	16.40	224	512	19	48	43	104	129	62
65.0	16.95	227	535	18	47	43	106	129	60
67.0	17.46	226	519	18	48	42	104	128	61
69.0	17.95	228	530	18	49	40	103	128	61
71.5	18.74	228	540	18	51	40	101	128	59

Table 3.32 Loch Goil core GD2 XRF trace element results

DEPTH (cm)	g cm^{-2}	Cu (ppm)	Zn (ppm)	Pb (ppm)	Th (ppm)	Rb (ppm)	Sr (ppm)	Y (ppm)	Zr (ppm)	Nb (ppm)
0.5	0.20									
1.5	0.36	60	470	318	16	100	242	25	146	13
2.5	0.68	67	528	359	18	104	190	26	145	14
3.5	0.98	68	534	355	18	106	178	26	149	14
4.5	1.23	68	525	346	16	106	180	26	145	14
5.5	1.53	69	554	349	18	105	174	25	142	14
6.5	1.81	65	565	383	17	100	184	25	140	14
7.5	2.12	66	645	435	19	101	169	25	137	13
8.5	2.51	66	760	459	18	101	164	26	142	13
9.5	2.87	65	888	464	19	100	174	27	140	14
11.0	3.36	74	1081	479	19	103	213	29	148	14
13.0	4.08	68	1038	481	18	103	195	28	147	14
15.0	4.67	61	626	409	18	104	183	26	143	14
17.0	5.31	54	528	375	17	102	186	25	140	14
19.0	5.68	60	542	382	16	106	188	27	149	15
21.0	6.26	55	541	393	16	103	163	27	146	15
23.0	6.82	54	500	418	17	107	145	27	146	15
25.0	7.43	52	400	386	17	109	151	27	151	15
27.0	7.81	52	366	356	18	110	166	28	152	16
29.0	8.18	49	345	327	16	107	165	27	150	15
31.0	8.67	48	347	318	15	107	159	27	152	16
33.0	9.12	52	331	325	16	113	160	28	156	16
35.0	9.69	48	270	288	16	119	157	29	165	17
37.0	10.23	35	175	169	16	123	152	29	172	17
39.0	10.77	27	160	157	14	117	150	27	162	17
41.0	11.29	31	166	168	15	119	157	27	162	16
43.0	11.72	29	160	161	16	120	152	27	165	17
45.0	12.24	29	155	155	14	120	150	28	163	17
47.0	12.71	26	144	146	15	120	152	28	162	16
49.0	13.17	26	142	140	17	123	153	28	164	17
51.0	13.63	24	136	125	16	124	147	28	166	17
53.0	14.07	26	137	130	16	124	152	29	165	17
55.0	14.59	24	128	100	17	124	147	27	169	18
57.0	14.98	21	124	94	16	122	151	27	168	17
59.0	15.52	22	123	89	15	122	151	28	169	17
61.0	15.93	21	124	92	16	122	153	28	168	17
63.0	16.40	23	126	92	16	125	155	29	169	18
65.0	16.95	22	121	80	16	125	152	28	175	18
67.0	17.46	21	122	83	15	124	151	28	172	18
69.0	17.95	21	120	80	15	125	148	28	175	18
71.5	18.74	19	117	78	15	122	147	28	169	17

Table 3.32 Loch Goil core GD2, XRF trace element results (continued)

DEPTH (cm)	g cm^{-2}	Si (%)	Al (%)	Fe (%)	Mg (%)	Ca (%)	Na (%)	K (%)	Ti (%)	Mn (%)	P (%)
0.5	0.20										
1.5	0.36	16.30	7.51	5.82	1.68	1.78	3.57	2.08	0.53	1.97	0.392
2.5	0.68	17.48	8.15	6.58	1.73	1.87	2.96	2.07	0.58	1.45	0.347
3.5	0.98	18.12	8.42	6.57	1.73	1.64	2.52	2.12	0.60	0.93	0.219
4.5	1.23	18.30	8.47	6.58	1.74	1.53	2.67	2.15	0.60	0.95	0.177
5.5	1.53	18.05	8.47	6.56	1.78	1.58	2.90	2.28	0.59	1.16	0.172
6.5	1.81	17.74	8.69	6.49	1.74	1.57	2.94	2.23	0.59	1.08	0.166
7.5	2.12	16.96	8.08	6.84	1.71	1.81	2.56	2.00	0.57	1.69	0.173
8.5	2.51	17.34	8.38	6.89	1.72	1.38	2.57	2.02	0.59	1.05	0.179
9.5	2.87	17.68	8.58	6.64	1.71	1.24	2.52	2.10	0.60	0.72	0.146
11.0	3.36	17.83	8.67	6.07	1.75	1.43	2.42	2.06	0.61	1.02	0.169
13.0	4.08	18.03	8.90	6.65	1.75	1.79	2.20	2.03	0.63	1.52	0.150
15.0	4.67	17.92	8.65	6.87	1.78	1.79	2.27	2.09	0.62	1.74	0.152
17.0	5.31	17.64	8.64	6.89	1.82	1.87	2.50	2.05	0.60	1.63	0.147
19.0	5.68	17.43	8.61	6.73	1.81	2.07	2.37	2.00	0.60	2.11	0.152
21.0	6.26	18.30	8.97	7.16	1.86	2.02	2.57	2.21	0.63	1.98	0.151
23.0	6.82	18.24	8.84	7.05	1.82	1.38	2.50	2.16	0.62	1.09	0.138
25.0	7.43	18.94	9.21	6.47	1.81	0.99	2.56	2.27	0.66	0.48	0.121
27.0	7.81	19.00	9.35	6.43	1.84	1.15	2.54	2.26	0.67	0.65	0.119
29.0	8.18	18.75	9.33	6.63	1.83	1.44	2.46	2.29	0.66	1.01	0.125
31.0	8.67	18.74	9.19	6.51	1.83	1.46	2.49	2.22	0.66	1.18	0.126
33.0	9.12	18.82	9.14	6.37	1.75	1.32	2.36	2.22	0.66	1.16	0.125
35.0	9.69	19.32	9.53	6.68	1.77	1.24	2.25	2.31	0.68	1.02	0.129
37.0	10.23	19.88	10.04	7.38	1.87	0.94	2.46	2.44	0.70	0.62	0.120
39.0	10.77	20.26	10.27	6.99	1.78	0.85	2.32	2.52	0.73	0.51	0.110
41.0	11.29	19.77	10.07	6.26	1.75	0.97	2.33	2.44	0.72	0.77	0.116
43.0	11.72	20.30	10.44	6.35	1.88	1.09	2.49	2.47	0.71	0.96	0.123
45.0	12.24	19.86	10.08	6.43	1.75	0.92	2.35	2.49	0.72	0.61	0.122
47.0	12.71	19.94	10.19	6.44	1.75	0.88	2.34	2.51	0.72	0.58	0.114
49.0	13.17	20.00	10.16	6.16	1.72	0.97	2.23	2.50	0.72	0.73	0.120
51.0	13.63	19.94	10.23	6.51	1.71	0.89	2.31	2.49	0.72	0.59	0.116
53.0	14.07	20.22	10.38	6.46	1.72	0.72	2.28	2.52	0.74	0.31	0.112
55.0	14.59	20.17	10.33	6.56	1.69	0.86	2.15	2.50	0.73	0.53	0.116
57.0	14.98	20.08	10.33	6.76	1.69	0.76	2.19	2.56	0.73	0.42	0.112
59.0	15.52	19.79	10.18	6.66	1.69	0.92	2.15	2.50	0.73	0.80	0.117
61.0	15.93	19.85	10.29	6.85	1.66	0.89	2.08	2.50	0.73	0.68	0.120
63.0	16.40	19.74	10.19	6.82	1.68	0.93	2.08	2.47	0.73	0.80	0.118
65.0	16.95	19.97	10.32	7.12	1.65	0.85	2.09	2.54	0.73	0.60	0.116
67.0	17.46	19.83	10.25	7.02	1.63	0.84	2.17	2.55	0.73	0.57	0.116
69.0	17.95	19.97	10.35	6.93	1.65	0.83	2.11	2.55	0.73	0.63	0.116
71.5	18.74	19.58	10.21	7.19	1.68	0.73	2.18	2.56	0.74	0.38	0.111
		19.61	10.24	6.96	1.64	0.79	2.22	2.49	0.73	0.50	0.114

Table 3.33 Loch Goil core GD2, XRF major element results

DEPTH (cm)	g cm^{-2}	^{210}Pb	+/-	^{226}Ra	+/-	excess ^{210}Pb	+/-
0.5	0.28	65.8	5.4	21.6	1.0	47.3	4.4
1.5	0.60	72.5	6.3	22.5	1.1	54.3	5.5
2.5	1.05	46.6	4.2	18.5	0.9	30.6	3.1
3.5	1.59	69.5	5.9	21.6	1.1	52.0	5.2
4.5	2.27	62.4	5.9	20.6	1.1	45.5	4.9
5.5	2.86	45.5	4.2	20.6	1.0	27.0	2.8
6.5	3.46	52.8	4.0	21.8	1.2	33.7	3.2
7.5	4.12	56.6	5.2	21.2	1.0	38.5	4.0
8.5	4.84	43.4	4.0	22.4	1.1	22.9	2.4
9.5	5.50	53.9	4.8	18.1	0.9	39.0	4.0
11.0	6.74	26.3	2.6	25.2	1.2	1.3	0.1
13.0	7.99	32.4	3.1	22.9	1.2	10.4	1.1
15.0	9.18	26.8	2.4	19.4	1.0	8.1	0.8
17.0	10.50	16.4	1.6	17.8	0.9	-1.5	-0.2
19.0	11.80	15.4	1.5	22.2	1.1	-7.4	-0.8
21.0	12.87	20.9	1.9	25.6	1.2	-5.1	-0.5
23.0	13.90	37.5	3.5	21.9	1.1	17.0	1.8
25.0	15.02	13.6	1.3	21.6	1.1	-8.7	-1.0
27.0	16.11	20.0	2.0	25.2	1.3	-5.7	-0.6
29.0	17.17	28.2	2.9	23.9	1.2	4.6	0.5
31.0	18.26	19.8	1.9	26.0	1.3	-6.8	-0.8
33.0	19.29	26.5	2.6	29.0	1.4	-2.7	-0.3
35.0	20.38	37.0	3.5	28.1	1.4	9.8	1.0
37.0	21.48	14.0	1.5	27.0	1.4	-14.2	-1.7
39.0	22.49	30.6	2.8	27.3	1.4	3.6	0.4
41.0	23.38	21.9	2.3	29.2	1.6	-8.1	-0.9
43.0	24.39	19.6	1.7	29.6	1.4	-11.0	-1.1
45.0	25.49	-2.6	-0.3	25.8	1.3	-31.3	-3.7
47.0	26.46	21.9	1.9	29.4	1.4	-8.3	-0.8
49.0	27.51	1.0	0.1	28.5	1.4	-30.4	-3.5
51.0	28.62	43.3	4.0	33.1	1.6	11.2	1.2
53.0	29.65	41.2	3.5	28.7	1.5	13.9	1.4
55.0	30.69	35.5	2.9	31.3	1.5	4.6	0.4
57.0	31.66	23.4	2.1	32.0	1.7	-9.6	-1.0
59.0	32.65	34.8	3.0	32.7	1.6	2.3	0.2
61.0	33.60	35.6	3.2	28.5	1.5	7.7	0.8
63.0	34.53	5.3	0.5	12.7	0.6	-8.2	-0.9
65.0	35.65	27.1	2.7	31.4	1.6	-4.8	-0.5
67.0	36.97	36.7	3.4	31.3	1.5	5.9	0.6

Table 3.34 Loch Fyne core FS, natural radionuclide concentrations (Bq kg^{-1})

DEPTH (cm)	g cm^{-2}	^{228}Th	+/-	^{228}Ra	+/-	^{238}U	+/-
0.5	0.28	29.0	1.3	29.0	1.2	44.5	3.9
1.5	0.60	30.7	1.4	26.7	1.2	33.4	3.8
2.5	1.05	23.2	1.0	23.6	1.0	39.4	4.3
3.5	1.59	26.0	1.1	23.3	1.0	30.5	3.6
4.5	2.27	26.5	1.2	22.8	1.1	38.2	4.5
5.5	2.86	25.8	1.2	24.6	1.2	34.8	4.3
6.5	3.46	28.1	1.3	22.7	1.0	36.3	3.9
7.5	4.12	23.3	1.0	23.6	1.0	35.4	5.4
8.5	4.84	25.7	1.2	31.1	1.3	41.5	5.4
9.5	5.50	24.8	1.1	26.6	1.2	34.9	4.5
11.0	6.74	24.5	1.1	22.7	1.0	36.2	5.0
13.0	7.99	24.6	1.1	25.3	1.1	41.6	5.4
15.0	9.18	25.6	1.1	27.2	1.2	42.1	5.4
17.0	10.50	26.0	1.1	28.9	1.3	32.9	3.5
19.0	11.80	28.7	1.2	22.6	1.0	32.6	4.6
21.0	12.87	28.0	1.2	29.2	1.2	46.5	4.9
23.0	13.90	28.1	1.2	23.7	1.1	51.7	6.1
25.0	15.02	30.9	1.4	28.7	1.2	52.4	5.9
27.0	16.11	30.7	1.2	32.1	1.4	45.2	4.8
29.0	17.17	32.2	1.4	34.5	1.5	52.6	5.7
31.0	18.26	33.1	1.3	31.1	1.3	42.5	4.7
33.0	19.29	35.7	1.7	34.1	1.5	44.8	4.9
35.0	20.38	35.8	1.4	30.8	1.4	50.3	5.9
37.0	21.48	36.9	1.6	33.1	1.5	40.9	4.6
39.0	22.49	34.5	1.5	30.2	1.4	48.7	5.9
41.0	23.38	0.5	0.0	33.8	1.4	58.1	6.8
43.0	24.39	35.7	1.5	37.3	1.6	45.7	4.7
45.0	25.49	nd	nd	31.3	1.4	33.0	3.9
47.0	26.46	0.4	0.0	33.6	1.4	42.9	4.3
49.0	27.51	0.4	0.0	33.5	1.4	38.8	4.9
51.0	28.62	0.7	0.0	34.7	1.5	48.8	5.4
53.0	29.65	1.1	0.0	37.1	1.5	35.3	3.9
55.0	30.69	0.4	0.0	33.4	1.4	44.1	4.6
57.0	31.66	nd	nd	32.1	1.4	47.4	6.4
59.0	32.65	0.8	0.0	35.3	1.4	47.9	5.0
61.0	33.60	0.3	0.0	nd	nd	45.3	5.0
63.0	34.53	nd	nd	14.3	0.6	27.4	3.6
65.0	35.65	0.4	0.0	33.1	1.4	56.7	6.5
67.0	36.97	0.5	0.0	33.7	1.3	48.4	5.1

Table 3.34 Loch Fyne core FS, natural radionuclide concentrations (Bq kg^{-1}) (continued)

DEPTH (cm)	g cm^{-2}	^{137}Cs	+/-	^{134}Cs	+/-	^{241}Am	+/-
0.5	0.28	118.0	2.5	5.2	0.3	4.2	0.3
1.5	0.60	148.9	3.1	1.9	0.2	5.0	0.6
2.5	1.05	152.9	3.3	2.4	0.2	4.4	0.3
3.5	1.59	204.4	4.5	4.9	0.3	4.6	0.3
4.5	2.27	226.7	4.9	1.9	0.2	5.0	0.4
5.5	2.86	226.8	5.4	1.2	0.1	4.1	0.4
6.5	3.46	218.0	4.8	1.6	0.2	3.6	0.2
7.5	4.12	182.0	4.0	1.7	0.1	nd	nd
8.5	4.84	148.3	3.2	nd	nd	nd	nd
9.5	5.50	131.0	2.9	nd	nd	nd	nd
11.0	6.74	111.2	2.5	0.9	0.1	nd	nd
13.0	7.99	59.4	1.5	nd	nd	nd	nd
15.0	9.18	32.2	0.9	nd	nd	nd	nd
17.0	10.50	29.1	0.8	nd	nd	nd	nd
19.0	11.80	32.3	0.9	nd	nd	nd	nd
21.0	12.87	34.2	0.9	nd	nd	nd	nd
23.0	13.90	31.0	0.7	nd	nd	nd	nd
25.0	15.02	14.8	0.5	nd	nd	nd	nd
27.0	16.11	7.3	0.3	nd	nd	nd	nd
29.0	17.17	2.3	0.2	nd	nd	nd	nd
31.0	18.26	1.5	0.1	nd	nd	nd	nd
33.0	19.29	0.4	0.0	nd	nd	nd	nd
35.0	20.38	1.1	0.1	nd	nd	nd	nd
37.0	21.48	1.0	0.1	nd	nd	nd	nd
39.0	22.49	0.7	0.1	nd	nd	nd	nd
41.0	23.38	nd	nd	nd	nd	nd	nd
43.0	24.39	0.3	0.0	nd	nd	nd	nd
45.0	25.49	0.3	0.0	nd	nd	nd	nd
47.0	26.46	0.2	0.0	nd	nd	nd	nd
49.0	27.51	nd	nd	nd	nd	nd	nd
51.0	28.62	0.6	0.1	nd	nd	nd	nd
53.0	29.65	0.2	0.0	nd	nd	nd	nd
55.0	30.69	0.1	0.0	nd	nd	nd	nd
57.0	31.66	1.1	0.1	nd	nd	nd	nd
59.0	32.65	0.5	0.0	nd	nd	nd	nd
61.0	33.60	nd	nd	nd	nd	nd	nd
63.0	34.53	0.4	0.1	nd	nd	nd	nd
65.0	35.65	nd	nd	nd	nd	nd	nd
67.0	36.97	nd	nd	nd	nd	nd	nd

Table 3.35 Loch Fyne core FS, manmade radionuclide concentrations (Bq kg^{-1})

DEPTH (cm)	g cm^{-2}	V (ppm)	Ba (ppm)	Sc (ppm)	La (ppm)	Nd (ppm)	Ce (ppm)	Cr (ppm)	Ni (ppm)
0.5	0.28								
1.5	0.60	101	365	13	27	26	62	86	32
2.5	1.05	106	385	13	28	25	59	87	34
3.5	1.59	108	377	14	29	26	61	90	32
4.5	2.27	106	378	14	27	27	62	87	34
5.5	2.86	109	379	13	31	28	64	92	35
6.5	3.46	107	371	14	29	29	64	88	33
7.5	4.12	100	361	12	28	27	60	84	32
8.5	4.84	108	375	14	30	26	60	89	34
9.5	5.50	107	388	13	28	26	61	92	33
11.0	6.74	104	379	13	27	25	59	85	32
13.0	7.99	106	368	12	31	28	66	82	31
15.0	9.18	101	355	12	31	27	64	76	31
17.0	10.50	101	364	12	31	26	62	78	32
19.0	11.80	107	374	14	30	28	65	80	32
21.0	12.87	98	358	13	26	28	61	82	35
23.0	13.90	103	381	13	28	27	63	89	36
25.0	15.02	107	406	13	30	27	63	83	34
27.0	16.11	104	409	13	31	30	67	87	37
29.0	17.17	111	445	15	30	29	64	89	37
31.0	18.26	119	463	15	31	31	71	97	40
33.0	19.29	122	501	16	33	31	74	103	43
35.0	20.38	122	499	16	32	31	70	104	42
37.0	21.48	124	512	16	34	32	75	105	42
39.0	22.49	123	502	16	35	32	75	100	42
41.0	23.38	125	510	16	35	33	75	104	44
43.0	24.39	124	509	17	34	32	74	105	43
45.0	25.49	121	507	17	32	32	76	104	44
47.0	26.46	123	509	16	34	31	74	105	43
49.0	27.51	123	526	16	32	32	74	102	42
51.0	28.62	123	535	15	33	30	71	102	42
53.0	29.65	125	520	16	34	32	74	102	41
55.0	30.69	127	537	16	33	32	72	104	42
57.0	31.66	126	537	17	34	32	74	106	43
59.0	32.65	126	528	17	31	32	73	105	44
61.0	33.60	127	545	16	34	33	75	106	45
63.0	34.53	126	526	17	35	34	80	107	44
65.0	35.65	127	551	15	35	33	76	110	45
67.0	36.97	126	536	16	34	33	73	108	44

Table 3.36 Loch Fyne core FS, XRF trace element results

DEPTH (cm)	g cm^{-2}	Cu (ppm)	Zn (ppm)	Pb (ppm)	Th (ppm)	Rb (ppm)	Sr (ppm)	Y (ppm)	Zr (ppm)	Nb (ppm)
0.5	0.28									
1.5	0.60	11	133	42	10	71	195	19	206	12
2.5	1.05	14	137	43	9	73	196	21	222	12
3.5	1.59	14	138	44	9	74	192	20	211	12
4.5	2.27	12	139	46	9	75	190	20	221	12
5.5	2.86	13	141	47	10	76	191	21	220	13
6.5	3.46	12	143	46	9	77	191	21	225	12
7.5	4.12	11	133	42	9	73	204	21	219	12
8.5	4.84	12	135	45	9	74	193	21	230	12
9.5	5.50	12	134	44	10	75	192	20	220	12
11.0	6.74	12	125	39	8	71	188	20	214	12
13.0	7.99	9	106	36	9	70	216	21	220	12
15.0	9.18	7	80	23	8	67	226	20	221	12
17.0	10.50	7	76	20	8	72	218	20	214	12
19.0	11.80	6	75	20	10	73	200	20	212	12
21.0	12.87	7	74	21	9	74	205	21	237	12
23.0	13.90	5	73	18	10	77	203	21	223	13
25.0	15.02	4	73	15	9	80	203	22	228	13
27.0	16.11	6	79	17	10	86	204	21	226	14
29.0	17.17	5	79	15	9	88	207	22	231	13
31.0	18.26	7	87	18	10	97	207	22	215	14
33.0	19.29	6	93	17	10	105	210	24	222	14
35.0	20.38	6	92	17	11	105	209	24	219	14
37.0	21.48	6	95	18	11	107	209	24	217	15
39.0	22.49	5	95	17	11	106	205	24	214	14
41.0	23.38	6	95	17	11	108	205	23	214	14
43.0	24.39	6	99	18	12	107	206	24	214	15
45.0	25.49	7	94	18	10	107	207	24	215	15
47.0	26.46	6	95	16	11	109	209	24	214	14
49.0	27.51	6	95	17	11	107	208	24	224	15
51.0	28.62	6	95	16	11	109	210	23	225	14
53.0	29.65	6	96	18	11	110	210	24	222	14
55.0	30.69	6	96	18	11	111	211	24	225	14
57.0	31.66	7	98	17	10	111	212	23	217	14
59.0	32.65	6	99	17	11	112	212	25	219	14
61.0	33.60	7	99	18	11	113	209	24	215	14
63.0	34.53	7	100	18	11	113	211	24	215	14
65.0	35.65	7	101	16	11	115	210	25	214	14
67.0	36.97	7	101	18	11	114	210	24	218	15

Table 3.36 Loch Fyne core FS, XRF trace element results (continued)

DEPTH (cm)	g cm^{-2}	Si (%)	Al (%)	Fe (%)	Mg (%)	Ca (%)	Na (%)	K (%)	Ti (%)	Mn (%)	P (%)
0.5	0.28	30.73	6.09	3.35	1.23	1.99	2.03	1.49	0.56	0.184	0.089
1.5	0.60	30.55	6.08	3.34	1.19	2.00	1.96	1.51	0.56	0.125	0.088
2.5	1.05	31.65	6.31	3.45	1.23	2.04	2.02	1.57	0.58	0.084	0.089
3.5	1.59	30.50	6.19	3.40	1.21	2.01	1.88	1.56	0.57	0.074	0.088
4.5	2.27	30.04	6.29	3.43	1.24	1.96	1.91	1.59	0.59	0.070	0.084
5.5	2.86	30.44	6.34	3.47	1.24	1.98	1.91	1.62	0.59	0.070	0.091
6.5	3.46	30.03	6.40	3.52	1.27	1.95	1.91	1.68	0.59	0.071	0.087
7.5	4.12	30.24	6.12	3.36	1.18	2.52	1.84	1.56	0.57	0.068	0.085
8.5	4.84	30.49	6.28	3.44	1.21	1.99	1.90	1.63	0.59	0.066	0.084
9.5	5.50	30.54	6.26	3.45	1.22	1.97	1.83	1.63	0.59	0.064	0.085
11.0	6.74	30.95	6.17	3.36	1.21	1.94	1.87	1.59	0.58	0.062	0.083
13.0	7.99	30.17	5.89	3.28	1.15	2.72	1.75	1.51	0.56	0.063	0.085
15.0	9.18	30.55	5.81	3.28	1.13	2.82	1.75	1.47	0.56	0.061	0.082
17.0	10.50	30.04	6.11	3.38	1.20	2.72	1.77	1.56	0.58	0.060	0.081
19.0	11.80	30.63	6.24	3.41	1.22	2.14	1.86	1.62	0.60	0.063	0.080
21.0	12.87	30.60	6.25	3.44	1.24	2.20	1.86	1.63	0.60	0.063	0.081
23.0	13.90	30.24	6.42	3.54	1.26	2.18	1.87	1.70	0.59	0.060	0.078
25.0	15.02	29.88	6.60	3.66	1.34	2.12	1.87	1.80	0.60	0.059	0.081
27.0	16.11	29.19	6.91	3.80	1.44	2.11	1.85	1.92	0.61	0.066	0.082
29.0	17.17	29.07	7.05	3.86	1.49	2.17	1.87	1.97	0.62	0.062	0.081
31.0	18.26	27.87	7.49	4.12	1.60	2.18	1.88	2.16	0.62	0.069	0.078
33.0	19.29	27.27	7.92	4.33	1.72	2.15	1.90	2.32	0.63	0.070	0.079
35.0	20.38	27.45	7.88	4.31	1.72	2.15	1.87	2.30	0.63	0.068	0.081
37.0	21.48	27.07	8.00	4.36	1.77	2.08	1.87	2.39	0.64	0.070	0.081
39.0	22.49	27.19	7.99	4.32	1.76	2.05	1.91	2.36	0.63	0.075	0.078
41.0	23.38	26.85	8.03	4.38	1.78	2.10	1.90	2.41	0.64	0.077	0.080
43.0	24.39	26.79	8.02	4.33	1.78	2.11	1.91	2.39	0.63	0.074	0.078
45.0	25.49	26.95	8.06	4.33	1.79	2.10	1.88	2.40	0.63	0.069	0.082
47.0	26.46	26.96	8.12	4.38	1.78	2.12	1.94	2.41	0.64	0.074	0.079
49.0	27.51	27.03	8.06	4.31	1.78	2.04	1.86	2.40	0.64	0.073	0.079
51.0	28.62	26.90	8.10	4.28	1.78	2.18	1.92	2.41	0.64	0.077	0.079
53.0	29.65	26.63	8.14	4.39	1.81	2.14	1.86	2.44	0.64	0.115	0.080
55.0	30.69	26.70	8.20	4.40	1.83	2.15	1.91	2.46	0.64	0.087	0.080
57.0	31.66	26.44	8.23	4.45	1.85	2.22	1.90	2.49	0.64	0.072	0.079
59.0	32.65	26.38	8.31	4.49	1.86	2.20	1.87	2.51	0.64	0.072	0.079
61.0	33.60	26.27	8.31	4.56	1.85	2.17	1.86	2.53	0.64	0.077	0.079
63.0	34.53	26.06	8.34	4.54	1.85	2.22	1.93	2.53	0.64	0.079	0.081
65.0	35.65	26.00	8.41	4.53	1.92	2.17	1.78	2.56	0.65	0.073	0.078
67.0	36.97	26.24	8.33	4.45	1.89	2.17	1.88	2.53	0.64	0.074	0.080

Table 3.37 Loch Fyne core FS, XRF major element results

Depth (cm)	g cm^{-2}	^{210}Pb	+/-	^{226}Ra	+/-	excess ^{210}Pb	+/-
0.5	0.08	130.3	14.9	145.2	9.6	-16.0	-2.1
1.5	0.42	136.5	11.3	127.8	5.4	9.6	0.9
2.5	0.63	123.1	10.2	107.1	4.6	17.6	1.6
3.5	0.96	160.9	12.6	123.0	5.0	41.5	3.7
4.5	1.34	165.3	12.1	128.1	5.2	40.7	3.4
5.5	1.75	160.3	11.8	116.5	4.7	47.9	4.0
6.5	2.08	145.7	10.7	110.4	4.6	38.7	3.3
7.5	2.54	43.6	3.9	71.7	3.5	-30.9	-3.1
8.8	2.92	12.4	1.1	59.3	2.6	-51.3	-5.1
9.5	3.41	202.1	23.4	111.4	5.1	99.4	12.4
10.5	3.84	186.3	21.9	113.5	5.4	79.8	10.1
11.5	4.19	166.0	20.5	104.4	5.2	67.6	9.0
12.5	4.64	182.0	21.2	139.3	6.4	46.8	5.9
13.5	5.24	162.1	19.0	136.9	6.4	27.7	3.5
14.5	5.81	139.2	16.7	166.7	7.6	-30.1	-3.9
15.5	6.42	102.3	12.2	127.1	5.8	-27.1	-3.5
16.5	7.09	81.2	10.4	92.2	4.4	-12.1	-1.7
17.5	7.68	70.8	8.8	54.5	2.8	17.9	2.4
18.5	8.33	45.4	5.6	65.0	3.1	-21.5	-2.8
19.5	8.88	56.1	8.0	68.5	3.4	-13.6	-2.0
21.0	9.81	34.3	4.3	63.8	3.0	-32.5	-4.3
23.0	10.94	57.1	7.1	72.6	3.5	-17.0	-2.3
25.0	12.22	60.6	7.6	75.0	3.8	-15.8	-2.1
27.0	13.20	27.3	3.6	62.9	3.0	-39.2	-5.4
29.0	14.02	30.9	3.9	66.3	3.4	-39.0	-5.3
31.0	15.06	45.3	5.7	60.6	2.9	-16.8	-2.3
33.0	15.91	65.8	8.5	61.1	3.0	5.2	0.7
35.0	16.97	26.3	3.5	65.0	3.3	-42.6	-6.0
37.0	18.28	13.4	1.8	62.8	3.0	-54.4	-7.6
39.0	19.24	36.0	4.5	61.2	3.1	-27.8	-3.8
41.0	20.39	30.3	4.1	65.0	3.2	-38.2	-5.4
43.5	21.88	43.3	5.4	69.2	3.4	-28.6	-3.8

Table 3.38 Loch Fyne core FD, natural radionuclide concentrations (Bq kg^{-1})

Depth (cm)	g cm^{-2}	^{228}Th	+/-	^{226}Ra	+/-	^{238}U	+/-
0.5	0.08	33.2	2.0	24.3	1.5	52.7	6.1
1.5	0.42	40.1	1.8	33.2	1.5	43.5	5.0
2.5	0.63	35.9	1.6	33.4	1.6	57.8	4.6
3.5	0.96	31.1	1.3	24.2	1.0	47.6	3.7
4.5	1.34	27.9	1.2	28.7	1.3	47.3	3.2
5.5	1.75	24.5	1.1	25.0	1.1	42.4	4.3
6.5	2.08	27.8	1.2	27.0	1.2	43.0	3.7
7.5	2.54	11.7	0.6	10.9	0.6	29.8	6.0
8.8	2.92	3.8	0.2	nd	nd	nd	nd
9.5	3.41	24.9	1.1	25.3	1.1	34.4	3.4
10.5	3.84	25.1	1.1	20.8	0.9	41.6	3.6
11.5	4.19	24.0	1.0	24.0	1.1	60.4	5.0
12.5	4.64	24.9	1.0	27.1	1.3	36.1	2.8
13.5	5.24	24.1	1.0	24.9	1.2	40.4	3.7
14.5	5.81	24.9	1.1	23.7	1.1	23.8	1.9
15.5	6.42	29.8	1.3	31.1	1.4	22.3	2.4
16.5	7.09	24.2	1.1	22.8	1.1	25.6	2.3
17.5	7.68	29.3	1.3	28.6	1.2	29.8	3.3
18.5	8.33	27.0	1.2	26.3	1.2	40.0	3.1
19.5	8.88	30.0	1.2	25.9	1.1	40.6	3.8
21.0	9.81	31.5	1.3	31.5	1.3	37.1	2.0
23.0	10.94	30.4	1.3	32.2	1.5	52.8	4.5
25.0	12.22	34.8	1.5	31.0	1.5	63.6	4.2
27.0	13.20	34.6	1.5	32.7	1.4	54.2	3.1
29.0	14.02	38.2	1.6	38.5	1.7	54.2	4.2
31.0	15.06	34.8	1.5	36.0	1.6	59.7	4.6
33.0	15.91	36.4	1.5	33.2	1.4	58.1	4.3
35.0	16.97	37.3	1.6	34.1	1.4	48.6	3.6
37.0	18.28	36.3	1.5	32.8	1.4	60.3	3.5
39.0	19.24	36.6	1.5	37.3	1.8	37.0	4.1
41.0	20.39	37.8	1.7	33.7	1.5	41.2	3.9
43.5	21.88	44.6	1.9	41.4	1.8	48.9	2.9

Table 3.38 Loch Fyne core FD, natural radionuclide concentrations (Bq kg^{-1}) (continued)

DEPTH (cm)	g cm^{-2}	^{137}Cs	+/-	^{134}Cs	+/-	^{241}Am	+/-
0.5	0.08	122.4	3.0	nd	nd	nd	nd
1.5	0.42	159.4	3.8	2.0	0.2	11.0	0.7
2.5	0.63	198.3	4.3	nd	nd	9.2	0.5
3.5	0.96	226.2	4.9	nd	nd	6.5	0.4
4.5	1.34	212.5	4.5	nd	nd	4.0	0.3
5.5	1.75	160.4	3.4	nd	nd	nd	nd
6.5	2.08	152.0	3.2	nd	nd	nd	nd
7.5	2.54	48.2	1.1	nd	nd	nd	nd
8.8	2.92	47.9	1.1	nd	nd	nd	nd
9.5	3.41	84.0	1.9	nd	nd	nd	nd
10.5	3.84	61.7	1.5	nd	nd	nd	nd
11.5	4.19	39.9	1.2	nd	nd	nd	nd
12.5	4.64	25.4	0.7	nd	nd	nd	nd
13.5	5.24	8.4	0.3	nd	nd	nd	nd
14.5	5.81	4.5	0.3	nd	nd	nd	nd
15.5	6.42	4.8	0.3	nd	nd	nd	nd
16.5	7.09	3.5	0.3	nd	nd	nd	nd
17.5	7.68	1.8	0.1	nd	nd	nd	nd
18.5	8.33	1.9	0.1	nd	nd	nd	nd
19.5	8.88	1.7	0.2	nd	nd	nd	nd
21.0	9.81	0.8	0.1	nd	nd	nd	nd
23.0	10.94	nd	nd	nd	nd	nd	nd
25.0	12.22	1.1	0.1	nd	nd	nd	nd
27.0	13.20	1.2	0.1	nd	nd	nd	nd
29.0	14.02	0.7	0.1	nd	nd	nd	nd
31.0	15.06	0.7	0.1	nd	nd	nd	nd
33.0	15.91	0.3	0.0	nd	nd	nd	nd
35.0	16.97	1.9	0.2	nd	nd	nd	nd
37.0	18.28	0.5	0.0	nd	nd	nd	nd
39.0	19.24	0.8	0.1	nd	nd	nd	nd
41.0	20.39	nd	nd	nd	nd	nd	nd
43.5	21.88	0.3	0.0	nd	nd	nd	nd

Table 3.39 Loch Fyne core FD, manmade radionuclide concentrations (Bq kg^{-1})

Depth (cm)	g cm^{-2}	V (ppm)	Ba (ppm)	Sc (ppm)	La (ppm)	Nd (ppm)	Ce (ppm)	Cr (ppm)	Ni (ppm)
0.5	0.08								
1.5	0.42	177	438	13	35	32	79	103	46
2.5	0.63	159	398	12	35	30	80	97	43
3.5	0.96	168	451	15	33	30	72	123	53
4.5	1.34	167	424	13	35	31	79	104	50
5.5	1.75	163	441	15	35	31	83	92	51
6.5	2.08	176	468	16	37	31	83	100	54
7.5	2.54	173	446	15	36	31	80	97	54
8.8	2.92	184	499	14	36	32	83	96	59
9.5	3.41	170	620	15	33	31	82	90	57
10.5	3.84	155	451	13	28	29	76	83	57
11.5	4.19	145	403	12	28	28	72	73	52
12.5	4.64	166	504	14	33	28	77	71	60
13.5	5.24	172	499	11	32	27	79	70	60
14.5	5.81	146	535	11	30	25	83	62	69
15.5	6.42	153	515	12	29	29	93	76	67
16.5	7.09	128	391	10	28	24	72	66	54
17.5	7.68	133	392	11	31	27	81	76	56
18.5	8.33	147	420	13	30	29	76	81	58
19.5	8.88	149	435	14	33	31	86	84	60
21.0	9.81	148	473	13	34	31	83	91	64
23.0	10.94	134	484	14	31	28	68	83	61
25.0	12.22	158	546	14	33	31	78	98	67
27.0	13.20	141	497	15	33	33	80	96	61
29.0	14.02	138	527	15	37	32	77	105	63
31.0	15.06	134	510	17	35	33	78	103	58
33.0	15.91	126	493	16	35	33	80	101	55
35.0	16.97	128	531	17	34	33	74	104	53
37.0	18.28	122	517	15	33	32	74	102	48
39.0	19.24	122	531	16	34	31	71	101	48
41.0	20.39	127	540	16	37	32	75	106	49
43.5	21.88	139	608	20	40	37	86	123	58

Table 3.40 Loch Fyne core FD, XRF trace element results

Depth (cm)	g cm^{-2}	Cu (ppm)	Zn (ppm)	Pb (ppm)	Th (ppm)	Rb (ppm)	Sr (ppm)	Y (ppm)	Zr (ppm)	Nb (ppm)
0.5	0.08									
1.5	0.42	20	204	123	9	71	196	19	133	9
2.5	0.63	18	189	120	9	76	189	20	131	9
3.5	0.96	22	214	110	9	85	232	21	139	10
4.5	1.34	20	185	100	8	84	221	20	127	10
5.5	1.75	14	126	68	9	84	205	21	147	11
6.5	2.08	11	113	53	10	88	192	20	147	11
7.5	2.54	13	108	49	11	89	198	20	151	11
8.8	2.92	13	108	51	8	89	204	21	156	11
9.5	3.41	60	105	48	9	89	249	21	143	10
10.5	3.84	11	86	46	9	83	219	20	153	10
11.5	4.19	11	82	42	8	81	231	19	146	10
12.5	4.64	10	84	44	8	80	228	20	142	9
13.5	5.24	9	82	46	9	78	225	19	144	10
14.5	5.81	11	80	48	7	69	222	19	136	9
15.5	6.42	14	83	49	10	79	200	19	148	9
16.5	7.09	12	77	36	9	73	203	18	148	9
17.5	7.68	13	83	34	9	80	188	20	162	9
18.5	8.33	14	87	31	9	87	185	21	164	10
19.5	8.88	14	89	33	10	91	183	21	165	11
21.0	9.81	15	89	27	11	96	180	23	177	11
23.0	10.94	12	82	22	9	91	188	21	173	11
25.0	12.22	23	95	22	10	103	230	24	173	12
27.0	13.20	13	92	22	9	102	203	23	162	11
29.0	14.02	14	96	22	11	108	203	24	169	12
31.0	15.06	14	98	24	11	108	197	23	172	13
33.0	15.91	13	95	22	12	107	196	23	163	12
35.0	16.97	13	95	20	11	111	199	23	170	12
37.0	18.28	13	89	18	10	104	188	23	169	12
39.0	19.24	14	93	19	12	110	197	24	166	13
41.0	20.39	12	94	20	11	112	195	24	177	13
43.5	21.88	15	111	22	15	131	215	26	160	14

Table 3.40 Loch Fyne core FD, XRF trace element results (continued)

Depth (cm)	g cm^{-2}	Si (%)	Al (%)	Fe (%)	Mg (%)	Ca (%)	Na (%)	K (%)	Ti (%)	Mn (%)	P (%)
0.5	0.08	29.63	4.83	4.17	1.18	2.25	1.25	1.40	0.39	1.83	0.11
1.5	0.42	29.57	5.14	4.19	1.19	2.25	1.28	1.47	0.42	1.22	0.10
2.5	0.63	27.55	5.70	4.26	1.37	2.63	1.28	1.68	0.45	2.19	0.09
3.5	0.96	27.14	5.70	4.21	1.39	2.92	1.29	1.65	0.44	1.74	0.09
4.5	1.34	28.14	5.81	4.17	1.38	2.47	1.20	1.68	0.46	1.74	0.09
5.5	1.75	28.35	5.96	4.24	1.39	2.40	1.40	1.75	0.47	1.18	0.08
6.5	2.08	27.28	6.14	4.21	1.49	2.77	1.34	1.77	0.48	1.49	0.08
7.5	2.54	27.25	6.06	4.24	1.47	2.55	1.37	1.76	0.47	1.75	0.08
8.8	2.92	26.60	6.05	4.21	1.51	2.95	1.36	1.79	0.48	1.80	0.08
9.5	3.41	27.31	5.68	4.02	1.44	3.10	1.26	1.68	0.45	2.11	0.08
10.5	3.84	26.45	5.56	3.84	1.45	4.00	1.25	1.59	0.44	2.14	0.08
11.5	4.19	26.18	5.34	3.83	1.47	3.48	1.33	1.60	0.43	3.29	0.08
12.5	4.64	26.30	5.25	3.68	1.45	3.73	1.24	1.55	0.42	3.21	0.08
13.5	5.24	24.17	4.68	3.22	1.51	4.40	1.08	1.36	0.37	5.80	0.09
14.5	5.81	26.99	5.34	3.51	1.47	3.47	1.20	1.68	0.42	2.92	0.08
15.5	6.42	24.74	4.96	3.17	1.54	4.99	1.03	1.53	0.39	4.31	0.08
16.5	7.09	26.18	5.43	3.45	1.57	4.13	1.17	1.68	0.42	2.97	0.08
17.5	7.68	26.19	5.93	3.54	1.63	3.90	1.29	1.91	0.45	2.29	0.07
18.5	8.33	27.14	6.16	3.65	1.60	3.48	1.24	1.97	0.47	1.44	0.07
19.5	8.88	28.43	6.63	3.80	1.69	3.08	1.31	2.10	0.50	0.55	0.06
21.0	9.81	27.60	6.15	3.52	1.59	3.54	1.20	1.99	0.47	1.35	0.06
23.0	10.94	28.98	7.09	4.03	1.92	4.76	1.45	2.26	0.52	2.17	0.08
25.0	12.22	26.09	6.90	3.94	1.78	3.70	1.38	2.22	0.50	0.95	0.06
27.0	13.20	25.86	7.35	4.16	1.87	3.45	1.41	2.39	0.53	0.55	0.06
29.0	14.02	26.17	7.37	4.24	1.85	3.30	1.48	2.38	0.53	0.45	0.06
31.0	15.06	26.19	7.29	4.15	1.83	3.39	1.38	2.34	0.52	0.46	0.06
33.0	15.91	26.44	7.45	4.28	1.83	3.27	1.37	2.43	0.53	0.22	0.06
35.0	16.97	27.24	7.04	4.07	1.74	3.15	1.36	2.27	0.52	0.19	0.06
37.0	18.28	26.47	7.49	4.25	1.83	3.22	1.43	2.40	0.53	0.19	0.06
39.0	19.24	26.30	7.55	4.32	1.84	3.20	1.44	2.46	0.53	0.17	0.06
41.0	20.39	23.55	8.72	4.86	2.16	3.45	1.60	2.85	0.58	0.20	0.07
43.5	21.88										

Table 3.41 Loch Fyne core FS, XRF major element results

DEPTH (cm)	g cm^{-2}	Li (ppb)	Cu (ppb)	Ba (ppb)	B (ppm)	Rb (ppb)	Al (ppb)	Sr (ppm)	Mn (ppm)	Mo (ppb)	U (ppb)	Fe (ppm)
0.5	0.18	193	38	16	5	124	37	7	8	52	2.9	3
1.5	0.65	201	66	20	6	130	71	8	11	32	2.9	3
2.5	1.14	210	67	23	6	136	32	8	12	33	2.6	3
3.5	1.56	215	74	17	6	138	55	8	14	35	2.9	4
4.5	1.93	214	78	20	6	142	42	8	16	34	2.1	4
5.5	2.50	218	79	24	6	139	74	8	15	37	1.9	5
6.5	2.92	187	56	30	6	136	31	8	14	32	1.0	6
7.5	3.43	193	82	36	6	143	94	8	15	25	0.9	10
8.5	3.99	197	86	33	6	140	64	8	16	25	0.7	10
9.5	4.56	197	83	34	6	143	69	8	15	21	0.6	10
11.0	5.16	184	83	32	6	133	101	8	14	23	0.5	11
13.0	5.69	195	84	31	6	144	74	8	12	19	0.4	13
15.0	6.19	169	27	33	5	171	47	7	12	11	0.6	6
17.0	6.74	85	24	18	2	95	46	4	5	12	0.4	3
19.0	7.32	160	48	29	4	166	52	8	8	18	0.8	4
21.0	7.95	160	54	33	4	169	65	8	10	19	0.6	7
23.0	8.47	167	48	34	5	174	86	8	11	16	0.8	6
25.0	8.99	157	53	36	4	165	39	8	13	14	0.5	9
27.0	9.53	234	43	37	7	185	62	8	16	4	0.8	9
29.0	10.13	249	61	34	7	170	83	8	17	3	0.4	19
31.0	10.69	264	68	36	8	182	96	8	13	4	1.1	12
33.0	11.19	264	61	38	8	189	72	8	14	5	1.1	12
35.0	11.78	258	59	37	8	185	40	8	13	4	1.1	11
37.0	12.34	236	57	37	7	177	34	8	14	2	1.0	7
39.0	13.04	239	51	38	7	182	45	8	12	4	1.9	5
41.0	13.65	230	39	37	7	207	72	7	10	25	3.5	3
43.0	14.34	238	54	34	7	196	58	8	9	28	3.8	4
45.0	14.91	238	70	34	8	202	125	8	8	35	4.7	5
47.0	15.52	242	57	31	8	207	13	8	8	38	5.0	3
49.0	15.88	240	58	33	8	213	119	8	8	41	4.7	4
51.0	16.44	239	51	30	7	203	34	8	7	39	5.0	3
53.0	16.95	238	52	31	8	208	88	8	7	42	4.9	3
55.0	17.56	219	41	31	7	195	569	7	6	46	10.5	2
57.0	18.14	225	48	30	7	189	88	8	6	35	9.1	3
59.0	18.72	228	40	29	7	181	71	8	6	28	9.6	2
61.0	19.26	231	48	32	7	189	180	8	6	34	9.5	3
63.0	19.86	241	52	31	8	201	64	8	6	52	11.0	3
65.0	20.44	228	58	30	7	198	49	8	6	34	10.1	3
67.0	21.03	252	39	30	7	199	57	7	6	59	8.1	2

Table 3.42 Loch Long core LL1, pore water results

DEPTH (cm)	g/cm2	Li (ppb)	Cu (ppb)	Ba (ppb)	B (ppm)	Rb (ppb)	Al (ppb)	Sr (ppm)	Mn (ppm)	Mo (ppb)	U (ppb)	Fe (ppm)
0.5	0.20	175	60	44	5	139	27	9	39	30	3.9	2
1.5	0.36	183	64	73	6	141	190	9	23	19	0.8	5
2.5	0.68	199	76	78	6	155	87	10	18	24	0.8	6
3.5	0.98	186	69	61	5	142	32	9	14	17	1.3	4
4.5	1.23	211	40	40	7	156	26	8	8	7	1.1	3
5.5	1.53	213	48	37	7	157	48	8	7	9	1.6	4
6.5	1.81	52	24	9	2	38	12	2	2	4	0.3	2
7.5	2.12	93	31	15	3	69	56	3	3	4	0.8	3
8.5	2.51	na	na	na	na	na	na	na	na	na	na	na
9.5	2.87	na	na	na	na	na	na	na	na	na	na	na
11.0	3.36	70	62	16	2	57	46	3	2	4	1.0	1
13.0	4.08	81	59	19	2	64	111	4	3	4	1.0	2
15.0	4.67	63	74	13	2	51	47	3	2	4	1.0	1
17.0	5.31	64	75	13	2	52	80	3	2	4	1.0	2
19.0	5.68	28	68	5	1	24	53	2	1	3	0.0	1
21.0	6.26	60	72	10	1	60	85	2	1	6	1.0	1
23.0	6.82	69	79	13	2	59	88	3	2	11	1.0	2
25.0	7.43	64	81	12	2	54	120	3	2	8	1.0	2
27.0	7.81	47	86	10	1	40	53	2	1	8	1.0	2
29.0	8.18	33	91	6	1	26	115	2	1	9	0.0	2
31.0	8.67	72	75	15	2	77	102	3	2	9	1.0	2
33.0	9.12	51	69	11	2	45	37	2	2	7	1.0	1
35.0	9.69	94	113	22	3	90	217	5	3	17	2.0	3
37.0	10.23	217	152	34	7	193	160	9	7	13	2.0	6
39.0	10.77	216	152	34	7	181	67	9	6	20	2.0	6
41.0	11.29	216	157	36	6	17	100	9	6	12	2.0	6
43.0	11.72	215	149	34	6	173	82	9	6	11	2.0	7
45.0	12.24	210	141	35	6	165	153	8	6	42	4.0	5
47.0	12.71	203	144	37	7	183	56	9	6	134	5.0	5
49.0	13.17	181	139	33	6	155	71	8	5	14	3.0	4
51.0	13.63	176	139	35	6	145	80	8	5	13	3.0	5
53.0	14.07	89	99	17	3	72	19	4	2	12	3.0	3
55.0	14.59	53	63	11	2	46	19	2	1	10	2.0	1
57.0	14.98	na	na	na	na	na	na	na	na	na	na	na
59.0	15.52	na	na	na	na	na	na	na	na	na	na	na
61.0	15.93	na	na	na	na	na	na	na	na	na	na	na
63.0	16.40	na	na	na	na	na	na	na	na	na	na	na
65.0	16.95	na	na	na	na	na	na	na	na	na	na	na
67.0	17.46	na	na	na	na	na	na	na	na	na	na	na
69.0	17.95	80	146	21	3	80	38	36	3	11	1.0	4
71.5	18.74	104	176	29	4	104	64	5	3	22	4.0	5

Table 3.43 Loch Goil core GD2 pore water results

DEPTH (cm)	g cm^{-2}	Li (ppb)	Cu (ppb)	Ba (ppb)	B (ppm)	Rb (ppb)	Al (ppb)	Sr (ppm)	Mn (ppm)	Mo (ppb)	U (ppb)	Fe (ppm)
0.5	0.28	244	70	16	5.4	136	37	8.6	9.7	33	2.2	3.1
1.5	0.60	230	83	19	5.3	135	44	7.8	12.2	33	2.9	3.1
2.5	1.05	233	88	23	5.2	138	70	7.9	11.6	27	2.8	3.2
3.5	1.59	234	102	23	5.4	141	48	7.8	8.4	26	2.3	3.2
4.5	2.27	220	113	19	4.9	135	96	7.3	5.9	20	2.5	4.7
5.5	2.86	198	77	20	5.1	143	70	7.9	5.6	19	2.0	4.2
6.5	3.46	194	78	17	4.9	137	58	7.6	4.7	24	2.0	3.3
7.5	4.12	210	90	15	4.9	148	49	8.0	5.3	33	1.7	3.9
8.5	4.84	212	80	16	5.1	144	84	8.0	4.7	22	2.0	4.1
9.5	5.50	206	83	17	5.1	144	64	7.7	4.6	25	1.6	4.7
11.0	6.74	159	68	9	2.7	71	42	4.0	2.0	15	0.7	2.7
13.0	7.99	199	79	17	5.1	137	77	7.9	4.7	19	1.3	3.7
15.0	9.18	193	74	17	4.9	133	36	7.7	4.2	27	2.0	3.1
17.0	10.50	198	80	18	5.4	133	55	7.6	4.2	23	1.8	3.1
19.0	11.80	195	79	17	5.2	139	50	7.8	4.0	25	1.8	2.9
21.0	12.87	250	79	18	5.2	136	65	7.1	3.4	16	2.3	2.7
23.0	13.90	272	89	20	5.1	141	99	7.1	3.6	20	2.4	2.8
25.0	15.02	248	96	20	5.1	142	131	7.1	4.0	18	1.7	2.9
27.0	16.11	240	100	21	4.9	142	67	7.3	4.6	21	1.9	2.6
29.0	17.17	228	103	21	4.8	143	88	7.2	4.7	20	2.0	2.7
31.0	18.26	174	34	21	5.4	157	17	8.0	5.0	26	4.3	1.6
33.0	19.29	169	63	22	5.0	159	31	8.3	5.3	22	2.9	2.6
35.0	20.38	165	67	21	4.9	155	33	7.9	5.4	25	1.6	2.7
37.0	21.48	182	70	25	5.2	169	95	8.5	5.6	28	2.8	3.2
39.0	22.49	186	81	28	4.9	175	113	8.3	5.2	45	7.3	3.1
41.0	23.38	194	86	28	4.9	179	211	8.6	5.3	50	6.6	3.0
43.0	24.39	189	93	29	5.4	161	196	7.7	4.9	81	6.1	2.3
45.0	25.49	200	96	32	5.7	162	231	8.0	4.8	48	6.5	2.4
47.0	26.46	196	79	27	5.5	151	57	7.7	4.6	39	6.5	2.0
49.0	27.51	210	81	29	6.4	162	87	8.3	5.0	41	5.6	2.0
51.0	28.62	214	88	30	5.8	164	111	8.3	5.2	42	5.1	2.1
53.0	29.65	188	59	28	7.0	147	33	7.6	4.8	31	4.4	2.2
55.0	30.69	188	76	30	7.2	153	38	8.0	5.0	32	5.6	2.4
57.0	31.66	195	85	32	7.2	160	103	8.0	4.9	38	6.1	2.9
59.0	32.65	186	89	32	6.7	151	96	7.8	4.7	41	7.1	2.7
61.0	33.60	186	100	29	6.8	154	77	7.6	5.0	41	4.7	2.5
63.0	34.53	202	106	35	6.4	163	165	7.6	4.9	89	8.0	2.5
65.0	35.65	227	103	34	7.3	160	236	8.0	5.0	98	5.2	3.0
67.0	36.97	195	121	59	5.5	140	839	6.8	4.0	48	7.2	3.6

Table 3.44 Loch Fyne core FS, pore water results

DEPTH (cm)	g cm^{-2}	Li (ppb)	Cu (ppb)	Ba (ppb)	B (ppm)	Rb (ppb)	Al (ppb)	Sr (ppm)	Mn (ppm)	Mo (ppb)	U (ppb)	Fe (ppm)
0.5	0.08	208	23	13	5.1	129	144	7.8	0.1	12	2.5	1.6
1.5	0.42	358	49	14	10.6	225	193	13.6	4.4	45	3.1	2.9
2.5	0.63	179	31	15	5.5	127	385	7.0	7.3	31	2.5	2.1
3.5	0.96	217	38	12	7.1	152	108	8.0	11.7	43	2.5	1.8
4.5	1.34	210	42	12	6.8	141	120	8.5	12.1	42	2.8	2.1
5.5	1.75	181	28	15	6.3	136	99	7.3	11.7	37	3.0	1.4
6.5	2.08	178	24	17	6.1	127	103	6.8	10.6	34	2.4	1.4
7.5	2.54	191	43	25	6.8	137	303	7.4	11.3	33	2.6	1.8
8.8	2.92	196	38	28	6.8	137	906	7.4	11.6	38	2.4	4.4
9.5	3.41	194	167	37	7.0	144	693	7.2	12.4	35	2.4	3.6
10.5	3.84	178	29	48	6.2	134	546	7.9	10.0	32	2.9	2.7
11.5	4.19	184	36	61	7.0	139	263	8.3	10.2	31	2.7	2.1
12.5	4.64	181	27	62	6.5	134	94	8.0	9.5	28	2.6	1.6
13.5	5.24	198	29	88	7.2	150	41	8.6	12.0	29	2.5	1.8
14.5	5.81	184	22	89	5.5	131	64	7.1	10.4	27	2.3	1.1
15.5	6.42	178	30	90	6.5	136	211	7.2	10.6	28	2.1	1.3
16.5	7.09	190	44	99	7.1	153	112	8.0	12.2	30	2.4	1.7
17.5	7.68	181	46	106	6.5	134	85	8.1	12.4	28	2.2	1.7
18.5	8.33	173	32	99	6.3	132	85	7.5	12.0	34	1.7	1.7
19.5	8.88	167	32	89	5.7	119	73	7.6	10.5	25	3.1	1.7
21.0	9.81	171	24	92	5.1	123	34	7.1	10.4	22	3.5	1.2
23.0	10.94	184	27	87	6.0	128	32	7.2	11.1	24	3.1	1.3
25.0	12.22	151	19	65	4.4	108	20	5.6	8.7	18	2.2	1.0
27.0	13.20	187	28	76	6.1	126	50	7.3	10.1	23	3.9	1.4
29.0	14.02	166	26	64	5.3	118	31	6.2	8.3	24	4.2	1.3
31.0	15.06	199	28	77	6.0	134	67	7.7	10.2	29	4.6	1.7
33.0	15.91	187	63	82	6.9	138	888	7.4	11.0	37	5.0	4.2
35.0	16.97	194	62	68	7.2	146	108	7.6	10.5	42	5.0	2.7
37.0	18.28	188	69	64	7.1	144	243	7.4	10.6	49	3.4	3.1
39.0	19.24	186	73	62	7.3	146	481	7.6	10.1	72	2.9	3.8
41.0	20.39	184	71	65	7.4	151	64	8.0	10.1	90	3.8	3.0
45.0	21.88	178	78	67	7.2	150		7.9	9.5	93	3.3	3.6

Table 3.45 Loch Fyne core FD, pore water results

nodule	^{210}Pb	^{226}Ra	^{232}Th	^{228}Th	^{228}Ra	^{234}U	^{234}Th	^{137}Cs
A	678.4	989.5	20.8	88	146.3	89.3	nd	72.3
B	610.2	893.5	19.8	24.4	97.6	109.5	36.4	71.5
C	542.0	689.1	13.3	nd	49.6	73.2	29.0	61.0
D	435.2	443.3	11.7	nd	45.6	70.3	56.5	50.3
E	391.0	373.8	9.8	nd	21.4	77.5	70.7	48.1

Table 3.46 Loch Fyne core FD, manganese nodule results

LE1		LE 2		LE3		LL1		GD2		FS		FD	
g/cm2	Mo (mg kg^{-1})	g/cm2	Mo (mg kg^{-1})	g/cm2	Mo (mg kg^{-1})	g/cm2	Mo (mg kg^{-1})	g/cm2	Mo (mg kg^{-1})	g/cm2	Mo (mg kg^{-1})	g/cm2	Mo (mg kg^{-1})
0.1		0.2	2.4	0.1		0.2	3.9	0.2		0.3		0.1	
0.2	2.0	0.5	3.2	0.1		0.6	4.4	0.4	2.0	0.6	1.6	0.4	8.8
0.4	2.8	0.7	3.2	0.3		1.1	2.3	0.7	2.1	1.1	0.8	0.6	5.0
0.6	2.9	1.1	2.5	0.4		1.6	3.0	1.0	1.9	1.6	0.1	1.0	8.6
0.8	1.5	1.4	2.2	0.5	1.5	1.9	2.1	1.2	2.9	2.3	1.1	1.3	6.9
1.0	1.2	1.8	2.0	0.7	2.6	2.5	2.0	1.5	3.9	2.9	0.5	1.7	5.3
1.3	2.7	2.1	2.3	0.8	5.0	2.9	8.1	1.8	4.0	3.5	1.1	2.1	3.3
1.5	2.6	2.4	1.9	1.0	5.0	3.4	2.3	2.1	2.1	4.1	0.7	2.5	4.0
1.8	3.0	2.8	2.2	1.2	5.8	4.0	3.5	2.5	0.8	4.8	1.0	2.9	5.3
2.2	4.3	3.1	2.3	1.3	5.3	4.6	2.1	2.9	2.6	5.5	1.3	3.4	4.8
2.9	4.7	3.7	2.7	1.7	5.9	5.2	1.7	3.4	3.2	6.7	1.6	3.8	6.1
3.4	3.1	4.2	2.5	2.1	3.7	5.7	2.3	4.1	3.0	8.0	1.2	4.2	4.7
3.8	4.0	4.8	2.7	2.5	4.6	6.2	2.8	4.7	1.3	9.2	3.0	4.6	6.6
4.3	3.2	5.4	3.2	2.8	3.4	6.7	3.1	5.3	2.5	10.5	2.2	5.2	6.9
4.8	3.6	5.9	3.4	3.2	4.0	7.3	2.7	5.7	2.4	11.8	2.6	5.8	7.9
5.3	2.7	6.5	3.4	3.5	4.7	8.0	2.3	6.3	2.4	12.9	2.4	6.4	4.9
5.8	3.9	7.1	4.3	3.9	5.6	8.5	3.0	6.8	3.5	13.9	1.7	7.1	2.6
6.3	3.6	7.6	4.1	4.3	5.0	9.0	1.5	7.4	4.0	15.0	1.8	7.7	2.6
6.9	4.5	8.1	4.0	4.7	6.6	9.5	3.6	7.8	3.4	16.1	1.5	8.3	1.9
7.4	5.0	8.8	4.3	5.2	6.8	10.1	3.5	8.2	4.2	17.2	2.4	8.9	1.2
7.9	5.1	9.4	5.7	5.7	8.3	10.7	3.7	8.7	3.9	18.3	2.3	9.8	1.7
8.4	8.0	10.1	5.5	6.1	8.1	11.2	3.0	9.1	5.1	19.3	1.2	10.9	1.3
9.0	6.8	10.7	5.3	6.6	9.2	11.8	2.9	9.7	3.3	20.4	2.4	12.2	1.4
9.5	9.5	11.4	5.3	7.1	7.6	12.3	3.0	10.2	4.2	21.5	2.1	13.2	1.1
10.0	9.7	12.0	4.9	7.5	5.5	13.0	2.6	10.8	4.4	22.5	1.6	14.0	2.4
10.5	6.9	12.6	5.4	8.0	7.2	13.6	3.3	11.3	3.0	23.4	2.7	15.1	3.1
11.1	8.0	13.3	4.4	8.4	6.8	14.3	3.7	11.7	4.0	24.4	1.5	15.9	2.0
11.6	9.7	14.0	6.3	8.8	5.5	14.9	5.6	12.2	4.0	25.5	1.7	17.0	2.0
12.2	10.8	14.7	5.1	9.2	4.3	15.5	5.1	12.7	3.7	26.5	1.4	18.3	2.4
12.9	13.2	15.4	5.2	9.6	4.6	15.9	5.2	13.2	4.1	27.5	1.6	19.2	5.5
	11.2	16.2	5.7	10.3	8.2	16.4	24.9	13.6	2.6	28.6	2.0	20.4	4.4
		17.1	5.2	10.8	4.8	17.0	4.3	14.1	3.8	29.6	1.3	21.9	5.8
				11.2	5.3	17.6	3.5	14.6	3.3	30.7	1.1		
						18.1	3.1	15.0	2.9	31.7	2.4		
						18.7	2.9	15.5	1.7	32.7	2.5		
						19.3	2.7	15.9	2.2	33.6	2.6		
						19.9	1.6	16.4	3.5	34.5	2.8		
						20.4	2.4	16.9	2.3	35.6	1.6		
						21.0	5.0	17.5	3.5	37.0	1.4		
						21.6	3.8	18.0	2.3				
						22.2	3.2	18.7	4.4				
						22.8	4.0						
						23.4	2.1						
						24.0	4.7						
						24.7	3.9						

Table 3.47 Loch Etive and Clyde Sea cores, Mo results

CHAPTER 4

Discussion

4.1 *Loch Etive surface transect*

This aspect of the research constituted a preliminary investigation of natural and manmade radionuclide concentrations in the surface sediments of Loch Etive and was carried out using archived samples collected at approximately 1 km intervals along the length of the sea loch in November 1981. The results for the surface transect samples, given in Chapter 3, have been discussed in detail in Williams et al., (1988) and this section will therefore only focus on the main points of interest.

The bathymetric profile of the loch, sampling stations, ^{210}Pb, ^{137}Cs and % organic concentration results are shown in Figure 4.0. The sampling stations are numbered 1 to 25 with station 1 representing open sea conditions. No samples could be obtained at stations 4 and 9.

4.1.1 *Surface transect ^{210}Pb concentrations*

The unsupported ^{210}Pb concentrations in the sediments of Loch Etive are in general higher than the value of 250 Bq kg^{-1} for open sea conditions (sample 1). Three distinct minima are observed in the unsupported ^{210}Pb concentration at stations 10, 17 and 21 which correspond to river inlets, with concentrations of unsupported ^{210}Pb of 107 Bq kg^{-1}, 136 Bq kg^{-1} and 125 Bq kg^{-1} respectively. The unsupported ^{210}Pb concentrations show a strong linear correlation with the sediment organic content ($r = 0.85$) which also has three distinct minima occurring at stations 10, 17 and 21. This observation could indicate a genuine chemical association of ^{210}Pb with organics or may simply reflect dilution of both species at the same locations as a consequence of enhanced input of terrigenous material.

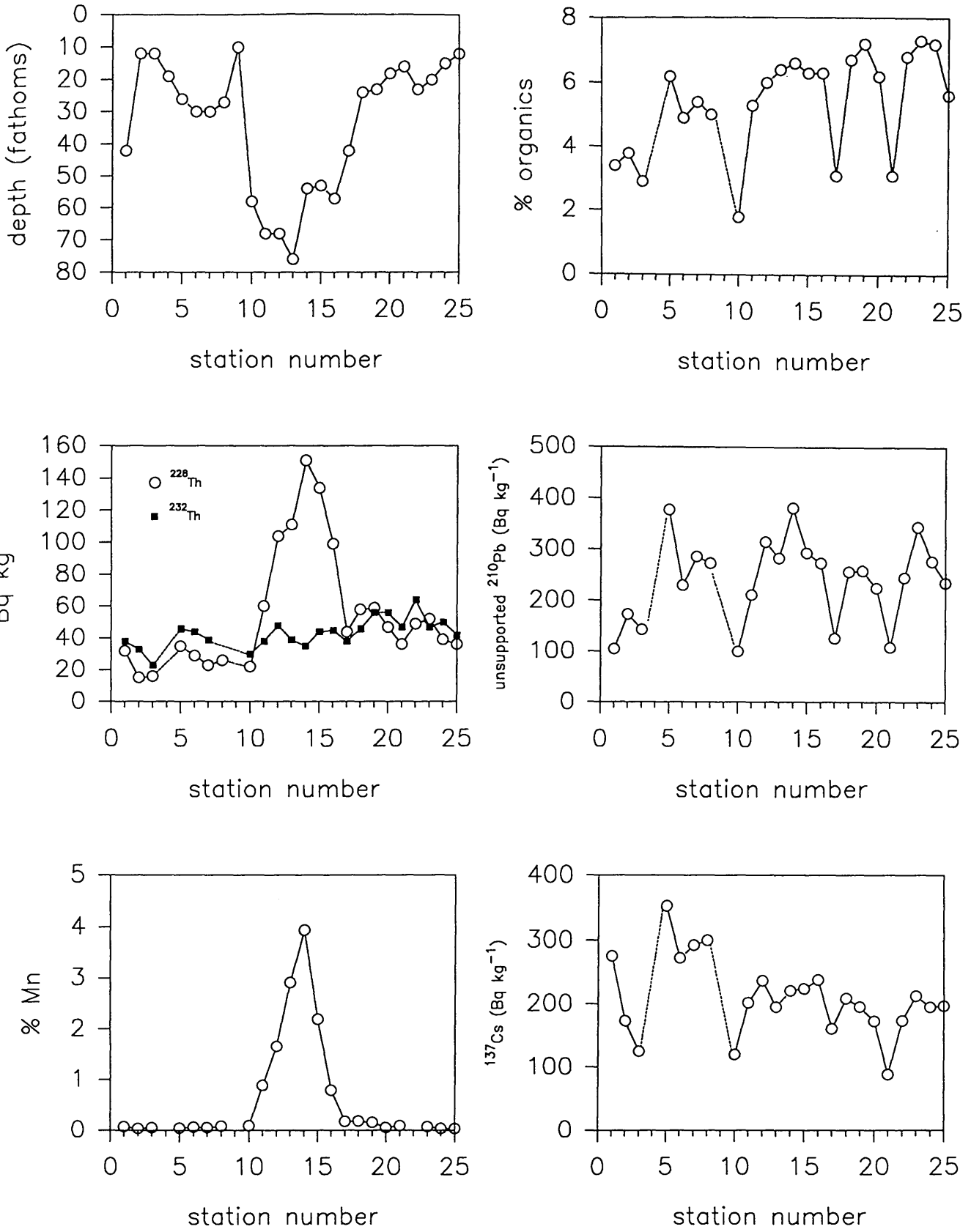

Figure 4.0.

Loch Etive surface transect, depth, % organics, ^{232}Th, ^{228}Th, unsupported ^{210}Pb, ^{137}Cs and % Mn profiles (November 1981)

4.1.2 *Surface transect ^{137}Cs concentrations*

The ^{137}Cs transect has concentrations in the range 88 to 353 Bq kg^{-1}, with the maximum concentration of 353 Bq kg^{-1} occurring at station 5. The concentrations of ^{137}Cs are higher in the outer basin than in the inner basin. As with the ^{210}Pb and % organics profiles the ^{137}Cs profile has minimum values at stations 10, 17 and 21 of 120 Bq kg^{-1}, 160 Bq kg^{-1} and 88 Bq kg^{-1} respectively which again would be considered with deposition of coarser river borne material at these locations.

4.1.3 *Surface transect unsupported ^{228}Th concentrations*

The unsupported ^{228}Th concentrations for the sediments of the surface transect were calculated by subtracting the ^{232}Th concentration from the total ^{228}Th concentration. The ^{228}Th profile shows an excess of ^{228}Th in the inner basin of the loch with a pronounced maximum in concentration (151 Bq kg^{-1}) at the deepest part of the inner basin (station 14) which correlates well with the Mn concentrations of the surface transect ($r = 0.9$). In contrast the outer basin shows a deficiency of ^{228}Th relative to ^{232}Th in the surface sediment.

In summary, the surface transect results indicated that there were major variations in natural and manmade radionuclides along the length of Loch Etive and suggested a possible association of ^{210}Pb with organics, with implications of the mechanism of transfer of lead to the sediment.

4.2 *Loch Etive sediment core studies*

Three gravity cores were collected from Loch Etive and the sampling methods and site locations are described in section 2.1.2. The sample preparation and analytical techniques used are described in Chapter 2 and the results are tabulated in Chapter 3. The results for sediment cores throughout this work, will be discussed in terms of cumulative weight (g cm^{-2}) rather than linear depth to account for difference in porosity with depth in the sediment. For convenience, cumulative weight will be referred to as depth in

the discussion. The linear depth for any quoted cumulative weight will be given in parenthesis.

4.2.1 *Geochemical characteristics of core LE 1*

The sampling location of core LE 1 was the same as that of the surface transect sample 5. In order to characterise the geochemical properties of the sediment and to evaluate changes in sediment type and texture with depth, or between cores, each of the sediment cores studied was analysed by XRF analysis as indicated in section 2.4.1. This generated a large set of analytical data which, for completeness, is presented in Chapter 3. Similar data sets have previously been produced in comprehensive investigations of sediment geochemistry in Loch Etive using XRF (Malcolm,1981; Ridgway, 1983), and detailed interpretation of all of the data is therefore not attempted here. Rather, the results are used selectively to provide information on variations in sediment type and grain size, and in some cases, on redox conditions in the sediment.

In this approach, selected elements were chosen to reflect the input of particular types of material to the sediment e.g. Al is primarily associated with the alumino-silicate fraction, Rb with clays, K with clays and feldspars, Ca with lithogenic and biogenic calcites and Ti with clays and heavy minerals. Si can be taken to represent the sand fraction, but it must be borne in mind that it also has a biogenic source. In order to determine whether there were any major changes in sediment input with time, element/Al ratios and K/Rb ratio were considered, with variations in these ratios being taken to indicate changes in sediment characteristics as follows. To assess changes in grain size Si/Al, Zr/Al, Ti/Al and K/Rb ratios were employed. The Ca/Al ratio was used to indicate the position of shell bands, and the Mn/Al, Fe/Al and P/Al ratios were used to assess the redox condition of the sediment. Fe, with a well established redox chemistry as described in section 1.1.3., has an obvious role in this context, while phosphorus is associated with the organic component of the sediment (Redfield et al., 1963) and is released as the organic matter is degraded by bacteria. Thereafter, the P may become

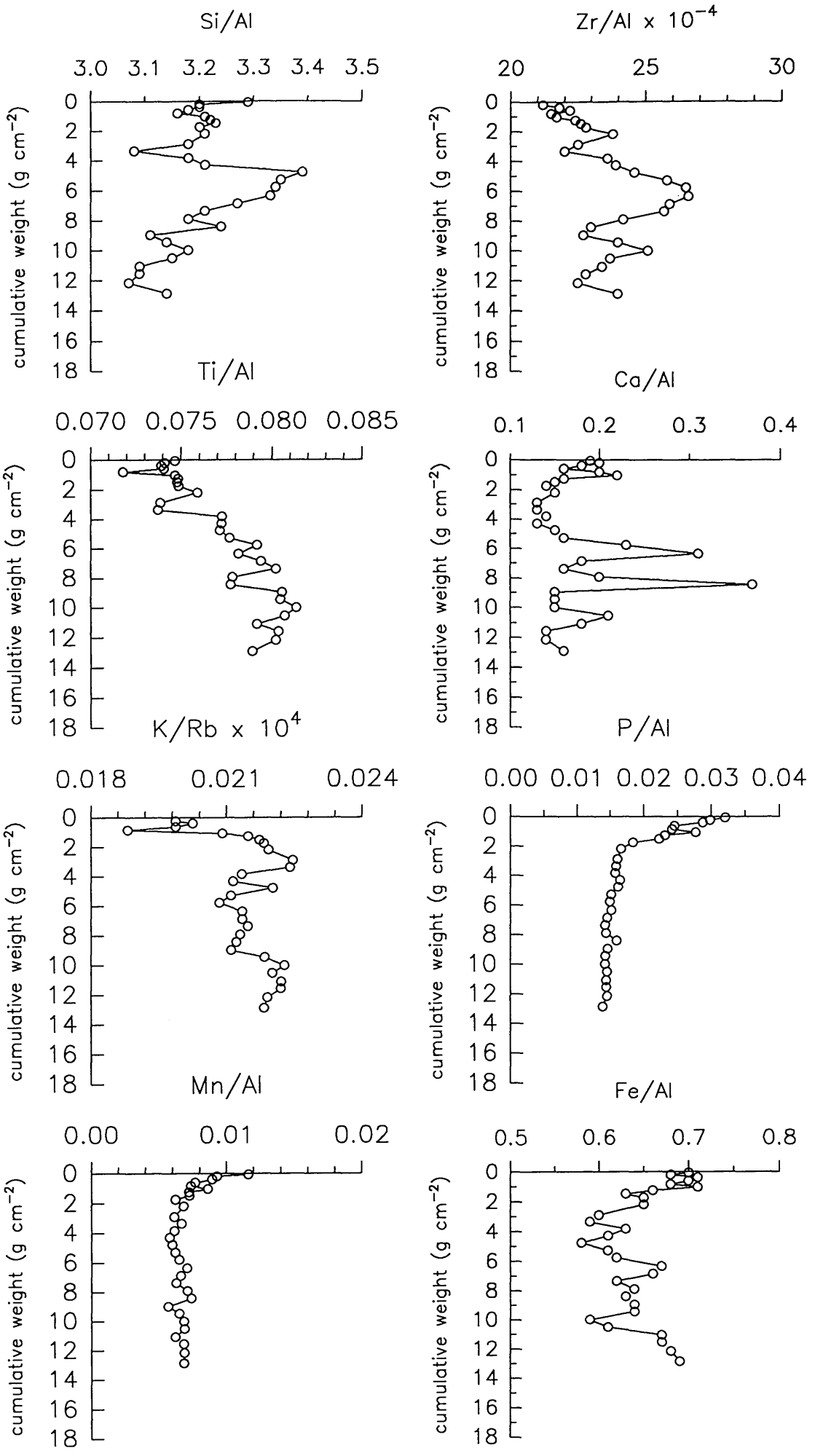

Figure 4.1. Loch Etive core 1 element/Al and K/Rb ratios.

associated with Fe oxyhydroxides and its degradation is thus also controlled by the redox cycling of Fe.

Selected element/Al ratios and K/Rb ratios for core LE 1 are shown in Figure 4.1. The Ti/Al ratio shows a general increase with depth, indicating a trend to coarser grain size with depth and this is also reflected in the Zr/Al and K/Rb ratios. There is an increase in the Si/Al ratio from 3.08 to 3.39 over the depth range 3.4 to 4.8 g cm^{-2} (15 to 21 cm) and the Si/Al profile indicates that a band of coarser material exists over the depth range 3 to 9 g cm^{-2}. If the Si is equated with sand this would imply an input of coarser material, indicating a possible change in sediment type. The Ca/Al ratio indicates the occurrence of shell bands at approximately 6, 8 and 11 g cm^{-2} (corresponding to 27, 35 and 43 cm depth) with a minor band near the surface at approximately 1 g cm^{-2}(6 cm). There is a general trend of increasing grain size with depth (with the exception of Si/Al profile which begins to decrease below 4 g cm^{-2}) indicating that the accumulating sediment type has changed with time. The ratios of Si/Al and Zr/Al, exhibit a sharp change from 3.4 to 5.8 g cm^{-2} (15 to 25 cm) indicating a relatively sudden change in the nature of the sediment deposited over this depth range.

The Mn/Al ratio decreases from a maximum of 0.012 at the surface to 0.006 at 1.8 g cm^{-2} (8.5 cm) after which it remains at a relatively constant value. In comparison, the Fe/Al ratio decreases more slowly from 0.70 at the surface to a minimum value of 0.58 at 4.8 g cm^{-2} (21 cm), below which there is a sharp increase (cf. Si/Al), with irregular but generally higher levels, possibly indicating the formation of Fe sulphides. Both the Mn/Al and Fe/Al ratio profiles indicate the effects of redox recycling near the surface of the sediment. The profiles suggest that the reduction of Mn is complete by 1.75 g cm^{-2} (8.5 cm) and Fe by 3.4 g cm^{-2} (15 cm) reflecting the differences in the Mn and Fe redox couples (Barrow, 1966). The P/Al ratio decreases from 0.032 at the surface, to 0.017 at 2.2 g cm^{-2} (10.5 cm) which probably indicates organic degradation and the involvement of P with Fe cycling. The decrease below this depth does not appear to be related to Fe and therefore probably represents continuous, slow organic degradation.

4.2.2 *^{210}Pb and ^{226}Ra profiles of core LE 1*

^{210}Pb and ^{226}Ra concentrations were measured to establish the sediment mixing and accumulation characteristics of core LE 1. Unsupported ^{210}Pb was calculated by subtracting the ^{226}Ra concentration from the total ^{210}Pb concentration at each depth. The plots of unsupported ^{210}Pb and ln unsupported ^{210}Pb against depth in g cm^{-2} are shown in Figure 4.2.

The ^{226}Ra results are tabulated in Chapter 3 (Table 3.5). The ^{226}Ra concentration has a surface value of 13.2 Bq kg^{-1} and increases to 35.9 Bq kg^{-1} at a depth of 1.26 g cm^{-2} (6.5 cm), below which irregular variations in the range 25.1 to 40.8 Bq kg^{-1} are observed. The low ^{226}Ra value at the surface may be due to loss of Ra from the surface sediment as discussed in Chapter 1. The ^{226}Ra inventory for core LE 1 was 3900 ± 350 Bq m^{-2}.

The unsupported ^{210}Pb concentration profile exhibited a surface maximum of 347.8 Bq kg^{-1} with irregular variations (but constant within the limits of experimental error) to a depth of 1.04 g cm^{-2} (5.5 cm), below which there was a systematic decrease in concentration with depth, falling to 8.1 Bq kg^{-1} at a depth of 6.9 g cm^{-2} (29 cm). This was interpreted as indicating a mixed zone of sediment to 1.04 g cm^{-2} (5.5 cm) and the sedimentation rate was obtained by plotting the natural logarithm of the unsupported ^{210}Pb concentration against depth in g cm^{-2} and linear regression fitting of a straight line to the data for samples from below the mixed layer, giving a correlation coefficient (r) of 0.96. A constant initial concentration (below the mixed layer) calculation (i.e. gradient = -λ/s see section 1.2.2.) was performed to give a sedimentation rate of 0.10 g cm^{-2} y^{-1}. The inventory of unsupported ^{210}Pb was calculated to be 9500 ± 1500 Bq m^{-2}, implying a steady state flux of 296 ± 47 Bq m^{-2} y^{-1} (calculated by multiplication of the total inventory by the decay constant). This flux can be compared to atmospheric ^{210}Pb fluxes of 71.3 to 150 Bq m^{-2} y^{-1} obtained by Sugden (1993) from Scottish peat cores, with the highest value of 150 Bq m^{-2} y^{-1} being for a core from North Uist. Appleby et al. (1990) obtained a ^{210}Pb flux, for Loch Sionascraig, north west Scotland of 148 Bq m^{-2} y^{-1} while Krishnaswamay and Lal (1978) estimated

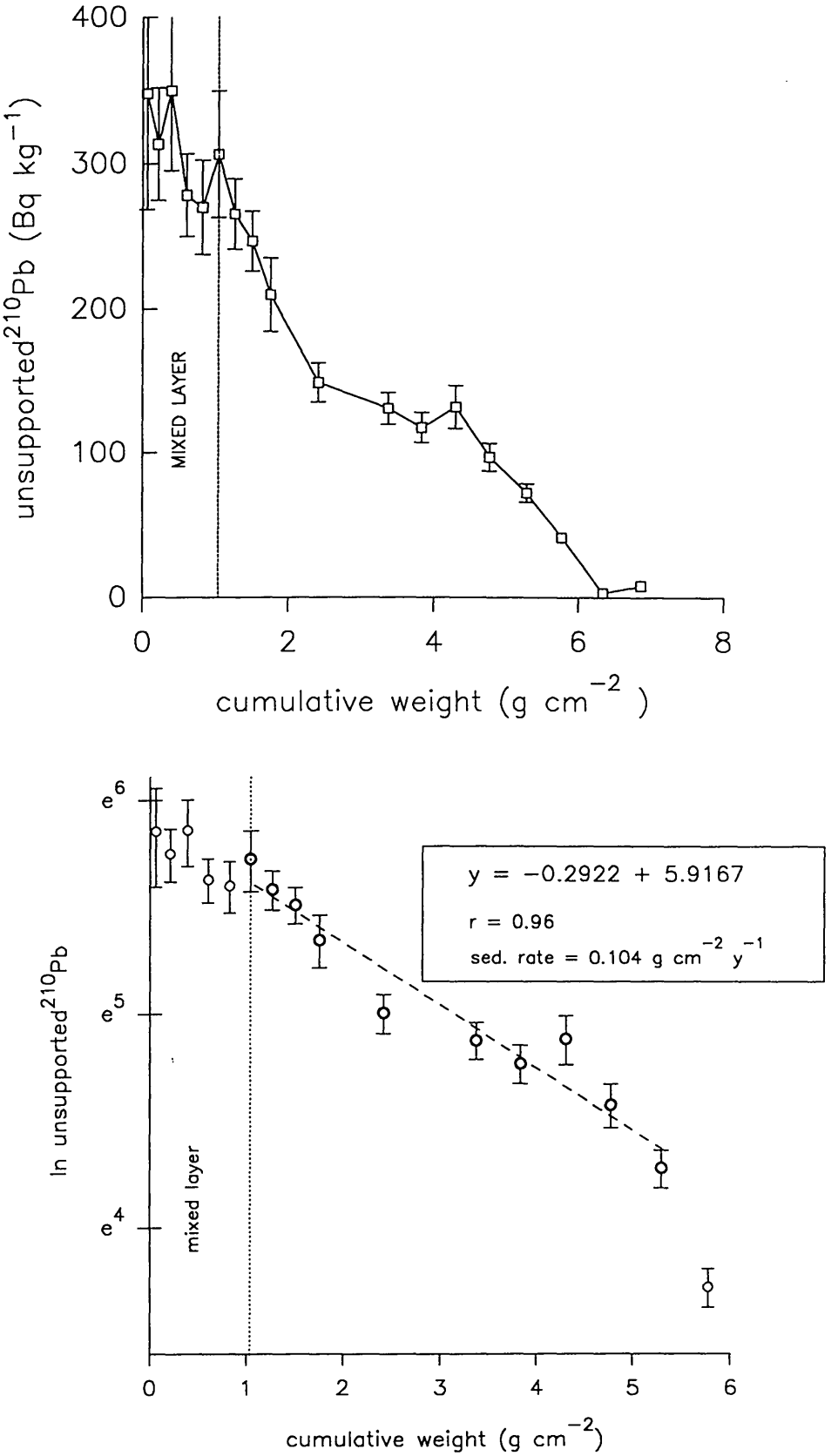

Figure 4.2. Loch Etive core LE1 unsupported ^{210}Pb concentrations

the mean global ^{210}Pb flux onto the land surface of the earth to be 166.5 Bq m^{-2} y^{-1}. Therefore, if the atmospheric flux of ^{210}Pb to the surface of Loch Etive is assumed to be approximately 150 Bq m^{-2} y^{-1}, it can be seen that the flux to LE 1 is approximately twice that expected from atmospheric deposition.

The flux of unsupported ^{210}Pb from in-situ production in the water column can be estimated by using a mean value of 0.002 Bq l^{-1} for the dissolved ^{226}Ra concentration (MacKenzie; 1977) and the volume of water overlying unit area of sediment. For LE 1 this gives a water column inventory of 112 Bq m^{-2} of ^{226}Ra which would generate 3.5 Bq m^{-2} y^{-1} of ^{210}Pb, setting this as an upper limit to the flux to the sediment from this source. Therefore, there is a greater flux of ^{210}Pb to LE 1 than can be accounted for by the expected atmospheric flux plus that from water column in-situ production. This suggests either a far greater atmospheric flux than expected or another source of unsupported ^{210}Pb to the sediment which could be due to solution input (from the Atlantic), particulate input from sea or land, sediment focusing or preferential deposition of ^{210}Pb at this location. The high ^{210}Pb flux for core LE 1 can be compared to the surface transect for Loch Etive (section 4.1) which has surface ^{210}Pb concentrations in the range 107 to 407 Bq kg^{-1}, with the concentration of ^{210}Pb at the surface transect site corresponding to that of LE 1 being 368 Bq kg^{-1}. This is the highest surface ^{210}Pb concentration observed for the surface samples and, in view of the trends in the transect, may add support for the suggestion of sediment focusing or preferential deposition of ^{210}Pb at this location.

On the basis of the calculated sedimentation rate it is possible to date some of the horizons seen in the element/Al ratios profiles (Fig. 4.1.) although it must be borne in mind that the profiles will have been influenced by the effects of mixing. Thus, the Si/Al ratio profile indicates a change in the type of sediment being deposited from 7.9 to 3.4 g cm^{-2} (33 to 15 cm) with the maximum value occurring at 4.8 g cm^{-2} (21 cm). These depths can be given (mid section dates) of 1912 to 1956 and 1942 respectively, however the effects of mixing must be considered. Mixing would damp the magnitude of a peak and spread it but not affect its position within the sediment column,

however mixing would smear downwards the effects of a change in sediment type. Therefore, after taking into account the effect of mixing the above depths correspond to correspond to 1921 to 1965 and 1942. The maxima in the Ca/Al ratio profile, indicate possible shell bands at depths of 6.3, 8.4 and 10.5 g cm^{-2} 1928, 1907 and 1887 respectively. The bottom of the mixed layer at a depth of 1.04 g cm^{-2} (5.5 cm) corresponds to 1977, giving a time of approximately 9 years for accumulation of a quantity of sediment equivalent to the mixed layer.

4.2.3 *^{137}Cs, ^{134}Cs and ^{241}Am profiles of core LE 1*

As described in Chapter 1 the three major inputs of radiocaesium to the environment of the west coast of Scotland have been Sellafield discharges, weapons testing fallout and Chernobyl fallout. The Sellafield discharge has been by far the most significant and the general features of the ^{137}Cs profile shown in Fig 4.3 follow the trends of temporal variations in the Sellafield discharge which had a pronounced maximum in 1975. (Fig. 1.4.). The ^{134}Cs/ ^{137}Cs activity ratio data can potentially be used to distinguish between Sellafield, weapons fallout and Chernobyl inputs as the ratio values for both the Sellafield discharge and Chernobyl fallout are well characterised and weapons testing fallout did not contain ^{134}Cs. However, as detailed below the effects of mixing limit the applicability of this approach in the present situation.

The ^{137}Cs profile has a concentration of 297.6 Bq kg^{-1} at the surface with a subsurface maximum of 312.9 Bq kg^{-1} at 0.6 g cm^{-2} (3.5 cm), below which the concentration decreases to 2.7 Bq kg^{-1} at a depth of 11.6 g cm^{-2} (47 cm). The maximum ^{137}Cs concentration occurs within the mixing depth of 1.04 g cm^{-2} indicated by the unsupported ^{210}Pb profile and the broad maximum in ^{137}Cs concentrations over the range 0.6 to 1.26 g cm^{-2} (3.5 - 6.5 cm) with the mid point at 0.93 g cm^{-2} (5 cm) suggests that the ^{137}Cs distribution in the sediment has been influenced by the mixing. This observation is consistent with the different effects of mixing on the steady state ^{210}Pb system and the non steady state input of ^{137}Cs. Thus, as indicated by Berner (1980), the effects

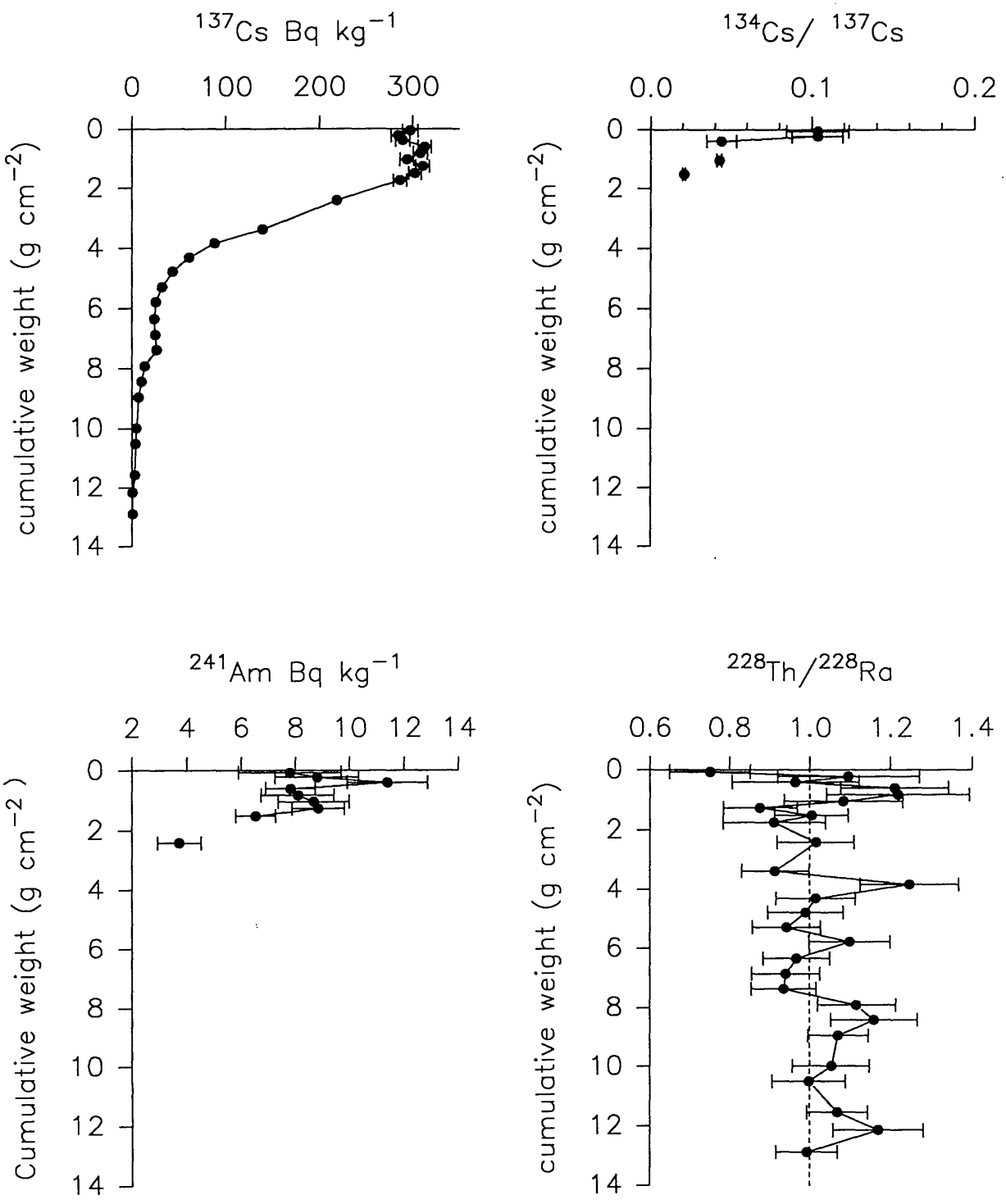

Figure 4.3. Loch Etive core LE1 radionuclide concentrations and activity ratios.

of mixing on a pulsed input of a species to a sediment will be to broaden and damp the amplitude of the peak but leave it in its correct vertical position in the sediment column.

In principle, both the shape of the ^{137}Cs profile and the total depth of penetration afford an opportunity to derive a sedimentation rate by equating the sub surface maximum with peak discharges from Sellafield (Swan et al.,1982), or by relating the start date of 1952 for the Sellafield discharge to the depth of maximum penetration of ^{137}Cs in the sediment (Ridgway and Price, 1987). Assuming that the maximum discharge of 1975 reached Loch Etive in 1977 (i.e two years transport time; McKinley et al., 1981; McKay, 1983) and that this corresponds to the mid point of the maximum (at a depth of 0.93 g cm^{-2}) then a sedimentation rate of 0.10 g cm^{-2} y^{-1} is obtained which is in excellent agreement with the sedimentation rate of 0.10 g cm^{-2} y^{-1} obtained from the unsupported ^{210}Pb.

The sedimentation rate obtained for core LE 1 from the depth of penetration of ^{137}Cs is 0.34 g cm^{-2} y^{-1}, which is clearly inconsistent with the previous two estimates. If mixing to a depth of 1.04 g cm^{-2} is taken into account the sedimentation rate based upon the first appearance of ^{137}Cs becomes 0.31 g cm^{-2} y^{-1} which is still considerably higher than the sedimentation rates of 0.10 g cm^{-2} y^{-1} obtained from the unsupported ^{210}Pb profile and 0.10 g cm^{-2} y^{-1} obtained from the position of the ^{137}Cs maximum. In recent years it has been accepted that caesium diffuses in the pore waters of sediments (Sholkovitz et al., 1983; Santschi et al., 1983; Torgersen and Longmore, 1984; Sholkovitz and Mann, 1984). Thus, diffusion of ^{137}Cs, along with the effects of mixing, invalidates the use of the depth of penetration of ^{137}Cs to calculate accumulation rates in this sediment. Therefore, in conclusion, the unsupported ^{210}Pb and the position of the ^{137}Cs maximum give consistent sedimentation rates but the depth of penetration of ^{137}Cs does not.

The inventory of ^{137}Cs in core LE 1 is 10100 $\pm$ 290 Bq m^{-2} which, allowing for decay and subsequent inputs, is in good agreement with a value of 12300 Bq m^{-2} reported by McKay (1983) for a Craib core collected from the inner basin

of Loch Etive.

The $^{134}Cs/^{137}Cs$ ratio reflects the input of radiocaesium from Chernobyl fallout at the surface of the sediment. The $^{134}Cs/^{137}Cs$ ratio of Chernobyl fallout (26/4/86) was 0.55 (Horrill et al., 1988; Fowler et al., 1987), which, when decay corrected to the time of collection of the core (12/9/86), gives a value of 0.49. The decay corrected $^{134}Cs/^{137}Cs$ ratio for the Sellafield discharge from 1984 (assuming a 2 year transit time) was 0.043 (BNFL, 1985). The ratios for the top two samples of core LE 1 are 0.103 and 0.104 below which it drops to 0.02 at a depth of 1.5 g cm^{-2}. The data therefore reveal that Chernobyl radiocaesium was mixed from the surface of the core to approximately 0.21 g cm^{-2} (1.5 cm) in a time span of 5 months. The depth of mixing indicated by the $^{134}Cs/^{137}Cs$ ratio is in good agreement with the depth of the mixing zone obtained from the unsupported ^{210}Pb profile. The amounts of Chernobyl derived ^{134}Cs and ^{137}Cs in the surface sample were calculated to be 19.8 Bq kg^{-1} and 40.4 Bq kg^{-1} respectively, representing 63 % of the total ^{134}Cs and 14 % of the ^{137}Cs in the surface sediment. However, mixing is taking place in the upper 1.04 g cm^{-2} (5.5 cm) of this core and as a result the $^{134}Cs/^{137}Cs$ ratio from the Sellafield discharge for 1984 will have been modified and thus, the calculated amounts of radiocaesium resulting from Chernobyl fallout can only be taken as an estimate. The inventory of ^{134}Cs for core LE 1 was 128 $\pm$ 6 Bq m^{-2}.

Using the ^{210}Pb chronology the depths (g cm^{-2}) corresponding to the onset of Sellafield discharge in 1954 (i.e. 1952 +2 years) and the maximum weapons testing fallout in 1963 can be calculated as 3.3 and 2.4 g cm^{-2} respectively. ^{137}Cs was in fact detectable to a depth of 11.6 g cm^{-2} which is considerably deeper than the calculated depths. If the effect of mixing is taken into account then the depth of penetration becomes 4.3 g cm^{-2} which suggests that the ^{137}Cs has diffused by a depth of 7.3 g cm^{-2}. However it must be remembered that although great care was taken in the sampling the cores, it is possible that some smearing of the sediment has occurred.

The ^{241}Am concentration profile exhibits a surface value of 7.8 Bq kg^{-1} and a

maximum of 11.4 Bq kg^{-1} at 0.39 g cm^{-2} (2.5 cm). ^{241}Am was only detectable to a depth of 2.41 g cm^{-2} (11 cm). As discussed in Chapter 1, ^{241}Am is particle reactive and it has been established that transport of Sellafield waste radionuclides to this area effectively occurs exclusively by solution transport (MacKenzie et al., 1987). Thus, since ^{241}Am is almost entirely taken up by the sediment of the Irish Sea, there will be little or no direct transfer of this nuclide to Loch Etive. In contrast, plutonium exists in two oxidation states in the marine environment, with the more soluble oxidised form being reasonably soluble (Nelson and Lovett, 1978), Therefore the ^{241}Am detected in Loch Etive will be dominantly from the grow in of ^{241}Am from ^{241}Pu from Sellafield waste, approximately 10% of which remains in the soluble Pu^{5+} form (Jefferies et al., 1973; Livingston et al., 1982; Pentreath et al., 1984; Hunt, 1985) and is transported out of the Irish Sea. ^{241}Pu from bomb fallout may also contribute to a lesser extent. The $^{137}Cs/\ ^{241}Am$ ratio for Irish sea sediments is in the range 1 to 10 (McDonald et al., 1990) whereas for LE 1 the ratio has values in the range 25-46 which substantiates the argument for solution transport of the Sellafield discharge nuclides to Loch Etive.

The "grow in" to 1986 of ^{241}Am from annual discharges of ^{241}Pu from Sellafield shows two maxima; one of 42 T Bq from discharges in 1973 and the other of 19 T Bq from discharges in 1978. The ^{241}Am profile for LE 1 also shows two maxima, with mid section dates of 1983 and 1975 respectively, which correspond to 1981 and 1973 when taking into account the transport time of two years. Therefore, the two maximum concentrations of ^{241}Am in the sediment correspond well with the dates of maximum ^{241}Am "grow in" from yearly discharges of ^{241}Pu from Sellafield. The maximum ^{241}Am concentration of 8.8 Bq kg^{-1} corresponding to the 1973 discharge of 42 T Bq is, however, lower than the value of 11.4 Bq kg^{-1} which corresponds to the 1978 discharge of 19 T Bq. This could be a consequence of the fact that the material deposited in 1975 has passed through the mixed zone and, as discussed above, the amplitude of the peak will therefore have been damped, reducing its concentration. Hence, the ^{241}Am profile supports the chronology obtained from the ^{210}Pb dating. Therefore, the radiocaesium and ^{241}Am provide two independent radionuclide chronologies that agree with the ^{210}Pb chronology

derived for LE 1.

If it is assumed that directly discharged ^{241}Am is retained entirely within the Irish Sea, the inventory of ^{241}Am in areas outwith the Irish Sea will be controlled by the amount of ^{241}Pu present. For Sellafield discharges to 1984, the ratio of the cumulative environmental inventory of ^{137}Cs (33538 Tb) to that of ^{241}Am grown in from the decay of ^{241}Pu (261 Tb) was 128. If it is assumed that approximately 90% of the ^{137}Cs and 10% of the ^{241}Pu remain in solution and are transported out of the Irish Sea, then outwith the Irish Sea this would have generated a total environmental inventory with a $^{137}Cs/^{241}Am$ ratio of about 1150. The in-situ production of ^{241}Am in the water column will be negligible so that the ^{241}Am detected in the sediment will be derived mainly from ^{241}Pu decay in the sediment. Thus, the $^{137}Cs/^{241}Am$ ratio will be controlled primarily by the relative transfer of ^{137}Cs and ^{241}Pu from the water column to the sediment and equal transfer of ^{137}Cs and ^{241}Pu would therefore give an inventory ratio of approximately 1150. Hetherington (1975) observed an effectively constant ratio of Cs:Pu in sea water over a distance of the order of 100 km within the Irish Sea indicating similar behaviour of ^{137}Cs and the dissolved component of the Pu, so this assumption of similar behaviour is not unreasonable, but is clearly inconsistent with the observed ratio of 75. Assuming a factor of 10 greater uptake of ^{241}Pu than ^{137}Cs by the sediment, an integrated $^{137}Cs/^{241}Am$ ratio of approximately 115 would be obtained which is in reasonable agreement with the observed value but is inconsistent with the similarity in behaviour of ^{137}Cs and Pu^{5+}. However in recent years research has shown that there has been up to 80% re-dissolution of ^{137}Cs from the sediments of the Irish Sea (Hunt and Kershaw, 1990; McCartney et al., 1992; Comans et al., 1989; Jones et al., 1988) and the $^{137}Cs/\ ^{241}Am$ ratio for core LE 1 could be interpreted as indicating the effects of re-dissolution of ^{137}Cs from the sediments of this core. This magnitude of re-dissolution would, however, be difficult to reconcile with the shape of the ^{137}Cs profile. Therefore, there is not an obvious explanation for this observation and the assumptions that, either there may be a greater uptake of Pu in comparison with ^{137}Cs, or that there is significant re-dissolution of ^{137}Cs may not be valid.

4.2.4 *^{228}Th and ^{228}Ra profiles of core LE 1*

The ^{228}Th/ ^{228}Ra profile for core LE 1 is shown in figure 4.3. The ratio has a value of 0.75 in the surface sediment then increases to a maximum of 1.21 at 0.6 g cm^{-2} (3.5 cm) depth below which it is within error of equilibrium to the bottom of the core. The inventories for ^{228}Th and ^{228}Ra are however essentially the same, with values of 4920 ± 230 and 4760 ± 380 respectively, indicating that there is no excess of either radionuclide in the sediment core. The ^{228}Th/ ^{228}Ra profile and the inventories suggest that ^{228}Ra is mobile and has been redistributed within the core, probably being controlled by the Mn distribution within the sediment. The variations in the activity ratio profile occur within the mixed zone suggested by the unsupported ^{210}Pb, indicating that the redistribution of ^{228}Ra must be more rapid than the rate of mixing. ^{232}Th concentration data for individual samples are not available, however an average ^{232}Th inventory for core LE 1 was calculated by using the ^{232}Th concentration for the surface transect sample 5, which corresponded to the sampling site of core LE 1 and assuming that the same concentration applied throughout the core. The ^{232}Th inventory of 5300 Bqm^{-2} obtained by this method is within error, the same as the ^{228}Th inventory of 4920 Bq m^{-2} indicating that there is no significant excess or deficiency of ^{228}Ra or ^{228}Th relative to ^{232}Th in this core in contrast to the conclusion derived in section 4.1.1. from consideration of surface samples only.

4.2.5 *Stable Pb and Pb isotope ratios of core LE 1*

In recent years, as discussed in Chapter 1, the immobility of Pb in sediments has been questioned and this casts doubt upon the validity of ^{210}Pb dating (Elbaz-Poulichet et al., 1984; Ridgway and Price, 1987; Wan et al, 1987; Beniot and Hemond, 1990; Beniot and Hemond, 1991; Urban et al., 1990). It is therefore essential that Pb mobility in sea-loch sediments be investigated with respect to assessing pollutant Pb inputs and using ^{210}Pb dating. In this context stable Pb concentrations and stable Pb isotope ratios were determined and the profiles compared with the chronologies obtained from ^{210}Pb dating.

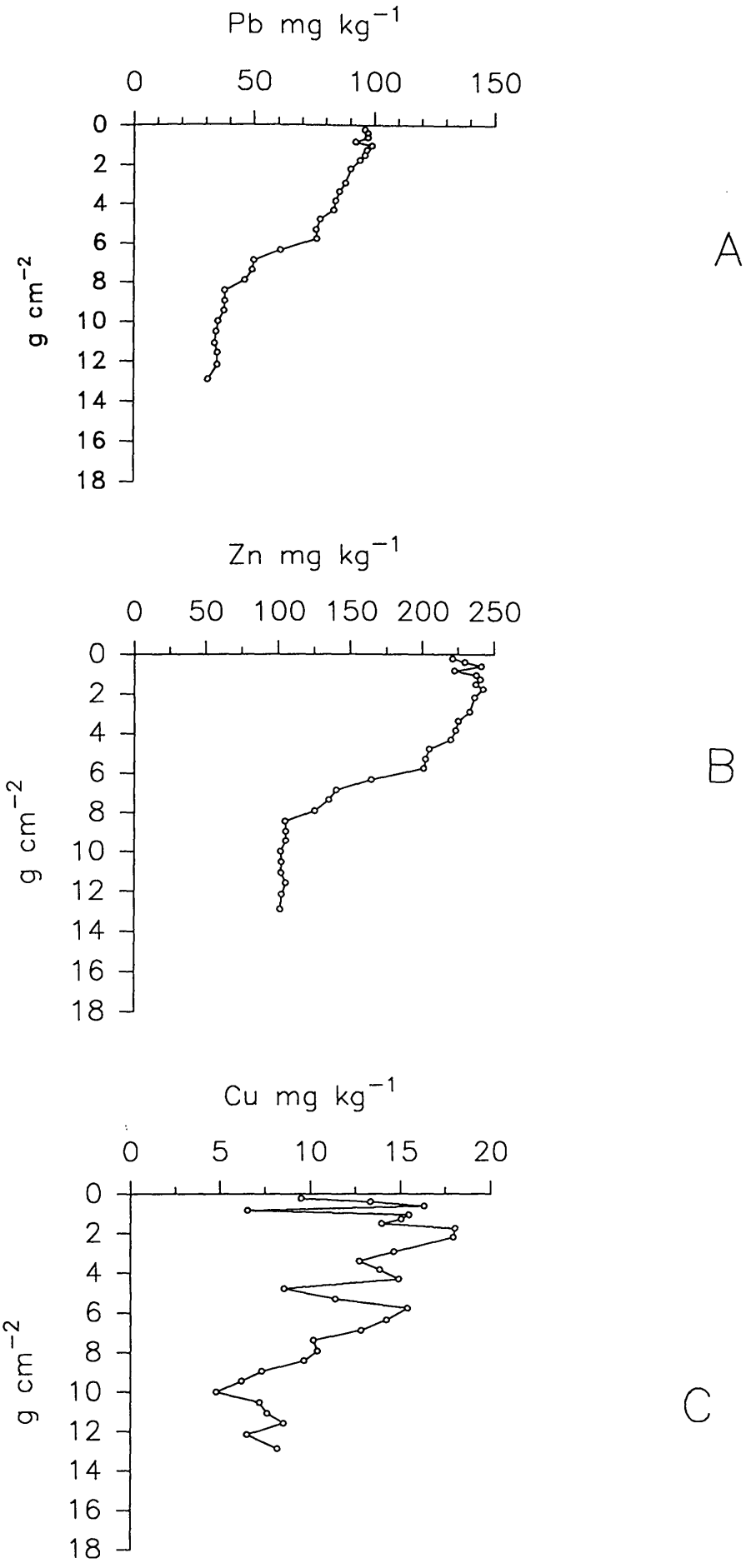

Figure 4.4. Loch Etive core LE1 Pb, Zn and Cu concentrations (mg kg^{-1})

The total stable Pb concentration data are presented in Table 3.8 and the plot of total Pb versus cumulative weight (g cm^{-2}) is shown in Figure 4.4. A. The Pb concentration is essentially constant at a value of about 96 mg kg^{-1} to a depth of 1.04 g cm^{-2} (5.5 cm), which corresponds to the bottom of the mixed layer as defined by the ^{210}Pb distribution. The Pb concentration then decreases to 83 mg kg^{-1} at a depth of 4.3 g cm^{-2} (19 cm), below which there is a more rapid decrease to 38 mg kg^{-1} at a depth of 8.4 g cm^{-2} (35 cm). Thereafter, the Pb concentration decreases slowly to a value of 31 mg kg^{-1} at 12.9 g cm^{-2} (52.5 cm). Pb was detectable to the bottom of the core at a mid section date of 1866 (using the ^{210}Pb chronology) which, after considering mixing corresponds to 1875. The sediment from a depth of 10 g cm^{-2} (41 cm) to the bottom of the core (12.9 g cm^{-2}; 52.5 cm) has a relatively constant Pb concentration ranging from 35 to 31 mg kg^{-1} which was considered to be representative of the non pollutant Pb in this sediment and the pollutant Pb concentration was calculated by subtracting a mean value of 34 mg kg^{-1} from the total Pb concentration. However, it was recognised that this assumption was limited by the depth of the sediment core and that the value of 34 mg kg^{-1} probably represents the natural lead level plus a contribution from early pollution and inventories and fluxes should therefore be regarded as lower limits.

The excess Pb flux results are given in Table 4.1. and the flux of pollutant Pb versus time for core LE 1 is shown in Figure 4.5 A.

Excess Pb is first detected in core LE 1 at a depth corresponding to deposition in 1872 (which is considered to be an upper limit for the date), with an implied lead flux of 0.004 g cm^{-2} y^{-1}. The Pb flux then increases slowly to a value of 0.006 g cm^{-2} y^{-1} by 1907. Above the 1907 horizon, there is a sharp increase in the excess Pb flux until 1933. In sediment deposited since 1933, the Pb flux continues to increase towards the surface but at a slower rate, to reach a maximum of 0.063 g cm^{-2} y^{-1} in 1977, after which it decreases slightly to a value of 0.06 g cm^{-2} y^{-1} at the surface of the sediment. The effects of mixing on the Pb profile would affect the position at which the onset of excess Pb is observed but would not affect the position of the

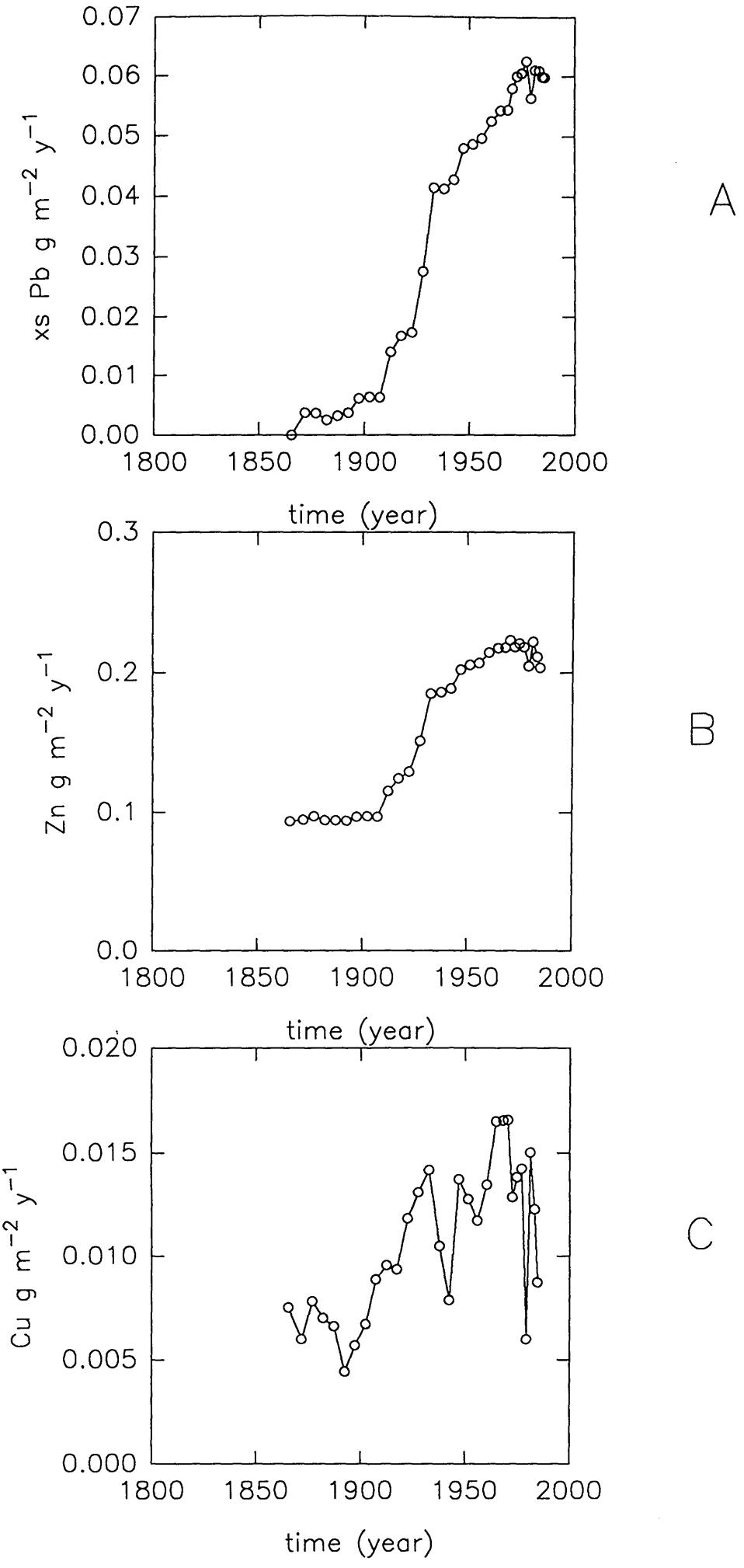

Figure 4.5. Loch Etive core LE1 Pb, Zn and Cu flux data

maximum flux (although it would damp the amplitude of the peak). If mixing to the base of the mixed zone defined by ^{210}Pb is assumed, the onset of excess Pb deposition in LE 1 would occur at 1881. As discussed above, the flux of Pb quoted must be considered as a lower limit by the probable contribution of early pollution to the assumed natural baseline Pb level but the trends in deposition will not be altered by this effect.

The inventory of excess Pb in core LE 1 is 3.8 g m^{-2} which is higher than the inventory of 0.52 g m^{-2} of total Pb observed in a North Uist peat core (Sugden, 1993) but is very similar to that of 3.38 g m^{-2} for a peat core from Flanders Moss in Stirlingshire, where the higher inventory was attributed to the proximity of the sample site to the industrial area of Central Scotland (Sugden, 1993). The fluxes of Pb to LE 1 are also similar to those found by Sugden (1993) in Loch Lomond (0.19 g m^{-2} y^{-1}, 1964) a freshwater loch lying 70 km south east of Loch Etive. Therefore, the peat core from Flanders Moss, sediment from Loch Lomond and Loch Etive all have very similar inventories which suggests that the supply of Pb to all three is by atmospheric deposition and that there is no significant additional input in any case.

As detailed in Section 1.4.2., the $^{206}Pb/^{207}Pb$ isotope ratio can potentially be used to characterise the source of pollutant Pb (Petit et al., 1984; Delves, 1988; Elbaz-Poulichet et al, 1986; Maring et al., 1987; Sturges and Barrie, 1987; Flegal et al., 1989; Sugden, 1993). The plot of $^{206}Pb/^{207}Pb$ ratio versus ^{210}Pb chronology for core LE 1 is shown in figure 4.6.A. along with the excess Pb flux (g m^{-2} y^{-1}). The surface sediment has a $^{206}Pb/^{207}Pb$ ratio of 1.149, and below the surface the ratio increases systematically with depth to a value of 1.182 at 12.89 g cm^{-2}. The trend in $^{206}Pb/^{207}Pb$ can readily be interpreted in terms of the input of Pb from different pollutant sources (Delves, 1989; Sugden, 1993). Thus if it is assumed that the profile is dominated by pollutant Pb, and that $^{206}Pb/^{207}Pb$ values of about 1.18 and 1.09 are appropriate for heavy industry and UK petrol derived Pb respectively (Sugden, 1993), then the decreasing ratio towards the sediment surface can be attributed to the increasing influence of vehicle exhaust emissions on

SAMPLE	DEPTH	cum. g cm^{-2}	date for mid section	excess Pb g cm^{-2} y^{-1}
LE1 0-1	0.5	0.06	1986	0.060
LE1 1-2	1.5	0.21	1985	0.060
LE1 2-3	2.5	0.39	1983	0.061
LE1 3-4	3.5	0.60	1981	0.061
LE1 4-5	4.5	0.82	1979	0.056
LE1 5-6	5.5	1.04	1977	0.063
LE1 6-7	6.5	1.26	1975	0.061
LE1 7-8	7.5	1.50	1973	0.060
LE1 8-9	8.5	1.75	1970	0.058
LE1 9-10	9.5	1.97	1968	0.054
LE1 10-12	11.0	2.41	1965	0.054
LE1 12-14	13.0	2.90	1960	0.052
LE1 14-16	15.0	3.37	1956	0.050
LE1 16-18	17.0	3.83	1951	0.049
LE1 18-20	19.0	4.30	1947	0.048
LE1 20-22	21.0	4.77	1942	0.043
LE1 22-24	23.0	5.29	1938	0.041
LE1 24-26	25.0	5.77	1933	0.041
LE1 26-28	27.0	6.34	1928	0.027
LE1 28-30	29.0	6.87	1922	0.017
LE1 30-32	31.0	7.37	1918	0.017
LE1 32-34	33.0	7.91	1912	0.014
LE1 34-36	35.0	8.43	1907	0.006
LE1 36-38	37.0	8.96	1902	0.006
LE1 38-40	39.0	9.45	1897	0.006
LE1 40-42	41.0	9.99	1892	0.004
LE1 42-44	43.0	10.52	1887	0.003
LE1 46-48	47.0	11.08	1882	0.003
LE1 46-48	47.0	11.56	1877	0.004
LE1 48-50	49.0	12.16	1872	0.004
LE1 50-55	52.5	12.89	1866	0.000

Table 4.1 Loch Etive core LE 1 Pb flux data

pollutant Pb fluxes to the sediment during this century. On the basis of the ^{210}Pb chronology, the onset of the change in $^{206}Pb/\ ^{207}Pb$ ratio took place at

approximately 1928 if mixing is ignored. If the effect of mixing is included for this core, an offset of 1.04 g cm^{-2}, which is equivalent to 9 years, would be applied. Thus, when mixing is taken into consideration the onset of the influence of Pb in petrol is seen in this sediment at approximately 1937. This date corresponds well with the onset of use of Pb in petrol as an 'antiknock' agent in 1922 (Guthrie, 1960).

It is now apparent that for this core there is independent chronological agreement between ^{210}Pb dating, ^{137}Cs dating, the ^{241}Am distribution and recorded trends in the stable Pb isotope input to the environment. The agreement between these independent parameters gives considerable confidence in the chronology and the immobility of Pb in this sediment.

The $^{206}Pb/ ^{207}Pb$ isotope results obtained for this core can be compared to the profile obtained by Sugden (1993) (Fig 4.5 B.) for a peat core from North Uist in the Outer Hebrides which was considered to reflect atmospheric deposition of pollutants. The $^{206}Pb/ ^{207}Pb$ profile for the peat shows the change in $^{206}Pb/ ^{207}Pb$ ratio occurring at approximately 1908 which is earlier than that found in core LE 1 and is in fact earlier than the date of introduction of Pb to petrol. The date of 1908 used by Sugden was, however, obtained without considering any mixing effects in the peat and must therefore be taken as a lower limit. The surface $^{206}Pb/ ^{207}Pb$ value for the North Uist peat core was 1.143 which is similar to, but slightly lower than, that of core LE 1 which reflects the predominantly petrol pollutant source to the peat in this remote location (Sugden, 1993). The lower surface $^{206}Pb/ ^{207}Pb$ ratio of the peat core also reflects the lower mineral content of the peat and hence the lower intrinsic Pb contribution from minerals in comparison to the sediment core.

It can be concluded that there is generally very good agreement between the $^{206}Pb/ ^{207}Pb$ profiles of the sediment core LE 1 and the peat core from North Uist which provides even more confidence in the chronology and behaviour of Pb in this sediment core.

Sugden (1993) used the following three component model to calculate the

percentage contributions of petrol, heavy industry and intrinsic Pb to the total Pb content of sediment. This model has the advantage of considering the intrinsic, industrial and petrol components but has the disadvantage of not allowing for variations in the ^{208}Pb concentration, although this will be a small effect.

$$R_s \times C_s = (R_i \times C_i) + [\, R_{Hi}(C_e - C_p)\,] + (R_p \times C_p)$$

where R_s= $^{206}Pb/\ ^{207}Pb$ of section

C_s=Pb concentration of section

R_i= $^{206}Pb/\ ^{207}Pb$ at depth

C_i= baseline Pb concentration

RH_i= $^{206}Pb/\ ^{207}Pb$ from historical industrial input (1.172 peat core)

C_E= excess Pb per section

$R_{P=}$ $^{206}Pb/\ ^{207}Pb$ in petrol (1.09)

C_P = Pb concentration in sediment derived from petrol.

The figures for core LE 1 are given in Table 4.2.

It should be noted here and in subsequent use of this model that the calculation of the percentage of the Pb derived from petrol depends very heavily on the choice of values for the ratios R_i and R_{Hi}. For core LE 1 R_i= 1.176 (mean of ratios at depth) and R_{Hi}= 1.172 were assumed and the results show the onset of deposition of pollutant Pb from petrol in 1933 at 4% which, after considering mixing, becomes 1942. However the contribution of petrol increases rapidly, reaching 40% in the late 1960's.

Comparison of the date of the onset of deposition of pollutant Pb from petrol from the above equation with those obtained by visual inspection of the $^{206}Pb/\ ^{207}Pb$ ratio profile (1928 and 1937 for a mixing and a no mixing situation) reveals a difference of 7 years in the estimated date of onset of petrol Pb deposition, which probably arises from the fact that a small change in either

of the ratios R_i and R_{Hi} will induce a discernable difference in the estimated percentage of the total Pb that arises from petrol Pb. Moreover, the probable contribution of early pollution to the bottom of the core means that the value assumed for R_i will probably be inaccurate.

Use of a single isotope ratio only utilises part of the available data and there are two independent ratios measured. An alternative approach which does employ all of the data is to plot the $^{208}Pb/^{206}Pb$ against the $^{206}Pb/^{207}Pb$ ratio. In the use of such diagrams, if there is a two component lead system, each component having its own characteristic $^{206}Pb/^{207}Pb$ and $^{208}Pb/^{206}Pb$ ratios, then mixing of the two will occur along a "tie line" between the end members representing the two pure components. Figure 4.12.B. indicates the positions of petrol, coal and mined ores from Scotland (Sugden, 1993) on such a diagram. A plot of this type is shown for core LE 1 in Figure 4.6.C. and the samples are numbered 1 to 31 reflecting the sequence of samples from surface to depth.

The results suggest a three component system (A, B and C) with two tie lines joining the end members. Samples deposited post 1900 form one group with an apparently two component system (A and B). All of these samples have Pb concentrations which are greater than 34 mg kg^{-1} and it is reasonable to assume that the Pb content is dominated by pollutant Pb. Thus the results indicate a mixing of pollutant sources from the older samples which are dominated by "heavy industry" signature (B) (c.f. $^{206}Pb/^{207}Pb$= 1.172-1.187, $^{208}Pb/^{206}Pb$= 2.075-2.109 Sugden, 1993.) to recent samples which have a significant input of petrol lead (A) (c.f. $^{206}Pb/^{207}Pb$= 1.093, $^{208}Pb/^{206}Pb$= 2.146, Sugden,1993.) with mixing occurring along tie line A-B.

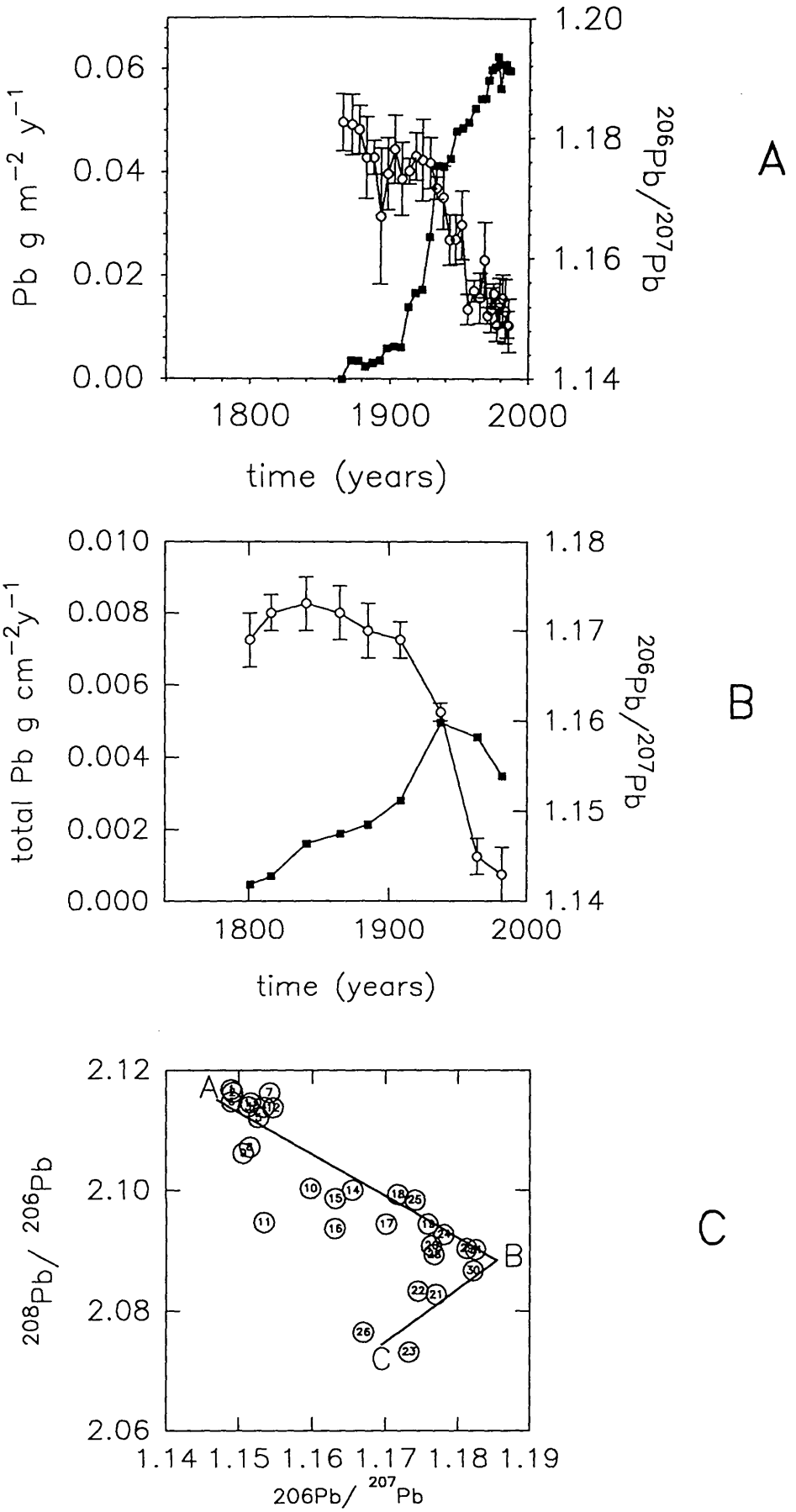

Figure 4.6. Loch Etive core LE1 Pb flux and Pb isotope ratio plots

SAMPLE	DEPTH	cum. g cm^{-2}	date for mid section	% Pb petrol
LE1 0-1	0.5	0.06	1986	44
LE1 1-2	1.5	0.21	1985	44
LE1 2-3	2.5	0.39	1983	39
LE1 3-4	3.5	0.60	1981	36
LE1 4-5	4.5	0.82	1979	38
LE1 5-6	5.5	1.04	1977	43
LE1 6-7	6.5	1.26	1975	34
LE1 7-8	7.5	1.50	1973	39
LE1 8-9	8.5	1.75	1970	41
LE1 9-10	9.5	1.97	1968	25
LE1 10-12	11.0	2.41	1965	37
LE1 12-14	13.0	2.90	1960	35
LE1 14-16	15.0	3.37	1956	42
LE1 16-18	17.0	3.83	1951	15
LE1 18-20	19.0	4.30	1947	20
LE1 20-22	21.0	4.77	1942	21
LE1 22-24	23.0	5.29	1938	7
LE1 24-26	25.0	5.77	1933	4
LE1 26-28	27.0	6.34	1928	
LE1 28-30	29.0	6.87	1922	
LE1 30-32	31.0	7.37	1918	
LE1 32-34	33.0	7.91	1912	
LE1 34-36	35.0	8.43	1907	
LE1 36-38	37.0	8.96	1902	
LE1 38-40	39.0	9.45	1897	
LE1 40-42	41.0	9.99	1892	
LE1 42-44	43.0	10.52	1887	
LE1 46-48	47.0	11.08	1882	
LE1 46-48	47.0	11.56	1877	
LE1 48-50	49.0	12.16	1872	
LE1 50-55	52.5	12.89	1866	

Table 4.2 % Pb in sediment from Pb in petrol

In the deeper section of the core, deposited before 1900, the data appear to follow a different tie lie, in this case probably reflecting mixing of "heavy industry" (B) pollutant Pb and natural Pb in the system (C) with mixing occurring along the tie line B-C.

4.2.6 *Zn and Cu profiles of core LE 1*

Zn and Cu also occur ubiquitously in the environment as atmospherically deposited industrial pollutants (Nriagu, 1991; Ducastel et al., 1991; Berg et al., 1991), with world wide industrial discharges into the air during 1983 of $132x10^9$ and $35x10^9$ g y^{-1} respectively (c.f. Pb= $332x10^9$ g y^{-1}) (Nriagu and Pacyna, 1988), and concentration profiles of these metals in core LE 1 are shown in Figures 4.4.B. and 4.4.C. The Zn profile is very similar to the total Pb profile, with the concentration increasing from a surface value of 221 mg kg^{-1} to 241 mg kg^{-1} at a depth of 0.6 g cm^{-2} (3.5 cm) then remaining essentially constant (with the exception of one point at 0.8 g cm^{-2}) to a depth of 2.19 g cm^{-2} (10.5 cm). Beneath this level, the concentration decreases to a value of 201 mg kg^{-1} at a depth of 5.8 g cm^{-2} (25 cm), after which it decreases more rapidly to 105 mg kg^{-1} at a depth of 8.4 g cm^{-2} (35 cm). Thereafter the concentration remains constant to the bottom of the core at 12.9 g cm^{-2} (52.5 cm). Assuming that the excess Pb profile represents the distribution of pollutant Pb during the 19^{th} and 20^{th} centuries, then the strong similarity of the Zn profile to that of the Pb, suggests that Zn has a similar behaviour, with the sediment profile providing a historical record of the deposition of industrial pollutants (modified by mixing). Using the ^{210}Pb chronology the maximum concentration of Zn occurs at a mid section date of 1981 and the constant value of 105 mg kg^{-1} at 1907 which, after considering mixing, corresponds to 1916. The sharp change of the Zn concentration occurs between 1907 and 1947, which after taking account of mixing, becomes 1916 to 1956.

The Cu profile is much more irregular but follows the same general trend as the total Pb and Zn profiles. The more variable structure of the profile probably reflects the low concentrations of Cu in the sediment which were

close to the limits of the XRF analysis. The sample at 0.6 g cm^{-2} (3.5 cm) has a low concentration of Pb, Zn and Cu. This minimum is also reflected in the Si/Al, Zr/Al, Ca/Al and Rb/Al ratios which could reflect a change in the sediment type at this depth. The pollutant metal data suggest that there was a major change in input starting at 8.4 g cm^{-2} (35 cm) which continued to 4.3 g cm^{-2} (approximately 19 cm). These trends can be compared with those of the element/Al ratios over the same depth range (Fig 4.1.) e.g. the Si/Al and Zr/Al ratios both have maximum values over this depth range and the Ca/Al ratio indicates shell bands at the top and bottom of the range. By using the ^{210}Pb chronology the depth ranges give a time span of 1907 (8.4 g cm^{-2}) to 1947 (4.3 g cm^{-2}) which after taking into account mixing, corresponds to 1916 and 1956. The geochemical and the pollutant metal data therefore indicate that there was a major change in material supplied, both directly and atmospherically, to the loch during the period spanning the two world wars, reflecting the change in industrial activity over this time. The increase in Pb, Zn and Cu concentrations is consistent with the increase of heavy industry during this time.

The fluxes of excess Pb, total Zn and total Cu are given in Table 4.3. and illustrated in Figure 4.6. As discussed before, the dates applied to changes in the fluxes may be subject to an approximately 9 year offset due to mixing within the core, but peak values will probably be in their correct position although the magnitude of the flux will be reduced.

The Zn flux profile is very similar to that of the Pb flux and follows even the fine structure of the Pb profile up to approximately 1950. Thereafter the Zn flux levels off whereas the Pb flux continues to increase. This is consistent with a post war decline in metal deposition from heavy industry but an increased Pb input from petrol. The Zn flux is relatively constant from 1866 to 1907, which corresponds to 1876 to 1916 after accounting for mixing, with a value of about 0.09 g m^{-2} y^{-1} after which it rises rapidly to 0.202 g m^{-2} y^{-1} around 1950 and thereafter more slowly to maxima of 0.223 and 0.222 g m^{-2} y^{-1} in 1970 and 1981. The total inventory of Zn in this core was 21.1 g m^{-2}.

SAMPLE	DEPTH	cum. g cm^{-2}	date for mid section	Cu g m^{-2} y^{-1}	Zn g m^{-2} y^{-1}
LE1 0-1	0.5	0.06	1986		
LE1 1-2	1.5	0.21	1985	0.009	0.204
LE1 2-3	2.5	0.39	1983	0.012	0.211
LE1 3-4	3.5	0.60	1981	0.015	0.222
LE1 4-5	4.5	0.82	1979	0.006	0.205
LE1 5-6	5.5	1.04	1977	0.014	0.219
LE1 6-7	6.5	1.26	1975	0.014	0.221
LE1 7-8	7.5	1.50	1973	0.013	0.218
LE1 8-9	8.5	1.75	1970	0.017	0.223
LE1 9-10	9.5	1.97	1968	0.017	0.218
LE1 10-12	11.0	2.41	1965	0.017	0.218
LE1 12-14	13.0	2.90	1960	0.013	0.214
LE1 14-16	15.0	3.37	1956	0.012	0.207
LE1 16-18	17.0	3.83	1951	0.013	0.206
LE1 18-20	19.0	4.30	1947	0.014	0.202
LE1 20-22	21.0	4.77	1942	0.008	0.189
LE1 22-24	23.0	5.29	1938	0.010	0.186
LE1 24-26	25.0	5.77	1933	0.014	0.185
LE1 26-28	27.0	6.34	1928	0.013	0.151
LE1 28-30	29.0	6.87	1922	0.012	0.129
LE1 30-32	31.0	7.37	1917	0.009	0.125
LE1 32-34	33.0	7.91	1912	0.010	0.115
LE1 34-36	35.0	8.43	1907	0.009	0.096
LE1 36-38	37.0	8.96	1902	0.007	0.097
LE1 38-40	39.0	9.45	1897	0.006	0.097
LE1 40-42	41.0	9.99	1892	0.004	0.094
LE1 42-44	43.0	10.52	1887	0.007	0.094
LE1 46-48	47.0	11.08	1882	0.007	0.094
LE1 46-48	47.0	11.56	1877	0.008	0.097
LE1 48-50	49.0	12.16	1872	0.006	0.094
LE1 50-55	52.5	12.89	1866	0.008	0.093

Table 4.3 Cu and Zn fluxes for core LE 1

LOCATION (depth of sample)	Pb (mg kg^{-1})	Zn (mg kg^{-1})	Cu (mg kg^{-1})_
Loch Etive, inner basin [1]	35	105	21
Loch Etive, outer basin [1]	35	103	17
Loch Etive, inner basin [10] (87.5 cm)	40	93	15
Loch Etive, inner basin [10] (82.5 cm)	43	83	14
Loch Etive, inner basin [10] (77.5 cm)	40	94	14
Loch Etive, inner basin [10] (82.5 cm)	37	83	8
Loch Etive, outer basin [10] (87.5 cm)	22	94	9
Loch Etive, outer basin [10] (77.5 cm)	40	98	14
Firth of Lorne [10] (87.5 cm)	20	63	2
Loch Etive, inner basin [11] (52.5 cm)	31	102	8
Loch Etive, inner basin [11] (57.5 cm)	21	92	5
Loch Etive,outer basin [11] (62.5 cm)	38	95	7
Baltic Sea, Eckernforderbucht [2]	21	119	36
Baltic Sea, Bornholm Basin [2]	27	105	29
Chesapeake Bay, CHSP 1411 [3]	25	100	20
California Borderlands, Santa Barbara [4]	11	100	30
California Borderlands, San Martin [4]	9	130	45
California Border lands, San Pedro [4]	10	110	45
Loch Duich, Scotland [5]	26	97	20
Oslo Fjord, Norway [6]	24	227	39
Narangansett Bay [7]	12	69	15
Mofjord, Norway [8]	16	90	18
Average Shale [9]	20	95	45

Table 4.4 Baseline sediment concentrations of Pb, Zn and Cu in Loch Etive and other coastal marine sediments

The Cu fluxes for core LE 1 show a generally similar trend to Pb and Zn but in this case the curve is irregular and there are several minima that do not correspond to the Pb and Zn profiles. As discussed above this could reflect errors in the analysis as the concentrations of Cu are an order of magnitude lower than those of Pb and two orders of magnitude lower than those of Zn.

As with the Pb and Zn, the Cu flux increases rapidly to 1942 (taking account of mixing) and thereafter increases more slowly. This corresponds to the large change in the Si/Al profile and correlates with the maximum Si/Al ratio. The inventory of Cu in this core is 1.4 g m^{-2}.

As has been discussed above the estimation of natural levels of Pb are limited due to the length of the core and this is also true of the estimation of natural levels of Zn and Cu. Malcolm (1981) compiled a table of baseline concentrations of Zn, Pb and Cu in Loch Etive and other polluted and non polluted coastal marine sediments which is reproduced in Table 4.4. with some added information.

(references: 1. Malcolm, 1981; 2. Erlenkeuser et al., 1974; 3. Goldberg et al., 1978; 4. Bruland et al., 1974; 5. Krom, 1976; 6. Doff, 1969; 7. Goldberg et al., 1977; 8. Hamilton-Taylor, 1974; 9. Turkeian and Wedepohl, 1972; 10. Ridgway, 1984; 11. present study.)

It can be seen from the above table that the Pb concentration ranges from 21 to 43 mg kg^{-1} for the inner basin and 22 to 38 mg kg^{-1} for the outer basin of Loch Etive. The Zn concentration ranges from 83 to 105 mg kg^{-1} and 94 to 103 mg kg^{-1} for the inner and outer basins respectively and the Cu concentration range from 5 to 21 mg kg^{-1} and 7 to 17 mg kg^{-1} for the inner and outer basins of Loch Etive. Therefore, by assuming values of 103 and 7 mg kg^{-1} for the natural levels of Zn and Cu in core LE 1 the excess inventories of these metals were calculated to be 7.8 and 0.5 g m^{-2}, which can be compared to the total inventories of 21.1 g m^{-2} and 1.4 g m^{-2}.

Iron smelting and quarrying have been the only industrial activities in the vicinity of Loch Etive (Malcolm, 1981). The iron smelting started in 1730 with a furnace in Glen Kinglass, after which a furnace was built at Bonawe which operated until 1870. Quarrying of granite has only been undertaken on a large scale in this century at the quarry sited at Bonawe. The granite is crushed on site for use as roadstone and is mainly shipped out by small coasters. It is possible that the element/Al ratios are reflecting peak quarrying

times and/ or increased road building at these times.

4.2.7 *Summary of core LE 1*

In summary, the results for core LE 1 suggest that ^{210}Pb, ^{137}Cs, ^{241}Am, heavy metals and $^{206}Pb/ ^{207}Pb$ isotope ratio give chronologically consistent profiles, indicating that ^{210}Pb dating is valid and that Pb is not mobile in this core. The core is mixed to a depth of 1.04 g cm^{-2} which is equivalent to (5.5 cm) and has an accumulation rate of 0.104g $cm^{-2} y^{-1}$ equivalent to a time interval from the surface of the sediment to the bottom of the mixed zone of 9 years.

The manmade radionuclides present in the sediment are dominated by the Sellafield discharge with the influence of Chernobyl fallout being restricted to a depth of 0.39 g cm^{-2} (2.5 cm). The ^{134}Cs and ^{137}Cs profiles indicated mobility of Cs by means of mixing and diffusion and ^{137}Cs is detectable to far greater depths than would be expected due to mixing alone, which limits its use in chronology.

The deposition of pollutant Pb increased dramatically from the early 1900's reflecting the increase in heavy industry. Pollutant Pb from petrol can be detected in the mid 1930's and had increased to 40% of the total pollutant Pb by the 1960's. Temporal trends in pollutant Pb flux correlate well with those derived from a peat profile from North Uist, although the magnitude of the pollutant Pb flux is an order of magnitude greater in core LE 1 than in the peat core. The Zn and Cu fluxes exhibit similar temporal variations to the Pb flux.

4.3.1 *Loch Etive core LE 2*

The sample site, sampling methods and preparation of core LE 2 are described in Chapter 2 which also includes detailed descriptions of the analytical techniques used. The results for this core are tabulated in Chapter 3. The sampling location of core LE 2 was the same as that of the surface transect sample 10.

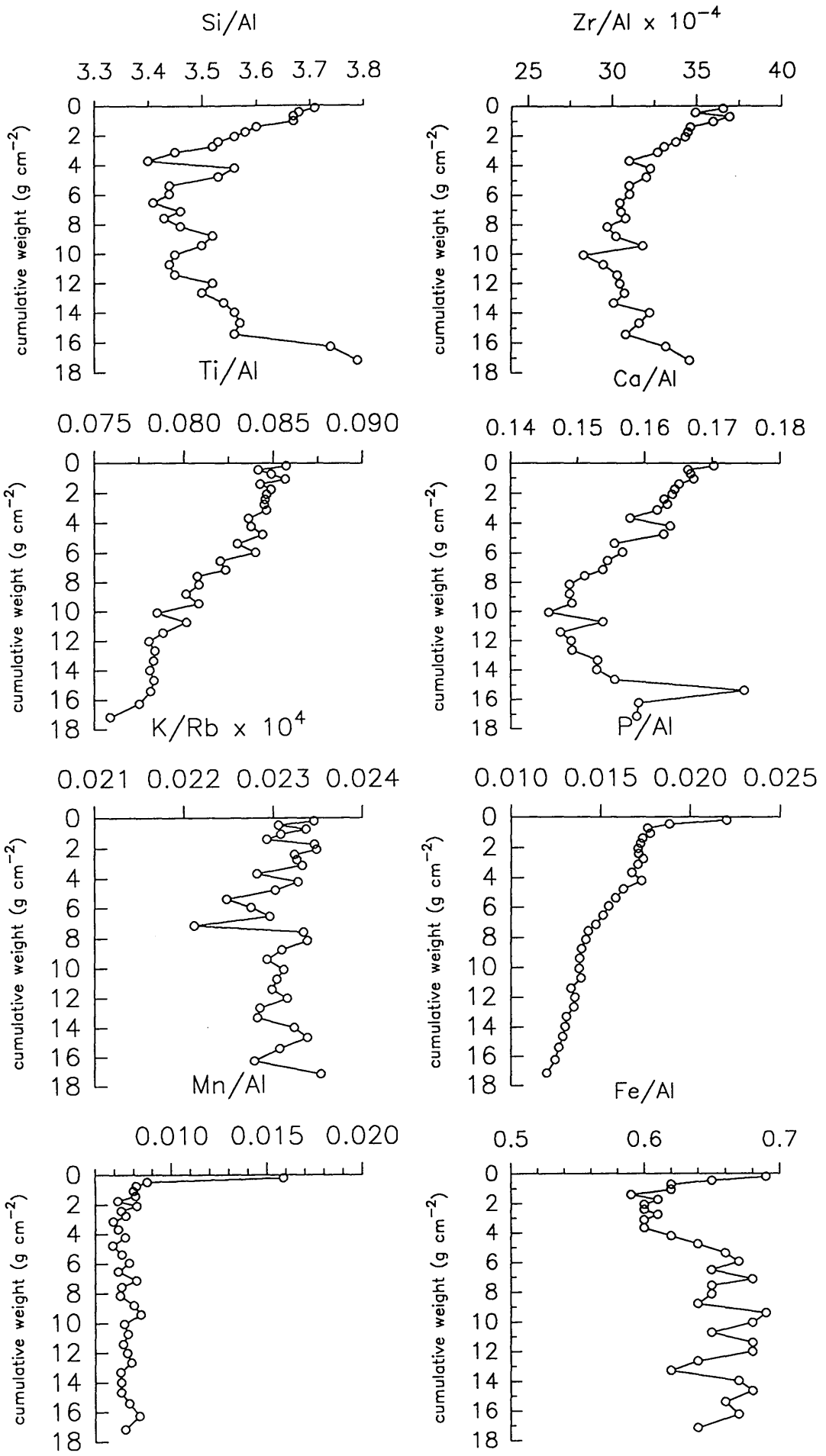

Figure 4.7. Loch Etive core 2 element/Al and K/Rb ratios.

4.3.2 *Geochemical characteristics of core LE 2*

The sampling site for core LE 2 is given in Figure 2.1. This core was obtained from the inner basin of Loch Etive close to the sill on the steep side of the basin and, as such, may be affected by winnowing .

Selected element/Al ratios and K/Rb ratios for core LE 2 are shown in Figure 4.7. The Ti/Al ratio of LE 2 is essentially constant at approximately 0.085 (which is higher than the surface ratio of 0.075 of LE 1) to a depth of 3.1 (9.5 cm) g cm^{-2} and then decreases with depth to 0.076 at 17.1 g cm^{-2} (57.5 cm) indicating that the sediment at the top of the core consists of coarser grains. This is also reflected in the Si/Al and Zr/Al ratios which decrease with depth. However the Si/Al, Zr/Al and Ca/Al all increase rapidly again at a depth of 16.2 g cm^{-2} (52.5 cm), and this is most marked in the Si/Al and the Ca/Al ratios which have very similar profiles. The Ca/Al ratio shows a small peak with its maximum at approximately 4.8 g cm^{-2} (15 cm), which possibly indicates a shell band. The Si/Al ratio has a value of 3.7 in the surface sediment and falls to a minimum of 3.4 at 3.7 g cm^{-2} (11 cm) (cf maximum Si/Al ratio for LE 1 = 3.4). The Zr/Al ratio is also greater in core LE 2 than in LE 1. The K/Rb ratio profile is erratic but suggests a decrease from the surface with a value of 235 to 222 at a depth of 7.56 g cm^{-2} (25 cm), after which it increases to 235 and remains at a relatively constant value to the bottom of the core. Therefore the Ti/Al, Si/Al and Zr/Al ratios all suggest a trend moving from coarser grain size at the top of the core to finer grain size at depth, which contrasts with LE 1, which contained a band of coarser sediment from 3 g cm^{-2} to 9 g cm^{-2}.

The Mn/Al ratio has a value of 0.016 at the surface, but decreases rapidly to 0.0087 at 0.45 g cm^{-2} (1.5 cm) consistent with diagenetic recycling of Mn. The Fe/Al ratio also reflects the effect of redox recycling, with the ratio decreasing from 0.69 at the surface to 0.59 at 1.4 g cm^{-2} (4.5 cm). The ratio remains relatively constant at about 0.6 to a depth of 3.7 g cm^{-2} (11 cm) after which it increases to 0.67 and remains around this level to the bottom of the core, indicating that re-dissolution of Fe occurs within the depth range 1.4 to 3.7

g cm^{-2} (4.5 to 11 cm), with re-deposition above and below this level. The rate of decrease of both the Mn/Al and Fe/Al ratios is faster than in LE 2, probably indicating that this sediment is attaining more reducing conditions nearer to the surface. As in LE 1, the Mn/Al ratio, reaches a constant value at a shallower depth than the Fe/Al ratio, consistent with the differences in the Mn and Fe redox couples.

The P/Al ratio decreases rapidly from a value of 0.022 at the surface of the sediment to 0.018 at 0.72 g cm^{-2} (0-2.5 cm) and then remains relatively constant to 4.2 g cm^{-2} (13 cm), after which it decreases systematically with depth to a value of 0.012 at 17.14 g cm^{-2}.

4.3.2 *^{210}Pb and ^{226}Ra profiles of core LE 2*

The ^{226}Ra and ^{210}Pb results are tabulated in Chapter 3 (Table 3.5.). The ^{226}Ra profile has a surface concentration of 29.9 Bq kg^{-1} and is essentially constant to a depth of 2.42 g cm^{-2} (7.5 cm) after which it increases to 39 Bq kg^{-1} at a depth of 3.7 g cm^{-2} (11 cm). This corresponds to the depth at which the minimum Si/Al ratio occurs, indicating that the coarser material has a lower ^{226}Ra content, and is also the depth corresponding to the bottom of the Fe re-dissolution zone. The profile of ^{226}Ra below this depth has values in the range 27.4 to 42.7 Bq kg^{-1} with two maxima at 5.8 and 16.2 g cm^{-2} (25 and 52.5 cm). The unsupported ^{210}Pb concentration for core LE 2 exhibited a surface maximum of 74.6 Bq kg^{-1} (which is considerably less than that of 347.8 Bq kg^{-1} for LE 1) with effectively constant values to 1.06 g cm^{-2} (3.5 cm), below which there is a systematic decrease to 1.8 Bq kg^{-1} at 4.76 g cm^{-2} (15 cm). The profile for this core thus suggests a mixed layer to a depth of 1.06 g cm^{-2} (3.5 cm). The ^{226}Ra inventory for LE 2 is 5700 $\pm$ 390 Bq m^{-2} which is greater than that of core LE 1 (3900 $\pm$ 346 Bq m^{-2}).

In this case, calculation of the sedimentation rate was not straightforward since the plot of ln unsupported ^{210}Pb (Fig. 4.8) could be taken to consist of three components. Thus, as shown in Figure 4.8, the mixed layer extends to 1.06 g cm^{-2} (3.5 cm), and below this are two sections with different

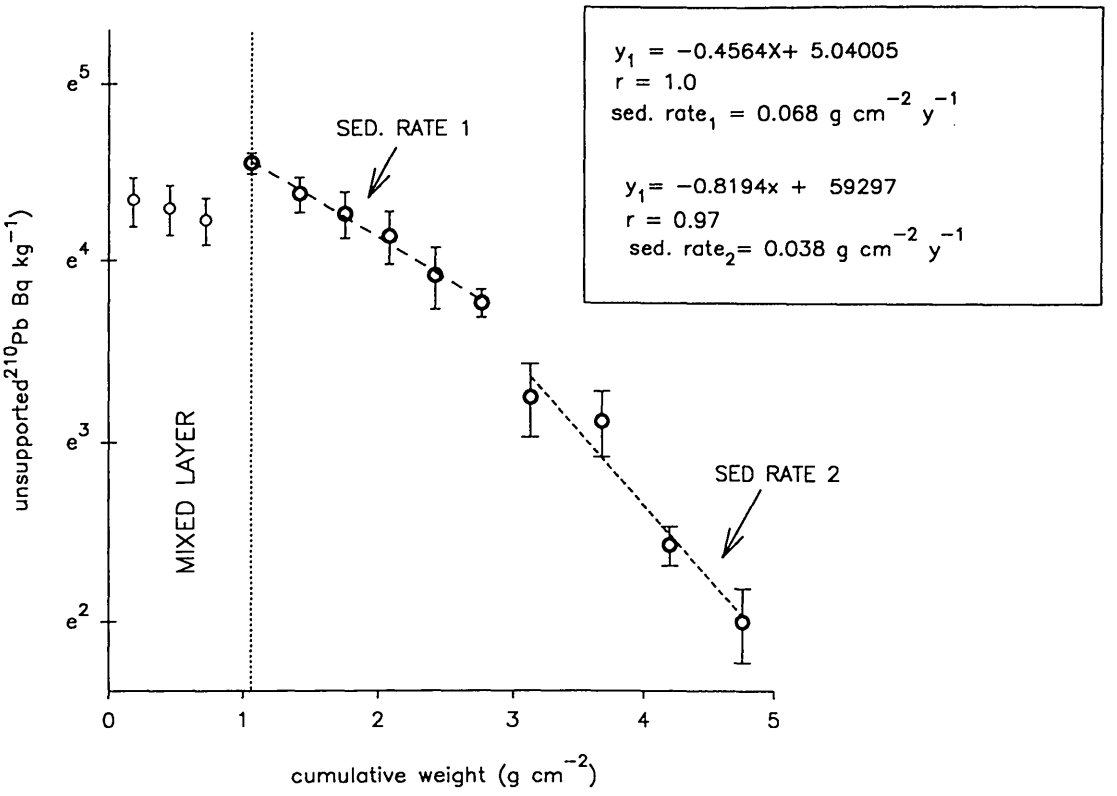

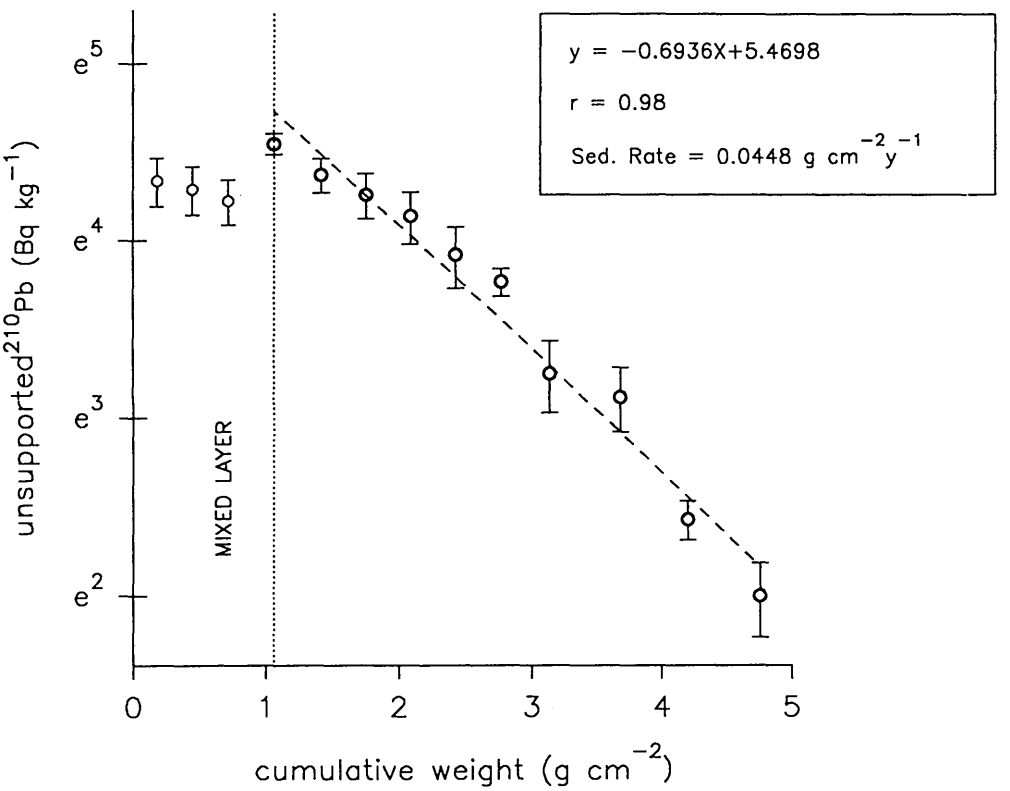

Figure 4.8. Loch Etive core LE2 unsupported ^{210}Pb concentrations

gradients, one from 1.06 to 2.76 g cm^{-2} (3.5 to 8.5 cm) and the second from 2.76 to 4.76 g cm^{-2} (8.5 to 15 cm). The sedimentation rate was first calculated using all 10 data points from beneath the mixed layer which gave a correlation coefficient (r) of 0.98 and a sedimentation rate of 0.045 g cm^{-2} y^{-1}. In comparison the sedimentation rate can be calculated from the two gradients to give values of 0.068 g cm^{-2} y^{-1} with a correlation coefficient of 0.996 (for sections 1.06 to 2.76 g cm^{-2}) and 0.038 g cm^{-2} y^{-1} with a correlation coefficient of 0.97 for sections (2.76 to 4.76 g cm^{-2}). The change in gradient occurs at approximately the same depth as the increase in the Ca/Al ratio and the presence of a shell band at this point may be influencing the unsupported ^{210}Pb profile. The sedimentation rates of 0.068 g cm^{-2} y^{-1} and 0.038 g cm^{-2} y^{-1} were used to determine the chronology of this core. The bottom of the mixed layer at a depth of 1.06 g cm^{-2} (3.5 cm) occurs at 1970 giving a mixed layer depth corresponding to an accumulation time of approximately 16 years.

The inventory of unsupported ^{210}Pb was 2200 ± 280 Bq m^{-2} implying a flux of 68 ± 9 Bq m^{-2} y^{-1}, which is considerably less than the corresponding values for LE 1 (9500 ± 1400 Bq m^{-2}, 294 ± 45 Bq m^{-2} y^{-1}). The flux for this core falls at the lower end of the range of 71.3 to 150 Bq m^{-2} for ^{210}Pb fluxes obtained by Sugden (1993) from Scottish peat cores and is considerably less than the mean global ^{210}Pb flux onto the land surface of 166.5 Bq m^{-2} obtained by Krishnaswamay and Lal (1978). The low ^{210}Pb flux can be compared to the surface transect concentrations of ^{210}Pb in Loch Etive (section 4.1.) which ranged from 107 to 407 Bq kg^{-1}, with station 10, closest to that of the sampling site of core LE 2, occurring at one of the pronounced minima in the ^{210}Pb transect (107 Bq kg^{-1}). The selected element/Al ratios for this core indicate that a coarser sediment is accumulating at this part of Loch Etive. Values for percentage loss on ignition (% L.O.I.) for LE 2 (Table 3.3a, Chapter 3), are lower than those for LE 1, with a % L.O.I. of 12.4% for the surface sediment increasing to a maximum of 14.7% at depth. This can be compared to a value of 19.0 % for the surface sediment of LE 1 and values at depth in the core falling within the range 15 to 20 %. Therefore the element/Al ratios and the % L.O.I. show that there is less organic material

accumulating in LE 2. Taken in conjunction with the surface transect results (as described in 4.1) which showed a strong correlation between ^{210}Pb and organics and also indicated a pronounced minimum in percentage organics at this part of the loch, these results could be taken to indicate that Pb is dominantly removed to the sediment by organic matter and that the organic flux determines the excess ^{210}Pb flux. This can be compared to the deep ocean situation where inorganic fluxes are low, and there is a direct link between productivity and ^{210}Pb flux (Moore and Diamond 1988). However, it must be remembered that the input to core LE 2 consists of coarser material in comparison to LE 1 and this may also be influencing the excess ^{210}Pb flux.

Using the chronology obtained from the sedimentation rates of 0.068 g cm^{-2} y^{-1} and 0.038 g cm^{-2} y^{-1}, it is possible to date some of the horizons observed in the profiles of the selected element/Al ratios. The Si/Al ratio starts to increase at approximately 5.9 g cm^{-2}, which could indicate the onset of the deposition of coarser sediment, after which a minimum occurs at 3.7 g cm^{-2} (11 cm). The onset of deposition of the coarser material for core LE 2 as indicated by the Si/Al ratio occurs at 1869, which after considering mixing (equal to 16 years) corresponds to 1885. However the mixing depth assuming a constant linear depth at the lower sedimentation rate of 0.038 g cm^{-2} y^{-1} would correspond to 28 years and would date the onset of deposition of the coarser material at 1907. This can be compared to LE 1 where the onset of deposition of coarser material (as indicated by an increase in the Si/Al ratio) occurs at approximately 8.4 g cm^{-2} (35 cm) which corresponds to 1905 or 1914, after considering mixing, which is later than that of LE 2. The Si/Al, Zr/Al and Ca/Al ratios decrease to a depth of approximately 10 g cm^{-2} (33 cm) after which they begin to increase. This point has a date of 1762 which, after considering mixing corresponds to 1790. The rapid increase at depth in the Si/Al and Ca/Al profiles occurs at a depth of 15.4 g cm^{-2} (49 cm) which corresponds to a mid section date of 1623, or 1651 with mixing.

4.2.3 ^{137}Cs, ^{134}Cs and ^{241}Am profiles of core LE 2

As with core LE 1 (section 4.2.3.) the ^{137}Cs profile for core LE 2 can be taken dominantly to reflect trends in the Sellafield discharge. The concentration profiles for ^{137}Cs and ^{241}Am and the activity ratio profile for $^{134}Cs/\ ^{137}Cs$ are shown in Figure 4.8. The ^{137}Cs concentration has a value of 128.8 Bq kg^{-1} at the surface, a subsurface maximum of 198.8 Bq kg^{-1} at 2.08 g cm^{-2} (6.5 cm) and then decreases to 4.4 Bq kg^{-1} at a depth of 9.41 g cm^{-2} (31 cm). Thereafter it remains between 0.7 and 2.0 Bq kg^{-1} to the bottom of the core at 17.14 g $cm^{-2.}$ (57.5 cm). As with core LE 1 the mixing identified from the ^{210}Pb data appears to have affected the ^{137}Cs profile, with the maximum occurring as a broad peak over the range 1.06 to 2.08 g cm^{-2} (3.5 to 6.5 cm) and a mid point at 1.57 g cm^{-2}. The inventory of ^{137}Cs in LE 2 is 7500 $\pm$ 220 Bq m^{-2} which is less than that for core LE 1 (10100 $\pm$ 290 Bq m^{-2}) and is consistent with coarser sediment occurring here. Assuming that the maximum discharge of ^{137}Cs from Sellafield reached Loch Etive in 1977 and that this corresponds to the mid point of the maximum (at a depth of 1.57 g cm-^{2} (5 cm)) then a sedimentation rate of 0.174 g cm^{-2} y^{-1} is obtained for core LE 2 which is considerably higher than the sedimentation rates of 0.068 g cm^{-2} y^{-1} and 0.038 g cm^{-2} y^{-1} derived from the ^{210}Pb profile and suggests an increasing sedimentation rate towards the surface. Thus, the structure of the upper section of the ^{210}Pb profile could be the result (at least in part) of more rapid accumulation rather than mixing. The sedimentation rate obtained for LE 2 from the depth of penetration of ^{137}Cs is 0.245 g cm^{-2} y^{-1}. However, if account is taken of mixing to a depth of 1.06 g cm^{-2} this becomes 0.219 g cm^{-2} y^{-1} which is also higher than the ^{210}Pb sedimentation rate.

The $^{134}Cs/\ ^{137}Cs$ ratio of LE 2 does not reflect significant input of radiocaesium from Chernobyl fallout, with a value of 0.04 (Sellafield discharge for 1984 had $^{134}Cs/\ ^{137}Cs$ = 0.043) at the surface, indicating that the Chernobyl radiocaesium concentration in core LE 2 is below detection limits. The $^{134}Cs/\ ^{137}Cs$ ratio decreases rapidly to 0.01 at a depth of 1.06 g cm^{-2} (3.5 cm) which corresponds to the depth of the bottom of the mixed layer implied by the unsupported ^{210}Pb profile. Below 1.06 g cm^{-2} (3.5 cm), there are

irregular appearances of ^{134}Cs down to 6.5 g cm^{-2} (21 cm), possibly indicating rapid advective movement e.g by burrow flushing. The inventory of ^{134}Cs for core LE 2 is 87 ± 17 Bq m^{-2} which is significantly lower than the 128 Bq m^{-2} observed for LE 1. The depth of penetration of ^{134}Cs, combined with the high sedimentation rate obtained from the ^{137}Cs could be taken to suggest that radiocaesium is more mobile in this core than in LE 1. This may result from the fact that the coarser material being deposited at the surface of core LE 2 has a lower clay content and consequently has a lower uptake and retention of radiocaesium.

Using the ^{210}Pb chronology the depth at which the onset of the Sellafield discharge in 1954 should occur can be calculated as 2.4 g cm^{-2} which becomes 3.5 g cm^{-2} after taking into account the depth of mixing. ^{137}Cs can in fact be detected to a depth of 14 g cm^{-2} (57.5 cm) which suggests a depth of diffusion of 10.5 g cm^{-2} which is greater than that found for core LE 1.

Only one result was obtained for ^{241}Am in this core, with a concentration of 2.4 Bq kg^{-1} at a depth of 1.06 g cm^{-2} (3.5 cm). Clearly no significant conclusion can be drawn from this single observation but the failure to detect ^{241}Am implies that there has been a lower uptake or a greater dilution of ^{241}Am in LE 2 than in LE 1.

4.3.4 *^{228}Th and ^{228}Ra profiles of core LE 2*

The $^{228}Th/^{228}Ra$ activity ratio profile for core LE 2 is shown in figure 4.9. The surface sediment has a ratio of 1.76, after which the ratio falls rapidly to 1.14 at a depth of 1.06 g cm^{-2} and is then generally greater than unity throughout the length of the core. The ^{228}Ra results for this core show an approximately constant value of 33 Bq kg^{-1} from the surface to 1.75 g cm^{-2}, with a generally higher value than this to the bottom of the core. The inventories for ^{228}Th and ^{228}Ra are 8000 ± 350 Bq m^{-2} and 6600 ± 470 Bq m^{-2} respectively. This again reflects the differences between LE 2 and LE 1 in which the ^{228}Th and ^{228}Ra inventories were essentially the same, with values of 4290 and 4760 Bq m^{-2} respectively which are also considerably lower than those of LE 2. The ^{232}Th

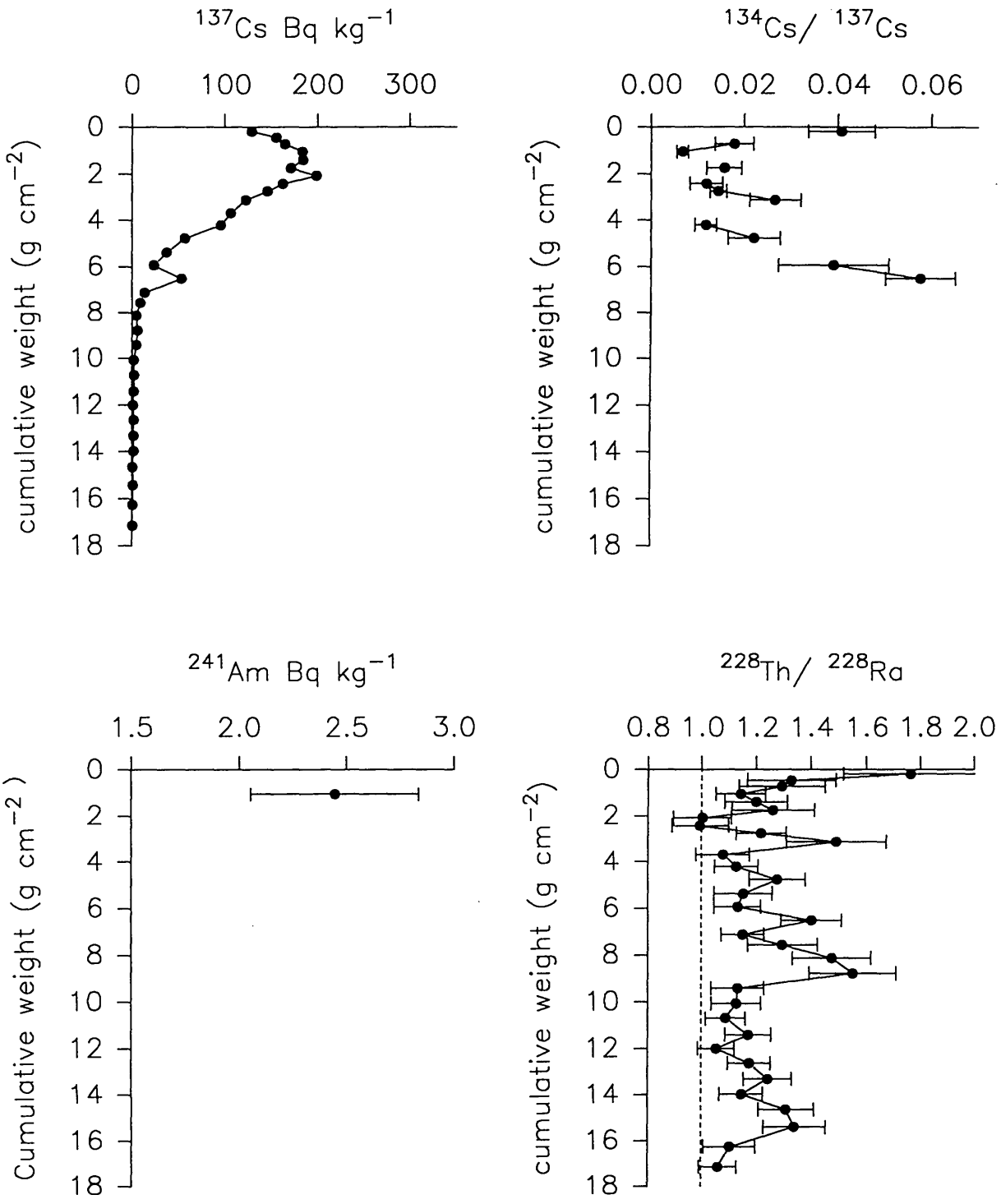

Figure 4.9. Loch Etive core LE2 radionuclide concentrations and activity ratios.

inventory for core LE 2 was 5100 Bq m^{-2} (calculated as described in section 4.2.4.) and indicates that there was an excess of approximately 3000 Bq m^{-2} of ^{228}Th in the sediments of core LE 2 which suggests either excess ^{228}Th deposition or transient equilibrium between ^{228}Ra and ^{228}Th in this sediment.

4.3.5 *Stable Pb and Pb isotope ratios of core LE 2*

The total stable Pb concentration data are presented in Table 3.5. and the plot of the total Pb concentration versus cumulative weight (g cm^{-2}) is shown in Figure 4.10.A. The Pb concentration is 55 mg kg^{-1} at the surface and increases to a maximum value of 60 mg kg^{-1} at a depth of 1.06 g cm^{-2} (3.5 cm). The concentration then remains constant to a depth of 2.8 g cm^{-2} (8.5 cm) after which it decreases rapidly to a value of 28 mg kg^{-1} at a depth of 6.5 g cm^{-2} (21 cm). The Pb concentration below this depth decreases slowly to a value of 21 mg kg^{-1} at the bottom of the core. The concentration of Pb in core LE 2 is far lower than in LE 1, which had a maximum concentration of 96 mg kg^{-1} decreasing to a minimum of 31 mg kg^{-1}. Using the ^{210}Pb chronology the maximum Pb value at 1.06 g cm^{-2} (3.5 cm) corresponds to a mid section date of 1973. Pb was detectable to the bottom of the core at 17.1 g cm^{-2} (57.5 cm) with a mid section date of 1579, or 1607 after mixing which is considerably older than the date of the bottom of core LE 1 which was 1875. The sediment from a depth of 10.7 g cm^{-2} (35 cm) down has relatively constant Pb concentrations ranging from 21 to 24 mg kg^{-1} and was considered to be representative of the non pollutant Pb in this sediment. The pollutant Pb concentrations were therefore calculated by subtracting a mean value of 24 mg kg^{-1} from the total Pb concentration. The lower concentration of Pb in this core compared to that of LE 1 (34 mg kg^{-1}) may simply reflect the difference between the inner and outer basins or, more likely, reflect the fact that core LE 2 extends to a date of 1607 which is 268 years earlier than core LE 1. The sharp rise in Pb concentration in core LE 2 takes place over a depth range of 6.5 to 2.8 g cm^{-2} which corresponds to 1881 to 1964 after considering mixing. This can be compared with LE 1 where the rapid increase in Pb concentration occurred over a depth range of 8.43 to 3.4 g cm^{-2} which corresponds to 1916 to 1964. Thus, the results indicate a

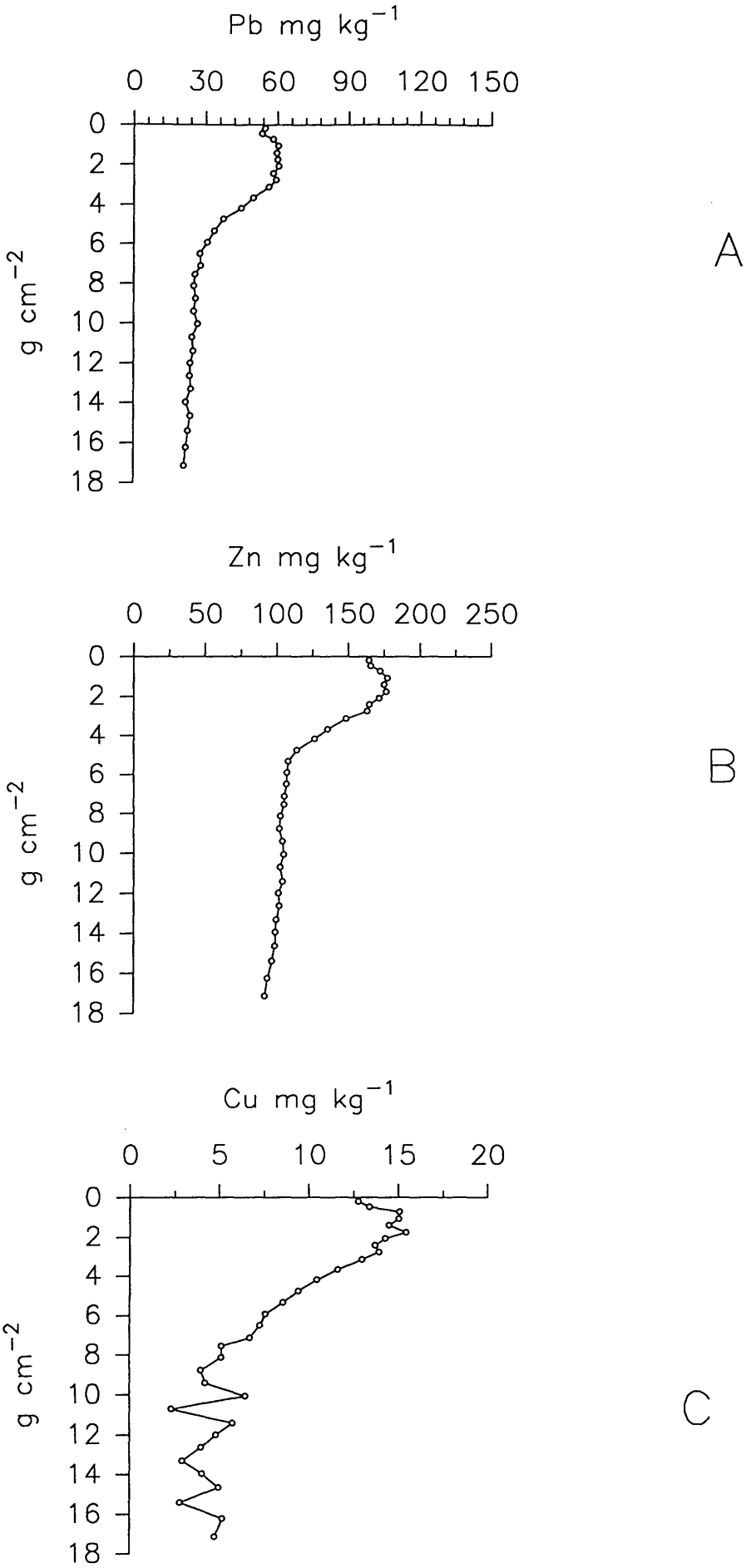

Figure 4.10. Loch Etive core LE2 Pb, Zn and Cu concentration (mg kg^{-1})

significant difference in temporal variations in pollutant Pb flux at the two sites. Alternatively, either, the chronology used for the deeper sections of core LE 2 may be erroneous and the change in sedimentation rate to 0.038 g cm^{-2} y^{-1} below 3 g cm^{-2} y^{-1} may not be reflecting a true change in accumulation rate, but an artefact due to the change in sediment type at this depth, and/or as indicated by the ^{137}Cs there has been a recent change to a higher sedimentation rate. The flux of pollutant Pb versus time (on the basis of the ^{210}Pb chronology) for core LE 2 is shown in figure 4.11.A. The excess Pb flux results are given in Table 4.5. Excess Pb is first observed in sediment deposited in 1727 (0.0005 g cm^{-2} y^{-1}) and the flux increases slowly to 1825 (0.0011 g cm^{2} y^{-1}). From 1825 there is a sharp increase to a value of 0.024 g cm^{-2} y^{-1} in 1948. Maximum fluxes for this core are observed from 1958-1977 after which they decrease. After considering the effects of mixing (28 years) a date of 1755 is obtained for the onset of deposition of excess Pb, which is earlier than a peat core from North Uist (1800) (Sugden, 1993).

The inventory of excess Pb for this core is 1.6 g m^{-2} which is considerably less than that for core LE 1 (3.8 g m^{-2}). As discussed in Chapter 1, sea lochs exhibit large variations in conditions over short distances which is reflected here in the very different inventories of Pb within cores LE 1 and LE 2. The excess stable Pb ratio of LE 1_{Pb}/LE 2_{Pb} is 2.4 and the excess ^{210}Pb ratio for LE $1_{Pb\text{-}210}$/LE $2_{Pb\text{-}210}$ is 4.3 which suggests that there is a source of Pb and ^{210}Pb other than that atmospherically deposited, to the sediments of Loch Etive which has a greater affect on core LE 1 from the outer basin. The difference between the excess Pb inventory ratio (2.4) and the excess ^{210}Pb inventory ratio (4.3) suggest that relative to ^{210}Pb deposition, LE 2 is receiving relatively more pollutant Pb than LE 1 which may indicate that LE 2 has been influenced by an early, small local Pb pollutant input. Iron smelting was first carried out in 1730 by Irish iron-masters with a furnace in Glen Kinglass and in 1870 a furnace was built at Bonawe. This early industrial activity may have resulted in a source of Pb to the sediment of core LE 2. The Pb flux for LE 2 begins to decrease at 0.72 g cm^{-2} which corresponds to 1977, and this decrease is more pronounced than for core LE 1.

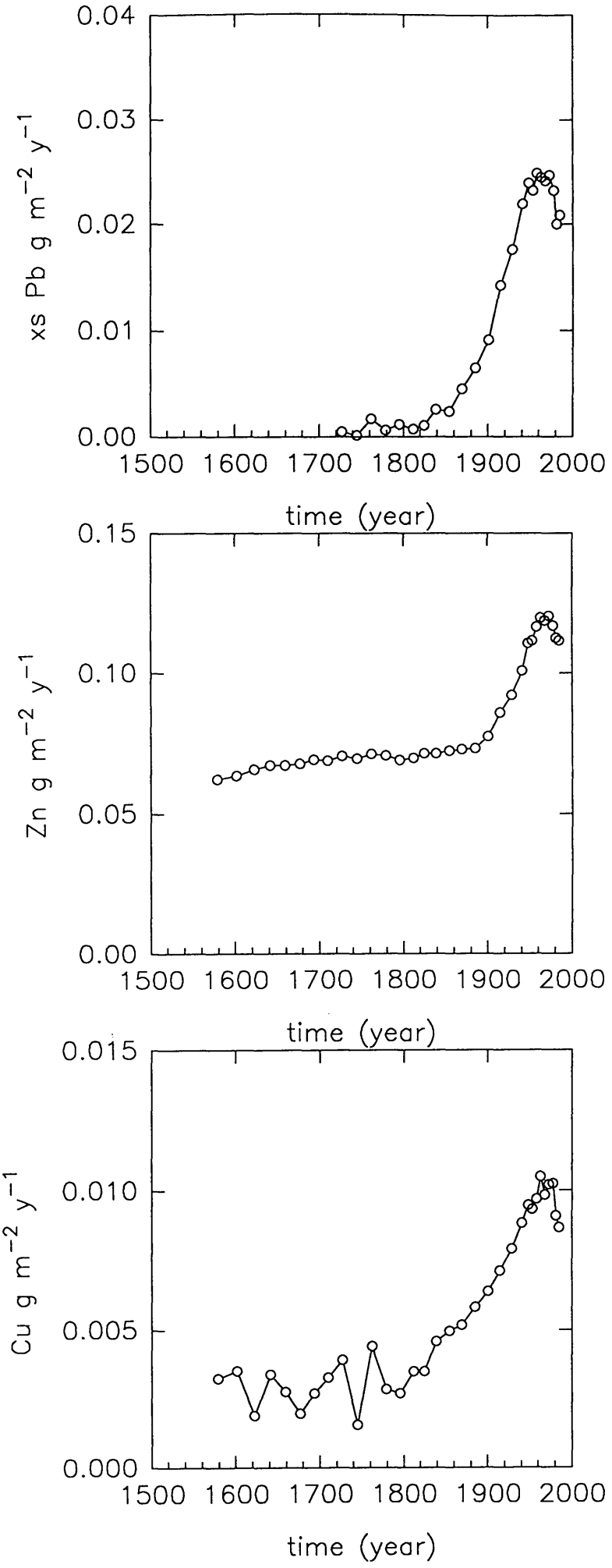

Figure 4.11. Loch Etive core LE2 Pb, Zn and Cu flux data

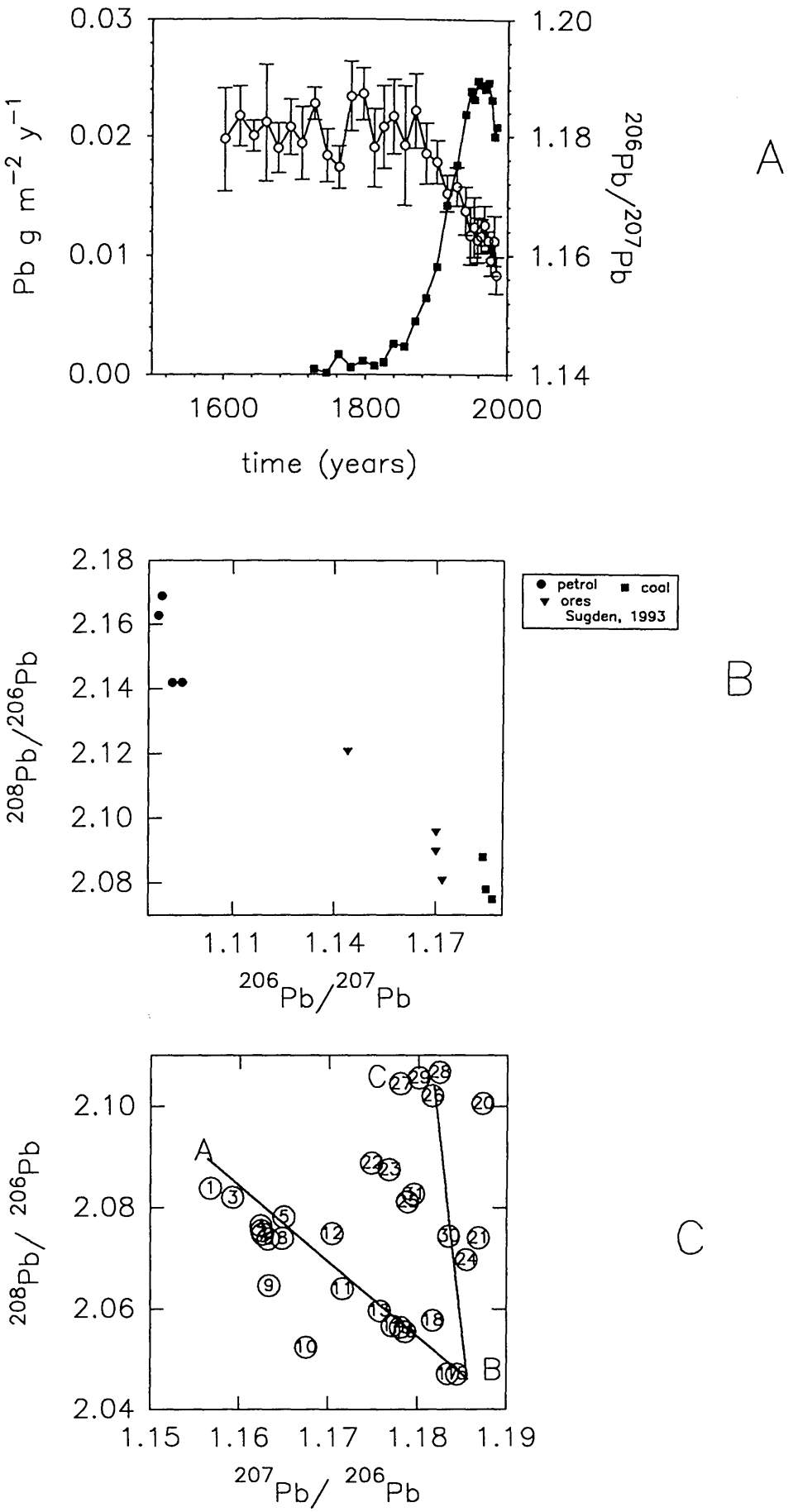

Figure 4.12. Loch Etive core LE2 flux, and Pb isotope ratio plots.

The $^{206}Pb/^{207}Pb$ versus ^{210}Pb chronology profile and excess Pb flux (g cm^{-2} y^{-1}) for LE 2 are shown in Figure 4.12.A. The surface sediment has a $^{206}Pb/^{207}Pb$ of 1.157 and with increasing depth the ratio increases to 1.180 at 16.24 g cm^{-2} (52.5 cm). Thus, the Pb flux and $^{206}Pb/^{207}Pb$ trends are similar for both LE 1 and LE 2, but the ^{210}Pb chronology for core LE 2 dates major changes in the profiles prematurely. As discussed in 4.2.3 the ratio at depth reflects heavy industrial $^{206}Pb/^{207}Pb$ combined with the natural $^{206}Pb/^{207}Pb$ signature from the sediment. The surface sediment of core LE 2, from the inner basin, has a significantly higher $^{206}Pb/^{207}Pb$ ratio compared to LE 1 (from the outer basin) and, on the assumption that the pollutant input is similar this suggests that the terrigenous input to LE 2 has a different $^{206}Pb/^{207}Pb$ ratio from that to LE 1.

The onset of the effect of the addition of pollutant Pb from petrol to the sediment occurs at a depth of 5.36 g cm^{-2} (17 cm) which is equivalent to 1885 if no mixing is assumed. If mixing is taken into account (mixing to 1.06 g cm^{-2}, equivalent to 28 years), this becomes 1913 which is 29 years earlier than the date obtained for core LE 1 from the outer basin of 1942 and too early to agree with the known historical record. This could be indicating that the accumulation rate is increasing towards the surface as is suggested by the sedimentation rate obtained from the ^{137}Cs concentration maximum (0.176 g cm^{-2} y^{-1}). If a three component system is applied to obtain a chronology, (i.e. 0-1.57 g cm^{-2}= 0.176 g cm^{-2} y^{-1}; 1.57 to 2.76 g cm^{-2}= 0.068 g cm^{-2} y^{-1}; 2.76- 5.36 g cm^{-2}= 0.038 g cm^{-2} y^{-1}) and mixing to a depth of 1.06 g cm^{-2} which is equivalent to 28 years is considered, then the onset of the effect of pollutant Pb from petrol is 1929 which is in good agreement with the historical record of addition of alkyl lead to petrol which occurred in 1922. By applying the chronology obtained from this three component system to the excess Pb profile, the sharp rise in Pb concentration occurs from 1924 to 1964, which is in reasonable agreement with core LE 1.

SAMPLE	DEPTH	cum. g cm^{-2}	date for mid section	excess Pb g m^{-2} y^{-1}
LE2 0-1	0.5	0.18	1985	0.0208
LE2 1-2	1.5	0.45	1981	0.0200
LE2 2-3	2.5	0.72	1977	0.0232
LE2 3-4	3.5	1.06	1973	0.0246
LE2 4-5	4.5	1.41	1968	0.0241
LE2 5-6	5.5	1.75	1963	0.0244
LE2 6-7	6.5	2.08	1958	0.0248
LE2 7-8	7.5	2.42	1953	0.0232
LE2 8-9	8.5	2.76	1948	0.0239
LE2 9-10	9.5	3.13	1941	0.0219
LE2 10-12	11.0	3.68	1928	0.0176
LE2 12-14	13.0	4.20	1914	0.0142
LE2 14-16	15.0	4.76	1900	0.0091
LE2 16-18	17.0	5.36	1885	0.0065
LE2 18-20	19.0	5.93	1869	0.0045
LE2 20-22	21.0	6.51	1854	0.0024
LE2 22-24	23.0	7.13	1839	0.0026
LE2 24-26	25.0	7.56	1825	0.0011
LE2 26-28	27.0	8.13	1812	0.0008
LE2 28-30	29.0	8.77	1796	0.0012
LE2 30-32	31.0	9.41	1779	0.0007
LE2 32-34	33.0	10.06	1762	0.0017
LE2 34-36	35.0	10.71	1745	0.0002
LE2 36-38	37.0	11.41	1727	0.0005
LE2 38-40	39.0	12.01	1710	
LE2 40-42	41.0	12.64	1694	
LE2 42-44	43.0	13.31	1677	
LE2 44-46	45.0	13.97	1659	
LE2 46-48	47.0	14.65	1641	
LE2 48-50	49.0	15.40	1623	
LE2 50-55	52.5	16.24	1602	
LE2 55-60	57.5	17.14	1579	

Table 4.5 Loch Etive core LE 2 Pb flux data

The calculation of the percentage Pb due to petrol was carried out as

described in 4.2.5. with R_I= 1.81 and R_{Hi}=1.172 and the results of this calculation are given in Table 4.6.

SAMPLE	DEPTH	cum. g cm^{-2}	date for mid section	% Pb petrol
LE2 0-1	0.5	0.18	1985	42
LE2 1-2	1.5	0.45	1981	30
LE2 2-3	2.5	0.72	1977	34
LE2 3-4	3.5	1.06	1973	27
LE2 4-5	4.5	1.41	1968	22
LE2 5-6	5.5	1.75	1963	25
LE2 6-7	6.5	2.08	1958	26
LE2 7-8	7.5	2.42	1953	23
LE2 8-9	8.5	2.76	1948	25
LE2 9-10	9.5	3.13	1941	18
LE2 10-12	11.0	3.68	1928	11
LE2 12-14	13.0	4.20	1914	17
LE2 14-16	15.0	4.76	1900	7
LE2 16-18	17.0	5.36	1885	5
LE2 18-20	19.0	5.93	1869	
LE2 20-22	21.0	6.51	1854	
LE2 22-24	23.0	7.13	1839	
LE2 24-26	25.0	7.56	1825	
LE2 26-28	27.0	8.13	1812	
LE2 28-30	29.0	8.77	1796	
LE2 30-32	31.0	9.41	1779	
LE2 32-34	33.0	10.06	1762	
LE2 34-36	35.0	10.71	1745	
LE2 36-38	37.0	11.41	1727	
LE2 38-40	39.0	12.01	1710	
LE2 40-42	41.0	12.64	1694	
LE2 42-44	43.0	13.31	1677	
LE2 44-46	45.0	13.97	1659	
LE2 46-48	47.0	14.65	1641	
LE2 48-50	49.0	15.40	1623	
LE2 50-55	52.5	16.24	1602	
LE2 55-60	57.5	17.14	1579	

Table 4.6 % Pb in core LE 2 from Pb in petrol

The % of the total Pb from petrol increases to a maximum of 42 % at the surface, however the % Pb from petrol at lower depths in the core is generally less than for equivalent dates for core LE 1 and probably reflects the fact that the inventory of excess Pb in this core is considerably less than that for LE 1 or indicates a local source of non-petrol pollutant Pb for LE 2.

The $^{208}Pb/^{206}Pb$ versus $^{206}Pb/^{207}Pb$ plot for core LE 2 is shown in Figure 4.12.C. The samples are numbered 1 to 31 according to increasing depth. Figure 4.12.B. illustrates the relative positions of "heavy industry" represented by coal and mined ores and petrol Pb with respect to their Pb isotope ratios (Sugden, 1993).

A three component system with two tie lines, as observed for core LE 1 is again apparent in this core but with a different characteristic $^{206}Pb/^{207}Pb$, $^{208}Pb/^{206}Pb$ signature for the natural (unpolluted) sediment, consistent with the two basins being in geologically distinct bedrock units. The upper samples i.e. post 1900, are dominated by pollutant Pb, and mixing of heavy industry (B) and petrol Pb (A) occurs along tie line A-B. The samples which have less pollutant Pb (pre-1900) are mixed along a tie line B-C representing the mixing of heavy industry (B) and natural Pb (C). The surface results are still clustered together, although at a lower $^{208}Pb/^{206}Pb$ ratio and a higher $^{206}Pb/^{207}Pb$ ratio than LE 1, reflecting the smaller effect of Pb from petrol in core LE 2. The intermediate samples tend towards a lower $^{208}Pb/^{206}Pb$ and higher $^{206}Pb/^{207}Pb$ ratio, again reflecting the decreasing contribution of petrol Pb in the deeper samples in the core. Finally samples 20-31 tend towards a higher $^{208}Pb/^{206}Pb$ ratio and a higher $^{206}Pb/^{207}Pb$ ratio, representative of the natural signature of the Pb in samples at depth.

4.3.6 *Zn and Cu profiles of core LE 2*

The Zn and Cu concentration profiles for core LE 2 are shown in Figure 4.10.B. and 4.10.C. respectively. The trends in the Zn profile are very similar to those of the total Pb profile. The Zn concentration has a surface value of 164 mg kg^{-1} which is lower than that of LE 1 (221 mg kg^{-1}) and increases to

a maximum of 177 at 1.06 g cm^{-2} (3.5 cm) depth. The Zn concentration then decreases systematically to 108 mg kg^{-1} at a depth of 5.36 g cm^{-2} (17 cm), after which it decreases slowly to 92 mg kg^{-2} at 17.1 g cm^{-2} (57.5 cm). Using the ^{210}Pb chronology the period of pronounced increase in the Zn flux occurs from 5.4 to 2.8 g cm^{-2} which corresponds to 1885 to 1948 or 1913 to 1964 after mixing is taken into account which is in good agreement with core LE 1 (1916 to 1956). The maximum concentration of Zn occurs at a mid section date of 1973. The change in rate of increase of Zn occurs at 1885 which, after accounting for mixing, becomes 1913 (the same time as the onset of Pb in petrol).

The Cu profile is smoother than that of LE 1 and follows the same trends as the Pb and Zn profiles. The concentration of Cu is 13 mg kg^{-1} at the surface, increasing to 15 mg kg^{-1} at 0.72 g cm^{-2} (2.5 cm) depth and remaining essentially constant to 2.8 g cm^{-2} (8.5 cm), below which it decreases to a mean value of 4 mg kg^{-1} at depth.

The fluxes of excess Pb, total Zn and total Cu are given in Figure 4.10. with the results being presented in Table 4.7. The fluxes are generally lower than those for LE 1 and the Zn profile is again very similar to that of Pb, with a flux of 0.062 g cm^{-2} y^{-1} at depth increasing to a maximum of 0.120 g cm^{-2} y^{-1}. The Cu flux for LE 2, as with all the other elements considered, is lower than that of LE 1. However, the profile is less irregular than that for LE 1 and again is in good agreement with the Pb and Zn profiles. The inventories of Cu and Zn are 19.8 and 1.2 g m^{-2} respectively which compare favourably with those of LE 1 (21.1 g m^{-2} for Zn and 1.4 g m^{-2} for Cu). The excess Zn and Cu inventories were calculated by subtracting natural values of 96 and 4 mg kg^{-1} respectively. This gave values of 3.4 and 0.6 g m^{-2} for the excess Zn and Cu inventories which can be compared to those of LE 1 of 7.8 g m^{-2} for Zn and 0.5 g m^{-2} for Cu. It is apparent that the excess Cu inventories for both cores are essentially the same but the excess Zn inventory of core LE 2 is less than half that of core LE 1.

Comparison of the ratios of the inventories of Zn and Cu for cores LE 1 and

SAMPLE	DEPTH	cum. g cm^{-2}	date for mid section	Cu g $m^{-2}y^{-1}$	Zn g $m^{-2}y^{-1}$
LE2 0-1	0.5	0.18	1985	0.009	0.112
LE2 1-2	1.5	0.45	1981	0.009	0.113
LE2 2-3	2.5	0.72	1977	0.010	0.117
LE2 3-4	3.5	1.06	1973	0.010	0.121
LE2 4-5	4.5	1.41	1968	0.010	0.119
LE2 5-6	5.5	1.75	1963	0.010	0.120
LE2 6-7	6.5	2.08	1958	0.010	0.117
LE2 7-8	7.5	2.42	1953	0.009	0.112
LE2 8-9	8.5	2.76	1948	0.009	0.111
LE2 9-10	9.5	3.13	1941	0.009	0.101
LE2 10-12	11.0	3.68	1928	0.008	0.092
LE2 12-14	13.0	4.20	1914	0.007	0.086
LE2 14-16	15.0	4.76	1900	0.006	0.077
LE2 16-18	17.0	5.36	1885	0.006	0.073
LE2 18-20	19.0	5.93	1869	0.005	0.073
LE2 20-22	21.0	6.51	1854	0.005	0.072
LE2 22-24	23.0	7.13	1839	0.005	0.071
LE2 24-26	25.0	7.56	1825	0.004	0.071
LE2 26-28	27.0	8.13	1812	0.004	0.070
LE2 28-30	29.0	8.77	1796	0.003	0.069
LE2 30-32	31.0	9.41	1779	0.003	0.071
LE2 32-34	33.0	10.06	1762	0.004	0.071
LE2 34-36	35.0	10.71	1745	0.002	0.070
LE2 36-38	37.0	11.41	1727	0.004	0.071
LE2 38-40	39.0	12.01	1710	0.003	0.069
LE2 40-42	41.0	12.64	1694	0.003	0.068
LE2 42-44	43.0	13.31	1677	0.002	0.068
LE2 44-46	45.0	13.97	1659	0.003	0.067
LE2 46-48	47.0	14.65	1641	0.003	0.067
LE2 48-50	49.0	15.40	1623	0.002	0.066
LE2 50-55	52.5	16.24	1602	0.004	0.064
LE2 55-60	57.5	17.14	1579	0.003	0.062

Table 4.7 Cu and Zn fluxes for LE 2

LE 2 gives values of LE 1_{Zn}/LE 2_{Zn} = 1.1 and LE 1_{Cu}/LE 2_{Cu} = 1.2 with the excess inventories giving values of LE 1_{xsZn}/LE 2_{xsZn} = 2.3 and LE 1_{xsCu}/LE 2_{xsCu} = 0.8 which can be compared to the excess Pb inventory ratios of LE

1_{xsPb}/LE 2_{xsPb} = 2.4 and the LE $1_{xsPb\text{-}210}$/LE $2_{xsPb\text{-}210}$ = 4.3. If the inventory due to Pb from petrol is subtracted from the total excess Pb inventory, residual excess Pb inventories of 2.9 and 1.3 g m^{-2} are obtained for cores LE 1 and LE 2 respectively. The ratio of the inventories of the residual excess Pb is LE $1_{res.Pb}$/LE $2_{res.Pb}$= 2.2 which is similar to the ratio of the excess Pb inventories of 2.4 and indicates that there is a slightly greater input of petrol Pb to core LE 1. Assuming that Zn and Cu are present in the sediments as a result of atmospheric deposition, then the ratios suggest that the supply of atmospherically deposited Cu is the same for both the inner and outer basin but that there is either another source of Pb and Zn to the outer basin or that the transfer of Pb and Zn from the water to the sediments involves a different mechanism than that of Cu.

4.3.7 *Summary of core LE 2*

In summary, the results for core LE 2 suggest that by applying three sedimentation rates (0.176 g cm^{-2} y^{-1}, ^{137}Cs; 0.068 g cm^{-2} y^{-1}, ^{210}Pb and 0.038 g cm^{-2} y^{-1}, ^{210}Pb) to this core gives a good chronology when compared to the Pb concentration and ^{206}Pb/ ^{207}Pb isotope ratio trends, although there is a discrepancy of 10 to 15 years between the observed onset of pollutant Pb from petrol and the historical trend. The sedimentation rate obtained by relating the maximum ^{137}Cs concentration to the peak Sellafield discharge gave a sedimentation rate that was far greater than those obtained from the ^{210}Pb dating method, suggesting that the accumulation rate for this core increases towards the surface. The core is mixed to a depth of 1.06 g cm^{-2} (3.5 cm) and has an accumulation rate of 0.176 g $cm^{-2}y^{-1}$ to a depth of 1.57 g cm^{-2} giving a time interval from the surface of the sediment to the bottom of the mixed zone of 6 years, however, the depth of the mixed zone would have been equivalent to 28 years at the lower sedimentation rate of 0.038 g $cm^{-2}y^{-1}$.

As with core LE 1 the manmade radionuclides present in the sediment are dominated by the Sellafield discharge. The inventories of manmade radionuclides are 7500 Bq m^{-2} of ^{137}Cs, 87 Bq m^{-2} of ^{134}Cs which are lower

than those calculated for LE 1 but there is good agreement between (^{134}Cs)LE 1/(^{137}Cs)LE 1 = 0.013 and (^{134}Cs)LE 2/(^{137}Cs)LE 2 = 0.012.

The plot of pollutant Pb flux versus time is very similar to that of LE 1 but the magnitude of the pollutant Pb inventory is less, being 1.6 g m^{-2} compared to that of 3.8 g m^{-2} for LE 1. The onset of the input of pollutant Pb from petrol can be detected in 1913 on the basis of the ^{210}Pb chronology, which is earlier than LE 1. However, if a three component system using the ^{137}Cs and both of the ^{210}Pb sedimentation rates is applied the chronology obtained, dates the onset of the effect of pollutant Pb from petrol at 1929 which is in good agreement with the known historical trend. The petrol Pb contribution in core LE 2 increased to 42 % of the total Pb content by 1985. The percentage of Pb from petrol is generally lower than that of LE 1. The Zn and Cu flux profiles are very similar to the Pb flux profile and core LE 2 has inventories of Zn and Cu of 19.8 and 1.4 g m^{-2} respectively which are similar to those calculated for core LE 1. However the excess inventories of Zn and Cu are 3.4 and 0.6 g m^{-2} giving excess inventory ratios between LE 1 and LE 2 of 2.3 and 0.8 respectively. The inventories for ^{210}Pb and excess Pb are considerably lower than those of LE 1. The ^{137}Cs, ^{134}Cs and ^{241}Am inventories are also lower than those found in LE 1.

The major changes in the Si/Al ratio indicate that the onset of deposition of coarser sediment occurred around 1913 (using the three component chronology). This can be compared to LE 1 where the onset of deposition of coarser material (as indicated by an increase in Si/Al ratio) occurs at a depth corresponding to 1914. Thus, a change in the type of sediment entering the loch at approximately 1914 is reflected in both cores LE 1 and LE 2. The change thus affected both the inner and outer basin around the start of the first world war and could represent the effects of industrial activity, road building or change in land use. It has also been suggested that there may have been some dredging of the Falls of Lora around 1915 (Price, pers.com.) to allow for the navigation of ships to Bonawe quarry. This date of the change in sediment input also coincides with the largest shell band that occurred in LE 1 at 1916, and it could be speculated that the change in sediment input

to Loch Etive affected the macrobenthos resulting in deposition of the shell band.

4.4 *Loch Etive core LE 3*

Core LE 3 was from the deepest part of the inner basin (Figure 2.1) and the sampling site, sampling analytical methods are described in Chapter 2. The results for core LE 3 are tabulated in Chapter 3. The sampling location of core LE 3 was the same as that of the surface transect sample 14.

4.4.1 *Geochemical characteristics of core LE 3*

To determine whether there were any major changes in sediment input to LE 3, selected element/Al ratios and K/Rb ratio were considered, the profiles of which are shown in Figure 4.13.

The Ti/Al ratio for core LE 3 has a surface value of 0.072 which is similar to that of core LE 1 (0.075) and lower than that of LE 2 (0.85), and increases to 0.085 at approximately 10 g cm^{-2} depth, indicating a change to coarser grain size with increasing depth. This trend is also reflected by the Zr/Al and K/Rb ratios. The Si/Al ratio has a value of 3.23 at the surface (which is similar to LE 1 but lower than LE 2) and remains reasonably constant to a depth of 1.7 g cm^{-2} (11 cm) after which the ratio increases to 3.29 and then decreases with depth. The Ca/Al ratio has a surface value of 0.17, which is essentially the same as both LE 1 (0.19) and LE 2 (0.17), and systematically increases with depth to a value of 0.26, with a maximum of 0.33 at a depth of 0.14 g cm^{-2} (1.5 cm). There is, therefore, a general trend of increasing grain size with depth which is similar to core LE 1, which had a subsurface band of coarser material, but opposite to core LE 2 which has a coarser grain size at the top of the core.

The Mn/Al ratio decreases from a maximum value of 0.25 at the sediment surface, which is an order of magnitude greater than either LE 1 (0.012) or LE 2 (0.016), to 0.067 at a depth of 0.5 g cm^{-2} (4.5 cm) indicating that there

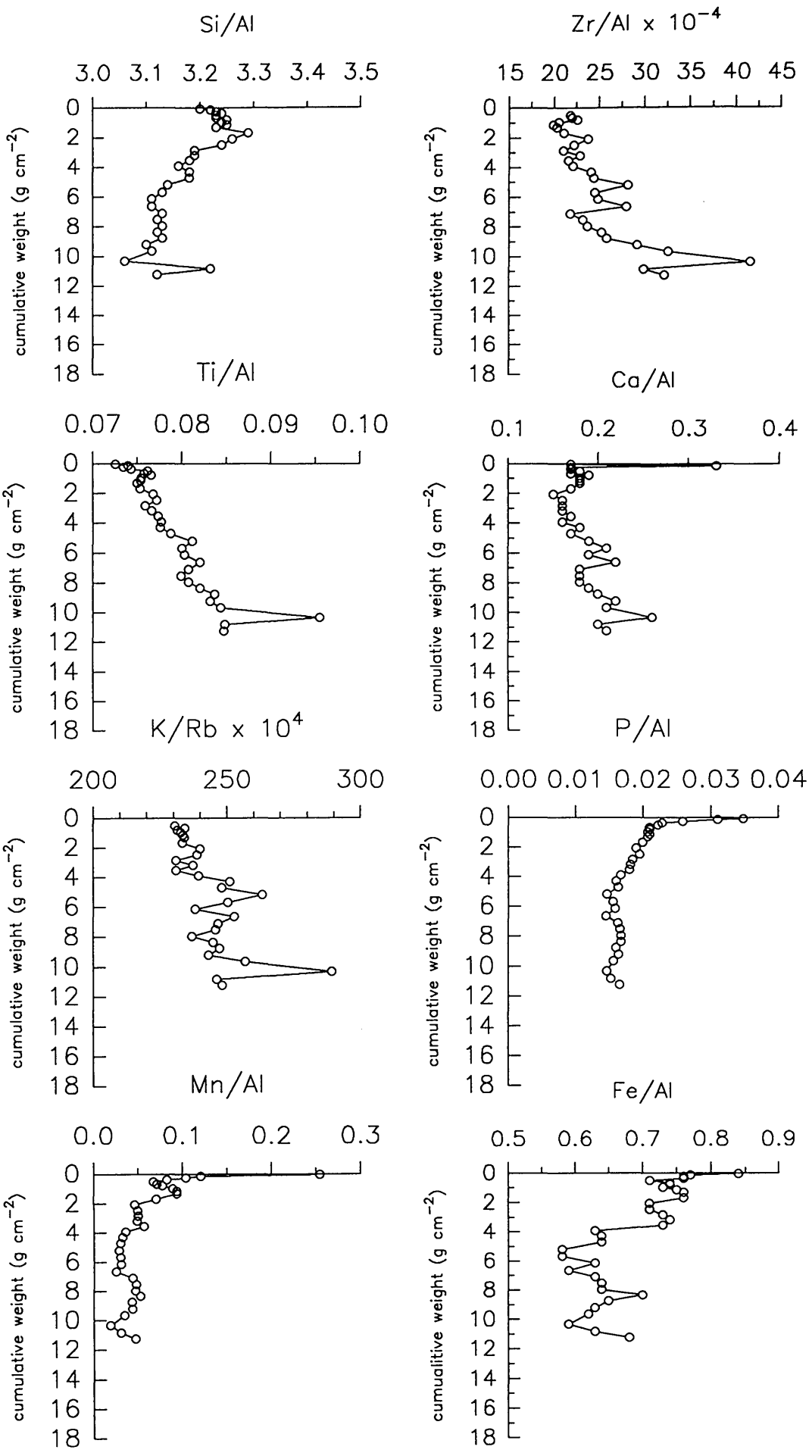

Figure 4.13. Loch Etive core LE3 element/Al and K/Rb ratios.

is extensive redox recycling of Mn near the surface of the sediment. The ratio then increases to a value of 0.094 at 1.15 g cm^{-2} (8.5 cm), below which it decreases again, with the average value at depth being 0.035 which is still greater than the surface values in cores LE 1 and 2 and may indicate that a stable Mn mineral such as Mn carbonate is forming at depth in this core. The Fe/Al ratio is 0.84 at the surface, which is higher than both LE 1 (0.70) and LE 2 (0.69), and reaches a minimum value of 0.58 at 5.2 g cm^{-2} (29 cm) depth. The P/Al ratio at the surface is 0.035 which is similar to LE 1 (0.032), but is higher than LE 2 (0.022). The P/Al ratio decreases rapidly to 0.002 at 0.5 g cm^{-2} (4.5 cm) and then decreases more slowly to 0.015 at depth. The Mn/Al, Fe/Al and P/Al ratios all indicate that organic matter is being degraded and that redox recycling of Mn and Fe is taking place in this sediment. The Mn/Al ratio also indicates that there is a far greater concentration of Mn in this core than in LE 1 and LE 2.

4.4.2 *^{210}Pb and ^{226}Ra profiles of core LE 3*

The unsupported ^{210}Pb concentrations and sedimentation rate for LE 3 were calculated as for LE 1. The plots of unsupported ^{210}Pb and ln unsupported ^{210}Pb versus depth in g cm^{-2} are shown in Figure 4.14.

The ^{226}Ra and ^{210}Pb results are tabulated in Chapter 3 (Table 3.15.). The ^{226}Ra concentration at the surface of core LE 3 is 276.9 Bq kg^{-1} which is an order of magnitude greater than either LE 1 (13.2 Bq kg^{-1}) or LE 2 (29.9 Bq Kg^{-1}) and indicates a significant enrichment of ^{226}Ra in the surface sediment. This large enrichment of ^{226}Ra in the sediments of sea lochs has also been observed by MacKenzie (1977) and Swan (1978) in their studies of Loch Goil. which like the inner basin of Loch Etive, is subject to transient oxygen depletion of the water column and has Mn rich surface sediments. This reflects the mobility of ^{226}Ra in core LE 3 and its involvement with Mn oxyhydroxide complexes (Ku and Broecker, 1969; Moore et al., 1980, 1981; Deal et al, 1981; Huh and Ku, 1984; Kadko et al., 1987; Todd et al., 1988). The concentration of ^{226}Ra falls to a value of 27.2 Bq kg^{-1} at 0.14 g cm^{-2} (1.5 cm) and then increases to 45.3 Bq kg^{-1} at a depth of 0.67 g cm^{-2} (5.5 cm).

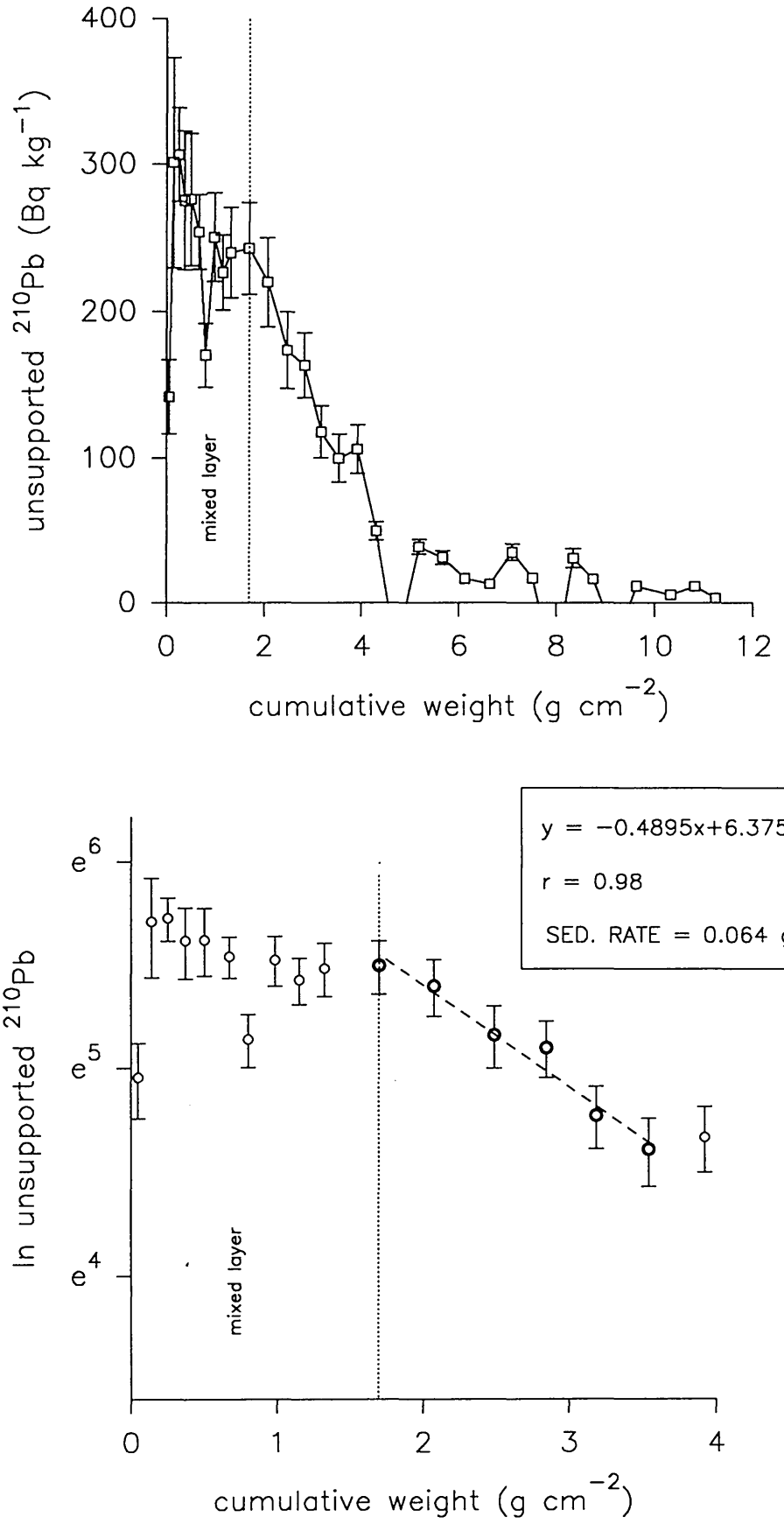

Figure 4.14. Loch Etive core LE3 unsupported ^{210}Pb concentrations

Thereafter the profile is irregular, with values falling in the range 27 to 52 Bq kg^{-1}. The inventory of ^{226}Ra in this core is 4200 ± 350 Bq m^{-2} which is within error the same as that of LE 1 (3900 Bq m^{-2}) and lower than LE 2 (5700 Bq m^{-2}).

The unsupported ^{210}Pb concentration is 141.8 Bq kg^{-1}, at the surface and increases to 301.1 Bq kg^{-1} at 0.14 g cm^{-2} depth (1.5 cm). The low unsupported ^{210}Pb surface value is a result of the high surface concentration of ^{226}Ra (276.9 Bq kg^{-1}), which is much greater than the average value of 40 Bq kg^{-1} for this core. The unsupported ^{210}Pb is restricted to the top 4 g cm^{-2} (23 cm) at which depth the concentration is 50.2 Bq kg^{-1}. The concentrations of unsupported ^{210}Pb are within error constant to a depth of 1.69 g cm^{-2} (11 cm) with the exception of one point at 0.8 g cm^{-2} (6.5 cm) which has a value of 170.5 Bq kg^{-1} and possibly represents surface sediment that has been redistributed by bioturbation. The ^{210}Pb profile was interpreted as representing a mixed zone of sediment to 1.69 g cm^{-2} and the sedimentation rate was obtained by plotting the natural log of the unsupported ^{210}Pb concentration against depth in g cm^{-2} and linear regression fitting of a straight line to the data below the mixed layer giving a correlation coefficient (r) of 0.98 and a sedimentation rate of 0.064 g cm^{-2} y^{-1}. The inventory of unsupported ^{210}Pb was 7700 ±1100 Bq m^{-2}, implying a steady state flux of 238 ± 33 Bq m^{-2} y^{-1} which, within error is the same as that of LE 1(294 ± 45 Bq m^{-2} y^{-1}) but far greater than that of LE 2 (68 ± 9 Bq m^{-2} y^{-1}). Taking account of an average atmospheric flux of 150 Bq m^{-2} y^{-1} and a flux of ^{210}Pb from the water column (128 m) of 8 Bq m^{-2} the inventory is approximately 80 Bq m^{-2} greater than can be accounted for by atmospheric deposition plus water column in-situ production and indicates that there must be another source of ^{210}Pb to this sediment. A significant observation is that cores LE 1 and LE 3 which are subject to markedly different geochemical conditions in the outer and inner basins of the loch have similar fluxes and inventories, indicating that the ^{210}Pb deposition and retention is the same in both cases despite the different geochemical condition.

Having obtained a sedimentation rate it is possible to date the horizons in the

profiles of the selected element/Al ratios. Using the sedimentation rate of 0.064 g cm^{-2} y^{-1} for LE 3 it is apparent that an increase in the Si/Al ratio occurs at 6.1 g cm^{-2} (33 cm) and there is a maximum at 1.69 g cm^{-2} (11 cm) corresponding to mid section dates of 1894 and 1960 respectively. Taking mixing into account, the onset of change of the Si/Al ratio has a date of 1920 which is slightly later than similar changes in cores LE 1 (1916) and LE 2 (1913). Therefore, all three cores from different parts of the loch are indicating that something has occurred around 1914-1920 which has affected the complete loch at this time. The maximum Ca/Al ratio at 0.14 g cm^{-2} has a date of 1984 and the maximum Zr/Al ratio at 10.33 g cm^{-2} (52.5 cm) has a mid section date of 1830. The bottom of the mixed layer at a depth of 1.69 g cm^{-2} (11 cm) occurs at 1959 giving a mixed layer depth of approximately 26 years.

4.4.3 *^{137}Cs, ^{134}Cs and ^{241}Am profiles of core LE 3*

The concentration profiles of ^{137}Cs and ^{241}Am and the activity ratio profile for ^{134}Cs/ ^{137}Cs are shown in Figure 4.15. The ^{137}Cs concentration is 248.2 Bq kg^{-1} at the surface of LE 3 and decreases to 2.3 Bq kg^{-1} at a depth of 9.64 g cm^{-2} (49 cm). The maximum concentration of 302.7 Bq kg^{-1} occurs at 0.50 g cm^{-2} (4.5 cm) which is within the mixed layer indicated by the ^{210}Pb profile. As with the two previous cores, LE 1 and LE 2 the mixing has affected the ^{137}Cs profile, with the maximum occurring as a broad peak over the depth range 0.37 to 0.98 g cm^{-2} (3.5 to 7.5 cm). The inventory of ^{137}Cs in LE 3 is 7700 ± 230 Bq m^{-2} which is within error the same as LE 2 (7500 Bq m^{-2}) but is significantly lower than that of LE 1 (10100 Bq m^{-2}). As discussed in sections 4.2.3. and 4.3.3. it is possible to obtain a sedimentation rate by relating the maximum ^{137}Cs discharge from Sellafield with the maximum ^{137}Cs concentration in the sediment and for core LE 3 this gives a value of 0.075 g cm^{-2} y^{-1} which is in reasonable agreement with the sedimentation rate of 0.064 g cm^{-2} y^{-1} obtained from ^{210}Pb dating. However the sedimentation rate from the depth of penetration is 0.284 g cm^{-2} y^{-1} which becomes 0.223 g cm^{-2} y^{-1} after taking into account the extent of mixing. Therefore LE 3 is similar to core LE 1 in that the sedimentation rates obtained from ^{210}Pb and ^{137}Cs

(using the maximum ^{137}Cs concentration) give consistent values but that obtained from the depth of penetration of ^{137}Cs is far greater.

The $^{134}Cs/^{137}Cs$ activity ratio reflects the input of radiocaesium from Chernobyl fallout at the sediment surface where a value of 0.091 is observed. Below this, the ratio falls rapidly to 0.015 at 0.25 g cm^{-2} (2.5 cm) depth. The $^{134}Cs/^{137}Cs$ ratio continues to decrease with depth to a value of 0.008 at 0.67 g cm^{-2} (5.5 cm). The surface ratio is similar to that of LE 1 ($^{134}Cs/^{137}Cs$ = 0.103) but higher than that of LE 2 ($^{134}Cs/^{137}Cs$ ratio = 0.04). The amounts of ^{134}Cs and ^{137}Cs present in the surface sample from Chernobyl fallout were calculated to be 13.1 Bq kg^{-1} and 27.7 Bq kg^{-1} respectively, which represent 58 % of the total ^{134}Cs and 11 % of the total ^{137}Cs in the surface sediment. These figures are similar to those for core LE 1 (63% and 14%), however it must be remembered that the effects of mixing on the ratios has not been taken into account. The inventory of ^{134}Cs for core LE 3 is 27 $\pm$ 6 Bq m^{-2}. The ^{134}Cs inventories decrease in the sequence 128, 87 to 27 Bq m^{-2} for LE 1, LE 2 and LE 3, while the corresponding ^{137}Cs inventories are 10100, 7500 and 7700 Bq m^{-2} and this decrease in the ^{134}Cs inventories could possibly reflect a difference in the Chernobyl input to different parts of the loch.

Using the ^{210}Pb chronology, the depth at which the onset of the Sellafield discharge and the maximum weapons fallout deposition, which occurred in 1963, should occur can be calculated as 2.05 and 1.5 g cm^{-2} respectively. ^{137}Cs was detectable to a depth of 9.64 g cm^{-2} which is considerably deeper than the calculated depths. Taking into account the effects of mixing, the depth of penetration becomes 3.7 g cm^{-2} which suggests that the ^{137}Cs has diffused by a depth of 5.9 g cm^{-2}.

^{241}Am was not detectable in the two samples nearest the surface as there was only a small weight of sediment available for these depths. Below this level, the ^{241}Am profile for LE 3 is similar to that of LE 1 with a maximum concentration of 9.2 Bq kg^{-1} at a depth of 0.50 g cm^{-2} (4.5 cm) and with ^{241}Am being detectable to 2.07 g cm^{-2} (13 cm) depth. The maximum concentration of ^{241}Am occurs at a depth corresponding to deposition in 1979 (using the

^{210}Pb chronology) which, after considering the transport time, would relate to the 1977 discharge. The maximum therefore provides a good match with ^{241}Am "grow in" value of 19 T Bq which occurred in 1978 and which would have reached Loch Etive at approximately 1980. A second maximum of 7.6 Bq kg^{-1} occurs at a depth of 0.98 g cm^{-2} (7.5 cm) corresponding to 1972, which after considering transport time of two years, corresponds to 1970. This is three years earlier than the occurrence of the second maximum ^{241}Am "grow in" from the Sellafield discharge in 1973 (42 T Bq) but is still in reasonable agreement with the expected date.

The ratio of the inventories of ^{137}Cs and ^{241}Am has a value of 73 which is in good agreement with that obtained for core LE 1 (^{137}Cs/^{241}Am inventory ratio = 75) and by the arguments advanced in section 4.2.3. suggests that there may have been significant re-dissolution of ^{137}Cs from the sediments, however, as discussed in section 4.2.3., there is not an obvious explanation for this observation.

4.4.4 *^{228}Th and ^{228}Ra profiles of core LE 3*

The ^{228}Th / ^{228}Ra profile is shown in Figure 4.15. The surface sediment has a ratio of 0.49 indicating an excess of ^{228}Ra. The ^{228}Ra concentration has a value of 379.7 Bq kg^{-1} in the surface sediment but falls rapidly to 57.5 Bq kg^{-1} at a depth of 0.25 g cm^{-2} (2.5 cm) after which the concentration fluctuates between 38 and 61 Bq kg^{-1}. The high concentration of ^{228}Ra in the surface sediment reflects the redistribution of ^{228}Ra within core LE 3 and its involvement in the redox recycling of Mn. This is similar to the ^{226}Ra in this core which also has an elevated concentration at the surface of the sediment. The ^{228}Th/ ^{228}Ra ratio increases to 1.97 at 0.37 g cm^{-2} (3.5 cm) indicating an excess of ^{228}Th at this depth. The ^{228}Th concentration is also high in the surface sediment but decreases more slowly with depth than the ^{228}Ra. The ^{228}Th concentration falls to 51.6 Bq kg^{-1} at a depth of 0.80 g cm^{-2} (6.5 cm) below which it remains relatively constant. The ratio tends to a value slightly greater than 1 at a depth of 2.84 g cm^{-2} (17 cm) below which it is with in error of unity. The inventories for ^{228}Th and ^{228}Ra are 5500 ± 360 Bq m^{-2} and 5300

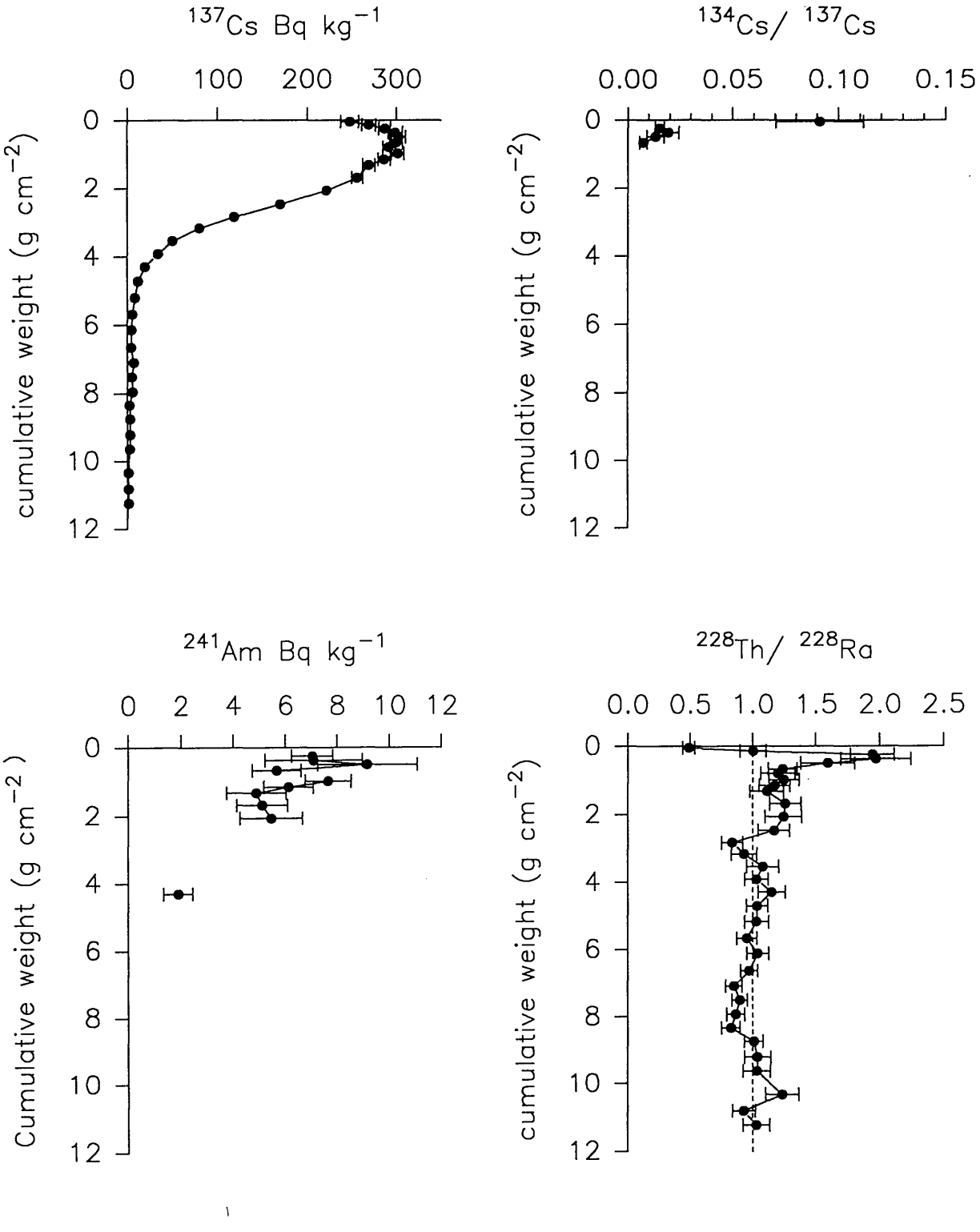

Figure 4.15. Loch Etive core LE3 radionuclide concentrations and activity ratios.

± 400 Bq m^{-2} which indicate that there is no loss of ^{228}Ra from this core but a redistribution of ^{228}Ra within it. Both ^{226}Ra and ^{228}Ra show enrichments in the surface sediment of core LE 3 where the concentration of Mn is highest (1.7%), indicating that the radium is mobile in the pore waters with scavenging by Mn oxyhydroxides near the surface and release at depth upon reduction of the Mn. Alternatively the excess ^{228}Ra may be being scavenged from the overlying water by Mn oxyhydroxides. Again, as with cores LE 1 and LE 2, there is structure in the profile within the mixed zone defined by the ^{210}Pb profile, indicating that rate of movement of Ra is more rapid than the rate of mixing. The ^{232}Th inventory of core LE 3 is 3900 Bq m^{-2} indicating that there is an excess of ^{228}Th within core LE 3 in the deep station of the inner basin and this is in agreement with the surface transect results where there was a large excess of ^{228}Th within the inner basin and a deficiency in the outer basin. This probably reflects the release of ^{228}Ra from the oxidising sediments of the loch which is being scavenged by Mn oxyhydroxides at the sites within the inner basin where Mn redox cycling is taking place. However the excess ^{228}Th was far greater in core LE 2 (3000 Bq m^{-2}) which is surprising as the Mn, organic content ^{210}Pb and Pb concentrations are all lower at this site.

4.4.5 *Stable Pb and Pb isotope ratios of core LE 3*

The total stable Pb concentration data are presented in Table 3.18. and the total Pb concentration versus cumulative weight (g cm^{-2}) profile is shown in Figure 4.16.A. The concentration of Pb has a surface value of 75 mg kg^{-1}, increases to a maximum of 98 mg kg^{-1} at a depth of 0.5 g cm^{-2} (4.5 cm), then remains essentially constant at a value of about 86 mg kg^{-1} to a depth of 1.69 g cm^{-2} 9 (11 cm), which is the depth of the mixed layer as indicated by the ^{210}Pb profile. The Pb concentration then decreases to a minimum of 28 mg kg^{-1} at a depth of 10.3 g cm^{-2} (52.5 cm). The maximum Pb concentration occurred in 1979 and Pb was detectable to the bottom of the core which had a mid section date of 1814 (using the ^{210}Pb chronology) which corresponds to input in 1840 after taking into account mixing. The pollutant Pb concentration was calculated by subtracting 28 mg kg^{-1} from the total Pb

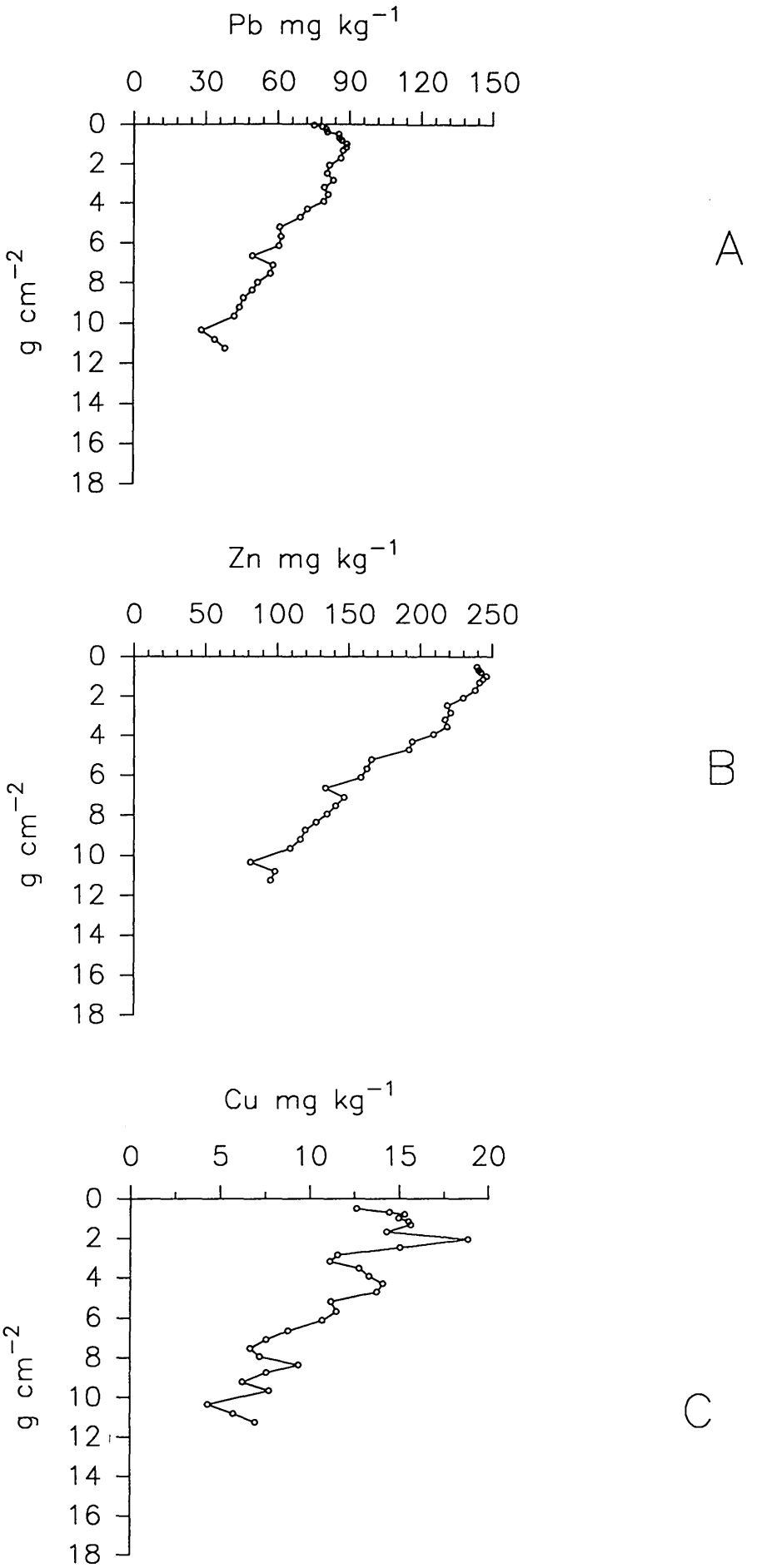

Figure 4.16. Loch Etive core LE3 Pb, Zn and Cu concentrations (mg kg^{-1})

concentration. As with cores LE 1 and LE 2 it was recognised that this figure could include an early pollution component and, if so, the excess Pb concentration calculated would represent a lower limit but this would not affect the trends within the Pb profile.

The flux of pollutant Pb versus time is shown in figure 4.17.A. and the flux values are given in Table 4.9. Excess Pb first appears in 1814, which, after considering the effects of mixing, corresponds to 1830. Unlike cores LE 1 and LE 2 the Pb flux increases relatively uniformly to a value of 0.038 g m^{-2} y^{-1} in 1934, which is probably a consequence of the relatively high degree of mixing in this core, and then decreases to 0.034 g m^{-2} y^{-1} in 1986. The maximum flux of 0.035 g m^{-2} y^{-1} occurs over the time span from 1969 to 1972.

The inventory of excess Pb for this core is 3.8 g m^{-2} which is the same as LE 1 and higher than that of LE 2 (1.6 g m^{-2}). This trend is also reflected in the ^{210}Pb inventories and fluxes. Therefore cores LE 1 (outer basin) and LE 3 (inner basin) which have accumulated under different geochemical conditions have the same inventory of pollutant Pb and, within error, the same ^{210}Pb inventory which strongly suggests that the geochemistry of pollutant Pb is the same in both cores. The distribution of pollutant Pb in core LE 3 is different from that in both LE 1 and LE 2 as is indicated by both the Pb concentration and the Pb flux profiles which both suggest that the high degree of mixing is redistributing the pollutant Pb down the sediment core.

Temporal trends in $^{206}Pb/^{207}Pb$ ratio and pollutant Pb fluxes for core LE 3 on the basis of the ^{210}Pb chronology are shown in Figure 4.18. The $^{206}Pb/^{207}Pb$ ratio is 1.152 at the surface and increases with depth to 1.179 at 10.3 g cm^{-2} (52.5 cm). The $^{206}Pb/^{207}Pb$ ratio starts to decrease at a depth of 5.2 g cm^{-2} (29 cm) which is equivalent to 1909. After accounting for the mixing of 1.69 g cm^{-2} this corresponds to an input starting in approximately 1935 which is good agreement with cores LE 1 and LE 2, with dates for onset of petrol Pb deposition of 1937 and 1929 respectively and indicates a lack of diagenetic mobility of Pb in this core.

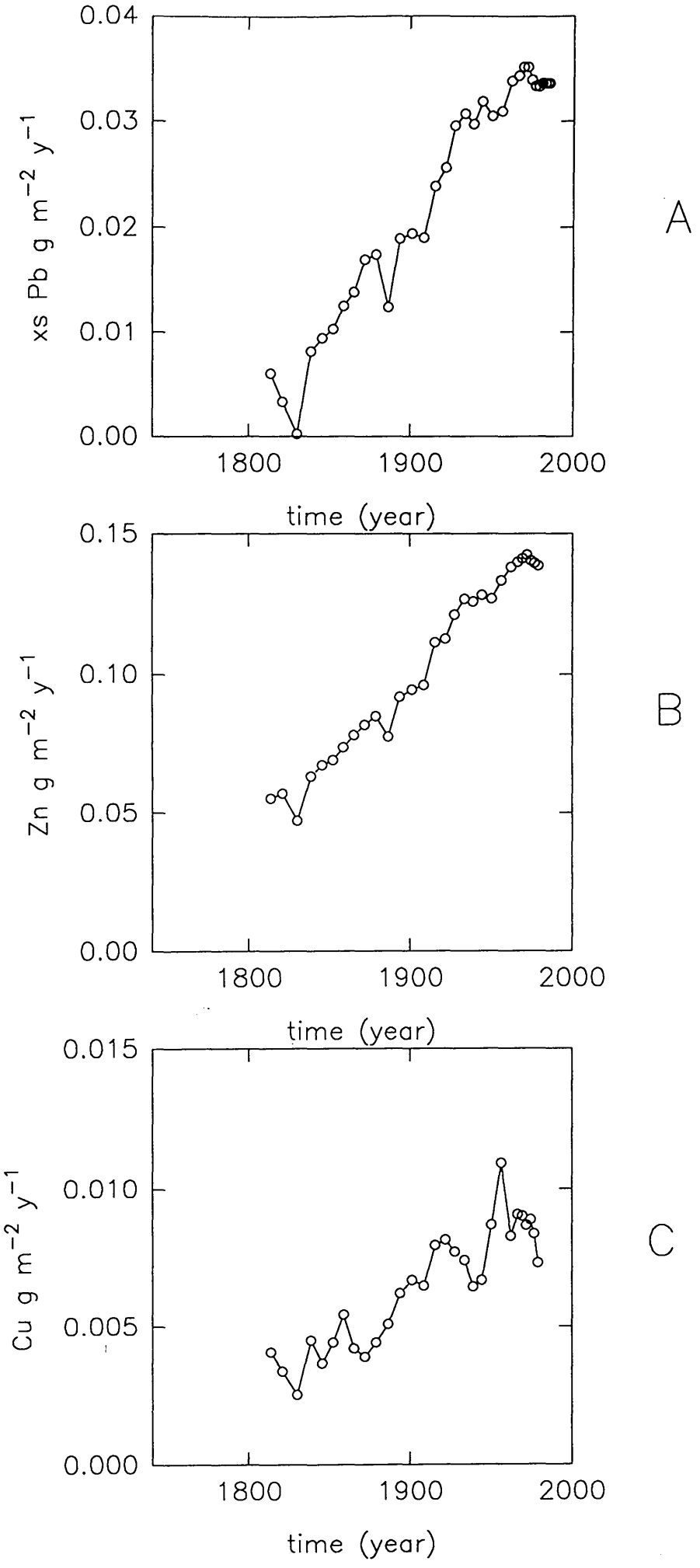

Figure 4.17. Loch Etive core LE3 Pb, Zn and Cu flux data

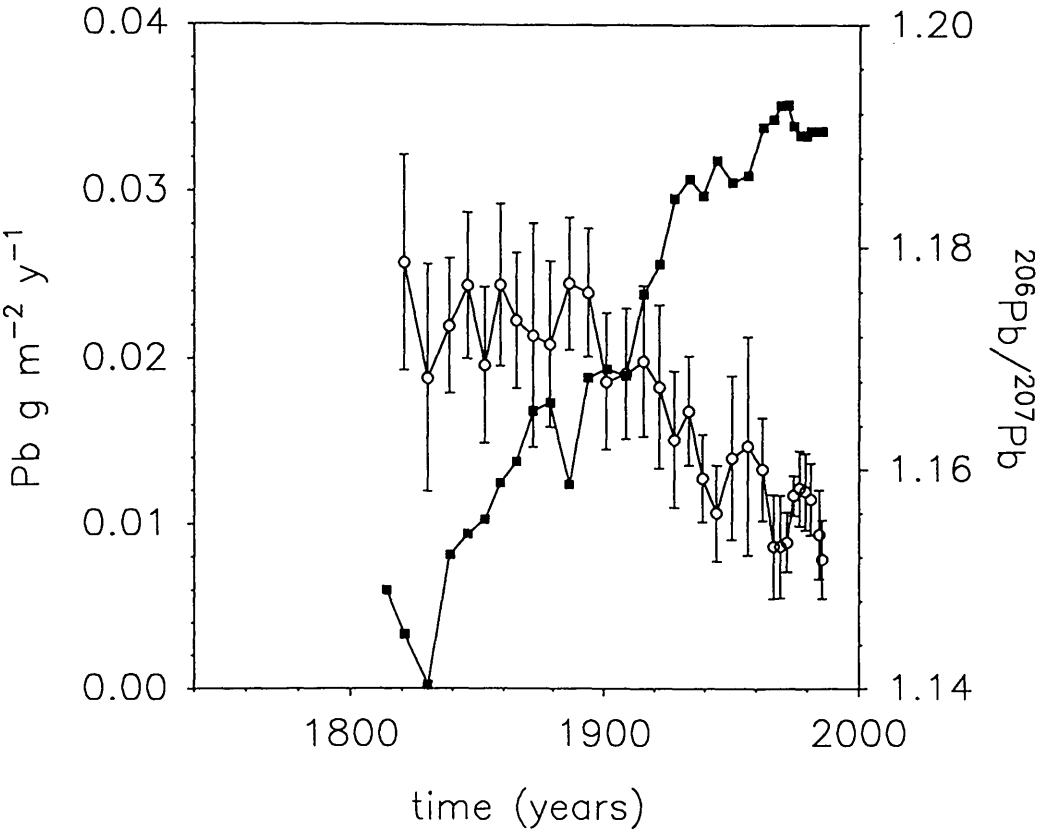

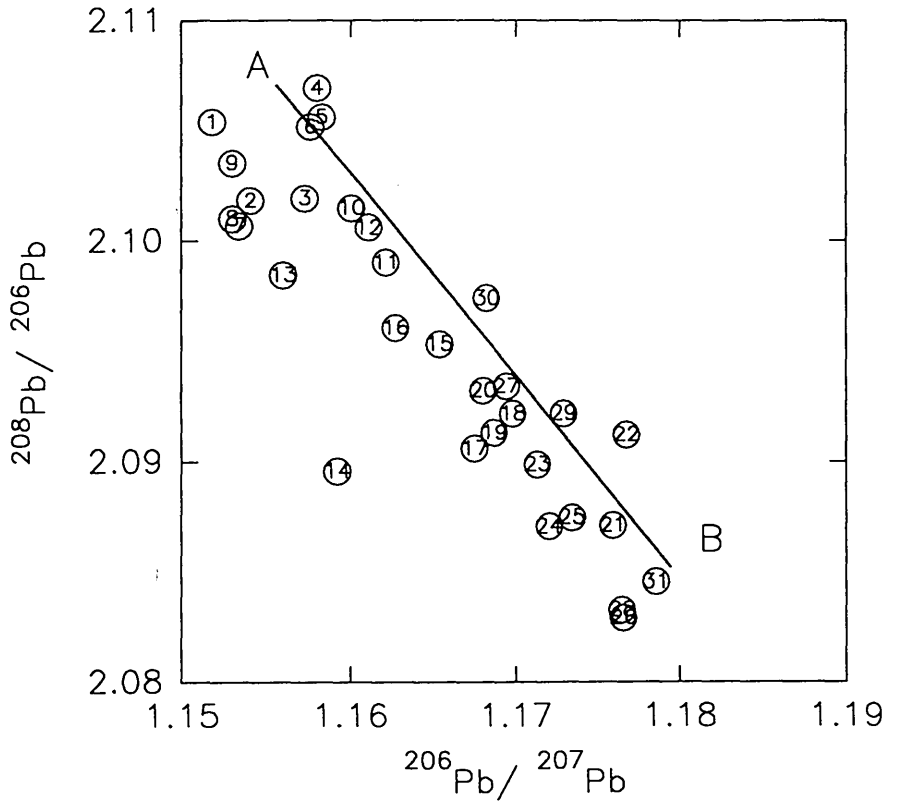

Figure 4.18. Loch Etive core LE3 Pb flux and Pb isotope ratio plots

SAMPLE	DEPTH	cum g cm^{-2}	date for mid section	excess Pb g m^{-2} y^{-1}
LE3 0-1	0.5	0.05	1986	0.0336
LE3 1-2	1.5	0.14	1984	0.0336
LE3 2-3	2.5	0.25	1983	0.0336
LE3 3-4	3.5	0.37	1981	0.0336
LE3 4-5	4.5	0.50	1979	0.0334
LE3 5-6	5.5	0.67	1977	0.0334
LE3 6-7	6.5	0.80	1974	0.0339
LE3 7-8	7.5	0.98	1972	0.0352
LE3 8-9	8.5	1.15	1969	0.0352
LE3 9-10	9.5	1.32	1967	0.0343
LE3 10-12	11.0	1.69	1962	0.0339
LE3 12-14	13.0	2.07	1957	0.0310
LE3 14-16	15.0	2.48	1950	0.0306
LE3 16-18	17.0	2.84	1944	0.0319
LE3 18-20	19.0	3.18	1939	0.0298
LE3 20-22	21.0	3.54	1934	0.0308
LE3 22-24	23.0	3.92	1928	0.0296
LE3 24-26	25.0	4.30	1922	0.0257
LE3 26-28	27.0	4.71	1911	0.0239
LE3 28-30	29.0	5.19	1909	0.0190
LE3 30-32	31.0	5.68	1901	0.0194
LE3 32-34	33.0	6.13	1894	0.0189
LE3 34-36	35.0	6.64	1886	0.0124
LE3 36-38	37.0	7.10	1879	0.0174
LE3 38-40	39.0	7.52	1872	0.0169
LE3 40-42	41.0	7.95	1865	0.0138
LE3 42-44	41.0	8.35	1859	0.0125
LE3 44-46	43.0	8.75	1852	0.0103
LE3 46-48	45.0	9.21	1846	0.0094
LE3 48-50	47.0	9.64	1839	0.0081
LE3 50-55	52.5	10.33	1830	0.0002
LE3 55-60	57.5	10.82	1821	0.0033
LE3 60-65	63.5	11.24	1814	0.0060

Table 4.8 Loch Etive core LE 3 Pb flux data

Calculation of the percentage Pb due to petrol was carried out as described in 4.2.5 with R_i= 1.174 and R_{Hi}= 1.172 and the results are given in Table

4.10. The onset of deposition of Pb from petrol occurs at 1909 which, after mixing is considered, becomes 1935, 7 years earlier than core LE 1(1942, 4%) and 7 years later than LE 2 (1929, 5%). The dates calculated using the above equation for cores LE 2 and LE 3 agree with the onset of petrol Pb as indicated by the change in the $^{206}Pb/\ ^{207}Pb$ ratio, but the date calculated for core LE 1 is 5 years later than that indicated by the $^{206}Pb/\ ^{207}Pb$ ratio. The maximum % Pb from petrol is 47 % at the surface of the sediment which is similar to both LE 1 (42%) and LE 2 (44%).

The $^{208}Pb/\ ^{206}Pb$ versus $^{206}Pb/\ ^{207}Pb$ plot for core LE 3 is shown in Figure 4.18., with the samples numbered 1 to 31 in the sequence of increasing depth. The three component system with two tie lines that was apparent in both LE 1 and LE 2 does not apply to this core which instead, exhibits a two component system with one tie line. This may be due either to pollutant Pb being dominant throughout the core with the result that the natural ratio is not being seen or, more likely, to the natural Pb ratio being similar to that of heavy industry pollution. Samples 1-9 (A) are grouped in a high $^{208}Pb/^{206}Pb$ ratio and low $^{206}Pb/^{207}Pb$ ratio position, which indicates a significant contribution of Pb from petrol. Samples 21-31 (B) tend to lower $^{208}Pb/^{206}Pb$ and higher $^{206}Pb/^{207}Pb$ ratios, with samples 10-21 lying on a tie line (A-B) between the two as would be seen if there were only two end members.

SAMPLE	DEPTH	cum. g cm^{-2}	date for mid section	% Pb petrol
LE3 0-1	0.5	0.05	1986	47
LE3 1-2	1.5	0.14	1984	40
LE3 2-3	2.5	0.25	1983	33
LE3 3-4	3.5	0.37	1981	31
LE3 4-5	4.5	0.50	1979	29
LE3 5-6	5.5	0.67	1977	31
LE3 6-7	6.5	0.80	1974	39
LE3 7-8	7.5	0.98	1972	39
LE3 8-9	8.5	1.15	1969	39
LE3 9-10	9.5	1.32	1967	25
LE3 10-12	11	1.69	1962	21
LE3 12-14	13	2.07	1957	25
LE3 14-16	15	2.48	1950	35
LE3 16-18	17	2.84	1944	28
LE3 18-20	19	3.18	1939	16
LE3 20-22	21	3.54	1934	21
LE3 22-24	23	3.92	1928	11
LE3 24-26	25	4.30	1922	7
LE3 26-28	27	4.71	1916	10
LE3 28-30	29	5.19	1909	14
LE3 30-32	31	5.68	1901	
LE3 32-34	33	6.13	1894	
LE3 34-36	35	6.64	1886	
LE3 36-38	37	7.10	1879	
LE3 38-40	39	7.52	1872	
LE3 40-42	41	7.95	1865	
LE3 42-44	41'	8.35	1859	
LE3 44-46	43	8.75	1852	
LE3 46-48	45	9.21	1846	
LE3 48-50	47	9.64	1839	
LE3 50-55	52.5	10.33	1830	
LE3 55-60	57.5	10.82	1821	
LE3 60-65	63.5	11.24	1814	

Table 4.9 % Pb in core LE 3 from Pb in petrol

4.4.6 *Zn and Cu profiles of core LE 3*

The Zn and Cu concentration profiles for LE 3 are shown in Figure 4.16.B. and 4.16.C. respectively. There are no values for Zn and Cu concentrations to a depth of 3.5 cm as the sample weights over this depth range were too small to analyse by XRF. The trends in the Zn profile are very similar to those of the Pb profile. The concentration has a value of 239 mg kg^{-1} at a depth of 0.5 g cm^{-2} (4.5 cm) and decreases uniformly to a value of 95 mg kg^{-1} at 11.2 g cm^{-2} (62.5 cm). Zn is detectable to the bottom of the core which has a date of 1814, or, considering the effects of mixing represents input in 1840. The Cu profile is more structured than either the Pb or Zn profiles but follows the same general trend. The Cu concentration is 13 mg kg^{-1} at 0.5 g cm^{-2} (4.5 cm) and increases to a maximum of 19 mg kg^{-1} at 2.1 g cm^{-2} (13 cm) which corresponds to 1957. The concentration then decreases somewhat erratically to 7 mg kg^{-1} at 11.2 g cm^{-2} (63.5 cm). The fluxes of excess Pb, total Zn and total Cu are given in Figure 4.17 with the results being presented in Table 4.11. The Zn flux increases relatively constantly from a depth of 11.24 g cm^{-2} to a maximum value of 0.143 at a depth of 0.98 g cm^{-2}, corresponding to a date of 1971. As with the previous two cores, the Zn profile is very similar to the Pb profile. The inventory of Zn for this core is 18.7 g m^{-2} which is similar to those of cores LE 1 (21.1 g m^{-2}) and LE 2 (19.8 g m^{-2}).

The plot of temporal variations in the Cu flux is again similar to the Pb and Zn flux plots and the total Cu inventory is 1.2 g m^{-2} which is similar to both LE 2 (1.2 g m^{-2}) and LE 1 (1.4 g m^{-2}). The ratio of the excess Pb, total Zn total Cu and ^{210}Pb inventories in core LE 1 to those of LE 3 have respective values of 1.0,1.1, 1.2 and 1.2, indicating very close agreement in all cases. The excess inventories of Zn and Cu for this core were calculated by assuming natural levels of 96 and 7 mg kg^{-1} for Zn and Cu respectively, and were 8.1 and 0.4 g m^{-2}. These values can be compared to cores LE 1 (Zn = 7.8, Cu = 0.5 g m^{-2}) and LE 2 (Zn = 3.4, Cu = 0.6 g m^{-2}) and once again it can be seen that the inventories of excess Cu are similar in all three cores and the excess Zn inventories are essentially the same for cores LE 1 and

LE 3, with the inventory for LE 2 being considerably lower. The ratio of the excess Zn and excess Cu inventories in core LE 1 to those of LE 3 have respective values of 1.0 and 1.2, indicating very close agreement between the inventories of excess Pb, ^{210}Pb, Zn and Cu of the outer and inner basin.

The residual Pb (i.e. excess Pb inventory - Pb inventory due to petrol) can be compared with that of LE 1 and the ratio LE $1_{res.Pb}$/LE $3_{res.Pb}$ has a value of 0.9. Therefore the above ratios suggest that Pb,^{210}Pb, Zn and Cu are all behaving effectively identically within the two sediments represented by cores LE 1 and LE 3, despite their markedly different geochemical conditions. The residual Pb ratio indicates that there is a higher proportion of pollutant Pb derived from petrol in core LE 1 than in core LE 3.

4.4.7 *Summary of core LE 3*

In summary, the results for core LE 3 suggest that ^{210}Pb dating, ^{137}Cs, ^{241}Am and ^{206}Pb/^{207}Pb isotope ratio trends give chronologically consistent profiles indicating that ^{210}Pb dating is valid and that Pb is not diagenetically mobile in this core, although the Pb concentration and flux profiles indicate that pollutant Pb has been redistributed downwards as a result of relatively intense mixing. The core is mixed to a depth of 1.69 g cm^{-2} (11 cm) and has an accumulation rate of 0.064 g cm^{-2} y^{-1} giving a time interval from the surface of the sediment to the base of the mixed zone of 26 years.

As with cores LE 1 and LE 2, the manmade radionuclides present in the sediment are dominated by the Sellafield discharge. The sedimentation rate derived from the position of the maximum ^{137}Cs concentration was 0.075 g cm^{-2} y^{-1} which is in reasonable agreement to that derived from ^{210}Pb dating. The ^{134}Cs and ^{137}Cs profiles indicated mobility of radiocaesium by means of mixing and diffusion and, as with cores LE 1 and LE 2, ^{137}Cs is detectable to far greater depths than would be expected due to mixing alone which limits its use in determining chronologies.

SAMPLE	DEPTH	cum g cm^{-2}	date for mid section	Cu g m^{-2} y-1	Zn g m^{-2} y^{-1}
LE3 0-1	0.5	0.05	1986		
LE3 1-2	1.5	0.14	1984		
LE3 2-3	2.5	0.25	1983		
LE3 3-4	3.5	0.37	1981		
LE3 4-5	4.5	0.50	1979	0.007	0.139
LE3 5-6	5.5	0.67	1977	0.008	0.139
LE3 6-7	6.5	0.80	1974	0.009	0.140
LE3 7-8	7.5	0.98	1972	0.009	0.143
LE3 8-9	8.5	1.15	1969	0.009	0.141
LE3 9-10	9.5	1.32	1967	0.009	0.140
LE3 10-12	11.0	1.69	1962	0.008	0.138
LE3 12-14	13.0	2.07	1957	0.011	0.133
LE3 14-16	15.0	2.48	1950	0.009	0.127
LE3 16-18	17.0	2.84	1944	0.007	0.128
LE3 18-20	19.0	3.18	1939	0.006	0.126
LE3 20-22	21.0	3.54	1934	0.007	0.127
LE3 22-24	23.0	3.92	1928	0.008	0.121
LE3 24-26	25.0	4.30	1912	0.008	0.113
LE3 26-28	27.0	4.71	1916	0.008	0.111
LE3 28-30	29.0	5.19	1909	0.007	0.096
LE3 30-32	31.0	5.68	1901	0.007	0.094
LE3 32-34	33.0	6.13	1894	0.006	0.092
LE3 34-36	35.0	6.64	1886	0.005	0.077
LE3 36-38	37.0	7.10	1879	0.004	0.085
LE3 38-40	39.0	7.52	1872	0.004	0.082
LE3 40-42	41.0	7.95	1865	0.004	0.078
LE3 42-44	41.0	8.35	1859	0.005	0.074
LE3 44-46	43.0	8.75	1852	0.004	0.069
LE3 46-48	45.0	9.21	1846	0.004	0.067
LE3 48-50	47.0	9.64	1839	0.005	0.063
LE3 50-55	52.5	10.33	1830	0.003	0.047
LE3 55-60	57.5	10.82	1821	0.003	0.057
LE3 60-65	63.5	11.24	1814	0.004	0.055

Table 4.10 Cu and Zn fluxes for core LE 3

Temporal variations in pollutant Pb flux are different from those of cores LE 1 and LE 2 in that there is not the same sharp increase in Pb flux (1916 to 1964), but a more uniform increase which probably reflects the extent and intensity of mixing in this core. The inventory of excess Pb in this core is 3.8 g m^{-2} which is the same as core LE 1 and considerably higher than that of LE 2 (1.6 g m^{-2}). The onset of deposition of pollutant Pb from petrol can be detected in 1935 at 14% which is higher than both LE 1 (4%) and LE 2 (5%). As with cores LE 1 and LE 2 the Zn and Cu flux profiles for core LE 3 are very similar to that of the Pb and core LE 3 has inventories of Zn and Cu of 18.7 and 1.2 g cm^{-2} respectively which are similar to those calculated for cores LE 1 and LE 2.

4.5 *Clyde Sea Area Sediment Cores*

As described in detail in chapter two, four gravity cores were collected within the Clyde Sea Area (CSA). The sampling locations are shown in Figure 2.2. Two cores were collected from Loch Fyne, one from a shallow station and one from a deep station, and one core from each of Loch Long and Loch Goil. The results for analysis of the cores are given in Chapter 3.

The Clyde Sea Area is described in detail in Chapter 1, however it is useful to recapitulate on some of the important features of the area which are pertinent to the following discussion. The Clyde Sea Area is a complex dynamic natural system which has been affected by anthropogenic pollution and physical disturbance and has two dumping sites within its boundaries. One is located at Garroch Head and sewage sludge from the Greater Glasgow area has been dumped at this site since 1904. The other dump site is situated at the entrance to Holy Loch and Clyde Port Limited (formerly The Clyde Port Authority) has dumped dredge spoil from the navigation channel of the Clyde estuary, which is highly contaminated with sewage and industrial effluent, at this location since 1939. Before 1939 the dredge was dumped south of the Cumbries (NERC, 1974). Although none of the four sampling sites was close to the dredge dump site it has the potential to affect the cores

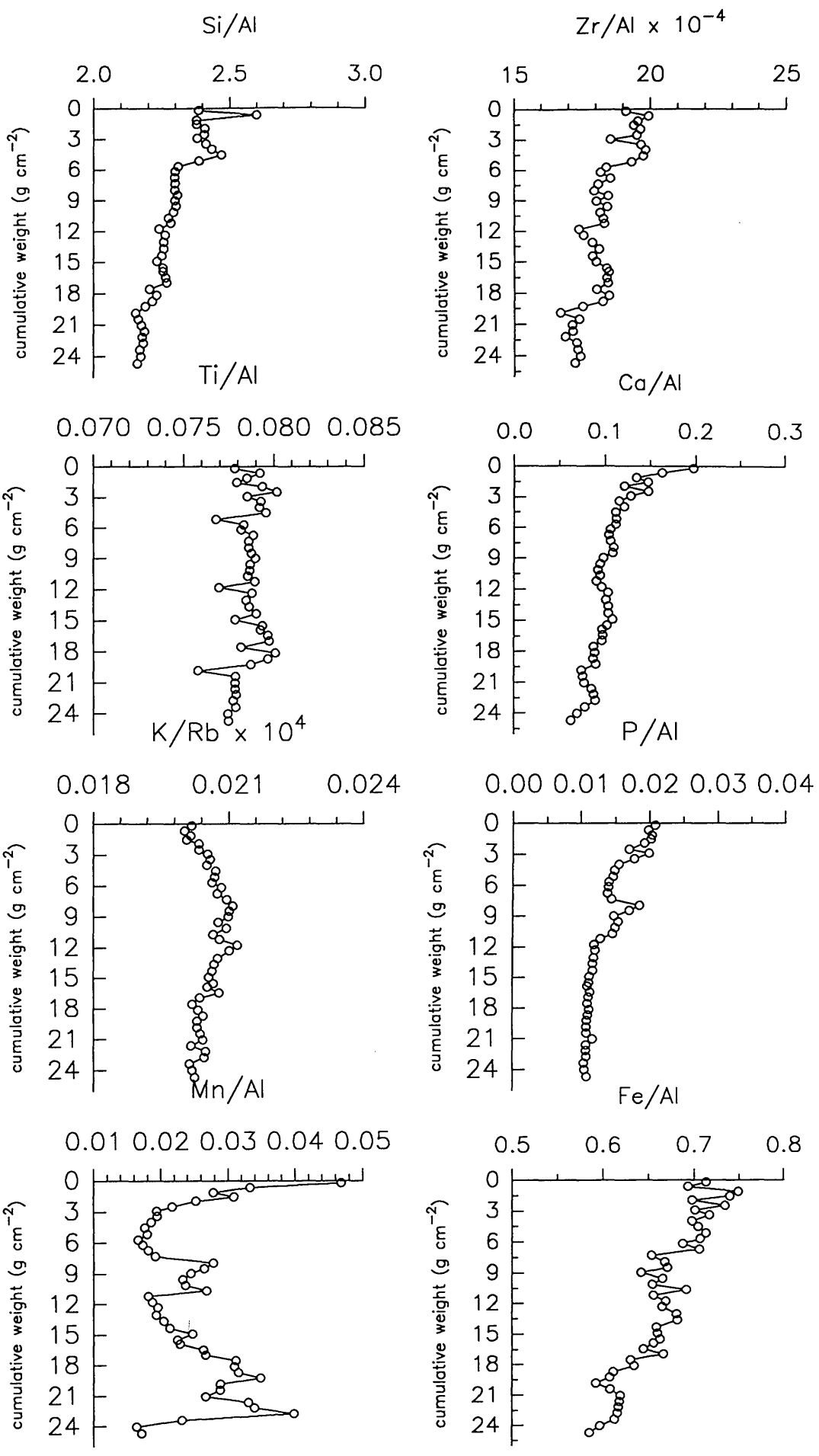

Figure 4.19 . Loch Long core LL1 element/Al and K/Rb ratios.

from Loch Long and Loch Goil.

4.5.1 *Geochemical characteristics of core LL1*

Selected element/Al ratios and K/Rb ratios for core LL1 are shown in Figure 4.19. The Si/Al, Zr/Al and Ti/Al profiles are all similar in that they have increased ratios above a depth of 5.7 g cm^{-2} (13 cm), signifying a change to coarser grain size sediment above this depth and also display a decrease in value from a depth of 19.9 g cm^{-2} (63 cm) possibly indicating a change to finer grain size sediment. The K/Rb ratio increases from a value of 200 at the surface to 210 at 7.95 g cm^{-2} (21 cm) depth, again indicating that there may have been a change in sediment type from finer to coarser grained material towards the surface of the core. This is also reflected in the Ca/Al ratio which decreases from a value of 0.20 at the surface to a value of 0.06 at 24.7 g cm^{-2} (79 cm).

The Mn/Al ratio decreases rapidly from a surface value of 0.05 to 0.017 at 5.7 g cm^{-2} (13 cm), indicating that diagenetic recycling of Mn is taking place in the surface sediment of core LL1. However the profile is complicated at depth and exhibits a maximum over the range 7 - 11 g cm^{-2}, possibly indicating the rapid burial of a former surface sediment enriched in Mn. The Mn/Al ratio then decreases to a value of 0.018, after which it increases with depth to a value of 0.04 at 22.8 g cm^{-2} (73 cm). Finally the ratio decreases to a value of 0.017 at 24.7 g cm^{-2} (79 cm). The Fe/Al ratio does not exhibit as rapid a decrease in value from the surface sediment as does the Mn/Al ratio, but decreases reasonably uniformly from a surface value of 0.71 to 0.59 at 24.7 g cm^{-2} (79 cm). There is, however, a step change at a depth of 7.3 g cm^{-2} (19 cm) which corresponds to a depth just above the horizon containing the elevated Mn/Al ratios. The P/Al ratio decreases from a surface value of 0.021 to 0.14 at 5.7 g cm^{-2} (13 cm) and remains at approximately this value to a depth of 6.7 g cm^{-2} (17 cm) after which it increases to 0.19 at 7.95 g cm^{-2} (21 cm). This corresponds to the depth at which the Mn/Al ratio increases and strengthens the argument for this section of the core having been a surface that has been buried rapidly. Below 7.95

g cm^{-2}, the P/Al ratio decreases systematically to a value of 0.012 at a depth of 11.8 g cm^{-2} (35 cm), and thereafter remains relatively constant to the bottom of the core. Therefore, the element/Al ratios indicate that changes have occurred in the type of accumulating material around 5.7 g cm^{-2} (13 cm) and 19.9 g cm^{-2} (63 cm). The ratios used to assess the redox condition of the sediment, namely Mn/Al, Fe/Al and P/Al, indicate that a possible former surface layer at a depth of 7.95 g cm^{-2} (21 cm) has been buried rapidly, indicative of an increase in sediment supply to this site, which could be due either to the influence of dumping, further south, of dredged sediment from the Clyde estuary or to a change in land use e.g deforestation of the area surrounding the loch or construction of roads.

4.5.2 *^{210}Pb and ^{226}Ra profiles of core LL1*

The plots of ^{226}Ra, unsupported ^{210}Pb and ln unsupported ^{210}Pb against depth in g cm^{-2} are shown in figure 4.20.

The ^{226}Ra results are tabulated in Chapter 3 (Table 3.24.). The ^{226}Ra concentration has a surface value of 23.9 Bq kg^{-1} and increases with depth to 28.3 Bq kg^{-1} at a depth of 6.19 g cm^{-2} (15 cm), with two maxima of 32.5 and 38.6 Bq kg^{-1} at depths of 0.65 (1.5 cm) and 2.92 g cm^{-2} (6.5 cm). The ^{226}Ra concentration then decreases to values of 20.3 and 22.5 Bq kg^{-1} at 6.74 (17 cm) to 7.32 g cm^{-2} (19 cm) respectively. The ^{226}Ra concentration below this depth fluctuates between 26.6 and 32.6 Bq kg^{-1} to the bottom of the core at 24.7 g cm^{-2} (79 cm). The ^{226}Ra inventory for core LL1 was 7000 $\pm$ 350 Bq m^{-2} which is higher than the ^{226}Ra inventory for any of the three Loch Etive cores.

The unsupported ^{210}Pb concentration profile exhibited a systematic decrease from the surface (124.9 Bq kg^{-1}) with a relatively regular pattern disrupted by anomalously low values between approximately 6 to 9 cm^{-2}, which corresponds to the section immediately overlying the horizon of enhanced Mn concentrations. This suggests an enhanced sedimentation rate giving depressed ^{210}Pb concentrations, consistent with the hypothesis of a rapidly

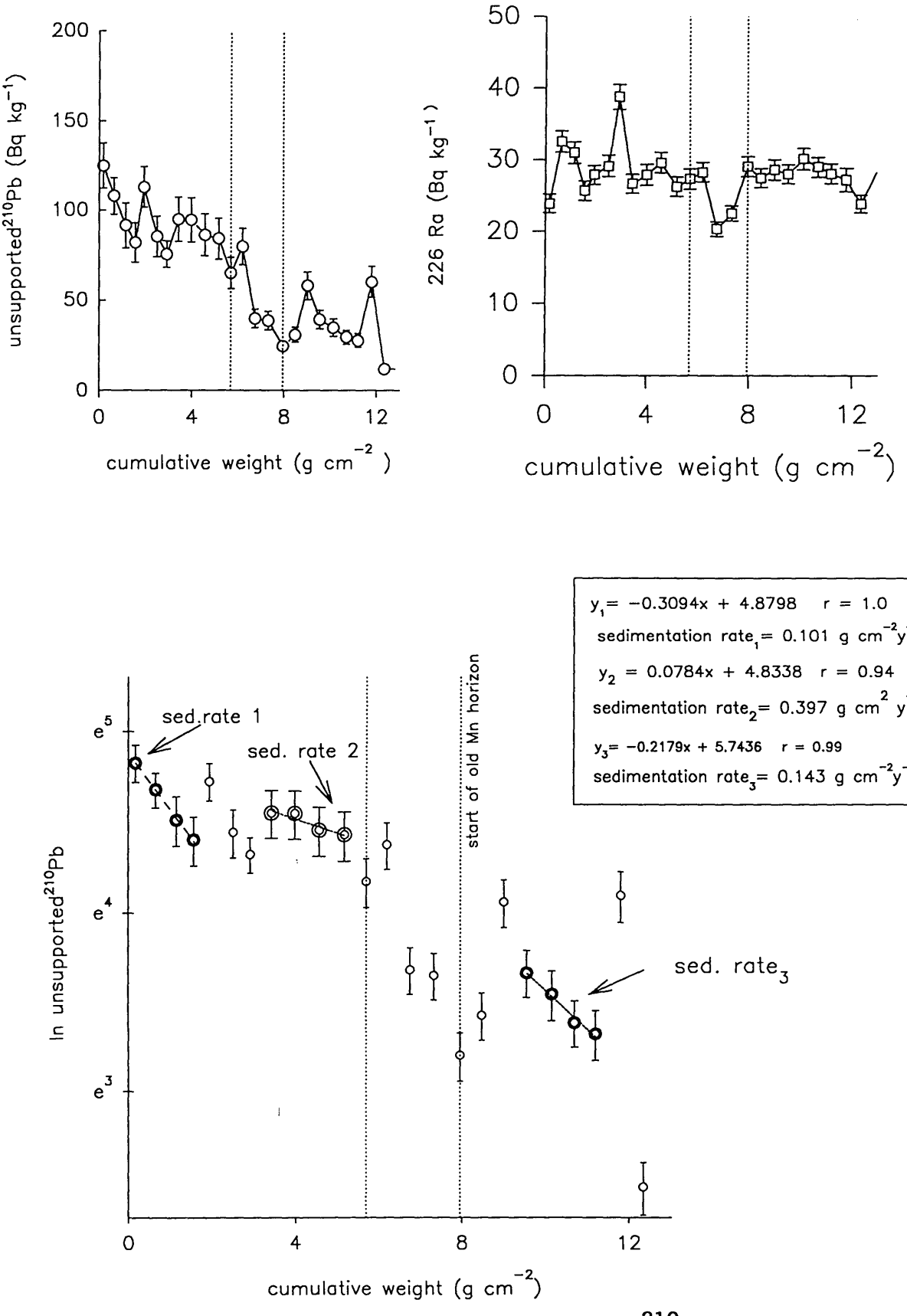

Figure 4.20 Loch Long core LL1 unsupported ^{210}Pb concentrations

buried surface. The unsupported ^{210}Pb profile exhibits an anomalously high value of 60.1 Bq kg^{-1} at 11.8 g cm^{-2} (35 cm) indicating perturbation of steady state deposition at this depth in the sediment.

While the plot of ln unsupported ^{210}Pb does decrease with depth, the profile is irregular and is clearly not suitable for application of a single C.I.C. calculation to obtain a sedimentation rate. The curve appears to consist of a number of sections, some of which show trends suggestive of periods of sediment accumulation, but with different rates of accumulation in each case. The bottom two points suggest irregular perturbation but the four points above this appear to reflect regular sedimentation at a rate of 0.14 g cm^{-2} y^{-1}. Above this level, decreased ^{210}Pb concentrations suggest a zone of enhanced sediment deposition from 8 to 5.7 g cm^{-2} (21 to 13 cm). Above this rapid accumulation zone, there is evidence of two sedimentation rates. From 5.2 to 3.4 g cm^{-2} (11 to 7.5 cm) rapid, accumulation at a rate of about 0.40 g cm^{-2} y^{-1} appears to have taken place, with a more recent decrease in accumulation rate to about 0.10 g cm^{-2} y^{-1} from 1.6 g cm^{-2} (3.5 cm) to the surface. It is not clear how long it took to accumulate the zone of sediment from 8 to 5.7 g cm^{-2} (21 to 13 cm) but a reasonable upper limit of 6 years can be applied if accumulation had taken place at the rate of 0.40 g cm^{-2} y^{-1} affecting the immediately overlying sediment. The anomalously low values in the perturbed section however suggest that the accumulation rate was significantly faster than this and, for the purposes of assigning a chronology, a deposition time of 1 year has been assumed. The effect of this could be to introduce a discrepancy of up to about 5 years in the chronology below this depth. The chronology for core LL1 using the above sedimentation rates is given in Table 4.11

SAMPLE	DEPTH	cum. g cm^{-2}	date for mid section	SAMPLE	DEPTH	cum. g cm^{-2}	date for mid section
LL1 0-1	0.5	0.18	1987	LL1 36-38	37	12.34	1934
LL1 1-2	1.5	0.65	1984	LL1 38-40	39	13.04	1929
LL1 2-3	2.5	1.14	1979	LL1 40-42	41	13.65	1924
LL1 3-4	3.5	1.56	1975	LL1 42-44	43	14.34	1920
LL1 4-5	4.5	1.93	1972	LL1 44-46	45	14.91	1916
LL1 5-6	5.5	2.50	1971	LL1 46-48	47	15.52	1912
LL1 6-7	6.5	2.92	1970	LL1 48-50	49	15.88	1908
LL1 7-8	7.5	3.43	1968	LL1 50-52	51	16.44	1905
LL1 8-9	8.5	3.99	1967	LL1 52-54	53	16.95	1901
LL1 9-10	9.5	4.56	1966	LL1 54-56	55	17.56	1897
LL1 10-12	11	5.16	1964	LL1 56-58	57	18.14	1893
LL1 12-14	13	5.69	1963	LL1 58-60	59	18.72	1889
LL1 14-16	15	6.19	1963	LL1 60-62	61	19.26	1885
LL1 16-18	17	6.74	1963	LL1 62-64	63	19.86	1881
LL1 18-20	19	7.32	1963	LL1 64-66	65	20.44	1877
LL1 20-22	21	7.95	1962	LL1 66-68	67	21.03	1873
LL1 22-24	23	8.47	1960	LL1 68-70	69	21.63	1869
LL1 24-26	25	8.99	1957	LL1 70-72	71	22.16	1865
LL1 26-28	27	9.53	1953	LL1 72-74	73	22.76	1861
LL1 28-30	29	10.13	1949	LL1 74-76	75	23.38	1857
LL1 30-32	31	10.69	1945	LL1 76-78	77	24.01	1852
LL1 32-34	33	11.19	1941	LL1 78-80	79	24.70	1848
LL1 34-36	35	11.78	1938				

Table 4.11 Chronology for core LL1 using a four zone system with a dumped section occurring over 1 year

The inventory of unsupported ^{210}Pb was calculated to be 7700 ± 980 Bq m^{-2} which is the same as that found in core LE 3 from Loch Etive and intermediate between those of LE 1 (9500 Bq m^{-2}) and LE 2 (2200 Bq m^{-2}). The unsupported ^{210}Pb inventory of core LL1 implies a steady state flux of 240 ± 30 Bq m^{-2} y^{-1} which is similar to the flux of unsupported ^{210}Pb (250 Bq m^{-2} y^{-1}) reported by Smith-Briggs (1983) for a core obtained from Loch Long (Craib core, 56° 2' 40"N; 4° 52' 30"W) in 1977. The unsupported ^{210}Pb flux for core LL1 is higher than either the atmospheric ^{210}Pb fluxes of 71.3 - 150 Bq m^{-2} y^{-1} obtained by Sugden (1993) from Scottish peat cores or the mean

global ^{210}Pb flux onto the land surface of the earth of 166.5 Bq m^{-2} y^{-1} estimated by Krishnaswamai and Lal (1987). The flux of ^{210}Pb to core LL1 is therefore considerably higher than that expected from atmospheric deposition, and the maximum flux of unsupported ^{210}Pb from in-situ production in the water column (70 m depth) can be estimated to be only about 4.4 Bq m^{-2} y^{-1}. This suggests either a far greater atmospheric flux than expected or another source of unsupported ^{210}Pb to the sediment, which could be due to solution input (from other parts of the Clyde Sea Area, the Atlantic, the Irish Sea or rivers), particulate input from sea or land or sediment focusing.

Using the chronology established for this core it is possible to date some of the horizons seen in the element/Al profiles (Figure 4.19). This core, although complicated due to differing sedimentation rates, did not show evidence of intense bioturbation or physical mixing at or near the surface.

The start of the increase of the Si/Al ratio occurs at a depth of 5.7 g cm^{-2} (13 cm) which corresponds to 1963, with the maximum ratio occurring in 1966. The K/Rb ratio begins to decrease at a depth of 7.95 g cm^{-2} (21 cm) which corresponds to 1962. The Mn/Al and P/Al ratios potentially indicate a former surface which has been rapidly buried and this occurs at 7.95 g cm^{-2} (21 cm) corresponding to 1962. Therefore, a section of rapidly accumulated material has been identified, which occurred over a depth range of 5.7 to 7.95 g cm^{-2} (13 to 21 cm), and a number of possible causes can be considered to explain this observation. The material could have resulted from a change in the land use surrounding the loch, from road building, from natural sediment slumping, from dumping of dredge spoil material or the redistribution of dumped material from the Holy Loch dumping site. For practical purposes the section of sediment from 7.95 to 5.69 g cm^{-2} (21 to 13 cm) will be referred to as a "dumped section" and the chronology for core LL1 suggests that the dumping started around 1962. The buried surface layer has Mn/Al and P/Al ratios which indicate that redox recycling of Mn was taking place in this sediment. The Si/Al ratio change at 5.7 g cm^{-2} (13 cm) corresponds to the top of the dumped section of material.

4.5.3 *^{137}Cs, ^{134}Cs and ^{241}Am concentration profiles of core LL1*

As discussed in previous sections, the ^{137}Cs concentration profile can be used to determine sedimentation rates by correlating the maximum concentration of ^{137}Cs with the Sellafield discharge, which had a pronounced maximum in 1975. In discussing the sediment cores from Loch Etive a transit time of Sellafield radiocaesium was taken to be 2 years. In the case of the Clyde Sea Area the transit time is considered to be approximately 1 year (McKinley et al., 1981; Baxter et al., 1979). Therefore, the maximum concentration of ^{137}Cs in the sediment cores from the Clyde Sea Area corresponds to a deposition date of 1976. As discussed in section 4.2.3. the $^{134}Cs/^{137}Cs$ ratio data can be used to some extent to distinguish between Sellafield and Chernobyl fallout in the surface sediment of these cores. However the cores from the Clyde Sea Area were obtained 2 years later than the cores from Loch Etive and the Chernobyl $^{134}Cs/^{137}Cs$ ratio would by then have decayed to 0.28.

The ^{137}Cs concentration (Figure 4.21) increases from 392.8 Bq kg^{-1} at the surface to a maximum of 666.1 Bq kg^{-1} at 4 g cm^{-2} (8.5 cm), below which it decreases to 127.4 Bq kg^{-1} at 6.7 g cm^{-2} (17 cm) and then increases to a subsidiary maximum of 180.3 Bq kg^{-1} at 7.95 g cm^{-2} (21 cm). This corresponds to the bottom of the dumped section and the top of the "buried surface" layer. Thereafter the ^{137}Cs decreases to a value of 2.5 at 24 g cm^{-2} (77 cm). If it is assumed that the maximum discharge from Sellafield which occurred in 1975, reached Loch Long in 1976 and this corresponds to the maximum ^{137}Cs concentration occurring at a depth of 4 g cm^{-2} then a sedimentation rate of 0.33 g cm^{-2} y^{-1} is obtained. This can be compared with the ^{210}Pb sedimentation rate for this depth range (i.e. zone 2; 1.56 to 5.69 g cm^{-2}) of 0.40 g cm^{-2} y^{-1}. Thus, despite the apparent complexity of the accumulation of this core, there is reasonable agreement between the sedimentation rates obtained from ^{210}Pb and the ^{137}Cs maximum.

The sedimentation rate obtained for core LL1 from the depth of penetration of ^{137}Cs is 0.69 g $cm^{-2}y^{-1}$ which is considerably higher than the highest

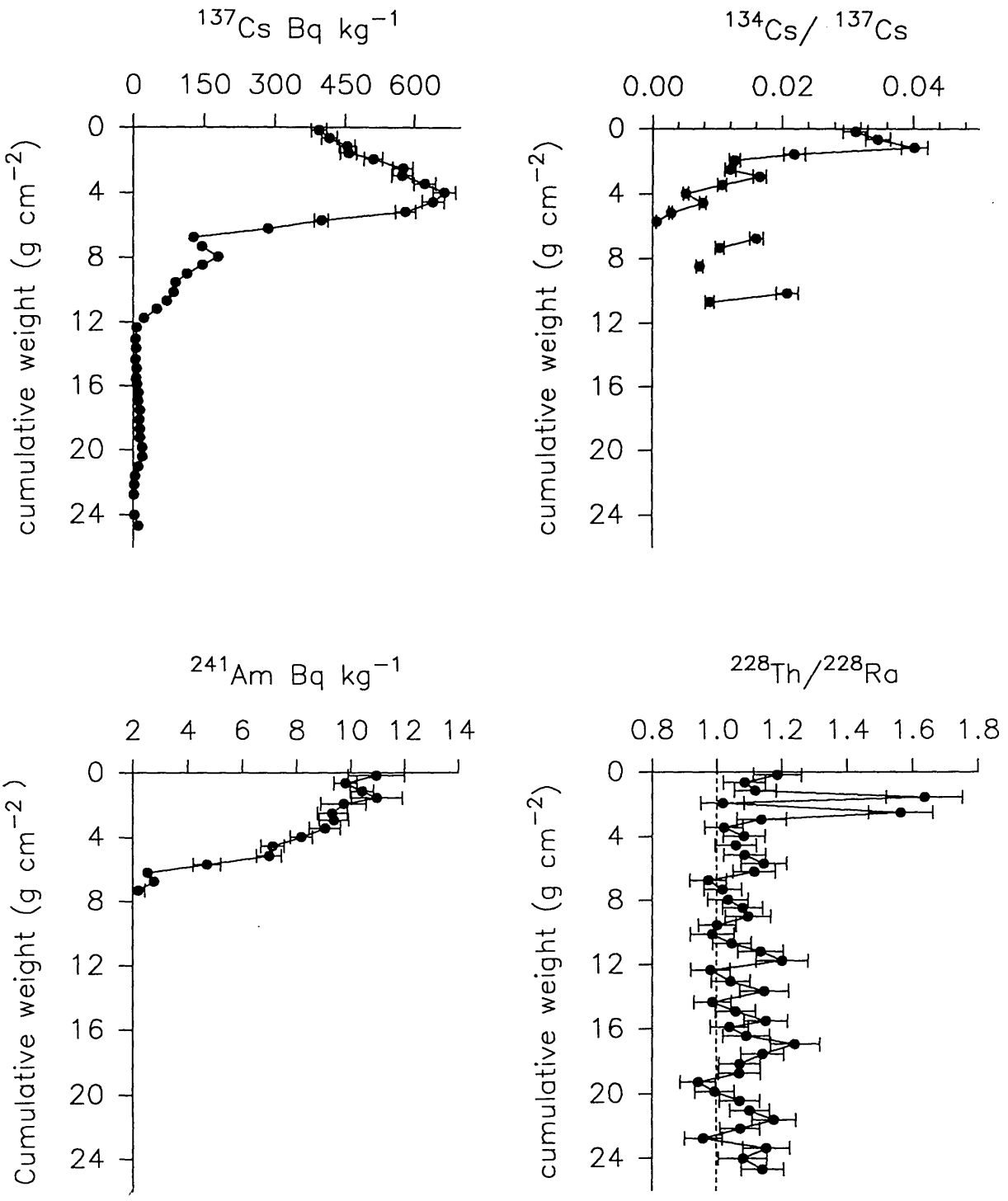

Figure 4.21. Loch Long core LL1 radionuclide concentrations and activity ratios.

sedimentation rate of 0.40 g $cm^{-2}y^{-1}$ obtained from the unsupported ^{210}Pb profile and 0.33 g $cm^{-2}y^{-1}$ obtained from the position of the ^{137}Cs maximum. Therefore, the unsupported ^{210}Pb and the position of the ^{137}Cs maximum give reasonably consistent sedimentation rates but the depth of penetration of ^{137}Cs does not.

The initial discharge from Sellafield occurred in 1952 which, taking into account a 1 year transit time, would reach Loch Long in 1953, this date corresponds to a depth of 9.53 g cm^{-2} using the ^{210}Pb chronologies. ^{137}Cs was detected to a depth of 24.7 g cm^{-2} which, assuming there is very little mixing in this core, suggests a depth of diffusion of 15.17 g cm^{-2}. This is considerably greater than any of the three cores from Loch Etive which had depths of diffusion of ^{137}Cs within the range 5.9 to 10.74 g cm^{-2} depth.

The inventory of ^{137}Cs in core LL1 is 39000 $\pm$ 1500 Bq m^{-2} which is considerably higher than any of the cores from Loch Etive. This can be compared to inventories obtained by Smith-Briggs (1983) of 34500 and 40333 Bq m^{-2} from cores obtained from Loch Long in 1977. The ratio of the ^{137}Cs inventory of core LL1 (39000 Bq m^{-2}) to the average of Smith-Briggs (1983) ^{137}Cs inventories for Loch Long (37400Bq m^{-2}) has a value of 1.04. This can be compared to the ratio of the cumulative environmental inventories of ^{137}Cs from the Sellafield discharge to 1987 and 1976 (31627 T Bq and 18870 T Bq respectively) which had a value of 1.7. If the supply of ^{137}Cs to this area of Loch Long had been continuously from the Sellafield discharge then the ratio of the sediment inventories should have been similar to that of the cumulative environmental inventories of ^{137}Cs. However the ratio of the inventories is lower than expected, which suggests that there has been another supply of ^{137}Cs to this sediment before 1977.

The values of the $^{134}Cs/^{137}Cs$ ratio that would be expected from the Sellafield discharge from 1985 to 1988 are given in Table 4.12.

date of Sellafield discharge	$^{134}Cs/^{137}Cs$ ratio of Sellafield discharge	date arrive at Loch Long (1 year transit)	Δt	decay corrected $^{134}Cs/^{137}Cs$ to 1988
1984	0.08	1985	4	0.023
1985	0.09	1986	3	0.035
1986	0.073	1987	2	0.039
1987	0101	1988	1	0.074

Table 4.12 Sellafield $^{134}Cs/^{137}Cs$ ratios decay corrected to 1988 (BNFL, 1985 to 1989)

The $^{134}Cs/^{137}Cs$ ratio at the surface of the sediment assuming a 1 year transit time and no mixing would be 0.074 and the Chernobyl $^{134}Cs/^{137}Cs$ ratio decay corrected to 1988 would be 0.28. The $^{134}Cs/^{137}Cs$ ratio has a value of 0.031 at the surface of core LL1 and increases to 0.04 at a depth of 1.14 g cm^{-2} (2.5 cm). Therefore, the $^{134}Cs/^{137}Cs$ ratio is lower than would be expected from the Sellafield discharge alone which suggests that the sediment system is mixed to some extent and that the $^{134}Cs/^{137}Cs$ of the surface sediment is reduced by mixing with older sediment with a lower ratio. However, mixing at the top of core LL1 does not seem to be reflected by the unsupported ^{210}Pb profiles. Unlike cores LE 1 and LE 3 from Loch Etive, core LL1 from Loch Long does not exhibit a significant Chernobyl input, however the radiocaesium associated with Chernobyl fallout was below detection limits in core LE 2 from Loch Etive which consisted of a coarser grain sediment. The element/Al profiles of core LL1 suggest a change to coarser grained material towards the surface and this may be the reason for the low concentration of Chernobyl radiocaesium in this core. The inventories of Sellafield radiocaesium for the Clyde Sea Area are much greater than those found in Loch Etive, and any Chernobyl input has probably been masked by the Sellafield radiocaesium. The inventory of ^{134}Cs for core LL1 was 460 ± 20 Bq m^{-2} which is far greater than the inventories found in Loch Etive. The $^{134}Cs/^{137}Cs$ ratio decreases to essentially zero at a depth of 5.7 g cm^{-2} (13 cm) which corresponds to the top of the dumped section and then increases to

values of 0.016 and 0.01 at depths of 6.74 and 7.32 g cm^{-2} (17, 19 cm) respectively, which are obviously too high, to correspond to Sellafield discharge ratios, after 26 years of decay. At 7.95 g cm^{-2} (21 cm) depth, ^{134}Cs again falls to the limit of detection, after which the $^{134}Cs/^{137}Cs$ ratio increases to 0.007 at 8.47 g cm^{-2} (23 cm) which is within the section considered to be an old surface. The ^{134}Cs detected below the dumped section may be due to ^{134}Cs from the dumped layer being redistributed at the time of dumping or to downward diffusion of radiocaesium. There are a number of possible arguments that can be used to explain these high $^{134}Cs/^{137}Cs$ ratios within the dumped section of material. Firstly, the results could be reflecting some analytical artefact, but this is thought to be unlikely as the $^{134}Cs/^{137}Cs$ values within the top of the sediment core range from 0.01 to 0.04 and compare favourably with values reported by Ben Shaban (1987) of 0.02 to 0.09 (after considering Chernobyl) for a core from Ardmore Bay, within the Clyde Sea Area. Another possibility is that the ^{210}Pb chronology is incorrect, which is feasible due to the complexity of the unsupported ^{210}Pb profile, and that the time of dumping occurred later than the ^{210}Pb chronology indicated. The sedimentation rate of 0.33 g cm^{-2} y^{-1} obtained from the ^{137}Cs maximum concentration can be applied to give an alternative chronology, and gives a date of 1968 for the sediment horizon at 6.74 g cm^{-2} (17 cm) containing the $^{134}Cs/^{137}Cs$ ratio of 0.16. This gives a decay time of 20 years and results in a $^{134}Cs/^{137}Cs$ ratio of 8.6 which is still abnormally high.

Having come to the conclusion that the section of core from 7.95 to 5.69 g cm^{-2} (13 to 21 cm) had been 'dumped', other possible indicators were examined in an attempt to substantiate the hypothesis. ^{60}Co was particularly effective in this context, and the ^{60}Co profile, shown in Figure 4.25., exhibits clearly enhanced values over the suggested "dumped" zone. Core LL1 was the only core in which detectable levels of ^{60}Co occurred. The ^{60}Co profile has a surface concentration of 38 Bq kg^{-1} which decreases rapidly with depth to 0.2 Bq kg^{-1} at 6.19 g cm^{-2} (15 cm). Below which, there is an increase in ^{60}Co concentrations to 20 Bq kg^{-1} within the 'dumped section'. ^{60}Co and ^{134}Cs are both activation products and the quantities of these nuclides present at depth in this core are too large, relative to the ^{137}Cs concentration to be

explained by Sellafield or ^{60}Co from weapons testing fallout inputs. The $^{134}Cs/^{137}Cs$ ratios within the dumped zone are high for a sediment of this age and if decay corrected to the time of deposition using the ^{210}Pb chronology give ratios in the order of 20 to 40. The most plausible alternative explanation for the presence of these activation products is that they originated from one of the two Naval bases which serviced nuclear submarines, namely Faslane and Holy Loch, of which only Faslane remains operational to this day. In this context, it may be significant that the dumped and rapidly accumulated layers of sediment correspond to the time of construction and early years of operation of these naval facilities. Therefore, the ^{134}Cs and ^{60}Co results suggest that the operation of the naval bases resulted in the dumping of sediment contaminated with ^{134}Cs and ^{60}Co. However, decay correction of the ^{134}Cs concentration of the ^{210}Pb chronology implies an initial concentration of the order of 10^4 Bq kg^{-1} of ^{134}Cs within the dumped section which is extremely high and limits the form of the discharge to solid phase. Comparison with the behaviour of the Sellafield discharged Cs and resultant concentration in areas such as the Ravenglass estuary suggests that an aqueous phase release of ^{134}Cs in the order of TBq would have been required to obtain such high concentrations in the Loch Long sediment. This suggests that the sediment was probably contaminated with some solid material containing high levels of ^{134}Cs. The water from the Clyde Sea Area has been monitored for radiocaesium since the 1970's and any aqueous discharge at such levels would have readily been detected.

The ^{241}Am concentration is 11 Bq kg^{-1} in the surface sediment below which it decreases to 9.8 Bq kg^{-1} at 0.65 g cm^{-2} (1.5 cm) and then increases to 10.4 Bq kg^{-1} at 1.14 g cm^{-2} (2.5 cm) and remains within error of this value to a depth of 1.93 g cm^{-2} (4.5 cm) after which it decreases to 2.2 Bq kg^{-1} at 7.3 g cm^{-2} (19 cm). The maximum discharges of ^{241}Pu from the Sellafield discharge which occurred in 1973 and 1978 would have reached the Clyde Sea Area one year later, i.e. 1974 and 1979 respectively. So the chronologies obtained from the unsupported ^{210}Pb profile (Table 4.11), indicate that the two maxima would have occurred at adjacent sections of the core namely at depths of 1.14 and 1.56 g cm^{-2} (2.5 and 3.5 cm) and this is reflected in the

essentially constant ^{241}Am concentration over this depth range. Therefore although the two distinct maxima of the Sellafield discharge could not be identified in this core (c.f. LE 1), the ^{241}Am profile is consistent with what would be expected taking into account the accumulation rate. The ratio of the cumulative environmental inventory of Sellafield ^{137}Cs to 1987 (31627 TBq) to that of ^{241}Am grown in from the decay of ^{241}Pu (322 TBq) was 98. If it is assumed that approximately 90% of the ^{137}Cs and 10% of the ^{241}Pu remain in solution and are transported out of the Irish Sea (Hunt, 1985; Pentreath et al., 1984; Livingston et al., 1982; Jefferies et al., 1973), then this would have generated a total environmental inventory with a ^{137}Cs/^{241}Am ratio of about 884 in areas out with the Irish Sea. Assuming that the ^{241}Am detected in the sediment is derived mainly from in-situ ^{241}Pu decay then the ^{137}Cs/^{241}Am ratio will be controlled primarily by the relative transfer of ^{137}Cs and ^{241}Pu from the water column to the sediment and equal transfer of ^{137}Cs and ^{241}Pu would therefore give an inventory ratio of approximately 880. The ratio of the inventories of ^{137}Cs and ^{241}Am for core LL1 has a value of 73 which is the same as the ^{137}Cs/^{241}Am inventory ratio found for cores LE 1 and LE 2 of 75 and 73 respectively which suggests that there is no differential removal of Cs and Pu during transit from the Clyde Sea Area to Loch Etive and that the removal mechanism from aqueous phase to the sediment is similar in Loch Long and Loch Etive. The ^{137}Cs/^{241}Am inventory ratio of 73 for core LL1 is far lower than the expected ratio of 880. Assuming that the uptake of ^{241}Pu is a factor of 10 greater then an integrated ^{137}Cs/^{241}Am ratio of approximately 88 would be expected which is close to the ratio of 73 found for this core. As discussed in previous sections (4.2.3.,4.3.3.) recent research has shown that there is up to 80% re-dissolution of ^{137}Cs from the sediments of the Irish Sea (Hunt and Kershaw, 1990; McCartney et al., 1992; Comans et al., 1989; Jones et al.:, 1988) and the ^{137}Cs/^{241}Am ratio for core LL1 could be interpreted as indicating the effects of re-dissolution of ^{137}Cs from the sediments of this core. Thus, the ^{137}Cs/^{241}Am ratios do not match the discharge and expected behaviour of Cs and Pu, however, comparison of Loch Etive and the Clyde Sea Area is comparable with similar behaviour. If re-dissolution was the major factor resulting in the observed values then some perturbation of the ^{137}Cs profiles would be expected which is not the case in either the Loch

Etive cores or in core LL1 from Loch Long. Therefore, it is not possible to obtain a definitive answer for the observed $^{137}Cs/^{241}Am$ ratios.

4.5.4 *^{228}Th and ^{228}Ra profiles of core LL1*

The $^{228}Th/^{228}Ra$ profile for core LL1 is shown in Figure 4.21. The ratio has a value of 1.19 in the surface sediment then increases to two maxima of 1.64 and 1.56 occurring at depths of 1.56 g cm^{-2} (3.5 cm) and 2.50 g cm^{-2} (5.5 cm) respectively, below which the ratio is mainly within error of unity to the bottom of the core. There are a few samples throughout the core that have $^{228}Th/^{228}Ra$ ratios slightly higher than unity. The inventories for ^{228}Th and ^{228}Ra are 10200 ± 450 Bq m^{-2} and 9300 ± 400 Bq m^{-2} which are essentially the same, suggesting secular equilibrium with ^{232}Th. The analysis of core LL1 for ^{232}Th concentrations has not been completed and will be reported in full elsewhere.

4.5.5 *Stable Pb and Pb isotope ratios of core LL1*

The total stable Pb concentration data are presented in Chapter 3 and the plot of the total Pb concentration versus cumulative weight (g cm^{-2}) is shown in Figure 4.22.A. The Pb concentration is 318 mg kg^{-1} at the surface and increases to a maximum value of 425 mg kg^{-1} at a depth of 6.74 g cm^{-2} (17 cm). The concentration then decreases to a value of 125 mg kg^{-1} at the bottom of the core (24.7 g cm^{-2}, 79 cm), with the exception of a single point at a depth of 11.8 g cm^{-2} (35 cm) has a higher concentration of 398 mg kg^{-1}. This point is also elevated in unsupported ^{210}Pb concentration (Figure 4.20) and may reflect some advective mixing at the time when this section of sediment was near the surface. The "dumped section" of sediment (5.69 to 7.95 g cm^{-2}) has concentrations of Pb, in excess of 400 mg kg^{-1}, which are high even for this highly polluted core. The concentration of Pb in this core is far greater than in any of the Loch Etive cores which had maximum Pb concentrations in the range 55 to 98 mg kg^{-1} and reflects the high degree of pollution in this system as a consequence of proximity to the industrial Clydeside area. The concentration of Pb at the bottom of the core (24.7gcm^{-2},

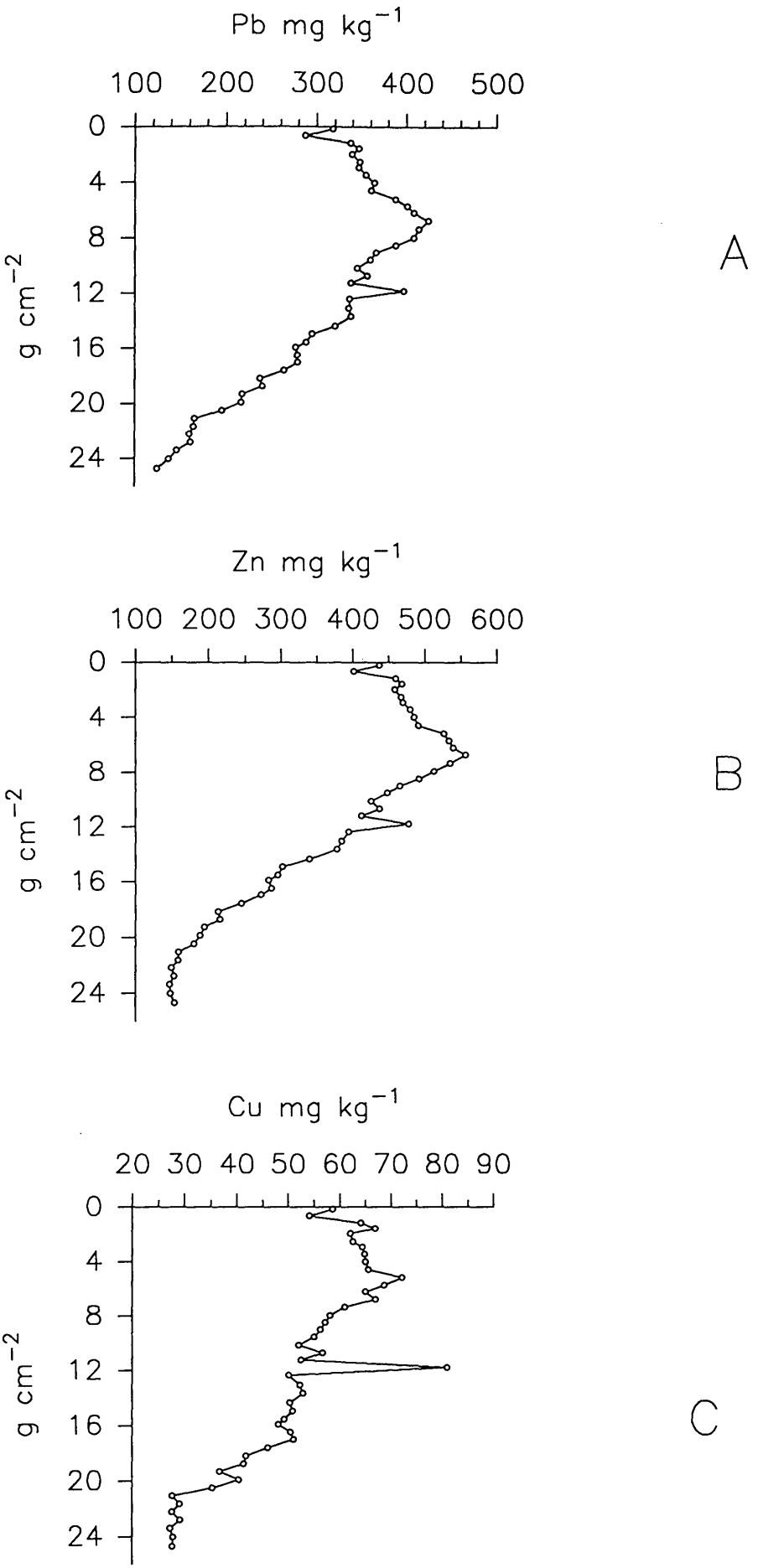

Figure 4.22. Loch Long core LL1 Pb, Zn and Cu concentrations (mg kg^{-1})

79 cm) is 125 mg kg^{-1} which indicates that pollutant Pb is still present at this depth. Smith-Briggs (1983) reported a maximum Pb concentration of 388 mg kg^{-1} at a depth of 4.8 g cm^{-2} (11-12 cm) from a Craib core, obtained from Loch Long (56° 2' 40"N; 4° 52' 30"W) in 1977, with a calculated sedimentation rate of 0.25 g cm^{-2}, which dates the maximum Pb concentration at 1960. This is in reasonable agreement with the date of the horizon of maximum Pb concentration found in core LL1 of 1963, giving support for the dating of this core. Smith-Briggs (1983) also reported a baseline concentration of Pb in Loch Long of 22 mg kg^{-1} which was obtained from the bottom section of a gravity core of length 121 cm. Thus, assuming a value of 22 mg kg^{-1} for the natural Pb concentration, the bottom of core LL1 is still indicating that there is 103 mg kg^{-1} of excess Pb in the sediment at a depth of 24.7 g cm^{-2} (79 cm) which corresponds to a date of 1848. The maximum Pb concentrations occur within the 'dumped section' of core LL1, and above this the Pb concentration decreases to 361 mg kg^{-1} at 4.6 g cm^{-2} (9.5 cm) which corresponds to 1966. The sharp rise in Pb concentration around 1900 that was observed in both LE 1 and LE 2 is not observed in LL1, reflecting the earlier onset and the greater magnitude of early pollutant Pb fluxes in this core due to the proximity of the sampling site to a major industrial area.

The flux of pollutant Pb versus time (on the basis of the ^{210}Pb chronology) for core LL1 is shown in Figure 4.23.A. The excess Pb flux results are given in Table 4.13. Excess Pb is observed in the sediment from the bottom of the core corresponding to 1848 (0.15 g m^{-2} y^{-1}) and the flux increases relatively uniformly to 0.52 g m^{-2} y^{-1} by 1962. Thereafter the flux increases dramatically, within the dumped section, to a maximum of 9.1 g m^{-2} y^{-1} in 1963. Enhanced deposition of this magnitude is highly unlikely to be due to atmospheric deposition at a time of declining industrial activity and improving air quality. The increase in the number and use of cars may have had some influence, but, comparison with fluxes obtained for Loch Lomond (0.19 g m^{-2} y^{-1}, 1964) and Flanders Moss (0.33 g m^{-2} y^{-1} for 1966-1990) (Sugden, 1993) does not support this, so there must be some source of pollutant Pb to this site other than atmospheric deposition. The radionuclide data discussed above indicate

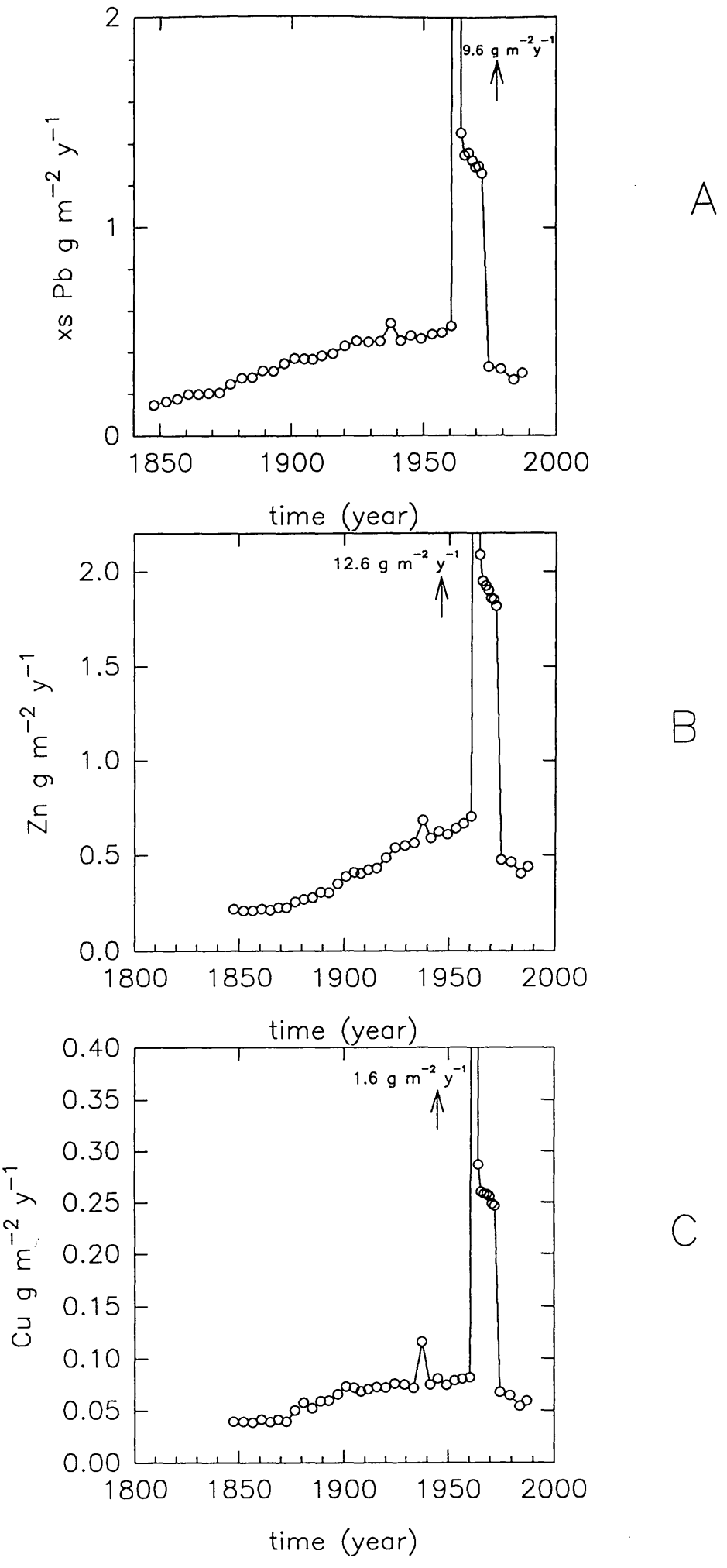

Figure 4.23. Loch Long core LL1 Pb, Zn and Cu flux data

that the most likely source is deposition of contaminated sediment from more polluted areas of the Clyde Sea Area, possibly representing the effects of dumping of highly contaminated dredged sediment at or near this location over a short period of time (assumed to be approximately 1 year). After the anomalously high input, the flux decreases to 1.45 g $m^{-2}y^{-1}$ at 5.16 g cm^{-2} (11 cm) corresponding to a date of 1964, and remains at a level greater than 1 g $m^{-2}y^{-1}$ until 1.93 g cm^{-2} (4.5 cm) corresponding to 1972. This increased flux occurs over the depth range 1.93 to 5.16 g cm^{-2} (4.5 to 11 cm) which corresponds to the section which has the higher sedimentation rate of 0.40 g $cm^{-2}y^{-1}$ derived from the unsupported ^{210}Pb profile and 0.33 g cm^{-2} y^{-1} calculated from the ^{137}Cs maximum concentration. This high sedimentation rate may indicate that deposition or redistribution of dumped sediment from dredging continued to affect this site over the time period (1964-1972). The excess Pb flux decreases to 0.33 g m^{-2} y^{-1} at a depth of 1.56 g cm^{-2} (3.5 cm), corresponding to 1975, and continues to decrease to a value of 0.3 g m^{-2} y^{-1} at the surface sediment.

The inventory of excess Pb in this core is 68.3 g m^{-2} which is far greater than those found in Loch Etive (1.6 to 3.8 g m^{-2}). A previous study of Loch Long reported an average pollutant Pb flux of 0.62 g m^{-2} y^{-1} (Smith-Briggs, 1983). It is apparent however from the present study that there have been large temporal variations in the Pb flux, which makes an average flux of limited use. It must also be remembered that the flux determined by Smith-Briggs was derived from a box core of only 29 cm length and this value may therefore be an over estimation of the average flux.

As detailed in section 1.4.2. the $^{206}Pb/^{207}Pb$ ratio can potentially be used to characterise the source of pollutant Pb (Sugden, 1993; Flegal et al., 1989; Maring et al., 1987; Sturges and Barrie, 1987; Delves, 1986; Elbaz-Poulichet et al, 1986; Petit et al., 1984). The plot of the $^{206}Pb/^{207}Pb$ ratio versus ^{210}Pb chronology for core LL1 is shown in Figure 4.24., along with the excess Pb flux (g $m^{-2}y^{-1}$). The surface sediment has a $^{206}Pb/^{207}Pb$ ratio of 1.155 which is higher than LE 1 (1.149) and essentially the same as LE 2 (1.157) and LE

SAMPLE	DEPTH (cm)	cum g cm^{-2}	date for mid section	excess Pb g m^{-2} y^{-1}
LL1 0-1	0.5	0.18	1987	0.30
LL1 1-2	1.5	0.65	1984	0.27
LL1 2-3	2.5	1.14	1979	0.32
LL1 3-4	3.5	1.56	1975	0.33
LL1 4-5	4.5	1.93	1972	1.26
LL1 5-6	5.5	2.50	1971	1.29
LL1 6-7	6.5	2.92	1970	1.29
LL1 7-8	7.5	3.43	1968	1.32
LL1 8-9	8.5	3.99	1967	1.36
LL1 9-10	9.5	4.56	1966	1.34
LL1 10-12	11	5.16	1964	1.45
LL1 12-14	13	5.69	1963	8.57
LL1 14-16	15	6.19	1963	8.74
LL1 16-18	17	6.74	1963	9.10
LL1 18-20	19	7.32	1963	8.87
LL1 20-22	21	7.95	1962	8.74
LL1 22-24	23	8.47	1960	0.52
LL1 24-26	25	8.99	1957	0.49
LL1 26-28	27	9.53	1953	0.48
LL1 28-30	29	10.13	1949	0.46
LL1 30-32	31	10.69	1945	0.48
LL1 32-34	33	11.19	1941	0.45
LL1 34-36	35	11.78	1938	0.54
LL1 36-38	37	12.34	1934	0.45
LL1 38-40	39	13.04	1929	0.45
LL1 40-42	41	13.65	1924	0.45
LL1 42-44	43	14.34	1920	0.43
LL1 44-46	45	14.91	1916	0.39
LL1 46-48	47	15.52	1912	0.38
LL1 48-50	49	15.88	1908	0.36
LL1 50-52	51	16.44	1905	0.37
LL1 52-54	53	16.95	1901	0.37
LL1 54-56	55	17.56	1897	0.35
LL1 56-58	57	18.14	1893	0.31

SAMPLE	DEPTH (cm)	cum g cm^{-2}	date for mid section	excess Pb g m^{-2} y^{-1}
LL1 58-60	59	18.72	1889	0.31
LL1 60-62	61	19.26	1885	0.28
LL1 62-64	63	19.86	1881	0.28
LL1 64-66	65	20.44	1877	0.25
LL1 66-68	67	21.03	1873	0.21
LL1 68-70	69	21.63	1869	0.20
LL1 70-72	71	22.16	1865	0.20
LL1 72-74	73	22.76	1861	0.20
LL1 74-76	75	23.38	1857	0.18
LL1 76-78	77	24.01	1852	0.17
LL1 78-80	79	24.70	1848	0.15

Table 4.13 Loch Long core LL1 Pb flux data

3 (1.152) after which the ratio remains constant within error to a depth of 5.69 g cm^{-2} (13 cm). The ratio then increases to a value of 1.162 and remains high, until returning to a value of 1.151 at a depth of 7.95 g cm^{-2}. Below this depth the $^{206}Pb/^{207}Pb$ ratio increases uniformly to a value of 1.170 at 14.9 g cm^{-2} (45 cm), after which it is within error constant to the bottom of the core at 24.7 g cm^{-2} (79 cm). The $^{206}Pb/^{207}Pb$ temporal trend for core LL1 is similar to those of Loch Etive and also to the trends reported by Sugden (1993) for Loch Lomond and Flanders Moss and is consistent with a trend reflecting the change from heavy industry to petrol pollution, which gives a reasonable degree of confidence in the ^{210}Pb chronology for this core. However a deviation from the trend occurs over the zone of "dumped" sediment containing very high Pb concentrations and the $^{206}Pb/^{207}Pb$ signature reflects a greater heavy industry component (corresponding to 1940's to 1950's for this core) consistent with the suggestion that the "dumped" material consists of dredged near surface sediment. Therefore the Pb isotope ratio profile is consistent with other observations and lends strong support to a) the chronology and b) the hypothesis of the existence of a dumped zone from 5.7 to 7.95 g cm^{-2} (13 to 21 cm). As discussed in section 4.2.5. the

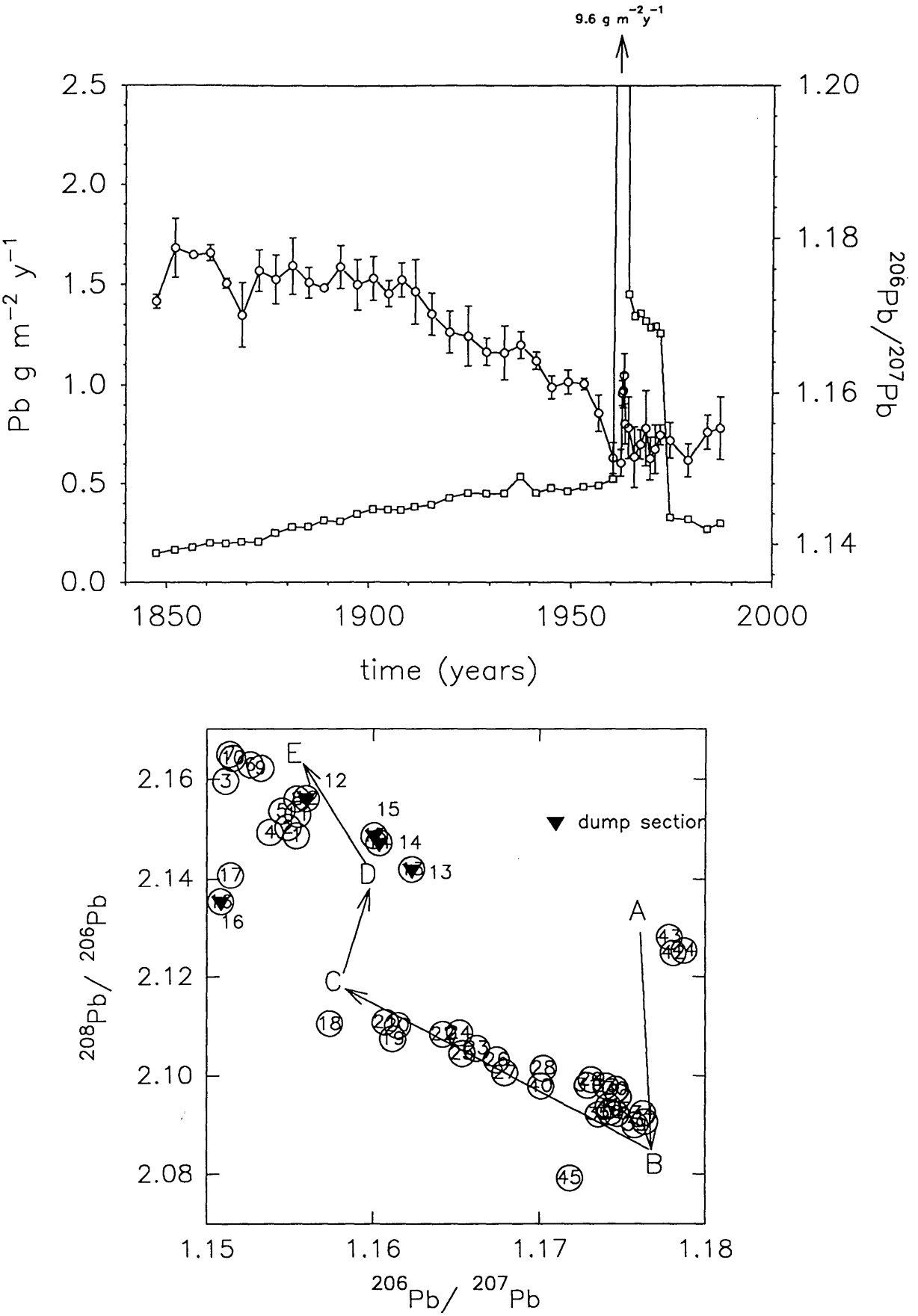

Figure 4.24. Loch Long core LL1 Pb flux and Pb isotope ratio plots

SAMPLE	DEPTH (cm)	cum. g cm^{-2}	date for mid section	% Pb petrol
LL1 0-1	0.5	0.18	1987	22
LL1 1-2	1.5	0.65	1984	23
LL1 2-3	2.5	1.14	1979	27
LL1 3-4	3.5	1.56	1975	24
LL1 4-5	4.5	1.93	1972	23
LL1 5-6	5.5	2.50	1971	26
LL1 6-7	6.5	2.92	1970	27
LL1 7-8	7.5	3.43	1968	22
LL1 8-9	8.5	3.99	1967	25
LL1 9-10	9.5	4.56	1966	27
LL1 10-12	11	5.16	1964	22
LL1 12-14	13	5.69	1963	21
LL1 14-16	15	6.19	1963	13
LL1 16-18	17	6.74	1963	15
LL1 18-20	19	7.32	1963	16
LL1 20-22	21	7.95	1962	28
LL1 22-24	23	8.47	1960	27
LL1 24-26	25	8.99	1957	19
LL1 26-28	27	9.53	1953	14
LL1 28-30	29	10.13	1949	14
LL1 30-32	31	10.69	1945	15
LL1 32-34	33	11.19	1941	10
LL1 34-36	35	11.78	1938	8
LL1 36-38	37	12.34	1934	9
LL1 38-40	39	13.04	1929	9
LL1 40-42	41	13.65	1924	6
LL1 42-44	43	14.34	1920	6
LL1 44-46	45	14.91	1916	3
LL1 46-48	47	15.52	1912	
LL1 48-50	49	15.88	1908	
LL1 50-52	51	16.44	1905	
LL1 52-54	53	16.95	1901	
LL1 54-56	55	17.56	1897	
LL1 56-58	57	18.14	1893	
LL1 58-60	59	18.72	1889	
LL1 60-62	61	19.26	1885	
LL1 62-64	63	19.86	1881	
LL1 64-66	65	20.44	1877	
LL1 66-68	67	21.03	1873	
LL1 68-70	69	21.63	1869	
LL1 70-72	71	22.16	1865	
LL1 72-74	73	22.76	1861	
LL1 74-76	75	23.38	1857	
LL1 76-78	77	24.01	1852	
LL1 78-80	79	24.70	1848	

Table 4.14 % Pb in sediment from Pb in petrol for core LL1

decreasing $^{206}Pb/^{207}Pb$ ratio towards the surface sediment can be attributed to the increasing influence of vehicle exhaust emissions on pollutant Pb fluxes to the sediment during this century. The onset of the change in ratio at 14.9 g cm^{-2} (45 cm) corresponds to a date of 1916 which is earlier than was observed for this change in the cores from Loch Etive and earlier than would be expected due to the onset of the use of alkyl leads in petrol as an anti-knock agent which was introduced in the mid-1920's. Therefore, the $^{206}Pb/^{207}Pb$ ratio profile would suggest that there has been some perturbation of the Pb isotope ratio profile resulting in the indication of the use of Pb in petrol approximately 10-15 years too early. However, considering the complexity of this core the date of 1916 is reasonable and again confirms that the chronology that has been applied to this core is realistic.

The calculation of the percentage Pb due to petrol was carried out as described in 4.2.5. with R_i= 1.175 and R_{Hi}= 1.172 and the results of this calculation are given in Table 4.14. The results from the calculation of percentage Pb in the sediment due to petrol indicate that the onset of deposition of Pb from petrol occurs at 1916 which is approximately 10 years earlier than expected, and is also earlier than the dates obtained for Loch Etive cores of LE 1= 1942; LE 2= 1928 and LE 3= 1935. The percentage of Pb from petrol is 3% in 1916 increasing to 27 % in the late 1970's to early 1980's and then beginning to decrease from 1984 to give a value of 22 % at the surface sediment. It is interesting to note that the % of Pb from petrol occurring at 7.95 g cm^{-2} (21 cm) was 28 % but the petrol Pb contribution decreased to 13 % within the 'dumped section' of sediment and then increased again to 21% at the top of the "dumped" zone. This is further evidence that this sediment is near surface material which has been dredged and dumped at or near this site. It is also of interest to note that a major change in the $^{208}Pb/^{206}Pb$ profile occurs at 8.47 g cm^{-2} (23 cm) (Table 3.26) indicating that there has been an increase in the ^{208}Pb concentration of the sediment from this depth to the surface.

The $^{208}Pb/^{206}Pb$ versus $^{206}Pb/^{207}Pb$ plot for core LL1 is shown in Figure 4.24. The samples are numbered 1 to 45 according to increasing depth. The

samples from the 'dumped section' namely, 12 to 16 are indicated on the diagram. The diagram indicates a five component system The tie line A→B represents a move from a geological Pb isotope signature to a heavy industry Pb signature, while the tie line B→C indicates the increasing influence of Pb from petrol relative to heavy industry. The tie line C→D illustrates the sudden addition of a new material i.e. Pb from a different source, and finally D→E represents the continued influence of Pb from petrol. The increase in the $^{208}Pb/^{206}Pb$ ratio which occurs at a depth of 8.47 g cm^{-2} (23 cm, identified by number 17) corresponds to 1960 and indicates that a change in the input of pollutant Pb occurred at this time. This effect is not observed in any of the Loch Etive cores and must therefore be considered to be a local effect to Loch Long.

4.5.6 *Zn and Cu profiles of core LL1*

The Zn and Cu concentration profiles for core LL1 are shown in Figures 4.22.B and 4.22.C. respectively and in both cases, the trends in the profiles are very similar to those of the Pb profile. The Zn concentration has a surface value of 436 mg kg^{-1} which is greater than that for the sediment cores from Loch Etive (164 to 239 mg kg^{-1}). A previous study reported Zn concentrations of 516 and 614 mg kg^{-1} in surface samples from sediment cores taken from Loch Long in 1977 and 1980 respectively (Smith-Briggs, 1983). The Zn concentration in core LL1 increases to a maximum of 556 mg kg^{-1} at a depth of 6.74 g cm^{-2} (17 cm) which is within the "dumped" zone, illustrating that Zn concentrations are also particularly enhanced in the "dumped" material. The Zn concentration then decreases systematically to 159 mg kg^{-1} at 21.03 g cm^{-2} (67 cm) which corresponds to a date of 1873 and then remains effectively constant to the bottom of the core. The mean concentration of Zn in the sediment of depth range 21.03 to 24.7 g cm^{-2} (67 to 79 cm) is 152 mg kg^{-1} which is lower than that obtained by Smith-Briggs (1983) (Zn=199 mg kg^{-1}) for sediment at 121 cm from a gravity core (56° 2' 30"N, 4° 52' W) from Loch Long in 1977.

The Cu concentration has a surface value of 59 mg kg^{-1} (c.f. Loch Etive

surface sediment Cu concentrations of 9-15 mg kg^{-1}) then increases to 72 mg kg^{-1} at a depth of 5.16 mg cm^{-2} (11 cm), corresponding to a date of 1964, which is one year later than the maximum concentrations of Pb and Zn. Smith-Briggs (1983) reported surface concentrations of 74 and 128 mg kg^{-1} for Cu concentrations in cores obtained from Loch Long in 1977 (Box core; 56° 2' 40"N 4° 52'48"W) and 1980 (Craib core 56° 2'40"N 4° 52' 30"W) with a concentration of 36 mg kg^{-1} at a depth of 121 cm (which was considered to be representative of unpolluted sediment Cu concentrations). The Cu concentration decreases to 28 mg kg^{-1} at a depth of 21.03 g cm^{-2} (67 cm), which corresponds to a date of 1873, and then remains constant to the bottom of the core. The Pb and Zn profiles indicate that there were pollutant levels of Pb and Zn present to the bottom of the core and this implies that the concentration of Cu at depth (28 mg kg^{-1}) still reflects the influence of very early pollution.

The Zn and Cu inventories in core LL1 of 87.3 and 12.6 g m^{-2} respectively are far greater than those found in the sediments of Loch Etive which were 18.7 to 21.1 g m^{-2} and 1.2 to 1.4 g m^{-2} of Zn and Cu respectively. It was more difficult to calculate excess inventories for both Zn and Cu as the base line values reported by Smith-Briggs for Zn and Cu were higher than the concentrations in the bottom sample of LL1, which was still considered to be polluted. Natural concentrations of 100 mg kg^{-1} and 20 mg kg^{-1} for Zn and Cu were assumed for the sediments from Loch Long which were similar to Loch Etive and Loch Duich (c.f. Table 4.4). Therefore the excess inventories are open to error as the natural levels may have been under or over estimated. The excess inventories of Zn and Cu in core LL1 were 62.6 and 7.6 g m^{-2}, considerably higher than those from Loch Etive which were in the range 3.4 to 8.1 g m^{-2} for Zn and 0.4 to 0.6 g m^{-2} for Cu.

The fluxes of excess Pb and total Zn and Cu are given in Table 4.15. and are illustrated in Figure 4.23.

SAMPLE	DEPTH	g cm^{-2}	date for mid section	Cu g m^{-2} y^{-1}	Zn g m^{-2} y^{-1}
LL1 0-1	0.5	0.18	1987	0.06	0.44
LL1 1-2	1.5	0.65	1984	0.05	0.41
LL1 2-3	2.5	1.14	1979	0.06	0.46
LL1 3-4	3.5	1.56	1975	0.07	0.47
LL1 4-5	4.5	1.93	1972	0.25	1.82
LL1 5-6	5.5	2.50	1971	0.25	1.86
LL1 6-7	6.5	2.92	1970	0.26	1.86
LL1 7-8	7.5	3.43	1968	0.26	1.90
LL1 8-9	8.5	3.99	1967	0.26	1.93
LL1 9-10	9.5	4.56	1966	0.26	1.95
LL1 10-12	11	5.16	1964	0.29	2.09
LL1 12-14	13	5.69	1963	1.55	12.05
LL1 14-16	15	6.19	1963	1.47	12.19
LL1 16-18	17	6.74	1963	1.51	12.57
LL1 18-20	19	7.32	1963	1.38	12.09
LL1 20-22	21	7.95	1962	1.32	11.58
LL1 22-24	23	8.47	1960	0.08	0.70
LL1 24-26	25	8.99	1957	0.08	0.67
LL1 26-28	27	9.53	1953	0.08	0.64
LL1 28-30	29	10.13	1949	0.07	0.61
LL1 30-32	31	10.69	1945	0.08	0.62
LL1 32-34	33	11.19	1941	0.08	0.59
LL1 34-36	35	11.78	1938	0.12	0.68
LL1 36-38	37	12.34	1934	0.07	0.56
LL1 38-40	39	13.04	1929	0.07	0.55
LL1 40-42	41	13.65	1924	0.08	0.54
LL1 42-44	43	14.34	1920	0.07	0.49
LL1 44-46	45	14.91	1916	0.07	0.43
LL1 46-48	47	15.52	1912	0.07	0.42
LL1 48-50	49	15.88	1908	0.07	0.40
LL1 50-52	51	16.44	1905	0.07	0.41
LL1 52-54	53	16.95	1901	0.07	0.39
LL1 54-56	55	17.56	1897	0.07	0.35
LL1 56-58	57	18.14	1893	0.06	0.30
LL1 58-60	59	18.72	1889	0.06	0.31

SAMPLE	DEPTH	g cm^{-2}	date for mid section	Cu g m^{-2} y^{-1}	Zn g m^{-2} y^{-1}
LL1 60-62	61	19.26	1885	0.05	0.28
LL1 62-64	63	19.86	1881	0.06	0.27
LL1 64-66	65	20.44	1877	0.05	0.26
LL1 66-68	67	21.03	1873	0.04	0.23
LL1 68-70	69	21.63	1869	0.04	0.23
LL1 70-72	71	22.16	1865	0.04	0.21
LL1 72-74	73	22.76	1861	0.04	0.22
LL1 74-76	75	23.38	1857	0.04	0.21
LL1 76-78	77	24.01	1852	0.04	0.21
LL1 78-80	79	24.70	1848	0.04	0.22

Table 4.15 Cu and Zn fluxes for Loch Long core LL1

The temporal trends of the Zn and Cu fluxes are very similar to the Pb flux profile and all three are dominated by the apparent large fluxes occurring around the early 1960's which are considered to be due to the dumping of a highly contaminated dredged surface material which was thought to have settled in a time span of approximately 1 year.

The Zn flux has a value of 0.22 g $m^{-2}y^{-1}$ in 1848 and remains at this value to 1873. The flux then increases to a value of 0.7 g $m^{-2}y^{-1}$ in 1960 after which it increasesto a maximum of 12.57 g $m^{-2}y^{-1}$ in 1963. The flux rapidly decreases to 2.09 g $m^{-2}y^{-1}$ in 1964 but remains at a value greater than 1g $m^{-2}y^{-1}$ until 1975 when it decreases to 0.47 g $m^{-2}y^{-1}$. The flux of Zn to the surface sediment is 0.44 g $m^{-2}y^{-1}$.

The Cu flux profile follows similar trends to those of Pb and Zn, with a value of 0.04 g $m^{-2}y^{-1}$ in 1848 increasing to a maximum of 1.55 g $m^{-2}y^{-1}$ in 1963 and finally a surface flux of 0.06 g $m^{-2}y^{-1}$. The fluxes of Zn and Cu to the sediments of Loch Long can be compared to average Zn and Cu fluxes respectively of 0.5 and 0.09 g $m^{-2}y^{-1}$ reported by Smith-Briggs (1983). The average fluxes of Zn and Cu to core LL1 are 0.58 and 0.08 g $m^{-2}y^{-1}$ respectively which compare very well with those obtained for the sediment

core from 1977.

4.5.7 *Summary of core LL1*

In summary, the unsupported ^{210}Pb profile for core LL1 indicates that the sedimentation rate has been variable with time and that ^{210}Pb dating can be used with care, to give a chronology for this core. However as this core is highly perturbed any chronology applied must be used with care. This chronology is broadly supported by the $^{206}Pb/^{207}Pb$ ratio profile and the position of the maximum in the ^{137}Cs profile which agree with the ^{210}Pb chronology to within 6-10 years. The $^{206}Pb/^{207}Pb$ ratio profile suggests that mixing has affected core LL1. The unsupported ^{210}Pb, heavy metal, Pb isotope, $^{134}Cs/^{137}Cs$ ratio, and ^{60}Co profiles all suggest that the section of the core from 7.95 g cm^{-2} to 5.69 g cm^{-2} consists of dredged sediment which was dumped at or near this location during the early 1960's.

The manmade radionuclides present in the sediment are dominated by the Sellafield discharge and any input from Chernobyl fallout cannot be identified in this core. The inventories of manmade radionuclides at the time of collection were 39000 ± 1500 Bq m^{-2} of ^{137} Cs, 460 ± 20 Bq m^{-2} of ^{134}Cs and 531 ± 35 Bq m^{-2} of ^{241}Am. The ^{137}Cs profiles indicated mobility of Cs by diffusion and ^{137}Cs is detectable to far greater depths than would be expected which limits its use in chrono-stratigraphy.

The deposition of pollutant Pb is far greater at this site than in Loch Etive, reflecting the highly polluted condition of this sediment. The effect of pollutant Pb can be detected to the bottom of the core which corresponds to a date of 1848. The effect of pollutant Pb from petrol can be detected in 1916 which is earlier than expected and indicates that some mixing has taken place in this core. The inventory of pollutant Pb for this core was 68.3 g m^{-2} which is at least a factor of 20 times higher than the pollutant Pb inventories found in Loch Etive. The total Zn and Cu inventories were 87.3 g cm^{-2} and 12.6 g cm^{-2} respectively and the excess Zn and Cu inventories were 62.6 and 7.6 g m^{-2} which are approximately 8 times and 10 times that of Loch Etive.

Therefore core LL1 from Loch Long reflects the anthropogenic influence on the sediments of the Clyde sea Area (physical and pollutant) and indicates the problems of interpreting sediment core data from this type of situation. From the results it would appear that a realistic chronology can be obtained from ^{210}Pb, however other indicators of chronology, such as Pb isotope ratios and profiles from the Sellafield discharge were required to confirm this chronology.

4.6 *Loch Goil core GD2*

The sample site, sampling methods and preparation of core GD2 are described in Chapter 2 which also includes detailed descriptions of the analytical techniques used. The results for this core are tabulated in Chapter 3. Due to a lack of material for the surface sample no XRF trace element analysis was carried out on the 0-1 cm sample and to simplify the discussion the 1-2 cm sample will be treated as the surface sample.

4.6.1 *Geochemical characteristics of core GD2*

Selected element/Al ratios and K/Rb ratios for core GD2 are shown in Figure 4.26. The Si/Al ratio decreases from a surface value of 2.17 to 2.04 at a depth of 1.53 g cm^{-2} (5.5 cm). The ratio then fluctuates within the range 2.01 to 2.10 to a depth of 9.12 g cm^{-2} (33 cm) after which there is a decrease in value to 1.98 at 9.69 g cm (35 cm) depth. Thereafter the ratio decreases uniformly to a value of 1.92 at the bottom of the core (18.74 g cm^{-2}, 71.5 cm). The Si/Al ratio decreases with depth, suggesting that there has been an overall change from finer to coarser grain size towards the surface of the core with several thin coarse grain units in the upper 9.69 g cm^{-2} (35 cm) of the core. The Zr/Al ratio decreases from a surface value of $17.91x10^{-4}$ to $16.37x10^{-4}$ at 1.53 g cm^{-2} (5.5 cm) after which it decreases to a minimum value of $15.54x10^{-4}$ at a depth of 11.29 g cm^{-2} (41 cm) depth. The Zr/Al ratio then increases with depth to a value of $16.53x10^{-4}$ at 18.74 g cm^{-2} (71.5 cm). The Zr/Al ratio profile again suggests a change to coarser grain size towards the surface of the core with the trend above 9.69 g cm^{-2} (35 cm) being similar

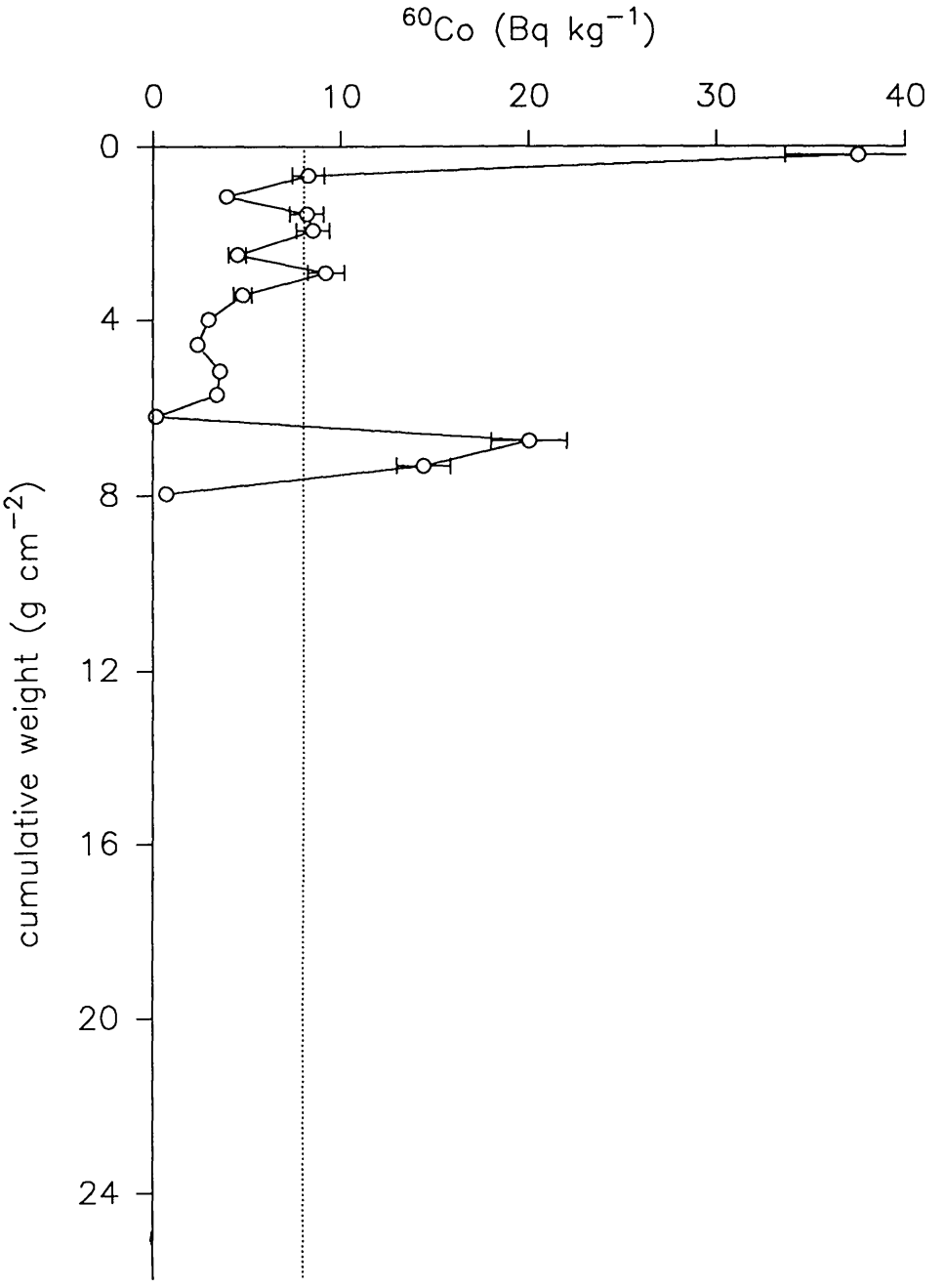

Figure 4.25. Loch Long core LL1 ^{60}Co concentrations (Bq kg^{-1})

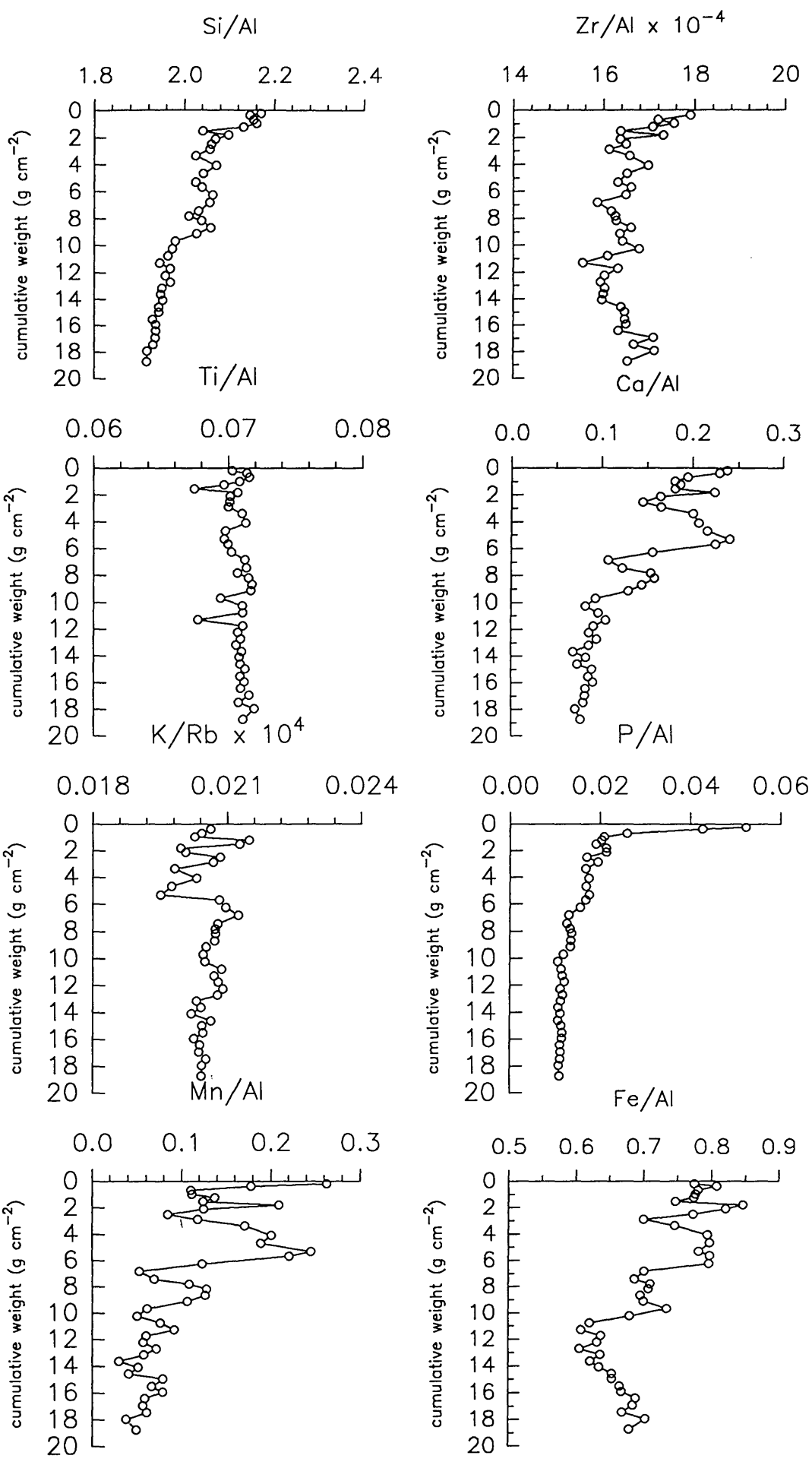

Figure 4.26. Loch Goil core GD2 element/Al and K/Rb ratios.

to that of Si/Al. The Ti/Al ratio has a surface value of 0.070, decreases to 0.068 at a depth of 1.53 g cm^{-2} (5.5 cm), and then remains relatively constant with depth with minima occurring at 5.31 (17 cm), 9.69 (35 cm) and 11.29 g cm^{-2} (41 cm). The Ca/Al ratio decreases irregularly from a surface value of 0.24 to 0.1 at the base of the core with maxima, possibly indicating the presence of shell bands or diagenetic carbonate, at the surface, 2 g cm^{-2}, 5 g cm^{-2} and 8 g cm^{-2} and a pronounced decrease in concentrations below approximately 10 g cm^{-2}(c.f. Si/Al profile). The K/Rb ratio decreases irregularly from a value of 206 at the surface to a minimum of 195 at 5.31 g cm^{-2} (17 cm), below which it increases sharply to 208 at 5.68 g cm^{-2} (19 cm) indicating a change in the type of sediment at this depth. Therefore the above element/Al and K/Rb ratios indicate that there has been a change in sediment type with depth, and that the more recently accumulated sediment has a coarser grain size.

The Mn/Al profile has a complex structure, exhibiting a general, but irregular decrease with depth, with pronounced maxima at the surface, 2 g cm^{-2}, 5 g cm^{-2} and 8 g cm^{-2} and lower concentrations below approximately 10 g cm^{-2}. The Mn/Al ratio follows the Ca/Al ratio trends remarkably closely, and in fact linear regression analysis of the two ratios gives a correlation coefficient (r) of 0.94 indicating that there is extremely good agreement between the two profiles and suggesting that solid phase $MnCO_3$ is being formed at depth. The Fe/Al ratio has a surface value of 0.78, increases to 0.81 at 0.36 g cm^{-2} (1.5 cm) and then remains constant to a depth of 1.53 g cm^{-2} (5.5 cm). The Fe/Al ratio profile follows a similar trend to the Ca/Al and Mn/Al ratio plots although agreement is not as good as that of the Ca/Al and Mn/Al profiles and this is reflected in the correlation coefficients which are 0.84 for the Ca/Al to Fe/Al plot and 0.75 for the Mn/Al to Fe/Al plot. However the similarity of the Fe/Al ratio profile to both the Ca/Al and Mn/Al profiles suggests that it is also involved in the formation of a solid phase material at depth. The P/Al ratio decreases rapidly from a surface value of 0.052 to 0.019 at a depth of 1.53 g cm^{-2} (5.5 cm), indicating the zone of degradation of organic matter within the surface sediment of core GD2. The ratio then decreases to a value of 0.012 at a depth of 9.69 g cm^{-2} (35 cm), after which it remains

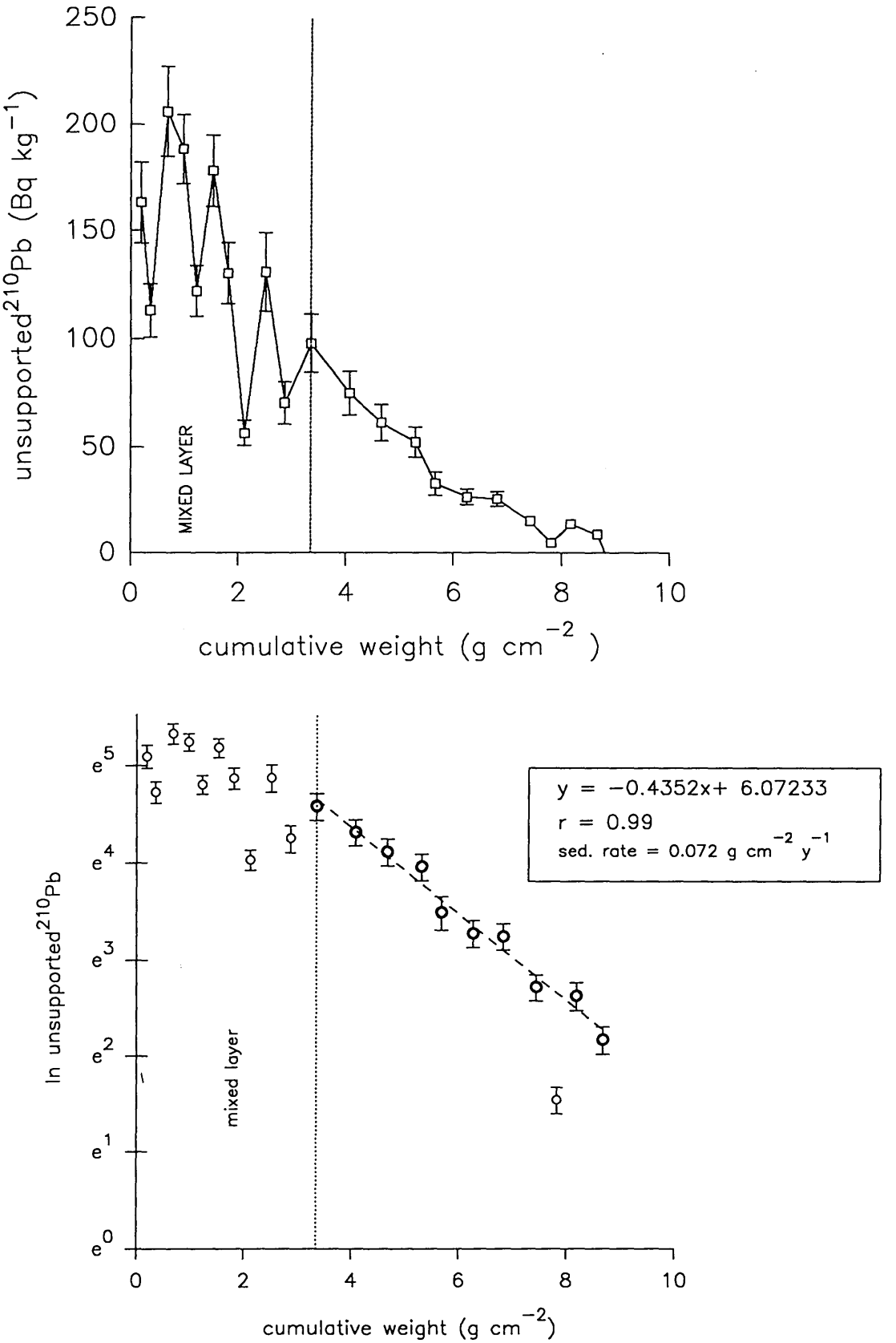

Figure 4.27. Loch Goil core GD2 unsupported ^{210}Pb concentrations

constant to the bottom of the core. Therefore the Mn/Al, Fe/Al and P/Al indicate that there is degradation of organic matter and redox recycling of Mn taking place within the surface sediments of core GD2. However, the Mn/Al, Fe/Al and Ca/Al profiles suggest that Mn is forming a solid phase material at depth, other than Mn oxyhydroxide which is probably $MnCO_3$ and that Fe is also be involved in this process. Calvert and Price (1970) found that both Mn oxyhydroxides and Mn carbonate were present in the sediments of Loch Fyne and this is probably the case for core GD2.

4.6.2 *^{210}Pb and ^{226}Ra profiles of core GD2*

The plots of unsupported ^{210}Pb and ln unsupported ^{210}Pb against depth in g cm^{-2} are shown in Figure 4.27. The ^{226}Ra results are tabulated in Chapter 3 (Table 3.29.). ^{226}Ra has a surface concentration of 118.2 Bq kg^{-1} and increases to 137.8 Bq kg^{-1} at a depth of 0.36 g cm^{-2} (1.5 cm), below which it decreases rapidly to 80.5 Bq kg^{-1} at 0.68 g cm^{-2} (2.5 cm). Thereafter the ^{226}Ra concentration decreases relatively uniformly to 53.2 Bq kg^{-1} at 3.36 g cm^{-2} (11 cm) depth and then remains within the concentration range 45.2 to 53.3 Bq kg^{-1} to the bottom of the core. High ^{226}Ra concentration of the surface sediment, was also observed in previous studies of Loch Goil (MacKenzie, 1977; Swan, 1978) and is probably due to the scavenging of radium from the pore waters and overlying waters by Mn oxyhydroxides (Ku and Broecker, 1969; Moore et al., 1980, 1981; Deal et al, 1981; Huh and Ku, 1984; Kadko et al., 1987; Todd et al., 1988). The association of ^{226}Ra with Fe-Mn oxyhydroxides has been well documented (Moore et al.,1981; Huh and Ku, 1984). The ^{226}Ra inventory for the core is 10300 $\pm$ 500 Bq m^{-2} which is higher than that of 7000 Bq m^{-2} for core LL1 from Loch Long and considerably higher than any of the cores from Loch Etive which were within the range 3900 to 5700 Bq m^{-2}.

The unsupported ^{210}Pb concentration varies irregularly in the range 157.6 Bq kg^{-1} to 94.6 Bq kg^{-1} from the surface to a depth of 3.36 g cm^{-2} (11 cm), below which there is a systematic decrease with depth to a value of 4.5 Bq kg^{-1} at 7.81 g cm^{-2} (27 cm). The unsupported ^{210}Pb profile for the section above 3.36

g cm^{-2} (11 cm) appears to be affected both by mixing and diagenetic influences on ^{226}Ra, making this part of the profile difficult to interpret. For practical purposes, the section of the core above 3.36 g cm^{-2} (11 cm) was treated as a mixed layer and an accumulation rate of 0.072 g cm^{-2} y^{-1} (r = 0.99) was obtained by plotting the natural log of the unsupported ^{210}Pb concentration against depth in g cm^{-2} and linear regression fitting of a straight line to the data for samples below the mixed layer. The inventory of unsupported ^{210}Pb was 6700 ± 800 Bq kg^{-1} implying a steady state flux of 208 ± 25 Bq m^{-2} y^{-1} which is within error the same as core LL1 and core LE 3 from Loch Etive, lower than core LE 1 and higher than core LE 2. The flux is once again higher than would be expected if the atmospheric flux is approximately 150 Bq m^{-2} y^{-1} and there is a maximum flux of 4.9 Bq m^{-2} y^{-1} from in-situ production in the water column (depth = 79 m and ^{226}Ra = 0.002 Bq l^{-1}). This suggests either a far greater atmospheric flux than expected or another source of unsupported ^{210}Pb to the sediment which could be due to solution input, particulate input or sediment focusing. Smith-Briggs (1983) and Swan (1978) reported ^{210}Pb fluxes of 423 Bq m^{-2} y^{-1} and 417 Bq m^{-2} y^{-1} respectively, for Loch Goil which are considerably higher than the value of 208 Bq m^{-2} y^{-1} for core GD2. However the cores studied by Swan and Smith-Briggs were obtained from the deepest part of the loch and this may have a bearing on the ^{210}Pb fluxes obtained.

On the basis of the calculated sedimentation rate it is possible to date some of the horizons seen in the element/Al ratio profiles (Figure 4.26) as follows. The change in the Si/Al ratio at 9.69 g cm^{-2} corresponds to 1857 which after considering the effects of mixing to a depth of 3.36 g cm^{-2} (equivalent to 47 years) becomes 1904. The other change in the Si/Al ratio occurs at 1.53 g cm^{-2} (within the mixed zone) which corresponds to a date of 1969. The change in K/Rb occurs at 5.31 g cm^{-2} corresponding to 1919, which after considering mixing, becomes 1963. The bottom of the mixed layer at a depth of 3.36 g cm^{-2} (11 cm) occurs at 1941 giving a mixed layer depth corresponding to an accumulation time of approximately 47 years.

4.6.3 ^{137}Cs, ^{134}Cs and ^{241}Am profiles of core GD2

As with the previous cores the ^{137}Cs profile for core GD2 can be taken dominantly to reflect trends in the Sellafield discharge and the $^{134}Cs/^{137}Cs$ ratio data can be used to distinguish between Sellafield and Chernobyl inputs.

The concentration profiles for ^{137}Cs and ^{241}Am and the activity ratio profile for $^{134}Cs/^{137}Cs$ are shown in Figure 4.28. The ^{137}Cs concentration has a value of 666.6 Bq kg^{-1} at the surface, a subsurface maximum of 920.3 Bq kg^{-1} at 1.23 g cm^{-2} (4.5 cm) and then decreases to 79.2 Bq kg^{-1} at 4.08 g cm^{-2} (13 cm) after which it increases to 118.6 Bq kg^{-1} at 5.31 g cm^{-2} (17 cm). Thereafter the ^{137}Cs concentration decreases to 1.7 Bq kg^{-1} at a depth of 14.07 g cm^{-2} (53 cm) and remains at a concentration less than 1 Bq kg^{-1} to the bottom of the core at 18.74 g cm^{-2} (71.5 cm) depth. The maximum ^{137}Cs concentration occurs within the mixed zone and the ^{137}Cs concentrations for depths 0.68 to 1.53 g cm^{-2} are in fact all within error the same. By taking the mid-point depth of 1.10 g cm^{-2} and assuming that the maximum discharge of ^{137}Cs from Sellafield reached Loch Goil in 1976, a sedimentation rate of 0.092 g cm^{-2} y^{-1} is obtained for core GD2 which is in reasonably good agreement with the ^{210}Pb sedimentation rate of 0.072 g cm^{-2} y^{-1}. The sedimentation rate for GD2 estimated from the depth of penetration of ^{137}Cs is 0.402 g $cm^{-2}y^{-1}$, which becomes 0.306 g $cm^{-2}y^{-1}$ after mixing has been taken into account and is thus far higher than either of the above estimates of sedimentation rate, indicating that there has probably been downwards diffusion of ^{137}Cs in this core. Using the ^{210}Pb sedimentation rate of 0.072 g cm^{-2} y^{-1} and assuming that the first ^{137}Cs would have appeared in the sediments 35 years ago, then the ^{137}Cs depth of penetration would be 2.52 g cm^{-2} which after considering the depth of mixing of 3.36 g cm^{-2} would be 5.88 g cm^{-2}. The depth of penetration of ^{137}Cs for this core was 14.07 g cm^{-2} which suggests a diffusion of 8.19 g cm^{-2}. Therefore, for this core, the calculated ^{137}Cs (max.) and ^{210}Pb sedimentation rates are in good agreement and can be compared to sedimentation rates of 0.200 g cm^{-2} y^{-1} (^{210}Pb) and 0.180 g $cm^{-2}y^{-1}$ (^{137}Cs depth.) obtained by Swan (1978) from a core collected in 1976. However these sedimentation rates

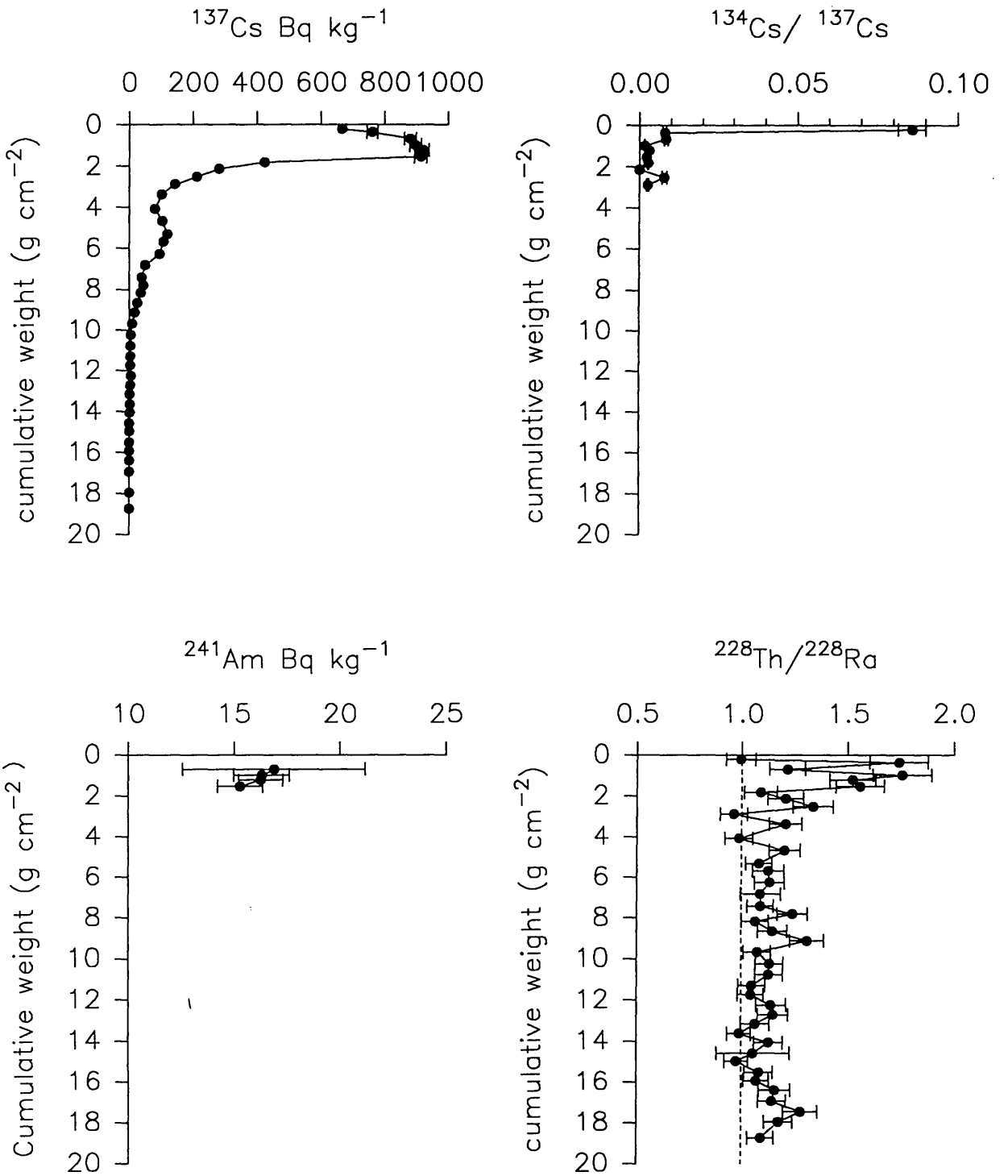

Figure 4.28. Loch Goil core GD2 radionuclide concentrations and activity ratios

were calculated from Craib cores which had maximum depths of 20 cm and therefore possibly only reflect the mixed area of the core for the ^{210}Pb concentrations.

The inventory of ^{137}Cs in GD2 is 21100 ± 500 Bq m^{-2} which is lower than core LL1 (39000 ± 1500 Bq m^{-2}) but considerably higher than any of the cores from Loch Etive (7500 to 10100 Bq m^{-2}). McKinley (1979) reported an inventory of 12133 Bq m^{-2} of ^{137}Cs for a core from the deepest part of Loch Goil obtained in 1979, however the inventory of a core from a shallower part of the loch gave a higher inventory of 17933 Bq m^{-2}. The comparison of results from previous studies and the present study indicate that there are differences between the sediments from the deeper part of the loch which have a higher ^{210}Pb flux and a lower ^{137}Cs inventory (423 Bq m^{-2} y^{-1} and 121133 Bq m^{-2}) than the sediments from the shallower station nearer to the mouth of loch which had a lower ^{210}Pb flux and a higher ^{137}Cs inventory (208 Bq m^{-2} y^{-1} and 21100 Bq m^{-2} (present study) and 17933 Bq m^{-2} (McKinley,1979)). These results suggest that there is a different supply of material to the shallow and deep stations of Loch Goil, and that the type of material being deposited is influencing the inventories of ^{210}Pb and ^{137}Cs in the sediments. The results for core GD2 and those of LE 2 suggest focusing of organic rich material to the deeper stations and the inventories of Loch Goil suggest that there is a higher percentage of clay rich material in the shallower stations.

The $^{134}Cs/^{137}Cs$ ratio has a surface value of 0.086 and decreases rapidly to a value of 0.008 at a depth of 0.36 g cm^{-2} (1.5 cm) after which it decreases to essentially zero at 2.12 g cm^{-2} (7.5 cm). The ratio then increases to 0.008 (2.51 g cm^{-2}, 8.5 cm) and then falls to 0.003 at 2.87 g cm^{-2} (9.5 cm), ^{134}Cs is not detectable below this depth. The surface $^{134}Cs/^{137}Cs$ ratio indicates that Chernobyl ^{134}Cs is detectable in the sediments of core GD2. Comparing the surface ratio of 0.086 with the value of 0.074 expected from the decay corrected Sellafield discharge (assuming no mixing) (Table 4.12.) it is possible to calculate the amount of radiocaesium present in the surface sediment from Chernobyl fallout, assuming that the decay corrected

$^{134}Cs/^{137}Cs$ ratio of the Chernobyl fallout was 0.28 in 1988. The amounts of ^{134}Cs and ^{137}Cs present in the surface sample from Chernobyl fallout were calculated to be 10.8 Bq kg^{-1} and 38.6 Bq kg^{-1} respectively which represent 19 % and of the total ^{134}Cs and 6% of the total ^{137}Cs, indicating that the Sellafield discharge remains the dominant source of radiocaesium in the surface sediment. The $^{134}Cs/^{137}Cs$ ratio at a depth of 2.51 g cm^{-2} (8.5 cm) has a ratio of 0.008 which corresponds to 1956 if no mixing is considered. The $^{134}Cs/^{137}Cs$ ratio for the Sellafield discharge for 1955 was 0.33 which after 33 years of decay would be not be detectable, therefore the $^{134}Cs/^{137}Cs$ ratio indicates mixing to a depth of 2.51 to 2.87 g cm^{-2} (8.5, 9.5 cm). The inventory of ^{134}Cs for core GD2 is 180 $\pm$ 10 Bq m^{-2} which is significantly lower than core LL1 (460 $\pm$ 20 Bq m^{-2}) and higher than any of the cores from Loch Etive (27 to 128 Bq m^{-2}).

^{241}Am was detected at a depth of 0.68 g cm^{-2} at a concentration of 16.9 Bq kg^{-1} and remains within error of this value to a depth of 1.53 g cm^{-2} below which was not detected. The two maximum discharges of ^{241}Pu occurred in 1973 and 1978 and would have reached Loch Goil in 1974 and 1979 respectively. These dates correspond to depths of 0.68 g cm^{-2} (bottom of section corresponds to 1979, mid section = 1981) and 0.98 g cm^{-2} (bottom of section corresponds to 1974, mid section = 1976) and therefore the first appearance of ^{241}Am at a depth of 0.68 g cm^{-2} coincides with the date of a maximum discharge of ^{241}Am and as with core LL1, core GD2 was not sampled with enough resolution to allow the two maxima from the Sellafield to be identified. The profile indicates a constant concentration of ^{241}Am to a depth of 1.53 g cm^{-2} (5.5 cm) and this may be due to mixing. As previously outlined (section 4.5.3.), the $^{137}Cs/^{241}Am$ inventory ratio for areas outwith the Irish Sea in 1987 can be estimated to be 880 whereas the $^{137}Cs/^{241}Am$ ratio of the inventories for core GD2 is 111. The $^{137}Cs/^{241}Am$ ratio for core GD2 is higher than LL1 and the Loch Etive cores which all gave the same value of approximately 73. The results therefore indicate, as discussed in section 4.5.3., either that ^{241}Pu is incorporated approximately ten times more efficiently in the sediment than ^{137}Cs or that there has been significant re-dissolution of ^{137}Cs from the sediment or that the $^{137}Cs/^{241}Am$ inventory ratio

of 880 for areas outwith the Irish Sea is incorrect.

4.6.4 *^{228}Th and ^{228}Ra profiles of core GD2*

The ^{228}Th/^{228}Ra profile for core GD2 is shown in Figure 4.26. The ratio has a value of 1.0 in the surface sediment then increases to 1.74 at 0.36 g cm^{-2} (1.5 cm) depth. The ratio decreases to a value within error of unity at a depth of 1.81 g cm^{-2} (6.5 cm) after which the profile is irregular with values above unity occurring. The inventories for ^{228}Th and ^{228}Ra are 8300 ± 360 Bq m^{-2} and 7300 ± 350 Bq m^{-2} respectively indicating that there is a small excess of ^{228}Th in this core. Both the ^{228}Ra and ^{228}Th concentrations are high in the surface sediments, probably reflecting the involvement of radium with the Mn oxyhydroxides. ^{232}Th data were not available for this sediment.

4.6.5 *Stable Pb and Pb isotope ratios*

The stable Pb concentration data are presented in Chapter 3 and the plot of the total Pb concentration versus cumulative weight (g cm^{-2}) is shown in Figure 4.29.A. The Pb concentration is 318 mg kg^{-1} at a depth of 0.36 g cm^{-2} (1.5 cm) and increases to a maximum of 481 mg kg^{-1} at 4.08 g cm^{-2} (13 cm). The concentration then decreases to 375 mg kg^{-1} at 5.31 g cm^{-2} (17 cm) after which it increases to 418 mg kg^{-1} at a depth of 6.82 g cm^{-2} (23 cm) and then decreases rapidly to 157 mg kg^{-1} at a depth of 10.77 g cm^{-2} (39 cm). Finally the Pb concentration continues to decrease more slowly to a value of 78 mg kg^{-1} at a depth of 18.74 g cm^{-2} (71.5 cm). The maximum concentration of 481 mg kg^{-1} of Pb in this core is higher than that of core LL1 from Loch Long (425 mg kg^{-1}) and far greater than the Pb concentration in the cores from Loch Etive, which had maximum Pb concentrations within the range 55 to 98 mg kg^{-1}. The concentration at the bottom of the core is 78 mg kg^{-1} which indicates that pollutant Pb is still present at this depth. Smith-Briggs (1983) reported baseline concentrations for two sites in Loch Goil, one from the deep part of the loch and another from a shallower site, which were 27 and 15 mg kg^{-1} respectively giving a mean value of 21 mg kg^{-1}. The pollutant Pb concentration of core GD2 was therefore calculated by subtracting 21 mg kg^{-1}

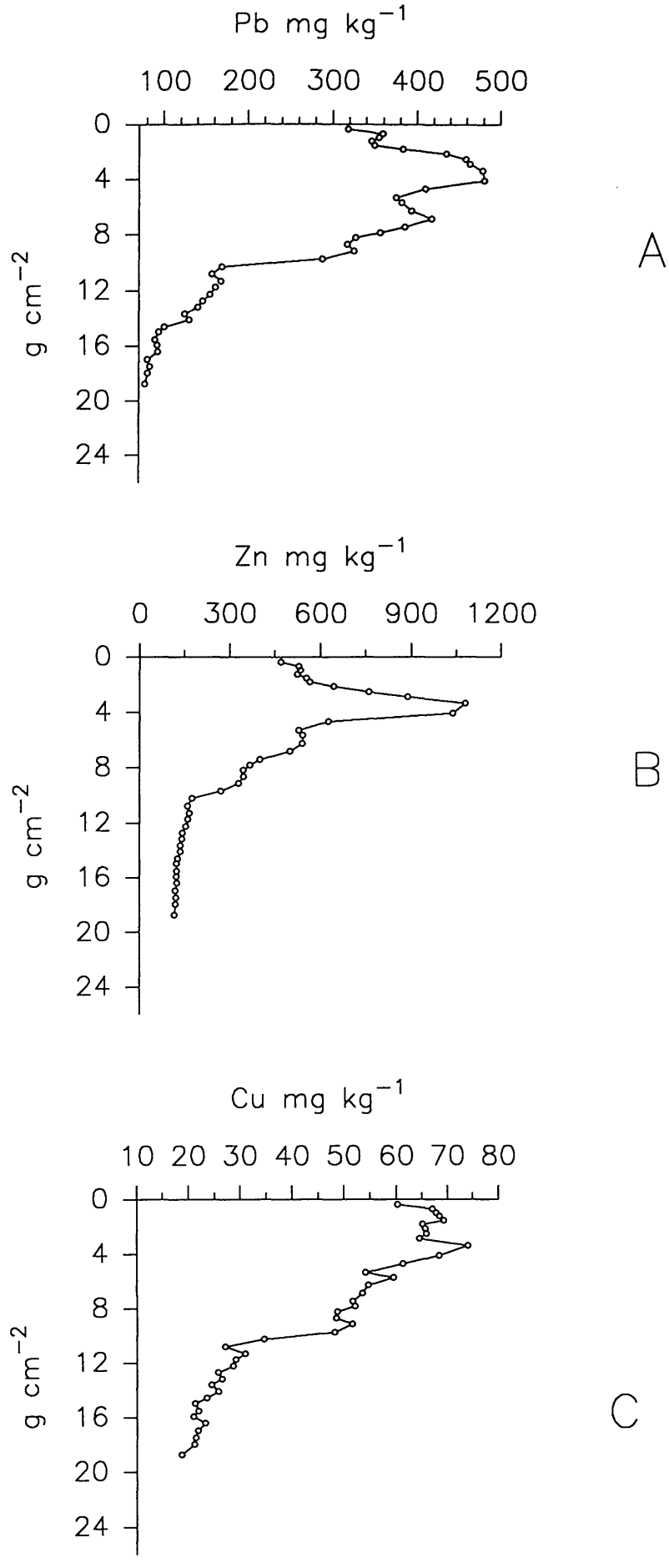

Figure 4.29. Loch Goil core GD2 Pb, Zn and Cu concentrations (mg kg^{-1})

from the total Pb concentration indicating that at a depth of 18.74 g cm^{-2} (71.5 cm) which corresponds to 1780 (after taking account of mixing equivalent to 47 years) there is approximately 57 mg kg^{-1} of pollutant Pb. This figure is high for the 18^{th} century and reflects the highly polluted nature of the Clyde Sea Area, or could be taken to suggest that there is, or has been mixing to a greater depth than is indicated by the present profiles, or that the calculated ^{210}Pb sedimentation rate is too low.

By using the calculated ^{210}Pb sedimentation rate it is possible to date the maximum Pb concentrations that occur in core GD2. The two maxima occurring at 6.82 and 4.08 g cm^{-2} (23 and 11 to 13 cm) correspond to dates of 1897 and approximately 1940 respectively. The minimum Pb concentration occurring between the two Pb maxima corresponds to the depth at which the maximum values for the Mn/Al, Fe/Al and Ca/Al Pb profiles occur and could possibly reflect dilution by an authigenic Mn/Fe/Ca carbonate-oxyhydroxide phases.

The flux of pollutant Pb versus time (on the basis of the ^{210}Pb chronology) for core GD2 is shown in Figure 4.30.A. The excess Pb flux results are given in Table 4.16.

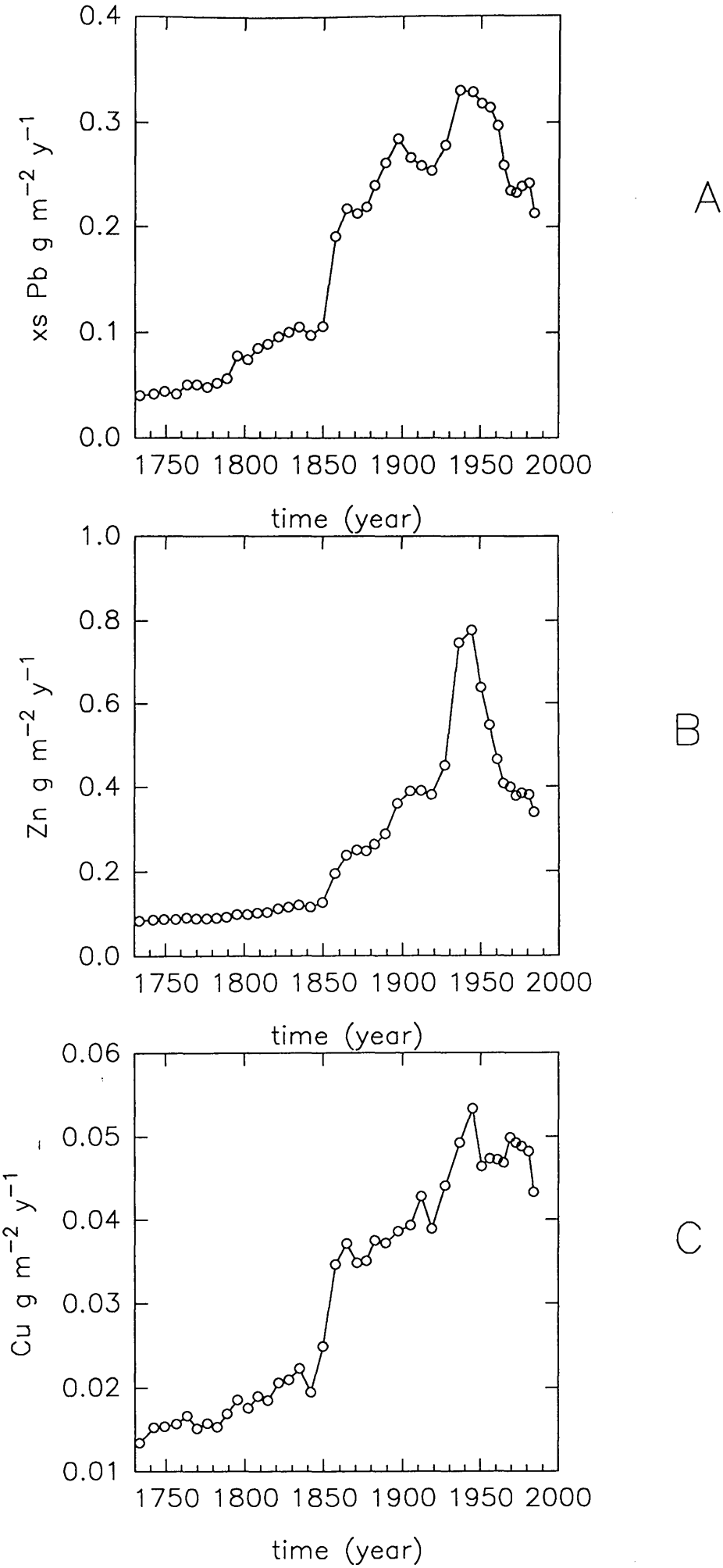

Figure 4.30. Loch Goil core GD2 Pb, Zn and Cu flux data

SAMPLE	DEPTH (cm)	cum g cm^{-2}	date for mid section	excess Pb g m^{-2} y^{-1}
GD2 0-1	0.5	0.20	1987	
GD2 1-2	1.5	0.36	1984	0.213
GD2 2-3	2.5	0.68	1981	0.243
GD2 3-4	3.5	0.98	1976	0.240
GD2 4-5	4.5	1.23	1973	0.233
GD2 5-6	5.5	1.53	1969	0.235
GD2 6-7	6.5	1.81	1965	0.260
GD2 7-8	7.5	2.12	1961	0.297
GD2 8-9	8.5	2.51	1956	0.315
GD2 9-10	9.5	2.87	1951	0.318
GD2 10-12	11	3.36	1945	0.329
GD2 12-14	13	4.08	1936	0.330
GD2 14-16	15	4.67	1927	0.279
GD2 16-18	17	5.31	1919	0.254
GD2 18-20	19	5.68	1912	0.259
GD2 20-22	21	6.26	1905	0.267
GD2 22-24	23	6.82	1897	0.285
GD2 24-26	25	7.43	1889	0.262
GD2 26-28	27	7.81	1882	0.240
GD2 28-30	29	8.18	1877	0.220
GD2 30-32	31	8.67	1871	0.213
GD2 32-34	33	9.12	1864	0.218
GD2 34-36	35	9.69	1857	0.192
GD2 36-38	37	10.23	1850	0.106
GD2 38-40	39	10.77	1842	0.097
GD2 40-42	41	11.29	1835	0.105
GD2 42-44	43	11.72	1828	0.100
GD2 44-46	45	12.24	1822	0.096
GD2 46-48	47	12.71	1815	0.089
GD2 48-50	49	13.17	1808	0.085
GD2 50-52	51	13.63	1802	0.074
GD2 52-54	53	14.07	1796	0.078
GD2 54-56	55	14.59	1789	0.056
GD2 56-58	57	14.98	1783	0.052
GD2 58-60	59	15.52	1776	0.048
GD2 60-62	61	15.93	1770	0.050
GD2 62-64	63	16.40	1764	0.050
GD2 64-66	65	16.95	1756	0.042
GD2 66-68	67	17.46	1749	0.044
GD2 68-70	69	17.95	1742	0.042
GD2 70-73	71.5	18.74	1733	0.040

Table 4.16 Loch Goil core GD2 Pb flux data

Excess Pb is observed in the sediment from the bottom of the core which corresponds to 1780 (after mixing) at 0.04 g m^{-2} y^{-1} and increases slowly to 0.106 g m^{-2} y^{-1} by 1897 (taking account of 47 years of mixing). Two maxima occur corresponding to dates of 1897 and approximately 1940. The excess flux of Pb decreases towards the surface of the sediment with a value of 0.23 g m^{-2} y^{-1} at 0.36 g cm^{-2} (1.5 cm) indicating that, as with core LL1 and the Loch Etive cores, the flux of excess Pb to the sediment has decreased in recent years. The excess Pb flux in the surface sediment of core GD2 is lower than LL1 (0.30 g m^{-2} y^{-1}) and considerably higher than cores LE 1 (0.06 g m^{-2} y^{-1}), LE 2 (0.02 g m^{-2} y^{-1}) and LE 3 (0.03 g m^{-2} y^{-1}). The onset of the rapid rise in the excess Pb flux occurs in 1897 which correlates well with the sharp rise in excess Pb flux that occurs in core LE 2 (1887) and is earlier than that of LE 1 (1907). Neither core LE 3 nor LL1 exhibits a sharp rise in excess Pb flux.

The inventory of excess Pb for core GD2 is 43.3 Bq m^{-2} which is significantly less than that of core LL1 (68.3 g m^{-2}) and considerably higher than the excess Pb inventory of the Loch Etive cores which were in the range 1.6 to 3.8 g m^{-2}. The differences in the excess Pb inventories for the Etive cores were also reflected in higher ^{210}Pb inventory and flux values for the Clyde Sea Area cores. Cores LL1 from Loch Long and GD2 from Loch Goil have similar ^{210}Pb inventories and fluxes but significantly different excess Pb inventories. If as the ^{210}Pb fluxes suggest, the amount of ^{210}Pb entering Loch Long and Loch Goil (at the sampling sites) is the same then the efficiency of removal of Pb to the sediment is essentially the same at both sites. If this is the case then it suggests that there has been an additional source of pollutant Pb to the sediments of core LL1. If the interpretation of core LL1 is correct an additional source of Pb has been identified in the form of the dumped section containing 11.4 g m^{-2} of excess Pb. Subtraction of the dumped section Pb from the total excess Pb inventory for LL1 leaves an inventory of 56.9 g m^{-2} which is still higher than core GD2.

The plot of $^{206}Pb/^{207}Pb$ ratio versus ^{210}Pb chronology for core GD2 is shown in figure 4.31. along with the excess Pb flux (g m^{-2} y^{-1}). The $^{206}Pb/^{207}Pb$ profile

is consistent with previous cores and shows a distinct petrol Pb influence towards the surface. The surface sediment has a $^{206}Pb/^{207}Pb$ ratio of 1.145 which is lower than that of LL1 (1.155), LE 2 (1.157) and LE 3 (1.152) and essentially the same as LE 1 (1.149). The ratio remains within error of this value to a depth of 1.23 g cm^{-2} (4.5 cm) after which it increases relatively uniformly to a value of 1.173 at a depth of 8.18 g cm^{-2} (29 cm). The ratio does suggest a decrease in $^{206}Pb/^{207}Pb$ ratio over the depth range 4.08 to 5.31 g cm^{-2} (13 to 17 cm) which corresponds to the depth at which the maximum Pb flux (4.08 g cm^{-2}, 13 cm) is observed and indicates an increased effect of Pb from petrol at this time which corresponds to the late 1970's to early 1980's (if mixing of 47 years is taken into account). An alternative argument may be considered that, as in core LL1, this sediment may have been physically disturbed by the effects of dumping of dredged material farther south in Loch Long. However the other profiles such as Mn/Al, P/Al, unsupported ^{210}Pb profile and the $^{134}Cs/^{137}Cs$ profile do not support this. The $^{206}Pb/^{207}Pb$ ratio is within error the same from a depth of 8.18 g cm^{-2} (29 cm) to 18.74 g cm^{-2} (71.5 cm) which was the bottom of the core. As discussed in section 4.2.5. the decreasing $^{206}Pb/^{207}Pb$ ratio towards the surface sediment can be attributed to the increasing influence of vehicle exhaust emissions on pollutant Pb fluxes to the sediment during this century. The onset of the change in ratio occurs at 8.18 g cm^{-2} (29 cm), corresponding to a date of 1877 or 1924 allowing for mixing, which is later than LL1 (1916) and earlier than the cores from Loch Etive (1929 to 1937). The date of 1924 is in good agreement with the historical date for the onset of pollutant Pb of the mid to late 1920's to give a reasonable degree of confidence in the applied ^{210}Pb chronology for this core.

The assessment of the percentage Pb due to pollutant Pb from petrol was calculated as described in 4.2.5. with R_i = 1.172 and R_{Hi}= 1.172 and the results of this calculation are given in Table 4.17.

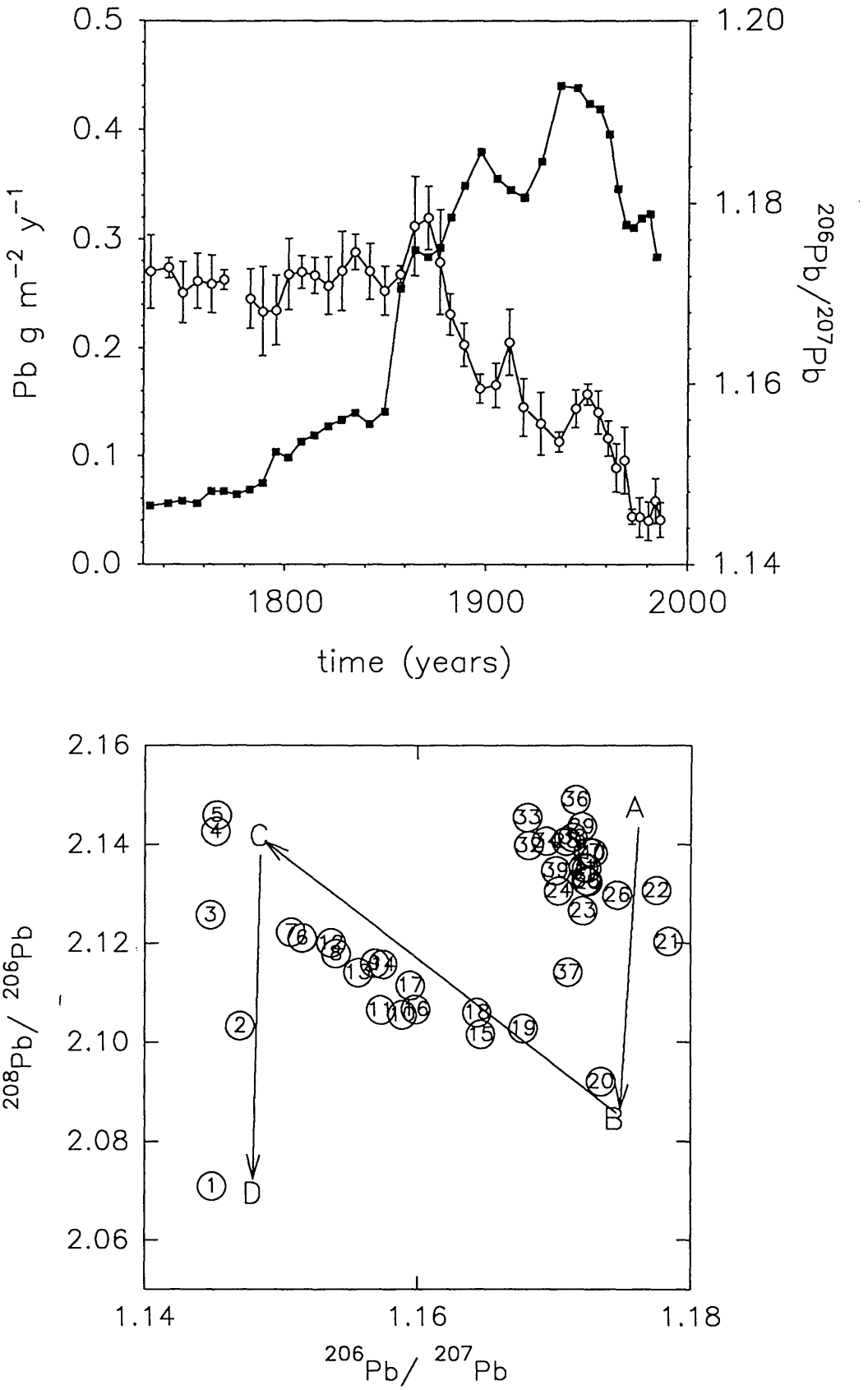

Figure 4.31. Loch Goil core GD2 Pb flux and Pb isotope ratio plots

sample	DEPTH (cm)	cum. g cm^{-2}	date for mid section	% Pb from petrol
GD2 0-1	0.5	0.20	1987	
GD2 1-2	1.5	0.36	1984	33
GD2 2-3	2.5	0.68	1981	35
GD2 3-4	3.5	0.98	1976	35
GD2 4-5	4.5	1.23	1973	35
GD2 5-6	5.5	1.53	1969	27
GD2 6-7	6.5	1.81	1965	28
GD2 7-8	7.5	2.12	1961	23
GD2 8-9	8.5	2.51	1956	19
GD2 9-10	9.5	2.87	1951	17
GD2 10-12	11	3.36	1945	19
GD2 12-14	13	4.08	1936	24
GD2 14-16	15	4.67	1927	21
GD2 16-18	17	5.31	1919	19
GD2 18-20	19	5.68	1912	10
GD2 20-22	21	6.26	1905	16
GD2 22-24	23	6.82	1897	16
GD2 24-26	25	7.43	1889	10
GD2 26-28	27	7.81	1882	5
GD2 28-30	29	8.18	1877	
GD2 30-32	31	8.67	1871	
GD2 32-34	33	9.12	1864	
GD2 34-36	35	9.69	1857	
GD2 36-38	37	10.23	1850	
GD2 38-40	39	10.77	1842	
GD2 40-42	41	11.29	1835	
GD2 42-44	43	11.72	1828	
GD2 44-46	45	12.24	1822	
GD2 46-48	47	12.71	1815	
GD2 48-50	49	13.17	1808	
GD2 50-52	51	13.63	1802	
GD2 52-54	53	14.07	1796	
GD2 54-56	55	14.59	1789	
GD2 56-58	57	14.98	1783	
GD2 58-60	59	15.52	1776	
GD2 60-62	61	15.93	1770	
GD2 62-64	63	16.40	1764	
GD2 64-66	65	16.95	1756	
GD2 66-68	67	17.46	1749	
GD2 68-70	69	17.95	1742	
GD2 70-73	71.5	18.74	1733	

Table 4.17 % Pb in sediment from Pb in petrol for core GD2

The results from the calculation of percentage Pb in the sediment due to the input of pollutant Pb from petrol indicate that the onset of deposition of Pb from petrol occurs at 1882 (5%). After accounting for mixing this becomes 1929 which is later than LL1 (1916) and in very good agreement with the Loch Etive cores (1929 to 1942). The % of Pb from Pb in petrol is 5% in 1929 increasing to 35 % in the 1970's and early 80's and then begins to decrease from 1984 to a value of 33% near the surface of the core. The percentages of Pb from petrol are higher than those calculated for core LL1 and lower than the cores from Loch Etive, which again reflects the greater pollution in the Clyde Sea Area due to heavy industry and coal burning with core LL1 being more polluted than GD2. The residual excess Pb inventory for this core (i.e. excess Pb inventory -Pb from petrol) is 37.9 g m^{-2}. The ratios of the inventories of excess ^{210}Pb, excess Pb and residual excess Pb of cores LL1 and GD2, are as follows;

$LL1_{210}/GD2_{210}$= 1.2, $LL1_{xsPb}/GD2_{xsPb}$= 1.6, $LL1_{res\text{-}Pb}/GD2_{res\text{-}Pb}$= 1.6.

The above ratios illustrate numerically that the ^{210}Pb inventories for the two cores are essentially the same and that there is a greater amount of pollutant Pb in core LL1, interestingly they also demonstrate that the proportion of pollutant Pb which arises from Pb from petrol is the same for the two cores, suggesting that the dumped material in Loch Long contained Pb from pollutant sources similar to those that had affected Loch Goil.

The $^{208}Pb/^{206}Pb$ versus $^{206}Pb/^{207}Pb$ plot for core GD2 is shown in Figure 4.31. The samples are numbered 1 to 41 according to increasing depth. The diagram indicates a four component system with the ratio for the samples at depth (21 to 41) reflecting the dominant Pb pollutant as heavy industry. The tie line A→B reflects the increasing effect of heavy industry, B→C (20 to 6) reflects the increasing effect of petrol and C→D reflects a recent input of low ^{208}Pb material. The reason for this major change in the ^{208}Pb ratio is unknown. The decrease in the $^{208}Pb/^{206}Pb$ ratio occurs at a depth of 1.23 g cm^{-2} (4.5 cm) which corresponds to a date of 1973. A change in the $^{208}Pb/^{206}Pb$ a ratio was also seen in core LL1, but in this case the ratio

increased, not decreased, at a depth corresponding to 1960. This change in the ^{208}Pb concentration is unexplained and as there is no evidence of a similar effect in the cores from Loch Etive it is thought to be a local effect.

4.6.6 *Zn and Cu profiles of core GD2*

The Zn and Cu concentration profiles for core GD2 are shown in Figures 4.29.B. and 4.29.C. respectively. The Zn profile has a concentration of 470 mg kg^{-1} at a depth of 0.36 g cm^{-2} (1.5 cm), and increases to a maximum of 1081 mg kg^{-1} at a depth of 3.36 g cm^{-2} which corresponds to a date of 1945. This may reflect the increase in metal ore smelting during the second world war or an increase in industrial activity in general. The Zn profile then decreases sharply to a value of 345 mg kg^{-1} at a depth of 8.18 g cm^{-2} (29 cm) corresponding to a date of 1924 (accounting for mixing) after which the concentration decreases more slowly to 128 mg kg^{-1} at a depth of 14.59 g cm^{-2} (55 cm) which corresponds to 1836. The concentration of Zn below 14.59 g cm^{-2} (55 cm) remains within the range 117 to 128 mg kg^{-1}. Smith-Briggs (1983) reported baseline concentrations of Zn for two cores from Loch Goil of 86 and 68 mg kg^{-1} respectively giving a mean value of 77 mg kg^{-1} which suggests that the sediment at depth in core GD2 may still be affected by pollutant concentrations of Zn, although not to the same degree as Pb. The depth of the maximum Zn concentration is the same as that of the first (and largest) maximum in the Pb concentration profile (Figure 4.29.A.), however the second maximum, which is present in th Pb profile at a depth of 6.82 g cm^{-2} (23 cm) is not as well defined in the Zn profile. Below this depth the profile follows similar trends to that of Pb.

The Cu profile has a concentration of 60 mg kg^{-1} at a depth of 0.36 g cm^{-2} (1.5 cm) and increases to a maximum of 74 mg kg^{-1} at a depth of 3.36 g cm^{-2} (11 cm) which is the depth of the maximum Pb and Zn concentrations and corresponds to a date of 1945. The Cu concentration profile then decreases to 48 mg kg^{-1} at 9.69 g cm^{-2} (35 cm) corresponding to 1892 and then more rapidly to 27 mg kg^{-1} at 10.77 g cm^{-2} (39 cm). Below this the concentration decreases slowly to 19 mg kg^{-1} at the bottom of the core (18.74 g cm^{-2}, 71.5

cm). Smith-Briggs (1983) reported baseline concentrations of Cu of 27 and 10 mg kg^{-1} for two cores from Loch Goil giving a mean value of 18 mg kg^{-1}, which suggests that unlike Pb and Zn the Cu concentration may have reached natural levels by the bottom of the core, corresponding to a date of 1780 after taking into account 47 years of mixing However if the baseline concentration of 10 mg kg^{-1} (Smith-Briggs, 1983) is taken to be representative of the natural Cu concentration then elevated Cu concentrations are still being detected. Although the Cu profile is much more irregular it follows very similar trends to the Pb profile. The trends in the Zn profile are similar to those of the Cu and Pb except that the Zn decreases much more rapidly towards the surface. If the profiles do represent temporal trends in deposition, this implies a much greater reduction in the use of Zn than of Pb and suggests that the extremely high Zn concentrations corresponding to 1945 may have resulted from a specific, local use of Zn at this time, (c.f. Loch Etive where the decline in Zn flux is similar to that of Pb). The pollutant metal data suggest that there were major changes in input over the depth ranges 10.23 to 5.31 g cm^{-2} (37 to 17 cm) and 5.31 to 3.36 g cm^{-2} (17 to 11 cm) corresponding to dates of 1850 to 1919 and 1919 to 1945.

The fluxes of total Zn and total Cu are given in Figures 4.30.B. and 4.30.C. respectively, with the results being presented in Table 4.18. The fluxes are higher than the Loch Etive cores which had maximum values in the range 0.12 to 0.22 g m^{-2} y^{-1} for Zn and 0.01 to 0.017 g m^{-2} y^{-1} for Cu. The fluxes for both Zn and Cu for core GD2 are, however, lower than those for core LL1 from Loch Long. The temporal variation in the Pb and Cu fluxes for GD2 are very similar, while the Zn flux exhibits similar trends to Pb and Cu, but with a sharper increase in the Zn flux to 1945 and sharper decrease since then. The Zn profile has a flux of 0.084 g m^{-2} y^{-1} at a depth of 18.74 g cm^{-2} which corresponds to 1780 when taking the effects of mixing into consideration, increasing to a maximum flux of 0.78 g m^{-2} y^{-1} in 1945, after which it decreases to a value of 0.34 g m^{-2} y^{-1} in the mid 1980's. An excess Zn flux of 0.99 g m^{-2} y^{-1} has been reported by Farmer (1982). The Cu flux for GD2 is 0.013 g m^{-2} y^{-1} in 1780, increases to a maximum of 0.49 g m^{-2} y^{-1} in 1945 and then decreases to a value of 0.1 g m^{-2} y^{-1} by the mid 1980's. The

inventories for Zn and Cu for core GD2 are 66.8 and 7.8 g m^{-2} respectively which are lower than those of LL1 of 87.3 and 12.6 g m^{-2} for Zn and Cu. The excess Zn and Cu inventories were calculated by subtracting the mean baseline values of 77 and 18 mg kg^{-1} of Zn and Cu respectively obtained by Smith-Briggs (1983). The excess Zn and Cu inventories for core GD2 are 52.5 and 4.5 g cm^{-2} respectively, which are lower than those of LL1 but considerably higher than the excess Zn and Cu inventories obtained for Loch Etive.

Comparison of the ratios of the inventories of Zn and Cu for cores LL1 and GD2 gives values of $LL1_{Zn}/GD2_{Zn}$=1.3, $LL1_{Cu}/GD2_{Cu}$=1.6 and $LL1_{xsZn}/GD2_{xsZn}$=1.2, $LL1_{xsCu}/GD2_{xsCu}$= 1.7, which can be compared to the Pb inventory ratios of $LL1_{Pb\text{-}210}/GD2_{Pb\text{-}210}$= 1.2, $LL1_{xsPb}/GD2_{xsPb}$= 1.6, $LL1_{res\text{-}Pb}/GD2_{res\text{-}Pb}$= 1.6. It can be seen from these ratios that the excess Pb, residual Pb and the Cu inventory ratios are all the same, despite differences in the lochs, indicating that the atmospherically derived pollutants Pb and Cu are behaving similarly in the sediments and that both Pb and Cu inventories are enhanced within the sediments of core LL1 from Loch Long with respect to core GD2 from Loch Goil. The ratio of the Zn inventories for cores LL1 and GD2 is lower than the respective Pb and Cu inventories which is probably due to the enhanced Zn flux around 1945 and suggests that this may have been a local input to Loch Goil.

SAMPLE	DEPTH (cm)	cum g cm^{-2}	date for mid section	Cu g m^{-2} y^{-1}	Zn g m^{-2} y^{-1}
GD2 0-1	0.5	0.20	1987		
GD2 1-2	1.5	0.36	1984	0.043	0.338
GD2 2-3	2.5	0.68	1981	0.048	0.380
GD2 3-4	3.5	0.98	1976	0.049	0.384
GD2 4-5	4.5	1.23	1973	0.049	0.378
GD2 5-6	5.5	1.53	1969	0.050	0.399
GD2 6-7	6.5	1.81	1965	0.047	0.407
GD2 7-8	7.5	2.12	1961	0.047	0.465
GD2 8-9	8.5	2.51	1956	0.047	0.547
GD2 9-10	9.5	2.87	1951	0.046	0.639
GD2 10-12	11	3.36	1945	0.053	0.778
GD2 12-14	13	4.08	1936	0.049	0.747
GD2 14-16	15	4.67	1927	0.044	0.451
GD2 16-18	17	5.31	1919	0.039	0.380
GD2 18-20	19	5.68	1912	0.043	0.390
GD2 20-22	21	6.26	1905	0.039	0.389
GD2 22-24	23	6.82	1897	0.039	0.360
GD2 24-26	25	7.43	1889	0.037	0.288
GD2 26-28	27	7.81	1882	0.038	0.264
GD2 28-30	29	8.18	1877	0.035	0.248
GD2 30-32	31	8.67	1871	0.035	0.250
GD2 32-34	33	9.12	1864	0.037	0.238
GD2 34-36	35	9.69	1857	0.035	0.194
GD2 36-38	37	10.23	1850	0.025	0.126
GD2 38-40	39	10.77	1842	0.020	0.115
GD2 40-42	41	11.29	1835	0.022	0.120
GD2 42-44	43	11.72	1828	0.021	0.115
GD2 44-46	45	12.24	1822	0.021	0.111
GD2 46-48	47	12.71	1815	0.019	0.103
GD2 48-50	49	13.17	1808	0.019	0.102
GD2 50-52	51	13.63	1802	0.018	0.098
GD2 52-54	53	14.07	1796	0.019	0.098
GD2 54-56	55	14.59	1789	0.017	0.092
GD2 56-58	57	14.98	1783	0.015	0.089
GD2 58-60	59	15.52	1776	0.016	0.089
GD2 60-62	61	15.93	1770	0.015	0.089
GD2 62-64	63	16.40	1764	0.017	0.091
GD2 64-66	65	16.95	1756	0.016	0.087
GD2 66-68	67	17.46	1749	0.015	0.088
GD2 68-70	69	17.95	1742	0.015	0.086
GD2 70-73	71.5	18.74	1733	0.013	0.084

Table 4.18 Cu and Zn fluxes for Loch Goil core GD2

4.6.7 *Summary of core GD2*

In summary, the results for core GD2 suggest that ^{210}Pb dating, ^{137}Cs maximum, heavy metals and $^{206}Pb/^{207}Pb$ isotope ratio trends give chronologically consistent profiles, indicating that ^{210}Pb dating is valid and that Pb is not mobile in this core. The ^{210}Pb, ^{137}Cs and $^{134}Cs/^{137}Cs$ profiles all indicate that mixing is taking place in the top 3.36 g cm^{-2} of this core. The mixing could be the result of human activity since the sediment of the loch has many cables running across its surface which have been laid by the navy and the presence of such cables restricted the choice of sampling and prevented coring in the deepest part of the loch. Swan (1978) reported evidence of worm burrows extending to a depth of a least 4 cm in a sediment core from Loch Goil and concluded that mixing was taking place within the surface sediment. The core has an accumulation rate of 0.072 g cm^{-2} y^{-1} giving a time interval from the surface of the sediment to the bottom of the mixed zone of approximately 47 years.

The manmade radionuclides present in the sediment are dominated by the Sellafield discharge, with the influence of Chernobyl fallout being seen in the surface sediment. The ^{137}Cs profile indicated mobility of Cs by means of mixing and diffusion and ^{137}Cs is detectable to far greater depths than would be expected due to mixing alone which limits its use in chronology. However, the method of correlating the maximum concentration of ^{137}Cs in the sediment with the maximum Sellafield discharge gives a sedimentation rate which is consistent with that obtained from ^{210}Pb dating.

The deposition of pollutant Pb increased dramatically from the late 1880's probably as a result of the increase in heavy industry in the greater Glasgow area. The effect of pollutant Pb from petrol can first be detected around 1917 and had increased to 35 % of the total pollutant Pb by the early 1970's. This is later than the date at which maximum % Pb from petrol was seen in Loch Etive and probably reflects the close proximity of the CSA to a large heavy industrial centre. The inventory of pollutant Pb for core GD2 was 43.9 g m^{-2} with a maximum flux of 0.33 g m^{-2} y^{-1} occurring in the early 1970's. The Cu

flux profile is very similar to the Pb flux profile, however the Zn profile has an increased flux around 1945 which would seem to be very local in nature.

4.7 *Loch Fyne core FS*

The sample site, sampling methods and analytical methods for core FS are described in Chapter 2. The results for this core are tabulated in Chapter 3.

4.7.1 *Geochemical characteristics of core FS*

Selected element/Al ratios and K/Rb ratios for core FS are shown in Figure 4.32. The Si/Al, Zr/Al and Ti/Al ratios all exhibit a pronounced increase at 19.3 g cm^{-2} (33 cm) indicating a change to coarser material above this depth. The profiles also begin to show a decrease in ratio towards the surface sediment at a depth of at 9.2 g cm^{-2} (15 cm). As with the above ratios, the Ca/Al ratio displays higher values above 19.2 g cm^{-2} (33 cm), with distinct peaks at 4.12 g cm^{-2} (7.5 cm), again indicating that a change in sediment type is occurring at 19.2 g cm^{-2} (33 cm). Therefore, the Ca/Al, Si/Al, Zr/Al and Ti/Al ratios all indicate a change in sediment type from finer to coarser material occurring at 19.2 g cm^{-2} (33 cm) depth. The K/Rb ratio has a value of 212 at a depth of 0.6 g cm^{-2} (1.5 cm) which increases to a value of 224 at 6.74 g cm^{-2} (11 cm) and then remains essentially constant to the bottom of the core.

The Mn/Al ratio has a surface value of 0.03 and decreases rapidly to 0.011 at 2.27 g cm^{-2} (4.5 cm), indicating that redox recycling of Mn is taking place in the surface sediments. The Mn/Al ratio remains effectively constant from 2.27 g cm^{-2} (4.5 cm) downwards except for a minor increase at approximately 30 g cm^{-2}. The P/Al ratio has a surface value of 0.015 and decreases to 0.01 at 18.3 g cm^{-2} (31 cm) depth after which it remains constant to the bottom of the core. The Fe/Al ratio has a value of 0.55 at the surface and remains constant to a depth of 6.74 g cm^{-2} (11 cm) after which it increases to a maximum of 0.57 at 9.2 g cm^{-2} (15 cm) and then remains within the range 0.53 to 0.56 to the bottom of the core. The above selected element/Al ratios

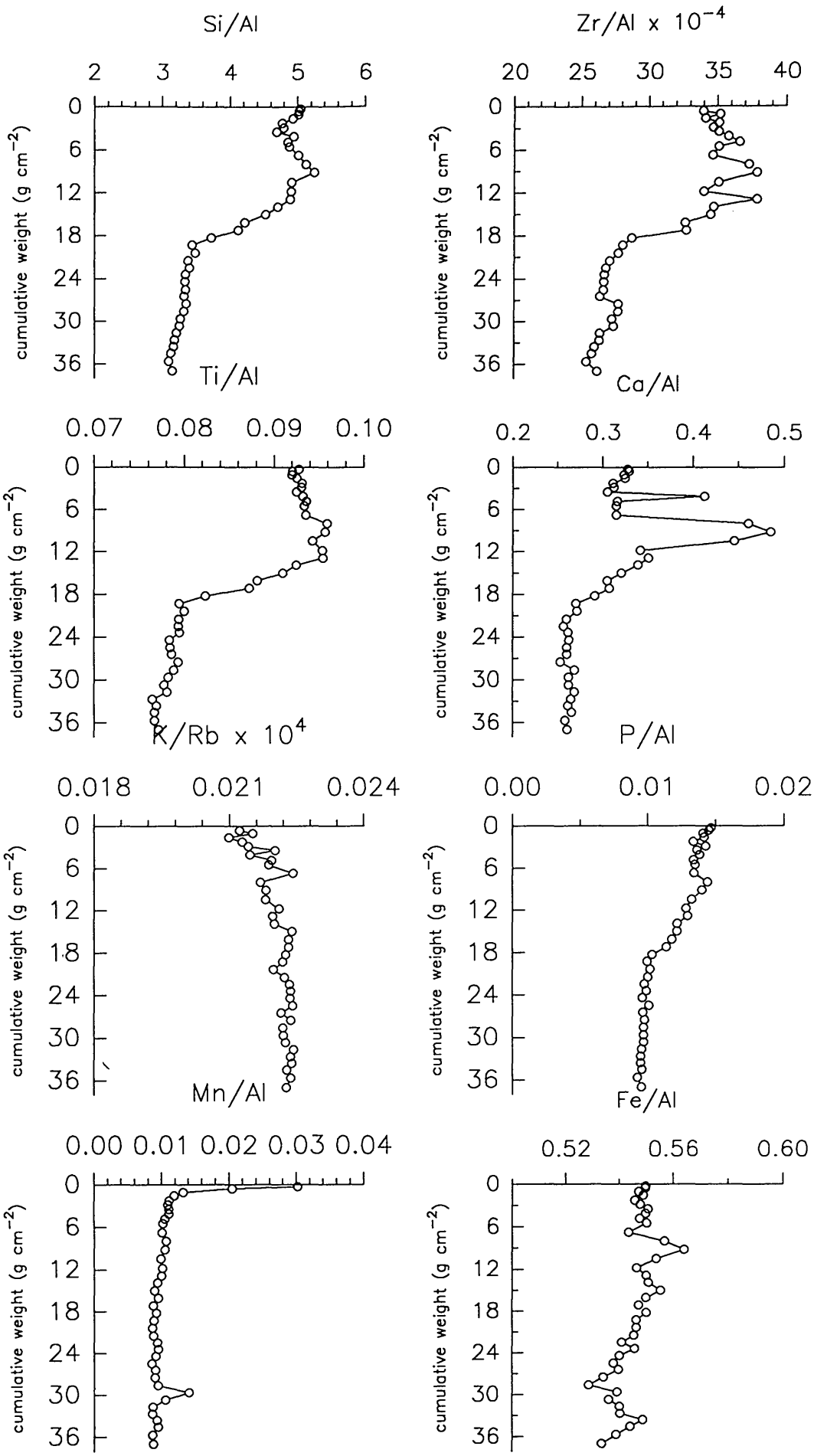

Figure 4.32. Loch Fyne core FS elemental/Al and K/Rb ratios

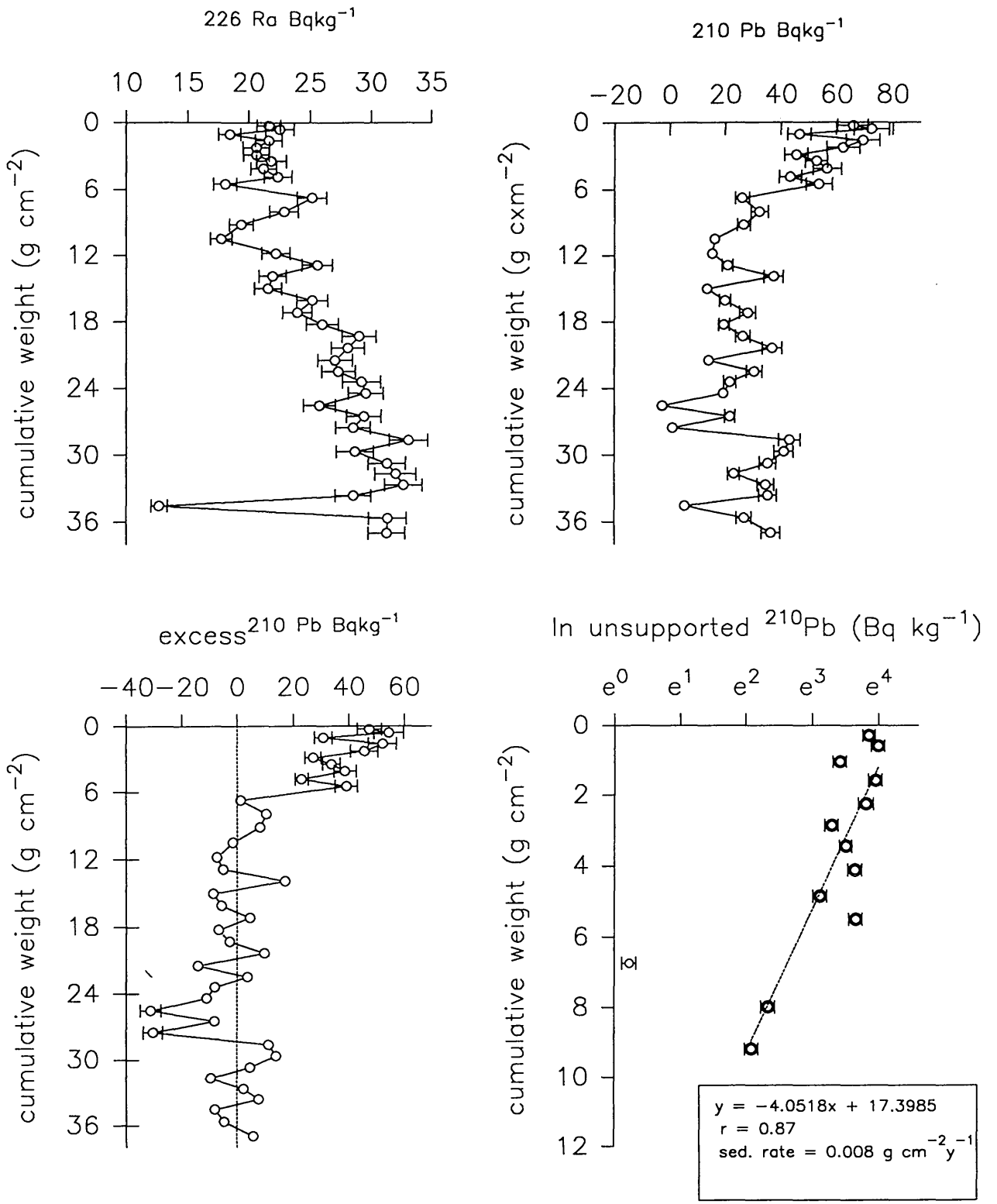

Figure 4.33.. Loch Fyne core FS unsupported ^{210}Pb concentrations

indicate that there has been a definite change in the type of accumulating sediment from finer to coarser grains in more recent times and that redox recycling of Mn but not Fe occurs at the surface of this core.

4.7.2 *^{210}Pb and ^{226}Ra profiles of core FS*

The plots of ^{226}Ra, ^{210}Pb and unsupported ^{210}Pb versus depth in g cm^{-2} are shown in Figure 4.33. The ^{226}Ra concentration has a surface value of 21.6 Bq kg^{-1} and exhibits an irregular but systematic increase with depth to a value of 31.3 Bq kg^{-1} at the bottom of the core (37 g cm^{-2}, 67 cm). Noticeably, ^{226}Ra concentrations above 19.2 g cm^{-2} (33 cm) are lower than those below this depth, consistent with the indication from the XRF data that the upper sediment is of a coarser, probably sandier nature. The ^{226}Ra inventory for core FS was 9400 ± 500 Bq m^{-2} which is higher than Loch Long (7000 ± 350 Bq m^{-2}) and similar to Loch Goil (10300 ± 500 Bq m^{-2}).

The ^{210}Pb concentration profile exhibits an irregular decrease from a surface value of 65.8 Bq kg^{-1} to 15.4 Bq kg^{-1} at 11.8 g cm^{-2} (19 cm), below which it exhibits an irregular trend to increasing ^{210}Pb concentrations towards the bottom of the core. The surface concentration of ^{210}Pb for core FS is lower than corresponding concentrations for Loch Long and Loch Goil (141.2 and 275.8 Bq kg^{-1} respectively). Similarly the surface ^{210}Pb concentrations for the Loch Etive cores (LE 1 = 292.3 Bq kg^{-1}, LE 2 = 98.6 Bq kg^{-1} and LE 3 = 418.7 Bq kg^{-1}) are also a higher than that of core FS. However, core LE 2 has a low surface ^{210}Pb concentration in comparison with LE 1 and LE 3 and the sediment type in LE 2 is similar to that of FS, in that there is a change to coarser material towards the surface. Thus, the low concentration of ^{210}Pb in cores FS and LE 2 may reflect a lower supply of fine particulates and organic material to these shallower sites. This is supported by the observation that core LE 2 had a lower % loss on ignition (12-15%) than LE 1 (15-20%) or LE 3 (14-20%). Core FS has even lower % loss on ignition values which are in the range 6 to 8%, indicative of the lower organic content of this sediment. The unsupported ^{210}Pb concentration profile exhibits an irregular but definite decline from 47.3 Bq kg^{-1} at the surface to reach the

limit of detection at 10.5 g cm^{-2} (17 cm). The profile suggests an irregular deposition pattern and is not well suited to ^{210}Pb dating but application of a C.I.C. calculation to the data gives an average accumulation rate of 0.008 g cm^{-2} y^{-1} (r = 0.87) (Figure 4.33.). This is extremely low sedimentation rate and would date the bottom of the core as 4621 years old if representative of continuous deposition throughout the core.

The irregular nature of the profile could be due to a change in the type of sediment that was accumulating over 0 to 6 g cm^{-2} depth (Si/Al, Ca/Al and K/Rb profiles indicate that some changes are taking place over this depth range), or it could indicate the effects of mixing or a combination of both. The unsupported ^{210}Pb data and geochemical data could be interpreted as indicating that there was negligible accumulation below 10.5 g cm^{-2} and irregular deposition of coarse material above this depth. The depth to which mixing occurs in this core was very difficult to assess, but two limits could be applied: no mixing, although from the ^{210}Pb and unsupported ^{210}Pb profile this was thought to be unlikely; and mixing to a depth of 5.5 g cm^{-2} (9.5 cm) which was thought to be the maximum depth to which mixing could occur as the unsupported ^{210}Pb concentration decreases rapidly to 1.2 Bq kg^{-1} below this depth. The unsupported ^{210}Pb plot also suggested that the mixing is not intense since distinct structure was preserved in the profile. As it was not possible to use the ^{210}Pb profiles to determine a mixing depth it was decided to consider some of the other profiles where mixing may be indicated such as ^{137}Cs, $^{134}Cs/^{137}Cs$ ratio, and $^{206}Pb/^{207}Pb$ ratio profiles as described below. The inventory of unsupported ^{210}Pb for core FS was 3100 $\pm$ 300 Bq m^{-2}, implying a steady state flux of 97 $\pm$ 10 Bq m^{-2} y^{-1} which is far lower than either core LL1 (240 Bq m^{-2} y^{-1}) or GD2 (208 Bq m^{-2} y^{-1}) but higher than that of core LE 2 (68 $\pm$ 9 Bq m^{-2}) from Loch Etive. The ^{210}Pb flux of 97 Bq m^{-2} y^{-1} (with the maximum flux of unsupported ^{210}Pb from in-situ production in the water column (86 m) being 5.4 Bq m^{-2} y^{-1}) for core FS falls at the lower end of the range of ^{210}Pb fluxes of 71.3 to 150 Bq m^{-2} y^{-1} obtained by Sugden (1993) from Scottish peat cores and is lower than the predicted average global atmospheric deposition of approximately 150 Bq m^{-2} y^{-1}. Therefore, the evidence from the cores discussed so far suggests that sites in which there

is a supply of finer material and/or organic material to the sediment have a higher ^{210}Pb flux than would be expected from atmospheric supply alone, and that the shallower sites which contain coarser material (LE 2 and FS) have a lower flux than would be expected from atmospheric deposition. This suggests that there is preferential deposition of ^{210}Pb in association with fine particulates and/or organics at sites of deeper locations.

4.7.3 *^{137}Cs, ^{134}Cs and ^{241}Am concentration profiles of core FS*

The concentration profiles for ^{137}Cs and ^{241}Am and the activity ratio profile for ^{134}Cs/^{137}Cs are shown in Figure 4.33. The ^{137}Cs concentration has a value of 118.0 Bq kg^{-1} at the surface, a subsurface maximum of 226.7 Bq kg^{-1} at 2.27 g cm^{-2} (4.5 cm) and then decreases to 59.4 Bq kg^{-1} at 7.99 g cm^{-2} (13 cm), after which it remains relatively constant with values between 29.1 to 34.2 Bq kg^{-1} to a depth of 15.02 g cm^{-2} (25 cm). Thereafter the ^{137}Cs concentration decreases to 1.0 Bq kg $^{-1}$ at a depth of 21.48 g cm^{-2} (37 cm), below which it is less than 1 Bq kg^{-1} to the bottom of the core. Assuming the maximum discharge of ^{137}Cs from Sellafield reached Loch Fyne in 1976, and taking the depth at which the maximum concentration of ^{137}Cs occurs to be 2.56 g cm^{-2}, a sedimentation rate of 0.214 g cm^{-2} y^{-1} is obtained for core FS. This sedimentation rate is very different from that obtained from the ^{210}Pb profile of 0.008 g cm^{-2} y^{-1}. The abrupt change in sediment type, the irregular ^{210}Pb profile and the discrepancy between ^{137}Cs and ^{210}Pb chronologies suggest that some change has been induced in the loch or its catchment, resulting in a change from a negligible rate of accumulation of fine sediment to a more recent increase in deposition of a coarse type of sediment. The radionuclide data indicate an increasing sedimentation rate towards the top of the core and it is not possible to derive a consistent chronology between the ^{210}Pb and the ^{137}Cs. Under these circumstances, the ^{137}Cs chronology was taken to represent recent deposition and is used in interpretation of the heavy metal profiles. However, as discussed above the chronology is open to errors especially below the depth of 19.29 g cm^{-2} (33 cm) where the major change in sediment type occurred, at a date of 1900 on the basis of the ^{137}Cs chronology. The sedimentation rate for FS estimated from the total depth of

penetration of ^{137}Cs is 0.614 g cm^{-2} y^{-1} which is far higher than that calculated from the position of the maximum concentration of ^{137}Cs, indicating that there has been downwards mixing and probably diffusion of ^{137}Cs in this core. The ^{137}Cs sedimentation rate of 0.214 g cm^{-2} y^{-1} would give a depth of penetration of ^{137}Cs of 7.14 g cm^{-2} (assuming the first waste discharge from Sellafield in 1952 reached Loch Fyne one year later in 1953) and a mixing depth of 2.27 g cm^{-2} is assumed this would give a maximum depth of penetration of ^{137}Cs of 9.41 g cm^{-2}. ^{137}Cs was detected to a depth of 21.48 g cm^{-2} which suggests a diffusion depth of 12.07 g cm^{-2} for this core, which is lower than the value obtained for LL1 (15.17 g cm^{-2}) and higher than for GD2 (9.04 g cm^{-2}) and the range of 5.9 to 10.74 g cm^{-2} for the Loch Etive cores.

The inventory of ^{137}Cs in FS is 14300 $\pm$ 300 Bq m^{-2} which is less than half that of core LL1 (39000 $\pm$ 1500 Bq m^{-2}) and considerably lower than core GD2 (21100 $\pm$ 500 Bq m^{-2}). However, as with the other cores from the Clyde Sea Area, the ^{137}Cs inventory for core FS is higher than any of the three cores from Loch Etive (7500 to 10100 Bq m^{-2}). As discussed in section 4.7.1. the sediment above 19.29 g cm^{-2} (33 cm) depth consists of a coarser material and this may have an influence in the ^{137}Cs inventory, as it is well established that ^{137}Cs has a higher affinity for clay particles and a lower uptake on coarser grain particles. The low ^{137}Cs inventory may also reflect a greater amount of dilution in the water column due to influence of the Atlantic water but, unfortunately, it was not possible to obtain salinity data for the Clyde Sea Area stations, and therefore it is not possible to confirm this.

The $^{134}Cs/^{137}Cs$ ratio has a value of 0.044 at the surface, below which it decreases rapidly to 0.013 at a depth of 0.6 g cm^{-2} (1.5 cm) and then increases to 0.024 at 1.59 g cm^{-2} (3.5 cm). Below this depth the $^{134}Cs/^{137}Cs$ values are within the range 0.005 to 0.009 to a depth of 4.12 g cm^{-2} (7.5 cm) after which ^{134}Cs is not detectable with the exception of one point at 6.74 g cm^{-2} (11 cm) which has a $^{134}Cs/^{137}Cs$ ratio value of 0.008. The depth of penetration of the ^{134}Cs as indicated by the $^{134}Cs/^{137}Cs$ profile is considered to be due to the combined effects of diffusion and mixing. The expected $^{134}Cs/^{137}Cs$ ratio from the Sellafield discharge that would have reached the

Clyde Sea Area by 1988 would be 0.074 (Table 4.12.) which is considerably higher than the $^{134}Cs/^{137}Cs$ ratio found for the surface sediment of core FS suggesting significant mixing of the sediment. The $^{134}Cs/^{137}Cs$ ratio at the surface suggests that this core has an insignificant Chernobyl input ($^{134}Cs/^{137}Cs$ ratio decay corrected to 1988 = 0.28).

^{241}Am concentrations increase from a surface value of 4.2 Bq kg^{-1} to a maximum of 5.1 Bq kg^{-1} at a depth of 2.27 g cm^{-2} (4.5 cm) and then decrease to 3.6 Bq kg^{-1} at 3.46 g cm^{-2} (6.5 cm), below which ^{241}Am is not detectable. The two maximum discharges of ^{241}Pu occurred in 1973 and 1978 and would have reached Loch Fyne in 1974 and 1979 respectively (see section 4.6.3.). These dates correspond to depths of 2.86 and 2.27 g cm^{-2} (5.5 and 4.5 cm) respectively. The ^{241}Am profile has a maximum at 2.27 g cm^{-2} (4.5 cm) which is equivalent to the time of the expected 1979 maximum discharge but the 1974 maximum is not apparent at 2.86 g cm^{-2} (5.5 cm) which may be due to mixing within the sediment. An alternative argument would be to assume that the two maxima present in the ^{241}Am profile at 0.6 and 2.27 g cm^{-2} represent the discharges of 1978 and 1973 (reaching the loch in 1979 and 1974) and this gives sedimentation rates of 0.07 and 0.162 g cm^{-2} suggesting that the sedimentation rate more than halved over 5 years which is contrary to previous indications of an increasing sedimentation rate towards the surface. As detailed in sections 4.2.3. and 4.6.3., the ratio of the cumulative environmental inventory of ^{137}Cs to that of the ^{241}Am grown in from the decay of $^{241}Pú$ from the Sellafield discharge can be estimated to be approximately 884 for areas outwith the Irish Sea. The ratio of the inventories of ^{137}Cs and ^{241}Am for core FS has a value of 94 which is higher than the $^{137}Cs/^{241}Am$ inventory ratio for cores LL1, LE 1 and LE 2 which were all approximately 75 and lower than GD2 which had a $^{137}Cs/^{241}Am$ inventory ratio of 111. Once again, the results suggest that the uptake of ^{241}Pu is a factor of 10 times greater than that of ^{137}Cs in these sediments or that there has been a substantial degree of re-dissolution of ^{137}Cs or that the assumptions of Cs and Pu retention in the Irish Sea are erroneous.

Having obtained a chronology for core FS from the calculated ^{137}Cs

sedimentation rate (assuming a linear accumulation) it is possible to date some of the horizons occurring in the element/Al ratios for this core (Figure 4.32). However as discussed before the ^{137}Cs chronology is probably over estimating the sedimentation rate and hence under estimating the age of the core, certainly below 19.29 g cm^{-2} (33 cm) but that the ^{137}Cs chronology is probably the best indicator of recent sedimentation processes. The major change in the Si/Al, Zr/Al and Ti/Al takes place at a depth of 19.3 g cm^{-2} which corresponds to a date of 1900. The two maxima of the Ca/Al profile occur at depths of 4.12 and 9.18 g cm^{-2} which correspond to 1970 and 1948 respectively. There is also a change in the Ca/Al profile occurring at a depth of 18.3 g cm^{-2} which corresponds to 1905. This is also the depth at which the P/Al ratio begins to increase. If mixing is assumed to be to a depth of 2.27 g cm^{-2} (4.5 cm), then the bottom of the mixed layer depth occurs at 1977, corresponding to approximately 11 years of accumulation.

4.7.4 *^{228}Th and ^{228} Ra profiles for core FS*

The $^{228}Th/^{228}Ra$ profile for core FS is shown in Figure 4.34. The ratio has a value of 1 in the surface sediment and remains within error of unity throughout the core with the exception of a few points. The inventories for ^{228}Th and ^{228}Ra are 11200 $\pm$ 600 Bq m^{-2} and 10700 $\pm$ 500 Bq m^{-2} respectively indicating that ^{228}Th and ^{228}Ra are in secular equilibrium with ^{232}Th in this core but ^{232}Th data are not available to confirm this.

4.7.5 *Stable Pb and Pb isotope ratios of core FS*

The total stable Pb concentration data are presented in Chapter 3 and the plot of the total Pb concentration versus cumulative weight (g cm^{-2}) is shown in Figure 4.35.A. The Pb concentration is 42 mg kg^{-1} at a depth of 0.6 g cm^{-2} (1.5 cm) and increases to a maximum of 47 mg kg^{-1} at 2.86 g cm^{-2} (5.5 cm). The concentration then decreases to 20 mg kg^{-1} at 10.5 g cm^{-2} (17 cm) and remains approximately at this value to 12.87 g cm^{-2} (21 cm) after which it decreases to 18 mg kg^{-1} at a depth of 13.9 g cm^{-2} (23 cm) and then remains within the concentration range 15 to 18 mg kg^{-1} to the bottom of the core.

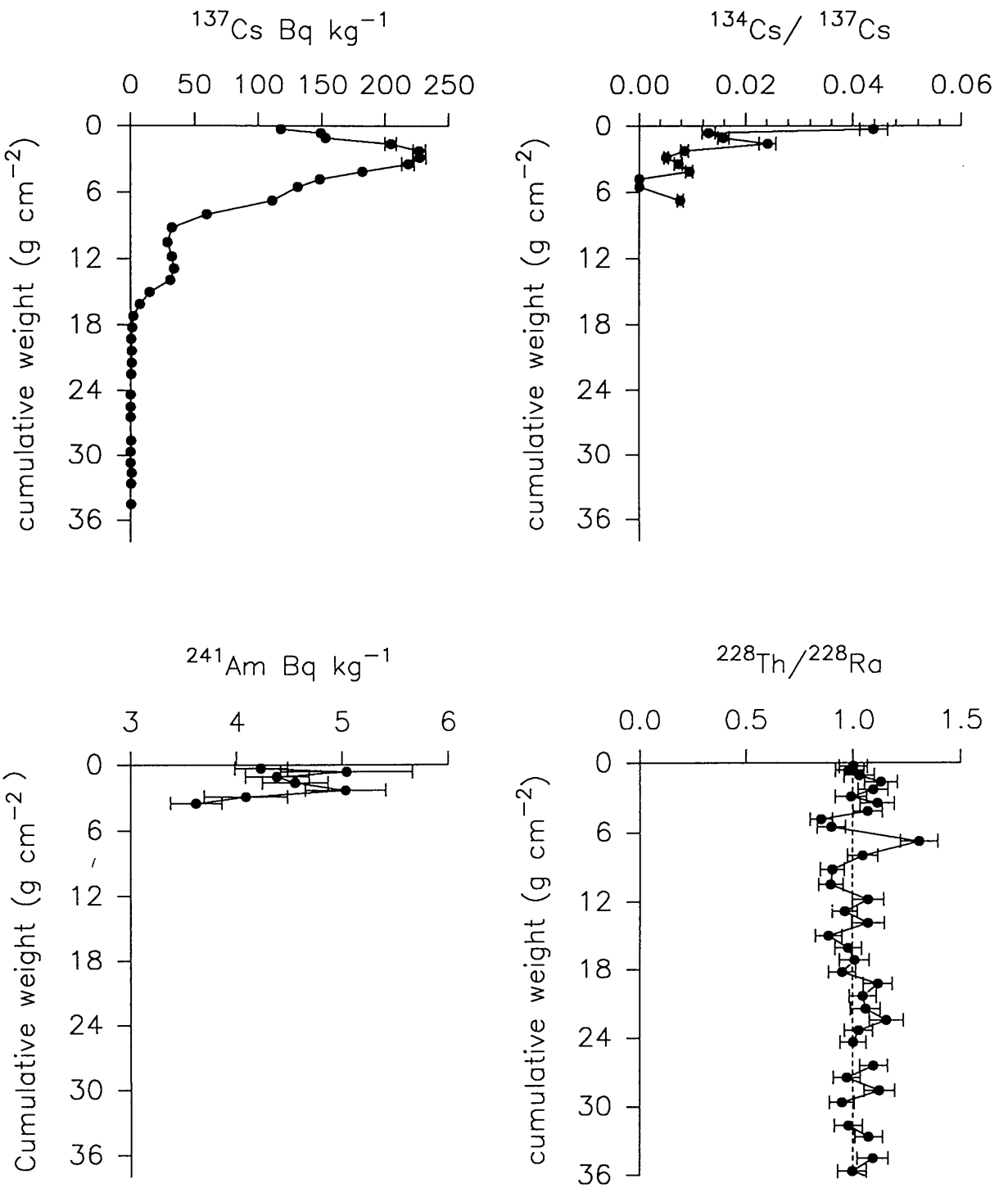

Figure 4.34. Loch Fyne core FS radionuclide concentrations and activity ratios

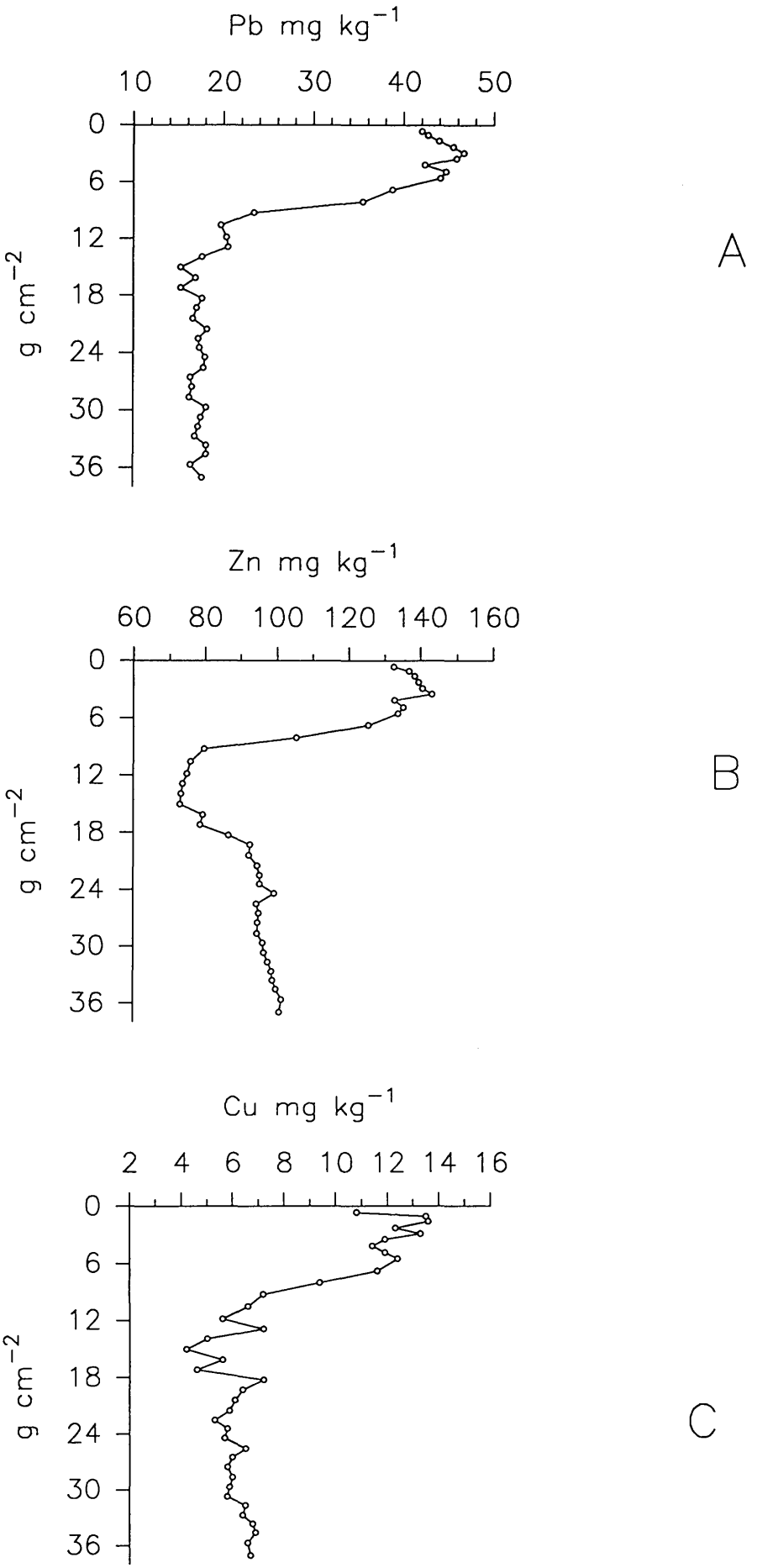

Figure 4.35. Loch Fyne core FS Pb, Zn and Cu concentrations (mg kg^{-1})

The maximum concentration of Pb in this core is 40 mg kg^{-1} which is far lower than even the minimum concentrations observed in cores LL1 (125 mg kg^{-1}) and GD2 (78 mg kg^{-1}). The cores from Loch Etive had maximum concentrations within the range 60 to 98 mg kg^{-1}, with LE 2 having a maximum concentration of 60 mg kg^{-1}, which is still higher than that of core FS. The mean Pb concentration for core FS over the depth range 13.9 to 37 g cm^{-2} (23 to 67 cm) was 17 mg kg^{-1} and this was considered to be representative of natural Pb concentration of this sediment. However, as the bottom of the core corresponds to a date of 1829 on the basis of the ^{137}Cs chronology and(taking account of mixing) the value of 17 mg kg^{-1} may reflect early industrial pollution and calculated excess Pb values therefore represent a lower limit. It is obvious from the Pb concentration profile that the sediment of core FS from Loch Fyne is not heavily polluted with respect to Pb, as are the other cores from the Clyde Sea Area, from Loch Long and Loch Goil. The low values of pollutant Pb concentrations in core FS illustrate the highly restricted nature of the pollution in Loch Long and Loch Goil and suggest that a major component of the pollutant Pb in the Loch Long and Loch Goil sediments is being supplied by either solution or particulate transport within the eastern branch of the Clyde Sea Area rather than atmospheric deposition which would also have affected Loch Fyne. The results from core FS also suggests that the coarser sediments from Loch Fyne have a low efficiency for uptake of Pb. The maximum Pb concentration occurs at a depth of 2.86 g cm^{-2} (5.5 cm) corresponding to a date of 1976, which is later than the maximum Pb concentrations found in core LL1 (early 1960's) and core GD2 (1936), but in good agreement with the dates corresponding to the maximum Pb concentration in the Loch Etive cores (1973-1979). Thus, the maximum Pb concentrations for the more remote locations in Loch Etive and Loch Fyne occur at similar times consistent with a dominantly atmospheric source of Pb, with peak deposition occurring at the same time.

The flux of pollutant Pb versus time (on the basis of the ^{137}Cs chronology) for core FS is shown in Figure 4.36.A. The excess Pb results are given in Table 4.19.

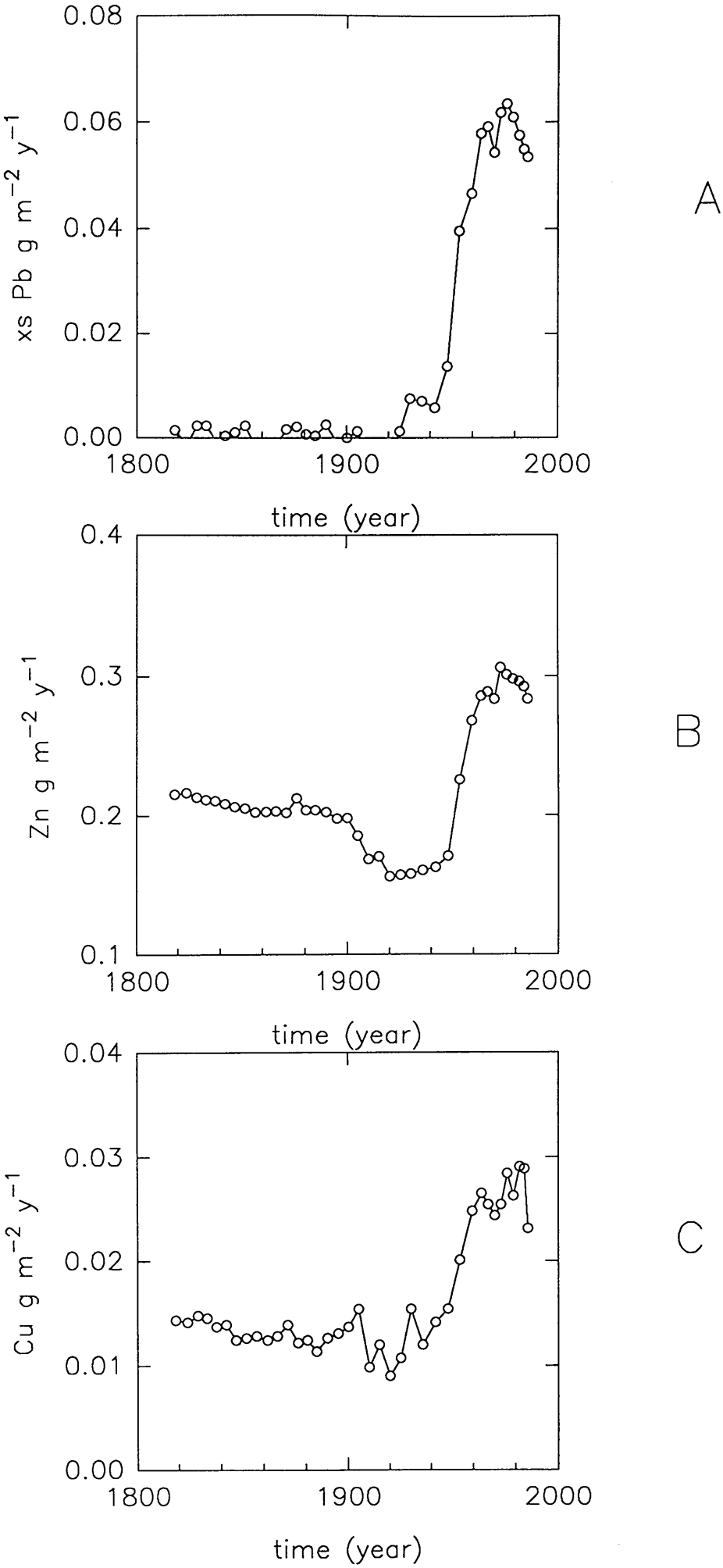

Figure 4.36 Loch Fyne core FS Pb, Zn and Cu flux data

SAMPLE	DEPTH (cm)	cum g cm^{-2}	date for mid section	excess Pb g m^{-2} y^{-1}
FS 0-1	0.5	0.28	1987	
FS 1-2	1.5	0.60	1986	0.054
FS 2-3	2.5	1.05	1984	0.055
FS 3-4	3.5	1.59	1982	0.058
FS 4-5	4.5	2.27	1979	0.061
FS 5-6	5.5	2.86	1976	0.064
FS 6-7	6.5	3.46	1973	0.062
FS 7-8	7.5	4.12	1970	0.054
FS 8-9	8.5	4.84	1967	0.059
FS 9-10	9.5	5.50	1984	0.058
FS 10-12	11.0	6.74	1959	0.047
FS 12-14	13.0	7.99	1954	0.040
FS 14-16	15.0	9.18	1948	0.014
FS 16-18	17.0	10.50	1942	0.006
FS 18-20	19.0	11.80	1936	0.007
FS 20-22	21.0	12.87	1930	0.007
FS 22-24	23.0	13.90	1926	0.001
FS 24-26	25.0	15.02	1920	-0.004
FS 26-28	27.0	16.11	1915	0.000
FS 28-30	29.0	17.17	1910	-0.004
FS 30-32	31.0	18.26	1905	0.001
FS 32-34	33.0	19.29	1900	0.000
FS 34-36	35.0	20.38	1895	-0.001
FS 36-38	37.0	21.48	1890	0.003
FS 38-40	39.0	22.49	1885	0.000
FS 40-42	41.0	23.38	1881	0.001
FS 42-44	43.0	24.39	1876	0.002
FS 44-46	45.0	25.49	1871	0.002
FS 46-48	47.0	26.46	1867	-0.001
FS 48-50	49.0	27.51	1862	-0.001
FS 50-52	51.0	28.62	1857	-0.002
FS 52-54	53.0	29.65	1852	0.002
FS 54-56	55.0	30.69	1847	0.001
FS 56-58	57.0	31.66	1842	0.000
FS 58-60	59.0	32.65	1838	0.000
FS 60-62	61.0	33.60	1833	0.002
FS 62-64	63.0	34.53	1829	0.002
FS 64-66	65.0	35.65	1824	-0.001
FS 66-68	67.0	36.97	1818	0.001

Table 4.19 Loch Fyne core FS excess Pb flux data

Excess Pb is first detected in 1818 which corresponds to 1829 taking into

account 11 years of mixing. However the flux is very low at 0.001 g m^{-2} y^{-1} and it is obvious from the negative results at various depths between 15.02 to 35.65 g cm^{-2} (25 to 65 cm) that the flux is very close to zero over this depth range. The first flux greater than 0.001 g m^{-2} y^{-1} occurs at a depth of 12.87 g cm^{-2} (21 cm) and corresponds to a date of 1920, or 1931, allowing for mixing, which is considerably later than any of the other cores analysed. The rise in flux is very sharp and the maximum value of 0.064 g $m^{-2}y^{-1}$ is reached by 1976 which correlates well with the dates of maximum fluxes in cores LE 1 (0.063 g m^{-2} y^{-1}, 1977), LE 2 (0.025 g m^{-2} y^{-1}, 1973) and LE 3 (0.052 g m^{-2} y^{-1}, 1972), but is somewhat later than the two previous cores from the Clyde Sea Area, LL1 and GD2 which have maximum fluxes of excess Pb in 1967 and 1945 respectively. The inventory of excess Pb for this core is 2.3 g m^{-2} which is far less than those for cores LL1 (68.3 g m^{-2}) and GD2 (43.9 g m^{-2}), but similar to those for cores LE 1 and LE 3 (both 3.8 g m^{-2}) and LE 2 (1.6 g m^{-2}). The Pb data thus show that the sediment of Loch Fyne has not been subjected to the high degree of pollution that affected cores LL1 and GD2 but has experienced a similar degree of pollution to Loch Etive, Loch Lomond, (Sugden, 1993) and the Flanders Moss peat bog (Sugden, 1993).

The plot of $^{206}Pb/^{207}Pb$ ratio versus ^{137}Cs chronology for core FS is shown in Figure 4.37., along with the excess Pb flux (g $m^{-2}y^{-1}$). The errors on the $^{206}Pb/^{207}Pb$ ratios for this core are higher than in the other cores from the Clyde Sea Area, reflecting the much lower concentration of Pb in this core, and interpretation of the data must therefore be carried out with care. The surface sediment has a $^{206}Pb/^{207}Pb$ ratio of 1.162 which is the highest of all the cores studied so far. The ratio remains within error the same to a depth of 2.27 g cm^{-2} (4.5 cm) and then decreases to a value of 1.146 at 3.46 g cm^{-2} (6.5 cm) depth. The ratio then increases with depth to 1.199 and remains within error of this value to 26.5 g cm^{-2} (47 cm). Finally the ratio decreases to 1.184 and remains within error of this value to the bottom of the core. The constant $^{206}Pb/^{207}Pb$ ratio from the surface to a depth of 2.27 g cm^{-2} (4.5 cm) suggests that there is mixing to this depth. Below the mixed layer, the ratio has a value of 1.146 (3.46 g cm^{-2}, 6.5 cm) and the higher ratio at the surface

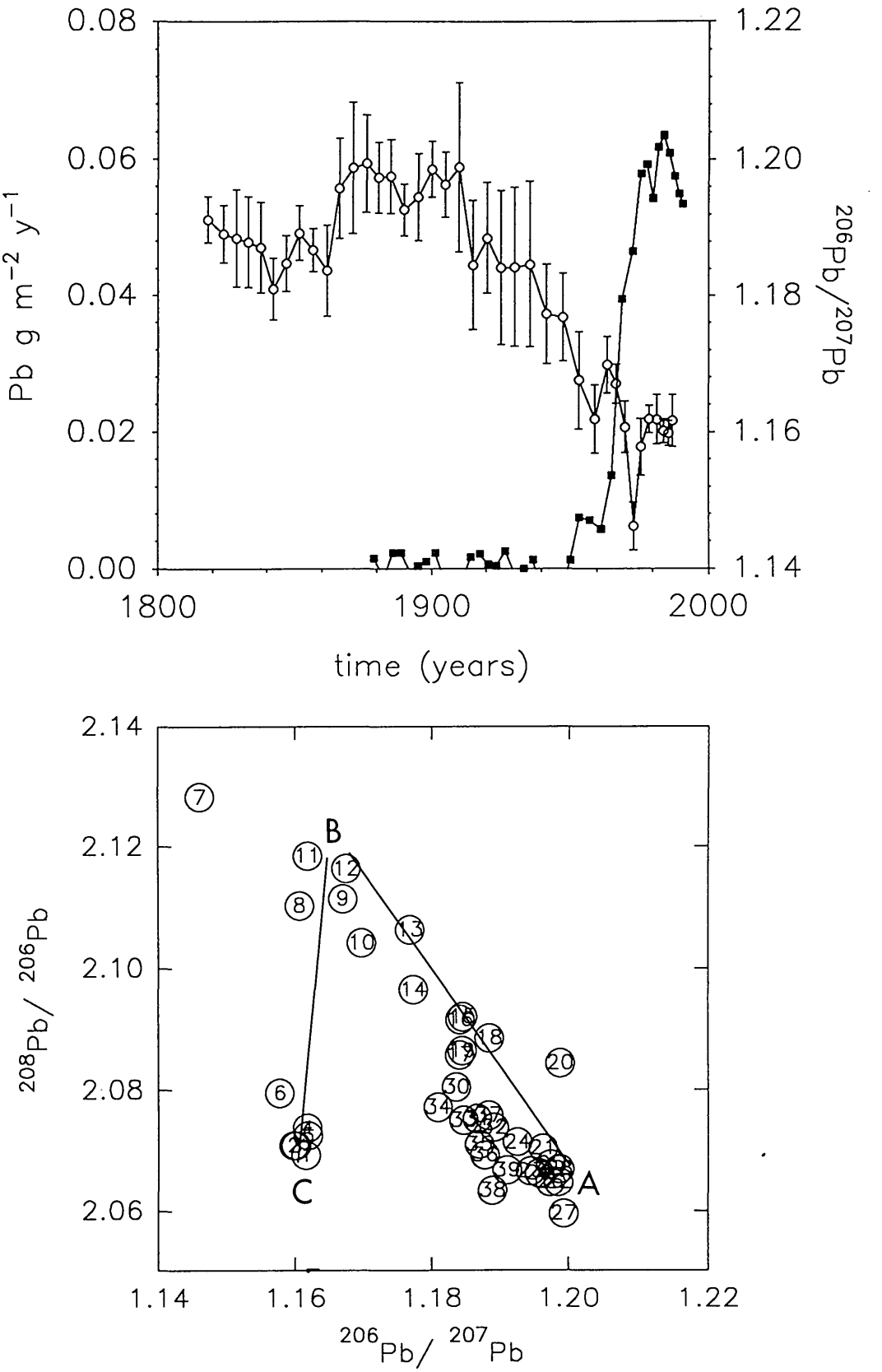

Figure 4.37. Loch Fyne core FS Pb flux and Pb isotope ratio plots

may reflect a decrease in the input of petrol derived Pb to the sediment due to the recent introduction of unleaded petrol. As discussed in section 4.2.5., the decreasing $^{206}Pb/^{207}Pb$ ratio towards the surface of the sediment can be attributed to the increasing influence of vehicle exhaust emissions on pollutant Pb fluxes to the sediment during this century. The onset of the change in $^{206}Pb/^{207}Pb$ ratio occurs at 11.8 g cm^{-2} (19 cm) which corresponds to 1936 or, 1947 allowing for mixing. This is later than expected, as is the apparent increase in Pb flux, probably indicating that the ^{137}Cs sedimentation rate is too high to apply over this length of the core.

Calculation of the percentage Pb due to petrol was carried out as described in 4.2.5. with R_i= 1.187 and R_{Hi}= 1.172 and the results are given in Table 4.20. The results from the calculation of percentage Pb in the sediment due to the input of pollutant Pb from petrol indicate that the onset of deposition of Pb from petrol occurs at 1936 (1%) which, allowing for mixing becomes 1947, but this chronology is subject to doubt as discussed above. The calculated percentage of Pb from petrol is very irregular with a maximum of 60% occurring in 1973. This high value for the % petrol Pb contribution reflects the fact that there is very little heavy industry pollution in core FS compared to the other cores analyses.

The residual excess Pb inventory for this core (i.e. excess Pb inventory -Pb from petrol) is 1.6 g m^{-2}. As with previous cores the ratios of the inventories of excess ^{210}Pb, excess Pb and residual excess Pb of cores LL1, GD2 and FS can be compared, as follows

$LL1_{210}/FS_{210}$= 2.5, $GD2_{210}/FS_{210}$= 2.2, $LL1_{xsPb}/FS_{xsPb}$=29.7, $GD2_{xsPb}/FS_{xsPb}$= 19.1, $LL1_{res\text{-}Pb}/FS_{res\text{-}Pb}$= 37.9, $GD2_{res\text{-}Pb}/FS_{res\text{-}Pb}$= 23.7.

Therefore the above ratios illustrate numerically that the ^{210}Pb inventories for LL1 and GD2 are more than twice that of FS and that LL1 and GD2 have experienced far greater non petrol Pb pollution than core FS.

SAMPLE	DEPTH (cm)	cum g cm^{-2}	Cs date for mid section	% Pb from petrol
FS 0-1	0.5	0.28	1987	34
FS 1-2	1.5	0.60	1986	37
FS 2-3	2.5	1.05	1984	36
FS 3-4	3.5	1.59	1982	32
FS 4-5	4.5	2.27	1979	30
FS 5-6	5.5	2.86	1976	37
FS 6-7	6.5	3.46	1973	61
FS 7-8	7.5	4.12	1970	36
FS 8-9	8.5	4.84	1967	21
FS 9-10	9.5	5.50	1984	16
FS 10-12	11.0	6.74	1959	36
FS 12-14	13.0	7.99	1954	27
FS 14-16	15.0	9.18	1948	29
FS 16-18	17.0	10.50	1942	60
FS 18-20	19.0	11.80	1936	1
FS 20-22	21.0	12.87	1930	
FS 22-24	23.0	13.90	1926	
FS 24-26	25.0	15.02	1920	
FS 26-28	27.0	16.11	1915	
FS 28-30	29.0	17.17	1910	
FS 30-32	31.0	18.26	1905	
FS 32-34	33.0	19.29	1900	
FS 34-36	35.0	20.38	1895	
FS 36-38	37.0	21.48	1890	
FS 38-40	39.0	22.49	1885	
FS 40-42	41.0	23.38	1881	
FS 42-44	43.0	24.39	1876	
FS 44-46	45.0	25.49	1871	
FS 46-48	47.0	26.46	1867	
FS 48-50	49.0	27.51	1862	
FS 50-52	51.0	28.62	1857	
FS 52-54	53.0	29.65	1852	
FS 54-56	55.0	30.69	1847	
FS 56-58	57.0	31.66	1842	
FS 58-60	59.0	32.65	1838	
FS 60-62	61.0	33.60	1833	
FS 62-64	63.0	34.53	1829	
FS 64-66	65.0	35.65	1824	
FS 66-68	67.0	36.97	1818	

Table 4.20 % Pb in sediment from Pb in Pb for core FS

The $^{208}Pb/^{206}Pb$ versus $^{206}Pb/^{207}Pb$ plot for core FS is shown in Figure 4.37. The samples are numbered 1 to 39 according to increasing depth. The diagram indicates a three component system: A (natural Pb component), B (heavy industry Pb) and C (petrol Pb) with tie lines joining the end members. Samples 39 to 29 form one group (A), which represents the natural Pb and/or very early pollution. The tie line A→B indicates the increasing effects of Pb from petrol, with tie line B→C indicating that there has been a recent decrease in the $^{208}Pb/^{206}Pb$ ratio. Thus, both core GD2 from Loch Goil and FS from Loch Fyne exhibit a recent decrease in the $^{208}Pb/^{206}Pb$ ratio and the onset of change occurs at 1973 in Loch Goil (GD2) and 1976 in core FS. The fact that the change in the $^{208}Pb/^{206}Pb$ ratio is reflected in the core from Loch Fyne which is obviously not affected by the highly polluted sediment from dredge spoil and sewage dumping suggests that the change in the ratio has come from either a solution pathway or from atmospheric deposition. Thus, although it is difficult to derive a chronology for this core, the trends in the Pb concentration and isotope ratios are consistent with those observed elsewhere and the results reveal a relatively low level of Pb contamination at this location.

4.7.6 *Zn and Cu profiles of core FS*

The total Zn and Cu concentration profiles for core FS are shown in Figure 4.35.B. and 4.35.C. respectively. The Zn profile has a concentration of 133 mg kg^{-1} at 0.6 g cm^{-2} (1.5 cm) and increases to a maximum of 143 mg kg^{-1} at 3.46 g cm^{-2} (6.5 cm) which corresponds to a date of 1973. The Zn concentration then decreases rapidly to a value of 80 mg kg^{-1} at 9.18 g cm^{-2} (15 cm) below which it decreases to a concentration of 73 mg kg^{-1} at 15.02 g cm^{-2} (25 cm) depth. This decrease in Zn concentration has not been seen in the other cores and possibly reflects the major change in sediment type, to coarser grain size, that occurs within core FS. Below 15.02 g cm^{-2} (25 cm), the concentration increases to a value of 101 mg kg^{-1} at the bottom of the core (37 g cm^{-2}, 67 cm). The Zn concentrations for core FS are lower than those of core LL1 and are an order of magnitude lower than those of GD2.

SAMPLE	DEPTH	cum g cm^{-2}	date for mid section	Cu g m^{-2} y^{-1}	Zn g m^{-2} y^{-1}
FS 0-1	0.5	0.28	1987		
FS 1-2	1.5	0.60	1986	0.023	0.284
FS 2-3	2.5	1.05	1984	0.029	0.293
FS 3-4	3.5	1.59	1982	0.029	0.296
FS 4-5	4.5	2.27	1979	0.026	0.298
FS 5-6	5.5	2.86	1976	0.028	0.301
FS 6-7	6.5	3.46	1973	0.025	0.306
FS 7-8	7.5	4.12	1970	0.024	0.284
FS 8-9	8.5	4.84	1967	0.025	0.289
FS 9-10	9.5	5.50	1984	0.027	0.286
FS 10-12	11.0	6.74	1959	0.025	0.268
FS 12-14	13.0	7.99	1954	0.020	0.226
FS 14-16	15.0	9.18	1948	0.015	0.170
FS 16-18	17.0	10.50	1942	0.014	0.162
FS 18-20	19.0	11.80	1936	0.012	0.160
FS 20-22	21.0	12.87	1930	0.015	0.158
FS 22-24	23.0	13.90	1926	0.011	0.157
FS 24-26	25.0	15.02	1920	0.009	0.156
FS 26-28	27.0	16.11	1915	0.012	0.170
FS 28-30	29.0	17.17	1910	0.010	0.168
FS 30-32	31.0	18.26	1905	0.015	0.185
FS 32-34	33.0	19.29	1900	0.014	0.198
FS 34-36	35.0	20.38	1895	0.013	0.198
FS 36-38	37.0	21.48	1890	0.013	0.202
FS 38-40	39.0	22.49	1885	0.011	0.204
FS 40-42	41.0	23.38	1881	0.012	0.204
FS 42-44	43.0	24.39	1876	0.012	0.213
FS 44-46	45.0	25.49	1871	0.014	0.202
FS 46-48	47.0	26.46	1867	0.013	0.203
FS 48-50	49.0	27.51	1862	0.012	0.203
FS 50-52	51.0	28.62	1857	0.013	0.202
FS 52-54	53.0	29.65	1852	0.013	0.205
FS 54-56	55.0	30.69	1847	0.012	0.206
FS 56-58	57.0	31.66	1842	0.014	0.209
FS 58-60	59.0	32.65	1838	0.014	0.211
FS 60-62	61.0	33.60	1833	0.015	0.212
FS 62-64	63.0	34.53	1829	0.015	0.213
FS 64-66	65.0	35.65	1824	0.014	0.217
FS 66-68	67.0	36.97	1818	0.014	0.215

Table 4.21 Cu and Zn fluxes for Loch Fyne core FS

The Cu profile follows the same trends as the Zn profile, with a value of 11 mg kg^{-1} at 0.6 g cm^{-2} (1.5 cm) and an increase to a maximum of 14 mg kg^{-1} at 1.59 g cm^{-2} (3.5 cm). Below this depth the concentration decreases irregularly to a value of 7 mg kg^{-1} at the bottom of the core.

The fluxes of total Zn and total Cu are given in Figures 4.36.B and 4.36.C. respectively, with the results being presented in Table 4.21. The fluxes are similar to those of LE 1, higher than LE 2 and LE 3 and considerably lower than LL1 and GD2. The profiles of excess Pb, total Zn and total Cu all have the same general trend from 1920 onwards. The Zn and Cu fluxes decrease between 1920 and 1948 which, after considering mixing, correspond to 1931 to 1959. The Zn profile has a flux of 0.215 g m^{-2} y^{-1} at the bottom of the core which corresponds to 1829 when taking the effects of mixing into consideration and has a maximum flux of 0.306 g m^{-2} y^{-1} which corresponds to 1973. After that, the flux decreases to a value of 0.284 in the mid 1980's.

The Cu flux for core FS is 0.014 g m^{-2} y^{-1} in 1829, increases to a maximum flux of 0.29 g m^{-2} y^{-1} in 1984 and then decreases to 0.023 g m^{-2} y^{-1} by 1986. The maximum flux of Cu is seen approximately 10 years later than the Pb and Zn maximum fluxes which is probably due to the irregularity of the profile and the relatively large error associated with the analysis of the low concentrations of Cu in this sediment. The inventories for total Zn and Cu for core FS are 36.4 and 2.7 g m^{-2} respectively which are lower than the Zn and Cu inventories for LL1 and GD2 (66.8 and 7.8 g m^{-2} and 87.3 and 12.6 g m^{-2} respectively) but higher than those for Loch Etive (Zn inventories in the range 18.7 to 21.1 g m^{-2} and Cu inventories in the range 1.2 to 1.4 g m^{-2}). The excess Zn and Cu inventories for core FS are 4.3 and 0.5 g cm^{-2} respectively which are considerably lower than cores LL1 (62.6 and 7.6 g cm^{-2}) and GD2 (52.5 and 4.5 g cm^{-2}) and similar to the Loch Etive cores which were within the range 3.4 to 8.1 g cm^{-2} for excess Zn and 0.4 to 0.6 g cm^{-2} for excess Cu. Therefore the excess Zn and Cu inventories for core FS reflect the unpolluted nature of Loch Fyne relative to cores from Loch Long and Loch Goil.

4.7.7 *Summary of core FS*

In summary, the results from core FS indicate that the sedimentation rate increased towards the surface and that ^{210}Pb dating could not be applied to give a useful chronology. However, by equating the maximum ^{137}Cs concentration to the maximum Sellafield discharge and assuming a 1 year transit time, it was possible to obtain a sedimentation rate of 0.214 g cm^{-2} y^{-1} for the section of sediment with the higher accumulation rate above a depth of about 19 g cm^{-2}. Since the sedimentation rate had increased towards the surface, it was recognised that there are doubts about the validity of applying this single value over an extended depth range. The depth of mixing could not be obtained from the ^{210}Pb profile but the ^{137}Cs and $^{134}Cs/^{137}Cs$ profiles indicated that mixing was taking place and an upper limit mixed layer depth of 2.27 g cm^{-2}, (equivalent to approximately 11 years of accumulation) was suggested by the $^{206}Pb/^{207}Pb$ profile. The chronology obtained from the ^{137}Cs sedimentation rate agreed well with the ^{241}Am profile and reasonably well with the heavy metal and Pb isotope profiles.

The manmade radionuclides present are dominated by the Sellafield discharge and for this core (as in the case of LL1) it was not possible to detect any significant Chernobyl input. The ^{137}Cs profile indicated mobility of Cs by means of mixing and diffusion and ^{137}Cs was detectable to far greater depths than would be expected due to mixing alone which limits its use in dating.

The deposition of pollutant Pb increased dramatically from the late 1940's which is later than the other cores studied and this could be a result of either an over estimated accumulation rate, resulting in an incorrect chronology being applied, or due to an increased amount of Pb from petrol in the atmosphere. From the excess Pb inventories and fluxes it is apparent that Loch Fyne is not as heavily polluted as the other cores from the Clyde Sea Area and that the pollution from heavy industry is very much a local input which is not reflected in the sediments of Loch Fyne.

4.8 *Loch Fyne core FD*

The sample site and sampling and analytical methods for core FD are described in Chapter 2. The results for this core are tabulated in Chapter 3. Core FD, from the deepest part of the inner basin of Loch Fyne, contained a great number of manganese nodules, mainly in the upper 7.68 g cm^{-2} of the sediment. At the time of sample processing the nodules were removed for separate analysis which is not, as yet, complete. The following discussion of this core therefore relates only to the sediment after removal of the nodules and this restricts the interpretation of the data.

Although the nodules from core FD have not yet been analysed, nodules from a bulk sample obtained from the same vicinity as core FD have been analysed and the results are tabulated in Chapter 3 (Table 3.46.). The nodules varied in size from < 1 mm to >15 mm in diameter and were separated into five size classes for analysis. The five size fractions were as follows; A = ≤0.7 mm; B = 0.7 - 2 mm; C = 2-4 mm; D = 4-10 mm and E = 10-15 mm.

4.8.1 *Geochemical characteristics of core FD*

The selected element/Al ratios and K/Rb ratio for core FD are shown in Figure 4.38. The Si/Al, Zr/Al and Ti/Al ratios all increase towards the surface indicating that coarser material has been deposited in more recent times. All three ratios have surface maxima, with the Si/Al surface value of 6.13 being far higher than any of the previous cores studied. The Si/Al, Zr/Al and Ti/Al ratios all have pronounced minima at 2.08 g cm^{-2} (6.5 cm) and subsurface peaks at 5.81 g cm^{-2} (14.5 cm). The Ca/Al ratio is 0.46 at 0.42 g cm^{-2} (1.5 cm) and fluctuates around this value to a depth of 2.54 g cm^{-2} (7.5 cm), after which it increases rapidly to two maxima of 0.94 and 1.01 occurring at 5.81 and 7.09 g cm^{-2} (14.5 and 16.5 cm) respectively. The ratio then decreases to 0.46 at 9.82 g cm^{-2} (21.0 cm), after which it increases to 0.67 at 12.22 g cm^{-2} (25 cm) and finally decreases to a value of 0.4 at the bottom of the core. There are, therefore two bands of increased Ca/Al ratio, the major band

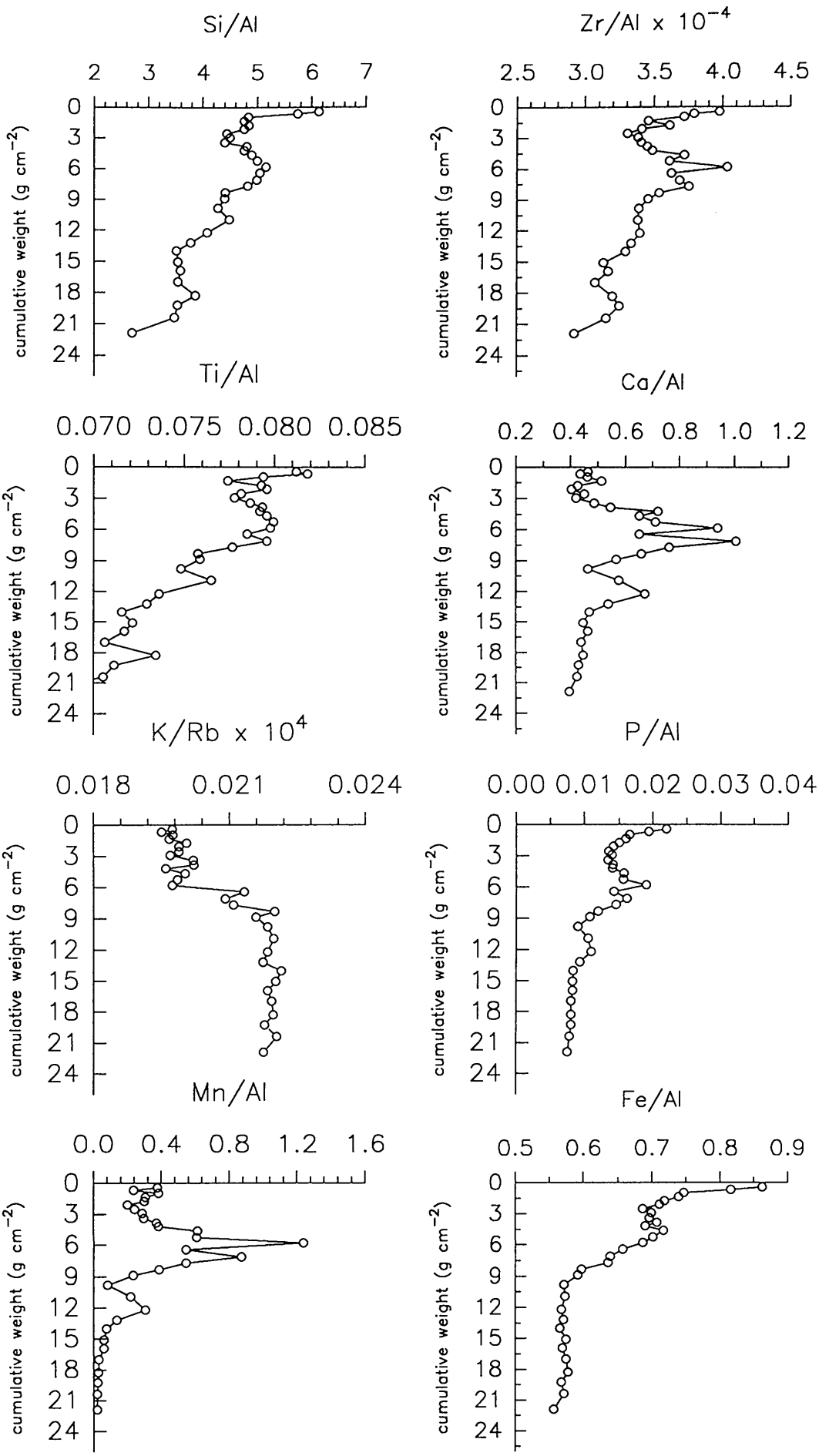

Figure 4.38. Loch Fyne core FD elemental/Al and K/Rb ratios

occurring from 2.54 g cm^{-2} to 9.82 g cm^{-2} (7.5 cm to 21.0 cm) and a minor band from 9.82 g cm^{-2} to 14.02 g cm^{-2} (21.0 cm to 29 cm), which could be taken to indicate the presence of shell bands. However, Calvert and Price (1970) analysed concretionary manganese carbonate from Loch Fyne and found the major components to be Ca (~13%), Mn (~19%) and CO_2 (~31%) and in view of the similarity of the Ca/Al and Mn/Al profiles, it is likely that the peaks in the Ca/Al ratio profile reflect the formation of this material. The K/Rb ratio has a value of 197 at 0.42 g cm^{-2} (1.5 cm) depth and remains within the range 195 to 202 to a depth of 5.81 g cm^{-2} (14.5 cm) after which it increases sharply to 213 at 6.42 g cm^{-2} (15.5 cm). The ratio reaches a maximum of 220 at 8.33 g cm^{-2}(18.5 cm) and remains around this value to the bottom of the core. The K/Rb ratio thus indicates that a change in sediment type took place at a depth of 5.81 g cm^{-2} (14.5 cm) which coincides with maxima that occur in the Si/Al, Zr/Al, Ti/Al and Ca/Al ratios.

The Mn/Al ratio profile is very similar to the Ca/Al ratio profile with the two ratios being related by a correlation coefficient of 0.86, again probably reflecting the formation of manganese calcium carbonate. The Mn/Al ratio has a value of 0.38 at a depth of 0.42 g cm^{-2} (1.5 cm) and then increases to a series of three maxima of 1.24 at of 5.81 g cm^{-2} (14.5 cm), 0.87 at 7.09 g cm^{-2} (16.5 cm) and 0.31 at 12.22 g cm^{-2} (25 cm), after which the ratio decreases to 0.023 at the bottom of the core. The Mn/Al ratios are far higher than those of any of the other cores considered which have the following surface values; LE 1 (0.012), LE 2 (0.016), LE 3 (0.025), LL1 (0.05) and GD2 (0.26) and the value at depth in core FD is greater than the surface values of LE 1 and LE 2. The Fe/Al ratio has a surface maximum value of 0.86 and a subsidiary peak at 4.6 g cm^{-2} (12.5 cm) depth which are separated by a minimum at 2.54 g cm^{-2} (7.5 cm). Below the subsurface peak the Fe/Al ratio decreases to a constant value of 0.57 at 9.81 g cm^{-2} (21 cm). The rapid decrease in the Fe/Al ratio near the surface of the sediment suggests that diagenetic recycling of Fe is taking place in this core. However, the Mn/Al profile does not reflect this, but as stated above the interpretation is difficult due to the removal of the Mn nodules from the core. The P/Al ratio has a surface maximum value of 0.022 and a subsurface peak at 5.81 g cm^{-2} (14.5

cm), separated by a minimum at 3.54 g cm^{-2} (7.5 cm). The ratio decreases to a value of 0.08 at 14.02 g cm^{-2} (29 cm) and remains constant to the bottom of the core. The P/Al profile has the same general trends as the Ca/Al and Mn/Al profile. It is obvious that the major changes taking place at depth in core FD are governed by the processes and elements involved in the formation of Mn nodules and Mn Ca concretions.

4.8.2 *^{210}Pb and ^{226}Ra profiles of core FD*

The plots of ^{226}Ra, ^{210}Pb and unsupported ^{210}Pb versus depth in g cm^{-2} are shown in Figure 4.39. ^{226}Ra has a pronounced surface enrichment with a value of 145.2 Bq kg^{-1} and a subsurface peak of 166.7 Bq kg^{-1} at 5.81 g cm^{-2} (14.5 cm) separated by a minimum at 2.92 g cm^{-2} (8.5 cm). The ^{226}Ra then decreases rapidly from the subsurface maximum to 54.5 Bq kg^{-1} at 7.68 g cm^{-2} (17.5 cm) after which it remains within the range 65 to 75 Bq kg^{-1} to the bottom of the core. It is worth noting that the minima occur where the maximum weight of nodules was removed (Figure 4.39.) which would be expected as Mn oxyhydroxides are known to scavenge radium (Ku and Broecker, 1969; Moore et al., 1980, 1981; Deal et al, 1981; Huh and Ku, 1984; Kadko et al., 1987; Todd et al., 1988). The nodules A to E had ^{226}Ra concentrations that ranged from 989.5 Bq kg^{-1} for nodule A to 373.8 Bq kg^{-1} for nodule E. (which are all much higher than is found in the sediment) indicating that the smaller nodules are more efficient at concentrating the ^{226}Ra which is probably a function of the surface area available. The ^{226}Ra inventory for this core was 17900 $\pm$ 800 Bq m^{-2} which is by far the largest ^{226}Ra inventory for any of the cores studied in this work.

The ^{210}Pb profile is very similar to the ^{226}Ra profile and has a value of 130.3 Bq kg^{-1} at the surface increasing to a maximum of 165.3 Bq kg^{-1} at 1.34 g cm^{-2} (4.5 cm), which is separated from a subsurface peak at 3.41 g cm^{-2} (9.5 cm) by a minimum at 2.92 g cm^{-2} (8.5 cm). The ^{210}Pb concentration decreases rapidly from the subsurface maximum to 34.3 Bq kg^{-1} at 9.81 g cm^{-2} (21 cm) after which it varies irregularly to the bottom of the core within the range 27 to 43 Bq kg^{-1}. The nodules A to E had ^{210}Pb concentrations that

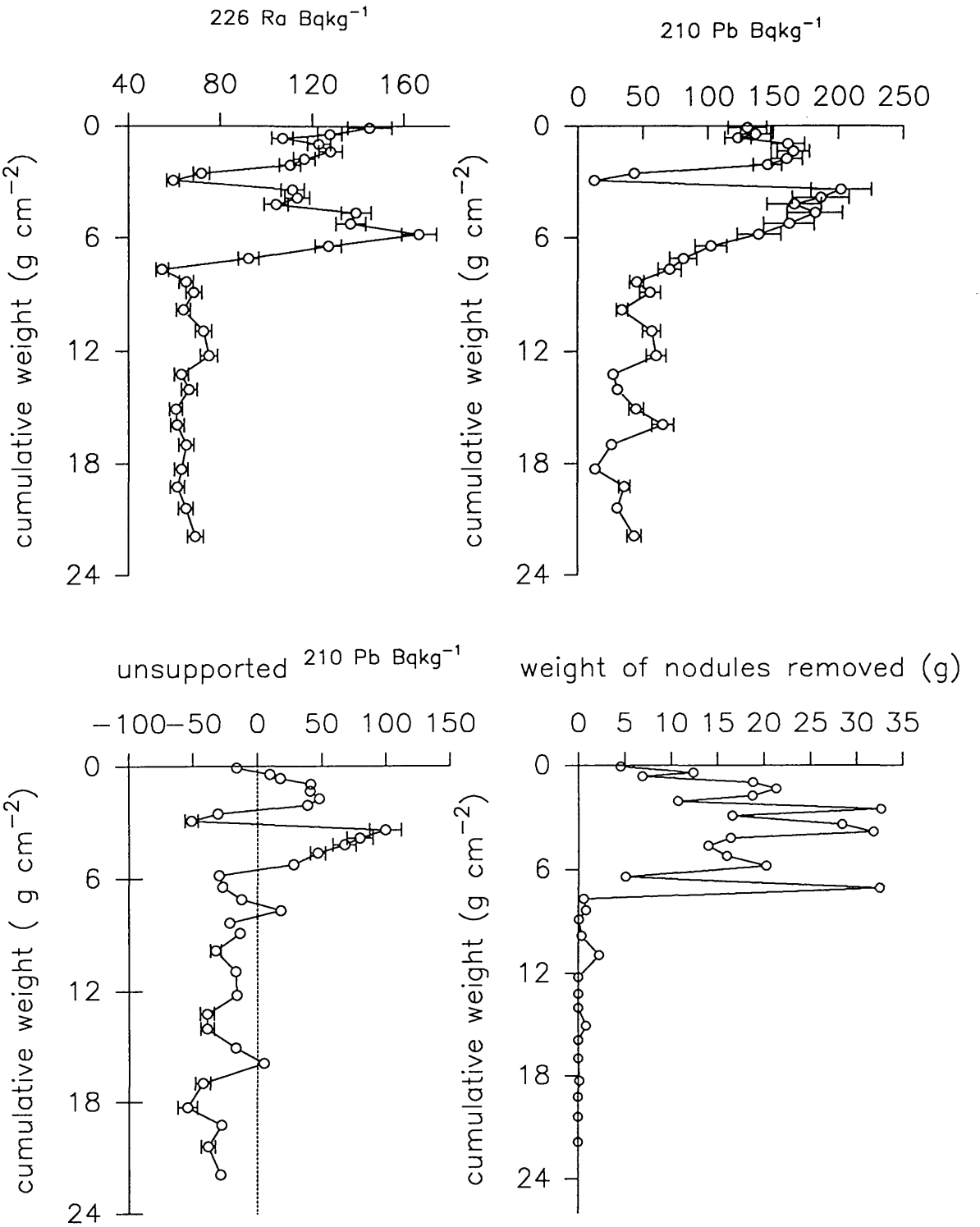

Figure 4.39. Loch Fyne core FD ^{226}Ra and ^{210}Pb concentrations and weight of nodules vs. depth

ranged from 678.4 Bq kg^{-1} for nodule A to 391 Bq kg^{-1} for nodule E.

The unsupported ^{210}Pb profile is similar to that of the total ^{210}Pb, with unsupported ^{210}Pb being restricted to the top 6 g cm^{-2} and subsurface maxima occurring at 1.75 (5.5 cm) and 3.41 g cm^{-2} (9.5 cm) separated by a minimum at 2.92 g cm^{-2} (8.5 cm). The ^{210}Pb and unsupported ^{210}Pb profiles are clearly dominated by the Mn/Ra system and do not represent steady state decay of ^{210}Pb in an accumulating system. Thus the ^{210}Pb data for this core are inherently unsuitable for investigation of mixing and accumulation processes. The unsupported ^{210}Pb profile at depth falls below zero, indicating that there is an excess of ^{226}Ra in this part of the core. The unsupported ^{210}Pb inventory for core FD was 2200 $\pm$ 250 Bq m^{-2} implying a steady state flux of 68 $\pm$ 8 Bq m^{-2} y^{-1} which is lower than core FS (3100 Bq m^{-2}, 97 Bq m^{-2} y^{-1}), LL1 (7700 Bq m^{-2}, 240 Bq m^{-2} y^{-1}), LE 1 (9500 Bq m^{-2}, 294 Bq m^{-2} y^{-1}), LE 3 (7700 Bq m^{-2}, 238 Bq m^{-2} y^{-1}) and the same as LE 2 (2200 Bq m^{-2}, 68 Bq m^{-2} y^{-1}). It is difficult to determine whether the supply and type of material to the core FD is the reason for the low unsupported ^{210}Pb inventory or due to the fact that the nodules have been removed from the sediment.

4.8.3 *^{137}Cs, ^{134}Cs and ^{241}Am concentration profiles of core FD*

As with the previous six sediment cores the ^{137}Cs profile for core FD can be taken to dominantly reflect trends in the Sellafield discharge and the $^{134}Cs/^{137}Cs$ ratio data can be used to distinguish between Sellafield and Chernobyl inputs.

The concentration profiles for ^{137}Cs and ^{241}Am and the activity ratio profile for $^{134}Cs/^{137}Cs$ are shown in Figure 4.40. The ^{137}Cs concentration has a value of 122.4 Bq kg^{-1} at the surface, a subsurface maximum of 226.2 Bq kg^{-1} at 0.96 g cm^{-2} (3.5 cm) and a smaller subsurface peak at 3.41 g cm^{-2} (9.5 cm) separated by a minimum at 2.54 g cm^{-2} (7.5 cm). Finally the ^{137}Cs concentration decreases to a value of 1.2 Bq kg^{-1} at a depth of 13.2 g cm^{-2} (27 cm) and below this the ^{137}Cs concentrations are below 1 Bq kg^{-1}. Following the previously defined procedure (section 4.2.3.) the position of the

maximum ^{137}Cs concentration (0.96 g cm^{-2}, 3.5 cm) implies a sedimentation rate of 0.08 g cm^{-2} y^{-1} but on this basis, the peak at 3.41 g cm^{-2} (9.5 cm) corresponds to a date of 1948, which does not relate to either the Sellafield discharge, which did not start until 1952, or the maximum fallout resulting from bomb testing which occurred around 1963. However the minimum ^{137}Cs concentration occurs at a similar depth to the minima that occur in the elemental/Al, ^{226}Ra and ^{210}Pb profiles, so the sharp decrease in ^{137}Cs concentration may be due to the same processes that are affecting the other profiles. The sedimentation rate for core FD from the depth of penetration of ^{137}Cs is 0.377 g cm^{-2} y^{-1} which is far higher than the sedimentation rate calculated from the depth of the maximum concentration of ^{137}Cs. Assuming that there is no mixing in this core and that the sedimentation rate is 0.08 g cm^{-2} y^{-1} then the expected depth of penetration of ^{137}Cs would be 2.8 g $cm^{-2}y^{-1}$. ^{137}Cs was detected to a depth of 13.2 g cm^{-2}, suggesting a diffusion depth of 10.4 g cm^{-2} for this core which is essentially the same as core LE 2 (10.74 g cm^{-2}) from Loch Etive and similar to core FS (12.07 g cm^{-2}). The nodules A to E had ^{137}Cs concentrations that ranged from 72.3 Bq kg^{-1} for A to 48.1 Bq kg^{-1} for E. which are generally lower than the concentration of ^{137}Cs in the upper sediment.

The inventory of ^{137}Cs in FD is 5400 $\pm$ 139 Bq m^{-2} which is far lower than any of the other three cores from the Clyde Sea Area which are within the range 14300 to 39000 Bq m^{-2} and lower than the cores from Loch Etive which were within the range 7500 to 10100 Bq m^{-2}. The low inventory can possibly be explained by the loss of ^{137}Cs from the sediment core due to the removal of nodules, as ^{137}Cs was detected in the nodules at reasonably high concentrations. Assuming the average ^{137}Cs concentration of the nodules is 60 Bq kg^{-1} and the weight of nodules removed was 312 g, then a total of 18.7 Bq of ^{137}Cs was removed from a core of area 77 cm^2, corresponding to removal of approximately 2400 Bq m^{-2}. Addition of this to the inventory for the sediment gives a combined inventory of 7800 Bq m^{-2}, which is similar to those of cores LE 2 and LE 3.

^{134}Cs was only detectable in the sediment at a depth of 0.42 g cm^{-2} (1.5 cm)

at a concentration of 2 Bq kg^{-1} giving a $^{134}Cs/^{137}Cs$ ratio of 0.012 and it is clearly not feasible to draw any conclusions from this single measurement.

^{241}Am was below detection limit in the surface sediment but was detectable at 11 Bq kg^{-1} at a depth of 0.42 g cm^{-2} (1.5 cm) below which the concentration of ^{241}Am decreased systematically to 4 Bq kg^{-1} at a depth of 1.34 g cm^{-2} (4.5 cm), ^{241}Am was not detected below this level. The ^{241}Am concentration decreases remarkably uniformly and is probably a true reflection of the Sellafield discharge.

4.8.4 *^{228}Th and ^{228}Ra profiles of core FD*

The $^{228}Th/^{228}Ra$ profile for core FD is shown in Figure 4.40. The ratio has a surface value of 1.36 then decreases to 0.97 at a depth of 1.34 g cm^{-2} (4.5 cm) below which the profile is irregular with a number of results being above unity. The high ratio at the surface indicates that there is an excess of ^{228}Th in the surface sediments, or alternatively that there is transient equilibrium between ^{228}Ra and ^{228}Th, but due to the complexity of this core and the removal of the Mn nodules it is difficult to speculate on the cause of the excess ^{228}Th. The nodules A to E had ^{228}Ra concentrations that ranged from 146.3 Bq kg^{-1} for A to 21.4 Bq kg^{-1} for E and ^{228}Th was only detectable in the two smaller sizes of nodule A and B at concentrations of 88 and 24.4 Bq kg^{-1} respectively. Therefore the nodules were removing ^{228}Ra as they were ^{226}Ra and the excess ^{228}Th in the surface sediments may reflect this. The inventories for ^{228}Th and ^{228}Ra are 7000 $\pm$ 300 Bq m^{-2} and 6700 $\pm$ 300 Bq m^{-2} indicating that throughout the length of the core there does not seem to be an excess of ^{228}Th but a redistribution of ^{228}Ra within the core. However, as stated before it is difficult to make any firm conclusions as the analysis of the nodules indicates removal of ^{228}Ra and to a lesser extent the removal of ^{228}Th.

4.8.5 *Stable Pb and Pb isotope ratios of core FD*

The total stable Pb concentration data are presented in Chapter 3 (Table

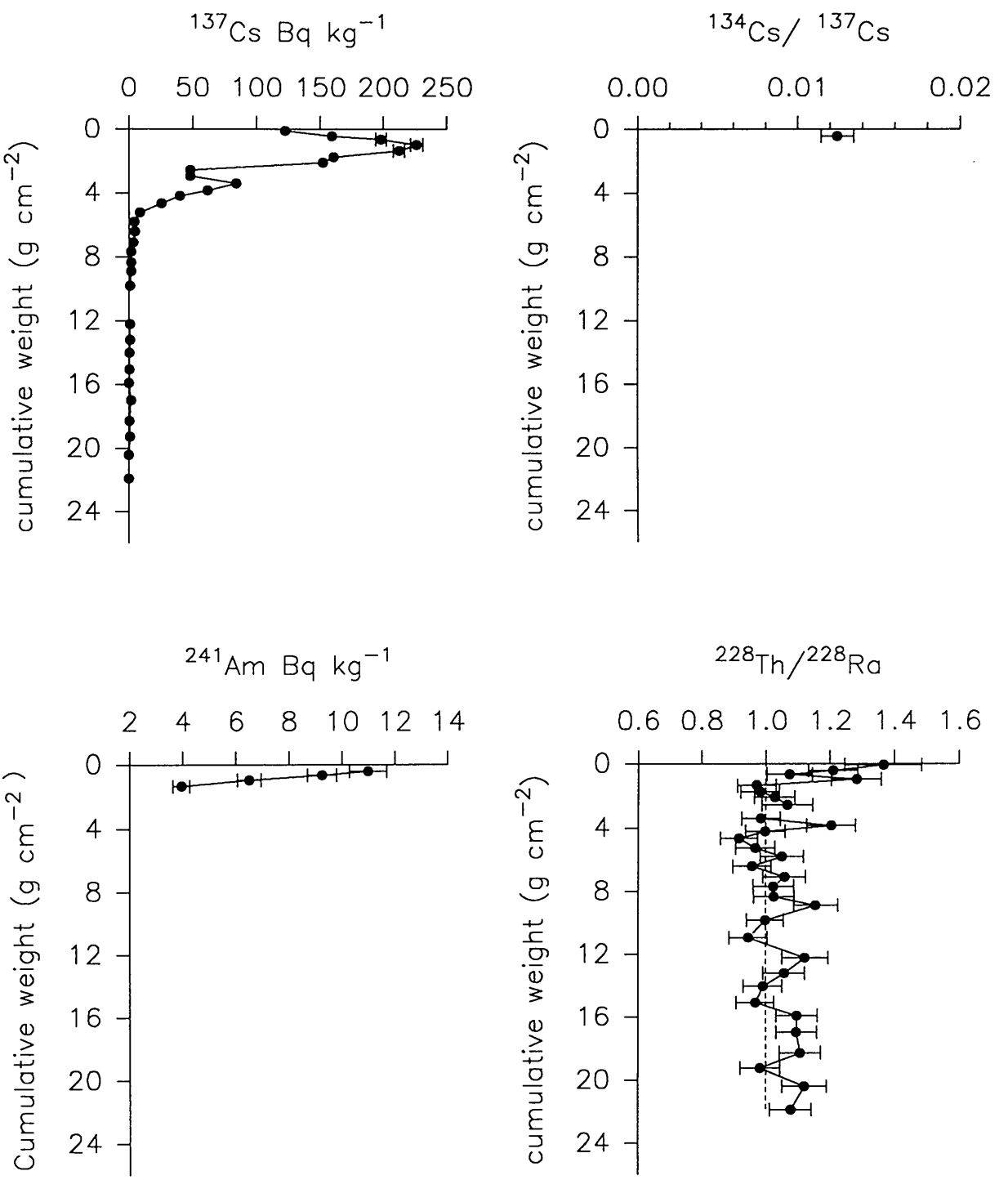

Figure 4.40. Loch Fyne core FD radionuclide concentrations and activity ratios

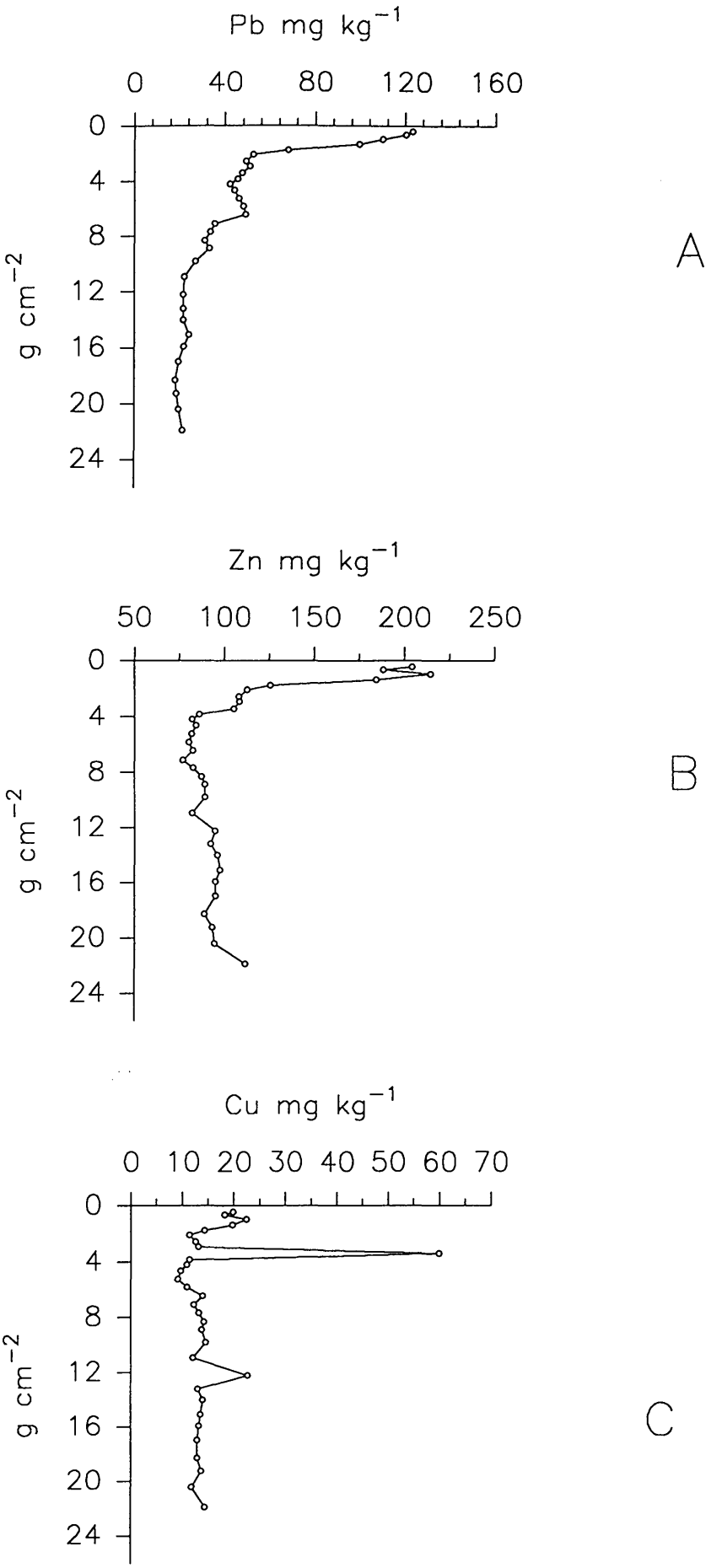

Figure 4.41. Loch Fyne core FD Pb, Zn and Cu concentrations (mg kg^{-1})

3.40) and the plot of the total Pb concentration versus cumulative weight (g cm^{-2}) is shown in Figure 4.41.A. The Pb profile has a surface maximum of 123 mg kg^{-1} and a small subsurface peak at 6.42 g cm^{-2} (15.5 cm) below which it decreases 22 mg kg^{-1} at the bottom of the core.

The maximum Pb concentration occurs at a depth of 0.42 g cm^{-2} (1.5 cm) which corresponds to a date of 1985. This is very different from the other cores which all exhibited a subsurface maximum in Pb concentration occurring at the following times LL1 (1962), GD2 (1936), FS (1976), LE 1 (this core had a constant value to a depth corresponding to 1977), LE 2 (1973) and core LE 3 (1979). Therefore the stable Pb profile again indicates that the profiles for this core are very different than those of the other six cores which is probably due to a combination of the unusual geochemical conditions which prevail within this sediment and the removal of the Mn nodules. The change in rate of increase in Pb concentration occurs at a depth of 2.08 g cm^{-2} (6.5 cm) which corresponds to 1964. The start of the increase in Pb pollution occurs at a depth of 10.94 g cm^{-2} (25 cm) corresponding to a date of 1858.

The flux of pollutant Pb versus time is shown in Figure 4.42.A. The excess flux results are given in Table 4.22. Excess Pb was first detected in 1794 at a value of 0.001 g m^{-2} y^{-1}, however, this was just above natural levels and the Pb flux did not begin to increase above this level until 1871 after which it increased to 0.022 g $m^{-2}y^{-1}$ around 1919. The Pb flux decreased after this date to 0.017 g $m^{-2}y^{-1}$ around 1939 and then increased to 0.025 g $m^{-2}y^{-1}$ in 1964. Thereafter the Pb flux increased rapidly to a maximum value of 0.082 g $m^{-2}y^{-1}$ by the mid 1980's. As the surface sample was not analysed for Pb it is not possible to say whether the flux began to decrease after this date, but if the trend for Pb flux for this core is similar to the previous six cores then it would expect to do so.

The inventory of excess Pb for core FD is 3.1 g m^{-2} which is similar to cores FS (2.3 g m^{-2}) and within the range of excess Pb found for cores LE 1 to LE 3 (1.6 to 3.8 g m^{-2}). It is, however, considerably lower than cores LL1 (68.3

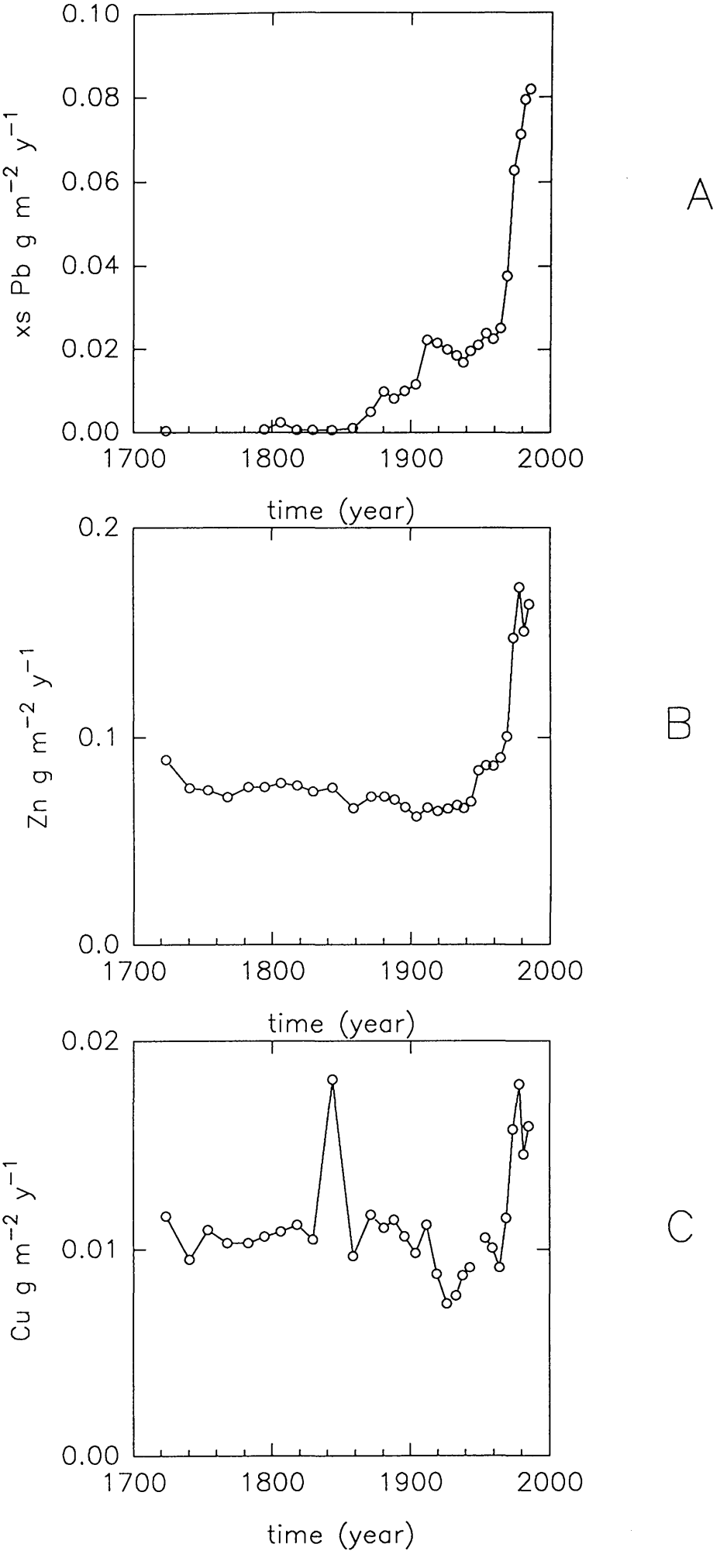

Figure 4.42. Loch Fyne core FD PB, Zn and Cu flux data

g m^{-2}) and GD2 (43.9 g m^{-2}). The inventory of core FD indicates that this sampling site in Loch Fyne, as with site FS, is not affected by the gross pollution that is experienced by cores LL1 and GD2. Therefore it is now apparent that the 'remote' lochs have excess Pb inventories of approximately 2 to 4 g cm^{-2} which can be compared to the excess Pb inventories of Loch lomond (2.91 g cm^{-2}), a freshwater loch, and peat cores from Flanders Moss (3.38 g m^{-2}) and North Uist (0.52 g m^{-2}) (Sugden, 1993). The similarity of the excess Pb inventories between these sea lochs and the freshwater loch and peat cores, suggests that the input is close to atmospheric and that there is no discernable marine influence as would be expected from the relatively short residence time of Pb in seawater.

The plot of $^{206}Pb/^{207}Pb$ ratio versus the ^{137}Cs chronology for core FD is shown in Figure 4.43.A. along with the excess Pb flux (g m^{-2} y^{-1}). The surface sediment has a $^{206}Pb/^{207}Pb$ ratio of 1.170 then decreases to a value of 1.165 in 1978 after which the ratio increases to 1.183 in 1964. The $^{206}Pb/^{207}Pb$ ratio profile is somewhat erratic but continues to increase to a mean of 1.191 in 1938. Below this depth the profile is irregular with a mean $^{206}Pb/^{207}Pb$ ratio value of 1.184. As discussed in section 4.2.5. the decreasing $^{206}Pb/^{207}Pb$ ratio towards the surface of the sediment can be attributed to the increasing influence of vehicle exhaust emissions on pollutant Pb fluxes to the sediment during this century. On the basis of the change in ratio, the onset of the deposition of petrol derived Pb was estimated to occur in 1938 which correlates well with cores LE 1 (1937), LE 2 (1928) and LE 3 (1935) and the known historical use of alkyl lead compounds in petrol. However it is later than cores LL1(1916) and GD2 (1912) which give dates that are too early when compared to the date of the known use of Pb in petrol. The date of the onset of pollutant Pb from petrol is seen in 1947 for core FS from the shallow station in Loch Fyne which is later than expected and may be due to either an over estimation of mixing in this core or that the sedimentation rate calculated from the ^{137}Cs profile is too high, or due to the unsuitability of applying the ^{137}Cs sedimentation rate over an extended depth. Therefore, although some care must be taken in drawing conclusions from core FD due to its sample preparation, the sediment from this core would seem to reflect

SAMPLE	DEPTH (cm)	cum .g cm^{-2}	date for mid section	excess Pb g m^{-2} y^{-1}
FD 0-1	0.5	0.08	1988	
FD 1-2	1.5	0.42	1985	0.082
FD 2-3	2.5	0.63	1981	0.079
FD 3-4	3.5	0.96	1978	0.071
FD 4-5	4.5	1.34	1974	0.063
FD 5-6	5.5	1.75	1969	0.038
FD 6-7	6.5	2.08	1964	0.025
FD 7-8	7.5	2.54	1959	0.023
FD 8-9	8.8	2.92	1954	0.024
FD 9-10	9.5	3.41	1948	0.021
FD 10-11	10.5	3.84	1943	0.020
FD 11-12	11.5	4.19	1939	0.017
FD 12-13	12.5	4.64	1933	0.019
FD 13-14	13.5	5.24	1926	0.020
FD 14-15	14.5	5.81	1919	0.022
FD 15-16	15.5	6.42	1912	0.022
FD 16-17	16.5	7.09	1904	0.012
FD 17-18	17.5	7.68	1896	0.010
FD 18-19	18.5	8.33	1888	0.008
FD 19-20	19.5	8.88	1880	0.010
FD 20-22	21.0	9.81	1871	0.005
FD 22-24	23.0	10.94	1858	0.001
FD 24-26	25.0	12.22	1843	0.001
FD 26-28	27.0	13.20	1829	0.001
FD 28-30	29.0	14.02	1818	0.001
FD 30-32	31.0	15.06	1806	0.002
FD 32-34	33.0	15.91	1794	0.001
FD 34-36	35.0	16.97	1782	0
FD 36-38	37.0	18.28	1768	0
38-40	39.0	19.24	1754	0
FD 40-42	41.0	20.39	1740	0
FD 42-46	45.0	21.88	1724	0

Table 4.22 Loch Fyne core FD excess flux data

the pollution history of Pb from petrol and gives a degree of confidence in the sedimentation rate used to obtain the chronology for this core. The

$^{206}Pb/^{207}Pb$ profile for core FD is very similar to core FS with only the time axis being different and this strongly suggests that the sedimentation rate applied to core FS was too high and that there is a discrepancy in the chronology.

Calculation of the percentage Pb due to petrol was carried out as described in section 4.2.5. with R_i = 1.184 and R_{Hi}= 1.172, and the results given in Table 4.23, indicate that the onset of Pb from petrol does not take place until 1969 with the maximum %Pb (15%) occurring in 1978. Therefore there is a discrepancy in the onset of Pb from petrol between the $^{206}Pb/^{207}Pb$ ratio profile and the above calculation which may be due to the $^{206}Pb/^{207}Pb$ ratio chosen to represent R_i and R_{Hi}. It is interesting to note that the $^{206}Pb/^{207}Pb$ ratio increases slightly in the top 3 samples, suggesting a recent decrease in the relative significance of petrol Pb. This could be a genuine reduction in Pb from this source or could represent an increase in Pb from other sources. The residual Pb inventory for this core (ie the excess Pb inventory - Pb from petrol) is 2.9 g m^{-2} indicating that under 10% of the pollutant Pb is from petrol in this core. As with previous cores we can compare the ratios of the inventories of excess ^{210}Pb, excess Pb and residual excess Pb of cores FS and FD from Loch Fyne. FS_{210}/FD_{210}= 1.4, FS_{xsPb}/FD_{xsPb}= 0.7, $FS_{res\text{-}Pb}/FD_{res\text{-}Pb}$= 0.6. The ratios suggest that core FS, from the shallow station, was receiving a greater flux of ^{210}Pb which is not what would have been expected from the results of the previous cores, however the analysis of bulk nodules has indicated a higher ^{210}Pb concentration than the surrounding sediment so, due to the removal of the nodules, comparison of the excess ^{210}Pb inventories for the two cores cannot be made. The ratios of the excess Pb and residual Pb inventories suggest that core FD has more pollutant Pb than core FS and that the amount of Pb from petrol is similar in both cores. Again these results may have been affected by the removal of the Mn nodules.

SAMPLE	DEPTH (cm)	cum g cm^{-2}	date for mid section	% Pb from petrol
FD 0-1	0.5	0.08	1988	
FD 1-2	1.5	0.42	1985	12
FD 2-3	2.5	0.63	1981	13
FD 3-4	3.5	0.96	1978	15
FD 4-5	4.5	1.34	1974	13
FD 5-6	5.5	1.75	1969	5
FD 6-7	6.5	2.08	1964	
FD 7-8	7.5	2.54	1959	
FD 8-9	8.8	2.92	1954	
FD 9-10	9.5	3.41	1948	
FD 10-11	10.5	3.84	1943	
FD 11-12	11.5	4.19	1939	
FD 12-13	12.5	4.64	1933	
FD 13-14	13.5	5.24	1926	
FD 14-15	14.5	5.81	1919	
FD 15-16	15.5	6.42	1912	
FD 16-17	16.5	7.09	1904	
FD 17-18	17.5	7.68	1896	
FD 18-19	18.5	8.33	1888	
FD 19-20	19.5	8.88	1880	
FD 20-22	21.0	9.81	1871	
FD 22-24	23.0	10.94	1858	
FD 24-26	25.0	12.22	1843	
FD 26-28	27.0	13.20	1829	
FD 28-30	29.0	14.02	1818	
FD 30-32	31.0	15.06	1806	
FD 32-34	33.0	15.91	1794	
FD 34-36	35.0	16.97	1782	
FD 36-38	37.0	18.28	1768	
FD 38-40	39.0	19.24	1754	
FD 40-42	41.0	20.39	1740	
FD 42-46	45.0	21.88	1724	

Table 4.23 % Pb in sediment from Pb for core FD

The $^{208}Pb/^{206}Pb$ versus $^{206}Pb/^{207}Pb$ plot for core FD is shown in Figure 4.43. The samples are numbered 1 to 32 according to increasing depth. There is not an obvious tie line apparent between end member groups with this core, although the sample most affected by petrol are clustered together with samples 7 to 25 forming a group in which there is a general increase in the

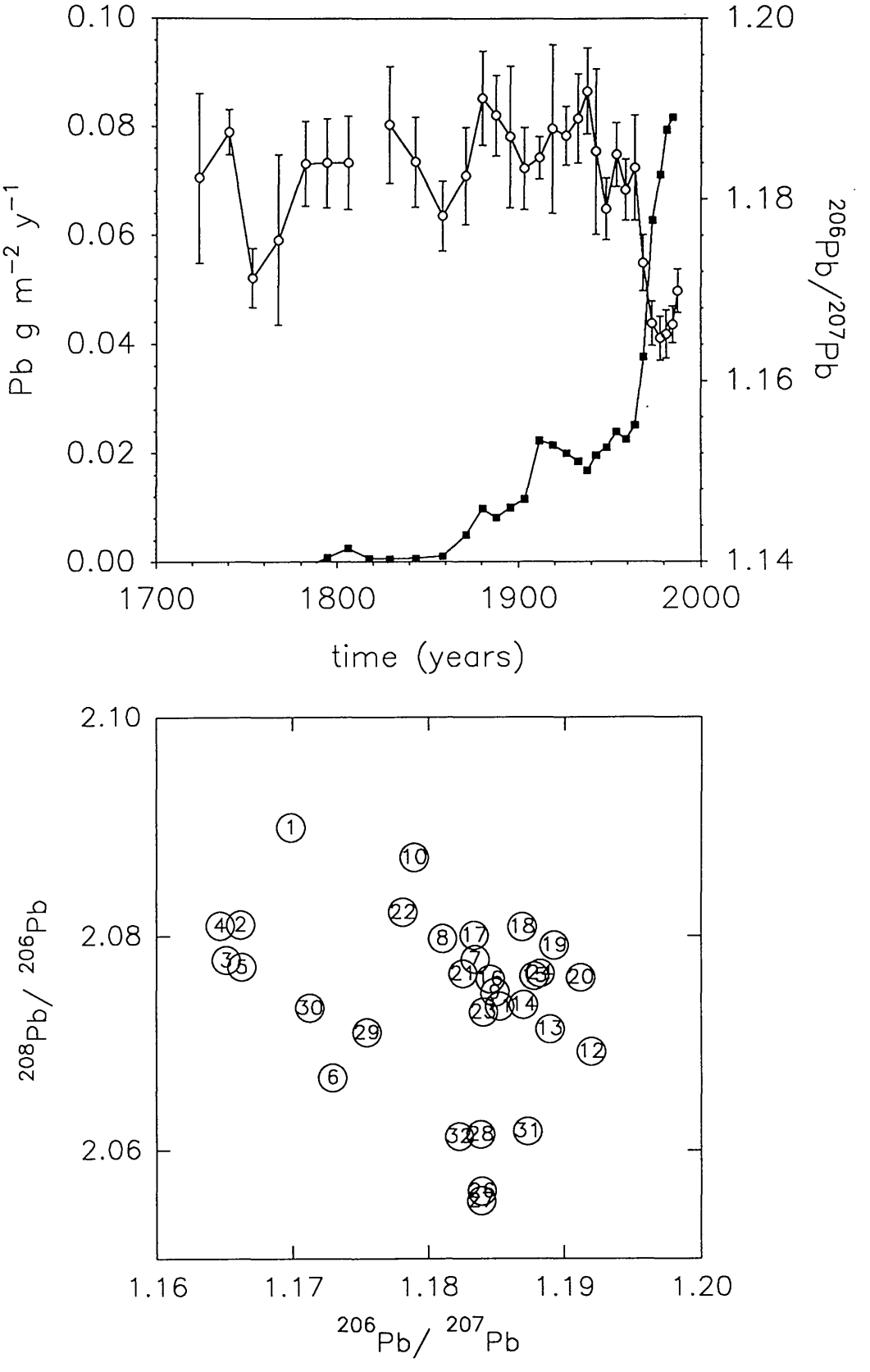

Figure 4.43. Loch Fyne core FD Pb flux and Pb isotope ratio plots

$^{206}Pb/^{207}Pb$ ratio and decrease in the $^{208}Pb/^{206}Pb$ ratio as would be expect from a combination of natural Pb, industrial Pb and increasing amounts of Pb from petrol. Samples 25 to 32 are possibly representative of the natural signature of the sediment, however samples 29 and 30 are anomalous in that they lie to the "petrol end" of the graph. The pronounced decrease in $^{208}Pb/^{206}Pb$ seen in cores FS and GD2 is not apparent here suggesting that there has been a local release of low lead with a ^{208}Pb concentration that has affected cores FS and GD2 but not core FD.

4.8.6 *Zn and Cu profiles of core FD*

The total Zn and Cu concentration profiles for core FD are shown in Figures 4.41.B. and 4.41.C. respectively. The Zn profile has a concentration of 204 mg kg^{-1} at a depth of 0.42 g cm^{-2} (1.5 cm) with a subsurface maximum of 214 mg kg^{-1} at 0.96 g cm^{-2} (3.5 cm), after which it decreases rapidly to 108 mg kg^{-1} at a depth of 2.54 g cm^{-2} (7.5 cm). The Zn concentration then decreases more slowly to a value of 83 mg kg^{-1} at a depth of 6.42 g cm^{-2} (15.5 cm). Below this depth the Zn concentration is within the range 77 to 111 mg kg^{-1}. Using the chronology obtained from the ^{137}Cs sedimentation rate, the maximum Zn concentration occurs in 1978 and the rapid increase starts in 1964.

The Cu concentration profile has a value of 20 mg kg^{-1} at 0.42 g cm^{-2} (1.5 cm) depth, then increases to 22 mg kg^{-1} at 0.96 g cm^{-2} (3.5 cm) after which it decreases to 11 mg kg^{-1} at 2.08 g cm^{-2} (6.5 cm). There is an extremely high result of 60 mg kg^{-1} at a depth of 3.41 g cm^{-2} (9.5 cm) which was considered to be erroneous due perhaps to contamination or an incorrect XRF analysis. The Cu concentration decreases to 15 mg kg^{-1} at the bottom of the core (21.88 g cm^{-2}, 44 cm). Therefore the maximum Cu concentration occurs in 1976 and the increase in concentration occurs around 1964 as was the case with the Zn profile. The Zn and Cu concentration profiles are very similar and have the same general trends with depth.

The fluxes of total Zn and total Cu are given in Figures 4.42.B. and 4.42.C.

respectively with the results being presented in Table 4.24. The fluxes are similar to core FS and considerably lower than LL1 and GD2. The profiles of total Zn and total Cu fluxes are similar and indicate that the major increase in flux took place around the mid 1960's. The excess Pb profile does not show a decrease in flux in the early 1980's as does the Zn and Cu and it has more structure to it from 1880 to 1940. The Zn profile indicates a maximum flux of 0.172 g m^{-2} y^{-1} with a flux of 0.089 g m^{-2} y^{-1} at depth. The Cu profile indicates a maximum flux of 0.018 g m^{-2} y^{-1} (with the exception of the flux at 3.41 g cm^{-2} which is considered to be erroneous.) with the flux at the bottom of the core being 0.012 g m^{-2} y^{-1}.

The inventories of total Zn and Cu for core FD are 21.7 g m^{-2} and 3.3 g m^{-2}. The Zn inventory is lower than core FS and the Cu inventory is higher than core FS probably indicating that the inventories for these metals have been affected by the removal of the Mn nodules. The excess Zn and Cu inventories for core FD are 2.7 and 1.3 g cm^{-2} respectively, and have the same trends as the total Zn and Cu inventories with respect to core FS in that the excess Zn is lower and the excess Cu is higher than those of core FS.

4.8.7 *Summary of core FD*

The results from core FD must be considered with the fact that this sediment core was treated differently due to the removal of Mn nodules from the core. In summary, the results from core FD indicate that ^{210}Pb dating could not be applied. However a sedimentation rate of 0.08 g cm^{-2} y^{-1} was obtained from the position of the maximum ^{137}Cs concentration. There was no mixing apparent in this core. The chronology obtained from the ^{137}Cs sedimentation rate agreed well with the Pb isotope profiles.

SAMPLE	DEPTH (cm)	cum g cm^{-2}	date for mid section	Cu g m^{-2} y^{-1}	Zn g $m^{-2}y^{-1}$
FD 0-1	0.5	0.08	1988		
FD 1-2	1.5	0.42	1985	0.016	0.164
FD 2-3	2.5	0.63	1981	0.015	0.151
FD 3-4	3.5	0.96	1978	0.018	0.172
FD 4-5	4.5	1.34	1974	0.016	0.148
FD 5-6	5.5	1.75	1969	0.012	0.100
FD 6-7	6.5	2.08	1964	0.009	0.090
FD 7-8	7.5	2.54	1959	0.010	0.086
FD 8-9	8.8	2.92	1954	0.011	0.087
FD 9-10	9.5	3.41	1948	0.048	0.084
FD 10-11	10.5	3.84	1943	0.009	0.069
FD 11-12	11.5	4.19	1939	0.009	0.066
FD 12-13	12.5	4.64	1933	0.008	0.067
FD 13-14	13.5	5.24	1926	0.007	0.065
FD 14-15	14.5	5.81	1919	0.009	0.064
FD 15-16	15.5	6.42	1912	0.011	0.066
FD 16-17	16.5	7.09	1904	0.010	0.062
FD 17-18	17.5	7.68	1896	0.011	0.066
FD 18-19	18.5	8.33	1888	0.011	0.070
FD 19-20	19.5	8.88	1880	0.011	0.072
FD 20-22	21.0	9.81	1871	0.012	0.071
FD 22-24	23.0	10.94	1858	0.010	0.066
FD 24-26	25.0	12.22	1843	0.018	0.076
FD 26-28	27.0	13.20	1829	0.010	0.074
FD 28-30	29.0	14.02	1818	0.011	0.077
FD 30-32	31.0	15.06	1806	0.011	0.078
FD 32-34	33.0	15.91	1794	0.011	0.076
FD 34-36	35.0	16.97	1782	0.010	0.076
FD 36-38	37.0	18.28	1768	0.010	0.071
FD 38-40	39.0	19.24	1754	0.011	0.075
FD 40-42	41.0	20.39	1740	0.010	0.076
FD 42-46	45.0	21.88	1724	0.012	0.089

Table 4.24 Cu and Zn fluxes for Loch Fyne core FD

The manmade radionuclides present are dominated by the Sellafield discharge. The ^{137}Cs profile indicated mobility of Cs by means of diffusion and therefore the use of the depth of penetration of ^{137}Cs can not be used to determine a sedimentation rate.

The deposition of pollutant Pb increased rapidly from the early 1960's probably as a result of the increased activity within the Clyde Sea Area that resulted from the construction of the Holy Loch Naval base and roads at that time. From the excess Pb inventories and fluxes it is apparent that Loch Fyne is not as heavily polluted as the other cores from the Clyde Sea Area.

4.9 *Clyde Sea Area Pore Water analysis*

The following section deals with selected element concentrations within the pore waters of sediment cores, LL1, GD2, FS and FD from the Clyde Sea Area. The sampling techniques used are described in detail in section 2.1.3. The main objective was to obtain information on the redox condition of the sediment by analysing elements that have a well established redox chemistry and exhibit variable oxidation states in the environment, with marked differences in solubility between the oxidised and reduced forms. Of particular interest in the preset case were Mn, Fe, Mo and U. Mn and Fe are insoluble in the oxidised forms (Mn^{4+}, Fe^{3+}) and soluble in the reduced forms (Mn^{2+}, Fe^{2+}) whereas Mo and U are soluble in the oxidised forms (Mo^{6+}, U^{6+}) but insoluble in the reduced forms (Mo^{4+}, U^{4+}) (Price, 1976; Wedepohl, 1978; Shimmield and Pedersen, 1990). The results obtained for redox sensitive elements (Mn, Mo and U) within the pore waters of cores LL1, GD2 and FD were discussed in Shimmield et al., (1991) and this section will consider these elements along with a brief discussion of some other element concentrations within the pore waters of the four sediment cores. The pore waters were analysed for Mn, Fe, Mo, U, Al, Cu, Ba, Li, B, Sr, Hg, Pb Zn and Sn by ICP-MS. However, the latter four elements (Hg, Pb, Zn and Sn) gave very erratic profiles which was considered to be due to a combination of contamination and analytical interferences.

As discussed previously, coastal marine sediments are important as major sinks of pollutants, including heavy metals and an understanding of the complex geochemical and biogeochemical processes which occur in this environment is essential in attempting to evaluate the long term fate of such pollutants. Redox controlled diagenetic recycling in surface sediments is of particular importance in understanding the behaviour of heavy metals both directly, since some exhibit variable oxidation states and in general, the combination of Eh and pH governs the form and solubility of the metal (Henderson, 1982), and indirectly via the possible influence of Fe/Mn diagenetic recycling on other species, as discussed for ^{226}Ra in section 1.2.3. The traditional method of establishing the redox condition of a sediment is to use an electrode inserted directly into the sediment/pore water or extracted water, but such results are prone to error due to factors such as poisoning of electrodes and the selective response of electrodes to major ions in solution (Guppy and Atkinson, 1989). Information about redox variations in sediments can also be inferred from the solid phase distribution of redox sensitive elements, as illustrated by the preceding use of XRF data, but solid phase variations do not necessarily coincide with aqueous phase Eh changes. Therefore, it was considered that the analysis of dissolved concentrations of redox sensitive elements in the pore water could give a more accurate assessment of the redox condition of the sediment. The solution phase data also provide information about concentration gradients and can therefore indicate diffusion processes taking place within the porewater.

4.9.1 *Loch Long core (LL1) pore water profiles*

The element concentration profiles for core LL1 pore water are given in Figure 4.43 and are expressed as concentration (in ng l^{-1} or mg l^{-1}) versus cumulative weight (g cm^{-2}) rather than linear depth to allow comparison with the sediment depth profiles. As discussed in section 2.1.3. due to the limited availability the N_2, gas flow to the glove box was turned off before the end of sectioning the cores (although the box remained sealed) and the depths at which this occurred are indicated on each of the profiles. As it is possible

that oxygen may have penetrated into the glove box at any time after the N_2 was switched off detailed discussion of the pore water profiles will be restricted to the part of the profile above the cut off point of N_2 gas.

The standard electrode potentials in acid solution for Mn^{2+}/Mn^{4+}, Fe^{2+}/Fe^{3+} and U^{4+}/U^{6+} couples are given in Table 4.25.

Standard Electrode Potentials	(acid solution)
$Mn^{2+} \rightarrow Mn^{4+}$	+1.23 V
$Fe^{2+} \rightarrow Fe^{3+}$	+0.70 V
$U^{4+} \rightarrow U^{6+}$	+0.33 V

Table 4.25 Standard electrode potentials of Mn, Fe, U and Mo in acid solution (Barrow, 1966; Krauskopf, 1979)

The aqueous phase Mn profile for LL1 has a surface value of 7.7 mg l^{-1} which is considerably higher than that of sea water (0.2 μg l^{-1}, Chester, 1990) and indicates that oxidation of Mn is incomplete at the surface of this core. The Mn profile has two subsurface maxima indicating zones of dissolution, separated by a minimum which suggests that Mn is being deposited at this depth (6.19 g cm^{-2}, 15 cm) in the core. The upper maximum relates to surface processes and the high concentration of dissolved Mn at the surface indicates that reduction of Mn is taking place at or near the sediment/water interface in core LL1. The second maximum can be considered with respect to the "dumped section", which extends from 5.69 to 7.95 g cm^{-2} (13 to 21 cm), and the buried surface, that were identified in core LL1 (section 4.5.1). The minimum dissolved Mn concentration occurs within the "dumped section" and the second maximum of 17.4 mg l^{-1} of Mn occurs below the buried surface at 10.13 g cm^{-2} (29 cm), indicating that dissolution of Mn from the old surface is taking place, with diffusion above and below this point. If the chronology for core LL1 is correct the 'surface' was buried in the early 1960's and this suggests that after approximately 25 years Mn reduction is still

taking place. The aqueous Mn profile for core LL1 indicates that the sediment is not completely oxidised at the surface and that there are two zones in which reduction of Mn is taking place, consistent with the solid phase data (Figure 4.19). The aqueous Fe profile is very similar to the aqueous Mn profile, with a value of 3 mg l^{-1} at the surface and two subsurface maxima of 13 and 19 mg l^{-1} (c.f. sea water = 2 μg l^{-1}) occurring at 5.69 and 10.13 g cm^{-2} (13 and 29 cm) separated by a minimum at 6.19 g cm^{-2} (15 cm). The increase in aqueous Fe concentration from the surface is less rapid than that of the Mn, suggesting that Fe reduction is taking place deeper in the core, as would be expected from its lower redox potential. The second Fe maximum coincides with the second Mn maximum and again suggests that there is dissolution related to the buried surface taking place at this depth, with diffusion above and below the point of dissolution.

As mentioned above, Mo and U behave differently from Mn and Fe in that it is the oxidised forms of these elements that are soluble and the reduced forms insoluble. The aqueous phase Mo profile has a surface concentration of 52 μg l^{-1} which is considerably higher than the concentration found in sea water (10 μg l^{-1}) indicating either that Mo is being released from the dissolving Mn oxyhydroxide layer or that there is a surface aqueous phase input from the highly polluted water of the Clyde Sea Area. The concentration decreases to 2.9 μg l^{-1} at 10.13 g cm^{-2} (29 cm), indicating that the Mo is being reduced and removed to the sediment at this depth. The aqueous Mo profile also exhibits a minimum at 6.19 to 6.74 g cm^{-2} (11 μg l^{-1}) which is the same as the Mn and Fe profiles and coincides with the dumped section of sediment in this core. The aqueous U concentration at the surface is close to the seawater value of 3.2 μg l^{-1} and remains at this level to 1.56 g cm^{-2} (3.5 cm) below which it decreases to a minimum of 0.4 ng l^{-1} by 5.69 g cm^{-2} (13 cm). Therefore the aqueous phase profiles of Mn, Fe, U and Mo indicate that the redox couple for the respective elements occurs at increasing depths in the core as would be expected from their known redox potentials. It is interesting to note that the aqueous phase Mo and U concentrations both increase in the deeper sections of the core as would be expected if oxidation of the sediment had taken place after the N_2 gas was switched off. However,

the increase in concentration does not take place immediately at the depth at which the N_2 flow was turned off but occurs significantly deeper in the core at a depth of 13.65 g cm^{-2} (41 cm).

As stated above, the main objective in analysing the pore waters was to obtain some indication of the redox conditions of the sediment. The ICP-MS technique, however, provides multi-element analysis, and profiles for other elements detected in the pore water are illustrated in Fig 4.43. Detailed discussion of these profiles is, however, beyond the scope of the present work and the following discussion is restricted to highlighting salient interesting features. More detailed consideration of these results will be presented elsewhere. The aqueous profiles of Cu, Ba, Li, B, Sr and Rb all reflect a minimum at a depth of 6.74 g cm^{-2} (17 cm) which is within the "dumped zone", with the Li and B profiles being very similar. The pore water profiles for core LL1 indicate that all the elements considered have a minimum occurring within the "dumped zone" with the exception of U. The minimum could be a result of differing redox conditions within the dumped sediment but this would not affect the B, Li Sr or Rb profiles. Ba is not inherently redox sensitive but it could potentially provide information in the important sulphate/sulphide system in sediments since $BaSO_4$ is insoluble. Thus, in zones in which sulphate is reduced to sulphide Ba will be released into the pore water. The aqueous Ba profile for core LL1 has a surface concentration of 16.2 μg l^{-1} (c.f. seawater 20 μg l^{-1}) and increases to 35.7μg l^{-1} at 3.43 g cm^{-2} (7.5 cm) indicating that there is a release of Ba into the pore waters which suggests that this is the depth at which the sulphate/sulphide redox couple is operating. Below this depth a minimum concentration of 19 μg l^{-1} occurs at 6.74 g cm^{-2} (17 cm) depth which coincides with a small increase in the solid phase Ba and may suggest the deposition of $BaSO_4$. The increased concentration of Ba at depth in this core, in comparison to the sea water value indicates that there is a release of Ba into the pore waters, probably as a result of the reduction of $BaSO_4$.

4.9.2 *Loch Goil core (GD2) pore water profiles*

The pore water profiles for selected elements are given in Figure 4.45. The nitrogen was turned off at a depth of 11.72 g cm^{-2} (43 cm) which is indicated on the plots by a dotted line. The aqueous phase Mn profile had a surface concentration of 38.9 mg l^{-1} (c.f. seawater 0.2 μg l^{-1}) which indicated that the surface sediment of this core was reducing with respect to Mn and indicated that the redox potential of this sediment is lower than the redox potential for the reduction of Mn oxyhydroxides. The rapid decrease in aqueous phase Mn concentration with depth in association with high solid phase concentrations (up to 2%) indicates downward diffusion of Mn and deposition under reduced conditions, probably as the carbonate, which is also suggested by the solid phase profiles. The aqueous phase Fe profile has a surface concentration of 2.0 mg l^{-1} and increases to a maximum of 5.7 mg l^{-1} at a depth of 0.68 g cm^{-2} (2.5 cm) indicating that this is probably the depth at which the Fe redox couple is operating. The Fe concentration decreases to 1.4 mg l^{-1} at 9.12 g cm^{-2} (33 cm) after which it increases to a maximum of 6.8 mg l^{-1} at 11.72 g cm^{-2} (43 cm).

The aqueous Mo profile has a surface concentration of 30 μg l^{-1} then rapidly decreases to 3.7 μg l^{-1} at 1.81 g cm^{-2} (6.5 cm). The Mo profile over this depth range is very similar to that of Mn suggesting that the Mo is being released from dissolving Mn oxyhydroxides. The Mo concentration remains relatively constant to 6.26 g cm^{-2} (21 cm) after which it begins to increase. The Mo data are therefore consistent with the Mn and Fe profiles, indicating that the sediment is rapidly becoming more reducing with depth. The aqueous U profile for core GD2 has a surface concentration of 3.9 μg l^{-1} (c.f. seawater 3.2 μg l^{-1}) then rapidly decreases to 0.8 μg l^{-1} by 0.36 g cm^{-2} (1.5 cm) indicating that the U in solution is being reduced very close to the surface of the sediment and is removed to the solid phase. As with all the aqueous phase elemental profiles the concentration of U begins to increase at 9.69 g cm^{-2} (35 cm). Therefore the profiles of the redox sensitive elements indicate that the Mn redox couple is operating at the surface of the sediment, the Fe redox couple is operating just below the surface, at approximately 0.7 g cm^{-2}

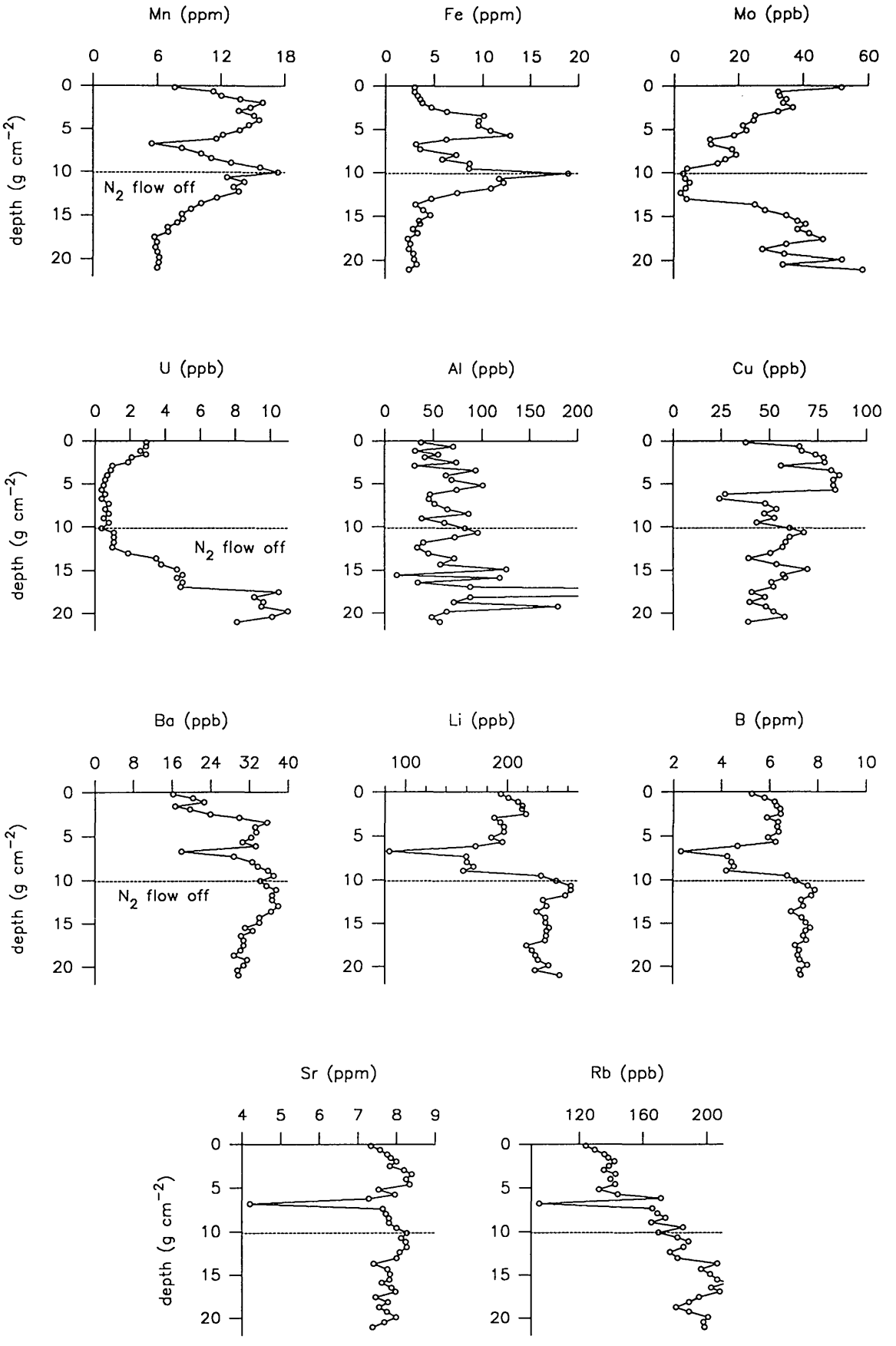

Figure 4.44 Loch Long core LL1 porewater results

(2.5 cm), the U redox couple is operating around 1 g cm^{-2} and finally the redox couple for Mo is operating at approximately 2 g cm^{-2}. The elements are following the expected trends of their redox couples which are all operating closer to the sediment surface than those of Loch Long indicating that the sediment of core GD2 is more reducing than that of LL1.

The aqueous Ba profile has a surface concentration of 44.2 μg l^{-1} which is twice that of seawater, and increases to a maximum of 78.4 μg l^{-1} at 0.68 g cm^{-2} (2.5 cm) after which it decreases rapidly to 8.5 μg l^{-1} at 1.81 g cm^{-2} (6.5 cm). The Ba profile indicates that dissolution is taking place at approximately 0.68 g cm^{-2} (2.5 cm) which is shallower than that of LL1 and, if equated with sulphate reduction, once again indicates that the sediment of GD2 is more reduced than that of LL1.

All of the other profiles show similar trends to those already discussed in that they have subsurface maximum concentrations decreasing to a minimum around 9 g cm^{-2} after which the concentration increases to and remains constant to below this. These samples were reanalysed to check for analytical error but gave the same results within error and it was therefore concluded that the increase at depth was a real observation and may be the result of re-dissolution of some authigenic phase at depth. There is an indication of a change to coarser material occurring around 9 g cm^{-2} and it is possible that the broad maximum in all the profiles is reflecting this.

4.9.3 *Loch Fyne core (FS) pore water profiles*

The pore water profiles for selected elements are given in figure 4.46. The nitrogen was turned off at a depth of 19.29 g cm^{-2} (30 cm) which is indicated on the plots by a dotted line.

The aqueous Mn profile has a surface concentration of 9.7 mg l^{-1}, increases to a maximum of 12.2 mg l^{-1} at 0.6 g cm^{-2} (1.5 cm) and then decreases to 3.6 mg l^{-1} at 13.9 g cm^{-2} (23 cm) depth. The aqueous phase Mn concentration below this depth begins to increase slightly. The Mn profile therefore

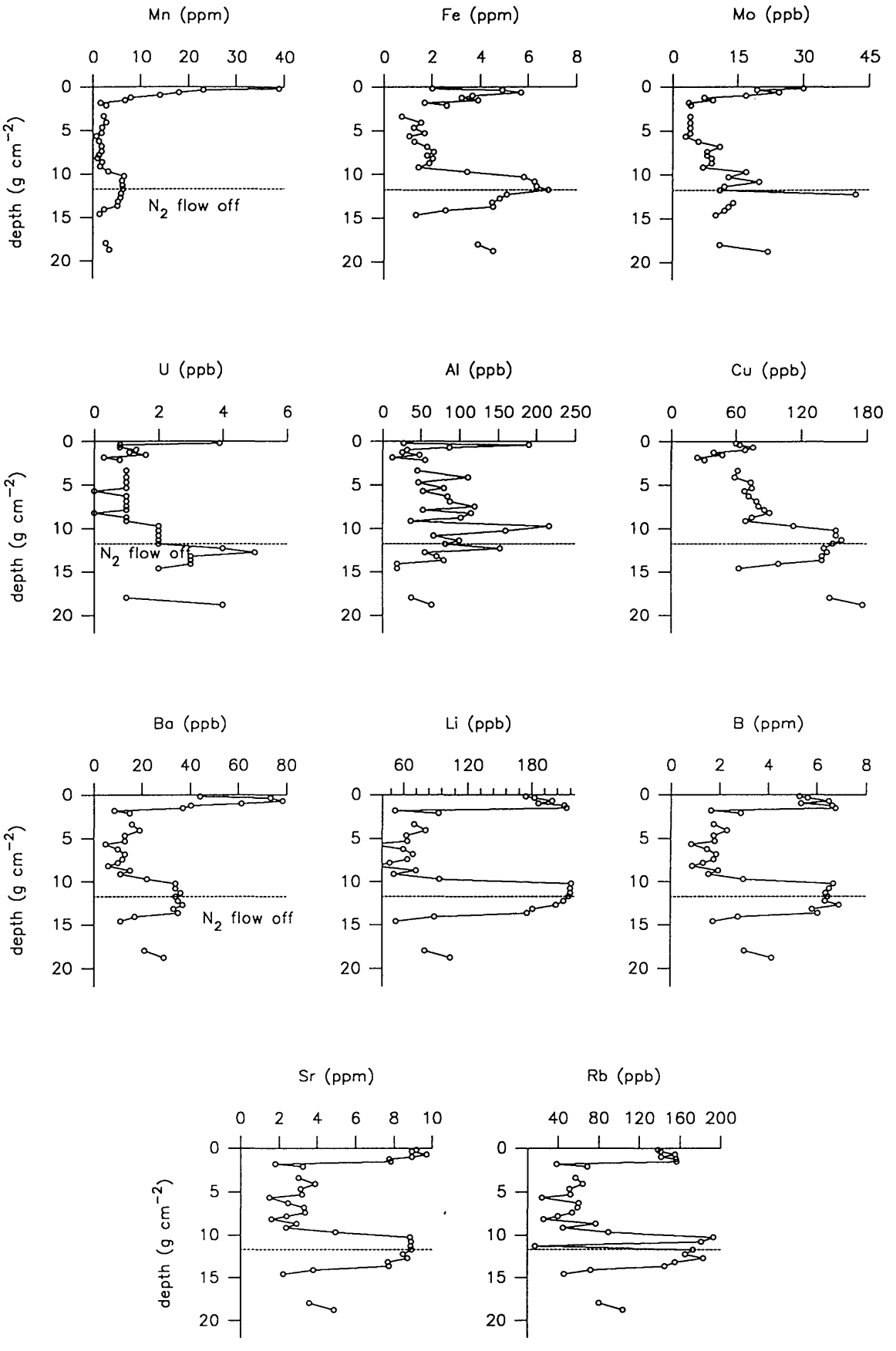

Figure 4.45 Loch Goil core GD2 porewater results

indicates that the sediment is reducing with respect to Mn at the surface as the Mn concentration is far greater than that of seawater. The aqueous phase Fe profile indicates that Fe is not being reduced until deeper in the core, at a depth of 2.27 g cm^{-2} (4.5 cm) suggesting that the Fe redox couple is operating at this depth.

The aqueous Mo profile has a surface concentration of 32.7 ng l^{-1} which is 1.5 times greater than that of seawater. The Mo concentration decreases to 14.5 ng l^{-1} at 6.74 g cm^{-2} (11 cm) and remains within the range 14 to 27 ng l^{-1} to a depth of 19.3 g cm^{-2} (33 cm). The aqueous U profile has a surface concentration of 2.2 ng l^{-1}, increases to 2.9 ng l^{-1} at 0.6 g cm^{-2} (1.5 cm) and then decreases to 0.7 ng l^{-1} at 6.74 g cm^{-2} (11 cm) indicating that the sediment is not reducing enough to affect the redox couple of U until a depth of 6.74 g cm^{-2} (11 cm) which is deeper than in cores GD2 and LL1.

The aqueous phase Ba profile indicates some enhancement with respect to seawater at a depth of 1.05 g cm^{-2} (2.5 cm) but does not show any obvious sign of sulphate reduction. The limited processes evidenced by the relatively consistent pore water profiles could indicate that little organic matter of a degradable nature is reaching this sediment which was also the reason suggested for the low ^{210}Pb fluxes of this sediment.

The remaining profiles show different trends, with the B, Sr and Rb profiles all exhibiting a minimum at the same depth. The aqueous Cu profile has a surface concentration of 70.3 μg l^{-1}, and then increases to 112.9 μg l^{-1} at 2.27 g cm^{-2} (4.5 cm). The Li profile decreases from the surface to a depth of 6.74 g cm^{-2} (11 cm) after which it increases to a maximum of 271.7 μg l^{-1} at a depth of 13.8 g cm^{-2} (23 cm).

4.9.4 *Loch Fyne core (FD) pore water profiles*

The pore water profiles for selected elements are given in figure 4.47. The nitrogen was used to the bottom of this core at a depth of 21.88 g cm^{-2} (45 cm).

The aqueous Mn profile has a surface concentration of 0.1 mg l^{-1} then increases rapidly to 12.1 mg l^{-1} at a depth of 1.34 g cm^{-2} (4.5 cm) after which it remains within the range 8.3 to 12.5 mg l^{-1} to the bottom of the core. The aqueous phase profile indicates very high values of around 10 mg l^{-1} for all samples below 1.34 g cm^{-2} (4.5 cm) indicating that Mn is reduced below this depth. Therefore the Mn profile indicates that the sediment is becoming more oxidising towards the surface. However the solid phase profiles of Mn and Ca for this core indicate that the surface enrichment in solid phase Mn is only partially attributable to deposition as a result of oxidation and that deposition of the carbonate is also a major factor. Nevertheless, the porewater data indicate a pronounced dissolution of Mn at 0.96 g cm^{-2} (3.5 cm) which is highly suggestive that this is the position of the Mn redox couple. The high aqueous phase concentrations of Mn below 0.96 g cm^{-2} (3.5 cm) do not appear to have been maintained by the bulk sediment and were probably produced by equilibrium with Mn nodules, which were removed before analysis. Above 0.96 g cm^{-2} (3.5 cm) the aqueous phase Mn concentration decreases rapidly to a value of 0.1 mg l^{-1} at the surface of the sediment indicating that the sediment is oxidising with respect to manganese at the surface. The aqueous phase Fe profile has a maximum concentration of at 2.92 g cm^{-2} (8.5 cm) depth. The band of elevated Fe concentrations occurs over the depth range 2.08 to 5.81 g cm^{-2} (6.5 to 14.5 cm) which probably indicates the depth at which re-dissolution of Fe and Mn oxyhydroxides was taking place and suggests that the Fe redox couple is operating at a depth of 2.5 g cm^{-2} (8.5 cm). The Fe concentration profile remains in the range 1 to 1.7 mg l^{-1} to a depth of 15.9 g cm^{-2} (33 cm) after which it increases to 4.2 mg l^{-1} and remains high to the bottom of the core. The aqueous Mo profile has a concentration of 11.9 μg l^{-1} which is lower than that of sea water (c.f. 20 μg l^{-1}) at the surface of the core and increases to 45.2 μg l^{-1} at 0.42 g cm^{-2} (1.5 cm), indicating dissolution of Mo. Concentrations then gradually decrease to 18 μg l^{-1} by 12.2 g cm^{-2} (25 cm), below which they increase again in parallel with an increase in the solid phase concentration (Table 4.47.), providing little evidence of Mo deposition as a consequence of reduction in this sediment. Therefore, the aqueous phase Mo profile is consistent with the concept of a relatively oxidising

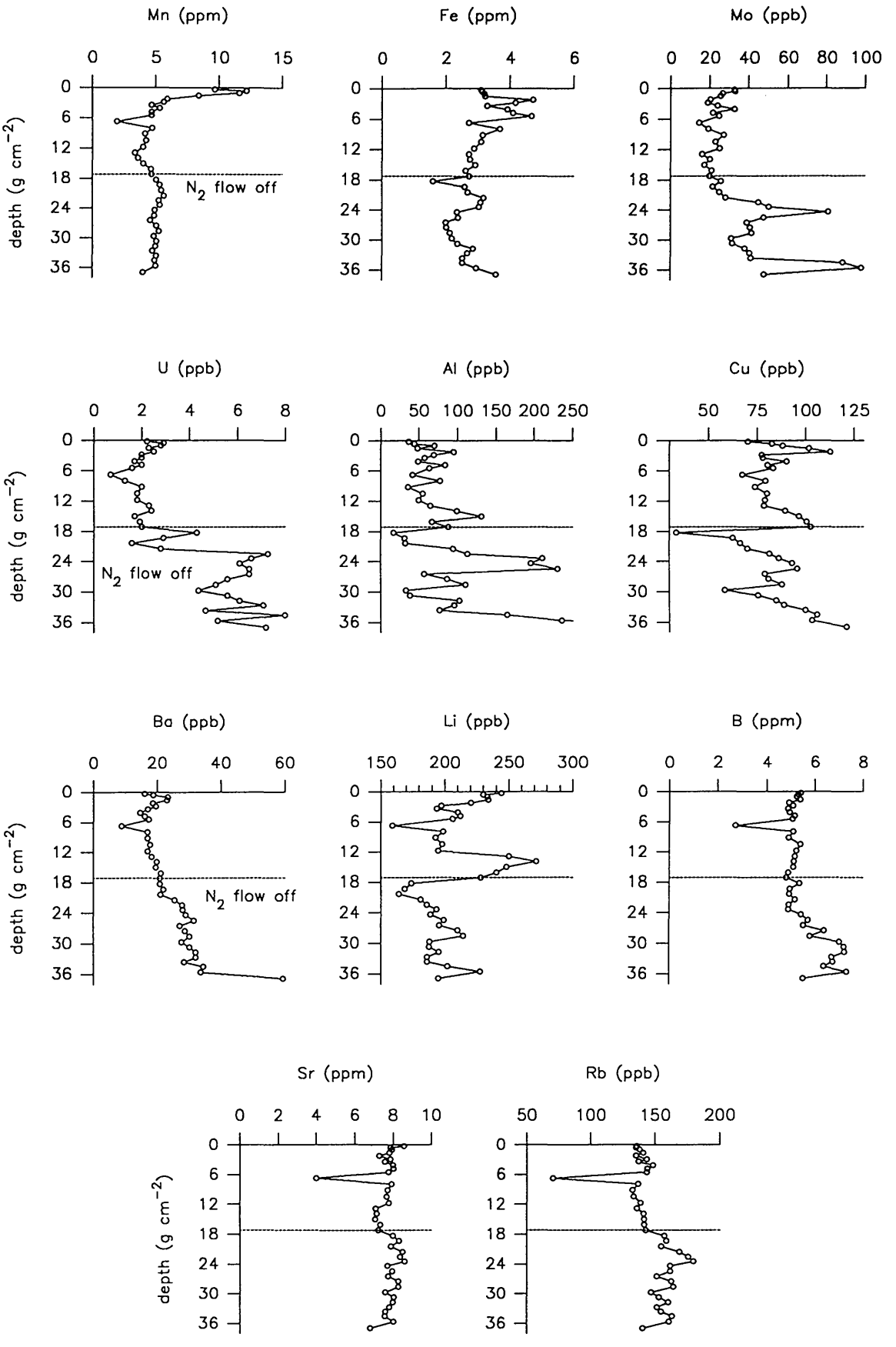

Figure 4.46. Loch Fyne core FS porewater results

sediment. The aqueous phase profile is similar to that of the Mn, suggesting that Mo may be released during re-dissolution of Mn nodules. In this core there is no evidence of U removal from the interstitial water, with all values being within error of the average sea water concentration of 3.2 μg l^{-1} to a depth of 14.02 g cm^{-2} (29 cm) indicating that the redox potential does not fall below that of the U redox couple. Below this depth the U concentration increases to 4.6 μg l^{-1} and has generally higher concentrations of U to the bottom of the core which is similar to the Mo and Fe pore water profiles. The above redox sensitive elements are indicating that the core is oxidising at the surface, below which there is reduction of Mn and Fe taking place. This reduction does not seem to affect the U and Mo concentrations which are probably being controlled by the re-dissolution of Mn nodules in this core.

The aqueous phase Ba profile has a value of 13 μg l^{-1} (c.f. sea water 20 μg l^{-1}) at the surface and remains below sea water values to 2.08 g cm^{-2} (6.5 cm) depth, after which it increases to a maximum of 106 μg l^{-1} at 7.68 g cm^{-2} (17.5 cm), indicating that Ba dissolution and hence reduction of sulphate to sulphide is taking place in this core. Below the maximum the concentration of Ba is in the range 62 to 98 μg l^{-1} below the maximum to the bottom of the core.

Of the remaining profiles Al, shows the largest changes, with maxima occurring at the same points as observed for Fe. This again could be due to the influences of the Mn nodules. The Cu profile also shows a maximum of 167 μg l^{-1} at 3.41 g cm^{-2} (9.5 cm) which correlates with the Fe maximum at that depth and possibly indicates the enhancement of Cu in the pore waters due to the dissolution of Mn nodules. The Cu profile also shows an increase in concentration below 15.91 g cm^{-2} (33 cm) depth. The Li, B, Sr and Rb profiles are all similar with a maximum occurring at 0.42 g cm^{-2} (1.5 cm) again with a suggestion of an increase in concentration at depth.

From this study it has been shown that ICP-MS is a useful and powerful technique in analysing pore waters and provides potentially extremely useful data. The use of the concentration of redox sensitive elements within the

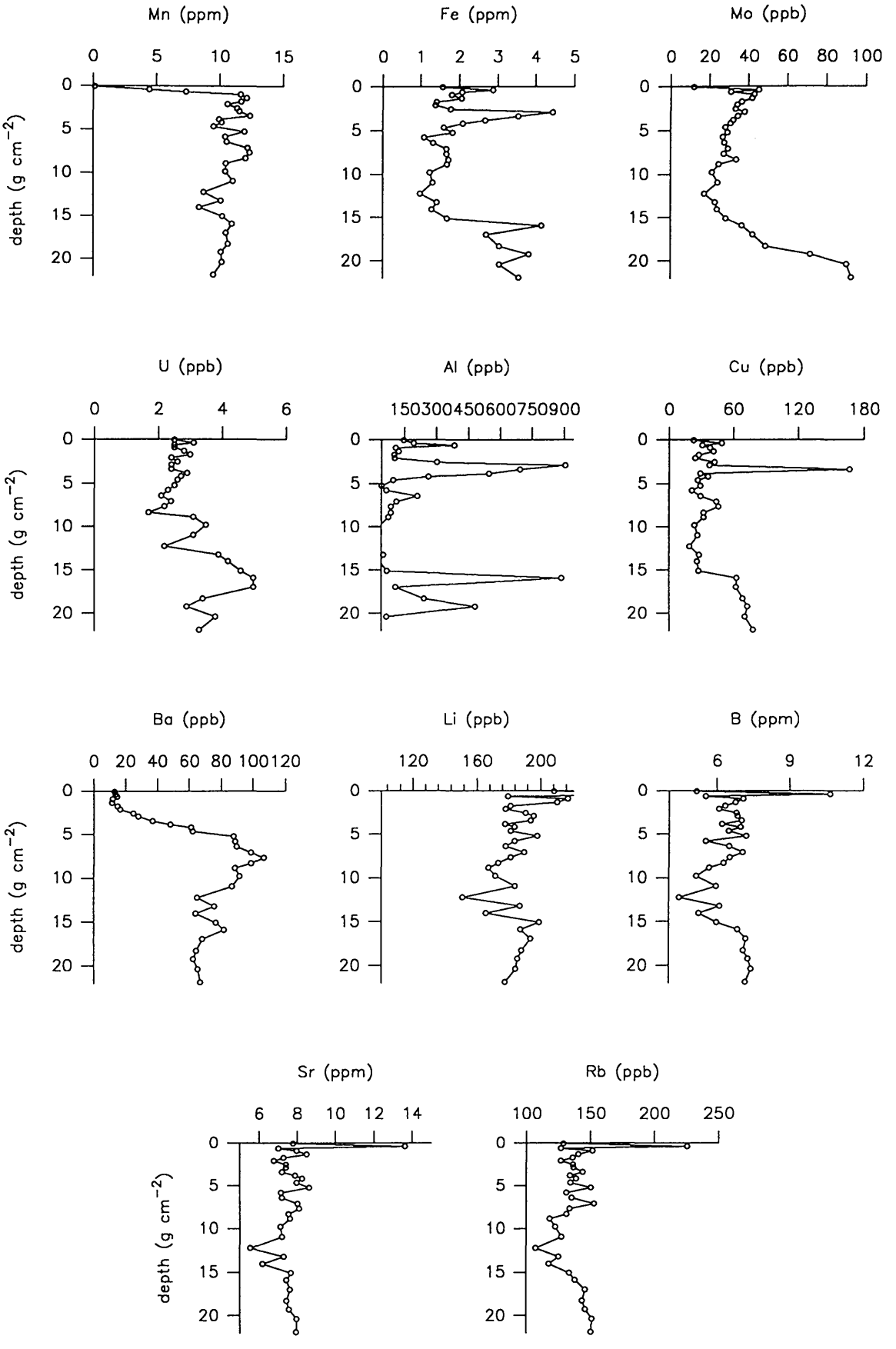

Figure 4.47. Loch Fyne core FD porewater results

pore water allows the assessment of the redox conditions of a sediment which may be difficult to do from solid phase data alone.

4.10 *Conclusions*

This work provided a number of significant conclusions that can be summarised as follows;

a) Radionuclide behaviour in sea lochs

The sedimentation rates obtained by application of ^{210}Pb dating, correlation of ^{137}Cs maximum concentrations with Sellafield discharge maxima and correlation of ^{137}Cs depths of penetration with onset of Sellafield discharge are summarised in Table 4.26.

Core	^{210}Pb sed. rate	^{137}Cs sed. rate (maximum)	^{137}Cs sed. rate (depth of penetration)
LE 1	0.10 g cm^{-2} y^{-1}	0.10 g cm^{-2} y^{-1}	0.31 g cm^{-2} y^{-1}
LE 2	0.07 g cm^{-2} y^{-1} 0.04 g cm^{-2} y^{-1}	0.18 g cm^{-2} y^{-1}	0.22 g cm^{-2} y^{-1}
LE 3	0.06 g cm^{-2} y^{-1}	0.07 g cm^{-2} y^{-1}	0.22 g cm^{-2} y^{-1}
LL1	0.10 g cm^{-2} y^{-1} 0.40 g cm^{-2} y^{-1} 0.14 g cm^{-2} y^{-1}	0.33 g cm^{-2} y^{-1}	0.69 g cm^{-2} y^{-1}
GD2	0.07 g cm^{-2} y^{-1}	0.09 g cm^{-2} y^{-1}	0.31 g cm^{-2} y^{-1}
FS	0.008 g cm^{-2} y^{-1}	0.21 g cm^{-2} y^{-1}	0.61 g cm^{-2} y^{-1}
FD	not applicable	0.08 g cm^{-2} y^{-1}	0.38 g cm^{-2} y^{-1}

Table 4.26 Sedimentation rates of the sediment cores studied.

These data clearly show that in cases where continuous accumulation (over limited sections of the core in some cases) applied, there is excellent agreement between the ^{210}Pb and ^{137}Cs maximum chronologies, i.e. cores LE1, LE3, LL1 and GD2. This is particularly significant in the case of LE3 since it implies that ^{210}Pb is not diagenetically mobile in this sediment. In the case of cores LE2 and FS, where an increase in sedimentation rate towards the surface was apparent, there is significant disagreement between the ^{210}Pb and ^{137}Cs max. chronologies, indicating that application of a single sedimentation rate to derive a chronology for these cores is not valid.

The ^{210}Pb data revealed mixing in the range 1 to 3.8 g cm^{-2} for the cores studied and clearly identified pronounced variations in sedimentation rate in core LL1, almost certainly as a consequence of anthropogenic redistribution of sediment .

In all cases studied, the XRF data suggested a change to coarser sediment near the surface, again probably resulting from human activity, and this could in several cases be related to an increasing sedimentation rate as indicated by ^{210}Pb and ^{137}Cs as demonstrated in cores LE 2, LL1 and FS.

^{241}Am concentrations profiles were also used to determine sedimentation rates, and in most cases where it was present at detectable levels, it was in reasonable agreement with the sedimentation rates obtained by ^{210}Pb dating. This was not the case in core FD which had an unusual profile, but as stated in the text this core has a unique geochemistry in which Mn nodules form and this may be influencing the distribution of ^{241}Am in this core.

The $^{134}Cs/^{137}Cs$ ratio profiles of the sediment cores were used along with the ^{210}Pb profiles to assess the extent of mixing within the cores. The amount of mixing varied considerably between cores and it was apparent that the assessment of the extent of mixing was important with respect to the determining sedimentation rates and interpretation of temporal trends of pollutant metals and Pb isotope ratios within the sediments of the sea lochs.

The radionuclide inventories and fluxes for the seven cores are given in Table 4.27.

Core	excess ^{210}Pb (Bq m^{-2})	^{210}Pb flux (Bq m^{-2} y^{-1})	^{228}Ra (Bq m^{-2})	^{228}Th (Bq m^{-2})	^{137}Cs (Bq m^{-2})	^{134}Cs (Bq m^{-2})	^{241}Am (Bq m^{-2})
LE 1	9500 ± 1400	294 ± 45	4800 ± 380	4900 ± 230	10100 ± 300	128 ± 6	135 ± 20
LE 2	2200 ± 280	68 ± 9	6700 ± 470	8000 ± 360	7500 ± 220	87 ± 17	8 ± 1
LE 3	7700 ± 1100	238 ± 33	5300 ± 400	5400 ± 360	7700 ± 220	276 ± 6	105 ± 20
LL1	7700 ± 980	240 ± 30	9300 ± 400	10200 ± 450	39000 ± 1500	460 ± 20	531 ± 35
GD2	6700 ± 800	208 ± 25	7300 ± 350	8300 ± 360	21100 ± 500	180 ± 10	190 ± 20
FS	3100 ± 300	97 ± 10	10700 ± 500	11200 ± 600	14300 ± 300	110 ± 8	150 ± 10
FD	2200 ± 250	68 ± 8	6300 ± 700	7000 ± 300	5400 ± 130	7 ± 1	94 ± 6

Table 4.27 Radionuclide inventories and fluxes

The excess ^{210}Pb inventories were in the range 2200 to 9500 Bq m^{-2}, with fluxes ranging from 68 to 294 Bq m^{-2} y^{-1}. The highest fluxes occurred within the deeper stations where the sediment had a greater organic content and consisted of finer sediment. In the cores where the sediment became coarser towards the surface and the organic content became less the ^{210}Pb flux was lower. In the deeper stations the ^{210}Pb flux was higher than expected from atmospheric deposition alone and it has been concluded that there has been sediment focusing of finer organic rich material to the deeper stations. Cores LE 1 and LE 3 are from very different geochemical environments but, the fluxes of ^{210}Pb to both cores were essentially the same which reinforces the conclusion that Pb is not mobile in the sea loch sediments studied. The ^{137}Cs inventories ranged from 5400 to 39000 Bq m^{-2} but did not vary between sites in the same manner as the ^{210}Pb flux, and indicating that the two radionuclides have a different mechanism for uptake in the sediments.

Therefore the radionuclides studied within these sediments have indicated that three of the sediment cores from the Clyde Sea Area (LL1, FS and FD) have had an increased supply of sediment in more recent times and core LL1 has been perturbed by dumping of dredged sediment at or close to the sampling site. It is concluded that the sediments of the sea lochs of the Clyde Sea Area reflect the increased affect of anthropogenic influences within the

area. The sediment cores of Loch Etive do not reflect the same level of anthropogenic disturbance but the chronology obtained from the radionuclides in conjunction with the geochemical data suggests that a major change in input to the loch occurred around 1915.

^{226}Ra was observed to mobile in some of the sediments studied and an excess of ^{228}Ra and ^{228}Th was observed in the inner basin of Loch Etive reflecting the involvement of radium in the Mn redox cycle.

b) Heavy metal distributions, geochemistry and historical trends in deposition.

Another aspect of this research was to investigate heavy metal distributions and geochemistry with particular respect to the potential diagenetic mobility of Pb. The total and excess inventories for Pb, Zn and Cu for the cores from Loch Etive, Loch Long, Loch Goil and Loch Fyne are given in Table 4.28.

Core	total Pb ($g\ m^{-2}$)	excess Pb ($g\ m^{-2}$)	total Zn ($g\ m^{-2}$)	excess Zn ($g\ m^{-2}$)	total Cu ($g\ m^{-2}$)	excess Cu ($g\ m^{-2}$)
LE 1	7.4	3.8	21.1	7.8	1.4	0.5
LE 2	5.6	1.6	19.8	3.4	1.2	0.6
LE 3	6.9	3.8	18.7	8.1	1.2	0.4
LL1	73.8	68.3	87.3	62.6	12.6	7.6
GD2	47.4	43.9	66.8	52.5	7.8	4.5
FS	8.5	2.3	36.4	4.3	2.7	0.5
FD	7.5	3.1	21.7	2.7	3.3	1.3

Table 4.28 Total and excess Pb, Zn and Cu inventories

The three pollutant metals investigated (Pb, Zn and Cu) all showed similar temporal trends consistent with the ^{210}Pb and ^{137}Cs chronologies, with an increase in the flux occurring in the early 1900's. The cores from the locations remote from industrial centres, that is Loch Etive and Loch Fyne indicate a sharp increase occurring in the pollutant flux around 1915. The one exception is core LE 3 which a more gradual increase and it was concluded that this was due to the extent of mixing within this core. The trends for LE 1 and LE 3 are entirely consistent with expected trends in historical input on

the basis of the ^{210}Pb and ^{137}Cs max chronologies. Therefore there is no evidence of diagenetic mobility of Pb in Loch Etive on this basis. The inventories for cores from Loch Etive and Loch Fyne had excess Pb inventories ranging from 1.6 to 3.8 g m^{-2}. The two cores which had coarser material at the surface, LE 2 and FS, had the lowest excess Pb inventories and as with the ^{210}Pb fluxes this suggests that the Pb is associated with the finer sediment and/or the organic matter of the sea lochs. The inventories of excess Pb for cores LE 1 and LE 3, which are from very differing geochemical environments (LE 1 oxic, LE 3 anoxic) were the same which suggests that there is no Pb loss from the anoxic sediment indicating that Pb is not diagenetically mobile in this environment. The excess Pb inventories for cores LL1 (Loch Long) and GD2 (Loch Goil) 68.3 and 43.9 g m^{-2} respectively, are considerably greater than those from the remoter locations indicating the extent of anthropogenic pollutant input to these sites. In contrast, the 'remote' lochs have excess Pb inventories of approximately 2 to 4 g cm^{-2} which can be compared to the excess Pb inventories of Loch Lomond (2.91 g cm^{-2}), a freshwater loch, and peat cores from Flanders Moss (3.38 g m^{-2}) and North Uist (0.52 g m^{-2}) (Sugden, 1993). The similarity of the excess Pb inventories between these sea lochs and the freshwater loch and peat cores, suggests that the input is close to atmospheric and that there is no discernible marine influence as would be expected from the relatively short residence time of Pb in seawater. The heavy metal data, ^{210}Pb and Pb isotope ratio profiles all indicated that there was a section of dumped surface material within core LL1 which was dumped around 1962 which correlates with the opening of an American Naval base at Holy Loch.

The excess Zn inventories ranged from 2.7 to 8.1 g m^{-2} for Loch Etive and Loch Fyne revealing a relatively low level of pollution. The excess Zn inventories for cores LE 1 and LE were essentially the same and that of core LE 2 was lower. The excess Zn inventories for cores LL1 and GD2 were 62.6 and 52.5 g m^{-2} again indicating that these site are heavily contaminated. The excess Cu inventories for Loch Etive and Loch Fyne range from 0.4 to 1.3 g m^{-2}, but in this case the excess Cu inventories are essentially the same for all three cores from Loch Etive and core FS from Loch Fyne. Core FD has a higher excess Cu inventory which probably reflects the influence of the

nodules within this core. The excess Cu inventories for cores LL1 and GD2 are 7.6 and 4.5 g m^{-2} again the higher values reflecting the highly contaminated nature of these sediments. There is a dump site located near Holy Loch where sewage sludge and dredged surface sediment is dumped and this may be spreading and affecting these two sites.

Therefore in conclusion, the heavy metal profiles show temporal trends that are consistent with increased industrial activity and indicate that the sediments from Loch Long and Loch Goil are heavily contaminated and that Pb is not mobile in these sediments. The excess Pb and Zn inventories show similar trends with the excess Zn to Pb inventory ratios being approximately 2 for cores LE 1, LE 2, LE 3 and FS, with cores LL1, GD2 and FD having a ratio around 1. Core FD is unusual in that it is from a remote site with a low level of pollution but has and excess Pb/excess Zn inventory ratio that is similar to the highly contaminated cores of LL1 and GD2, again this is thought to be due to a combination of the geochemical conditions and the removal of Mn nodules before analysis. The excess Pb/excess Cu inventory ratios range from 0.1 to 0.4 with the contaminated sediment from LL1 and GD2 having the same ratio as cores LE 1 and LE 3 indicating that either Cu has a different input source than Pb and Zn or that there is a different mechanism of removal to the sediments.

The Pb isotope profiles for all the cores indicate that there has been an increase in deposition of Pb from petrol over the last fifty years and the dates for the onset of deposition of Pb from petrol are given in Table 4.29.

The cores from the remote locations and cores LL1 and GD2 all indicate that the onset of the deposition of Pb from petrol occurs between 1916 to 1947 which agrees well with the known historical date of input in the late 1920's. Therefore the Pb isotope profiles are consistent with the chronologies obtained from ^{210}Pb and ^{137}Cs profiles and again reinforce the conclusion that Pb is not mobile in these sediments. The % of Pb from petrol is highest in the cores from Loch Etive and Loch Fyne (with the exception of FD), indicating that the major source of pollutant Pb to these sites is from atmospheric deposition with a large percentage resulting from pollutant Pb

from petrol. The lower % of pollutant Pb from petrol for cores LL1 and GD2 reflects the increased contamination of these sediments with non petrol Pb and indicates that there is an additional supply of pollutant Pb to these sediments which probably results from the redistribution of contaminated sediment.

Core	onset of Pb from Petrol from $^{206}Pb/^{207}Pb$ profile	onset of Pb from Petrol calculated from isotope ratio model	
LE 1	1937	1947	Petrol Pb= 4%(min); 44% (max)
LE 2	1928	1928	Petrol Pb=5%(min); 42%(max)
LE 3	1935	1935	Petrol Pb=14%(min); 47%(max)
LL1	1916	1916	Petrol Pb= 3%(min); 27%(max)
GD2	1924	1929	Petrol Pb= 5%(min); 25%(max)
FS	1947	1947	Petrol Pb= 1%(min); 61%(max)
FD	1938	1947	Petrol Pb= 5%(min); 15%(max)

Table 4.29 Date of onset of deposition of pollutant Pb from petrol

c) ICP-MS analysis of sediment pore water

This study also established that ICP-MS is a very useful technique in the study of pore waters and that a large amount of potentially useful information can be obtained which is not restricted to the redox sensitive elements. The analysis of the pore waters from the four cores from the Clyde Sea Area indicated that the redox couples of Mn, Fe , U and Mo were operating in there expected sequence and redox trends were established in each of the cores which were consistent with that of the solid phase profiles. The Mo pore water data suggested that the main controlling factor of Mo in these surface sediments was Mn and where the sediment was reducing with respect to Mn, the Mo concentration of the pore waters was high.

In summary, this research has validated the use of ^{210}Pb and ^{137}Cs in chronological and mixing studies of sediments, characterised such processes in four Scottish Sea Lochs and defined inventories and depositional trends for heavy metals in those locations. The work indicates that Pb is not diagenetically mobile in any of the sediments and demonstrates that ICP-MS

is potentially an extremely useful technique in the study of porewaters.

REFERENCES

Aaby, B., Jacobsen, J. and Jacobsen, O. S. Pb-210 dating and lead deposition in the ombrotrophic peat bog, Draved Mose, Denmark. D. G. U. arbog, 1978.

Appleby, P. G. and Oldfield, F. The calculation of lead-210 dates assuming a constant rate of supply of unsupported ^{210}Pb to the sediment. Catena, 5, 1-8, 1978.

Applications of inductively ccupled plasma mass spectrometry. Eds. A. R. Date and A. L. Gray. Publ. Blackie, Glasgow and London, 1989.

Assinder, D. J., Kelly, M. and Aston, S. R. Tidal Variations in Dissolved and Particulate Phase Radionuclide Activities in the Esk Estuary, England and their Distribution Coefficients and Particulate Activity Fractions. J. Environ. Radioactivity 2, 1-22, 1985.

Aston, S. R., Assinder, D. J., Stanners, D. A. and Rae, J. E. Plutonium Occurrence and Phase Distribution in Sediments of the Wyre Estuary, Northwest England. Marine Pollut. Bull., 12, 9, 308-314, 1981.

Aston, S. R. and Stanners, D. A. Local Variability in the Distribution of Windscale Fission Products in Estuarine Sediments. Est. Coastal Shelf Sci., 14, 167-174, 1982.

Aston, S. R. and Stanners, D. A. The transport to and deposition of americium in intertidal sediments of the Ravenglass estuary and its relationship to plutonium. Environ. Pollut. (Ser. B.), 3, 1-9, 1982.

Baas Becking, L. G. M., Kaplan, I. R. and Moore, D. Limits of the natural environment in terms of pH and oxidation-reduction potentials. Jour. of Geol., 68, 3, 1960.

Bacon, M. P., Spencer, D. W. and Brewer, P. G. $^{210}Pb/^{226}Ra$ and $^{210}Po/^{210}Pb$ disequilibria in seawater and suspended particulate matter. Earth Planet. Sci. Letts., 32, 277-296, 1976.

Baxter, M. S., McKinley, I. G., MacKenzie, A. B. and Jack, W. Windscale Radiocaesium in the Clyde Sea Area. Mar. Poll. Bull., 10, 116-120, 1979.

Baxter, M. S. and McKinley, I. G. Radioactive species in sea water. Proc. Roy. Soc. Edinburgh, 76B, 17-35, 1978.

Ben-Shaban, Y. A. Radionuclide movement and geochemistry in intertidal sediments in South West Scotland. PhD Thesis, SURRC, University of Glasgow, 1989.

Benninger, L. K., Aller, R. C., Cochran, J. K. and Turekian, K. K. Effects of biological sediment mixing on the ^{210}Pb chronology and trace metal distribution in a Long Island sound sediment core. Earth Planet. Sci. Letts., 43, 241-259, 1979.

Benoit, G. and Hemond, H. F. ^{210}Po and ^{210}Pb Remobilization from Lake Sediments

in Relation to Iron and Manganese Cycling. Environ. Sci. Technol., 24, 1224-1234, 1990.

Benoit, G. and Hemond, H. F. Evidence for diffusive redistribution of ^{210}Pb in lake sediments. Geochim. Cosmochim. Acta, 55, 1063-1975, 1991.

Berg, T., Hagen, L. O., Royset, O. and Steinnes, E. Elements in Airborne Particles at 24 Urban and Industrial Sites in Norway. In: Heavy Metals in the Environment, vol. 1. Ed. J. G. Farmer, CEP Consultants, Edinburgh, 1991.

Berger, W. H. and Heath, G. R. Vertical mixing in pelagic sediments. Jour. Mar. Research, 26, 134-143, 1968.

Berner, R. A. Early Diagenesis: A Theoretical Approach. Publ: Princeton University Press, Princeton, New Jersey, 1980.

Bewers, J. M. and Yeats, P. A. Oceanic residence times of trace metals. Nature, 268, 595-598, 1977.

Bjurman, B., Erlandsson, B. and Mattsson, S. Efficiency calibration of Ge spectrometers for measurements on environmental samples. Nucl. Instr. Methods Phys. Res. A262, 548-550, 1987.

BNFL plc. Annual report on radioactive discharges and monitoring of the environment, 1977-89. BNFL, Risley, Warrington. Issued by Director of Health and Safety, 1978-90.

Bonnett, P. J. P. and Cambray, R. S. The chronology of deposition of radionuclides as recorded in the sediments of Ponsonby Tarn, Cumbria. Proc. 5th Int. Symp. Palaeolimnology, Cumbria, 1989.

Bowen, V. T., Noshkin, V. E., Livingston, H. D. and Volchok, H. L. Fallout radionuclides in the Pacific Ocean: Vertical and horizontal distributions, largely from Geosecs stations. Earth Planet. Sci. Lett., 49, 411-434, 1980.

Broecker, W. S. and Bonebakker, E. R. The Vertical Distribution of Cesium 137 and Strontium 90 in the Oceans, 2. Jour. Geophys. Res., 71, 8, 1966.

Broecker, W. S., Kaufman, A. and Trier, R. M. The residence time of thorium in surface sea water and its implications regarding the rate of reactive pollutants. Earth Planet. Sci. Letts., 20, 35-44, 1973.

Brown, J. S. Ore leads and isotopes. Econ. Geol., 57, 673, 1962.

Bruland, K. W., Franks, R. P., Landing, W. M. and Soutar A. Southern California inner basin sediment trap calibration. Earth Planet. Sci. Letts., 53, 400-408, 1981.

Bruland, K. W., Bertine, K., Koide, M. and Goldberg, E. D. History of metal pollution in southern California coastal zone. Environ. Sci. Tech. 8, 425-432, 1974.

Bruno, J. and Sellin, P. Radionuclide solubilities to be used SKB 91. SKB Technical

Report 92-13, Stockholm, 1992.

Bryant, C. PhD Thesis, University of Edinburgh, 1993.

Buchowiecki, J. and Cherry, R. D. Thorium, radium and potassium in manganese nodules. Chem. Geol., 3, 111-117, 1968.

Burdige, D. J. and Gieskes, J. M. A pore water/solid phase diagenetic model for manganese in marine sediments. Am. J. Sci., 283, 29-47, 1983.

Calvert, S. H. and Price, N. B. Composition of Manganese Nodules and Manganese Carbonates from Loch Fyne, Scotland. Contr. Mineral and Petrol. 29, 215-233, 1970.

Cambray, R. S. Annual discharges of certain long-lived radionuclides to the sea and to the atmosphere from the Sellafield Works, Cumbria 1957-81. UKAEA Harwell Report AERE-M-3283. United Kingdom Atomic Energy Authority, Harwell, UK, 1982.

Cambray, R. S. and Eakins, J. D. Pu, ^{241}Am and ^{137}Cs in soil in West Cumbria and a maritime effect. Nature, 300, 1982.

Camplin, W. C., Mitchell, N. T., Leonard, D. R. P. and Jefferies, D. F. Radioactivity in surface and coastal waters of the British Isles. Monitoring of fallout from the Chernoybl Reactor Accident. In: Aquatic Environment Monitoring Report, no. 15, M.A.F.F., Lowestoft, 1986.

Carpenter, R. and Beasley, T. M. Plutonium and americium in anoxic marine sediments: Evidence against remobilization. Geochim. Cosmochim. Acta, 45, 1917-1930, 1981.

Carpenter, R., Beasley, T. M., Zahnle, D. and Somayajulu, B. L. K. Cycling of fallout (Pu, ^{241}Am, ^{137}Cs) and natural (U, Th, ^{210}Pb) radionuclides in Washington continental slope sediments. Geochim. Cosmochim. Acta, 51, 1897-1921, 1987.

Carpenter, R., Peterson, M L., Bennett, J. T. and Somayajulu, B. L. K. Mixing and cycling of uranium, thorium and ^{210}Pb in Puget Sound sediments. Geochim. Cosmochim. Acta, 48, 1949-1963, 1984.

Carter, M. W. and Moghissi, A. A. Three decades of nuclear testing. Health Phys. 33, 55-71, 1977.

Chanton, J. P., Martens, C. S. and Kipphut, G. W. Lead-210 sediment geochronology in a changing coastal environment. Geochim. Cosmochim. Acta, 47, 1791-1804, 1983.

Chester, R. Marine Geochemistry. Ed. Unwin Hyman, London, 1990.

Chung, Y. ^{210}Pb in the western Indian Ocean: distribution, disequilibrium and partitioning between dissolved and particulate phases. Earth Planet. Sci. Letts., 85, 28-40, 1987.

Clifton, R. J. and Hamilton, E. I. Lead-210 Chronology in Relation to Levels of Elements in Dated Sediment Core Profiles. Est. Coastal Marine Sci., 8, 259-269, 1979.

Clyde Study Group, Members of the. An Assessment of Present Knowledge. NERC Publ. Series C., 11, 1974.

Cochran, J. K., Carey, A. E., Sholkovitz, E. R. and Surprenant, L. D. The geochemistry of uranium and thorium in coastal marine sediments and sediment pore waters. Geochim. Cosmochim. Acta, 50, 663-680, 1986.

Cochran, J. K., Livingston, H. D., Hirschberg, D. J. and Surprenant, L. D. Natural and anthropogenic radionuclide distributions in the northwest Atlantic Ocean. Earth Planet. sci. Letts., 84, 135-152, 1987.

Comans, R. N. J., Middelburg, J. J., Zonderhuis, J., Woitticz, J. R. W., de Lange, G. J., Das, H. A. and van der Weijden, C. H. Mobilisation of radiocaesium in pore water of lake sediments. Nature, 339, 367-369, 1989.

Cook, G. T., Baxter, M. S., Duncan, H. J. and Malcolmson, R. Geochemical Associations of Plutonium and γ-Emitting Radionuclides in Caithness Soils and Marine Particulates. J. Environ. Radioactivity, 1, 119-131, 1984.

Cutshall, N. H., Larsen, I. L. and Olsen, C. R. Direct analysis of ^{210}Pb in sediment samples: self-absorption corrections. Nucl. Instr. Methods, 206, 309-312, 1983.

Date, A. R., Yuk Ying Cheung and Stuart, M. E. The influence of polyatomic ion interferences in analysis by inductively coupled plasma source mass spectrometry (ICP-MS). Spectrochimica Acta, 428, 1/2, 3-20, 1987.

Day, J. P. and Cross, J. E. ^{241}Am from the decay of ^{241}Pu in the Irish Sea. Nature, 292, 43-45, 1981.

Dean, J. R., Ebdon, L. and Massey, R. Selection of mode for the measurement of lead isotope ratios by inductively coupled plasma mass spectrometry and its application to milk powder analysis. Jour. Anal. Atomic Spec., 2, 1987.

Dean, W. E., Moore, W. S. and Nealson, K. H. Manganese cycles and the origin of manganese nodules, Oneida Lake, New York, USA. Chem. Geol., 34, 53-64, 1981.

Delves, H. T. Biomedical applications of ICP-MS. Chemistry in Britain, 1009-1012, 1988.

Delves, H. R. and Campbell, M. J. Measurements of total lead concentrations and of lead isotope ratios in whole blood by use of Inductively Coupled Plasma Source Mass Spectrometry. Jour. Anal. Atomic Spec., 3., 343-348, 1988.

Doff, D. H. The geochemistry of recent oxic and anoxic sediments of Oslo fjord, Norway. PhD Thesis, University of Edinburgh, 1969.

Ducastel, G., Maenhaut, W., Hillamo, R., Pakkanen, T. and Pacyna, J. M. Detailed

Size Distributions of Atmospheric Trace Elements in Southern Norway During Spring 1988 and 1989. In: Heavy Metals in the Environment, 1. Ed. J. G. Farmer, CEP Consultants, Edinburgh, 1991.

Dudley Stamp, L. Britain's Structure and Scenery. The Fontana New Naturalist, 1969.

Duinker, J. C. Formation and Transformation of Element Species in Estuaries. In: The Importance of Chemical "Speciation" in Environmental Processes. Eds. M. Bernhard, F. E. Brinckman and P. J. Sadler, 365-384, 1986.

Duinker, J. C., Wollast, R. and Billen, G. Behaviour of manganese in the Rhine and Scheldt estuaries. II. Geochemical cycling. Estuar. Coastal Shelf Sci. 9, 727-738, 1979.

Edgington, D. N. Characterization of transuranic elements at environmental levels. In: Techniques for Identifying Transuranic Speciation in Aquatic Environments. Proc. Joint CEC/IAEA Tech. Meeting, Ispra, 1980.

Edwards, A. and Edelsten, D. J. Deep Water Renewal of Loch Etive: A three basin Scottish Fjord. Est. and Coast. Mar. Sci. vol. 5, 575-595, 1977.

Edwards, A. and Sharples, F. Scottish Sea Lochs: A Catalogue. Dunstaffnage Marine Laboratory, 1991.

Ehmann, W. D. and Vance, D. E. Chemical Analysis, 116. Ed. John Wiley, New York, 531pp, 1991.

Elbaz-Poulichet, F., Holliger, P., Martin, J. M. and Petit, D. Stable lead isotopes ratios in major French rivers and estuaries. Sci. Tot. Env., 54, 61-76, 1986.

Elbaz-Poulichet, F., Holliger, P., Wei Wen Huang and Martin, J. M. Lead cycling in estuaries, illustrated by the Gironde estuary, France. Nature, 308, 1984.

Elsinger, R. J. and Moore, W. S. ^{226}Ra and ^{228}Ra in the Mixing Zones of the Pee Dee River-Winyah Bay, Yangtze River and Delaware Bay Estuaries. Est. Coastal Shelf. Sci. 18, 601-613, 1984.

Erlenkeuser, H., Suess, E. and Willkom, H. Industrialization affects, heavy metal and carbon isotope concentrations in Recent Baltic Sea sediments. Geochim. Cosmochim. Acta 38, 823-842, 1974.

Ertel, J. R. and Hedges, J. I. Sources of sedimentary humic substances: vascular plant debris. Geochim. Cosmochim. Acta 49, 2097-2107, 1985.

Farmer, J. G. Metal Pollution in Marine Sediment Cores from the West Coast of Scotland. Marine Env. Res., 8, 1-28, 1983.

Faure, G. Principles of isotope geology. Eds. John Wiley and Sons, New York, 1986.

Flegal, A. R., Nriagu, J. O., Niemeyer, S. and Coale, K. H. Isotopic tracers of lead contamination in the Great Lakes. Nature, 339, 455-460, 1989.

Flegal, A. R. and Stukas, V. J. Accuracy and precision of lead isotopic composition measurements in seawater. Marine Chemistry, 22, 163-177, 1987.

Fowler, S. W., Buat-Menard, P., Yokoyama, Y., Ballestra, S., Holm, E. and van Nguyen, H. Rapid removal of Chernobyl fallout from Mediterranean surface waters by biological activity. Nature, 329, 1987.

Friedlander, G., Kennedy, J. W., Macias, E. S. and Miller, J. M. Nuclear and Radiochemistry, 3rd Edition. Ed. John Wiley, New York, 684p, 1981.

Froelich, P. N, Klinkhammer, G. P., Bender, M. L., Luedtke, N. A., Heath, F. R., Cullen, D., Dauphin, P., Hammond, D., Hartman, B. and Maynard, V. Early oxidation of organic matter in pelagic sediments of the eastern equatorial Atlantic: suboxic diagenesis. Geochim. Cosmochim. Acta 43, 1075-1090, 1979.

Fry, F. A., Clarke, R. H. and O'Riordan, M. C. Early estimates of UK radiation doses from the Chernobyl reactor. Nature, 321, 1986.

Gäggeler, H., Von Gunten, H. R. and Nyffeler, U. Determination of ^{210}Pb in lake sediments and in air samples by direct gamma-ray measurement. Earth and Planet. Sci. Letts., 33, 119-121, 1976.

Galoway, F and Bender, M. Diagenetic models of interstitial nitrate profiles in deep-sea suboxic sediments. Limnol. Oceanogr. 27, 624-638, 1982.

Gillson, G. R., Douglas, D. J., Fulford, J. E., Halligan, K. W. and Tanner, S. D. Nonspectroscopic interelement interferences in inductively coupled plasma mass spectrometry. Anal. Chem., 60, 1472-1474, 1988.

Goldberg, E. D., Gamble, E., Griffin, J. J. and Koide, M. Pollution history of Narragansett Bay as recorded in its sediments. Est. Coast Mar. Sci. 5, 549-561, 1977.

Goldberg, E. D., Hodge, V., Koide, M., Griffin, J. J., Gamble, E., Bricher, V. P., Matisoff, G., Holdren, G. R. and Braun, R. A pollution history of Chesapeake Bay. Geochim. Cosmochim. Acta, 42, 1978.

Goldberg, E. D. and Koide, M. Geochronological studies of deep-sea sediments by the Io/Th method. Geochim. Cosmochim. Acta, 26, 417-450, 1962.

Greenwood, N. N. and Earnshaw, A. Chemistry of the Elements. Pergamon Press Ltd, Oxford, 1984.

Gubala, C. P., Engstrom, D. R. and White, J. R. Effects of Iron Cycling on ^{210}Pb Dating of Sediments in an Adirondack Lake, USA. J. Fish. Aquat. Sci., 47, 1990.

Guinasso, N. L. and Schink, D. R., 1975. Quantitative estimate of biological mixing rates in abyssal sediments. Jour. Geophys. Research, 80, 3032-3043, 1975.

Guppy, R. M. and Atkinson, A. The evolution of redox conditions in a repository: preliminary investigations. UK DOE Report DOE/RW/89/103. DOE, London, UK, 1989.

Hamilton-Taylor, J. The geochemistry of fjords in south west Norway. Unpubl. PhD Thesis, University of Edinburgh, 1974.

Hamilton-Taylor, J. and Price, N. B. The Geochemistry of Iron and Manganese in the Waters and Sediments of Bolstadfjord, S. W. Norway. Est. Coastal. Shelf Sci., 17, 1-19, 1983.

Hanor, J. S. and Marshall, J. S. Mixing of sediment by organisms. In: Trace Fossils. Ed: Bob F. Perkins, Louisiana State University Miscellaneous Publication 71-1, 127-135, 1971.

Harrison, R. M. and Laxen, D. P. H. Lead Pollution. University Press, Cambridge, 1981.

Henderson, P. Inorganic Chemistry. Ed. Pergamon Press, Oxford, 1982.

Hetherington, J. A. The behaviour of plutonium nuclides in the Irish Sea. In: Environmental Toxicity of Aquatic Radionuclides: Models and Mechanisms. Eds. M. W. Miller and J. N. Stannard, Ann Arbor Science Publishers Inc., 1975.

Hetherington, J. A. The uptake of plutonium nuclides by marine sediments. Mar. Sci. Comms., 4(3), 239-274, 1978.

Horrill, A. D., Lowe, V. P. W. and Hawson, G. Chernobyl fallout in Great Britain. DOE Report No DOE/RW/88.101, UK. Department of the Environment, London, 1988.

Houk, R. S. Mass spectrometry of inductively coupled plasmas. Anal. Chem., 58, 1, 1986.

Huh, C. A. and Ku, T.L. Radiochemical observations on manganese nodules from three sedimentary environments in the North Pacific. Geochim. Cosmochim. Acta, 48, 951-963, 1984.

Huh, Chih-An, Zahnle, D. L., Small, L. F. and Noshkin, V. E. Budgets and behaviours of uranium and thorium series isotopes in Santa Monica Basin sediments. Geochim. Cosmochim. Acta, 51, 1743-1754, 1987.

Hunt, G. J. Timescales for Dilution and Dispersion of Transuranics in the Irish Sea near Sellafield. Sci. Total Env., 46, 261-278, 1985.

Hunt, G. J. and Kershaw, P. J. Remobilisation of artificial radionuclides from the sediment of the Irish Sea. J. Radiol. Prot., 10, 2, 147-151, 1990.

Ivanovich, M. and Harmon, R. S. Uranium-series Disequilibrium: Applications to Earth, Marine and Environmental Sciences. 2nd Edition. Eds: Clarendon Press, Oxford, 1992.

Jahnke, R. A., Emerson, S. R. and Murray, J. W. A model of oxygen reduction, denitrification and organic matter mineralization in marine sediments. Limnol. Oceanogr. 27, 610-623, 1982.

Jarvis, K. E. Inductively coupled plasma mass spectrometry: a new technique for the rapid or ultra-trace level determination of the rare-earth elements in geological materials. Chemical Geology, 68, 31-39, 1988.

Jarvis, K. E., Gray, A. L., Houk, R. S., et al. Handbook of inductively coupled plasma mass spectrometry. Ed. Blackie, Glasgow and London.

Jefferies, D. F., Preston, A. and Steele, A. K. Distribution of Caesium-137 in British Coastal Waters. Mar. Poll. Bull., 4, 8, 1973.

Jones, D. G., Roberts, P. D. and Miller, J. M. The Distribution of Gamma-emitting Radionuclides in Surface Subtidal Sediments Near the Sellafield Plant. Estuarine, Coastal and Shelf Science, 27, 143-161, 1988.

Jones, D. G., Miller, J. M. and Roberts, P. D. The Distribution of ^{137}Cs in Surface Intertidal Sediments from the Solway Firth. Mar. Poll. Bull., 15, 5, 187-194, 1984.

Kadko, D., Cochran, J. K. and Lyle M. The effect of bioturbation and adsorption gradients on solid and dissolved radium profiles in sediments from the eastern equatorial Pacific. Geochimica Cosmochim. Acta, 51, 1613-1623, 1987.

Keller, C. Radiochemistry. Ellis Horwood Limited, Chichester, 1988.

Kemp. A. I. W., Thomas, R. I., Dell, G.I. and Jaquet, J. M. J. Fish resources Board, Canada, 33, 440, 1976.

Kershaw, P. J., Woodhead, D. S., Malcolm, S. J., Allington, D. J. and Lovett, M. B. A Sediment History of Sellafield Discharge. J. Environ. Radioactivity, 12, 201-241, 1990.

Kesler, S. E. Economic lead deposits. In: Nriagu, J. O. (ed). The Biochemistry of Lead in the Environment, Part A, pp73. Elsevier/North-Holland, Biomedical Press, Amsterdam, 1978.

Kester, D. R., Byrne, Jr, R. H. and Liang, Yu-Jean. Redox Reactions and Solution Complexes of Iron in Marine Systems. In: Marine Chemistry in the Coastal Environment. Ed: Robert F. Gould, 1975.

Kester, D. R. et al (Group report). Chemical Species in Marine and Estuarine Systems. In: The Importance of Chemical "Speciation" in Environmental Processes. Eds. M. Bernhard, F. E. Brinckman and P. J. Sadler, 275-299, 1986.

Kigoshi, K. Alpha-recoil thorium-234: dissolution into water and the uranium-234/uranium-238 disequilibrium in nature. Science, 173, 47-48, 1971.

Klinkhammer, G., Heggie, D. T. and Graham, D. W., 1982. Metal diagenesis in oxic marine sediments. Earth Planet. Sci. Lett., 61, 211-219, 1982.

Koide, M., Bruland, K. W. and Goldberg, E. D. Th-228/Th-232 and Pb-210 geochronologies in marine and lake sediments. Geochim. Cosmochim. Acta, 37, 1171-1187, 1973.

Kram, M. D. The geochemistry of Loch Duich, Scotland. Unpubl. PhD Thesis, University of Edinburgh, 1976.

Krauskopf, K. B., Introduction to Geochemistry, 2nd Edition. Ed. McGraw Hill, New York, 617pp., 1979.

Krylov, O. T., Novikov, P. D. and Nesterova, M. P. Calculation of Relative Amounts of Uranium Forms in Sea Water. Oceanology, 25, 2, 1985.

Ku, T. L. and Broecker, W. S. Radiochemical studies on manganese nodules of deep-sea origin. Deep Sea Res., 16, 625-637, 1969.

Ku, T. L. and Lin, M. C. ^{226}Ra distribution in the Antarctic Ocean. Earth Planet. Sci. Letts., 32, 236, 1976.

Li, Yuan-Hui, Burkhardt, L. and Teraoka, H. Desorption and coagulation of trace elements during estuarine mixing. Geochim. Cosmochim. Acta, 48, 1879-1884, 1984.

Li, Yuan-Hui, Feely, H. W. and Toggweiler, J. R. ^{228}Ra and ^{228}Th concentrations in GEOSECS Atlantic surface waters. Deep-Sea Res., 27A, 545-555, 1980.

Li, Yuan-Hui, Mathieu, G., Biscaye, P. and Simpson, H. J. The flux of ^{226}Ra from estuarine and continental shelf sediments. Plan. Sci. Letts., 37, 237-241, 1977.

Lillie, D. W. Our Radiant World. The Iowa State University Press, 1986.

Livingston, H. D., Bowen, V. T. and Kupferman, S. L. Radionuclides from Windscale discharges I: nonequilibrium tracer experiments in high-latitude oceanography. Jour. Marine Research, 40, part 1, 253-272, 1982.

Livingston, H. D. and Bowen, V. T. Windscale effluent in the waters and sediments of the Minch, Nature, 269, 586-588, 1977.

Long, S. E. and Brown, R. M. Optimisation in inductively coupled plasma mass spectrometry. Analyst, 111, 901-906, 1986.

Longerich, H. P., Fryer, B. J., Strong, D. F. and Kantipuly, C. J. Effects of operating conditions on the determination of the rare earth elements by inductively coupled plasma mass spectrometry (ICP-MS). Spectrochimica Acta, 428, 1/2, 75-92, 1987.

Lyon, T. D. B., Fell, G. S., McKay, K. and Scott, R. D. Accuracy of multi-element analysis of human tissue obtained at autopsy using inductively coupled plasma mass spectrometry. Jour. Anal. Atomic Spec., 6, 1991.

Lyon, T. D. B., Fell, G. S., Hutton, R. C. and Eaton, A. N. Evaluation of inductively coupled argon plasma mass spectrometry (ICP-MS) for simultaneous multi-element

trace analysis in clinical chemistry. Jour. Anal. Atomic Spec., 3, 265-271, 1988.

MacKenzie, A. B. A radionuclide study of the Clyde Sea Area. PhD Thesis, Department of Chemistry, University of Glasgow, 1977.

MacKenzie, A. B. Radiochemical Methods in Instrumental Analysis of Pollutants. Ed. C. N. Hewitt, Elsevier, New York, 367pp, 1991.

MacKenzie, A. B., Baxter, M. S., McKinley, I. G., Swan, D. S. and Jack, W. The determination of ^{134}Cs, ^{137}Cs, ^{210}Pb, ^{226}Ra and ^{228}Ra concentrations in nearshore marine sediments and seawater. Jour. Radioanal. Chem., 48, 29-47, 1979.

MacKenzie, A. B. and Scott, R. D. Sellafield waste radionuclides in Irish Sea intertidal and salt marsh sediments. (In press) 1993.

MacKenzie, A. B. and Scott, R. D. Artificial radionuclides in the coastal zone of southern Scotland. In: Transuranic cycling behaviour in the marine environment. IAEA TECDOC 265, 111-119, IAEA, Vienna, 1982.

MacKenzie, A. B., Scott, R. D., Allan, R. L., Ben Shaban, Y. A., Cook, G. T. and Pulford, I. D. Sediment radionuclide profiles: implications for mechanisms of Sellafield waste dispersal in the Irish Sea. (In press), 1993.

MacKenzie, A. B., Scott, R. D. and Williams, T. M. Mechanisms for northwards dispersal of Sellafield waste. Nature, 329, 6134, 42-45, 1987.

MAFF. Radioactivity in surface and coastal waters of the British Isles. Aquatic Environment Monitoring Reports. Ministry of Agriculture Fisheries and Food, Lowestoft, UK, 1990.

Malcolm, S. J. Early diagenesis of molybdenum in estuarine sediments. Marine Chem., 16, 213-225, 1985.

Malcolm, S. J. The Chemistry of Sediments of Loch Etive, Scotland. PhD Thesis, University of Edinburgh, 1981.

Marine Pollution Bulletin. Distribution of Caesium-137 in British Coastal Waters. Marine Pollution Bulletin, 4, 8, 1973.

Maring, H., Settle, M., Buat-Menard, P., Dulac, F. and Patterson, C. C. Stable lead isotope tracers of air mass trajectories in the Mediterranean region. Nature, 300, 154, 1987.

Martin, W. R. and Sayles, F. L. Seasonal cycles of particle and solute transport processes in nearshore sediments: $^{222}Rn/^{226}Ra$ and $^{234}Th/^{238}U$ disewuilibrium at a site in Buzzards Bay, MA. Geochim. Cosmochim. Acta, 51, 977-943, 1987.

McCartney, M., Kershaw, P. J., Woodhead, D. S. and Denoon, D. C. Artificial radionuclides in the surface sediments of the Irish Sea, 1968-1988. Sci. Total Environ. (in press), 1993.

McDonald, P., Cook, G. T., Baxter, M. S. and Thompson, J. C. The terrestrial distribution of artificial radioactivity in south-west Scotland. Sci. Tot. Environ., 111, 59-82, 1992.

McDonald, P., Cook, G. T., Baxter, M. S. and Thomson, J. C. Radionuclide Transfer from Sellafield to South-West Scotland. J. Environ. Radioactivity, 12, 285-298, 1990.

McKay, W. A. Marine Chemistry and Tracer Applications of Radiocaesium. PhD Thesis, University of Glasgow, 1983.

McKay, W. A. and Baxter, M. S. The Partitioning of Sellafield-derived Radiocaesium in Scottish Coastal Sediments. J. Environ. Radioactivity, 2, 93-114, 1985.

McKinley, I. G. Tracer applications of radiocaesium in a coastal marine environment. PhD Thesis, Department of Chemistry, University of Glasgow, 1978.

McKinley, I. G., Baxter, M. S., Ellett, D. J. and Jack, W. Tracer Applications of Radiocaesium in the Sea of the Hebrides. Est. Coastal. Shelf Sci. 13, 69-82, 1981.

McKinley, L. G., Baxter, M. S. and Jack, W. A Simple Model of Radiocaesium Transport from Windscale to the Clyde Sea Area. Estuarine Coastal and Shelf Science, 13, 59-67, 1981.

Miller, K. M. Self-absorption corrections for gamma ray spectral measurements of ^{210}Pb in environmental samples. Nucl. Instr. Methods Phys. Res. A258, 281-285, 1987.

Miller, J. M., Thomas, B. W., Roberts, P. D. and Creamer, S. C. Measurement of marine radionuclide distribution using a towed sea-bed spectrometer. Marine Pollution. Bull., 13, 315-319, 1982.

Milliman, J. D., Summerhayes, C. P. and Barreto, H. T. Oceanography and suspended matter of the Amazon River, February-March. J. Sed. Petrol. 45, 189-206, 1975.

Mitchell, N. T. Radioactivity in surface and coastal waters of the British Isles, 1975. Tech. Rep. Fish. Radiobiol. Lab., M.A.F.F., Direct. Fish. Res. (FRL 12) pp32, 1977.

Moorbath, S. Lead isotope abundance studies on mineral occurrences in the British Isles and their geological significance. Phil. Trans. R. Soc. Lon, 254, 295, 1962.

Moore, W. S. Oceanic concentrations of ^{228}Radium. Earth Planet. Sci. Letts. 6, 437-446, 1969.

Moore, W. S. Radium-228: Application to thermocline mixing studies. Earth Planet. Sci. Letts., 16, 421-422, 1972.

Moore W. S. and Dymond, J. Correlation of ^{210}Pb removal with organic carbon fluxes in the Pacific Ocean. Nature, 331, 1988.

Moore, W. S., Dean, W. E., Krishnaswami, S. and Borole, D. V. Growth rates of

manganese nodules in Oneida Lake, New York. Earth Planet. Sci. Lett., 46, 191-200, 1980.

Moore, W. S., Ku, T. L., MacDougall, J. D., Burns, V. M., Burns, R., Dymond, J., Lyle, m. W. and Piper, D. Z. Fluxes of metals to a manganese nodule: radiochemical, chemical, structural and mineralogical studies. Earth Planet. Sci. Lett., 52, 151-171, 1981.

Murray, J. and Irvine, R. On the chemical changes which take place in the composition of the seawater associated with blue muds on the floor of the ocean. Trans. R. Soc. Edin. 37, 481-507, 1985.

NERC. The Clyde Estuary and Firth, An Assessment of Present Knowledge. Publ. Series C. no. 11, 1974.

Nozaki, Y. and Tsunogai, S. ^{226}Ra, ^{210}Pb and ^{210}Po disequilibria in the Western North Pacific. Earth Planet. Sci. Letts, 32, 313-321, 1976.

Nozaki, Y., Cochran, J. K., Turekian, K. K. and Keller, G. Radiocarbon and ^{210}Pb distribution in submersible-taken deep-sea cores from Project Famous. Earth Planet. Sci. Letters, 34, 167-173, 1977.

Nozaki, Y., Thomson, J. and Turekian, K. K. The distribution of ^{210}Pb and ^{210}Po in the surface waters of the Pacific Ocean. Earth Planet. Sci. Letts., 32, 304-312, 1976.

Nriagu, J. O. Properties and the biogeochemical cycle of lead. In: Nriagu, J. O. (ed.). The Biochemistry of Lead in the Environment, Part A, pp1. Elsevier/North-Holland Biomedical Press, Amsterdam, 1978.

Nriagu, J. O. A global assessment of natural sources of atmospheric trace metals. Nature, 338, 47, 1989.

Nriagu, J. O. Human influence on the global cycling of trace metals. In: Heavy Metals in the Environment, 1. Ed. J. G. Farmer, CEP Consultants, Edinburgh, 1991.

Olivares, J. A. and Houk, R. S. Suppression of analyte signal by various concomitant salts in inductively coupled plasma mass spectrometry. Anal. Chem., 58, 20-25, 1986.

Paalman, M. A. A., Van de Meent-Olieman, G. C. and Van der Weijden, C. H. Porewater chemistry of estuarine Rhine-Meuse sediments; (re)mobilization of Cu, Zn and Ni. In: Heavy Metals in the Environment, 1. Ed: J. G. Farmer, CEP Consultants, Edinburgh, 1991.

Parry, S. J., 1991. Activation Spectrometry in Chemical Analysis, Chemical Analysis, vol. 119. Ed. John Wiley, New York, 531pp, 1991.

Pearson, T. H. and Stanley, S. O. Comparative Measurement of the Redox Potential of Marine Sediments as a Rapid Means of Assessing the Effect of Organic Pollution. Marine Biology, 53, 371-379, 1979.

Pedersen, T. F., Waters, R. D. and Macdonald, R. W. On the natural enrichment of cadmium and molybdenum in the sediments of ucluelet inlet, British Columbia. Sci. Tot. Environ., 79, 125-139, 1989.

Peng, T. H., Broecker, W. S., Kipphut, G. and Shackleton, N. Benthic mixing in deep sea cores as determined by ^{14}C dating and its implications regarding climate, stratigraphy and the fate of fossil fuel CO_2. In: The Fate of Fossil Fuel CO_2 in the Oceans. Eds. N. R. Andersen and A. Malahoff, Plenum, New York, 355-374, 1977.

Pentreath, R. J., Harvey, B. R. and Lovett, M. B. Chemical speciation of transuranium nuclides discharged into the marine environment. In: Speciation of fission and activation products in the environment. 312-324. Eds. R. A. Bulman and J. R. Cooper, Elsevier Applied Science Publishers, London and New York, 1986.

Pentreath, R. J., Lovett, M. B., Jefferies, D. F., Woodhead, D. S, Talbot, J. W. and Mitchell, N. T. Impact on public radiation exposure of transuranium nuclides discharged in liquid wastes from fuel element reprocessing at Sellafield, United Kingdom. In: Radioactive Waste Management, 5, IAEA, Vienna.

Peterson, M. L. and Carpenter, R. Arsenic distributions in porewaters and sediments of Puget Sound, Lake Washington, the Washington coast and Saanich Inlet, B. C. Geochim. Cosmochim. Acta. 50, 353-369, 1986.

Petit, D., Mennessier, J. P. and Lamberts, L. Stable lead isotopes in pond sediments as tracer of past and present atmospheric lead pollution in Belgium. Atmos. Env., 18, 6, 1189-1193, 1984.

Petroleum Products Handbook, 1st Edition. Ed. V. B. Guthrie, McGraw Hill Book Company, 1960.

Physical Chemistry, 2nd Edition. Ed. Gordon M. Barrow, McGraw Hill Book Company, New York, 1966.

Plasma source mass spectrometry. Proc. 3rd Surrey Conf. Univ. of Surrey. Eds. K. E. Jarvis, A. L. Gray, J. G. Williams and I. Jarvis. Publ. Roy. Soc. Chem., 1989.

Price, N. B. and Calvert, S. E. ICSU/SCOR Symp., Cambridge 1970. Inst. Geol. Sci. Rep. 70/16, 185, 1973.

Redfield, A. C., Ketchum, B. H. and Richards, F. A. The influence of organisms on the composition of seawater. In: The Sea, 2nd Edition. Ed. M. N. Hill, Wiley, New York, p26-77, 1963.

Reid, D. F., Moore, W. S. and Sackett, W. M. Temporal variation of ^{228}Ra in the near-surface Gulf of Mexico. Earth. Planet Sci. Letts., 43, 227-236, 1979.

Reuther, J. H. Chemical interactions involving the bioshpere and fluxes of organic material in estuaries. In: River inputs to ocean systems. Eds. J. M. Martin, J. D. Burton and D. Eisma, 243-249, Paris UNEP/Unesco, 1981.

Riddle, C., Vander Voet, A. and Doherty, W. Rock analysis using inductively

coupled plasma mass spectrometry: a review. Geostandards Newsletter, 12, 1, 203-234, 1988.

Ridgway, I. M. The Behaviour of Organic Matter and Minor Elements in Scottish Sea Lochs. PhD Thesis, University of Edinburgh, 1984.

Ridgway, I. M. and Price, N.B. Geochemical associations and post-depositional mobility of heavy metals in coastal sediments: Loch Etive, Scotland. Marine Chemistry, 21, 229-248, 1987.

Robbins, J. A. and Edgington, D. N. Determination of recent sedimentation rates in Lake Michigan using Pb-210 and Cs-137. Geochim. Cosmochim. Acta, 39, 285-304, 1975.

Santschi, P. H., Li, Y. H., Adler, D. M., Amdurer, M., Bell, J. and Nyffeler, U. P. The relative mobility of natural (Th, Pb and Po) and fallout (Pu, Am, Cs) radionuclides in the coastal marine environment: results from model ecosystems (MERL) and Narrangansett Bay. Geochemica et Cosmochimica Acta, 47, 201-210, 1982.

Sawlan, J. J. and Murray, J. W. Trace metal remobilization in the interstitial waters of red clay and hemipelagic marine sediments. Earth. Planet. Sci. Letts., 64, 213-230, 1983.

Schell, W. R. and Barnes, R. S. Environmental isotope anthropogenic tracers of recent lake sedimentation. In: The Terrestrial Environment, B. Chapt. 4., 1986.

Selby, M. and Hieftje G. M. Inductively coupled plasma-mass spectrometry: A status report. International Laboratory, 28-38, 1987.

Shimmield, G. B. and Pedersen, T. F. The Geochemistry of Reactive Trace Metals and Halogens in Hemipelagic Continental Margin Sediments. Aquatic Sciences, 3, issues 2 and 3, 255-279, 1990.

Shimmield, T. M., MacKenzie, A. B. and Price, N. B. ICP-MS analysis of trace element concentrations in interstitial waters of Scottish sea loch sediments. In: Heavy Metals in the Environment, 1. Ed. J. G. Farmer, CEP Consultants, Edinburgh, 1991.

Shishkina, O. V. and Pavlova, G. A. Geochemistry, 2, 559, 1965.

Sholkovitz, E. R. and Mann, D. R. The pore water chemistry of $^{239,240}Pu$ and ^{137}Cs in sediments of Buzzards Bay, Massachusetts. Geochim. Cosmochim. Acta, 48, 1107-1114, 1984.

Sholkovitz, E. R., Cochran, J. K. and Carey, A. E. Laboratory studies of the diagenesis and mobility of $^{239,240}Pu$ and ^{137}Cs in nearshore sediments. Geochim. Cosmochim. Acta, 47, 1369-1379, 1983.

Skei, J. Geochemical and sedimentological considerations of a permanently anoxic fjord -Framvaren, South Norway. Sed. Geol., 36, 131-145, 1983.

Smith, T. J., Parker, W. R. and Kirby, R. Sedimentation studies relevant to low-level radioactive effluent dispersal in the Irish Sea. Part 1: Radionuclides in marine sediments. IOS Report No 110, pp87. Institute of Oceanographic Sciences, Godalming, UK, 1980.

Smith-Briggs, J. L. A Combined Trace Metal/Radionuclide Study of the Clyde Sea Area. PhD Thesis, University of Glasgow, 1983.

Stanners, D. A. and Aston, S. R. ^{134}Cs: ^{137}Cs and ^{106}Ru: ^{137}Cs Ratios in Intertidal Sediments from the Cumbria and Lancashire Coasts, England. Est. Coastal Shelf Sci., 13, 409-417, 1981.

Starik, I. Ye and Kolyadin, L. B. Conditions of occurrence of uranium in ocean water. Geokhimiya, 3, 204-209, 1957.

Strickland, J. D. H. and Parsons, T. R. A practical Handbook of Seawater Analysis. Fisheries Research Board, Canada, 1968.

Stumm, W and Morgan, J. J. Aquatic chemistry. New York: Wiley, 1981.

Sugawara, K. and Terada, K. J. Earth Sci., Nagoya Univ. 5, 81, 1957.

Sugden, C. L. Isotopic studies of the environmental chemistry of lead. PhD Thesis, University of Edinburgh, 1993.

Swan, D. S. Some Geochronological Applications of ^{210}Pb in the Coastal marine and Freshwater Environments. PhD Thesis, University of Glasgow, 1978.

Swan, D. S., Baxter, M. S., McKinley, I. G. and Jack, W. Radiocaesium and ^{210}Pb in Clyde Sea Loch Sediments. Estuarine, Coastal and Shelf Science, 15, 515-536, 1982.

Thomson, J., Colley, S., Anderson, R., Cook, G. T. and MacKenzie, A. B. ^{210}Pb in the sediments and water column of the Northeast Atlantic from 47 to 59°N along 20°W. Earth Planet. Sci. Letts., 115, 75-87, 1993.

Todd, J. F., Elsinger, R. J. and Moore, W. S. The distributions of uranium, radium and thorium isotopes in two anoxic fjords: Framvaren Fjord (Norway) and Saanich Inlet (British Columbia). Marine Chemistry, 23, 393-415, 1988.

Torgersen, T. and Longmore, M. E. ^{137}Cs Diffusion in the Highly Organic Sediment of Hidden Lake, Fraser Island, Queensland. Aust. J. Mar. Freshw. Res., 35, 537-48, 1984.

Trefry, J. H. and Presely, B. J. Heavy metal transport from the Mississippi River to the Gulf of Mexico. In: Marine Pollutant Transport, H. L. Windom and R. A. Duce (eds), 39-76. Lexington, Mass: Lexington Books, 1976.

Urban, N. R., Eisenreich, S. J., Grigal, D. F. and Schurr, K. T. Geochim. Cosmochim. Acta, 54, 3329, 1990.

VG Elemental. PlasmaQuad System Manual, Version 2a, 1988.

Viczián, M., Lásztity and Barnes, R. M. Identification of potential environmental sources of childhood lead poisoning by inductively coupled plasma mass spectrometry. Verification and Case Studies. Jour. Anal. Atomic Spec., 5, 293-300, 1990.

Vinogradov, A. P. Tr. Biogeokhim Lab., Akad. Nauk SSSR, 5, 33, 1939.

Walker, M. I. and McKay, W. A. Radionuclide Distributions in Seawater around the Sellafield Pipeline. Est. Coastal Shelf. Sci., 32, 385-393, 1991.

Wan, G. J., Santschi, P. H., Sturm, M., Farrenkothen, K., Lueck, A., Werth, E. and Schuler, Ch. Natural (^{210}Pb, ^{7}Be) and fallout (^{137}Cs, ^{239,240}Pu, ^{90}Sr) radionuclides as geochemical tracers of sedimentation in Greifensee, Switzerland. Chem. Geol., 63, 181-196, 1987.

Wehr, M. R. and Richards, Jr. J. A. Physics of the Atom. Addison-Wesley Publishing Company, Inc, London, 1966.

Williams, T. M., MacKenzie, A. B., Scott, R. D., Price, N. B. and Ridgway, I. M. Radionuclide distributions in the surface sediments of Loch Etive. Proc. International Symposium, Cherbourg, France, 1-5 June 1987. Ed. Elsevier, New York, 1987.

Williams, P. J. Primary productivity and hetrotrophic activity in estuaries. In: River inputs to oceans systems. Eds. J. M. Martin, J. D. Burton and D. Eisma, 243-249, Paris UNEP/Unesco, 1981.

Wilson, D. A., Vickers, G. H. and Hieftje, G. M. Analytical characteristics of an inductively coupled plasma-mass spectrometer. Spectrochimica Acta, 428, 1/2, 29-38, 1987.

Wilson, T. S. R. Caesium-137 as a water movement tracer in the St Georges Channel, Nature, 248, 125-127, 1974.

Wilson, T. R. S., Thompson, J., Colley, S., Hydes, D. J. and Higgs, N. C. Early organic diagenesis: the significance of progressive subsurface oxidation fronts in pelagic sediments. Geochim. Cosmochim. Acta, 49, 811-822, 1985.

Krishnaswami, S. and Lal, D. Radionuclide limnochronology. In: Lerman, A. (ed.), Lakes, Chemistry Geology and Physics, 153. Springer-Verlag, New York, 1978.

Santschi, P. H. and Honeyman, B. D. Radionuclides in aquatic environments. Radiat. Phys. Chem. 34, 2, 213, 1989.

Sugden, C. L., Farmer, J. G. and MacKenzie, A.B. Lead and ^{206}Pb/^{207}Pb Profiles on ^{210}Pb-dated ombrotrophic peat cores from Scotland. In: Heavy Metals in the Environment, 1. Ed. J.G. Farmer, CEP Consultants, Edinburgh, 1991.